NASA SP-352

ROTORCRAFT DYNAMICS

A conference held at
AMES RESEARCH CENTER
Moffett Field, California
February 13–15, 1974

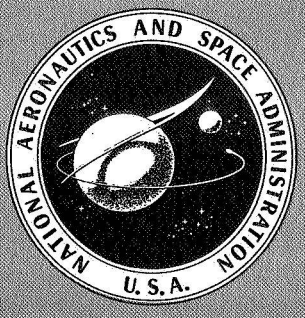

NATIONAL AERONAUTICS AND SPACE ADMINISTRATION

NASA SP-352

ROTORCRAFT DYNAMICS

A conference sponsored by
Ames Research Center and the American Helicopter Society
and held at Ames Research Center, Moffett Field, California
February 13–15, 1974

Prepared at Ames Research Center

Scientific and Technical Information Office 1974
NATIONAL AERONAUTICS AND SPACE ADMINISTRATION
Washington, D.C.

For sale by the National Technical Information Service
Springfield, Virginia 22151
Price $8.00

PREFACE

Events of recent years have clearly identified rotorcraft dynamics as one of the most critical technologies pacing the helicopter industry's efforts to develop new rotor concepts. And as rotary wing program investments have escalated, the financial stakes in the technical risks have become tremendous. The rotor dynamicist is suddenly very much in the critical path.

Fortunately Research and Development efforts by industry in rotorcraft dynamics have been greatly augmented in recent years by stepped up in-house efforts on the part of NASA and the U. S. Army. New computer tools and more complete experimental data coming from many quarters, are bringing us to the threshold of a far more complete understanding of the problem. This increased R&D is reflected in the number of high quality papers that have exceeded the capacity of the dynamics session at recent AHS Annual Forums.

With these thoughts in mind, the Specialists' Meeting on Rotorcraft Dynamics was organized to provide an opportunity for the principal investigators in the field to dialogue in greater depth than is possible at the American Helicopter Society Annual Forum. This is the first such meeting in the U. S. since the CAL/TRECOM Helicopter and V/STOL Dynamic Loads Symposium in 1963.

This volume contains the formal presentations of the first four sessions of the meeting. Presentations of the fifth session and transcriptions of questions and panel discussions are contained in the supplement to this volume.

E. S. Carter, Jr.
Meeting General Chairman

ORGANIZING COMMITTEE

General Chairman
Edward S. Carter, Jr., Sikorsky Aircraft

Technical Chairman
Robert A. Ormiston, U. S. Army Air Mobility R&D Laboratory, Ames Directorate

Administrative Chairman
James C. Biggers, NASA–Ames Research Center

Chairman, AHS Dynamics Technical Committee
E. Roberts Wood, Lockheed-California Company

Session Chairmen and Co-Chairmen

Session I
Kurt H. Hohenemser, Washington University
James R. Neff, Hughes Helicopters

Session II
E. Roberts Wood, Lockheed-California Company
G. Alvin Pierce, Georgia Institute of Technology

Session III
Peter J. Arcidiacono, Sikorsky Aircraft
William E. Nettles, U. S. Army Air Mobility R&D Laboratory Eustis Directorate

Session IV
James J. O'Leary, Boeing Vertol Company
William G. Flannelly, Kaman Aerospace Corporation

Session V
Troy M. Gaffey, Bell Helicopter Company

CONTENTS

SUPPLEMENT

HINGELESS ROTOR FREQUENCY RESPONSE WITH UNSTEADY INFLOW

David A. Peters
Research Scientist
Ames Directorate
U.S. Army Air Mobility R&D Laboratory
Moffett Field, Calif. 94035

Abstract

Hingeless rotor frequency response calculations are obtained by applying a generalized harmonic balance to the elastic blade flapping equations. Nonuniform, unsteady induced flow effects are included by assuming a simple three-degree-of-freedom description of the rotor wake. Results obtained by using various models of elastic blade bending and induced flow are compared with experimental data obtained from a 7.5-ft diameter wind tunnel model at advance ratios from 0.0 to 0.6. It is shown that the blade elasticity and nonuniform, unsteady induced flow can have a significant effect on the transient response characteristics of rotor systems. Good correlation between theory and experiment is obtained by using: (i) a single rotating mode shape description of the elastic blade bending, (ii) an empirical formula for the quasi-steady induced flow behavior, and (iii) the apparent mass terms from potential flow for the unsteady induced flow characteristics.

Notation

a	two-dimensional lift-curve slope, rad^{-1}
a_{jn}, b_{jn}	harmonics of jth flapping mode
b	number of blades
B	tip loss factor
c	blade chord, ft
$\bar{C}_T$	steady value of thrust coefficient, steady thrust/$\rho\pi\Omega^2R^4$
C_T	harmonic perturbation of thrust coefficient
C_L	harmonic perturbation of roll moment coefficient = roll moment/$\rho\pi\Omega^2R^5$, positive advancing blade down
C_M	harmonic perturbation of pitch moment coefficient = pitch moment/$\rho\pi\Omega^2R^5$, positive nose up
e	dimensionless flapping hinge offset
e_{pc}	dimensionless radius of pocket cutout
EI	rotor blade bending stiffness, $lb\text{-}ft^2$
$\{f\}$	generalized response vector
F,G	aerodynamic and inertial forces per unit blade span, lb/ft
g_o, g_s, g_c	nondimensional harmonics of inertial forcing function, Eq. (12)
i	$\sqrt{-1}$
I_A	apparent inertia of air, $slug\text{-}ft^2$
$[I]$	identity matrix
j	index referring to mode number
J	number of flap bending modes
K_m, K_I	nondimensional apparent mass and inertia of impermeable disk
$[K]$	control feedback matrix
$[L]$	nonuniform induced flow matrix
$[L_E]$	empirical value for quasi-steady portion of $[L]$
m	rotor blade mass distribution, slug/ft
$\bar{m}, m_{yy}, m_{yj}$	nondimensional blade parameters $\frac{1}{\rho acR^2}\int_o^R m\,dr$, $\frac{1}{\rho acR^4}\int_o^R mr^2\,dr$, $\frac{1}{\rho acR^3}\int_o^R mr\phi_j\,dr$
$[M],[M']$	rotor response matrix open loop, closed loop
dm	elemental apparent mass, slugs
$\dot{dm}$	elemental mass flow, slugs/sec
m_A	apparent mass of air, slugs
n	index referring to harmonic number
N	number of azimuthal harmonics
$[0]$	null matrix
p	first flap frequency divided by Ω
q_j	generalized coordinates
$\bar{q}_j$	steady values of q_j
r	rotor blade radius coordinate, ft
R	rotor blade radius, ft
$S(0,\psi)$	blade root moment, ft-lb
S_j	blade parameter $\frac{1}{\rho acR^2}\int_o^R m\phi_j\,dr$
$\{u\}$	generalized control vector $\langle\theta_o\theta_s\theta_c g_o g_s g_c \lambda_o \lambda_s \lambda_c\rangle$
U_P, U_T	perpendicular, tangential components of air speed in undeformed blade coordinate system, ft/sec
U_∞, V_∞	freestream airspeed perpendicular and parallel to rotor shaft (V_∞ positive down), ft/sec
v	induced flow parameter = $[\mu^2 + \bar{\lambda}(\bar{\lambda} + \bar{v})]/(\mu^2 + \bar{\lambda}^2)^{1/2}$
$V(0,\psi)$	blade root shear, lb
w	rotor blade flap deflection, ft
$[W]$	frequency transform, Eq. (23)
$\{x\}$	physical control vector $\langle\theta_o\theta_s\theta_c z\phi\alpha\rangle$
$[Y]$	control coupling matrix
z	hub plunge deflection divided by R, positive down
α	hub pitch angle, positive nose up, rad

Presented at the AHS/NASA-Ames Specialists' Meeting on Rotorcraft Dynamics, February 13-15, 1974.

γ	Lock number, $1/m_{yy}$
γ^*	equivalent Lock number, Eq. (35)
θ	blade pitch angle = $\bar{\theta} + (\theta_o + \theta_s \sin\psi + \theta_c \cos\psi)e^{i\omega\psi}$
$\bar{\theta}$	steady collective pitch angle
$\theta_o, \theta_s, \theta_c$	rotor pitch perturbations
λ	total inflow (including induced flow) $= \bar{\lambda} + \left(\lambda_o + \lambda_s \frac{r}{R} \sin\psi + \lambda_c \frac{r}{R} \cos\psi\right) e^{i\omega\psi}$
$\bar{\lambda}$	steady inflow ratio = $V_\infty/\Omega R + \bar{\nu}$
$\lambda_o, \lambda_s, \lambda_c$	inflow perturbations (including induced flow), Eq. (10)
μ	advance ratio = $U_\infty/\Omega R$
ν	total induced flow = $\bar{\nu} + \left(\nu_o + \nu_s \frac{r}{R} \sin\psi + \nu_c \frac{r}{R} \cos\psi\right) e^{i\omega\psi}$
$\bar{\nu}$	induced flow due to steady rotor thrust
ν_o, ν_s, ν_c	induced flow perturbations
ρ	air density, slug/ft^3
σ	rotor solidity, $bc/\pi R$
τ_T, τ_S	induced flow time constants, rad^{-1}
ϕ	hub roll angle, positive advancing blade down, rad
ϕ_j	orthogonal functions
ψ	rotor blade azimuth position, nondimensional time, rad
ω	excitation frequency divided by Ω
Ω	rotor blade angular velocity, rad/sec
$(\,)'$	$\partial/\partial r$
$\dot{(\,)}$	$\partial/\partial\psi$

The dynamic response characteristics of hingeless rotors are dependent upon the distributed structural properties of the rotor blades, the local aerodynamic properties of the blade sections, and the detailed description of the aerodynamic environment. It is generally believed, however, that reasonable predictions of rotor thrust and moments at low lift can be obtained by using some appropriately simplified models for the blade structure, section aerodynamics, and inflow distribution. The development of these simplified rotor models is useful for gaining insight into the basic dynamic mechanisms of rotor response. Detailed calculations of dynamic airloads, necessary for many applications, are usually too complex for use in basic dynamic research or preliminary design calculations.

The formulation of a minimum complexity rotor response model is the subject of several recent papers. One area of interest is the effect of mode shape and mode number on rotor flapping response. Shupe[1] addresses the effects of the second flap mode, Ormiston and Peters[2] compare various mode shape models for first and second flap modes, and Hohenemser and Yin[3] consider the effect of using rotating rather than nonrotating modes as generalized degrees of freedom. The fundamental conclusion, as clarified in Reference 3, is that for $\mu < 0.8$ a single rotating mode shape is adequate for modeling the steady rotor flapping response.

A second area of interest is the effect of induced flow perturbations on rotor flapping response. In Reference 1, a simple momentum theory predicts a significant effect of induced flow on steady rotor response. In Reference 2, a comparison of steady experimental and theoretical results indicates that, although there is a significant effect due to induced flow, momentum theory is inadequate for predicting this effect in forward flight. Alternate induced flow models are introduced and compared with the data, but no clear choice for the best model is found. In Reference 4, an unsteady momentum theory is used in hover to improve correlations with experimental frequency response data.

The work in References 1 through 4 indicates that a minimum complexity analytic model for rotor dynamics must include appropriate degrees of freedom for both structural and induced flow perturbations (certain flight dynamics programs presently include a simplified dynamic treatment of the induced flow[5]). Unfortunately, while some success has been achieved using simple models of the rotor induced flow in hover, a completely satisfactory induced flow model for forward flight has not been found, not even for the condition of steady response. In addition, neither the physical values of the induced flow time constants nor the frequency range in which they are important is known. The unsteady behavior of the induced flow contributes directly to the low frequency rotor control characteristics and to the coupled rotor/fuselage aeroelastic stability. In particular, induced flow perturbations contribute to the rotor damping available in pitch and roll (which is important for ground and air resonance calculations). It is consequently important to understand the dynamic characteristics of the induced flow.

The purpose of this paper is to provide additional insight into the question of rotor structural and induced flow modeling. To this end, experimental rotor frequency response data in hover and in forward flight are compared with theoretical results that are calculated by using several different models for the elastic blade bending and induced flow. The frequency response data provide a broad base of comparison so that the effects of mode shape and induced flow model can be clearly determined throughout the frequency range of interest.

Basic Equations

Analysis

The mathematical technique used here is a further generalization of the harmonic balance approach of Reference 2. In addition to an arbitrary number of bending modes (with an arbitrary number of azimuthal harmonics for each mode), the generalized harmonic balance allows for a

rational treatment of reversed flow aerodynamics and the possibility of harmonically oscillating control inputs.

The linear equation of motion for the deflection of an elastic beam subject to distributed aerodynamic and inertial loadings $F(r,\psi)$ and $G(r,\psi)$ is[6]

$$(EIw'')'' + m\Omega^2\ddot{w} + \Omega^2\left(mrw' - w''\int_r^R mr\,dr\right) = F(r,\psi) + G(r,\psi) \qquad (1)$$

The associated expressions for bending moment and shear at the blade root are

$$S(0,\psi) = \int_0^R (F + G - m\Omega^2\ddot{w} - m\Omega^2 w)r\,dr \qquad (2)$$

$$V(0,\psi) = \int_0^R (F + G - m\Omega^2\ddot{w})dr \qquad (3)$$

The blade root bending moment is transformed into a stationary coordinate system to yield the pitch and roll moment of the rotor. The solution of Eq. (1) yields directly the blade deflections, and substitution into Eqs. (2) and (3) then yields the forces and moments.

Application of the harmonic balance involves, first of all, an orthogonal expansion of w:

$$\frac{w}{R} = \sum_{j=1}^{J} q_j(\psi)\phi_j(r) \qquad (4)$$

For the present analysis, the ϕ_j are taken to be the exact mode shapes of the rotating beam without aerodynamics. Galerkin's method is then used to transform Eq. (1) into J ordinary differential equations (with periodic coefficients) for the modal coordinates q_j.[6] When the forcing terms contain a steady portion superposed onto periodic functions that are modulated by an excitation frequency ω (cycles per revolution), Floquet's theorem implies that the q_j have a solution of the form[7]

$$q_j = \bar{q}_j + \left\{a_{jo} + \sum_{n=1}^{\infty}\left[a_{jn}\cos(n\psi) + b_{jn}\sin(n\psi)\right]\right\}e^{i\omega\psi} \qquad (5)$$

where $\bar{q}_j$ are the steady coning displacements and the a_{jn} and b_{jn} are complex quantities indicating the magnitude and phase shift of each modulated harmonic of the perturbation response. The harmonic balance approach entails substituting Eq. (5) into the J ordinary differential equations for q_j and setting coefficients of like harmonics equal. When n is truncated at the highest harmonic of interest N, then $(2 \cdot N + 1) \cdot J$ linear algebraic equations are obtained for the a_{jn} and b_{jn}. Solution of these equations, followed by a substitution of Eq. (5) into Eqs. (2) and (3), results in the phase and magnitude of all desired harmonics of the flapping deflections and hub forces and moments.

Blade Loading

The aerodynamic loading of each blade is given by

$$F = \frac{\rho ac}{2}|U_T|\left(U_T\theta - U_P\right) \qquad (6)$$

where

$$U_T = \Omega r + \Omega R\mu\sin\psi \qquad (7)$$

$$U_P = \dot{w} + \Omega R\lambda + \Omega R\mu w'\cos\psi \qquad (8)$$

Eq. (8) contains the primary contributions of mode shape and induced flow to the flapping equations. The details of blade mode shape become important as μ increases because U_P depends upon both the blade deflection w and its first derivative w'. The induced flow is important because first order perturbations to the inflow λ create first order changes to U_P and F.

Although the inflow is in general a complicated function of radius and azimuth, as a first approximation, the total inflow can be represented by

$$\lambda = \bar{\lambda} + \left[\lambda_o + \lambda_s\frac{r}{R}\sin\psi + \lambda_c\frac{r}{R}\cos\psi\right]e^{i\omega\psi} \qquad (9)$$

The steady portion of the total inflow $\bar{\lambda}$ contains contributions from the freestream velocity $V_\infty/\Omega R$ and from the steady induced flow due to rotor thrust $\bar{\nu}$. The unsteady inflow components $\lambda_o,\lambda_s,\lambda_c$ contain contributions from harmonic plunging $ze^{i\omega\psi}$, rolling $\phi e^{i\omega\psi}$, and pitching $\alpha e^{i\omega\psi}$ of the shaft, as well as contributions from the unsteady induced flow components ν_o,ν_s,ν_c due to perturbations in rotor thrust and moments:

$$\left.\begin{aligned}\lambda_o &= -i\omega z + \nu_o - \mu\alpha\\ \lambda_s &= -i\omega\phi + \nu_s\\ \lambda_c &= -i\omega\alpha + \nu_c\end{aligned}\right\} \qquad (10\ a\text{-}c)$$

The blade pitch angle θ is given by

$$\theta = \bar{\theta} + \left[\theta_o + \theta_s\sin\psi + \theta_c\cos\psi\right]e^{i\omega\psi} \qquad (11)$$

where $\bar{\theta}$ is the steady value of θ and $\theta_o,\theta_s,\theta_c$ are control system perturbations. The inflow perturbations $\lambda_o,\lambda_s,\lambda_c$ are assumed to be

small compared with unity. This implies that the induced flow perturbations ν_o,ν_s,ν_c and the control perturbations $\theta_o,\theta_s,\theta_c,z,\phi,\alpha$ are also small quantities yielding linear perturbation equations.

The inertial loading of each blade is given by

$$G = -m\Omega^2 R\left[g_o + g_s \frac{r}{R}\sin\psi + g_c \frac{r}{R}\cos\psi\right]e^{i\omega\psi} \quad (12)$$

where

$$\left.\begin{aligned} g_o &= \omega^2 z \\ g_s &= \omega^2\phi + 2i\omega\alpha \\ g_c &= -2i\omega\phi + \omega^2\alpha \end{aligned}\right\} \quad (13\ a\text{-}c)$$

The inertial loading is a result of centrifugal, Coriolis, and gyroscopic forces which occur in the rotating reference frame of the blade due to hub motions z,ϕ,α in the inertial reference frame.

When Eqs. (6) through (12) are combined and appropriately integrated in Eqs. (1), (2), and (3), the steady deflections and forces $q_j,\bar{C}_T/\sigma a$ are obtained as linear functions of the steady inputs $\bar{\theta},\bar{\lambda}$; and the perturbation blade deflections and hub forces and moments are obtained as linear combinations of the generalized control variables

$$\langle u\rangle = \langle \theta_o\theta_s\theta_c g_o g_s g_c \lambda_o\lambda_s\lambda_c \rangle \quad (14)$$

Although g_o,g_s,g_c are simply related to the shaft motion through Eq. (13), they are retained as generalized controls so that the generalized controls can be separated into physical, inertial, and aerodynamic groupings. This will facilitate the calculation of rotor response when induced flow is included later.

Interpretation of Results

The results of the harmonic balance can be expressed in matrix form as

$$\{f\} = [M]\{u\} \quad (15)$$

where $\{f\}$ represents the perturbation harmonics of thrust, moments, and generalized coordinates. The elements of $[M]$, therefore, have direct physical significance. They are the partial derivatives of each of the response harmonics taken with respect to each of the generalized controls u_j. The generalized control variables are in turn functions of the physical controls x_j,

$$\langle x\rangle = \langle \theta_o\theta_s\theta_c z\phi\alpha \rangle \quad (16)$$

as evidenced in Eqs. (10) and (13).

The generalized control variables u_j are also coupled to the f_j, because the thrust and moments influence the induced flow. The induced flow, therefore, is a feedback loop of Eq. (15), causing the u_j to depend upon the f_j.

From the standpoint of calculation, it is convenient to express the coupling relation (between the generalized controls, the physical controls, and the rotor response) in matrix form:

$$\{u\} = [Y]\{x\} + [K]\{f\} \quad (17)$$

Eq. (17) is simply a set of linear equations describing: (i) the generalized control perturbations due to application of the physical controls $[Y]$ and (ii) the generalized control perturbations due to the effect that rotor response has on the induced flow $[K]$. The matrices $[Y]$ and $[K]$ will be obtained later by using an appropriate induced flow model. It follows that the partial derivatives of the f_j with respect to the physical controls x_j can be found (including induced flow effects) from Eqs. (15) and (17). The derivative matrix is designated $[M']$ and has the properties

$$\{f\} = [M']\{x\} \quad (18)$$

$$[M'] = \left[[I] - [M][K]\right]^{-1}[M][Y] \quad (19)$$

Although the higher harmonics are often necessary in the harmonic balance calculation of $[M]$, the subsequent calculation of $[M']$ by Eq. (19) may be performed for only those response and inflow harmonics of interest. In this paper, five harmonics are used in the calculation of $[M]$, but only first harmonics are retained in Eqs. (18) and (19), so that the f_j are taken to be

$$\langle f\rangle = \left\langle \frac{C_T}{\sigma a}\frac{C_L}{\sigma a}\frac{C_M}{\sigma a}\, a_{j0} b_{j1} a_{j1} \right\rangle \quad (20)$$

Induced Flow

Form of Induced Flow Model

A useful form of the induced flow model is given by[2]

$$\begin{Bmatrix}\nu_o\\ \nu_s\\ \nu_c\end{Bmatrix} = [L]\begin{Bmatrix}C_T/\sigma a\\ C_L/\sigma a\\ C_M/\sigma a\end{Bmatrix}\ \text{aerodynamic only} \quad (21)$$

Although not completely general, Eq. (21) can accommodate a variety of induced flow models. Only aerodynamic contributions are included on the right-hand side, because they are the only loads which produce reaction forces on the rotor wake. Using Eqs. (2) and (3), these aerodynamic forces and moments can be expressed in matrix form as

$$\begin{Bmatrix} C_T/\sigma a \\ C_L/\sigma a \\ C_M/\sigma a \end{Bmatrix}_{\substack{\text{aero-}\\ \text{dynamic}}} = \begin{Bmatrix} C_T/\sigma a \\ C_L/\sigma a \\ C_M/\sigma a \end{Bmatrix} + \begin{bmatrix} \bar{m} & 0 & 0 \\ 0 & -\frac{1}{2} m_{yy} & 0 \\ 0 & 0 & -\frac{1}{2} m_{yy} \end{bmatrix} \begin{Bmatrix} g_o \\ g_s \\ g_c \end{Bmatrix}$$

$$- [W] \begin{bmatrix} S_j & 0 & 0 \\ 0 & -\frac{1}{2} m_{yj} & 0 \\ 0 & 0 & -\frac{1}{2} m_{yj} \end{bmatrix} \begin{Bmatrix} a_{jo} \\ b_{j1} \\ a_{j1} \end{Bmatrix} \qquad (22)$$

where

$$[W] \equiv \begin{bmatrix} \omega^2 & 0 & 0 \\ 0 & \omega^2 & 2i\omega \\ 0 & -2i\omega & \omega^2 \end{bmatrix} \qquad (23)$$

With the induced flow ν described by Eqs. (21) and (22), the inflow relation follows directly from Eqs. (10), (13), and (21). The matrices [Y] and [K] of Eq. (17) may then be identified as

$$[Y] = \begin{bmatrix} I_{3\times3} & 0_{3\times3} \\ 0_{3\times3} & [W]_{3\times3} \\ 0_{3\times3} & [L][W] \begin{bmatrix} \bar{m} & 0 & 0 \\ 0 & -\frac{1}{2} m_{yy} & 0 \\ 0 & 0 & -\frac{1}{2} m_{yy} \end{bmatrix} - \begin{bmatrix} i\omega & 0 & \mu \\ 0 & i\omega & 0 \\ 0 & 0 & i\omega \end{bmatrix} \end{bmatrix} \qquad (24)$$

$$[K] = \begin{bmatrix} 0_{3\times3} & 0_{3\times3J} \\ 0_{3\times3} & 0_{3\times3J} \\ [L]_{3\times3} & -[L][W] \begin{bmatrix} S_j & 0 & 0 \\ 0 & -\frac{1}{2} m_{yj} & 0 \\ 0 & 0 & -\frac{1}{2} m_{yj} \end{bmatrix}_{3\times3J} \end{bmatrix} \qquad (25)$$

Eq. (24) represents the control coupling between the physical controls x_j and the generalized controls u_j. The presence of [L] in this matrix indicates that the λ's are indirectly coupled (through the induced flow), as well as geometrically coupled [Eqs. (10) and (13)] to the rotor plunge, pitch, and roll motions. Eq. (25) represents the induced flow caused by the dependence of λ upon the thrust and first harmonic flapping. If a suitable approximation to the inflow can be modeled in the form of Eq. (21), then Eqs. (24) and (25) may be substituted directly in Eq. (19) to obtain the complete rotor response to physical control inputs.

Unsteady Momentum Theory

An approximation of the induced flow that is suitable for Eq. (21) can be obtained as an extension of the momentum theory used in Reference 2. The differential force on an elemental area of rotor disk is written as

$$dF = 2\Omega R\nu d\dot{m} + \Omega^2 R\dot{\nu} dm \qquad (26)$$

where $2\Omega R\nu$ is the total change in velocity normal to the disk, $d\dot{m}$ is the differential mass flow through the element, dm is the apparent mass associated with the flow, and $\dot{\nu}$ is the time derivative of ν in the nonrotating system. The differential mass flow relation

$$d\dot{m} = \rho\Omega R \sqrt{\mu^2 + \lambda^2}\, r\, dr\, d\psi \qquad (27)$$

can be used to integrate the first term of Eq. (26) over the disk to obtain a quasi-steady induced flow relation for rotors that have combined conditions of thrust and forward speed. The evaluation of the second term in Eq. (26) (the unsteady effect) requires the additional knowledge of the apparent mass dm associated with the flow.

An approximation to the apparent mass terms of a lifting rotor can be made in terms of the reaction forces (or moments) on an impermeable disk which is instantaneously accelerated (or rotated) in still air. This approximation was used in Reference 8, giving good agreement with transient thrust measurements for an articulated rotor. The reactions on such an impermeable disk are given from potential flow theory in terms of elliptic integrals which are evaluated in the literature.[9] They result in apparent mass and inertia values

$$m_A = \frac{8}{3} \rho R^3 , \qquad I_A = \frac{16}{45} \rho R^5 \qquad (28)$$

(For $\nu = \nu_o\, r/R$, a radial velocity distribution, $m_A = \rho R^3$.) These values represent 64 percent of the mass and 57 percent of the rotary inertia of a sphere of air having radius R. It is emphasized that they are only approximations to the actual values for a lifting rotor.

Using this approximation, the steady induced flow equation and the unsteady induced flow perturbation equations can be derived from Eqs. (26) through (28):

$$2\bar{\nu} \sqrt{\mu^2 + \bar{\lambda}^2} = \bar{C}_T \qquad (29a)$$

$$\left.\begin{aligned} K_m \dot{\nu}_o + 2\nu\nu_o &= C_T \\ K_I \dot{\nu}_s + \tfrac{1}{2} \nu\nu_s &= -C_L \\ K_I \dot{\nu}_c + \tfrac{1}{2} \nu\nu_c &= -C_M \end{aligned}\right\} \qquad (29b\text{-}d)$$

where

$$v \equiv \frac{\mu^2 + \bar{\lambda}(\bar{\lambda} + \bar{\nu})}{\sqrt{\mu^2 + \bar{\lambda}^2}} \tag{29e}$$

and

$$\left.\begin{aligned} K_m &\equiv \frac{m_A}{\rho\pi R^3} = \frac{8}{3\pi} = 0.8488 \\ K_I &\equiv \frac{I_A}{\rho\pi R^5} = \frac{16}{45\pi} = 0.1132 \end{aligned}\right\} \tag{30a-b}$$

Eq. (29a) expresses the nonlinear relation between the steady thrust and the steady induced flow $\bar{\nu}$. Eqs. (29b-d) are then the linear perturbation equations for small changes in thrust, moments, and induced flow. In order for the perturbation equations to be valid, it is assumed that ν_o, ν_s, ν_c are much smaller than $(\mu^2 + \bar{\lambda}^2)^{1/2}$.

The time constants associated with the induced flow model in Eq. (29) are

$$\left.\begin{aligned} \tau_T &= \frac{K_m}{2v} = 0.4244/v \qquad (\text{for } \nu_o) \\ \tau_S &= \frac{2K_I}{v} = 0.2264/v \qquad (\text{for } \nu_s, \nu_c) \end{aligned}\right\} \tag{31a-b}$$

In Reference 4, the steady induced flow $\bar{\nu}$ and the time constant for ν_s, ν_c are obtained by correlating experimental hover frequency response data. Two operating conditions are considered, and the best fit in these cases is found to be $\bar{\nu} = .014$, $\tau_s = 8$ (with $\bar{\theta} = 2°$) and $\bar{\nu} = .028$, $\tau_s = 4$ (with $\bar{\theta} = 8°$). From the $\bar{\nu}$ values indicated for these cases, it can be shown that each τ_s implies the same value of $K_I = 0.112$. Thus, there is some experimental evidence that the potential flow value $K_I = 0.113$ is approximately valid.

By assuming simple harmonic motion, Eqs. (29b-d) can be brought into the form of Eq. (21), yielding the components of [L] for unsteady momentum theory.

$$[L] = \begin{bmatrix} \dfrac{\sigma a}{2v + K_m i\omega} & 0 & 0 \\ 0 & \dfrac{-\sigma a}{v/2 + K_I i\omega} & 0 \\ 0 & 0 & \dfrac{-\sigma a}{v/2 + K_I i\omega} \end{bmatrix} \tag{32}$$

(L_{22} and L_{33} differ by a factor of 4/3 from Reference 2, because ν_s and ν_c are taken uniform with r in that reference, whereas they are taken linear with r here.) The matrix [L] from Eq. (32) may now be substituted into Eqs. (24), (25), and (19) to obtain the rotor response that includes inflow.

Empirical Model

Experimental data have shown that momentum theory, although particularly simple to use, is qualitatively inaccurate for certain steady response derivatives in forward flight.[2] Reference 2 introduces an alternate induced flow model for forward flight in which the elements of [L] (with $\omega = 0$) are chosen to give the best fit of experimental response data for several configurations at conditions of near zero lift. If this empirical inflow model, $[L_E]$, is taken for the quasi-steady portion of the induced flow law, and if the theoretical apparent mass terms (from potential flow) are taken as a model for the unsteady portion of the induced flow law, then a complete induced flow equation can be expressed as

$$\frac{1}{\sigma a}\begin{bmatrix} K_m & 0 & 0 \\ 0 & -K_I & 0 \\ 0 & 0 & -K_I \end{bmatrix}\begin{Bmatrix} \dot{\nu}_o \\ \dot{\nu}_s \\ \dot{\nu}_c \end{Bmatrix} + [L_E]^{-1}\begin{Bmatrix} \nu_o \\ \nu_s \\ \nu_c \end{Bmatrix} = \begin{Bmatrix} C_T/\sigma a \\ C_L/\sigma a \\ C_M/\sigma a \end{Bmatrix} \tag{33}$$

The assumption that the apparent mass terms may be superposed on the quasi-steady terms is not rigorous, but it can be considered analogous to unsteady wing theory in which the apparent mass terms are theoretically independent of the free-stream velocity. Under the superposition assumption, the empirical inflow model modified for the unsteady case is

$$[L] = \left[\begin{bmatrix} K_m & 0 & 0 \\ 0 & -K_I & 0 \\ 0 & 0 & -K_I \end{bmatrix}\frac{i\omega}{\sigma a} + [L_E]^{-1}\right]^{-1} \tag{34}$$

Although this particular formulation of [L] is valuable for predicting the effects of induced flow, ultimately a more consistent formulation of [L] should be made, as discussed in Reference 10.

Equivalent Lock Number

Another method of accounting for the unsteady induced flow is the use of an equivalent Lock number γ^*, which can be derived from a single harmonic balance of the root moment equation:

$$\frac{\gamma^*}{\gamma} = 1 - \frac{1}{1 + 8v/\sigma a + 16K_I i\omega/\sigma a} \tag{35}$$

Although this approach is not a completely consistent treatment of the induced flow, since it does not give an exact harmonic balance of the blade flapping and thrust equations, it yields results which are nearly the same as those obtained from momentum theory.[2]

The practical use of Eq. (35) is somewhat limited because of the inaccuracies of momentum theory in forward flight, but a γ^* approach is nevertheless a valuable conceptual tool for understanding the effects of induced flow. In particular, Eq. (35) shows that one effect of induced flow perturbations is to decrease the effective Lock number (i.e., decrease the aerodynamic effectiveness). This decrease is most pronounced at low values of ν (i.e., low μ and $\bar{\theta}$) and low values of ω. For example, rotor roll moment is plotted in Figure 1 for two values of $\bar{\theta}$ and compared with the value from elementary theory (steady induced flow only, induced flow perturbations neglected, equivalent to $\lim \bar{\theta} \to \infty$). The curves for $\bar{\theta} = 0, 0.05$ result in values of roll moment well below the elementary value.

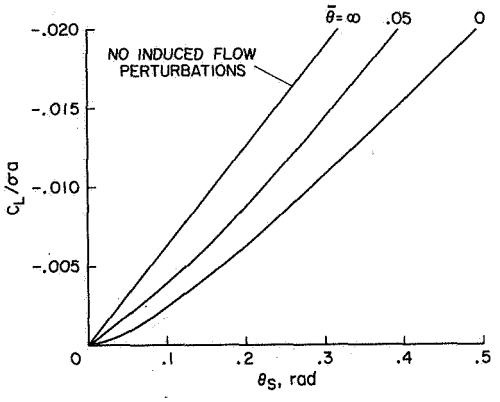

Figure 1. Effect of induced flow on steady rotor response in hover, $\mu = 0$, $\omega = 0$, $\sigma = 0.1$, $a = 2\pi$, $p = \infty$.

The effect of induced flow is most pronounced in the response derivative (the slope of the response curve at $\theta_s = 0$). For $p = \infty$, the derivative is given by

$$\partial\left[C_L/\sigma a\right]/\partial\theta_s\Big|_{\theta_s=0} \simeq -\frac{1}{16}\frac{\gamma^*}{\gamma}\left(1 + 3/2\ \mu^2\right) \quad (36)$$

indicating that $\gamma^*/\gamma < 1$ results in a reduction of the roll moment response (or control power) from the elementary value. When the rotor is in hover with no lift ($\nu = 0$), a quasi-steady perturbation of θ_s ($\omega = 0$) results in no response because of the zero slope of the curve in Figure 1. The mathematical justification for the vanishing response derivative can be seen in Eqs. (35) and (36). With $\omega = \nu = 0$, γ^*/γ and the response derivative must equal zero. As $\bar{\theta}$ increases, however, $\bar{\nu}$ and ν increase so that γ^*/γ approaches unity and the derivative approaches -1/16, as illustrated in Figure 2. Within the practical range of thrust coefficients, however, the response derivative never recovers more than about 80 percent of the elementary value. Eq. (35) also implies that increasing advance ratio (which increases ν) will result in a partial recovery of γ^*/γ (and of the response derivative). This recovery is evident in

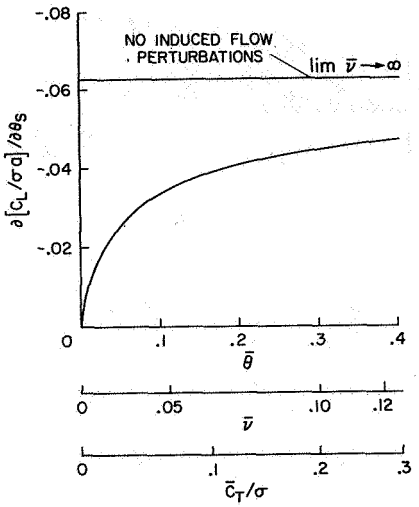

Figure 2. Effect of induced flow on steady rotor response derivatives in hover, $\mu = 0$, $\omega = 0$, $\sigma = 0.1$, $a = 2\pi$, $p = \infty$.

Figure 3, where the roll response is given versus μ; but no more than 90 percent of the elementary value is reached in the practical range of thrust and advance ratio.

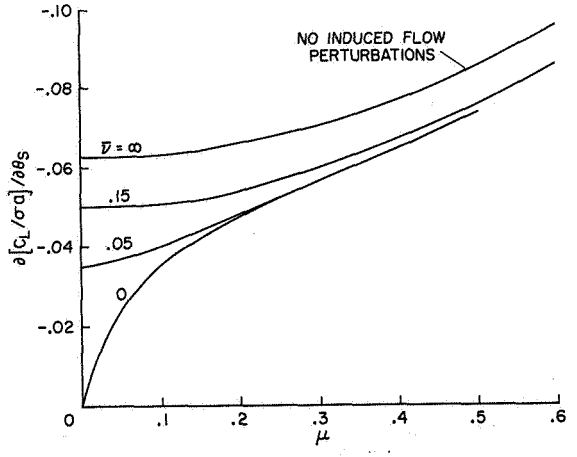

Figure 3. Effect of induced flow on steady rotor response derivatives in forward flight, $\omega = 0$, $\sigma = 0.1$, $a = 2\pi$, $p = \infty$.

The unsteady terms (apparent inertia K_I) also bring γ^*/γ closer to unity, as seen by the role of K_I in Eq. (35). This recovery with frequency is illustrated in Figure 4, where, as ω becomes large, the response derivative approaches the elementary value of -1/16. The rate at which the response approaches -1/16 is dependent upon the magnitude of the apparent inertia K_I. Large values of K_I result in a rapid return to the elementary value, and small values of K_I result in a slow return. For $K_I = 0.1132$ and $\omega < 0.3$, the unsteady terms provide only small contributions to the response. Thus, the quasi-

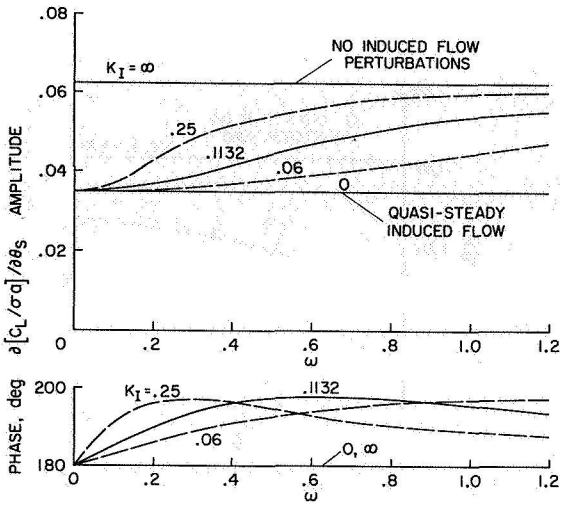

Figure 4. Effect of induced flow time constant on rotor frequency response derivatives, $\mu = 0$, $\sigma = 0.1$, $a = 2\pi$, $p = \infty$, $\bar{\nu} = \bar{\lambda} = 0.05$.

steady theory (with $K_I = 0$) would be adequate in this range. In the frequency range $0.3 < \omega < 1.0$, the unsteady terms have a more significant effect. Above $\omega = 1.2$, the total effect of induced flow diminishes so that the elementary theory and the unsteady theory give similar results; but the quasi-steady theory (with $K_I = 0$) is in considerable error in this region.

The frequency range in which unsteady induced flow is important is also dependent upon the thrust or mean inflow $\bar{\nu}$ as shown in Figure 5. For low values of $\bar{\nu}$, the unsteady effects dominate at low frequencies; and for large values of $\bar{\nu}$, the unsteady effects are delayed into the higher frequencies. This effect is implicit in Eq. (35) and is a direct result of the inverse dependence of time constant upon v, Eq. (31). Thus, a low $\bar{\nu}$ implies a slow induced flow response; and a high $\bar{\nu}$ implies a rapid induced flow response. Equation (35) shows that advance ratio (which also increases v) has a similar effect on the induced flow behavior. It follows that the relative importance of the unsteady and quasi-steady nonuniform induced flow terms depends upon both the rotor operating conditions and the frequency range of interest.

In Figure 6, the relative importance of these terms is presented qualitatively through a chart of the operating regimes in which (for no induced flow or quasi-steady induced flow) $|\gamma^*|$ differs by less than 10 percent from the unsteady value. This is a subjective criterion and is merely intended to illustrate the trends with thrust, advance ratio, and frequency. Four regions are defined: (i) at high ω and v, induced flow effects are small and either the elementary or quasi-steady approximation is adequate; (ii) at high ω and low v, although induced flow effects are small (no induced flow being a good approximation), the quasi-steady

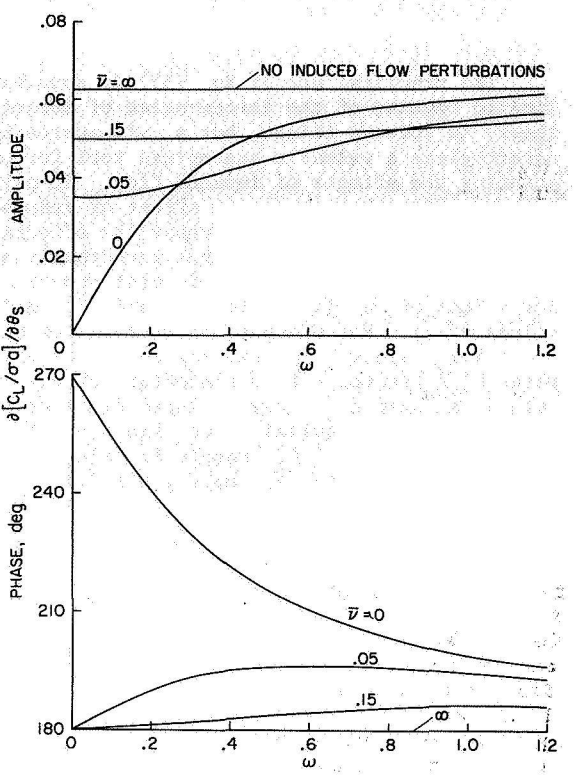

Figure 5. Effect of unsteady induced flow on rotor frequency response derivatives, $\mu = 0$, $\sigma = 0.1$, $a = 2\pi$, $p = \infty$, $K_I = 0.1132$.

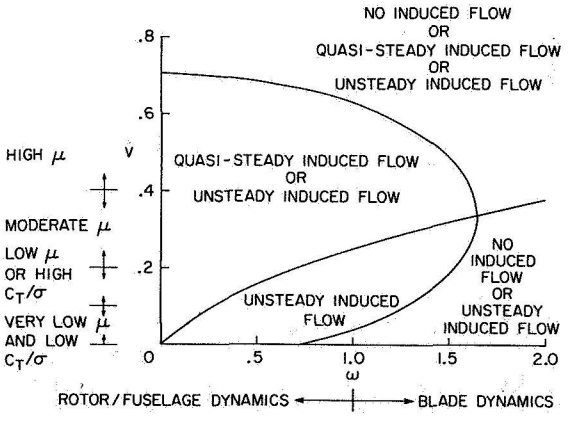

Figure 6. Regions of validity for steady (no induced flow perturbations) quasi-steady ($K_I = K_m = 0$), and unsteady ($K_I = 0.1132$, $K_m = 0.8488$) induced flow models based on γ^*, Eq. (35), $\sigma = 0.1$, $a = 2\pi$.

theory alone will be in error; (iii) at low ω and high v, the opposite is true (i.e., the quasi-steady nonuniform theory is required, whereas neglecting induced flow results in error); and (iv) for low ω and v, complete unsteady theory is required.

Comparison of Theory and Experiment

The experimental data used in the following correlations were obtained with a 7.5-ft-diameter hingeless rotor model tested in the USAAMRDL-Ames wind tunnel.[11] The model configuration and test conditions covered a wide range of parameters. The results included here are for $p = 1.15$ and advance ratios from 0.0 to 0.6.

Elastic Blade Bending

In Fig. 7, experimental values of roll and pitch moments due to θ_s are compared with theoretical results which are calculated neglecting induced flow perturbations. Two sets of theory are presented. The first theory employs a rigid centrally-hinged blade with root spring to model the elastic blade bending, and the second theory uses a similar model, except that hinge offset is allowed. The largest differences between the two theories occur near resonant frequencies, i.e., $\omega = 0.15, 1.15$. (The primary effect of mode shape is aerodynamic, Eq. (8); it causes dominance at resonance.) A surprising element in Figure 7 is that the centrally hinged model gives closer agreement with the high frequency response than does the hinge offset model. This reversal, however, is not a consistent trend in the data and may be somewhat coincidental.

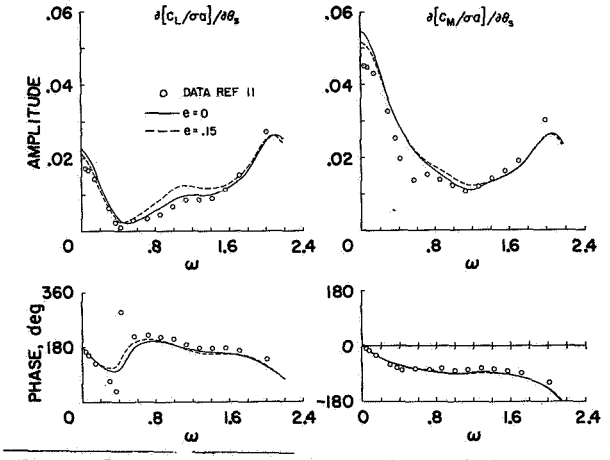

Figure 7. Comparison of experimental data with rigid blade approximations without induced flow, $p = 1.15$, $\gamma = 4.25$, $B = 0.97$, $e_{pc} = 0.25$, $\mu = 0.60$.

Similar frequency response comparisons have been made when the blade is modeled by one or two of the rotating elastic mode shapes. When $\mu < 0.8$ and ω is at least once-per-revolution below the second flap frequency, the one- and two-mode calculations are within a few percent of the hinge-offset results. At higher advance ratios and frequencies, the effects of second-mode bending can become significant; but in the range of operating conditions considered here, a single rotating mode is sufficient to model the blade.

Three major types of discrepancies between theory and experiment which are found in Figure 7 cannot be explained in terms of flapping mode shape effects. The first is the difference encountered at frequencies near one and two per revolution. This difference may be explained by the fact that the lead-lag frequency of this configuration is near two per revolution, causing resonance at these frequencies. The second discrepancy is the irregularity in the pitch response at $\omega = 0.6$. Here, a natural frequency of the rotor support stand is being excited and contaminates the data.[11] The third discrepancy is found at $\omega < 0.6$, and will be shown to result from unsteady inflow perturbations.

Effect of Induced Flow In Hover

The low-frequency hover data provide some insight into the effects of unsteady induced flow. In Figure 8, rotor roll and pitch moments versus θ_s are presented. The experimental results are for $\bar{\theta} = 4°$, $\bar{v} = 0.03$. The theoretical results are calculated using the actual blade rotating mode shape as a generalized coordinate and using three different representations of the induced flow. The first representation is the elementary model, which completely neglects induced flow perturbations. The second representation is quasi-steady momentum theory, which neglects the apparent inertia ($K_I = 0$), assuming that nonuniform induced flow perturbations instantaneously follow the blade dynamics. The third representation is unsteady momentum theory, which gives a time lag on the induced flow perturbations. (The empirical model is not applicable in hover.)

A comparison of theory and experiment reveals that the elementary theory is unsatisfactory below $\omega = 0.6$, failing to reproduce even the qualitative character of the data. On the other hand, the theories which include induced flow perturbations account for most of the important features of the response. The loss of aerodynamic effectiveness, which is a result of induced flow perturbations, causes a decrease in the excitation forces and an overall decrease in the response. But the loss of aerodynamic effectiveness also lowers the blade damping, causing a resonant peak effect near the blade natural frequency (with $p = 1.15$, $\omega = 0.15$).

The effect of the unsteady induced flow terms is also evidenced in Figure 8. The major contribution of K_I is the determination of how rapidly with ω the aerodynamic effectiveness returns to the elementary value. Above $\omega = 0.6$, the theoretical value of K_I gives the proper amplitude and phase for the hub moments, while the quasi-steady theory ($K_I = 0$) fails to return to the conventional value and does not agree with the data. Below $\omega = 0.6$ the comparison is less clear. In the roll-moment phase and amplitude, a K_I less than 0.1132 would give better correlation than does this theoretical value. In the pitch-moment response, however, a smaller K_I would give worse correlation than does $K_I = 0.1132$. Further work would be necessary to determine if this effect is due to experimental difficulties (such as recirculation) or to an actual deficiency in the induced flow model.

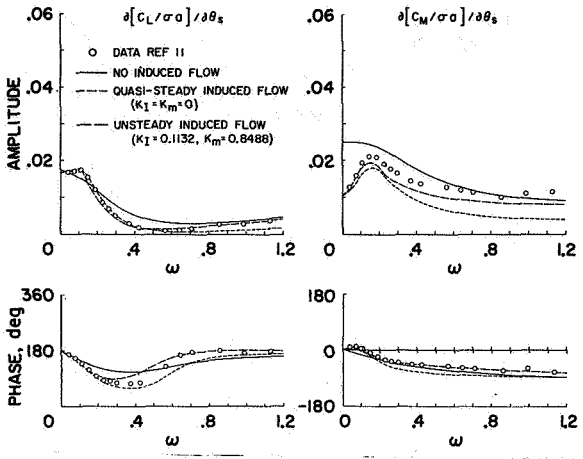

Figure 8. Rotor response to cyclic pitch in hover, $p = 1.15$, $\gamma = 4.25$, $B = 0.97$, $e_{pc} = 0.25$, $\mu = 0$, $\sigma a = 0.7294$, $\bar{\nu} = \bar{\lambda} = 0.03$, momentum theory, single rotating mode.

In Figure 9, rotor roll and pitch moments versus α are presented for the same test conditions as in Figure 8. Data are presented for shaft excitations in both roll and pitch, since in hover the response to these controls is ideally symmetric. A comparison of the two sets of data gives an indication of the experimental error due to test stand dynamics (and possibly recirculation). Although the data are questionable for $\omega > 0.3$, the lower frequency data substantiate three of the observations made from Figure 8. First, the elementary theory is qualitatively inaccurate for amplitude and phase response. Second, a major effect of induced flow is a resonant peak effect near $\omega = 0.15$. Third, $K_I < 0.1132$ would give better correlation than the theoretical value at low ω. Figure 9 also

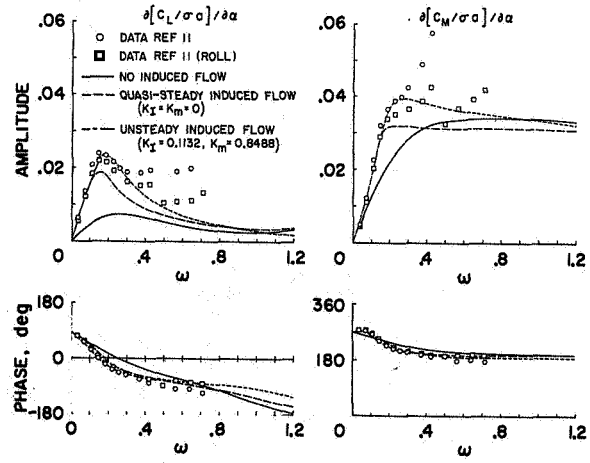

Figure 9. Rotor response to hub motions in hover, $p = 1.15$, $\gamma = 4.25$, $B = 0.97$, $e_{pc} = 0.25$, $\mu = 0$, $\sigma a = 0.7294$, $\bar{\nu} = \bar{\lambda} = 0.03$, momentum theory, single rotating mode.

shows that although induced flow decreases the blade damping, it can actually increase the rotor pitch/rate damping $= -\mathrm{Re}[\partial(C_M/\sigma a)/\partial\bar{\alpha}]$ and also increase the rotor pitch/roll coupling $= -\mathrm{Re}[\partial(C_L/\sigma a)/\partial\bar{\alpha}]$. The damping and coupling can be found by dividing the plotted curves by $-i\omega$, $\dot{\bar{\alpha}} = i\omega\bar{\alpha}$, which is approximately equivalent to taking the slope of the plotted curves with a 90-degree shift in phase angle. For this particular configuration, the damping and coupling are increased by induced flow effects, indicating that induced flow perturbations can be important in coupled rotor/fuselage dynamics.

Effect of Induced Flow in Forward Flight

In the next three figures, experimental data at high-advance ratio ($\mu = 0.51$) and very low lift ($\bar{\theta} \approx 0.5°$) are compared with theory using three induced flow descriptions. The first description is an analysis which neglects induced flow perturbations, the second description is the empirical model of Reference 2 with no time lag (quasi-steady, $K_I = K_m = 0$), and the third description is the empirical model of Reference 2 adapted to the unsteady case according to Eq. (34) (with the

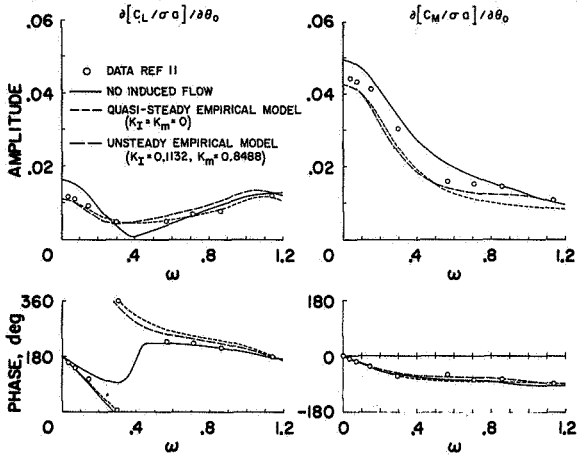

Figure 10. Rotor response to collective pitch in forward flight, $p = 1.15$, $\gamma = 4.25$, $B = 0.97$, $e_{pc} = 0.25$, $\mu = 0.51$, $\sigma a = 0.7294$, $\bar{\nu} = \bar{\lambda} = 0$, single rotating mode.

theoretical values of K_I and K_m). The first comparison of theory and experiment is shown in Figure 10 for the roll- and pitch-moment response due to θ_o. The elementary theory predicts a roll moment of 0.017 at $\omega = 0$ and a near-zero crossing (amplitude = 0, phase angle discontinuous) at $\omega = 0.4$. The data, however, displays a much lower steady value and completely avoids the zero crossing. The unsteady and quasi-steady empirical models provide a fairly accurate description of this behavior, showing quantitative agreement with phase and magnitude for $\omega < 0.6$. For the pitch moment derivative, the empirical models predict the qualitative (but not the quantitative) aspects of the reduction in moment (from the conventional value) due to induced flow.

Another comparison of theory and experiment is shown in Figure 11 for the roll- and pitch-moment response due to θ_s. The empirical models predict a roll-moment derivative which is less than the elementary value, exhibiting a near-zero crossing at $\omega = 0.26$. This characteristic is clearly evident in the magnitude and phase of the data, but it does not appear in the theory

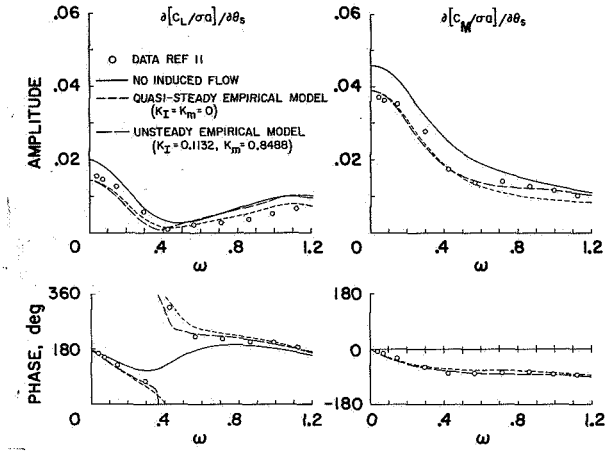

Figure 11. Rotor response to longitudinal cyclic pitch in forward flight, $p = 1.15$, $\gamma = 4.25$, $B = 0.97$, $e_{pc} = 0.25$, $\mu = 0.51$, $\sigma a = 0.7294$, $\bar{\nu} = \bar{\lambda} = 0$, single rotating mode.

without induced flow. For the pitch-moment derivative, the elementary theory agrees with the data only for $\omega > 1.2$; the quasi-steady theory shows good correlation for $0 < \omega < 0.6$, and the unsteady theory gives quantitative correlation at all frequencies.

The third comparison is shown in Figure 12 for the roll- and pitch-moment response due to θ_c. The data show that the roll-moment derivative is less than the elementary value at $\omega = 0$, displaying a resonant peak (near $\omega = 0.15$) which is greater than the elementary value and which is accompanied by a 10-degree phase shift. The empirical models predict the qualitative character of the resonant peak and quantitative character of the phase shift. The empirical models also correlate well with the pitch-moment response, for which the experiment shows the derivative to be greater than the elementary value for $\omega < 0.3$ and less than the elementary value for $\omega > 0.3$.

In general, the empirical inflow models show this same degree of correlation at all advance ratios considered ($\mu = 0.27, 0.36, 0.51, 0.60$). This substantiates one of the qualitative conclusions of Figure 6. For moderate advance ratios and $\omega < 1.0$, an appropriate unsteady or quasi-steady induced flow theory is adequate, but the theory without induced flow is in considerable error. Of course, Figure 6 only implies in which regions quasi-steady or unsteady terms may be significant. It does not imply that any particular quasi-steady or unsteady model will be

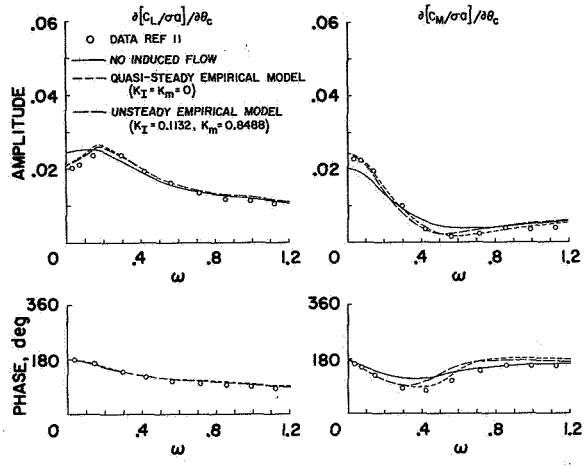

Figure 12. Rotor response to lateral cyclic pitch in forward flight, $p = 1.15$, $\gamma = 4.25$, $B = 0.97$, $e_{pc} = 0.25$, $\mu = 0.51$, $\sigma a = 0.7294$, $\bar{\nu} = \bar{\lambda} = 0$, single rotating mode.

adequate. For example, in Figure 13, pitch moment derivates (as calculated using the theory without induced flow, unsteady momentum theory, and unsteady empirical theory) are compared with the experimental data. The comparison shows that unsteady momentum theory can be in qualitative disagreement with the data even though empirical theory shows good correlation. Even the empirical model, however, does not show complete quantitative correlation; and further refinements in the induced flow model may be necessary.

Conclusions

1. On the basis of an equivalent Lock number relation and $p = \infty$, quasi-steady nonuniform induced flow perturbations can have a significant effect on rotor response throughout the entire thrust/advance ratio range; but the time lag of the induced flow is only important at low lift and low advance ratio.

2. In hover, unsteady momentum theory with apparent mass terms from potential flow provides a significant improvement in data correlation over the theory without induced flow perturbations; but further work is required to refine the induced flow model.

3. In forward flight and near-zero lift, the empirical inflow model of Reference 2, whether used with the unsteady time-lag effect or without the time-lag effect (quasi-steady), correlates well with most qualitative and some quantitative aspects of the data, while unsteady momentum theory and the theory without induced flow provide little agreement with the data.

4. A single rotating mode is sufficient for flapping response calculations when $\mu < 0.8$ and when the major excitation frequency is at least once-per-revolution below the second flapping frequency.

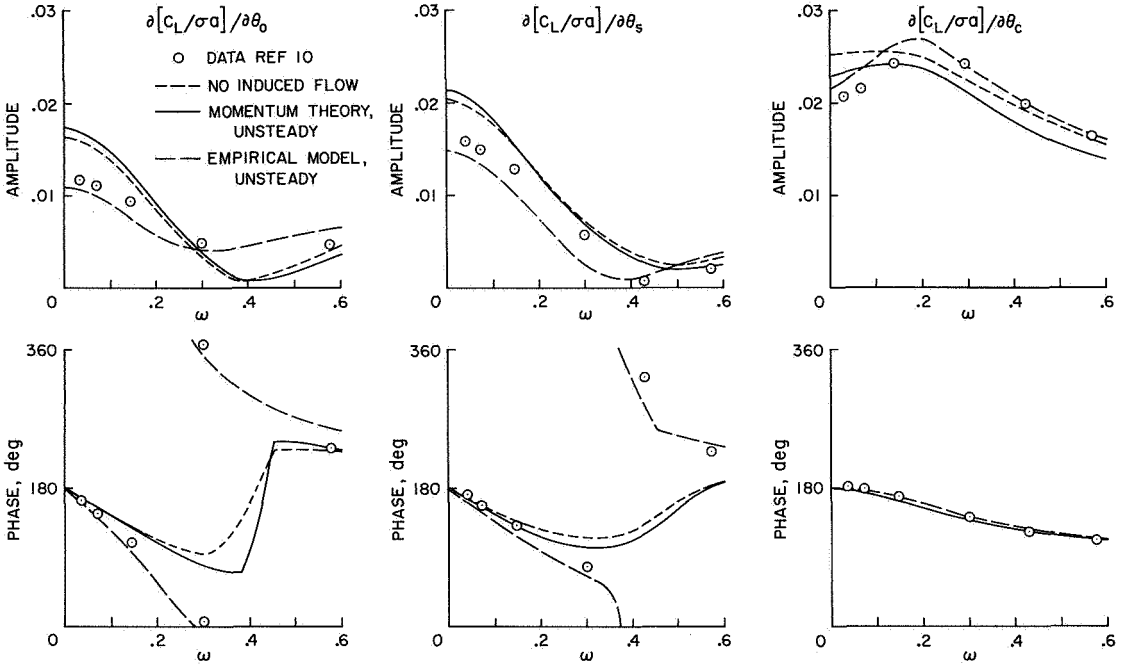

Figure 13. Effect of induced flow model on low frequency, roll response, p = 1.15, γ = 4.25, B = 0.97, e_{pc} = 0.25, μ = 0.51, σa = 0.7294, $\nu = \lambda$ = 0, K_I = 0.1132, K_m = 0.8488, single rotating mode.

References

1. Shupe, N. K., "A Study of the Dynamic Motions of Hingeless Rotored Helicopter," PhD. Thesis, Princeton Univ.

2. Ormiston, R. A. and Peters, D. A., "Hingeless Rotor Response with Nonuniform Inflow and Elastic Blade Bending," Journal of Aircraft, Vol. 9, No. 10, October 1972, pp. 730-736.

3. Hohenemser, K. H. and Yin, Sheng-Kwang, "On the Question of Adequate Hingeless Rotor Modeling in Flight Dynamics," 29th Annual National Forum of the American Helicopter Society, Preprint No. 732, May 1973.

4. Crews, S. T., Hohenemser, K. H., and Ormiston, R. A., "An Unsteady Wake Model for a Hingeless Rotor," Journal of Aircraft, Vol. 10, No. 12, December 1973.

5. Potthast, A. J., "Lockheed Hingeless Rotor Technology Summary - Flight Dynamics", Lockheed Report LR 259871, June 1973, p. 43.

6. Bisplinghoff, R. L., Ashley, H., and Halfman, R. L., Aeroelasticity, Addison-Wesley, Reading, Mass., c. 1955.

7. Peters, D. A. and Hohenemser, K. H., "Application of the Floquet Transition Matrix to Problems of Lifting Rotor Stability," Journal of the American Helicopter Society, Vol. 16, No. 2, April 1971, pp. 25-33.

8. Carpenter, P. J. and Fridovich, B., "Effect of Rapid Blade Pitch Increase on the Thrust and Induced Velocity Response of a Full Scale Helicopter Rotor," NACA TN 3044, Nov. 1953.

9. Tuckerman, L. B., "Inertia Factors of Ellipsoids for Use in Airship Design," NACA Report No. 210, 1925.

10. Ormiston, R. A., "An Actuator Disc Theory for Rotor Wake Induced Velocities," presented at AGARD Specialists' Meeting on the Aerodynamics of Rotary Wings, September 1972.

11. Kuczynski, W. A., "Experimental Hingeless Rotor Characteristics at Full Scale First Flap Mode Frequencies," NASA CR 114519, October 1972.

DYNAMIC STALL MODELING AND CORRELATION WITH EXPERIMENTAL DATA ON AIRFOILS AND ROTORS

R. G. Carlson, Supervisor
R. H. Blackwell, Dynamics Engineer
Rotor Dynamics Section
Sikorsky Aircraft Division of United Aircraft Corporation
Stratford, Connecticut

G. L. Commerford, Research Engineer
Aeroelastics Group, Fluid Dynamics Laboratory
United Aircraft Research Laboratories
East Hartford, Connecticut

P. H. Mirick, Aerospace Engineer
U. S. Army Air Mobility Research and Development Laboratory
Fort Eustis, Virginia

Abstract

Two methods for modeling dynamic stall have been developed at United Aircraft. The α, A, B Method generates lift and pitching moments as functions of angle of attack and its first two time derivatives. The coefficients are derived from experimental data for oscillating airfoils. The Time Delay Method generates the coefficients from steady state airfoil characteristics and an associated time delay in stall beyond the steady state stall angle. Correlation with three types of test data shows that the α, A, B Method is somewhat better for use in predicting helicopter rotor response in forward flight. Correlation with lift and moment hysteresis loops generated for oscillating airfoils was good for both models. Correlation with test data in which flexibly mounted two-dimensional airfoils were oscillated to simulate the 1P pitch variation of a helicopter rotor blade showed that both methods overpredicted the response, and neither gave a clear advantage. The α, A, B Method gave better correlation of torsional response of full scale rotors and remains the method in general use. The Time Delay Method has the potential to be applied more easily and probably can be improved by consideration of spanwise propagation of stall effects.

Stall-related phenomena limit the operational capabilities of the helicopter. Power, blade stress, and control system loads can all increase substantially due to blade stall. To predict such phenomena unsteady aerodynamics in stall must be modeled in blade aeroelastic analyses. A number of unsteady aerodynamic models have been developed. These include methods described in References 1 and 2. Reference 3 is a recent general survey article of rotor dynamic stall. The α, A, B Method and the Time Delay Method are two methods developed by United Aircraft. The α, A, B Method was developed to use airfoil test data obtained for a sinusoidally oscillating two-dimensional model airfoil. The Time Delay Method was developed to provide an empirical method that would agree with the lift and pitching moment hysteresis characteristics measured in oscillating airfoil tests for a number of airfoils and test conditions.

Evaluation of unsteady aerodynamic modeling techniques generally proceeds from correlation with data obtained in two-dimensional oscillating airfoil tests to correlation of full scale rotor blade torsional response. Two-dimensional rigid airfoil results are compared on the basis of aerodynamic pitch damping and lift and pitching moment hysteresis loops, and full scale correlation is judged on the basis of agreement in blade torsional moments or control rod loads. Evaluation of an unsteady model on the basis of full scale torsional response is made difficult by uncertainties in three-dimensional rotor inflow and blade bending and plunging motion. Correlation of the lift and pitching moment time histories of rigidly driven airfoils, on the other hand, is not the best method of comparison because it does not treat blade dynamic response to stall. As an intermediate approach, model test data were obtained for a flexibly mounted model airfoil which was dynamically scaled to simulate the dynamics of the first torsional mode of a rotor blade. This paper summarizes unsteady aerodynamic modeling techniques and includes comparisons based on two-dimensional aerodynamic pitch damping, lift and pitching moment hysteresis loops, two-dimensional flexured airfoil response, and full scale rotor blade torsional moments.

Description of the Unsteady Models

α, A, B Method

In the α, A, B method the aerodynamic moment is assumed to be a function of angle of attack and its first two time derivatives. Reference 4 demonstrated that unsteady normal force and moment data generated during sinusoidal airfoil tests and tabulated as functions of α, $A = \frac{b\dot{\alpha}}{U_o}$ and $B = \frac{b^2\ddot{\alpha}}{U_o^2}$ (where b is the airfoil semi-chord and U_o is the free stream velocity) could be used to predict the aerodynamic response of an airfoil executing

Presented at the AHS/NASA-Ames Specialists' Meeting on Rotorcraft Dynamics, February 13-15, 1974.

Based on work performed under U. S. Army Air Mobility Research and Development Laboratory Contract No. DAAJ02-72-C-0105.

a nonsinusoidal motion. In a limited number of flexured airfoil tests described in Reference 4, good correlation was achieved between measured and predicted airfoil dynamic response. The α, A, B lift and pitching moment data tabulations of Reference 4 were used in the calculation of torsional response for the dynamically scaled model airfoil. As applied in this investigation, two changes were made in the calculation. First, to consider the pitch axis of the model airfoil as a variable, provision was made to include pitching moment due to chordwise offset of the aerodynamic center from the pitch axis:

$$c_{m_{\bar{X}_{PA}}}(\alpha,A,B)=c_{m_{c/4}}(\alpha,A,B)+(\bar{X}_{PA}-.25)c_l(\alpha,A,B)$$

The second change involved scaling the unsteady data tables to account for differences in wind tunnel characteristics. The steady state lift and moment data for the present test program differed from the corresponding steady data obtained in Reference 4 because the tests were conducted in an open jet wind tunnel and because the airfoil effective aspect ratio was much higher. The method of scaling used for these analyses required a shift in the entire data tabulation by constant values of angle of attack, unsteady lift coefficient, and unsteady moment coefficient according to the following relations:

$$c_l(\alpha,A,B)_{\text{open jet}}=c_l(\alpha+\delta\alpha_l,A,B)_{TAB}+\delta c_l$$

and

$$c_m(\alpha,A,B)_{\text{open jet}}=c_m(\alpha+\delta\alpha_m,A,B)_{TAB}+\delta c_m$$

The constants $\delta\alpha_l$, $\delta\alpha_m$, δc_l and δc_m were established for each airfoil and were equal to the amount of shift necessary to make the open jet steady state stall points in lift and moment match the steady state stall points of the airfoil of Reference 4.

Time Delay Unsteady Model

Wind tunnel airfoil dynamic response was also calculated with the Sikorsky Time Delay unsteady aerodynamic method. This formulation was developed empirically by generalizing the results of a set of oscillating airfoil test programs. It is intended to predict the unsteady aerodynamic characteristics of arbitrary airfoils. Its aim is to provide the blade designer with unsteady lift and pitching moment characteristics of various airfoils without conducting extensive oscillating airfoil tests. This model, based on a hypothesis of the physical separation process, does not depend on an assumed harmonic variation of angle of attack. The basic assumption is that there exists a maximum quasi-static angle of attack at which the pressure distribution and the boundary layer are in equilibrium. During increases in angle of attack beyond this static stall angle, there are finite time delays before a redistribution of pressure causes first a moment break and then a loss of lift corresponding to flow separation. The relative phasing of the moment and lift breaks with angle of attack produces either positive or negative damping of the motion.

To test the Time Delay hypothesis, harmonic data from Reference 5 were examined. It was noted that the onset of stall can occur before, with, or after maximum amplitude of the oscillation. In accordance with the Time Delay hypothesis, the spread between the static moment stall angle and the dynamic lift break was evaluated in terms of elapsed time nondimensionalized by free stream velocity and chord length, $\tau^* = \Delta t_{SEP}(U_o/c)$. Typical results show that separation generally occurs when τ^* exceeds about 6.

Dynamic pitching moment stall has been handled similarly. Test data showed, in general, that the dynamic moment break occurred before the lift break. This has been noted in Reference 6 and attributed to the shedding of a vortex at the airfoil leading edge at the beginning of the separation process. Rearward movement of the vortex over the surface of the airfoil tends to maintain lift, but drastically alters the pitching moment.

To apply the Time Delay Model to a given airfoil, only static aerodynamic data are required. First, the airfoil static lift and pitching moment data are used to define the approximate variation in center of pressure between the static moment stall angle α_1 and an angle of attack α_2 above which the center of pressure is assumed fixed. Secondly, an approximation is made to the c_l versus α curve for fully separated flow. The sequence of events occurring during one stall-unstall cycle is detailed in Figure 1. Briefly stated, lift and pitching moment are determined from potential flow theory until the nondimensional time τ_2 (which begins counting when the angle of attack exceeds the static moment stall angle) reaches τ_s. At this point the pressure distribution begins to change, leading to rearward movement of the center of pressure and loss of potential flow pitching moment. Later, when $\tau_2 = \tau^*$, the lift breaks from the static line and decreases gradually with time to the fully separated value, $c_{l_{SEP}}(\alpha)$. For $\tau_2 > \tau^*$ the center of pressure coincides with $C.P._{SEP}(\alpha)$. At the point where $\dot{\alpha} = 0$, the rates at which c_l approaches $c_{l_{SEP}}(\alpha)$ and C.P. approaches $C.P._{SEP}(\alpha)$ (if it does not already equal $C.P._{SEP}(\alpha)$) are increased. When α falls back below the quasi-static stall angle α_1, the center of pressure returns to the quarter chord, potential flow pitching moment effects are reintroduced and a second time parameter τ_3 is recorded to govern the rate at which c_l returns to $c_{l_{POT}}$.

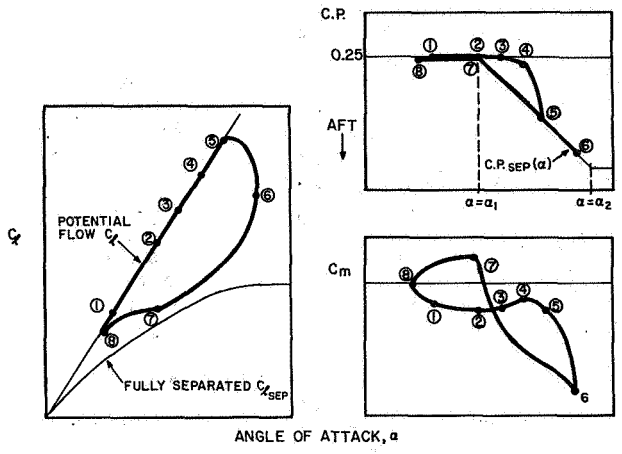

① $\alpha<\alpha_1$
- $c_l = c_{l_{POT}}$
- C.P. = 0.25
- $c_m = c_{m_{POT}} = -\frac{\pi}{4}\frac{d\theta}{d\tau}$

② $\alpha = \alpha_1$
- τ_2 counting begins $\tau_2 = \sum_{n=o}^{\text{at } \alpha=\alpha_1} \Delta t_n \frac{U_{on}}{c}$

③ τ_2 = moment stall time constant $\tau_s = 2.0$
- C.P. begins to move rearward with time toward $C.P._{SEP(\alpha)}$
- $c_{m_{POT}}$ is eliminated

④ $\tau_s<\tau_2<\tau^*$
- c_l remains equal to $c_{l_{POT}}$
- C.P. continues to shift aft with time, τ_2

$$C.P. = 0.25 + \left(\frac{\tau_2 - \tau_s}{\tau^* - \tau_s}\right)\left[C.P._{SEP}(\alpha) - 0.25\right]$$

- $c_m = c_l(C.P. - 0.25)$

⑤ τ_2 = lift stall time constant $\tau^* = 6.0$
- c_l begins to decay toward $c_{l_{SEP}}(\alpha)$

$$c_l = c_{l_{POT}} - \left[c_{l_{POT}} - c_{l_{SEP}}(\alpha)\right]\left[1 - e^{-(\tau_2-\tau^*)/4}\right]$$

- C.P. moves to $C.P._{SEP}(\alpha)$ independent of subsequent variation in α

⑥ $\dot{\alpha} = 0$
- the exponential rate at which c_l approaches $c_{l_{SEP}}(\alpha)$ is increased by a factor of 3
- if $\tau_s<\tau_2<\tau^*$ the rate at which C.P. approaches $C.P._{SEP}(\alpha)$ is increased by doubling the time increment

$$\tau_{2_{n+1}} = \tau_{2_n} + 2\Delta t_n\left(\frac{U_{on}}{c}\right)$$

⑦ $\alpha<\alpha_1$
- τ_3 counting begins $\tau_3 = \sum_{n=o}^{\text{at } \alpha=\alpha_1, \dot{\alpha}<o} \Delta t_n\left(\frac{U_{oc}}{c}\right)$
- c_l moves back toward $c_{l_{POT}}$
- C.P. returns to 0.25
- potential flow moment is reintroduced $c_m = c_{m_{POT}} e^{-\tau_3/4}$

⑧ $\dot{\alpha} = 0$
- $\tau_2 = \tau_3 = 0$
- $c_l = c_{l_{POT}}$
- C.P. = 0.25
- $c_m = c_{m_{POT}}$

Figure 1. Time Delay Unsteady Aerodynamic Model.

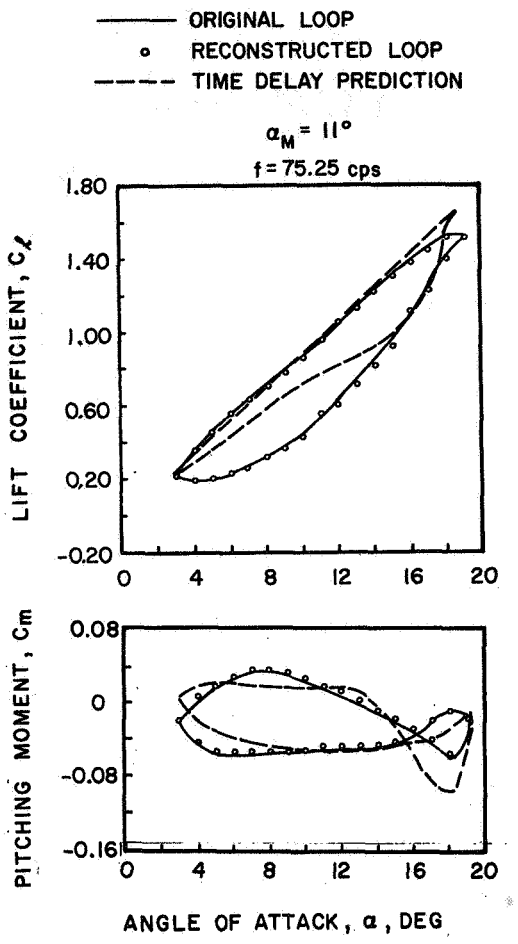

Figure 2. Correlation with NACA 0012 Lift and Pitching Moment Hysteresis Loops.

Although additional correlation studies must be made to identify the effects of airfoil type on the time delay constants and although refinements to the present model may be implemented, this rather simple model represents well the essential features of the dynamic stall process. Correlation typical of that claimed for other empirical methods (References 2 and 7) has been found with data from References 4, 5, and 8. Only the α, A, B Method has produced better correlation (Reference 4), but it suffers from the requirement for extensive testing and data processing. Figure 2 compares the NACA 0012 unsteady lift and pitching moment hysteresis loops measured in Reference 4 with Time Delay results. This correlation was achieved by setting the lift break time constant τ^* equal to 4.0 instead of 6.0. Three-dimensional effects encountered in this test apparently reduced the time interval between static stall and dynamic lift stall. Also shown are the hysteresis loops

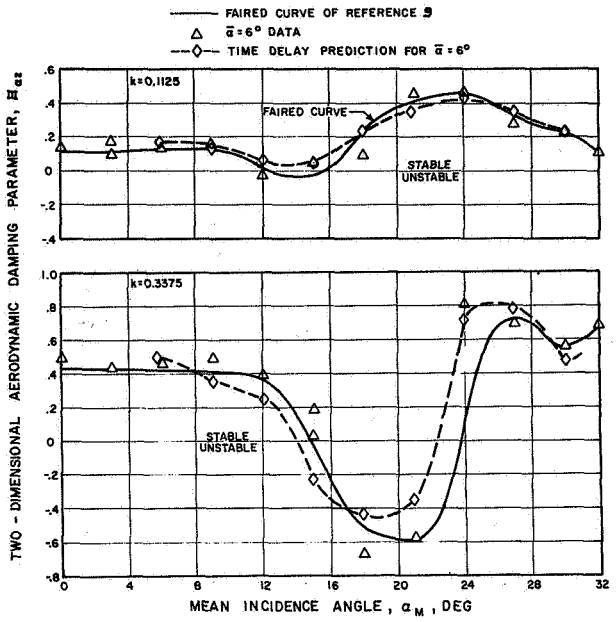

Figure 3. Correlation of Two-Dimensional Aero-Dynamic Pitch Damping.

predicted using the α, A, B Method. The α, A, B Method correlation is with the data from which the α, A, B coefficients were derived.

In addition to predicting the exact form of lift and moment hysteresis loops, an unsteady model should represent faithfully aerodynamic pitch damping. Accordingly, the Time Delay Model was used to calculate two-dimensional aerodynamic damping for the reduced frequency/mean angles of attack test points of Reference 9. Sample results plotted versus airfoil mean incidence angle of attack are shown in Figure 3. Generally excellent correlation of measured and predicted damping is noted.

Other correlation of the Time Delay Method with two-dimensional oscillating airfoil test data has been good. During development of the theory, correlation was carried out with forced oscillating airfoil data for a range of airfoils, frequencies of forced oscillation, Mach numbers, and angles of attack. Typical examples of the correlation obtained are shown in Figure 4 where measured and calculated hysteresis loops are shown for the V13006-7 airfoil. These test data taken from Reference 1 show the correlation with the Boeing Theory of Reference 1 as well. Correlation included hysteresis loops for different airfoils and covered a Mach number range from 0.2 to 0.6. In all cases, the general character and magnitude of the hysteresis loops were well matched. In particular, the method provides the sharp drop in pitching moment that is often found when stall occurs. The oscillation frequency in Figure 4 is constant for the two cases, but Mach number and mean angle of attack are changed. The lift break occurs before the angle of attack reaches its maximum value. In terms of the non-dimensional time parameter τ*, the τ* value of 6 at which lift stall occurs is reached before the maximum angle of attack is reached. The Time Delay and Boeing Methods show comparable correlation for lift. For the Mach number 0.4 case (Figure 4b) the return to potential flow occurs earlier for decreasing angle of attack than the return given by the Time Delay Method. Pitching moment correlation is better for the Time Delay Method. The triple loop characteristic is well duplicated. Similar correlation obtained with the Time Delay Method for a wide range of conditions demonstrated its promise as a practical method for analyzing unsteady aerodynamics.

Dynamic Stall Tests

In order to obtain data useful in evaluating the two unsteady aerodynamic methods dynamic stall wind tunnel tests were run using a two-dimensional airfoil model. The model was oscillated at a frequency simulating the cyclic pitch variation on a helicopter rotor blade. Torsional frequencies representative of helicopter blade frequencies were obtained by varying a torsional stiffness element between the drive system and the airfoil section. The airfoil models were made to be as stiff as possible along their span and light in weight to approximate scaled helicopter blade mass and inertia properties. Hence the non-dimensional coefficients in the equation of motion of the model airfoil were close to those of the helicopter blade torsional equation of motion based on the aerodynamics of the three-quarter radius on the retracting blade. Two different airfoils were fabricated, an NACA 0012 and an SC 1095.

The model airfoils and drive system were designed to permit investigation of the effects on torsional response of torsional natural frequency, chordwise pitch axis location and torsional inertia over a range of 1P frequencies for an NACA 0012 airfoil and a cambered SC 1095 airfoil. The oscillating mechanism provided an 8-degree amplitude of motion of the model with an adjustable mean angle of attack. The model has a span of 1.75 feet and a chord of 0.5 feet. The wind tunnel velocity was 275 fps for all tests. Time histories of the model angular motion were recorded at nominal driving frequencies of 8.0, 10.0, and 12.5 cps. Tests were run for the full range of angle of attack for all the combinations of pitch axis, torsional inertia, torsional natural frequency, and airfoil type. A typical set of time histories for a basic reference condition (NACA 0012 airfoil, 25 percent pivot axis, nominal blade inertia, and 5P natural frequency ratio) is shown for four mean angles of attack in Figure 5. These time histories represent the time average of ten cycles.

The elastic torsional deflection of the airfoil (difference between total angular motion and input angular motion) was obtained for each test condition by subtracting the input angular

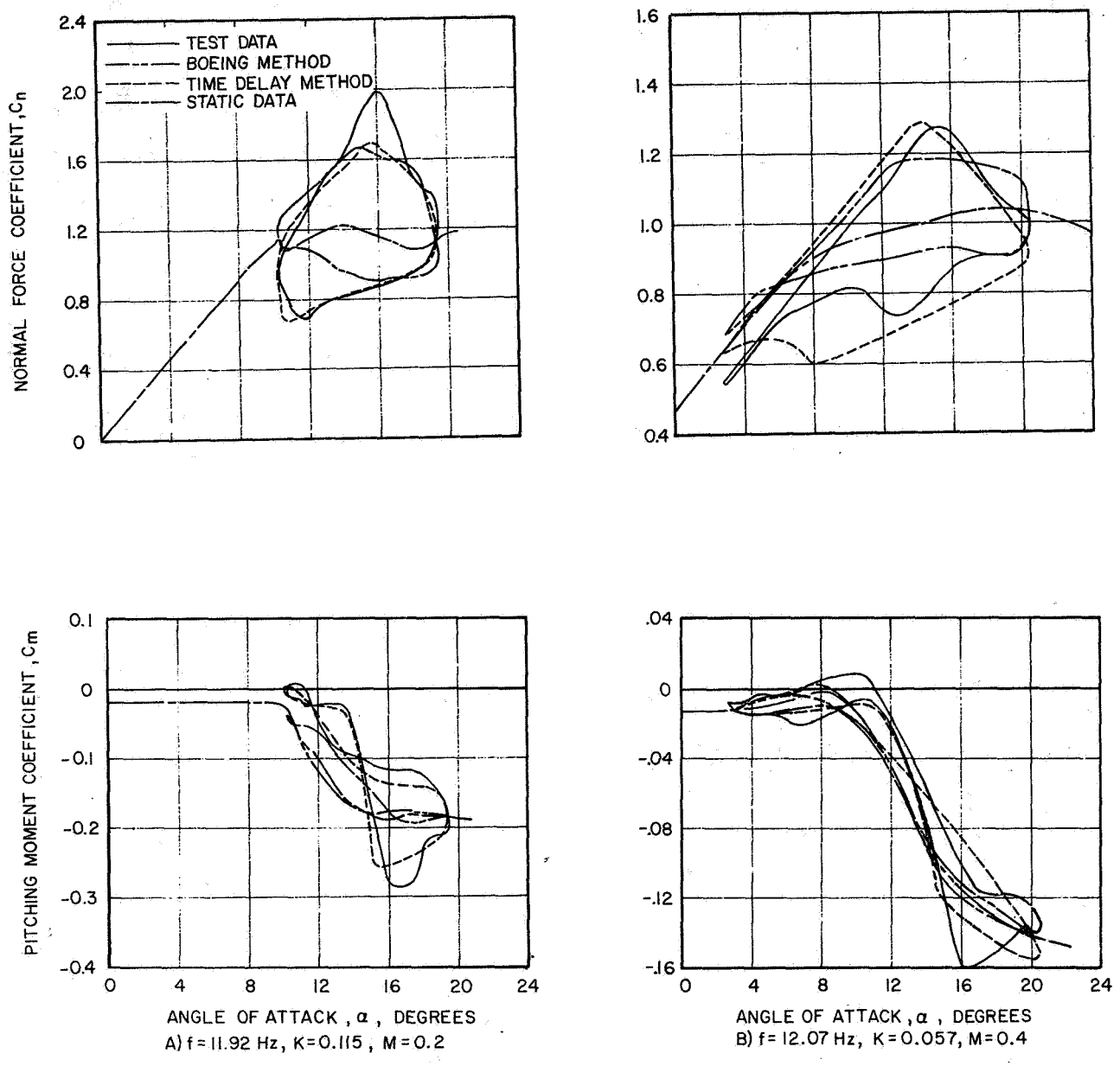

Figure 4. Correlation of Dynamic Loops for the V13006-7 Airfoil in Forced Pitch Oscillation.

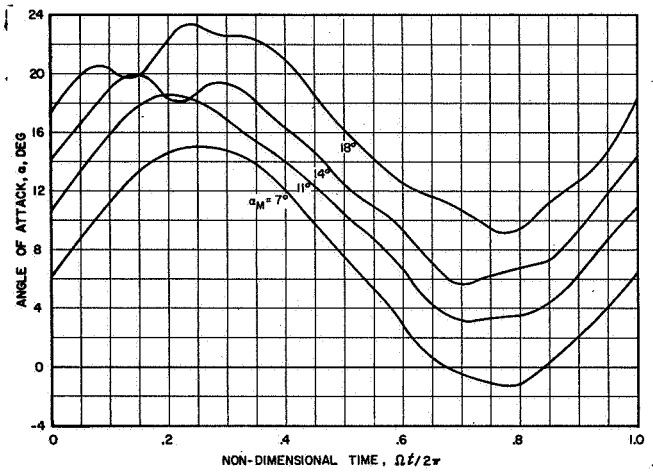

Figure 5. Averaged Time Histories of Angle of Attack for the Model Airfoil.

position time history from the averaged airfoil angular position time history:

$$\theta(\tau) = \alpha(\tau) - (\alpha_m + \bar{\alpha}\sin 2\pi\tau)$$

where $\theta(\tau)$ is the difference between the measured non-dimensional angular time history response $\alpha(\tau)$ and the input driving motion. The non-dimensional time τ is given by t/T, where the period, T, was established from the ten-cycle time-averaging process for that run. Some statistical variation in measured response was noted when stall flutter occurred, but in general the ten cycle time averaged response was representative of the measured data. Two measures of stall response amplitude were extracted from each of the $\theta(\tau)$ time histories. These were $\Delta\theta_1$ which is one-half of the initial response to stall and $\theta_{\frac{1}{2}PTP}$ which is one-half of the overall peak-to-peak elastic deflection.

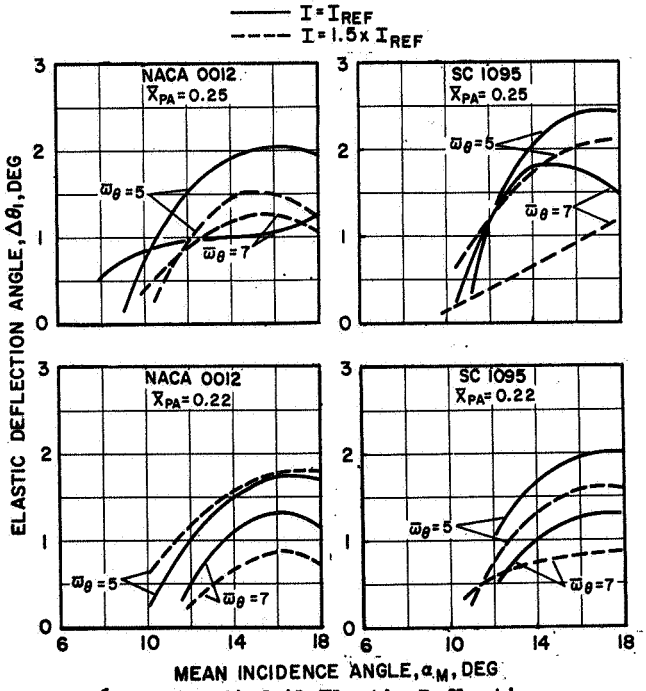

Figure 6. Model Airfoil Elastic Deflection.

It was found that the initial stall response parameter $\Delta\theta_1$ gave the most consistent indication of susceptibility to stall flutter. The possible reduction in flutter amplitude introduced by the time averaging procedure when there was cycle-to-cycle variation in phase made it somewhat difficult to assess the amplitude of flutter response. Fortunately, the initial stall deflection showed virtually no cycle-to-cycle variation. Figure 6 compares measured initial deflection angles for an excitation frequency Ω of 10 cps for the two airfoils at all combinations of airfoil natural frequency ratio ($\bar{\omega}_\theta = \omega_\theta/\Omega$), torsional inertia, and pitch axis. Certain general trends of deflection angle can be identified in the test results.

1. Elastic deflection increases with mean incidence angle.
2. For the same torsional inertia, response is generally greater for the lower frequency airfoil section.
3. The amplitude of response is inversely related to torsional inertia.
4. Forward movement of the pitch axis leads to a decrease in deflection.
5. SC 1095 airfoil dynamic stall response begins to build up at a higher mean incidence angle than the 0012, but the two airfoils have comparable responses once stall is penetrated.

Correlation Study of Two-Dimensional Results

The two-dimensional flexured airfoil test data were compared with predictions based on various unsteady aerodynamic methods. The single torsional degree of freedom differential equation of motion for the flexibly mounted airfoil section oscillating in the wind tunnel test section is given by

$$I\ddot{\alpha} + c\dot{\alpha} + K(\alpha-\alpha_m) = M(t) + K\bar{\alpha}\sin\Omega t$$

where c = equivalent mechanical damping per unit span
I = airfoil torsional inertia per unit span
K = torsional spring constant
M_t = applied aerodynamic moment
t = time
α = airfoil angle of attack
$\bar{\alpha}$ = amplitude of angular oscillation
α_M = mean angle of the oscillation
Ω = angular frequency of the applied torque

This equation was solved numerically using the unsteady aerodynamic models to calculate the applied aerodynamic moment M(t). For the α, A, B Method unsteady data tables obtained from earlier oscillating airfoil tests, Reference 4, were scaled for both airfoils. The measured steady state lift

and pitching moment data served as inputs in the Time Delay calculations. Additionally, the airfoil mean incidence angle used in the Time Delay solution was two degrees less than that set in the wind tunnel. The open jet flow deflection experienced at high unsteady lift coefficients was sufficient to decrease actual peak angles of attack to a value somewhat lower than the geometrically impressed pitch angle. The two-degree correction to α_M gave consistently better correlation of the initial stall time.

Correlation between measured wind tunnel model response and response calculated with the unsteady models was examined for thirty-six test conditions. The set of cases studied was sufficient to evaluate the independent effects on airfoil stall response of mean incidence angle,

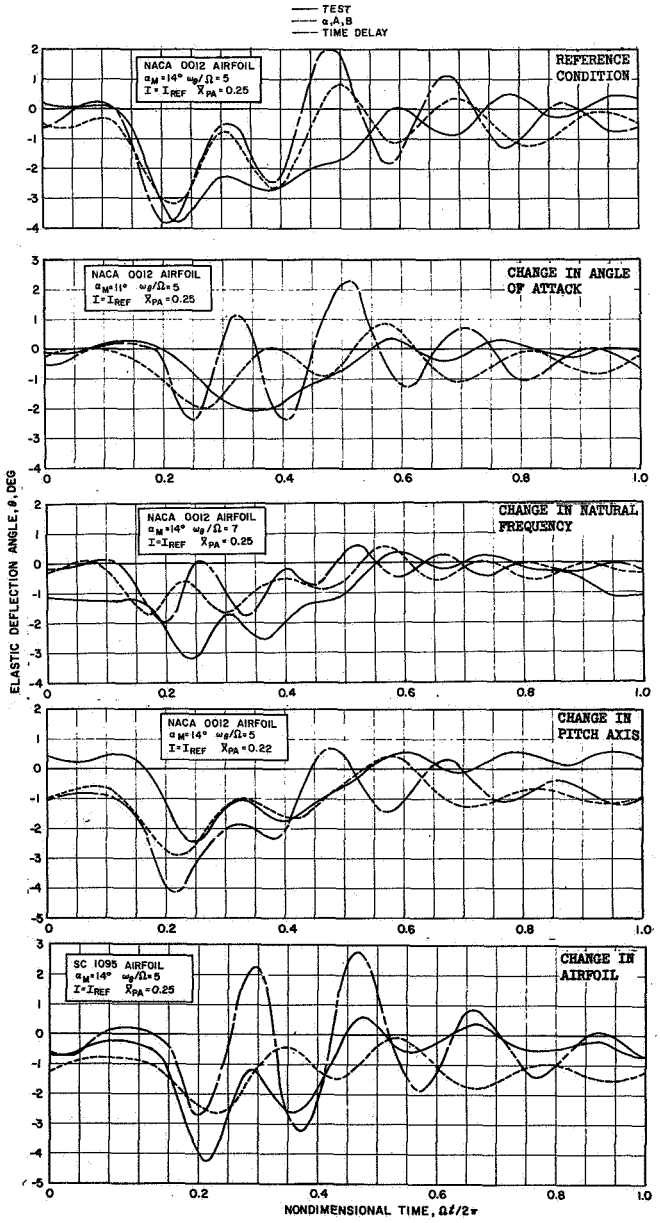

Figure 7. Effect of Parameters on Airfoil Response.

torsional natural frequency, chordwise pitch axis, torsional inertia, and airfoil type. Relative to a baseline case taken to be the NACA 0012 airfoil at $\alpha_M = 14^\circ$, $\omega_\theta/\Omega = 5$, $\bar{X}_{PA} = 0.25$, and $I = I_{REF}$, Figure 7 shows measured and predicted effects of mean angle, torsional natural frequency, pitch axis, and airfoil type on time histories of elastic deflection. Comparison of the measured and predicted effects of airfoil mean angle of attack indicates that deeper penetration into stall results in sharper initial stall deflection and larger residual stall flutter response. The two analyses predict these effects qualitatively, but each - especially the Time Delay model - overpredicts the amplitude of response. The main effects of an increase in torsional natural frequency are a shift in response frequency and a decrease in the amplitude of elastic deflection. Figure 7 shows good correlation of response amplitude, although both analyses predict an initial stall response earlier than that measured. Moving the airfoil pitch axis forward causes delay in initial stall time and reduction in amplitude of response. The analytical results do predict the reduction in response amplitude, but the Time Delay model still results in overpredicted response. Finally, a comparison between the NACA 0012 and the SC 1095 airfoils shows a delay in the initial stall time for the SC 1095 airfoil, which had a static stall angle measured in this wind tunnel to be about three degrees higher than that of the NACA 0012. However, the SC 1095 stall flutter amplitude was comparable to that experienced by the NACA 0012 at this condition.

The time history correlation was good in that the initial response and the frequency of the subsequent oscillations were predicted. The trends observed in test were well matched by the analysis, although the Time Delay model generally overpredicted stall flutter response. The basic effects of structural changes on blade response time histories were well predicted by either analysis.

Although torsional elastic deflection is important in determining rotor stability and performance, the torsional moments resulting from stall flutter are the designer's primary concern. To measure the trends of torsional moment with parameter changes, the twisting moment experienced by the flexible connector in the model airfoil drive system was calculated for each test condition. The torsion moment M_θ was calculated using the equivalent spring stiffness of the connector:

$$M_\theta = K_{eq}\theta = (I_{airfoil}\,\omega_\theta^2)\,\theta$$

The torsional moments corresponding to the initial stall deflection angle $\Delta\theta_1$ were used to show the effects of blade parameters on structural moments. Figure 8 presents typical results for three combinations of airfoil type and mean angle of attack. It was generally found that decreasing torsional natural frequency reduced stall flutter moments. Although the stiffer system experienced lower response amplitudes, the corresponding structural moments were increased:

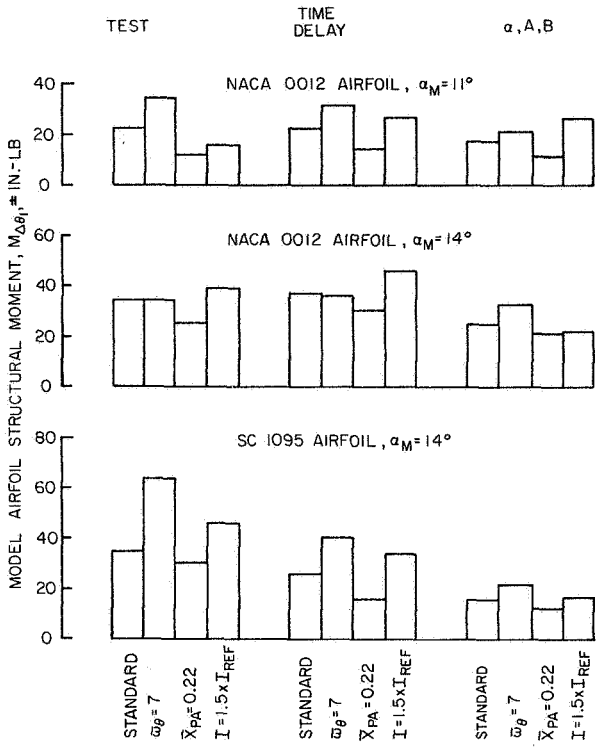

Figure 8. Effect of Airfoil Parameters on Model Airfoil Vibratory Torsional Moments.

$$\frac{M_{\theta 7p}}{M_{\theta 5p}} = \left(\frac{\omega_{\theta 7p}}{\omega_{\theta 5p}}\right)^2 \left(\frac{\theta_{7p}}{\theta_{5p}}\right) = \left(\frac{7}{5}\right)^2 \left(\frac{\theta_{7p}}{\theta_{5p}}\right)$$

Forward placement of the airfoil pitch axis generally decreased vibratory torsional moments. The two analyses predicted this trend with comparable accuracy. That forward movement of the airfoil pitch axis relative to the aerodynamic center reduces stall flutter moments can be understood based on lift and pitching moment hysteresis loops. For an airfoil with pitch axis forward of the center of pressure, positive lift forces cause negative moments about the pitch axis. For positive lift, the lift hysteresis loop is usually traversed in the clockwise direction, which contributes a negative pitching moment loop in the counterclockwise (stabilizing) direction. A decrease in torsional moment amplitude with decreasing torsional inertia was generally found throughout the testing. This trend, evident in two of the conditions shown in Figure 8, is predicted somewhat more correctly by the Time Delay Analysis. Finally the two airfoils are compared in Figure 9. For two different combinations of inertia and pitch axis, high stall flutter moments are delayed in mean angle with the SC 1095 airfoil.

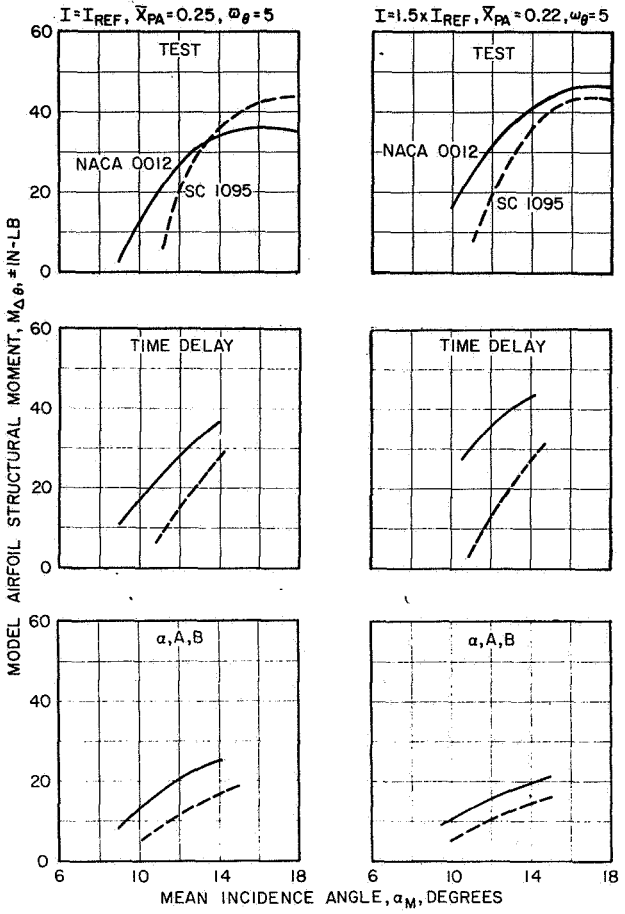

Figure 9. Effect of Airfoil Type on Structural Moments

Flight Test Correlation

Flight test data were correlated with the Normal Modes Blade Aeroelastic Analysis for both the CH-53A and CH-54B aircraft. Both models of unsteady aerodynamics were used. Information on the blade analysis used can be found in Reference 10.

Correlation of CH-53 control system loads, blade stresses and required power was studied at a nominal aircraft gross weight of 42,000 lb (C_m/σ = 0.083), a tip speed of 710 ft/sec, and a 3000 ft density altitude for airspeeds ranging from 100 knots to 170 knots. Inclusion of variable inflow was found to be essential in calculating the proper levels of blade bending moments. It also provided some improvement in the correlation of blade torsional moments.

The α, A, B and Time Delay aerodynamic models are compared at 137 knots in Figure 10. Figures 10a and 10b shows that the computed blade stresses are comparable for the two methods. However, the push rod loads calculated with the Time Delay Model are much less than values calculated with the α, A, B Method and measured values. The Time

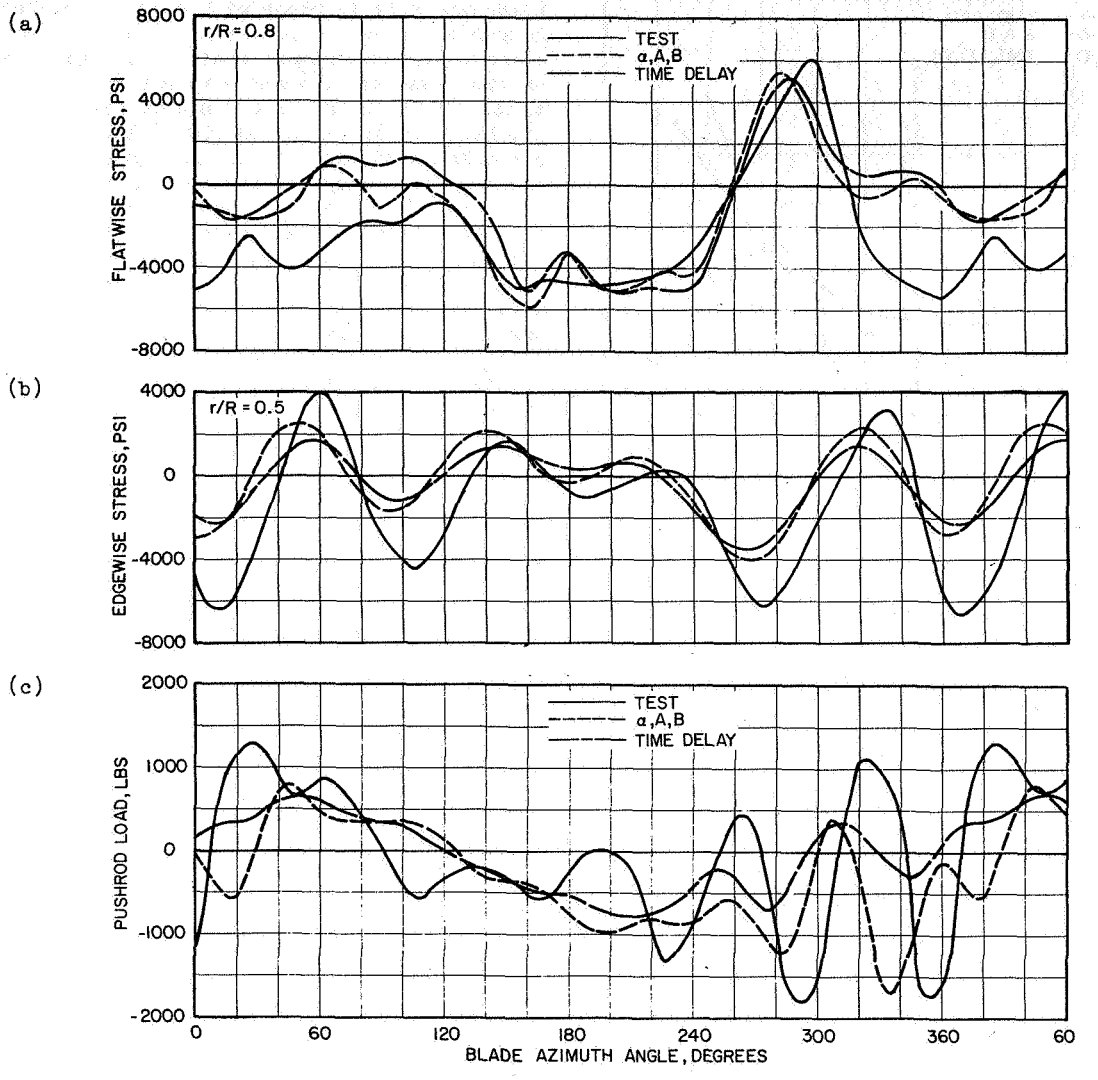

Figure 10. Correlation of CH-53A Blade Stresses and Pushrod Loads.

Delay results generally do not give sufficiently large oscillations in stall.

That better correlation of stall flutter moments was possible with the α, A, B Method is evident in Figure 11a which shows the buildup of vibratory pushrod load amplitude with airspeed. The α, A, B model predicts a buildup rate almost identical with the mean of the test data. A discrepancy of no more than 10 knots in the knee of the control load curve is evident at this thrust coefficient. Figure 11b shows the correlation of pushrod load amplitude achieved with the α, A, B Method at three thrust coefficients.

Calculated CH-54B control loads were also generally less than measured values. Figure 12 indicates that a definite stall boundary is predicted by the analysis. Relative to the CH-53A calculations, a decreased control load stall speed and an increased rate of buildup with airspeed are clearly predicted. Again, higher loads are computed based on the α, A, B Model. The comparison of measured and predicted push rod load time histories indicates that the α, A, B results reflect a buildup in the higher frequency loads much more accurately than do the Time Delay calculations.

It is not entirely clear why, relative to the α, A, B method, the Time Delay model underpredicts helicopter control loads while overpredicting the stall flutter oscillations of the two-dimensional wind tunnel model. Examination of several blade section pitching moment/angle of attack hysteresis loops indicates not so much

(a)

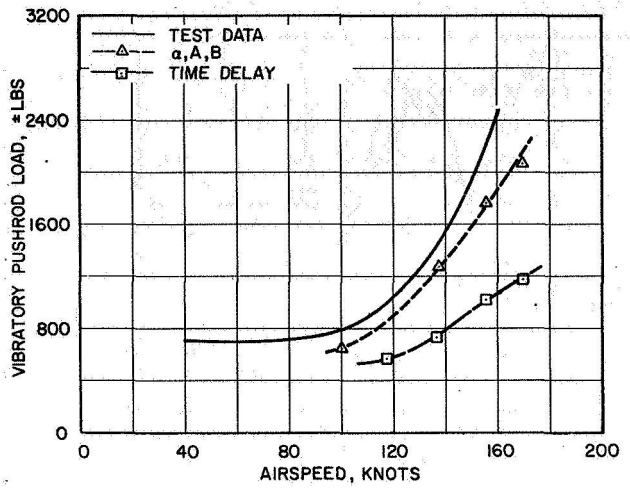

(b)

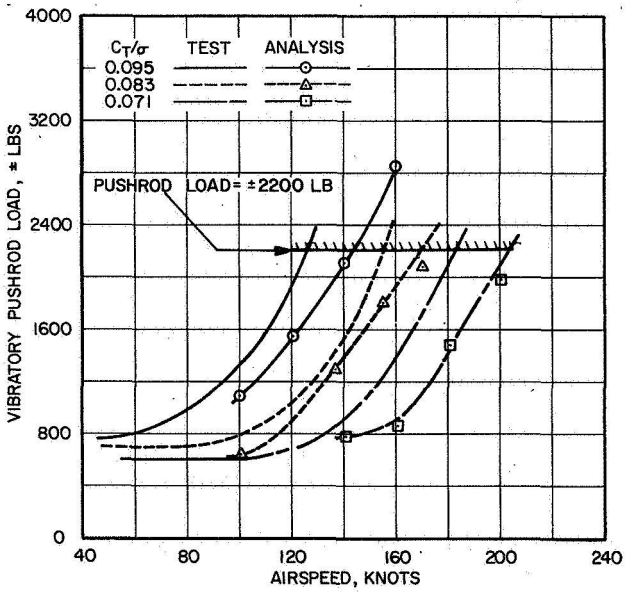

Figure 11. Correlation of CH-53A Vibratory Pushrod Loads.

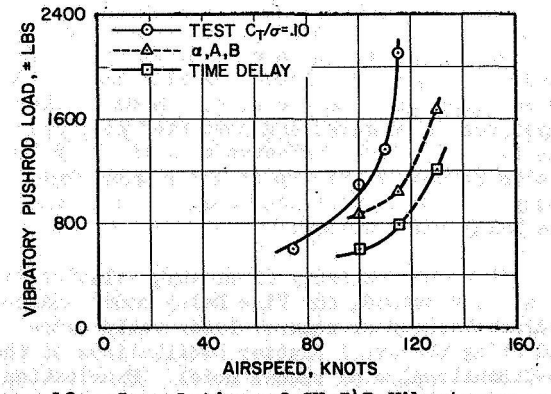

Figure 12. Correlation of CH-54B Vibratory Pushrod Loads.

that more negative pitch damping is present in the α, A, B results. Rather pitching moments along the blade are more in phase with each other, leading to larger modal excitation. In the α, A, B formulation, pitching moment coefficients are tabulated as functions of α, $\dot{\alpha}$ and $\ddot{\alpha}$ values all along the blade. This formulation leads to similarly phased pitching moments. In the Time Delay Model, moments are calculated based on the angles of attack exceeding the steady state stall angle for a certain interval of time and are not solely dependent on the instantaneous angle of attack characteristics. For small differences in calculated angles of attack, computed pitching moments for adjacent blade sections can be different in phase. Because the two-dimensional wind tunnel airfoil was modeled as a single panel for the calculation of aerodynamic forces, the effects of simultaneous spanwise stalling were not a factor in the correlation with that data.

Comparison of Methods

Because the α, A, B Method has demonstrated better correlation with flight test data, it continues to be the method in use for blade design analysis. However, development of both methods continues. The α, A, B Method provides a relatively direct and simple procedure for calculating unsteady aerodynamic loads. Correlation has been good with test data but its disadvantage centers largely on the apparent need for extensive tests to provide the body of tabulated data required for each airfoil. Some success has been obtained by scaling the NACA 0012 unsteady aerodynamic tables based on steady state differences between airfoils. Work is also being done on developing analytical expressions to replace the tabulated data. These may lead to the ability to synthesize the data required for a given airfoil, which would make the method more desirable for general applications.

The Time Delay Method has the great advantage of requiring only steady state airfoil data for its application. The correlation with forced oscillations of two-dimensional airfoils demonstrated its applicability over a wide range of conditions. Correlation with the tests described in this paper showed no clear advantage of the Time Delay Method over the α, A, B Method, and correlation with flight test data was definitely poorer with the Time Delay Method. Further work must be done to investigate the reasons for the poor flight test correlation. The problem may result from the assumption in the analysis that, on a blade, each radial section acts independently of its neighboring sections. This causes a more random stalling along the span with time, which smoothes out the changes in blade loading. The propagation of stall along the span for the three-dimensional case of a helicopter blade must be added to the Time Delay Method. The α, A, B Method does provide spanwise correlation in loading by use of torsional mode acceleration to calculate the B parameter. This acceleration is in phase for each point along the blade span. Incorporation of a suitable radial propagation model in the Time Delay Method may make this a more versatile, more easily applicable, and

more accurate model of unsteady aerodynamics. Until this can be shown the α, A, B Method continues in use in blade design.

Conclusions

1. The α, A, B and Time Delay unsteady aerodynamic models predict with good accuracy the lift and pitching moment hysteresis loops and the aerodynamic pitch damping of rigidly driven oscillating airfoils.

2. Two-dimensional stall flutter tests indicate that reducing blade torsional stiffness, reducing blade torsional inertia and moving blade pitch axis forward decrease stall flutter induced moments. Inception of stall flutter was delayed with the SC 1095 airfoil relative to the NACA 0012 airfoil; however, once initiated, stall flutter loads for the two airfoils were generally comparable.

3. Stall flutter response of the two-dimensional model airfoils and the effects of airfoil structural design parameters on blade torsional moments can be calculated using both unsteady models. The Time Delay method gives a high prediction of response amplitude.

4. Good correlation of CH-53A and CH-54B blade stresses and control loads was obtained with a rotor aeroelastic analysis employing variable rotor inflow and unsteady aerodynamics. Best correlation was achieved using the α, A, B unsteady model. The Time Delay method generally underpredicted full scale rotor stall flutter response.

5. The α, A, B model is in use for blade design analysis. Refinements to the Time Delay Method may make it a more versatile and more easily applied unsteady aerodynamic model.

References

1. Gormont, R. E., A MATHEMATICAL MODEL OF UNSTEADY AERODYNAMICS AND RADIAL FLOW FOR APPLICATION TO HELICOPTER ROTORS, USAAMRDL TR 72-67. U. S. Army Air Mobility Research and Development Laboratory, Fort Eustis, Virginia, May 1973.

2. Ericsson, L. E. and Reding, J. P., UNSTEADY AIRFOIL STALL REVIEW AND EXTENSION, AIAA Journal of Aircraft, Vol. 8, No. 8, August 1971.

3. McCroskey, W. J., RECENT DEVELOPMENTS IN ROTOR BLADE STALL, AGARD Conference Pre-Print No. 111 on Aerodynamics of Rotary Wings, September 1972.

4. Carta, F. O., Commerford, G. L., Carlson, R. G., and Blackwell, R. H., INVESTIGATION OF AIRFOIL DYNAMIC STALL AND ITS INFLUENCE ON HELICOPTER CONTROL LOADS, United Aircraft Research Laboratories; USAAMRDL TR 72-51, U. S. Army Air Mobility Research and Development Laboratory, Fort Eustis, Virginia, September 1972.

5. Gray, L. and Liiva, J., WIND TUNNEL TESTS OF THIN AIRFOILS OSCILLATING NEAR STALL, The Boeing Company, Vertol Division; USAAMRDL TR 68-89A and 68-89B, U. S. Army Aviation Materiel Laboratories, Fort Eustis, Virginia, January 1969.

6. Ham, N. D. and Garelick, M. S., DYNAMIC STALL CONSIDERATIONS IN HELICOPTER ROTORS, Journal of the American Helicopter Society, Vol. 13, No. 2, April 1968.

7. Tarzanin, F. J., PREDICTION OF CONTROL LOADS DUE TO BLADE STALL, American Helicopter Society, 27th Annual National Forum, May 1971.

8. Arcidiacono, P. J., Carta, F. O., Caselini, L. M., and Elman, H. L., INVESTIGATION OF HELICOPTER CONTROL LOADS INDUCED BY STALL FLUTTER, United Aircraft Corporation, Sikorsky Aircraft Division; USAAVLABS TR 70-2, U. S. Army Aviation Material Laboratories, Fort Eustis Virginia, March 1970.

9. Carta, F. O., and Niebanck, C. F., PREDICTION OF ROTOR INSTABILITY AT HIGH FORWARD SPEEDS, Volume III, STALL FLUTTER, USAAVLABS TR 68-18C, U. S. Army Aviation Materiel Laboratories, Fort Eustis, Virginia, February 1969.

10. Arcidiacono, P. J., PREDICTION OF ROTOR INSTABILITY AT HIGH FORWARD SPEEDS, Vol. I, Steady Flight Differential Equations of Motion for a Flexible Helicopter Blade with Chordwise Mass Unbalance, United Aircraft Corporation, Sikorsky Aircraft Division; USAAVLABS TR 68-18A, U. S. Army Aviation Materiel Laboratories, Fort Eustis, Virginia, February 1969.

COMPUTER EXPERIMENTS ON PERIODIC SYSTEMS IDENTIFICATION USING ROTOR BLADE TRANSIENT FLAPPING-TORSION RESPONSES AT HIGH ADVANCE RATIO

K. H. Hohenemser and D. A. Prelewicz°
Washington University, St. Louis, Missouri 63130

Abstract

Systems identification methods have recently been applied to rotorcraft to estimate stability derivatives from transient flight control response data. While these applications assumed a linear constant coefficient representation of the rotorcraft, the computer experiments described in this paper used transient responses in flap-bending and torsion of a rotor blade at high advance ratio which is a rapidly time varying periodic system. It was found that a simple system identification method applying a linear sequential estimator also called equation of motion estimator, is suitable for this periodic system and can be used directly if only the acceleration data are noise polluted. In the case of noise being present also in the state variable data the direct application of the estimator gave poor results, however after prefiltering the data with a digital Graham filter having a cut-off frequency above the natural blade torsion frequency, the linear sequential estimator successfully recovered the parameters of the periodic coefficient analytical model.

Notation+

B	Blade tip loss factor
$F \approx (I_1/16I_f)(c/R)^2$	First blade torsional inertia number
F(x,t)	State matrix
G(t)	Process noise modulating matrix
H(ω)	Fourier transform of weighting function
H(x,t)	Measurement matrix
H(ξ,a)	State matrix = measurement matrix
I_1	Blade flapping moment of inertia.
I_f	Blade feathering moment of inertia.
J	Quadratic cost function.
P(t) or P	Covariance matrix of conditional state vector probability distribution given measurements.
P	Blade flapping natural frequency.
$Q = (I_1/4I_f)c/R$	Second blade torsional inertia number.
R	Measurement noise covariance matrix.
R	Blade radius
a,b,c	Unknown parameters to be estimated in flapping-torsion problem.
a	Parameter vector.
c	Blade chord.
f	Blade torsional natural frequency.
t	Non-dimensional time.
v	Measurement noise vector
w(jΔt)	Smoothing weights.
w	Process noise vector
x	State vector
z	Measurement vector.
β	Flapping angle.
γ	Blade Lock number.
δ	Blade torsion deflection
ζ	Acceleration vector.
η	Rate of displacement vector.
θ	Blade pitch angle.
λ	Rotor inflow ratio, constant over disk.
μ	Rotor advance ratio.
ξ	Displacement vector.

Presented at the AHS/NASA-Ames Specialists' Meeting on Rotorcraft Dynamics, February 13-15, 1974. This work was sponsored by AMRDL, Ames Directorate, under Contract No. NAS2-4151.

°Now at the Westinghouse Bettis Atomic Power Lab. Westmifflin, Pennsylvania.

+In order to retain the conventional symbols in helicopter aerodynamics (Reference 7) and in systems analysis (Reference 9) some symbols are used in two different meanings.

Notation (cont')

σ	Standard deviation.
ω	Circular frequency.

Subscripts

o	Initial or mean value.
c,t	Beginning and end of filter cut-off frequencies.

Superscripts

$\dot{}$	Time differentiation.
-	Smoothed data after filtering.
^	Estimate
T	Matrix transpose

The question often arises, how to best select some parameters of a given analytical model of a dynamic system on the basis of transient responses to certain inputs either obtained analytically with a more complete math model or obtained experimentally. In rotorcraft flight dynamics one may want to use a linear constant coefficient math model and select the state matrix in an optimal way from the measured data obtained in a number of transient flight maneuvers. One also may have a more sophisticated non-linear analytical model of the rotorcraft. The problem then is how can the simpler linear math model be selected to best represent the responses of the more complete analytical model; or one may have the dynamic equations of a rotorcraft without the effects of dynamic inflow and one desires to modify some of the parameters in such a way that dynamic inflow effects are best approximated. It is known from theoretical studies, for example Reference 1, that a reduction in blade Lock number can approximately account for rotor inflow effects in steady conditions. The question then is whether changes in parameters can also account for inflow effects during transient conditions.

The idea of using transient response data to determine parameters of an analytical model is certainly not new. Recently, however, considerable interest in this area has been developed and a number of approaches have been studied which are unified under the title of "system identification". There is a considerable and rapidly growing literature in this field. System identification methods generally fall into two classes: (1) deterministic methods - usually some variation of the classical least squares technique and (2) probabilistic methods which determine the parameters as maximum likelihood estimates of random variables. Some methods can also be interpreted either on a deterministic or on a probabilistic basis. References 2 and 3 are typical of recent work using deterministic methods. Both of these studies illustrate the feasibility of determining coefficients in time invariant linear systems from transient response data. Reference 4 describes many of the probabilistic techniques. Reference 5 gives a detailed discussion of the various methods in their application to V/STOL aircraft and Reference 6 presents an identification method suitable for obtaining stability derivatives for a helicopter from flight test data in transient maneuvers. The studies of References 5 and 6 assume a linear constant coefficient representation of the system. A rotorcraft blade is, however, a dynamic system with rapidly changing periodic coefficients. It appeared, therefore, desirable to try out methods of system identification for a periodic dynamic system.

Selection of Identification Method

If one assumes that only the state variables have been measured but not the accelerations, one must use a non-linear estimator since the estimate of a system parameter and the estimate of a state variable appear as a product of two unknowns. A non-linear sequential estimator was tried on the simplest linear periodic system described by the Mathieu Equation. It was found that the non-linear estimating process diverged in most cases, unless the initial estimate and its standard deviation were selected within rather narrow limits. Reference 6 uses a sequential non-linear estimator but initializes the process by first applying a least square estimator, which needs in addition to the state variable measurements also measurements of the accelerations. In the case of the problem of Reference 6 the least square estimator yielded a rather good set of derivatives and the improvement from the much more involved non-linear estimation was not very pronounced. From this experience it would appear that one needs to apply the least square or an equivalent linear estimator any way and that in some cases it is doubtful whether or not the subsequent application of a non-linear estimator is worth the considerable effort.

After conducting the rather unsatisfactory computer experiments to identify a simple periodic system with the

non-linear estimator, all subsequent work was done with a linear sequential estimator. This estimator is equivalent to least square estimation but has the advantage of being usable for "on-line" system identification. The inversion of large matrices is avoided and replaced by numerical integration of a number of ordinary differential equations. The computer experiments were conducted with the system equations of Reference 7 for the flapping - torsion dynamics of a rotorblade operating at advance ratio 1.6. Reference 7 assumes a straight blade elastically hinged at the rotor center and stipulates linear elastic blade twist. The system used here for the computer experiments represents only a relatively crude approximation, since at 1.6 advance ratio blade bending flexibility is of importance, see for example Reference 8. The coefficients in the system equations are non-analytic periodic functions which include the effects of reversed flow.

The identification algorithm used in this report is easily derived using the extended Kalman filter discussed in the next section. Although the algorithm does not provide for noise in the state variables, one can nevertheless use it also for noisy data if one interprets the estimate, which normally is a deterministic variable, as a sample of a random variable. The effects on system identification of computer generated noise in both the acceleration data and in the state variable data were studied. However, no errors in modeling were introduced since their effects can only be evaluated on a case by case basis.

Extended Kalman Filter

The extended Kalman filter is an algorithm for obtaining an estimate $\hat{x}$ of a state vector x satisfying

$$\dot{x} = F(x,t) + G(t)w \qquad \text{Process Equation (1)}$$

given noisy measurements z related to x via

$$z = H(x,t) + v \qquad \text{Measurement Equation (2)}$$

In the above equations w represents zero mean white Gaussian process noise with covariance matrix Q, v represents zero mean white Gaussian measurement noise with covariance matrix R. An optimum estimate $\hat{x}$ of x can be obtained by solving the extended Kalman filter equations (see Reference 9)

$$\dot{\hat{x}} = F(x,t) + P\left(\frac{\partial H}{\partial x}\right)^T R^{-1}\left(z - H(\hat{x},t)\right) \qquad \text{Filter Equation (3)}$$

$$\dot{P} = \frac{\partial F}{\partial x} P + P\left(\frac{\partial F}{\partial x}\right)^T + GQG^T - P\left(\frac{\partial H}{\partial x}\right)^T R^{-1} \frac{\partial H}{\partial x} P$$

Covariance Equation (4)

$$\hat{x}(o) = x_o \quad , \quad P(o) = P_o$$

Initial Conditions (5)

$\hat{x}$ and P can be interpreted as vector mean and covariance matrix of a conditional probability distribution of the state vector x, given the measurement vector z.

However, since the extended Kalman filter is a biased estimator (see Reference 5) and since the correct value of P_o is not known, P cannot be used as a measure of the quality of the estimate. Rather, the rate of decrease of P is an indication of the amount of information being obtained from the data. When P approaches a constant value then no further information is being obtained.

The extended Kalman filter may also be interpreted as an algorithm for obtaining a least square estimate recursively. The estimate is such as to minimize the following quadratic cost function

$$J = 1/2 \left\{ (x_o - \hat{x}_o)^T P_o^{-1} (x_o - \hat{x}_o) + \int_o^t w^T Q^{-1} w + \left(z - H(x,t)\right)^T R^{-1} \left(z - H(x,t)\right) dt \right\}$$

Cost Function (6)

where now P_o, R and Q are arbitrary weighting matrices, which may be selected for good convergence of the algorithm. Since 1.) numerical methods for solving ordinary differential equations are well developed and 2.) R is usually a diagonal matrix so that R^{-1} is easy to obtain, this algorithm is computationally very efficient.

Estimation of Unknown Parameters

If we wish to estimate the vector a of unknown parameters we substitute a for x in the Kalman filter Eq. 3. For constant parameters we have

$$\dot{a} = o \qquad \text{Process Equation (7)}$$

so that F(x,t) = w = o. The system equation is then used as the measurement equation

$$\zeta = H(\xi,a) + v \qquad \text{Measurement Equation} = \text{System Equation (8)}$$

ζ is the vector of measured accelerations, ξ is the measured state vector and v can be interpreted as acceleration measurement noise or as system noise (including modeling errors). The Kalman filter equations are then

$$\dot{\hat{a}} = P\left(\frac{\partial H}{\partial a}\right)^T R^{-1} [\zeta - H(\xi,\hat{a})]$$

Filter Equation (9)

$$\dot{P} = -P\left(\frac{\partial H}{\partial a}\right)^T R^{-1} \frac{\partial H}{\partial a} P$$

Covariance Equation (10)

For $P \to o$ the measurements lose influence on the estimate and one obtains

$$\dot{\hat{a}} = o$$ Asymptotic Filter Equation (11)

which agrees with the process equation. Again P_o and R may be selected for good convergence. A convenient choice for the initial estimate is $\hat{a}(o) = o$. The elements of R should be large enough to prevent the elements of P from becoming negative due to computation errors in the numerical integration.

Note that ξ, the state vector, is also a measured quantity. If measurement errors are present then this estimation algorithm is biased by an amount approximately proportional to the noise to signal ratio in the state variable measurements, see Reference 5. It is therefore advantageous to reduce the noise ratio before using the estimator. Methods for doing this are discussed in a later section on filtering of the response data.

In practice, one can almost always choose the parameters to be identified in such a way that $H(\xi,a)$ is a linear function of a. The estimator (9), (10) is then linear and problems of nonuniqueness and filter divergence are easily avoided. For this case, we call the algorithm the linear sequential estimator.

The extended Kalman filter assumes that the noise processes w and v are white and Gaussian. This will never be the case in practice especially if w must account for the effects of modeling errors. Because the extended Kalman filter may also be interpreted as yielding a least squares estimate for a given sample of the state ξ and acceleration ζ, we can regard the resulting estimate as a sample from a random variable. Determination of this random variable would necessitate a complete simulation, i.e., mean and variance determined by averaging over many runs. Since this approach is expensive of computing time, efforts here have been directed toward recovering parameters from a single run of computer generated response data.

The above approach to parameter estimation allows the use of high order of accuracy numerical integration (i.e., predictor corrector) schemes to solve the system of ordinary differential equations provided that the response data are sufficiently smooth. The parameter estimation is rapid and requires little computer time. R and P_o can be freely selected to obtain good convergence. The reason for this benign behavior of the estimation method is the linearity of the filter equations in the unknowns. If the accelerations of the system are not measured, one must estimate state variables and parameters simultaneously from a nonlinear filter equation. This nonlinear estimation requires an order of magnitude more computer effort and it is very sensitive to the initializations and to the correct assumptions of process noise and measurement noise. As mentioned before, we began by applying the nonlinear estimator to the identification of parameters in Mathieu's equation for a periodic system. The results were unsatisfactory since filter divergence occured for many choices of P_o and R. However, for the linear sequential estimator divergence could be avoided by following simple rules in selecting $\hat{x}(o)$, P_o and R.

Identifiability of System Parameters

It is obvious from the filter equation (9) that $\hat{a}$ will asymptotically approach a constant value provided that $P \to o$. The covariance equation (10) can be solved explicitly (see Appendix A) to yield

$$P = \left[P_o^{-1} + \int_o^t \left(\frac{\partial H}{\partial a}\right)^T R^{-1} \frac{\partial H}{\partial a}\, dt \right]^{-1} \qquad (12)$$

If the integral is replaced by a sum, this is the error equation for the standard least square method. If $P_o \neq o$, then $P(t) \to o$ whenever the integrand in the above equation is positive definite for all t. This is then a sufficient condition for identifiability. Note that $\frac{\partial H}{\partial a}$ is a function of the system response and hence also of the excitation, so that the identifiability depends not only upon the system but also upon the type of excitation. From the measurement equation (8) we see that the matrix $\frac{\partial H}{\partial a}$ is a measure of the sensitivity of acceleration

measurements to changes in the parameters. For estimating parameters, a well designed excitation is obviously one which causes the elements of the P matrix to decrease rapidly. If any elements of P are decreasing slowly or not at all, then a different type of excitation is needed. A look at which elements of P are causing the trouble will give a clue as to which modes of the system are not being properly excited.

Filtering the Response Data

In practice, we usually have some knowledge of the character of the response data. For example, because of the damping present in physical systems, the true response will not contain much energy at high frequencies. We also know that the acceleration is the derivative of the velocity which is in turn the derivative of the displacement, etc. so that these responses are not independent.

To remove high frequency noise without effecting the signal a zero phase shift low band pass digital filter was used. This filter completely removes all of the signal and noise above a certain termination frequency ω_t without phase or amplitude distortion below a cutoff frequency ω_c. The digital filter used, due to Graham, Reference 10, generates the smoothed data as a numerical convolution of the raw data and a set of numerical smoothing weights, i.e.,

$$\tilde{f}(t_o + i\Delta t) = \sum_{j=-N}^{N} w(j\Delta t) f(t_o + (i + j)\Delta t) \qquad (13)$$

where $f(t_o + (i + j)\Delta t)$ are the sampled values of the signal, $\tilde{f}(t_o + i\Delta t)$ are the smoothed sampled values and where the smoothing weights are given by

$$w(j\Delta t) = \frac{\pi c}{2j\Delta t} \frac{\sin \omega_t j\Delta t + \sin \omega_c j\Delta t}{\pi^2 - (\omega_t - \omega_c)^2 j^2 \Delta t^2} \qquad j = -N, \ldots, +N \quad j \neq o$$

$$w(o) = \frac{c(\omega_t + \omega_c)}{2\pi} \qquad \omega_c < \omega_t \qquad (14)$$

where the constant c is chosen to satisfy the constraint

$$\sum_{j=-N}^{+N} w(j\Delta t) = 1 \qquad (15)$$

The continuous weighting function w(t), of which $w(j\Delta t)$ is a discretization, has the Fourier transform, i.e., frequency domain representation, shown in Figure 1. Convolution of this function with an arbitrary signal will obviously result in a smoothed signal which has all frequencies above ω_t completely suppressed and all signal components below ω_c undistorted. If ω_c and ω_t are properly selected then response data with low frequency signal and high frequency noise can be improved via digital filtering, that is, signal to noise ratio can be significantly increased.

In using the digital filter, it is tempting to achieve a "sharp" filter by taking $\omega_c \simeq \omega_t$. Graham, Reference 10, has determined empirically that the number of points N needed to achieve a given accuracy is approximately inversely proportional to $|\omega_t - \omega_c|$ at least over a limited frequency range. Since N = 40 points were used to filter the data, we selected $|\omega_t - \omega_c| \geq 1$ which according to Graham is sufficient to yield 2% accuracy.

In this study, the numerical convolution was accomplished by using a moving average, i.e., $\tilde{f}(t_o + i\Delta t)$ was computed separately for each i using Eq. (13). For long data records it is possible to achieve considerable savings in computer time by using the Fast Fourier transform algorithm to do this convolution, see Reference 11.

Improvements in the response data can also be obtained by making use of relationships among the various response signals. For the coupled flapping-torsion system considered in the next section the displacements ξ, velocities η and accelerations ζ are related by

$$\dot{\xi} = \eta$$
$$\dot{\eta} = \zeta + v \qquad (16)$$

We can use these equations as process equations in a Kalman filter along with measurement equations

$$\begin{bmatrix} \bar{\xi} \\ \bar{\eta} \end{bmatrix} = \begin{bmatrix} \xi \\ \eta \end{bmatrix} + \begin{bmatrix} v_1 \\ v_2 \end{bmatrix} \qquad (17)$$

where $\bar{\xi}$ and $\bar{\eta}$ denote smoothed measured values. In the process equation (16) replace ζ by its smoothed measured value $\bar{\zeta}$ and let R, the process noise covariance matrix account for remaining errors. Then the Kalman Filter is given by

$$\begin{bmatrix} \dot{\hat{\xi}} \\ \dot{\hat{\eta}} \end{bmatrix} = \begin{bmatrix} \hat{\eta} \\ \hat{\zeta} \end{bmatrix} + PR^{-1} \begin{bmatrix} \bar{\xi} - \hat{\xi} \\ \bar{\eta} - \hat{\eta} \end{bmatrix} \tag{18}$$

Note that $\dot{\hat{\eta}}$ is available when solving the above equations and can be used as an improved estimate of $\bar{\zeta}$. Although this technique has not been used in this study, a similar procedure has been used successfully in Reference 6 for helicopter derivative identification.

Computer Experiments

Coupled flapping-torsion vibrations of a rotor blade at high advance ratio are governed by the equations

$$\ddot{\beta} + P^2\beta = \frac{\gamma}{2}\left[M_{\theta_1}(t)\delta + M_\lambda(t)\lambda + M_{\theta_o}(t)\theta_o - C(t)\dot{\beta} - K(t)\beta\right]$$

$$\ddot{\delta} + f^2\delta = -\frac{3}{2}\ddot{\theta}_o - 3\gamma F\left[C_{\theta_o}(t)\dot{\theta}_o + C_\delta(t)\dot{\delta}\right] - 3\gamma Q\left[\ell_{r\dot{\beta}}(t)\dot{\beta} + \ell_{r\beta}(t)\beta + \ell_{r\lambda}(t)\lambda + \ell_{r\theta_o}(t)\theta_o + K_\delta(t)\delta\right] \tag{20}$$

where the periodic coefficients are defined in Reference 7. Responses to the gust excitations shown in Figure 2 were generated by solving Eq. (20) numerically using a fourth order Adams Moulton method with a time step of .05 and the following parameter values:

$$p^2 = 1.69 \quad \gamma = 4.0 \quad Q = 15.$$
$$f^2 = 64. \quad \mu = 1.6 \quad \theta_o = 0. \tag{21}$$
$$B = .97 \quad F = .24$$

Simulated noisy measurements were obtained by adding samples from zero mean computer generated Gaussian random sequences to the computer generated responses. First the noise was added only to accelerations using the standard deviations

$$\sigma_{\ddot{\beta}} = 1.0 \qquad \sigma_{\ddot{\delta}} = 10 \tag{22}$$

The following three parameters with the values

$$a = \gamma/2 = 2.0$$
$$b = -3\gamma F = -2.88 \tag{23}$$
$$c = -3\gamma Q = -180$$

were assumed to be unknown.

They represent blade flapping and torsional inertia numbers. Unsteady aerodynamic inflow effects may possibly be considered by modifications of these inertia numbers from transient rotor model wind tunnel tests. The linear sequential estimator was started with the initial values of the estimates and errors of the estimates

$$\begin{bmatrix} \hat{a}(o) \\ \hat{b}(o) \\ \hat{c}(o) \end{bmatrix} = o \qquad P(o) = \begin{bmatrix} 40 & 0 & 0 \\ 0 & 55 & 0 \\ 0 & 0 & 4000 \end{bmatrix} \tag{24}$$

The linear sequential estimator is, as mentioned before, quite insensitive to the initial standard deviations which could have been selected still much larger. The values for R used are the following

$$R = \begin{bmatrix} 10 & 0 \\ 0 & 10 \end{bmatrix} \tag{25}$$

The method allows wide variations in the assumptions of the noise covariance matrix R. The integration scheme for solving filter and covariance Eqs. (9) and (10) was again a 4th order Adams Moulton method with a time step of .05. Fig. 3, shows the estimates $\hat{a}$, $\hat{b}$, $\hat{c}$ normalized with the true values and the 3 diagonal terms of the error covariance matrix P normalized with the initial values vs. non-dimensional time t. The excitation for this case was a unit step gust at time t = o, as indicated in Fig. 2 by the dash line. In about one revolution ($t = 2\pi$) the diagonal components of the covariance matrix P_a P_b P_c are approximately zero and further improvements of the parameter estimates $\hat{a}$ $\hat{b}$ $\hat{c}$ are not obtained. There is a small bias error (deviation from the value 1) in two of the parameters, which have been recovered within about 5% error.

The next case assumes that not only the accelerations but also the state variables are noisy. The following standard deviations were used

$$\sigma_\beta = .2 \qquad \sigma_\delta = .5$$
$$\sigma_{\dot\beta} = .6 \qquad \sigma_{\dot\delta} = 3.0 \qquad (22a)$$
$$\sigma_{\ddot\beta} = 1.0 \qquad \sigma_{\ddot\delta} = 10$$

The linear sequential estimator was first applied to the raw data. In this case the responses are far from smooth so that the use of a high order numerical integration scheme was unjustified. A first order Euler's method was used for the integration of the estimator equations. The initial values were

$$\begin{bmatrix} \hat a(o) \\ \hat b(o) \\ \hat c(o) \end{bmatrix} = o \qquad P(o) = \begin{bmatrix} 30 & 0 & 0 \\ 0 & 35 & 0 \\ 0 & 0 & 1000 \end{bmatrix} \qquad (24a)$$

The values for the R used in the estimator were

$$R = \begin{bmatrix} 16 & 0 \\ 0 & 225 \end{bmatrix} \qquad (25a)$$

The excitation consisted of a upward unit step gust at t = 2.0 followed by a down step gust to λ = -1 at t = 6.0, as indicated in Fig. 2. The second gust was added in order to provide to the system another transient useful for the estimator process. Fig. 4 shows that though two of the diagonal covariance terms go to zero after the second gust, the associated parameter estimates remain quite erroneous. The linear sequential estimator cannot be used if noise is present in accelerations as well as in the state variables.

Next the same data were passed through a digital filter with cut-off frequencies $\omega_c = 12$, $\omega_t = 13$, see Fig. 1. These cut-off frequencies are about 50% higher than the torsional frequency of f = 8. Applying now the linear sequential estimator to the filtered data, the initial values were the same as before, Eq. (24a), however R was reduced:

$$R = \begin{bmatrix} 1 & 0 \\ 0 & 9 \end{bmatrix} \qquad (25b)$$

The results of the estimation are shown in Fig. 5. All diagonal terms of the covariance matrix go to zero soon after the second gust, the estimates stabilize in less than 2 rotor revolutions and have only a small bias error of about 5%; same as for the case with zero noise in the state variables. Digitally filtering the data to remove high frequency noise has thus appreciably extended the range of applicability of the linear sequential estimator. It might be argued that the success of the digital filter is due to the "white" character of the computer generated noise whereas real data will contain energy only at finite frequencies. It should be noted that the digital filter removes all of the signal above the truncation frequency and hence would be equally successful for any other distribution of the energy above ω_t.

In selecting the parameters for the digital filter it is important to keep ω_c large enough so that the responses are not significantly distorted. Initially, the noisy data was processed using different digital filters for the torsion and flapping responses. A digital filter with high cut-off frequency i.e., $\omega_c = 12.$ and $\omega_t = 13.$ was used for torsion responses while a lower bandpass filter with $\omega_c = 2.$ and $\omega_t = 3.$ was used to filter flapping responses. This resulted in poor identification of the parameter a in the flapping equation. When the same filter with high cut-off frequency was used for all of the data, adequate identification of all parameters was obtained. Although $\omega_c = 2.$ is above the natural frequency of flapping vibration, the flapping response obviously contains higher frequency components because of the coupling with torsion. This can easily be seen by inspection of the flapping response in Figure 6. For a good identification it is necessary that these higher frequency components not be removed from the signal. Fig. 6 compares the response without noise to the response with noise but after filtering. Also indicated are the standard deviations for flapping and torsion before filtering. It is seen that the filter was very effective in removing the noise corruption from the data.

Conclusions

1. The linear sequential estimator, also called equation of motion estimator, has been successfully applied to recover the system parameters of a periodic system representing rotor blade flapping-torsion dynamics at high rotor advance ratio with noise contaminated accelerations. Filtering of the noisy acceleration data was found to be not necessary.

2. If noise is present in the state variables as well as in the accelerations, the linear sequential

estimator performed very poorly.

3. Filtering both state variables and accelerations with a Graham digital filter with a low cut-off frequency for flapping and a high cut-off for torsion before estimation lead to a poor estimate for the flapping parameter.

4. Filtering both flapping and torsion response with a high cut-off frequency digital filter before estimation resulted in an adequate parameter recovery both in flapping and in torsion.

5. As compared to non-linear estimation methods which are applicable also if acceleration information is not available, the linear sequential estimator has the great advantage of being insensitive to the assumption of initial values for the estimate and for the error of the estimate. No matter what the actual measurement noise is, the assumed noise covariance matrix should be over-rather than underestimated.

6. As compared to the usual form of the least square estimation the linear sequential estimator does not require the inversion of large matrices but merely the numerical solution of a system of ordinary differential equations, thus allowing on-line application. The digital filter smoothes the data sufficiently so that high order of accuracy predictor corrector methods can be used for the integration.

7. The computer studies were performed assuming rather large measuring errors with standard deviations for the deflections of about 10% of the maximum measured values. The foregoing conclusions assume the absence of modeling errors, which would require special investigations.

References

1. Curtis, H.C. Jr., COMPLEX COORDINATES IN NEAR HOVERING ROTOR DYNAMICS, Journal of Aircraft Vol. 10 No. 5,May 1973, pp. 289-296.

2. Berman, A. and Flannelly, W.G., THEORY OF INCOMPLETE MODELS OF DYNAMIC STRUCTURES, AIAA Journal, Vol. 9 No. 4, August 1971, pp. 1481-87.

3. Dales, O.B. and Cohen, R., MULTI-PARAMETER IDENTIFICATION IN LINEAR CONTINUOUS VIBRATING SYSTEMS, Journal of Dynamic Systems, Measurement and Control, Vol. 93, No. 1, Ser. G. March 1971, pp. 45-52.

4. Sage, A.P. and Melsa, J.L., SYSTEM IDENTIFICATION, Academic Press, New York 1971.

5. Chen, R.T.N., Eulrich, B.J. and Lebacqz, J.V., DEVELOPMENT OF ADVANCED TECHNIQUES FOR THE IDENTIFICATION OF V/STOL AIRCRAFT STABILITY AND CONTROL PARAMETERS, Cornell Aeronautical Laboratory Report, No. BM-2820-F-1, August 1971.

6. Molusis, J.A., HELICOPTER STABILITY DERIVATIVE EXTRACTION FROM FLIGHT DATA USING THE BAYESIAN APPROACH TO ESTIMATION, Journal of the American Helicopter Society, Vol. 18, No. 2, April 1973, pp. 12-23.

7. Sissingh, G.J. and Kuczynski, W.A., INVESTIGATIONS ON THE EFFECT OF BLADE TORSION ON THE DYNAMICS OF THE FLAPPING MOTION, Journal of the American Helicopter Society, Vol. 15, No. 2, April 1970, pp. 2-9.

8. Hohenemser, K.H. and Yin, S.K., ON THE QUESTION OF ADEQUATE HINGELESS ROTOR MODELING IN FLIGHT DYNAMICS, Proceedings 29th Annual National Forum of the American Helicopter Society, Washington D.C., May 1973, Preprint No. 732.

9. Bryson, A.E. and Ho, Y.C., APPLIED OPTIMAL CONTROL, Ginn & Co., Waltham, Mass., 1969, p. 376.

10. Graham, R.J., DETERMINATION AND ANALYSIS OF NUMERICAL SMOOTHING WEIGHTS, NASA TR R-179, December 1963.

11. Gold, B. and Rader, C., DIGITAL PROCESSING OF SIGNALS, McGraw-Hill, New York, 1969.

12. Ried, W.T., RICATTI DIFFERENTIAL EQUATIONS, Academic Press, New York, 1971.

Appendix A

Solution of the Covariance Equation

The covariance equation of the linear sequential estimator

$$\dot{P} = -P\left(\frac{\partial H}{\partial a}\right)^T R^{-1} \frac{\partial H}{\partial a} P \qquad \text{(A-1)}$$

is a matrix Ricatti differential equation. It is well known that the general matrix Ricatti Equation with all matrices being time functions

$$\dot{P} = -PA - DP - PBP + C \qquad \text{(A-2)}$$

of which (A-1) is a special case, has the solution

$$P = VU^{-1} \tag{A-3}$$

where U and V satisfy

$$\begin{aligned} \dot{V} &= CU - DV \\ \dot{U} &= AU + BV \end{aligned} \tag{A-4}$$

This and other aspects of matrix Ricatti equations are discussed in Reference 12.

By comparing Eqs. (A-1) and (A-2) we see that Eq. (A-1) is of the form of Eq. (A-2) with A=C=D=0 and $B = \left(\frac{\partial H}{\partial a}\right)^T R^{-1} \frac{\partial H}{\partial a}$

Therefore, from Eq. (A-4) $V = V_o$, a constant matrix and

$$\dot{U} = BV_o \tag{A-5}$$

Integrating yields

$$U = U_o + \int_o^t B\, dt V_o \tag{A-6}$$

Now since from (A-3)

$$P_o = V_o U_o^{-1} \tag{A-7}$$

we can satisfy the initial condition by taking $V_o = I$ and $U_o = P_o^{-1}$. Hence

$$U = P_o^{-1} + \int_o^t B\, dt \tag{A-8}$$

and

$$P = \left[P_o^{-1} + \int_o^t \left(\frac{\partial H}{\partial a}\right)^T R^{-1} \frac{\partial H}{\partial a}\, dt\right]^{-1} \tag{A-9}$$

Minimizing the cost function Eq. (6) with w = o, x = a and z = ζ, one obtains the least square estimate

$$\hat{a} = [P_o^{-1} + \int_o^t \left(\frac{\partial H}{\partial a}\right)^T R^{-1} \frac{\partial H}{\partial a}\, dt]^{-1}[P_o^{-1} a_o + \int_o^t \left(\frac{\partial H}{\partial a}\right)^T R^{-1} \zeta dt] \tag{A-10}$$

where the first factor is the covariance P from Eq. (A-9). Eq. (A-10) is the equivalent of solving Eqs. (9) and (10) and has been used in Ref. 6 with $P_o^{-1} = o$ after replacing the integrals by sums. In this case the result is independent of R which cancels out.

Even in the general case of finite P(o) the error covariance matrix R need not be considered as a separate input. If R is a diagonal constant matrix it is evident that Eqs. (9) and (10) can be written in the form

$$\dot{\hat{a}} = P_r \left(\frac{\partial H}{\partial a}\right)^T [\zeta - H(\xi, \hat{a})] \tag{A-10}$$

$$\dot{P}_r = - P_r \left(\frac{\partial H}{\partial a}\right)^T \frac{\partial H}{\partial a} P_r \tag{A-11}$$

where $P_r = P R^{-1}$. This was pointed out to the authors by John A. Molusis.

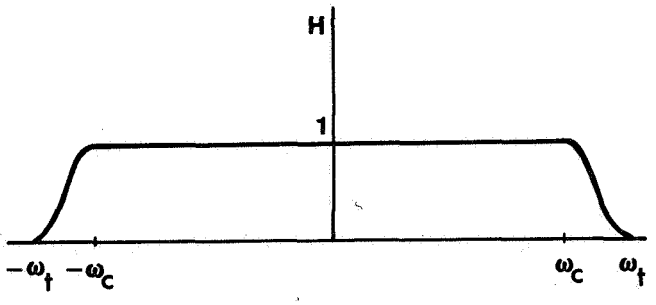

Fig. 1. Fourier Transform of Weighting Function

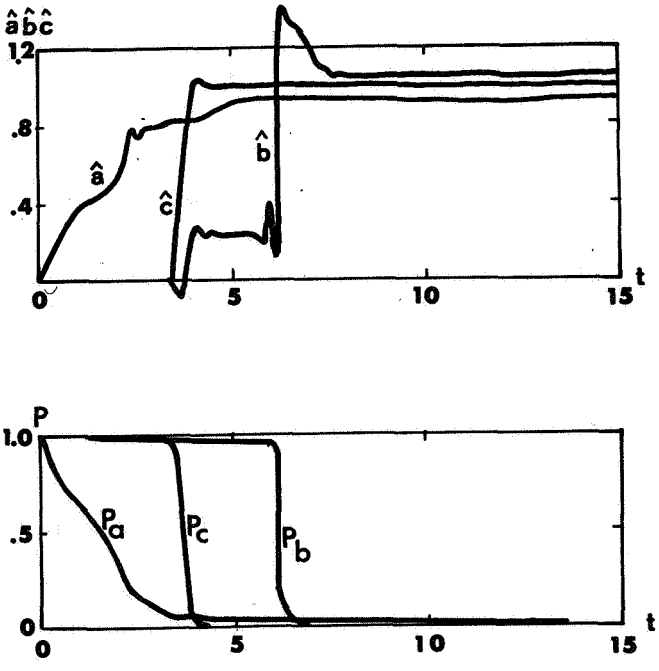

Fig. 3. Estimates & Covariances vs. Time, Acceleration Noise Only

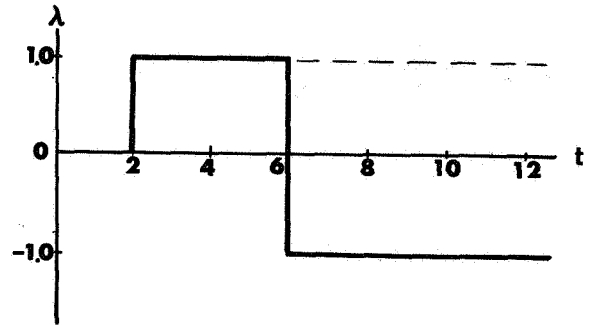

Fig. 2. Gust Excitations

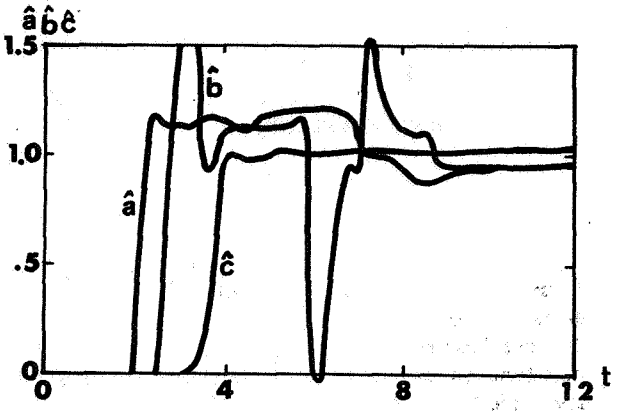

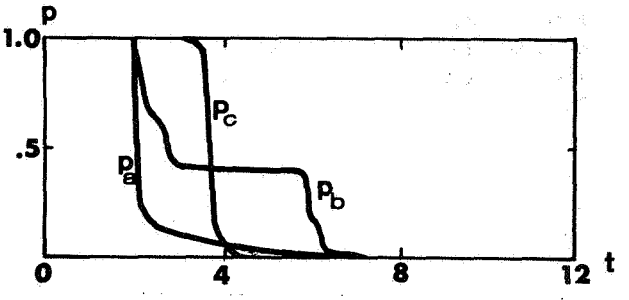

Fig. 5. Estimates & Covariances, Filtered Data

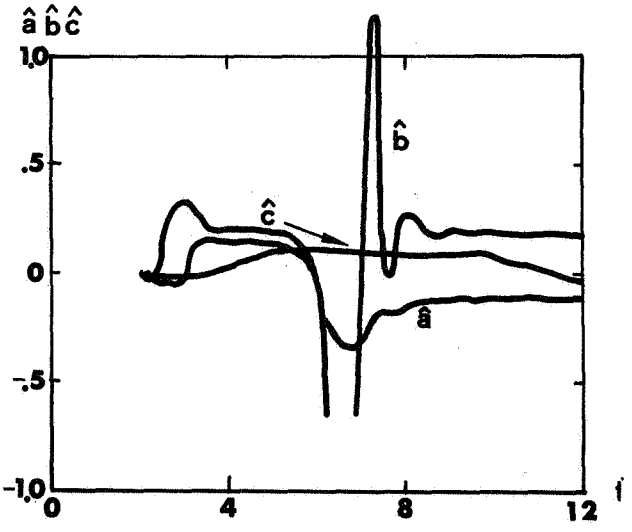

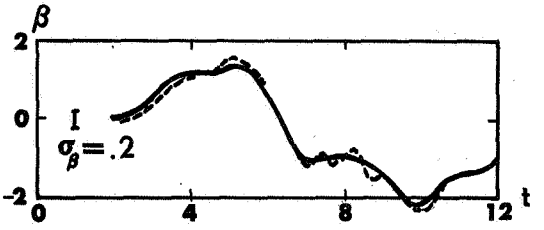

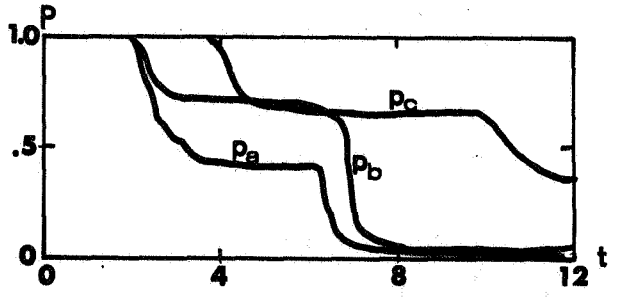

Fig. 4. Estimates & Covariances vs. Time, Acceleration and State Variable Noise

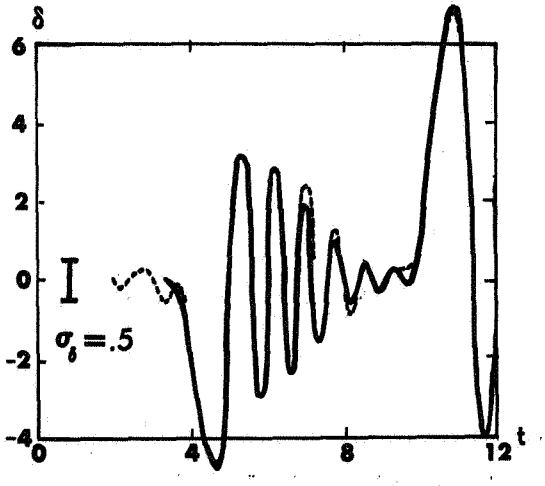

Fig. 6. Exact and Filtered Noisy Responses (Solid & dash line respectively)

DYNAMIC ANALYSIS OF MULTI-DEGREE-OF-FREEDOM SYSTEMS USING PHASING MATRICES

Richard L. Bielawa*
United Aircraft Research Laboratories
East Hartford, Connecticut

Abstract

A mathematical technique is presented for improved analysis of a wide class of dynamic and aeroelastic systems characterized by several degrees-of-freedom. The technique enables greater utilization of the usual eigensolution obtained from the system dynamic equations by systematizing the identification of destabilizing and/or stiffening forces. Included, as illustrative examples of the use of the technique, are analyses of a helicopter rotor blade for bending-torsion divergence and flutter and for pitch-lag/flap instability.

Notation

$[A]$, $[B]$, $[C]$	Inertia, damping and stiffness matrices, respectively, Eq. (1)
A_{v_k}	Pitch-lag coupling for k'th edgewise mode $(=\Delta\theta/\Delta q_{v_k})$
A_{w_m}	Pitch-flap coupling for m'th flatwise mode $(=\Delta\theta/\Delta q_{w_m})$
a	Section lift curve slope, /rad
a_{ij}, b_{ij}, c_{ij}	Elements of the [A], [B] and [C] matrices
C_{e_k}	Viscous equivalent structural damping of k'th edgewise mode
c	Blade chord, in.
EI_y, EI_z	Flatwise and edgewise bending stiffness, respectively, lb-in.^{2}
$\{F(t)\}$	Dynamic excitation force vector, Eq. (1)
f_n	Resultant driving force for n'th degree of freedom, Eq. (5)
$[G(\lambda_i)]$	Dynamic matrix for i'th eigenvalue, Eq. (3)
GJ	Torsional stiffness, lb-in.^{2}
K_c	Root feathering spring, in.-lb/rad
k_A	Polar radius of gyration of spar about its center, in.
$k_{y_{lo}}$, $k_{z_{lo}}$	Section thickness-wise and chordwise mass radii of gyration, respectively, about spar center, in.
m	Section mass distribution, lb-sec^2/in.^{2}
m_o	Reference mass distribution, (= 0.000776 lb-sec^2/in.^{2})
$[P_{A_i}]$, $[P_{B_i}]$, $[P_{C_i}]$	"Stability" Force Phasing Matrices for i'th eigenvalue, Eqs. (6) through (8)
$[\hat{P}_{A_i}]$, $[\hat{P}_{B_i}]$, $[\hat{P}_{C_i}]$	"Stiffness" Force Phasing Matrices for i'th eigenvalue, Eqs. (10) through (13)
q_{v_k}	k'th edgewise modal response variable
q_{w_i}	i'th flatwise modal response variable
q_{θ_j}	j'th torsional modal response variable, (j = 1, for rigid feathering)
R	Rotor radius, in.
r	Blade spanwise location, in.
T	Tension at r, lb
t	Time, sec
$\{x\}$	Vector of degrees of freedom
$y_{lo_{cg}}$, $y_{lo_{c/4}}$, $y_{lo_{3c/4}}$	Chordwise positions forward of spar center of mass center, quarter chord, and three-quarter chord, in.
α_o	Spanwise variable section angle of attack about which perturbations occur, rad
β	Blade pre-coning angle, rad
γ_i	Angle defined in Fig. 1 (= arg λ_i)
γ_{v_k}	k'th assumed edgewise mode shape
γ_{w_i}	i'th assumed flatwise mode shape
γ_{θ_j}	j'th assumed torsion mode shape
δ_o, δ_4	Coefficients describing quartic variation of profile drag coefficient with angle of attack
δ_{ij}	Kronecker delta
η	Number defined in Eq. (9)
θ	Geometric (collective) pitch angle at r, rad
θ_e	Elastic torsion deflection at r, rad
λ	(Uniform) rotor inflow
λ_i	i'th eigenvalue, /sec
ρ	Air density, lb-sec^2/in.^{4}
σ	Blade solidity
σ_i	Real part of i'th eigenvalue, /sec
$\{\phi^{(i)}\}$	i'th eigenvector of dynamic matrix equation
Ω	Rotor rotational speed, rad/sec
ω_i	Imaginary part of i'th eigenvalue, /sec

*Senior Research Engineer, Rotary Wing Technology Group.

$(^*)$	Differentiation with respect to (Ωt)
$(\ )'$	Differentiation with respect to $\mathbf{r}$
$(\bar{\ })$	Indicates quantity is nondimensionalized using combinations of R, m_o and Ω, as appropriate
$[\ ]$	Diagonal matrix

I. Introduction

Dynamic and aeroelastic analyses of aerospace structures typically involve deriving and solving sets of linear differential equations of motion generally written in matrix form:

$$[A]\{\ddot{x}\} + [B]\{\dot{x}\} + [C]\{x\} = \{F(t)\} \qquad (1)$$

In general, the A, B and C matrices are square and real-valued. A recognized hallmark of rotary wing and turbomachinery dynamics is an abundance of nonconservative forces (usually involving rotor rotation speed). Consequently, the resulting analyses produce matrix equations of motion of the above type which are highly nonsymmetrical, and often of large orders.

Although a large part of the dynamic analyst's job involves the calculation of dynamic loads and stresses due to explicit excitations, the scope of this paper will be limited to the equally important eigenproblem (F(t) = 0):

$$\{x\} = \sum_i \{\varphi^{(i)}\} e^{\lambda_i t} \qquad (2)$$

$$\left[[A]\lambda_i^2 + [B]\lambda_i + [C]\right]\{\varphi^{(i)}\} = [G(\lambda_i)]\{\varphi^{(i)}\} = \{0\} \qquad (3)$$

The eigenvalues λ $(= \sigma \pm i\omega)$, which give stability and natural frequency information are obtained from the familiar characteristic determinant:

$$|[A]\lambda^2 + [B]\lambda + [C]| = 0 \qquad (4)$$

by any of various well-established methods [1], [2], [3]. The "flutter" mode shapes, $\phi^{(i)}$, are obtained from Eq. (3) once the eigenvalues are known.

This paper presents an easily implemented technique for the improved analysis of dynamic systems of the type described above. The technique requires a reliable eigensolution and involves manipulations of the given dynamic equations, their eigenvalues and eigenvectors. Specifically, the technique systematizes the identification of destabilizing and/or stiffening forces by the calculation of "force phasing matrices". Applications of the technique to analyses of bending-torsion divergence and flutter and of pitch-lag/flap instability of a helicopter rotor blade are presented. Furthermore, this paper essentially represents an expansion of a portion of an earlier paper [4].

II. Mathematical Development

The principal function of the force-phasing matrix technique is to identify those force terms in the equations of motion which, for an unstable mode, are so phased by the mode shape as to be drivers of the motion. The technique is perhaps nothing more than a formalization of the intuitive use an experienced dynamicist would make of the eigenvector information. The basis of the technique can be seen by writing any single equation of the set represented by Eq. (3) as the sum of the mass, damper and spring forces of the diagonal degree-of-freedom and the remaining forces acting as a combined exciting force.

$$a_{nn}\lambda_i^2\varphi_n^{(i)} + b_{nn}\lambda_i\varphi_n^{(i)} + c_{nn}\varphi_n^{(i)} + \underbrace{\sum_{j\neq n}(a_{nj}\lambda_i^2 + b_{nj}\lambda_i + c_{nj})\varphi_j^{(i)}}_{f_n} = 0 \qquad (5)$$

For the usual case a_{nn}, b_{nn} and c_{nn} are all positive numbers; that is, each mass when uncoupled from the others is a stable spring-mass-damper system. Since the root, λ_i, is generally complex, Eq. (5) can then be interpretted as the sum of four complex quantities or vectors in the complex plane which must, furthermore, be in equilibrium. Assuming that the root with positive imaginary part is used throughout, the argument of the root, γ_i, is the angle by which the inertia force vector is rotated relative to the damper force vector and the damper force vector is rotated relative to the spring force vector. For an unstable root this angle will be less than 90 degrees. If a purely imaginary value is assigned to the spring force vector, unstable motion is assumed and it is recalled that the four vectors are in equilibrium, then

the real parts of the damper and inertia force vectors will be negative and the driving force must always have a positive real part. Figure 1, which demonstrates this argument, shows the four force vectors in the complex plane for an unstable oscillatory mode ($Re(\lambda_i) = \sigma_i > 0$) and for unit imaginary displacement:

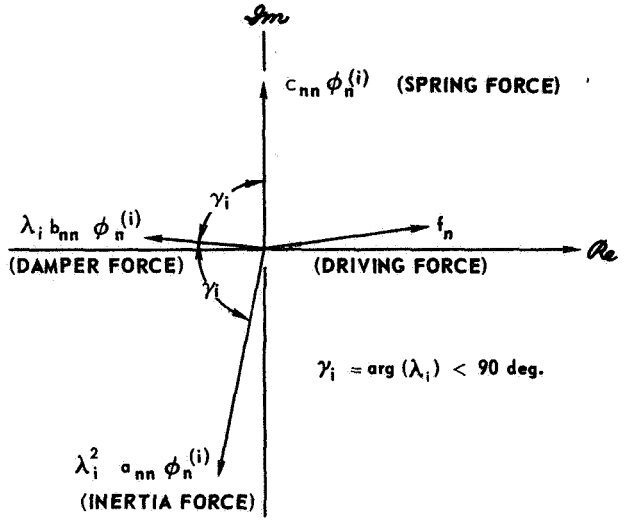

Figure 1. Force-Vector Diagram for n'th Degree-Of-Freedom, i'th Mode (Oscillatory Instability)

A secondary function of the technique is to identify those terms in the equations which, for any coupled mode, act as stiffness so as to increase the coupled frequency of the mode. Reference to Figure 1 shows that driving forces with positive imaginary parts will tend to reinforce the diagonal spring term and, hence, raise the frequency of the coupled mode. An interesting observation that can be made from Figure 1 is that, for unstable motion, the diagonal damper force also has a positive imaginary part. Hence, it tends to stiffen the (unstable) coupled mode in contrast to the frequency lowering effect of damping for stable motion.

Figure 2 shows the same forces as vectors for an unstable aperiodic mode (divergence) for negative unit real displacement:

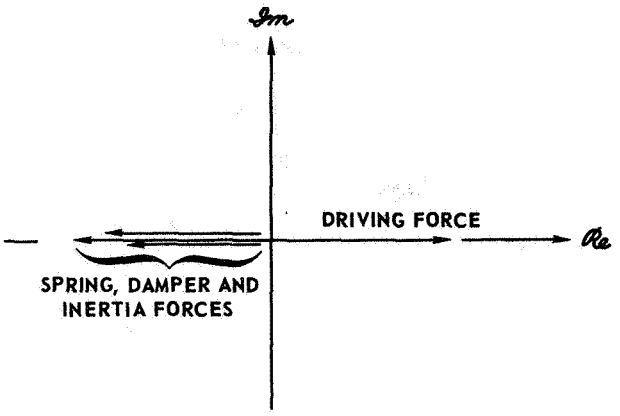

Figure 2. Force-Vector Diagram for n'th Degree-of-Freedom, Divergence Instability.

Again, the driving force is always a positive real number. Furthermore, for divergences, stiffening forces are by definition stabilizing; hence, those components of the driving force which are negative are also those that stiffen the coupled mode.

These interpretations of unstable motion can be quantitatively implemented first, by multiplying each of the dynamic equations (i.e., each row of the equation (1)) by a quantity which makes the diagonal stiffness force (stiffness matrix element x displacement) become pure imaginary and second, by representing the modal vector as a diagonal (square) matrix. This latter operation has the effect of evaluating the magnitudes of the component dynamic equation forces without numerically adding them together. The resulting "stability" force phasing matrices are then readily written as:

$$[P_{A_i}] = Re[\eta/\varphi^{(i)}]\lambda_i^2[A][\varphi^{(i)}] \quad (6)$$

$$[P_{B_i}] = Re[\eta/\varphi^{(i)}]\lambda_i[B][\varphi^{(i)}] \quad (7)$$

$$[P_{C_i}] = Re[\eta/\varphi^{(i)}][C][\varphi^{(i)}] \quad (8)$$

where

$$\eta = \begin{cases} i & \text{, for oscillatory instabilities} \\ -1. & \text{, for divergences} \end{cases} \quad (9)$$

and where the eigenvalue in the upper half plane is used.

In all cases, the real parts of the above indicated matrix expressions give instability driving force information. Forces defined by elements of the A, B and C dynamic equation matrices which are phased by the mode shape so as to be drivers of the motion then cause the corresponding elements of the P_{A_i}, P_{B_i} and P_{C_i} "stability" force phasing matrices, respectively, to be positive and proportional to their strength as drivers.

Stiffening driving force information is obtained differently for oscillatory motion and for aperiodic motion. Those elements of the dynamic equation matrices which are phased so as to be stiffeners of the coupled mode will cause the corresponding elements of the matrix expressions to be either positive imaginary for oscillatory motion, or negative real for aperiodic motion. The resulting "stiffness" force phasing matrices are then expressed as:

$$[\hat{P}_{A_i}] = \mathrm{Im}[\eta/\varphi^{(i)}]\lambda_i^2[A][\varphi^{(i)}] \qquad (10)$$

$$[\hat{P}_{B_i}] = \mathrm{Im}[\eta/\varphi^{(i)}]\lambda_i[B][\varphi^{(i)}] \qquad (11)$$

$$[\hat{P}_{C_i}] = \mathrm{Im}[\eta/\varphi^{(i)}][C][\varphi^{(i)}] \qquad (12)$$

for oscillatory motion, and:

$$[\hat{P}_{(\ )_i}] = [P_{(\ )_i}] \qquad (13)$$

for aperiodic motion.

It should be stressed that these force phasing matrices are no more than a more systematic and efficient interpretation of the all too often voluminous eigensolution information. The following sections illustrate the usage of the force phasing matrix technique in substantiating what is generally known of some rather fundamental, classical helicopter rotor blade instabilities.

III. Description of Illustrative Rotor Blade Example

For illustrative purposes, relatively simple linear equations of motion were formulated for a generalized untwisted helicopter rotor blade and then applied to a realistic nonarticulated rotor configuration. The blade is assumed to be operating in an unstalled hover condition at some collective angle and with a built-in coning angle. Perturbative elastic flatwise, edgewise and torsion motions are assumed to occur about the preconed position. The resulting linear aeroelastic equations are fairly standard [5], [6]; quasi-static aerodynamics (uniform inflow) is assumed and a normal mode description of the blade elasticity is employed. Thus, for the chosen configuration, two flatwise bending modes, one edgewise bending mode, and the rigid feathering degree-of-freedom are assumed. The resulting response vector, $\{x\}$, consists of the quantities q_{w_1}, q_{w_2}, q_{v_1}, and q_{θ_1} whose detailed dynamic equations are given in the Appendix. The dynamic equations then comprise a set of four differential equations written as a 4 x 4 matrix equation of the Eq. (1) type. The aeroelastic degrees-of-freedom together with the general parameters are shown in Figure 4:

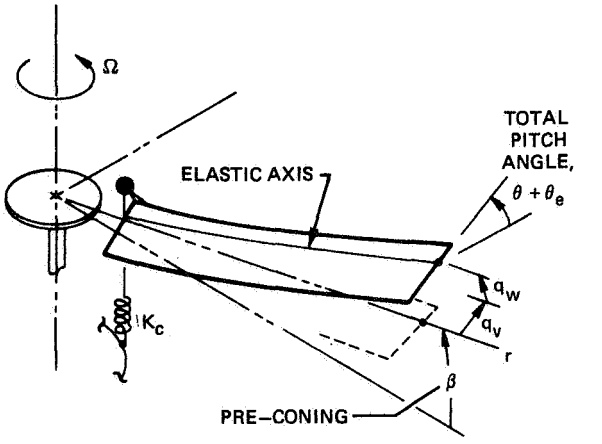

Figure 4. Schematic of Nonarticulated Rotor Configuration and Aeroelastic Degrees-of-Freedom.

The basic configuration incorporates a counterweight over the outer 70 percent of the blade, pitch-flap coupling (determined from the geometry of the pushrod attachment and flatwise modal deflection) and pitch-lag coupling of arbitrary magnitude. The chordwise position of the counterweight and the magnitude of pitch-lag coupling are purposely varied in the following analysis to establish known blade instabilities in order to illustrate the phasing matrix analysis technique. Table I below summarizes the pertinent geometric and aeroelastic data for the rotor blade configuration:

TABLE I - BLADE CHARACTERISTICS

Radius	210 in.
Chord (0.1R to tip)	13.5 in.
Tip Speed	650 fps
Pitch-Flap coupling, A_{w_m} $\begin{cases} m = 1 \\ m = 2 \end{cases}$	$\begin{matrix} 0. \\ 0.188 \end{matrix}$
Roof feathering spring rate	3.55×10^6 in.-lb/rad
Blade coning	2 deg.
Airfoil: (NACA 0012; Mach No. = 0):	
a	6.0/rad
δ_o	0.01
δ_4	$3.30/\text{rad}^4$
(Uniform) mass distribution	0.000776 lb-sec^2/in.^{2}
(Uncoupled) blade natural frequencies:	
first flatwise mode	1.092/rev
second flatwise mode	2.681/rev
first edgewise mode	1.390/rev
rigid feathering	3.820/rev
$\frac{\text{(edgewise mode structural damping)}}{\text{(critical damping)}}$	0.01
Flight condition (hovering)	sea level, standard
collective angle, θ	10 deg.
inflow ratio, λ	-.0601

The normal flatwise and edgewise mode shapes used are shown in Figure 5.

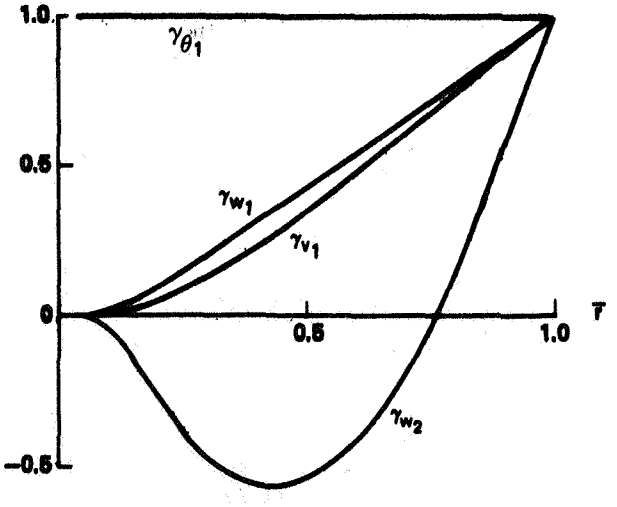

Figure 5. Spanwise Variation of Normal Mode Shapes.

IV. Application of Analysis to Illustrative Example

Basic Configuration

For purposes of comparison, the data in Table I was used together with a collective angle of 10 deg, inflow ratio of -0.0601, and with zero counterweight chordwise offset (from the quarter chord), and zero pitch-lag coupling. This basic case is stable in all modes as is shown by the following list of resulting eigenvalues:

$$\lambda_{1,2} = -0.504 \pm i10.960$$
$$\lambda_{3,4} = -0.411 \pm i2.610$$
$$\lambda_{5,6} = -0.027 \pm i1.398$$
$$\lambda_{7,8} = -1.472 \pm i3.506$$

While all the aeroelastic modes represented by the various eigenvalues comprise responses in all the four degrees of freedom, they could be characterized as follows: mode 1 ($\lambda_{1,2}$) is first flatwise bending, mode 2 ($\lambda_{3,4}$) is second flatwise bending, mode 3 ($\lambda_{5,6}$) is first edgewise bending, and mode 4 ($\lambda_{7,8}$) is rigid feathering.

Configuration With Rearward Chordwise Counterweight

If the 70 percent outer span counterweight is artificially shifted aft so as to place the chordwise section mass center at the 32 percent chord point, reference to the dynamic equations (A-1, A-2 and A-3) then yields the following A, B and C matrices (given in E format):

A (Inertia) Matrix:

.2909-00	-.0000	-.0000	-.1884-02
-.0000	.2006-00	-.0000	.3482-03
-.0000	-.0000	.2542-00	-.0000
-.1884-02	.3482-03	-.0000	.1133-03

B (Damping) Matrix:

.2887-00	.7757-01	-.4500-02	-.1256-01
.7992-01	.1665-00	-.8166-02	-.3309-03
.3099-01	.1943-01	.7901-02	-.2020-02
.1536-07	.6326-04	-.1058-03	.3370-03

C (Stiffness) Matrix:

.3382-00	-.5763-01	.4633-01	-.3067-00
-.8232-03	.1422+01	.7484-02	-.7080-01
.4633-01	-.2974-02	.4988-00	-.4396-01
-.2300-02	-.5423-02	-.2919-03	.1646-02

The first two rows of the matrix equation are the equations for the first and second flatwise bending modes, respectively. The third

row is the equation for the first edgewise mode, while the fourth is for rigid feathering. Correspondingly, elements in the first two columns of the matrices are terms multiplying the flatwise bending responses and their derivatives. Similarly, third and fourth column elements are terms multiplying edgewise bending and rigid feathering, respectively, and their derivatives.

The eigensolution for these matrices (see Eq. (4)) reveals the configuration to be unstable in both divergence and flutter:

$$\lambda_{1,2} = 0.408, \quad -4.466$$
$$\lambda_{3,4} = 0.300 \pm i1.789$$
$$\lambda_{5,6} = -0.0088 \pm i1.402$$
$$\lambda_{7,8} = -0.578 \pm i3.099$$

Since the equations are in nondimensional form, the units of these eigenvalues are per rotor revolution frequency or "p". Using Eqs. (6) through (9) the following "stability" force phasing matrices are written for the unstable divergence mode:

A Phasing Matrix, P_{A_1}

-.4840-01	-.0000	-.0000	.5061-03
-.0000	-.3338-01	-.0000	-.1726-02
-.0000	-.0000	-.4229-01	-.0000
.1941-03	-.1944-05	-.0000	-.1885-04

B Phasing Matrix, P_{B_1}

-.1178+00	-.1715-02	.4408-04	.8272-02
-.6016-00	-.6791-01	.1476-02	.4022-02
-.5265-00	-.1789-01	-.3223-02	.5540-01
-.3881-08	-.8660-06	.6418-06	-.1375-03

C Phasing Matrix, P_{C_1}

-.3382-00	.3123-02	-.1113-02	.4953-00
.1519-01	-.1422+01	-.3316-02	.2110+01
-.1929+01	.6710-02	-.4988-00	.2956+01
.1424-02	.1820-03	.4341-05	-.1646-02

The larger of the destabilizing driving forces, which show up as positive terms, have been underlined for clarity. A reasonable yard-stick for measuring the size of the destabilizing forces is to compare them to the size of the stabilizing element in each matrix equation row. For oscillatory instabilities that element would be the diagonal damping force; for divergences, it would be the diagonal stiffness force. As would be expected of a divergence instability, the major destabilizing forces are displacement dependent (i.e., appear in the C matrix). By making additional reference to Eqs. (A-1) and (A-2), and (A-3) and to their evaluation given above, the following interpretation can be drawn from these results:

1. The unstable mechanism involves a coupling mainly between first flatwise bending and rigid feathering. The mode shape, $\phi^{(1)}$ = (0.619, 0.0336, 0.0149, and 1.0), confirms this result.

2. The position of the chordwise mass center behind the elastic axis, as indicated by negative dynamic equation elements $a_{1,4}$ and $c_{4,1}$ and reference to the explicit statements of the equations in the Appendix, is a major link in the unstable coupling chain of events. This result confirms well-known results concerning the divergence of rotor blades [5]; specifically, that the torsion modes drive the flatwise modes aerodynamically (elements $c_{1,4}$ and $c_{2,4}$) while the flatwise modes drive the torsion modes with centrifugal inertial forces through the rearward mass center position (elements $c_{4,1}$ and $c_{4,2}$).

3. The first edgewise bending mode is being driven by the rigid feathering through aerodynamic and inertia terms (element $b_{3,4}$) but is not actively participating in the unstable mechanism.

In a similar manner the following force phasing matrices are written for the unstable oscillatory (flutter) mode, λ_3:

A Phasing Matrix, P_{A_3}

-.3125-00	-.0000	-.0000	-.1904-01
-.0000	-.2155-00	-.0000	-.1101-01
-.0000	-.0000	-.2731-00	-.0000
.1421-02	-.1114-04	-.0000	-.1217-03

B Phasing Matrix, P_{B_3}

-.5163-00	.7587-02	.2749-02	-.1968-01
.6947-00	-.2978-00	-.1561-01	.1282-01
-.1493-00	.1659-02	-.1413-01	-.4186-05
.5201-08	-.5155-05	-.6870-05	-.6027-03

C Phasing Matrix, P_{C_3}

-.1260-08	.6779-02	-.4386-02	.8548-00
-.4997-02	-.1325-08	.1751-01	-.1802-00
.3814-01	.1173-02	-.0000	.3956-00
-.6696-03	.2794-04	-.3155-04	-.0000

Again the major destabilizing terms have been underlined for clarity. With few exceptions the same interpretations can be made of the flutter force phasing matrices as were made for the divergence ones. While the feathering

degree-of-freedom again drives the first flatwise mode aerodynamically (element $c_{1,4}$), the flatwise mode now drives the feathering degree-of-freedom with vibratory inertia forces (element $a_{4,1}$). Again these results confirm well-known findings.

Configuration With Pitch-Lag Coupling

Using the reconfirmed knowledge that an aft chordwise center of mass is destabilizing, the configuration is altered back to the original quarter chord balanced configuration. In addition, unit pitch-lag coupling ($A_{v_1} = 1.$) is introduced into the configuration. The resulting dynamic equations are as follows:

A (Inertia) Matrix

.2909-00	-.0000	-.0000	-.0000
-.0000	.2006-00	-.0000	-.0000
-.0000	-.0000	.2542-00	-.0000
-.0000	-.0000	-.0000	.1133-03

B (Damping) Matrix

.2887-00	.7757-01	-.1622-01	-.1256-01
.7992-01	.1665-00	-.8596-02	-.3309-03
.3015-01	.1953-01	.1003-01	-.2169-02
.1536-07	.6326-04	.3801-03	.3370-03

C (Stiffness) Matrix

.3382-00	-.5763-01	-.2563-00	-.3049-00
-.8232-03	.1422+01	-.6358-01	-.7113-01
.4633-01	-.2974-02	.4431-00	-.4337-01
-.0000	-.0000	-.0000	.1646-02

The eigenvalues for this configuration reveal the configuration to be unstable in the edgewise bending mode:

$\lambda_{1,2} = -0.573 \pm i0.977$
$\lambda_{3,4} = -0.408 \pm i2.609$
$\lambda_{5,6} = 0.0119 \pm i1.324$
$\lambda_{7,8} = -1.449 \pm i3.505$

Again, the stability force-phasing matrices are formed for the unstable mode (λ_5) and the larger positive terms are underlined:

A Phasing Matrix, P_{A_5}

-.9137-02	-.0000	-.0000	-.0000
-.0000	-.6302-02	-.0000	-.0000
-.0000	-.0000	-.7985-02	-.0000
-.0000	-.0000	-.0000	-.3558-05

B Phasing Matrix, P_{B_5}

-.3822-00	.5003-02	-.2424-01	.8736-02
.2114+01	-.2204-00	.2079-00	-.4936-02
.1546-01	-.3974-03	-.1327-01	-.2946-03
-.3235-07	.6967-05	.4427-03	-.4461-03

C Phasing Matrix, P_{C_5}

.1260-08	-.4643-03	.3315-00	.7077-01
.2728-02	.5299-08	-.1886+01	-.2069-00
.2015-01	.7210-04	-.0000	-.1373-01
-.0000	-.0000	-.0000	-.0000

By referring to the explicit dynamic equations given in the Appendix, the following observations can be made:

1. The instability appears very similar to classic pitch-lag instability [7] and is mainly a three-way coupling between first flatwise and edgewise bending modes and the rigid feathering degree-of-freedom. The resulting coupled mode, $\phi^{(3)}$ = (-0.383 - i0.435, 0.015 + i0.024, 1., -0.100 - i.0317).

2. The edgewise bending mode is being driven by inertia forces generated by flatwise bending motion: coriolis forces proportional to precone and flatwise bending rate and forces proportional to pitch angle and flatwise bending deflection.

3. The flatwise bending mode is being driven by aerodynamic forces generated chiefly by pitch-lag coupled edgewise bending and to a lesser extent rigid feathering deflection.

4. The rigid feathering degree-of-freedom is being driven principally by a centrifugal force moment involving chordwise mass radii of inertia, pitch angle, and edgewise bending rate.

The stiffness force-phasing matrices for this mode are formed and the significant terms for the edgewise bending equation are underlined:

A Phasing Matrix, $\hat{P}_{A_3}$

-.5097-00	.0000	.0000	.0000
.0000	-.3516-00	.0000	.0000
.0000	.0000	-.4455-00	.0000
.0000	.0000	.0000	-.1985-03

B Phasing Matrix, $\hat{P}_{B_3}$

.3425-02	.7827-03	.2799-01	.3780-02
-.3696-00	.1975-02	-.3394-00	-.1230-02
.1722-01	-.6235-03	.1190-03	-.9064-03
.1469-07	-.1870-05	-.1450-02	.3998-05

C Phasing Matrix, $\hat{P}_{C_3}$

.3382-00	.2803-02	.2923-00	-.1596-00
.1647-01	.1422+01	-.1179+01	.7995-00
-.1777-01	-.4505-04	.4431-00	.4327-02
.0000	.0000	.0000	.1646-02

It can be seen that the principal stiffening terms are, not unexpectedly, the diagonal mass and stiffness terms. The only other significant stiffening terms are those involving flatwise bending rate and deflection which are also the drivers of the unstable edgewise motion.

That the flatwise bending deflection term is negative and numerically greater than the rate dependent term can be appreciated by noting that the unstable coupled edgewise mode frequency, 1.324, is lower than the original corresponding stable mode frequency, 1.398.

V. Concluding Remarks

The "force-phasing" matrices technique provides yet another tool for understanding dynamic/aerodynamic phenomena. While it does not, by itself, indicate stability levels such as are provided by the eigensolution, it does complement the eigensolution by giving insight into the details of the dynamic configuration which are not directly available from the eigenvalues and eigenvectors alone. Moreover, the technique requires, in particular, eigenvector information as a starting point. Hence, it is inherently incapable of answering the more fundamental question of why, for any one mode, the eigenvector elements are indeed phased as they are. It should also be stressed that the technique is a tool to be used with, and in support of, engineer/analyst judgement; the results have to be interpreted properly, generally in the context of the specific application. Finally, the relative simplicity of the formulation makes the incorporation of the technique in any aeroelastic eigensolution program a straightforward and easily implemented task.

Appendix - Details of Dynamic Equations

The linear dynamic equations used to represent the aeroelastics of the rotor blade in hover are formulated using an assumed modal approach; the derivation is standard and uses the nomenclature of Reference 6. The linearization and subsequent simplifications are based upon the following assumptions:

1. quasi-static, incompressible, nonstalled airloads.
2. coincident spar center, shear center and tension center.
3. zero twist.
4. two flatwise bending modes, one edgewise bending mode and the rigid feathering degree-of-freedom.
5. normal uncoupled bending mode shapes (zero twist and pitch angle).

The flatwise bending equations are then written as:

$$\int_0^1 \Big\{ (\bar{m}\gamma_{w_i}\gamma_{w_m})\,\ddot{q}_{w_m} + (\bar{m}\,\bar{y}_{1O_{cg}}\gamma_{w_i}\gamma_{\theta_j})\,\ddot{q}_{\theta_j} + [2\bar{m}\gamma_{w_i}(\beta\gamma_{v_k} + \bar{y}_{1O_{cg}}\sin\theta\gamma'_{v_k})]\,\dot{q}_{v_k} - (2\,\bar{m}\,\bar{k}^2_{y_{1O}}\cos\theta\,\gamma_{\theta_j}\gamma'_{w_i})\,\dot{q}_{\theta_j} + [\overline{EI}_y\gamma''_{w_i}\gamma''_{w_m} + \bar{T}\gamma'_{w_i}\gamma'_{w_m} - \bar{m}\sin^2\theta\,\gamma_{w_i}\gamma_{w_m}]\,q_{w_m} + (\bar{m}\gamma_{w_i}\gamma_{v_k}\sin\theta\cos\theta)\,q_{v_k} + [\bar{m}\gamma_{w_i}(\bar{y}_{1O_{cg}}\cos 2\theta - \bar{r}\beta\sin\theta)\gamma_{\theta_j}]\,q_{\theta_j} + \frac{\rho acR}{2m_o}\gamma_{w_i}\Big[-\bar{r}^2\big(\gamma_{\theta_j}q_{\theta_j} + A_{w_m}q_{w_m} + A_{v_k}q_{v_k}\big) + \bar{r}\big(\gamma_{w_m}\dot{q}_{w_m} + \bar{y}_{1O_{3c/4}}(\gamma_{\theta_j}\dot{q}_{\theta_j} + A_{w_m}\dot{q}_{w_m} + A_{v_k}\dot{q}_{v_k}) - \alpha_o\gamma_{v_k}\dot{q}_{v_k}\big)\Big]\Big\}\,d\bar{r} = 0 \qquad \text{(A-1)}$$

The edgewise equations are written as:

$$\int_0^1 \Big\{ (\bar{m}\gamma_{v_k}\gamma_{v_n})\,\ddot{q}_{v_n}^{**}$$

$$-[2\,\bar{m}\gamma_{w_m}(\beta\gamma_{v_k} + \bar{y}_{10_{cg}}\sin\theta\,\gamma'_{v_k})]\,\ddot{q}_{w_m}^{*}$$

$$-[2\,\bar{m}(\beta\bar{y}_{10_{cg}}\gamma_{v_k} + \bar{k}^2_{z_{10}}\sin\theta\,\gamma'_{v_k})\,\gamma_{\theta_j}]\,\ddot{q}_{\theta_j}^{*}$$

$$+(\bar{m}\gamma_{v_k}\gamma_{w_m}\sin\theta\,\cos\theta)\,q_{w_m} \qquad \text{(A-2)}$$

$$+[\overline{EI}_z\gamma''_{v_k}\gamma''_{v_n} + \bar{T}\gamma'_{v_k}\gamma'_{v_n} - \bar{m}\cos^2\theta\,\gamma_{v_k}\gamma_{v_n}]\,q_{v_n}$$

$$+[\bar{m}\gamma_{v_k}(\bar{r}\beta\,\cos\theta + \bar{y}_{10_{cg}}\sin 2\theta)\gamma_{\theta_j}]\,q_{\theta_j}$$

$$+\frac{\rho acR}{2m_o}\,\gamma_{v_k}\Big[-\bar{r}^2\Big(2\,\alpha_o - 4\,\frac{\delta_4}{a}\alpha_o^3\Big)(\gamma_{\theta_j}q_{\theta_j} + A_{w_m}q_{w_m}$$

$$+\,A_{v_n}q_{v_n}) + \bar{r}\Big(2\,\alpha_o - 4\,\frac{\delta_4}{a}\alpha_o^3 - 2\,\frac{\delta_o}{a}\theta\Big)\Big(\gamma_{w_m}\ddot{q}_{w_m}^{*}$$

$$+\,\bar{y}_{10_{3c/4}}\Big(\gamma_{\theta_j}\ddot{q}_{\theta_j}^{*} + A_{w_m}\ddot{q}_{w_m}^{*} + A_{v_n}\ddot{q}_{v_n}^{*}\Big)\Big)$$

$$+\,2\,\bar{r}\Big(\frac{\delta_o}{a} - \frac{\delta_4}{a}\alpha_o^4\Big)\gamma_{v_n}\ddot{q}_{v_n}^{*}\Big]\Big\}d\bar{r} + C_{e_k}\ddot{q}_{v_k}^{*} = 0$$

The torsion equations are written as:

$$\int_0^1 \Big\{ (\bar{m}\,\bar{y}_{10_{cg}}\gamma_{\theta_j}\gamma_{w_m})\,\ddot{q}_{w_m}^{**} + [\bar{m}(\bar{k}^2_{y_{10}} + \bar{k}^2_{z_{10}})\gamma_{\theta_j}\gamma_{\theta_k}]\,\ddot{q}_{\theta_k}^{**}$$

$$+(2\,\bar{m}\,\bar{k}^2_{y_{10}}\cos\theta\,\gamma_{\theta_j}\gamma'_{w_m})\,\ddot{q}_{w_m}^{*}$$

$$+[2\,\bar{m}(\beta\bar{y}_{10_{cg}}\gamma_{v_n} + \bar{k}^2_{z_{10}}\sin\theta\,\gamma'_{v_n})\,\gamma_{\theta_j}]\,\ddot{q}_{v_n}^{*}$$

$$+[\bar{m}\,\bar{y}_{10_{cg}}(\bar{r}\gamma'_{w_m} - \sin^2\theta\,\gamma_{w_m})\gamma_{\theta_j}]\,q_{w_m}$$

$$+[(\overline{GJ} + \bar{k}^2_{\bar{A}}\bar{T})\,\gamma'_{\theta_j}\gamma'_{\theta_k} + \bar{m}(\bar{k}^2_{z_{10}} - \bar{k}^2_{y_{10}})\cos 2\theta\,\gamma_{\theta_j}\gamma_{\theta_k}]q_{\theta_k}$$

$$+(\bar{m}\,\bar{y}_{10_{cg}}\sin\theta\,\cos\theta\,\gamma_{\theta_j}\gamma_{v_n})\,q_{v_n} \qquad \text{(A-3)}$$

$$+\frac{\rho acR}{2m_o}\,\gamma_{\theta_j}[-\bar{r}^2\bar{y}_{10_{c/4}}(\gamma_{\theta_k}q_{\theta_k} + A_{w_m}q_{w_m} + A_{v_n}q_{v_n})$$

$$+\,\bar{r}\,\bar{y}_{10_{c/4}}\Big(\gamma_{w_m}\ddot{q}_{w_m}^{*} - \alpha_o\gamma_{v_n}\ddot{q}_{v_n}^{*} + \bar{y}_{10_{3c/4}}(\gamma_{\theta_k}\ddot{q}_{\theta_k}^{*}$$

$$+\,A_{w_m}\ddot{q}_{w_m}^{*} + A_{v_n}\ddot{q}_{v_n}^{*})\Big) - \frac{\pi c}{2aR}\,\bar{r}\,\bar{y}_{10_{3c/4}}(\gamma_{\theta_k}\ddot{q}_{\theta_k}^{*}$$

$$+\,A_{w_m}\ddot{q}_{w_m}^{*} + A_{v_n}\ddot{q}_{v_n}^{*})]\Big\}d\bar{r} + \frac{K_c\delta_{j,1}}{m_oR^3\Omega^2}\,q_{\theta_1} = 0$$

where:

$$\alpha_o = \theta + \lambda/\bar{r} \qquad \text{(A-4)}$$

References

1. Wilkinson, J. H.: The Algebraic Eigenvalue Problem. Clarendon Press, Oxford, 1965.

2. Programmer's Manual: Subroutines ATEIG and HSBG. IBM System/360 Scientific Subroutine Package, Version III, GH20-0205-4, August 1970.

3. Leppert, E. L., Jr.: A Fraction Series Solution for Characteristic Values Useful in Some Problems of Airplane Dynamics. Journal of the Aeronautical Sciences, Vol. 22, No. 5, May 1955.

4. Bielawa, R. L.: Techniques for Stability Analysis and Design Optimization with Dynamic Constraints of Nonconservative Linear Systems. AIAA/ASME 12th Structures, Sturctural Dynamics and Materials Conference Paper No. 71-388, Anaheim, California, April 1971.

5. Miller, R. H. and C. W. Ellis: Blade Vibration and Flutter. Journal of the American Helicopter Society, Vol. 1, No. 3, July 1956.

6. Arcidiacono, P. J.: Prediction of Rotor Instability at High Forward Speeds. Vol. I, Differential Equations of Motion for a Flexible Helicopter Rotor Blade in Steady Flight Including Chordwise Mass Unbalance Effects. USAAVLABS Technical Report 68-18A, U. S. Army, February 1969.

7. Chou, P. C.: Pitch-Lag Instability of Helicopter Rotors. Journal of the American Helicopter Society, Vol. 3, No. 3, July 1958.

SOME APPROXIMATIONS TO THE FLAPPING STABILITY OF HELICOPTER ROTORS

James C. Biggers
Research Scientist
Ames Research Center, NASA
Moffett Field, California 94035

Abstract

The flapping equation for a helicopter in forward flight has coefficients which are periodic in time, and this effect complicates the calculation of stability. This paper presents a constant coefficient approximation which will allow the use of all the well known methods for analyzing constant coefficient equations. The flapping equation is first transformed into the nonrotating coordinate frame, where some of the periodic coefficients are transformed into constant terms. The constant coefficient approximation is then made by using time averaged coefficients in the nonrotating frame. Stability calculations based on the approximation are compared to results from a theory which correctly includes all of the periodicity. The comparison indicates that the approximation is reasonably accurate at advance ratios up to 0.5.

Notation

a	blade lift curve slope
B	tip loss factor
c	blade chord
I	blade flapping inertia
i	$\sqrt{-1}$
k_β	flapping spring stiffness
N	number of blades
R	rotor radius
t	time, sec
V	forward velocity
α	angle of attack of hub plane
β_i	flapping of ith blade relative to hub plane
$\underline{\beta}$	vector of rotor degrees of freedom in nonrotating coordinates
β_0	rotor coning angle
β_{1c}	rotor tilt forward (longitudinal flapping)
β_{1s}	rotor tilt to left (lateral flapping)
β_2	rotor differential flapping
γ	blade lock number, $\rho acR^4/I$
λ	eigenvalue or root, nondimensionalized by Ω, $\frac{\sigma}{\Omega} + j\frac{\omega}{\Omega}$
μ	rotor advance ratio, $V(\cos\alpha)/\Omega R$
ν	flapping natural frequency of rotating blade
σ	real part of eigenvalue
ρ	air density
ψ	azimuth angle, Ωt
Ω	rotor rotational speed
ω	imaginary part of eigenvalue
ω_β	flapping natural frequency of stationary blade, $\sqrt{k_\beta/I}$
$\dot{(\,)}$	derivative, $d(\,)/d\psi$
$\ddot{(\,)}$	derivative, $d^2(\,)/d\psi^2$

For helicopter stability and control studies, it is desirable to use as simple a math model as possible while retaining reasonable accuracy, both to reduce computation effort and to gain insight into system behavior. However, for a helicopter in forward flight, the rotor flapping motion is described by a differential equation having coefficients which are periodic in time (azimuth). This fact complicates the solution of the equation, requiring methods which use considerable numerical computation and which give little insight. Thus it is desirable to find a differential equation with constant coefficients (hence an approximation) which adequately represents the forward flight flapping dynamics of a helicopter rotor. If such an equation is found, all of the well known techniques for analyzing constant coefficient equations may be used.

The flapping equation may be transformed into the nonrotating coordinate frame, as done in References 1 and 2, where some of the periodicity is transformed into constant terms. This result suggests that the use of constant coefficients in the nonrotating frame will retain some of the periodic system behavior. The constant coefficient approximation examined herein is made by using time averaged coefficients in the nonrotating frame. A comparison is made between the eigenvalues (stability) obtained from the approximation and the results from a theory which correctly includes all of the periodicity. The comparison indicates that the approximation is a useful representation of helicopter flapping dynamics for both hingeless and articulated rotors. This approximation was briefly discussed in Reference 1 for one set of rotor parameters. The present paper discusses the approximation in a more general manner and gives more insight into its features, limits, and applicability.

The rotor math model used here is for fixed shaft operation and includes only first mode (rigid blade) flapping, with spring-restrained flapping hinges at the hub center. Flapping natural frequency may be matched by selecting the spring rate. Thus the only approximations are in the use of the aerodynamic terms for rigid blade motion. Uniform inflow is used, and for the advance ratios considered here ($\mu < 0.5$), reverse flow effects are not included.

Equations of Motion

In this section, the single blade homogeneous flapping equation is presented for a rigid, spring-restrained, centrally hinged blade. This equation is then transformed to a nonrotating coordinate frame, using a coordinate transformation which is briefly discussed. Insight into the fundamental behavior of the rotor is gained by examining the hovering ($\mu = 0$) eigenvalues of the equation in nonrotating coordinates.

Presented at the AHS/NASA-Ames Specialists' Meeting on Rotorcraft Dynamics, February 13-15, 1974.

For the single blade, the homogeneous equation of motion is

$$\ddot{\beta}_i + M_{\dot{\beta}}\dot{\beta}_i + (\nu^2 + M_\beta)\beta_i = 0 \qquad (1)$$

where

$$M_{\dot{\beta}} = \frac{\gamma}{8} B^4 + \mu \frac{\gamma}{6} B^3 \sin \psi_i$$

$$M_\beta = \mu \frac{\gamma}{6} B^3 \cos \psi_i + \mu^2 \frac{\gamma}{8} B^2 \sin 2\psi_i$$

$$\nu^2 = 1 + \frac{\omega_\beta^2}{\Omega^2} = 1 + \frac{k_\beta}{I\Omega^2}$$

Note that reverse flow has not been included here. Although it could be included, it would not significantly affect the results for $\mu < 0.5$, since the additional terms are fourth order in μ.

By a coordinate transformation of the Fourier type, the single blade equation may be written in terms of nonrotating coordinates. The transformation accounts for the motion of all blades, and the number of degrees of freedom is equal to the number of blades. For example, with a three-bladed rotor, the degrees of freedom are coning (all blades flapping together), rotor pitching (cosine ψ flapping), and rotor rolling (sine ψ flapping). Adding a fourth blade adds a differential flapping degree of freedom, where blades 1 and 3 flap in one direction while blades 2 and 4 flap in the other direction. This type of differential motion is a degree of freedom with rotors having any even number of blades. Adding more blades adds degrees of freedom which, in the nonrotating frame, warp the plane described by the sine ψ and cosine ψ flapping motion.

The coordinate for the single blade is β_i. For a three-bladed rotor, the corresponding nonrotating coordinates are

$$\vec{\beta} = \begin{pmatrix} \beta_0 \\ \beta_{1c} \\ \beta_{1s} \end{pmatrix}$$

where β_0, β_{1c}, and β_{1s} are rotor coning, pitching, and rolling motions. For a four-bladed rotor,

$$\vec{\beta} = \begin{pmatrix} \beta_0 \\ \beta_{1c} \\ \beta_{1s} \\ \beta_2 \end{pmatrix}$$

where β_2 is the differential flapping motion discussed above.

In general, the blade degrees of freedom in the transformation are

$$\beta_0 = \frac{1}{N}\sum_{i=1}^{N} \beta_i$$

$$\beta_{nc} = \frac{2}{N}\sum_{i=1}^{N} \beta_i \cos n\psi_i$$

$$\beta_{ns} = \frac{2}{N}\sum_{i=1}^{N} \beta_i \sin n\psi_i$$

$$\beta_{\frac{N}{2}} = \frac{1}{N}\sum_{i=1}^{N} \beta_i (-1)^i, \quad N \text{ even only}$$

Then the motion of the ith blade is

$$\beta_i = \beta_0 + \sum_{n=1}^{K} \left(\beta_{nc} \cos n\psi_i + \beta_{ns} \sin n\psi_i\right) + \beta_{\frac{N}{2}} (-1)^i;$$

$$K = \begin{cases} \frac{1}{2}(N-1), & N \text{ odd} \\ \frac{1}{2}(N-2), & N \text{ even} \end{cases}$$

The equations of motion (that is, eq. (1)) must also be converted from a rotating to a nonrotating frame by a similar procedure. This process is accomplished by operating on the equations with the summation operators

$$\frac{1}{N}\sum_i (\ldots), \quad \frac{2}{N}\sum_i (\ldots)\cos n\psi_i ,$$

$$\frac{2}{N}\sum_i (\ldots)\sin n\psi_i , \quad \frac{1}{N}\sum_i (\ldots)(-1)^i$$

This is virtually the same procedure used in Reference 1.

It may be seen that the transformation involves multiplication by $\sin\psi$, $\cos\psi$, $\sin 2\psi$, $\cos 2\psi$, etc. This changes some of the periodic terms of the equations in the rotating reference frame into constants (plus higher harmonics) due to products of periodic terms, and vice versa.

Performing the indicated operations for $N = 3$ yields the following equations for a three-bladed rotor.

$$\ddot{\vec{\beta}} + \begin{bmatrix} \frac{\gamma}{8}B^4 & 0 & \mu\frac{\gamma}{12}B^3 \\ 0 & \frac{\gamma}{8}B^4 + \mu\frac{\gamma}{12}B^3\sin 3\psi & 2 - \mu\frac{\gamma}{12}B^3\cos 3\psi \\ \mu\frac{\gamma}{6}B^3 & -2 - \mu\frac{\gamma}{12}B^3\cos 3\psi & \frac{\gamma}{8}B^4 - \mu\frac{\gamma}{12}B^3\sin 3\psi \end{bmatrix} \dot{\vec{\beta}}$$

$$+ \begin{bmatrix} \nu^2 & \mu^2\frac{\gamma}{16}B^2\sin 3\psi & -\mu^2\frac{\gamma}{16}B^2\cos 3\psi \\ \mu\frac{\gamma}{6}B^3 + \mu^2\frac{\gamma}{8}B^2\sin 3\psi & \nu^2 - 1 + \mu\frac{\gamma}{6}B^3\cos 3\psi & \frac{\gamma}{8}\left(B^4 + \frac{1}{2}\mu^2B^2\right) + \mu\frac{\gamma}{6}B^3\sin 3\psi \\ -\mu^2\frac{\gamma}{8}B^2\cos 3\psi & -\frac{\gamma}{8}\left(B^4 - \frac{1}{2}\mu^2B^2\right) + \mu\frac{\gamma}{6}B^3\sin 3\psi & \nu^2 - 1 - \mu\frac{\gamma}{6}B^3\cos 3\psi \end{bmatrix} \vec{\beta} = 0 \qquad (2)$$

Similarly, operating as above with $N = 4$, the equations of a four-bladed rotor are obtained.

$$\ddot{\beta} + \begin{bmatrix} \frac{\gamma}{8}B^4 & 0 & \mu\frac{\gamma}{12}B^3 & 0 \\ 0 & \frac{\gamma}{8}B^4 & 2 & \mu\frac{\gamma}{6}B^3\sin 2\psi \\ \mu\frac{\gamma}{6}B^3 & -2 & \frac{\gamma}{8}B^4 & -\mu\frac{\gamma}{6}B^3\cos 2\psi \\ 0 & \mu\frac{\gamma}{12}B^3\sin 2\psi & -\mu\frac{\gamma}{12}B^2\cos 2\psi & \frac{\gamma}{8}B^4 \end{bmatrix}\dot{\beta}$$

$$+ \begin{bmatrix} \nu^2 & 0 & 0 & \mu^2\frac{\gamma}{8}B^2\sin 2\psi \\ \mu\frac{\gamma}{6}B^3 & \nu^2 - 1 + \mu^2\frac{\gamma}{16}B^2\sin 4\psi & \frac{\gamma}{8}(B^4 + \frac{1}{2}\mu^2B^2 - \frac{1}{2}B^2\mu^2\cos 4\psi) & \mu\frac{\gamma}{6}B^3\cos 2\psi \\ 0 & -\frac{\gamma}{8}(B^4 - \frac{1}{2}\mu^2B^2 + \frac{1}{2}\mu^2B^2\cos 4\psi) & \nu^2 - 1 - \mu^2\frac{\gamma}{16}B^2\sin 4\psi & \mu\frac{\gamma}{6}B^3\sin 2\psi \\ \mu^2\frac{\gamma}{8}B^2\sin 2\psi & \mu\frac{\gamma}{6}B^3\cos 2\psi & \mu\frac{\gamma}{6}B^3\sin 2\psi & \nu^2 \end{bmatrix}\beta = 0 \qquad (3)$$

The three- and four-bladed rotors have similar behavior except for the terms which are periodic in ψ. The periodic terms are 3/rev for the three-bladed rotor, but are 2 and 4/rev for the four-bladed rotor.

The main advantage of the transformed equations is that it is easier to express the combined rotor and airframe motions because the rotor equations are now in a nonrotating reference frame and include the motions of all blades. Furthermore, rotor motions are more intuitively understood, since the degrees of freedom are those seen by an observer in or beside the helicopter.

In the nonrotating coordinates of equations (2) and (3), the equations are coupled by off-diagonal terms. Note however, these are actually independent blades (unless some sort of feedback is added) and the coupling is due to the coordinate transformation.

To gain understanding of these degrees of freedom, the hovering ($\mu = 0$) behavior is examined next. The hover equations for four blades are given below.

$$\ddot{\beta} + \begin{bmatrix} \frac{\gamma}{8}B^4 & 0 & 0 & 0 \\ 0 & \frac{\gamma}{8}B^4 & 2 & 0 \\ 0 & -2 & \frac{\gamma}{8}B^4 & 0 \\ 0 & 0 & 0 & \frac{\gamma}{8}B^4 \end{bmatrix}\dot{\beta}$$

$$+ \begin{bmatrix} \nu^2 & 0 & 0 & 0 \\ 0 & \nu^2 - 1 & \frac{\gamma}{8}B^4 & 0 \\ 0 & -\frac{\gamma}{8}B^4 & \nu^2 - 1 & 0 \\ 0 & 0 & 0 & \nu^2 \end{bmatrix}\beta = 0 \qquad (4)$$

For three blades, the hovering equations are identical, except that the β_2 equation is then absent. The β_0 and β_2 equations at hover are completely uncoupled and are both identical to that of the single blade in rotating coordinates.

$$\ddot{\beta}_i + \frac{\gamma}{8}B^4\dot{\beta}_i + \nu^2\beta_i = 0 \qquad (1), \text{ for } \mu = 0$$

$$\left.\begin{aligned} \ddot{\beta}_o + \frac{\gamma}{8}B^4\dot{\beta}_o + \nu^2\beta_o = 0 \\ \ddot{\beta}_2 + \frac{\gamma}{8}B^4\dot{\beta}_2 + \nu^2\beta_2 = 0 \end{aligned}\right\} \text{ from equation (4)}$$

Eigenvalues of these equations are easily calculated, and are shown on figure 1. These will be

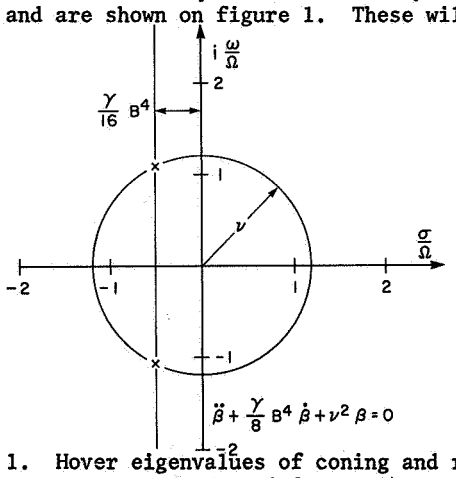

Figure 1. Hover eigenvalues of coning and reactionless modes ($\nu = 1.2$, $\gamma = 8$).

called coning and reactionless modes. The reactionless mode is so named because at hover it produces no net reaction at the hub. The equations for rotor pitching and rolling are,

$$\begin{pmatrix} \beta_{1c} \\ \beta_{1s} \end{pmatrix}'' + \begin{bmatrix} \frac{\gamma}{8}B^4 & 2 \\ -2 & \frac{\gamma}{8}B^4 \end{bmatrix}\begin{pmatrix} \beta_{1c} \\ \beta_{1s} \end{pmatrix}'$$

$$+ \begin{bmatrix} \nu^2 - 1 & \frac{\gamma}{8}B^4 \\ -\frac{\gamma}{8}B^4 & \nu^2 - 1 \end{bmatrix}\begin{pmatrix} \beta_{1c} \\ \beta_{1s} \end{pmatrix} = 0$$

and the characteristic equation is then,

$$\left(\lambda^2 + \frac{\gamma}{8}B^4\lambda + \nu^2 - 1\right)^2 + \left(2\lambda + \frac{\gamma}{8}B^4\right)^2 = 0$$

The eigenvalues for this equation are shown in figure 2. By analogy to a gyro, these modes will be called precession (the lower frequency mode) and nutation (the higher frequency mode). The damping, $-\gamma/16$, is the same as for the single blade of equation (1) and for the β_0 and β_2 modes discussed above. However, the coordinate transformation has resulted in the precession mode frequency being Ω lower than the single blade mode frequency in the

$$\begin{pmatrix}\beta_{1c}\\ \beta_{1s}\end{pmatrix}'' + \begin{bmatrix}\frac{\gamma}{8}B^4 & 2\\ -2 & \frac{\gamma}{8}B^4\end{bmatrix}\begin{pmatrix}\beta_{1c}\\ \beta_{1s}\end{pmatrix}' + \begin{bmatrix}\nu^2-1 & \frac{\gamma}{8}B^4\\ -\frac{\gamma}{8}B^4 & \nu^2-1\end{bmatrix}\begin{pmatrix}\beta_{1c}\\ \beta_{1s}\end{pmatrix} = 0$$

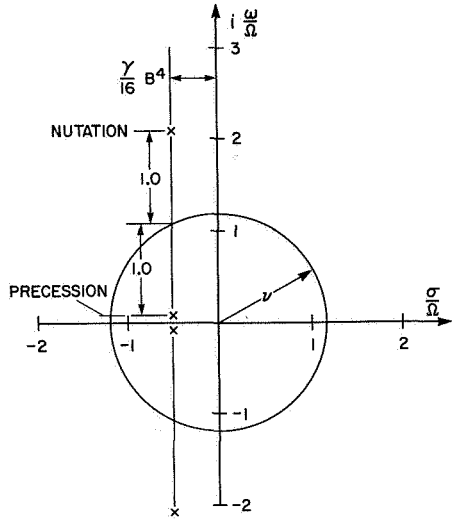

Figure 2. Hover eigenvalues of precession and nutation modes (ν = 1.2, γ = 8).

rotating frame. Similarly, the nutation mode frequency is Ω higher than that of the single blade in the rotating frame.

The coning mode (fig. 1) will excite vertical motions of the vehicle, while the precession mode will excite pitch and roll motions. Thus vehicle responses are more intuitively understood by use of the nonrotating coordinates. Also, these equations may be used to study feedback control systems such as rotor tilting or rotor coning feedback, which were discussed in Reference 1. Note (from eqs. (1) and (2)) that the performance of such systems will depend on the number of blades used, since the blade motions become coupled by the feedback terms and the coupling will vary with the number of blades.

To compare the various modes with each other and with other theories, it is necessary to transform all eigenvalues into the same reference frame. The obvious choice is the rotating coordinates of equation (1), since most other theories are applicable to this frame. As may be seen by comparing figures 1 and 2, the precession and nutation modes may be transformed back into the rotating frame by adding and subtracting Ω respectively. This process results in four identical eigenvalues, as expected, since the rotor is composed of four identical blades, each described in the rotating frame by equation (1). As noted above, the frequencies of the β_0 and β_2 modes do not change

The equations for $\mu = 0$ have been easily solved and the nonrotating coordinate system has been presented and discussed. In nonhovering flight, however, the equations have periodic coefficients, which makes the equations more difficult to solve, as well as giving the solutions some special characteristics. These will be discussed in the next section.

Periodic Coefficient Solutions

Floquet Theory

Eigenvalues of equations such as (1) may be found with Floquet theory, as for example in References 3 and 4. The equation is integrated for one period (ψ = 0,..., 2π) for each independent initial condition to obtain the state transition matrix. The frequency and damping of the system modes are then obtained by taking the logarithms of the state transition matrix eigenvalues.

This technique has been applied here to three cases, and the results are shown on figure 3 for

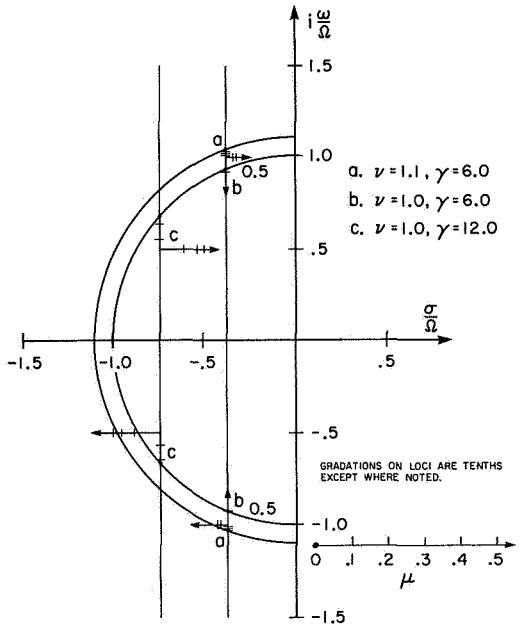

Figure 3. Floquet theory root loci for varying μ; single blade in rotating coordinates.

varying μ. Note that as μ is increased, the frequency (ω/Ω) decreases, while the damping (σ/Ω) remains constant at $-\gamma/16$ until the frequency reaches an integer multiple of 1/2 /rev. As μ is increased further, the frequency remains constant while the damping both decreases (the upper roots) and increases (the lower roots) as shown for cases a and c. This behavior may be surprising to those accustomed to constant coefficient equations, but is typical of periodic systems. The nonsymmetry about the real axis is analogous to the behavior of a constant coefficient equation root locus when the locus meets the real axis. At that point, the roots separate (no longer complex conjugates), one becoming less stable and the other becoming more stable. With periodic coefficient equations, the separation can occur at any multiple of 1/2 the frequency of the periodicity. Actually, the constant coefficient equation is a special case of the periodic one, where the frequency in the coefficients is zero. This behavior may be seen in more detail by plotting the eigenvalues versus μ, as in figure 4, which again shows results from Floquet theory.

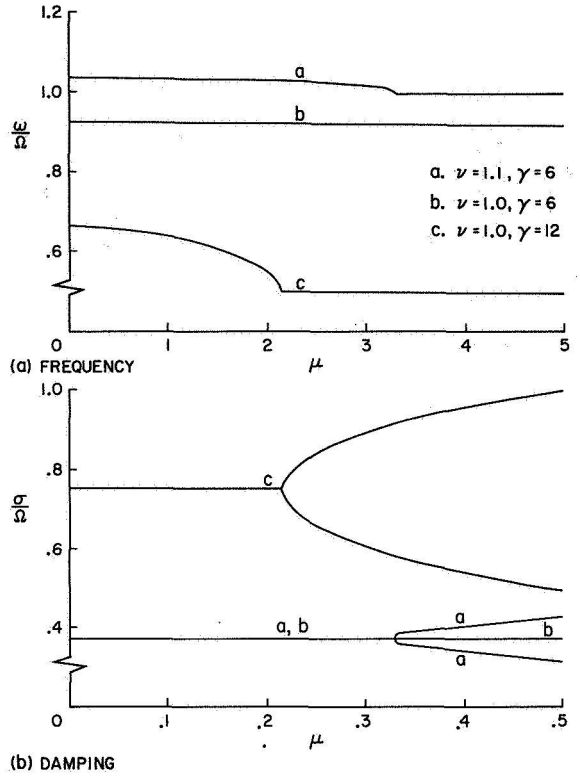

Figure 4. Floquet theory variation of frequency and damping with μ; single blade in rotating coordinates.

Figures 3 and 4 have shown the eigenvalues in the rotating coordinate system. These may be transposed into the nonrotating system to examine the behavior of the nonrotating modes. Choosing case c ($\nu = 1.0$, $\gamma = 12$) as an example, the root locus is plotted on figure 5. The coning mode has the same eigenvalues shown in the two previous figures. The nutation and precession modes have the same damping, but as mentioned before, their frequencies are Ω higher and lower, respectively, than the coning frequency.

The regions where the frequency remains constant while the damping changes, called critical regions, may be illustrated by constructing the $\gamma - \mu$ plane as in figure 6 (and discussed in References 3 and 4). In the 0/rev region, the behavior is like that of a constant coefficient equation when the root locus meets the real axis; there are two real roots, with order μ^2 changes in damping. In the $\frac{1}{2}$/rev region, the frequency is exactly half of the rotational frequency (fig. 3, case b), and the damping changes somewhat more rapidly. In the 1/rev region (fig. 3, case a) the frequency is the same as the rotational frequency (Ω), and again the damping changes are order μ^2. As previously noted, damping is constant at $-\gamma/16$ outside of the critical regions. Note that varying ν has little effect on the boundaries of the 0/rev and $\frac{1}{2}$/rev regions, but as ν is increased the 1/rev region moves upward.

In this section, the characteristics of the periodic coefficient solutions have been discussed

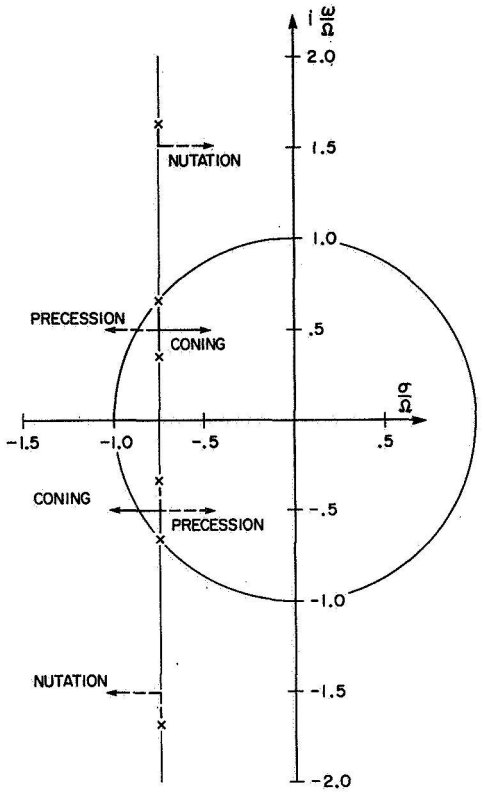

Figure 5. Floquet theory root loci for varying μ; three-bladed rotor in nonrotating coordinates ($\nu = 1.0$, $\gamma = 12$; case c).

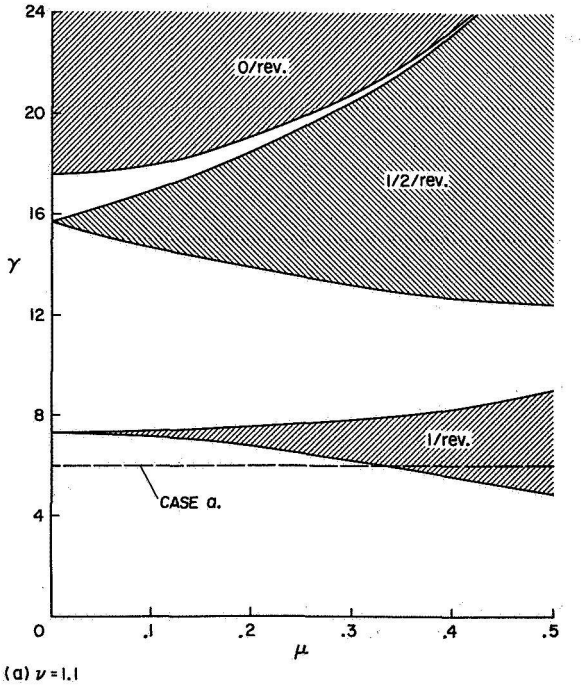

Figure 6. $\gamma - \mu$ plane for single blade in rotating coordinates based on Floquet theory.

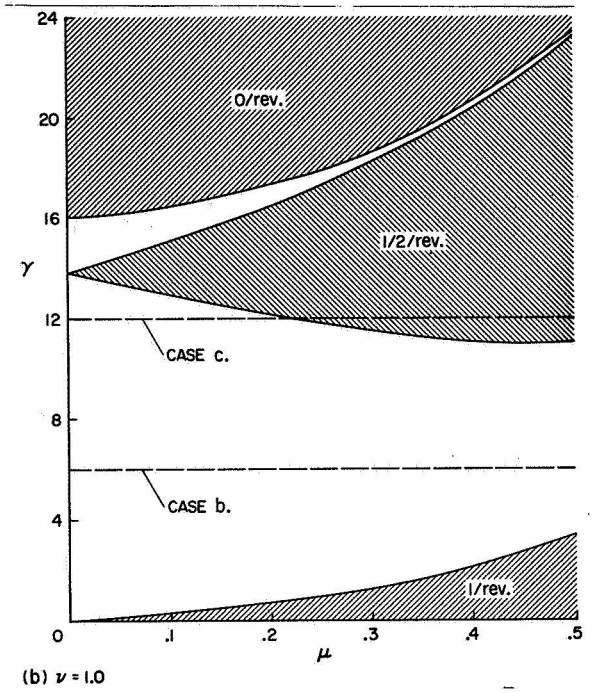

Figure 6. Concluded.

for nonhovering flight. The next sections will discuss an approximation which has constant coefficients, yet gives some of the behavior of the periodic coefficient system.

Constant Coefficient Approximation

In equation (1) the periodic coefficients are all of the speed (μ) dependent terms, and a constant coefficient approximation yields only the hover solution. However, in the nonrotating frame of equations (2) and (3), these periodic terms have been transformed into constants plus higher harmonic periodic terms. This result suggests that the primary effects of μ may be determined by using the average values of the coefficients. The constant coefficient approximation thus obtained for a four-bladed rotor is given in equation (5). The corresponding equation for three blades is identical, except that the β_2 motion is absent.

$$\ddot{\tilde{\beta}} + \begin{bmatrix} \frac{\gamma}{8}B^4 & 0 & \mu\frac{\gamma}{12}B^3 & 0 \\ 0 & \frac{\gamma}{8}B^4 & 2 & 0 \\ \mu\frac{\gamma}{6}B^3 & -2 & \frac{\gamma}{8}B^4 & 0 \\ 0 & 0 & 0 & \frac{\gamma}{8}B^4 \end{bmatrix} \dot{\tilde{\beta}} + \begin{bmatrix} \nu^2 & 0 & 0 & 0 \\ \mu\frac{\gamma}{6}B^3 & \nu^2-1 & \frac{\gamma}{8}\left(B^4+\frac{1}{2}\mu^2B^2\right) & 0 \\ 0 & -\frac{\gamma}{8}\left(B^4-\frac{1}{2}\mu^2B^2\right) & \nu^2-1 & 0 \\ 0 & 0 & 0 & \nu^2 \end{bmatrix} \tilde{\beta} = 0 \qquad (5)$$

Note that the β_2 equation is not coupled to the others and is the same as the β_2 equation for hover; hence it yields only the $\mu = 0$ roots. Therefore the β_2 equation will not be discussed further or included in subsequent figures. The β_0 equation has only one μ-dependent term, coupling it to the β_{1S} motion. The pitch and roll equations are coupled by both damping and aerodynamic spring terms.

Comparison

As noted earlier, eigenvalues may be compared by adding Ω to the precession frequency and subtracting Ω from the nutation frequency. In examining the constant coefficient approximation, any differences in eigenvalues will be due to the dropped periodicity. That is, all of the roots should approximate those obtained by using Floquet theory to solve equation (1). Using the comparison method mentioned above, the constant coefficient approximation is compared to Floquet theory results in figures 7, 8, and 9. The frequency scales have been expanded to exaggerate the effects of forward speed. Each of the three cases is discussed below.

Case a. ν = 1.1, γ = 6. (fig. 7)

This case corresponds to a hingeless rotor similar to the Lockheed XH-51. For this rotor the variations with μ of frequency and damping are small but significant since the 1/rev critical region is encountered (see fig. 6). All three modes of the approximation agree well with Floquet theory at low advance ratios, where the influence of the periodic coefficients is small. As the advance ratio is further increased, the precession mode displays the same type of behavior as the Floquet theory results, but the other two modes do not. For the precession mode (and the Floquet theory), the frequency becomes constant at 1/rev, and the damping then has two values as previously discussed. It is useful to examine why the constant coefficient approximation displays periodic

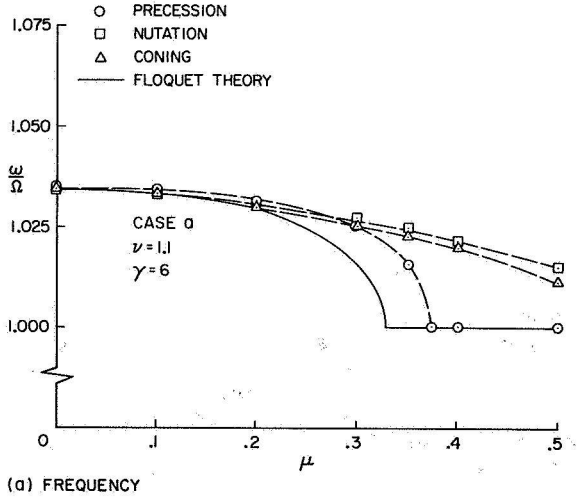

Figure 7. Comparison of constant coefficient approximation to Floquet theory (ν = 1.1, γ = 6).

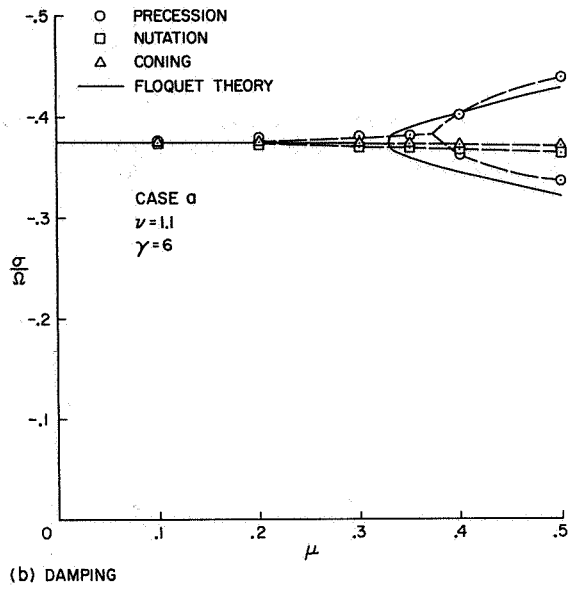

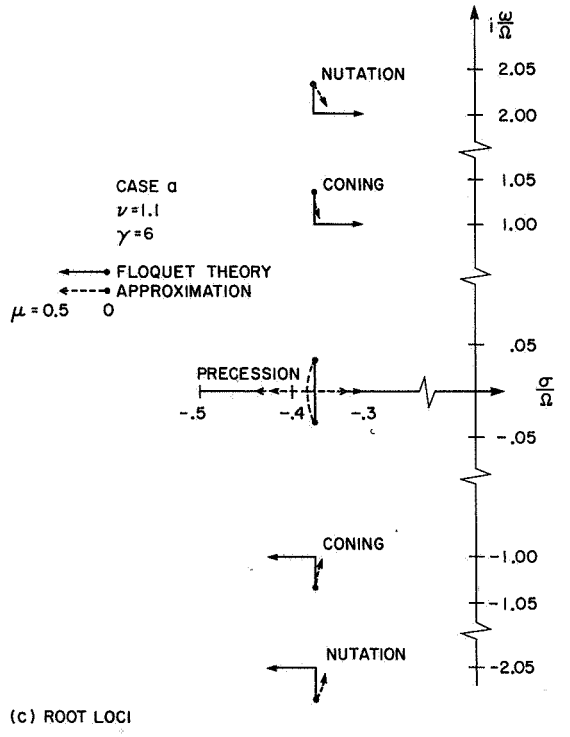

Figure 7. Concluded.

system (critical region) behavior. In this case, the precession roots at hover ($\mu = 0$) are very near the real axis due to the coordinate transformation. As μ is increased, the precession roots move toward the real axis and then split when they reach the axis, as usual with constant coefficient systems. Thus the damping both increases (the left branch) and decreases (the right branch).

Case b. $\nu = 1.0$, $\gamma = 6$. (fig. 8)

This case corresponds to an articulated rotor having relatively heavy blades, such as might be used for a high speed helicopter. This case is well removed from critical regions, and there are no significant changes in the eigenvalues for the μ range shown. The constant coefficient approximation agrees well with results from Floquet theory.

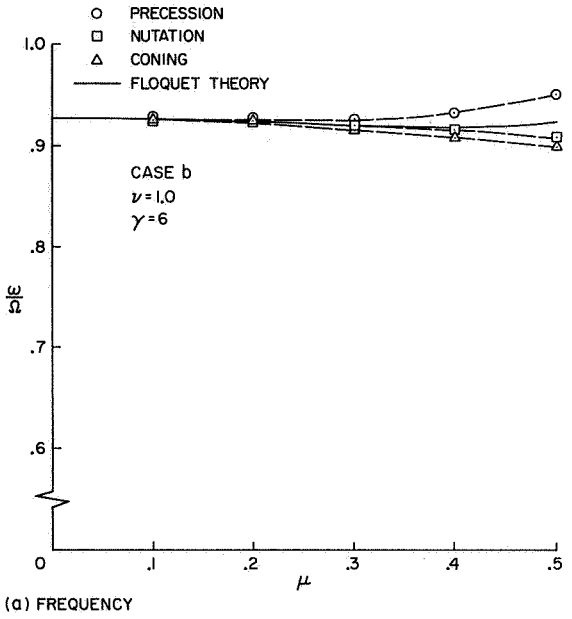

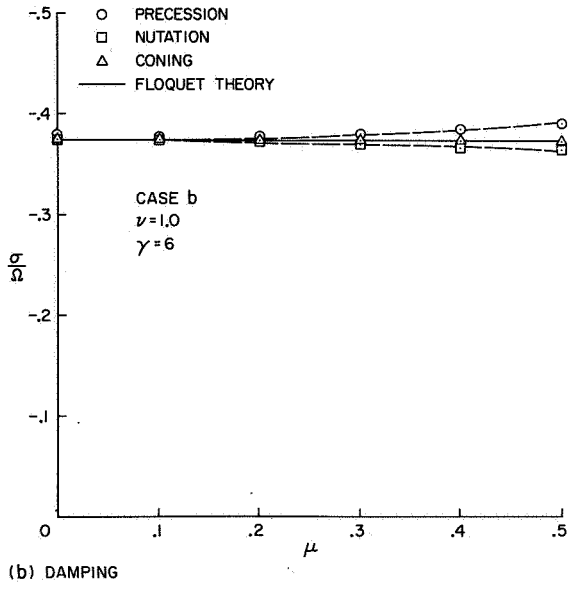

Figure 8. Comparison of constant coefficient approximation to Floquet theory ($\nu = 1.0$, $\gamma = 6$).

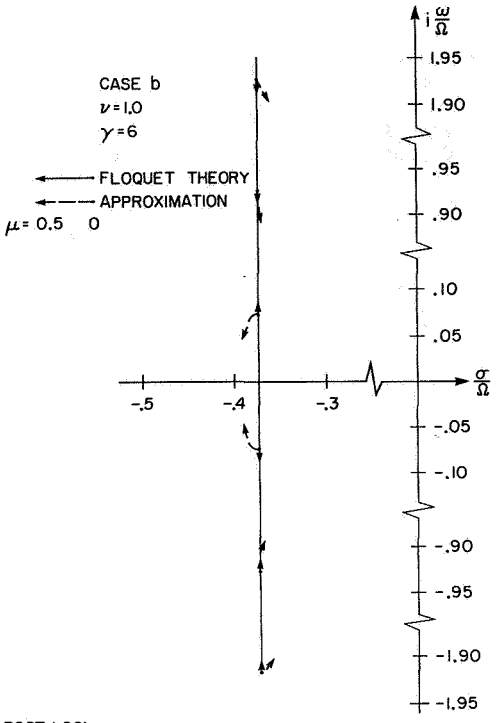

(c) ROOT LOCI

Figure 8. Concluded.

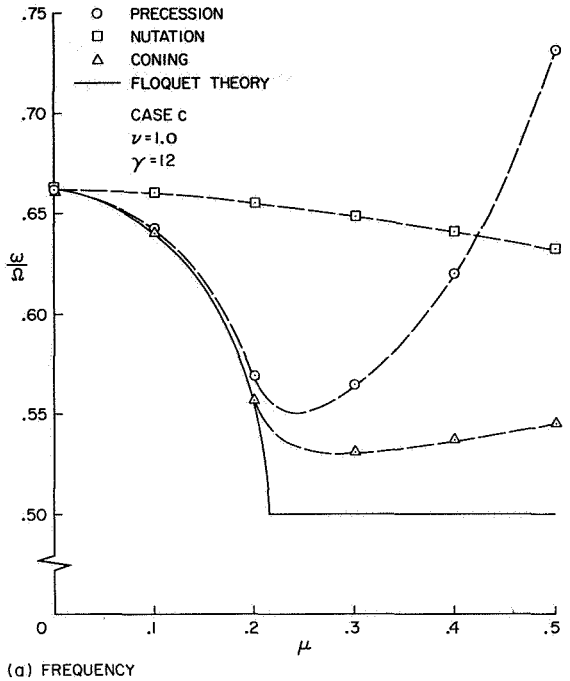

(a) FREQUENCY

Case c. $\nu = 1.0$, $\gamma = 12$. (fig. 9)

This case corresponds to a typical articulated rotor with blades similar to many aircraft flying today. The Floquet theory indicates that the $\frac{1}{2}$/rev region is encountered at $\mu = 0.215$. It is seen that the nutation mode is a poor approximation. Apparently, the constant coefficient approximation is not adequate for higher frequency modes if a critical region is encountered. The precession and coning modes (combined), however, do display the correct type of behavior: the frequency approaches $\frac{1}{2}$/rev and the damping both increases (the precession mode) and decreases (the coning mode). In this case, the correct behavior is obtained because two modes are involved. As may be seen in figure 9(c), the two sets of Floquet roots approach each other, meet at $\frac{1}{2}$/rev, and split (no longer complex conjugates). This behavior is approximated by the coning and precession modes, but in the approximation, the roots remain complex conjugates as shown in figure 9(c). The frequency of the precession mode does not agree well with Floquet results, but its damping is increasing; hence it is of less interest. The coning mode agrees well with the Floquet results, predicting the reduced damping very accurately.

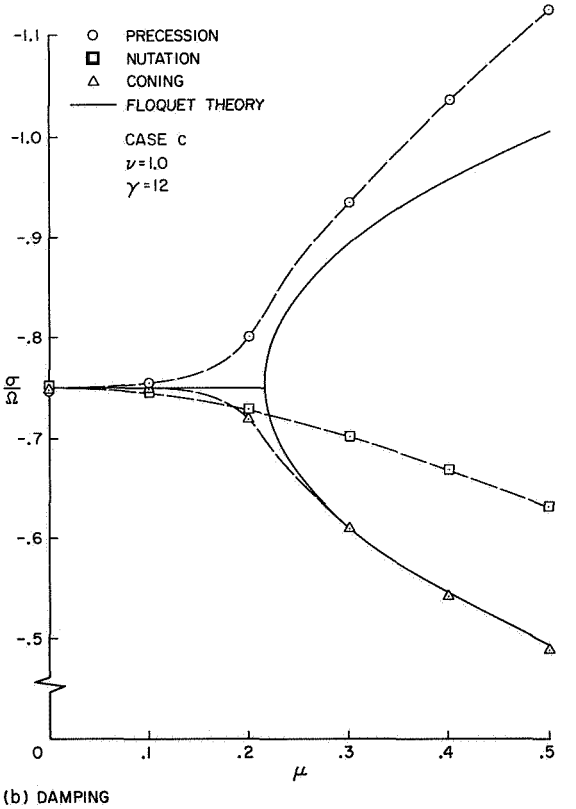

(b) DAMPING

Figure 9. Comparison of constant coefficient approximation to Floquet theory ($\nu = 1.0$, $\gamma = 12$).

Perturbation Theory

Equation (1) has also been studied in Reference 5, using a perturbation technique known as the method of multiple time scales. Analytic expressions are derived for the eigenvalues, with expressions valid near and within each of the critical regions and ones which are valid away from the critical regions. These results are very

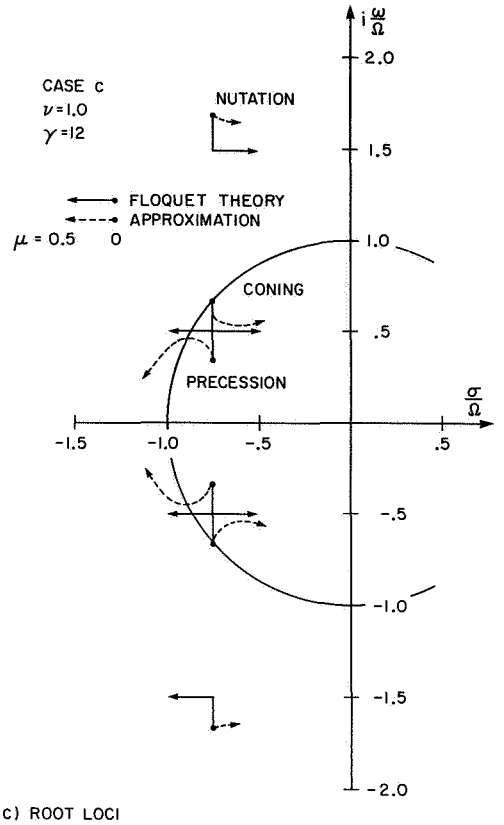

(c) ROOT LOCI

Figure 9. Concluded.

useful; they give additional insight into the behavior of periodic systems in general and equation (1) in particular. A comparison between the Floquet results of the present work and the analytic results from Reference 5 indicates that the latter are also useful quantitatively. An exception is near the $\frac{1}{2}$/rev region, where the perturbation solution was carried only to order μ. It should evidently be extended to order μ^2 as was the rest of the perturbation solution.

Discussion

Based on the cases described above, it is apparent that the constant coefficient approximation may be used to calculate rotor eigenvalues at advance ratios up to 0.5. A range of rotor parameters (γ and ν) have been studied which are representative of most conventional helicopters. The lower frequency modes agree well with Floquet results and display behavior approximating that of the Floquet theory critical regions. Therefore, there are many cases where the approximation may be used instead of more complicated methods.

The higher frequency modes of the approximation, however, do not display the correct behavior. Where these modes are important, for example, in using high gain feedback, the approximation should be used with caution.

The perturbation theory of Reference 5 is very easy to use for rotor stability calculations. However, the solutions are for uncoupled blades in the rotating coordinate frame. To account for inter-blade coupling (as with certain feedback schemes) one must either use another technique such as that described herein or rederive the solutions with the coupling included.

Conclusion

Transforming the flapping equation of a helicopter rotor in forward flight into the nonrotating coordinate frame results in a set of differential equations where some of the periodicity due to forward flight is transformed into constant terms. Using the time-averaged values of these, i.e., dropping the remaining periodicity, gives a constant coefficient approximation which retains some of the periodic effects. Comparison between results of the approximation and those of Floquet theory indicates that the approximation should be acceptably accurate for calculating flapping stability of most helicopters for the advance ratios shown herein. Use of the nonrotating coordinates has given insight into rotor behavior and indicates how the vehicle motion would be affected by the rotor modes.

The higher frequency modes of the approximation do not agree well with Floquet theory. Where these modes are important for example, in using high gain feedback control systems, the approximation should be used with caution.

References

1. Hohenemser, K. H. and Yin, S-K., SOME APPLICATIONS OF THE METHOD OF MULTIBLADE COORDINATES, Journal of the American Helicopter Society, Vol. 17, No. 3, July 1972, pp 3-12.

2. NASA CR-114290, RESEARCH PROGRAM TO DETERMINE ROTOR RESPONSE CHARACTERISTICS AT HIGH ADVANCE RATIOS, Kuczynski, W. A. and Sissingh, G. J., February 1971.

3. Peters, D. A. and Hohenemser, K. H., APPLICATION OF THE FLOQUET TRANSITION MATRIX TO PROBLEMS OF LIFTING ROTOR STABILITY, Journal of the American Helicopter Society, Vol. 16, No. 2, April 1971, pp 25-33.

4. Hall, W. Earl Jr., APPLICATION OF FLOQUET THEORY TO THE ANALYSIS OF ROTARY-WING VTOL STABILITY, SUDAAR No. 400, Stanford University, February 1970.

5. NASA TM X-62,165, A PERTURBATION SOLUTION OF ROTOR FLAPPING STABILITY, Johnson, W., July 1972.

FLAP-LAG DYNAMICS OF HINGELESS HELICOPTER BLADES AT MODERATE AND HIGH ADVANCE RATIOS

P. Friedmann
Assistant Professor

and

L.J. Silverthorn*
Research Assistant
Mechanics and Structures Department
School of Engineering and Applied Science
University of California, Los Angeles

Abstract

Equations for large amplitude coupled flap-lag motion of a hingeless elastic helicopter blade in forward flight are derived. Only a torsionally rigid blade exicted by quasi-steady aerodynamic loads is considered. The effects of reversed flow together with some new terms due to forward flight are included. Using Galerkin's method the spatial dependence is eliminated and the equations are linearized about a suitable equilibrium position.

The resulting system of equations is solved using multivariable Floquet-Liapunov theory, and the transition matrix at the end of the period is evaluated by two separate methods. Results illustrating the effects of forward flight and various important blade parameters on the stability boundaries are presented.

Notation

a	Two dimensional lift curve slope
$\bar{A}$	Tip loss coefficient
$\underset{\sim}{A}$	Periodic matrix with elements A_{ij}, defined in Appendix B
A_{Fi}, A_{Li}	Generalized aerodynamic force for i^{th} flap and lag mode respectively
$\bar{A}_{Fi}, \bar{A}_{Li}$	Same as above, in reverse and mixed flow regions.
b	Semi-chord nondimensionalized with respect to R
$\bar{B}$	Tip loss coefficient
$\bar{B}^i$	Generalized masses defined in Appendix A
C_T	Thrust coefficient
$\underset{\sim}{C}$	Constant matrix
C_{do}	Profile drag coefficient
$C(k)$	Theodorsen's lift deficiency function
e_1	Defined in Fig. 1
$F_{C1}, E_{C2}, \bar{\bar{E}}^s_{ik}, \bar{\bar{E}}^s_{im}, E^{\overline{cs}}_{im}, \bar{\bar{E}}^{cs}_{ik}$	Terms associated with elastic coupling defined in Appendix A
$(EI)_y$	Stiffness for flapwise bending
$(EI)_z$	Stiffness for inplane of rotation bending
F^i	Flap coefficients defined in Appendix A
g_k	Generalized coordinate, k^{th} normal flapping mode
g_k^o	Static value of g_k in hover
Δg_k	Perturbation in g_k about g_k^o
g_{SF}, g_{SL}	Viscous structural damping in flap and lag respectively
h_m	Generalized coordinate, m^{th} normal inplane mode
h_k^o	Static value of h_k in hover
Δh_k	Perturbation in h_k about h_k^o
$i = \sqrt{-1}$	
$\underset{\sim}{i}, \underset{\sim}{j}, \underset{\sim}{k}$	Unit vectors in x,y and z directions (Fig. 1)
I_b	Mass moment of inertia in flap, defined in Appendix A
$\underset{\sim}{I}$	Unit matrix
ℓ	Length of blade capable of elastic deflection
L_y, L_z	Aerodynamic load per unit length in the y and z directions respectively
L^i	Lag coefficients, defined in Appendix A
m	Mass of blade per unit length

Presented at the AHS/NASA-Ames Specialists' Meeting on Rotorcraft Dynamics, February 13-15, 1974.

*Presently, Dynamics Engineer, Hughes Helicopter Company, Culver City, California.

M,N	Number of modes in lag and flap respectively
$\overline{M}_{Fi},\overline{M}_{Li}$	Generalized mass for the i^{th} flap and lag mode respectively, defined in Appendix A
$(\overline{M_\eta})_{ik\ell},(\overline{M_\gamma})_{imr}$	Defined in Appendix A
p_x,p_y,p_z	Resultant total loading per unit length in the x,y and z direction respectively
$\overline{P}_{ikm}$	Defined in Appendix A
$\underset{\sim}{P}(t)$	Periodic matrix
R	Blade radius
$\underset{\sim}{R}$	Constant matrix used in Floquet-Liapunov theorem
$\underset{\sim}{Q}$	Constant matrix
T	Common nondimensional period
u,v,w	x,y and z displacement of a point on the elastic axis of the blade
U_P	Component of air velocity w.r.t. the blade at station x perpendicular to x-y plane (hub plane), positive down
U_T	Same as above, in the x-y plane, tangent to a circle having a radius x
v_e,v_{eo}	Elastic part of the displacement of a point on the elastic axis of the blade parallel to hub plane, (see Fig. 1), subscript o denotes the static equilibrium value
V	Velocity of forward flight of the whole rotor
w_e,w_{eo}	Elastic part of the displacement of a point on the elastic axis of the blade, in the k direction, approximately, (Fig. 1)
x,y,z	Rotating orthogonal coordinate system
$x_o = x - e_1$	Running spanwise coordinate for part of the blade free to deflect elastically
X_H,Y_G	Defined in Appendix B
α	Angle of reversed flow region (Fig. 2)
α_R	Angle of attack of the whole rotor
β_D	Droop, built in angle of the undeformed position of the blade measured from the feathering axis (Fig. 1)
β_P	Preconing, inclination of the feathering axis w.r.t. the hub plane measured in a vertical plane
γ	Lock number ($\gamma=2\rho_A bR^5 a/I_b$) for normal flow
γ_m	m^{th} inplane bending mode
ε_D	Symbolic quantity having the same order of magnitude like the displacements v and w
ζ_k	Real part of the k^{th} characteristic exponent
η_k	k^{th} flapwise bending mode
η_{SF_1},η_{SL_1}	Viscous structural damping coefficients defined in Appendix A
θ	Collective pitch angle measured from x-y plane
θ_C	Critical value of collective pitch at which the linearized coupled flap-lag system becomes unstable in hover
λ	Inflow ratio, induced velocity over disk, positive down, nondimensionalized w.r.t. $R\Omega$
$\underset{\sim}{\lambda}$	Diagonal matrix, containing eigenvalues λ_k of R
$\underset{\sim}{\Lambda}$	Diagonal matrix containing eigenvalues Λ_k of $\underset{\sim}{\Phi}(T,0)$
μ	Advance ratio
μ_C	Critical value of advance ratio at which flap-lag system becomes unstable
ρ_A	Density of air
σ	Blade solidity ratio
$\Phi(\psi,\psi_o)$	State transition matrix at ψ, for initial conditions given at ψ_o
ψ	Azimuth angle of blade ($\psi=\Omega t$) measured from straight aft position
ω_C	Flutter frequency
ω_k	Imaginary part of k^{th} characteristic exponent

$\bar{\omega}_{Fi}, \bar{\omega}_{Li}$	Natural frequency of i^{th} flap or lag mode, rotating
Ω	Speed of rotation

Special Symbols

$\bar{(\ )}$	Nondimensionalized quantity, length for elastic properties nondimensionalized w.r.t. ℓ; all other w.r.t. R frequencies w.r.t. Ω; mass properties w.r.t. I_b
$(\ )'$	Differentiation w.r.t. $\bar{x}_o$
$(\ ^*)$	Differentiation w.r.t. ψ
$(\ )_R$, $(\ )_I$	Subscripts, denoting real and imaginary parts of the appropriate quantity
$\underset{\sim}{(\ )}$	The symbol beneath a quantity denotes a vector or a matrix
$\underset{\sim}{(\ )}^{-1}$	Denotes the inverse of a matrix

The dynamics of a helicopter blade in forward flight are usually described by a system of linear differential equations with periodic coefficients. A growing acceptance of hingeless helicopter blades for conventional helicopters flying at relatively high forward flight speeds has intensified the need for fundamental research on the aeroelastic stability of such systems.

Studies dealing with the effect of forward flight (or periodic coefficients) have been primarily devoted to the study of flapping instability at high advance ratios.[1-8] A limited number of studies dealing with the effect of periodic coefficients on coupled flap-lag[9,10] or coupled flap-lag-pitch[11] motion were also conducted. The case of coupled flap-lag motion has been, somewhat inconclusively, investigated by Hall[10] using multivariable Floquet theory, the same problem was also considered by Friedmann and Tong[9] but the treatment was limited to low advance ratios ($\mu<0.3$). The coupled, linearized, flap-lag-torsion motion has been investigated by Crimi[11] using a modified Hill method. In both cases[10,11] only a limited number of numerical results were obtained and the physical mechanism of the aeroelastic instabilities has not been clearly identified, in particular the degree of freedom which triggers the instability was not identified and the results for forward flight were not compared with those for hover.

Recent investigation of the aeroelastic stability of hingeless blades in hover[12] indicated that the aeroelastic stability boundaries are quite sensitive to the number of degrees of freedom employed in the analysis. Therefore it is important to determine how the flapping behavior of a blade at high advance ratios is modified by the lag degree of freedom. This important problem, which has not received adequate treatment before, is one of the main topics of the present study.

The mathematical methods used in previous studies dealing with the effects of forward flight were: (a) The rectangular ripple method[1], (b) Analog computer simulation,[3,4] (c) Various forms of Hill's method,[2,11] (d) Multivariable Floquet-Liapunov theory,[6,7,10] (e) Perturbation method in multiple time scales.[8,9] The mathematical method employed in the present study is the Floquet-Liapunov theorem, and the transition matrix is evaluated by two separate methods. It is also shown that careful use of this method enables one to circumvent problems associated with identifying the results encountered in previous studies.[10]

In addition, a new and convenient approximation for the reversed flow region is developed, this approximation is believed to be adequate for most blade stability analyses. Finally, the effects of various important parameters such as collective pitch setting, structural damping, droop and preconing on the instability associated with forward flight is investigated.

1. The Equations of Motion

1.1 Basic Assumptions

The present study is based upon a consistently derived system of equations of motion for the linearized coupled flap-lag motion of a cantilevered rotor blade at arbitrary advance ratios.

The derivation itself is algebraically tedious, thus only a brief outline will be given in this paper, the complete details of the derivation can be found elsewhere.[13]

The geometry of the problem is shown in Fig. 1. The following basic assumptions were used in deriving the equations of motion: (a) The blade is cantilevered at the hub. It can have an angle of droop β_D at the root. In addition, the feathering axis can be preconed by an angle β_P. The angles β_D and β_P are small. (b) The blade can bend in two directions normal to the elastic axis and is torsionally rigid. (c) The deflections of the blade are moderately small so that terms of $O(\epsilon_D^2)$ can be neglected compared to one. (d) Moderately large deflections have only a small effect on the tension due to elastic effects on the blade since one of its ends is free, thus a linear treatment of the elastic restoring forces is adequate. (e) Two dimensional quasi-steady aerodynamic strip theory is used $C(k)=1$ and apparent mass effects are neglected. (f) Reversed flow is included using an approximate model for reversed flow described in Appendix C. (g) Stall and compressibility effects are neglected.

Using the assumptions given above a system of nonlinear partial differential equations for the coupled flap-lag motion of the blade is derived, with respect to an x,y, and z coordinate system rotating with the blade. The derivation follows essentially along the lines of Reference 14, all the details can be found in Reference 13.

1.2 Brief Derivation of the Equations of Motion

The differential equation for the dynamic stability of a cantilevered rotor blade can be written as

$$\frac{\partial^2}{\partial x_o^2}\left\{[(EI)_y + E_{Cl}]\frac{\partial^2 w_e}{\partial x_o^2} + E_{C2}\frac{\partial^2 v_e}{\partial x_o^2}\right\} - \frac{\partial}{\partial x_o}[T\frac{\partial w}{\partial x_o}] = P_z$$

$$\frac{\partial^2}{\partial x_o^2}\left\{[(EI)_z - E_{Cl}]\frac{\partial^2 v_e}{\partial x_o^2} + E_{C2}\frac{\partial^2 w_e}{\partial x_o^2}\right\} - \frac{\partial}{\partial x_o}[T\frac{\partial v}{\partial x_o}] = P_y \qquad (1)$$

where the quantities E_{Cl}, E_{C2} are given in Appendix A.

The distributed loading terms in the x,y and z directions with terms up to $O(\varepsilon_D^3)$ in displacements can be written as

$$P_x = \frac{T}{x_o} = m\Omega^2[(x_o + e_1) + 2\overset{*}{v}]$$

$$P_y = L_y - m\Omega^2[\overset{**}{v} - (e_o + v) + 2\overset{*}{u}] - g_{SL}\Omega\overset{*}{v}$$

$$P_z = L_z - m\Omega^2\overset{**}{w} - g_{SF}\Omega\overset{*}{w} \qquad (2)$$

The boundary conditions for this kind of blade are well known.[14] The displacement field of the blade with $\sin\theta \cong \theta$ and $\cos\theta \cong 1$ can be written as[13,14]

$$u = -w_e(\beta_p+\beta_D) - \frac{x_o}{2}(\beta_p+\beta_D)^2 - \frac{1}{2}\int_o^{x_o}\left[\left(\frac{\partial v_e}{\partial x_1}\right)^2 + \left(\frac{\partial w_e}{\partial x_1}\right)^2\right]dx_1$$

$$v = v_e - x_o\beta_D\theta \qquad (3)$$

$$w = w_e + x_o(\beta_p + \beta_D)$$

and

$$w_e = \sum_{k=1}^{N} \ell\,\eta_k(x_o)g_k(t) = \ell\,\eta_k g_k$$

$$v_e = -\sum_{m=1}^{M} \ell\,\gamma_m(x_o)h_m(t) = -\ell\,\gamma_m h_m \qquad (4)$$

where it is understood that repeated indices imply summation unless otherwise stated.

The aerodynamic loads L_z and L_y are given by[13,14]

$$L_z = a\rho_A bR\,U_T(U_T\theta - U_p) \qquad (5)$$

$$L_y = a\rho_A bR\left[U_p(U_T\theta - U_p) + \frac{C_{do}}{a}U_T^2\right] \qquad (6)$$

where the velocities U_p and U_T are given by

$$U_p = \Omega\overset{*}{w} + \Omega R\left(\lambda + \mu\cos\psi\frac{\partial w}{\partial x_o}\right) \qquad (7)$$

$$U_T = \Omega\overset{*}{v} + \Omega R\left(\bar{x} + \mu\sin\psi + \mu\cos\psi\frac{\partial v}{\partial x_o}\right) \qquad (8)$$

The last term in Equation (8) is due to the radial flow along the blade. This term has been neglected in some previous analyses. For arbitrary advance ratios this is an important and non-negligible term.

Combination of Equations (1) through (8) and application of Galerkin's method to eliminate the spatial variable reduces the problem to a system of ordinary differential equations.

$$M_{Fi}\overset{**}{g}_i + 2\bar{\omega}_{Fi}\bar{M}_{Fi}\eta_{SFi}\overset{*}{g}_i + \bar{E}^s_{ik}g_k + \bar{\omega}^2_{Fi}M_{Fi}g_i = \overline{E^{cs}_{im}}h_m$$
$$+2\bar{P}_{ikm}g_k\overset{*}{h}_m - (\beta_D+\beta_P)\bar{B}^1_i + 2(\beta_P+\beta_D)\bar{B}^3_{im}h_m + A_{Fi} \qquad (9)$$

$$\bar{M}_{Li}\overset{**}{h}_i + 2\bar{M}_{Li}\bar{\omega}_{Li}\eta_{SLi}\overset{*}{h}_i + \bar{M}_{Li}\bar{\omega}^2_{Li}h_i - \bar{\bar{E}}^s_{im}h_m = \bar{\bar{E}}^{cs}_{ik}g_k$$
$$-2\bar{B}^7_{ik}(\beta_P+\beta_D)\overset{*}{g}_k + \overline{B^{11}_i}\beta_D\theta + 2[\bar{S}_{imr} - (\bar{M}_\gamma)_{imr}]\overset{*}{h}_m h_r$$
$$-2(\bar{M}_\eta)_{ik\ell}\overset{*}{g}_k g_\ell - \overline{B^{10}_i}\beta_D\theta + 2\,\overline{B^8_{im}}\beta_D\theta\,\overset{*}{h}_m + A_{Li} \qquad (10)$$

where the various quantities $\bar{M}_{Fi}$, $\bar{P}_{ikm}$, $\bar{M}_{Li}$, $\bar{S}_{imr}$, $(\bar{M}_\eta)_{ik\ell}$ are generalized mass integrals given in References 13 and 14, and also in Reference 12 (for i=k=ℓ=m=r=1). While the quantities $\bar{B}^1_i$, $\bar{B}^3_{im}$, $\bar{E}^s_{ik}$, $\bar{E}^{cs}_{im}$, $\bar{E}^s_{im}$, $\bar{E}^{cs}_{ik}$, $\bar{B}^{11}_i$, $\bar{B}^7_{ik}$, $\bar{B}^{10}_i$ amd $\bar{B}^8_{im}$ etc. are given in Appendix A. The quantities A_{Fi}, A_{Li} are generalized aerodynamic forces defined by

$$A_{Fi} = \ell^2\int_{\bar{A}}^{\bar{B}} L_z\,\eta_i\,d\bar{x}_o/\Omega^2 I_b \qquad (11)$$

$$A_{Li} = \ell^2\int_{\bar{A}}^{\bar{B}} L_y\,\gamma_i\,d\bar{x}_o/\Omega^2 I_b \qquad (12)$$

Equations (9) and (10) are coupled nonlinear ordinary differential equations. In the present study these equations will be linearized about a suitable equilibrium position, which is taken to be the steady state equilibrium position of the blade in hover. Through this process of linearization many nonlinear terms are transformed into coupling terms. At this stage one encounters a considerable number of terms which are small and therefore negligible. In order to neglect the appropriate terms a rational ordering scheme is used which enables one to neglect terms in a systematic manner. In this scheme all the important parameters of the problem are assigned orders of magnitudes in terms of a typical displacement quantity ε_D thus:

$$\frac{v}{R} = O(\varepsilon_D);\ \frac{w}{R} = O(\varepsilon_D);\ \bar{x}=O(1);\ \mu=O(1);$$
$$\lambda=O(\varepsilon_D);\ \theta=O(\varepsilon_D)$$

$$\frac{\partial w}{\partial x_o} = O(\varepsilon_D);\ \frac{\partial v}{\partial x_o} = O(\varepsilon_D);\ \beta_D=\beta_P=O(\varepsilon_D);$$
$$\frac{C_{do}}{a} = O(\varepsilon_D^2) \qquad (13)$$

An order of magnitude analysis of the equations indicates that in general terms up to and including $O(\varepsilon_D^2)$ must be included in the linearized flap equations, while for lag equations some $O(\varepsilon_D^3)$ terms have to be retained.

The process of the linearization consists of expressing the elastic part of the displacement field as

$$w_e = w_{eo} + \Delta w_e = \eta_k(g_k^o + \Delta g_k)$$
$$v_e = v_{eo} + \Delta v_e = -\gamma_m(h_m^o + \Delta h_m) \qquad (14)$$

where the static equilibrium condition in hover is given by

$$\bar{E}^s_{ik} g^o_k + \bar{\omega}^2_{Fi} M_{Fi} g^o_i - \bar{\bar{E}}^{cs}_{im} h^o_m = -(\beta_P + \beta_D)\bar{B}^1_i + \frac{\gamma}{2}\left(\frac{\ell}{R}\right)^2(\theta F^1_i - \lambda F^2_i)$$

where $i = 1,2,\ldots,N$

$$-\bar{E}^{cs}_{ik} g^o_k + \bar{M}_{Li}\bar{\omega}^2_{Li} h^o_i - \bar{\bar{E}}^s_{im} h^o_m = \beta_D\theta(\overline{B^{11}} - \overline{B^{10}})$$
$$+ \frac{\gamma}{2}\left(\frac{\ell}{R}\right)^2[\lambda(\theta L^1_i - \lambda L^2_i) + \frac{C_{do}}{a} L^4_i] \quad i=1,2,\ldots M \qquad (15)$$

The various quantities F^i, L^i are defined in Appendix A. Next, for the sake of simplicity, the equations are specialized to the case of one elastic mode for each degree of freedom, i.e. one flapping and one lead-lag mode.

Furthermore for mathematical convenience the equations of motion have to be transformed into a system of first order equations. This is achieved by using the following notation

$$\Delta g_1 = y_1 \quad ; \quad \Delta \overset{*}{h}_1 = y_3$$
$$\Delta g_1 = y_2 \quad ; \quad \Delta h_1 = y_4 \qquad (16)$$

For the stability analysis, only the homogeneous part of the equations of motion is required, thus the equations of motion in their final form can be written as

$$\overset{*}{\underset{\sim}{y}} = \underset{\sim}{A}(\psi)\underset{\sim}{y} \qquad (17)$$

where $\underset{\sim}{A}$ is a 4x4 matrix defined in Appendix B.

The equations of motion (17) will have a different form for the normal flow region and for the reversed flow region. The representation of the reversed flow together with its effect on the form of Equations (17) is described in Appendix C.

2. Method of Solution

The stability investigation of the blade motions is based upon the Floquet-Liapunov theorem[15] which states the knowledge of the state transition matrix over one period is sufficient in order to determine the stability of a periodic system having a common period T. Based upon the Floquet-Liapunov theorem, the transition matrix for the periodic system can be written as[15]

$$\underset{\sim}{\Phi}(\psi,\psi_o) = \underset{\sim}{P}^{-1}(\psi) e^{\underset{\sim}{R}(\psi-\psi_o)} \underset{\sim}{P}(\psi_o) \qquad (18)$$

where

$$\underset{\sim}{P}(\psi+T) = \underset{\sim}{P}(\psi) \qquad (19)$$

where $\underset{\sim}{R}$ is a constant matrix and $\underset{\sim}{P}(t)$ is a periodic matrix. Clearly the stability of the system is determined by the matrix $\underset{\sim}{R}$, where $\underset{\sim}{R}$ is given by following relation

$$\underset{\sim}{\Phi}(T,0) = e^{\underset{\sim}{RT}} = \underset{\sim}{C} \qquad (20)$$

A direct result of the Floquet-Liapunov theorem is that the knowledge of the transition matrix over one period determines the solution to the homogeneous system everywhere through the relation

$$\underset{\sim}{\Phi}(\psi+sT,0) = \underset{\sim}{\Phi}(\psi,0)(e^{\underset{\sim}{RT}})^s \qquad (21)$$

where $0 \leq \psi \leq T$, s any integer.

In general $\underset{\sim}{R}$ is a fully populated (nxn) square matrix. If it has n independent eigenvalues, it is well known from elementary linear algebra[15] that a similarity transformation can be found such that

$$\underset{\sim}{Q}^{-1}\underset{\sim}{R}\,\underset{\sim}{Q} = \underset{\sim}{\lambda} \qquad (22)$$

where the columns of Q are the n-linearly independent eigenvectors of $\underset{\sim}{R}$ and $\underset{\sim}{\lambda}$ is a diagonal matrix whose elements are the eigenvalues of $\underset{\sim}{R}$. Combining Equations (20) and (22) and using the definition of the matrix exponential[15] one has

$$e^{\underset{\sim}{RT}} = \underset{\sim}{Q}\, e^{\underset{\sim}{\lambda T}}\, \underset{\sim}{Q}^{-1} = \underset{\sim}{C}$$

or

$$e^{\underset{\sim}{\lambda T}} = \underset{\sim}{\Lambda} = \underset{\sim}{Q}^{-1}\underset{\sim}{C}\,\underset{\sim}{Q} = \underset{\sim}{Q}^{-1}\underset{\sim}{\Phi}(T,0)\underset{\sim}{Q} \qquad (23)$$

where $\underset{\sim}{\Lambda}$ is a diagonal matrix containing the eigenvalues of the transition matrix at the end of one period. The eigenvalues of $\underset{\sim}{\Phi}(T,0)$ or the characteristic multipliers are related to the eigenvalues of $\underset{\sim}{R}$, denoted characteristic exponents, through the relation

$$e^{\lambda_k T} = \Lambda_k \qquad k=1,2,\ldots r \qquad (24)$$

Clearly λ_k and Λ_k are both complex quantities in general, thus

$$\lambda_k = \zeta_k + i\omega_k$$
$$\Lambda_k = \Lambda_{kR} + i\,\Lambda_{kI} \qquad (25)$$

from which

$$\zeta_k = \frac{1}{2T}\ell n[\Lambda^2_{kR} + \Lambda^2_{kI}] \qquad (26)$$

and

$$\omega_k = \frac{1}{T}\tan^{-1}\frac{\Lambda_{kI}}{\Lambda_{kR}} \qquad (27)$$

the quantity ω_k can be determined according to the Floquet-Liapunov theory only within an integer multiple of the nondimensional period.

The stability criteria for the system is related to the eigenvalues of $\underset{\sim}{R}$ or the real part of the characteristic exponents ζ_k. The solutions of the Equation (17) approach zero as $\psi \to \infty$ if

$$|\Lambda^2_{kR} + \Lambda^2_{kI}| < 1 \quad \text{or} \quad \zeta_k < 0 \quad k=1,2,\ldots,n$$

Finally a brief description of the numerical implementation of the scheme described above will be given. The transition matrix at the end of one period $\underset{\sim}{\Phi}(T,0)$ is evaluated using direct numerical integration. Equations (17) are integrated for the set of initial conditions corresponding to $\underset{\sim}{\Phi}(0,0) = \underset{\sim}{I}$. The numerical integration is performed using a fourth order Runge Kutta method. The eigenvalues of the transition matrix are evaluated by a Jacobi type eigenvalue routine. For some of the cases the value of $\underset{\sim}{\Phi}(T,0)$ has been evaluated using Hsu's method.[13,17] This was done in order to obtain results by two different numerical schemes and also because Hsu's method was found to be more efficient numerically. Both methods yield identical results, therefore it is not specified on the plots which scheme was used to evaluate $\underset{\sim}{\Phi}(T,0)$.

3. Results and Discussion

3.1 Numerical Quantities Used in the Calculations

In computing the numerical results the following assumptions were made,

Mass and stiffness distribution was assumed to be constant along the span of the blade. Two different kinds of mode shapes were used:

(a) For most of the cases for which essentially trend type studies were conducted an assumed mode shape in flap and lap was used as given by the appropriate expression in Reference 12. When an assumed mode shape is used the elastic coupling effect[16] is neglected.

(b) For a few cases an exact rotating mode shape in flap and lag was employed. These mode shapes were generated by using Galerkin's method based upon five nonrotating cantilever mode shapes for each flap or lag degree of freedom. For these cases the elastic coupling effect was included.

The coefficients F^i, L^i and $\bar{B}^i$ defined in Appendix A and in References 12 through 14 were evaluated using seven point Gaussian integration. For the region of reversed flow these coefficients were treated in a special manner as explained in Appendix C.

For the cases computed the inflow was evaluated using an expression for constant inflow ratio in hover, given by

$$\lambda = \frac{a\sigma}{16}\left[\sqrt{1 + \frac{24\theta}{a\sigma}} - 1\right] \tag{28}$$

This inflow relation is equivalent to taking the induced velocity of 3/4 blade radius as representative of a constant induced velocity over the whole disk. It is clear that for forward flight one should use the expression

$$\lambda = \mu \tan\alpha_R + C_T/2\sqrt{\mu^2+\lambda^2} \tag{29}$$

Use of this relation would have required the use of a trim procedure in the calculations. It can be seen from Reference 14 that the requirement of trimmed flight at a fixed C_T results in an increase of θ at advance ratios of $\mu > .3$ and it also requires continuous changes in θ_{1c}* and θ_{1s}. The experience gained when using this approach in Reference 14 indicates that when the trim requirement is included in the calculation, the value of μ_c at which instability will occur will be usually lower. Furthermore, when using this approach it was found that it is difficult to determine which part of the degradation in stability is related to the increase in θ, θ_{1s} and θ_{1c} and which part is due to the periodic coefficients. This added complication is not warranted in a trend study such as the present one, and it is not consistent with the stated purpose of this paper, which is; a clear illustration of the effects of the periodic coefficients when the lag degree of freedom is included in the formulation of the problem.

Finally, in all the computations the following values were used:

$$C_{do} = .01;\ a = 2\pi;\ \sigma = .05;\ e_1 = 0;\ \bar{A} = 0.\ ;\ \bar{B} = 1$$

Various other pertinent quantities are specified on the plots.

3.2 Results

The results obtained in the present study usually are given in form of plots representing the variation of the real part of the characteristic exponent ζ_k with the advance ratio μ. Most of the cases presented in this study were evaluated using an assumed mode shape, as described in the previous section, and neglecting the elastic coupling effect.

For some cases an exact rotating mode shape in flap and lead-lag was used and the elastic coupling was included, when this approach was used a statement to this effect appears on the appropriate plots. When no such statement appears it is to be understood that the assumed mode shape is used and the elastic coupling is neglected.

A typical case is shown in Figure 3 for a collective pitch setting of $\theta = .15$. Starting the computation at $\mu = 0$, enables one to easily identify the instabilities encountered, by using results previously obtained for hover. As shown the lag degree becomes unstable and the frequency of the oscillation is $\omega_k = 1.28119$. This result clearly indicates that by neglecting the lag degree of freedom one could obtain completely incorrect stability boundaries.

The importance of the reversed flow region is illustrated by Figure 4. As shown with the reversed flow region the instability occurs at higher values of μ than without the reversed flow region. Similar trends were observed in previous studies when only the flapping motion was considered,[5] indicating that by neglecting the reversed flow region one could expect conservative results from a stability point of view. It also

*θ_{1c}, θ_{1s} cyclic pitch changes.

indicates that in this particular case the reversed flow region starts being important above advance ratios of $\mu = 0.8$.

It is important to note that the frequency at which the lag degree of freedom becomes unstable is not 1/2 or 1 as is usual for the case of parametric excitation. Thus it seemed important to identify the source of this destabilizing effect. The results of this study are presented in Figures 5 and 6. The effect of neglecting the radial flow terms on the real part of the characteristic exponent, associated with the flap degree of freedom, is shown in Figure 5. As shown, the radial flow terms have a stabilizing effect on the flapping motion with the radial flow forms suppressed the flap degree of freedom becomes unstable at μ=1.33. The effect of the radial flow terms on the lead-lag degree of freedom is illustrated by Figure 6, as shown without the radial flow terms the instability in the lag degree of freedom is completely eliminated and the system becomes unstable in flap. When the radial flow terms are included, the lag degree of freedom is the critical one and the system becomes unstable at μ=.754. This matter was pursued further by identifying the actual destabilizing term in the equations of motion, which was found to be an aerodynamic coupling term. This term couples the flap motion with the lag motion in the flap equation, its form is

$$\mu^2 \cos^2\psi \frac{\partial w}{\partial x_o} \frac{\partial u}{\partial x_o}$$

This term is due to the $U_T U_P$ term in Equation (5). The term shown above is the complete nonlinear one, clearly the one retained in the equations of motion is the coupling term obtained from linearizing this expression.

As mentioned in the previous section the results presented in Figures 3 through 6 were obtained by neglecting the elastic coupling effect. In order to asses the effect of this assumption the typical case has been also recomputed with the exact mode shape and the elastic coupling effect, the results are shown in Figure 11. From Figure 11 it is clear that use of the exact rotating mode in flap and lag reduces the value of μ_c to $\mu_c = 0.653$, when the elastic coupling is also included μ_c is further reduced to $\mu_c = .583$. Thus, for this case, μ_c seems to be more sensitive to the type of mode shape used than to the inclusion of the elastic coupling effect. It is also interesting to note, that for this case the elastic coupling effect is destabilizing, while for hover its effect on θ_c is quite stabilizing.

Previous studies[12] dealing with the effect of viscous type of structural damping on the stability boundaries for hover indicated that this parameter has an important stabilizing. The effect of this parameter for forward flight is shown by Figures 7 and 8. The stabilizing effect of structural damping in the lag degree of freedom is evident from Figure 7, where the real part of the characteristic exponent associated with the lead-lag degree of freedom is plotted as a function of the advance ratio μ, again only the structural damping in lag is important. A summary of these results is presented in Figure 8 showing the variation of μ_c as a function of the structural damping. It is interesting to note that this plot indicates that the greatest stabilizing effect due to structural damping is obtained in the range $0 < \eta_{SL1} < .02$ (2% of critical damping), after which, the gain in stability tends to level off. Similar trends were obtained from stability studies in hover.[12]

Again in order to illustrate the sensitivity of the results to the mode shape and elastic coupling, the results have been recomputed with these effects included; these results are also shown in Figure 8. As seen the use of the correct mode shape and the elastic coupling effect reduce the value of μ_c, at which instability occurs.

The sensitivity of the results, to different collective pitch settings is illustrated by Figure 9. Comparison of Figures 3 and 9 indicates that by decreasing the collective pitch setting from $\theta = .15$ to $\theta = .05$ eliminated the instability associated with thelead-lag motion. The instability in this case occurs at $\mu_c = 1.88$ with a frequency of 0 or 1. This is a typical flapping instability due to the periodic coefficients. Comparison of Figures 3 and 9 seems to indicate that the assumption of nonlifting rotors used in some forward flight studies[7] can be nonconservative.

Finally, Figure 10 shows the dependence of μ_c on the angle of droop β_D. As shown μ_c is relatively insensitive to β_D. On the other hand β_D has a very important effect on the value of θ_c at which the linearized system in hover becomes unstable.

It should be also noted that a considerable number of additional numerical results, including the effects of elastic coupling can be found in Reference 13.

4. Conclusions

The major conclusions obtained from the present study are summarized below. They should be considered indicative of trends and their application to the design of a helicopter blade should be limited by the assumptions used.

(1) Flapping instability and response studies at high advance ratios can be inaccurate and misleading due to the neglection of the lag degree of freedom. The effect of the periodic coefficients on the coupled flap-lag system shows that in general instability can occur at lower values of advance ratios than when the flap degree of freedom is considered by itself.

(2) In addition to the instabilities associated with the periodic coefficients (i.e. with frequencies of 0, 1 or 1/2) the coupled flap-lag

system has the tendency to become unstable due to an aerodynamic coupling effect associated with the radial flow terms. This instability which has a frequency close to the rotating lag frequency of the system, occurs usually at values of μ_c much lower than those for which the flapping degree of freedom becomes unstable.

(3) Viscous type of structural damping in the lead-lag degree of freedom has a stabilizing effect on the instability discussed in previous conclusion.

(4) The value of the collective pitch setting has a considerable effect on the value of the advance ratio at which instabilities due to the periodic coefficients or the radial flow aerodynamic coupling terms occur. Increase in collective pitch is destabilizing, therefore high advance ratio studies which do not include this effect (nonlifting rotors) may yield nonconservative results.

(5) The numerical results obtained in the present study agree with the analytical results obtained previously[9] indicating that hingeless blades with a rotating lag stiffness of 1/2 or 1 can easily become unstable due to the effect of periodic coefficients.

(6) While droop has a very strong effect on the stability boundaries of hingeless blades in hover, it has a very minor effect on the stability boundary in forward flight.

References

1. Horvay, G. and Yuan, S.W., STATILITY OF ROTOR BLADE FLAPPING MOTION WHEN THE HINGES ARE TILTED. GENERALIZATION OF THE 'RECTANGULAR RIPPLE' METHOD OF SOLUTION, Journal of the Aeronautical Sciences, October 1947, pp. 583-593.

2. Shulman, Y., STABILITY OF A FLEXIBLE HELICOPTER ROTOR BLADE IN FORWARD FLIGHT, Journal of the Aeronautical Sciences, July 1956, pp. 663-670, 693.

3. Sissingh, G.J., DYNAMICS OF ROTOR OPERATING AT HIGH ADVANCE RATIOS, Journal of American Helicopter Society, July 1968, pp. 56-63.

4. Sissingh, G.J., and Kuczynski, W.A., INVESTIGATIONS ON THE EFFECT OF BLADE TORSION ON THE DYNAMICS OF THE FLAPPING MOTION, Journal of the American Helicopter Society, April 1970, pp. 2-9.

5. R & M No. 3544, THE STABILITY OF ROTOR BLADE FLAPPING MOTION AT HIGH TIP SPEED RATIOS, Lowis, O.J., 1968.

6. Peters, D.A., and Hohenemser, K.H., APPLICATION OF THE FLOQUET TRANSITION MATRIX TO PROBLEMS OF LIFTING ROTOR STABILITY, Journal of the American Helicopter Society, April 1971, pp. 25-33.

7. Hohenemser, K.H., and Yin, S.K., SOME APPLICATIONS OF THE METHOD OF MULTIBLADE COORDINATES, Journal of American Helicopter Society, July 1972, pp. 3-12.

8. Johnson, W., A PERTURBATION SOLUTION OF ROTOR FLAPPING STABILITY, AIAA Paper 72-955.

9. Friedmann, P. and Tong, P., NONLINEAR FLAP-LAG DYNAMICS OF HINGELESS HELICOPTER BLADES IN HOVER AND IN FORWARD FLIGHT, Journal of Sound and Vibration, September 1973.

10. SUDAAR No. 400, APPLICATION OF FLOQUET THEORY TO THE ANALYSIS OF ROTARY WING VTOL STABILITY, HALL, W.E., Stanford University, February 1970.

11. NASA CR-1332, A METHOD FOR ANALYZING THE AEROELASTIC STABILITY OF A HELICOPTER ROTOR IN FORWARD FLIGHT, Crimi, P., August 1969.

12. Friedmann, P., AEROELASTIC INSTABILITIES OF HINGELESS HELICOPTER BLADES, AIAA Paper 73-193 January 1973, (also Journal of Aircraft, October 1973).

13. UCLA School of Engineering and Applied Science Report, AEROELASTIC STABILITY OF COUPLED FLAP-LAG MOTION OF HELICOPTER BLADES AT ARBITRARY ADVANCE RATIOS, Friedmann, P., and Silverthorn, J.L., to be published January 1974.

14. NASA-CR-114 485, DYNAMIC NONLINEAR ELASTIC STABILITY OF HELICOPTER ROTOR BLADES IN HOVER AND FORWARD FLIGHT, Friedmann, P., and Tong, P., May 1972.

15. Brockett, R.W., FINITE DIMENSIONAL LINEAR SYSTEMS, John Wiley and Sons, 1970.

16. Ormiston, R.A., and Hodges, D.H., LINEAR FLAP-LAG DYNAMICS OF HINGELESS HELICOPTER ROTOR BLADES IN HOVER, Journal of the American Helicopter Society, Vol. 17, No. 2, April 1972, pp. 2-14.

17. Hsu, C.S., and Cheng, W.H., APPLICATION OF THE THEORY OF IMPULSIVE PARAMETRIC EXCITATION AND NEW TREATMENTS OF GENERAL PARAMETRIC EXCITATION PROBLEMS, Journal of Applied Mechanics, March 1973, pp. 78-86.

Appendix A. Definitions of the Generalized Masses, Aerodynamic Integtals and other Quantities

The quantities, $\overline{P}_{111}, \overline{M}_{FI}, \overline{M}_{L1}, \overline{S}_{111}, (\overline{M}_{\eta})_{111}, (\overline{M}_{\gamma})_{111}$ are generalized masses given, in Appendix A of Reference 12, with the general i,m,k indices these quantities can be found in References 13 and 14.

$$\bar{B}_i^1 = \ell^3 \int_0^1 \left[\int_{\bar{x}_o}^1 m(\bar{x}_1+\bar{e}_1)d\bar{x}_1\right]\eta_i' \, d\bar{x}_o/I_b$$

$$\bar{B}_{im}^3 = \ell^3 \int_0^1 \eta_i'\left[\int_{\bar{x}_o}^1 m\,\gamma_m d\bar{x}_1\right] d\bar{x}_o/I_b$$

$$\bar{B}_{im}^7 = \ell^3 \int_0^1 m\,\eta_i\gamma_m d\bar{x}_o/I_b;$$

$$\bar{B}_{im}^8 = \ell^3\left[\int_{\bar{x}_o}^1 m\,\gamma_m d\bar{x}_1\right] d\bar{x}_o/I_b$$

$$\bar{B}_{im}^{10} = \ell^3 \int_0^1 \gamma_i\left[\int_{\bar{x}_o}^1 m(\bar{x}_1+\bar{e}_1)d\bar{x}\right] d\bar{x}_o/I_b;$$

$$\bar{B}_i^{11} = \ell^3 \int_0^1 \bar{x}_o m\gamma_i \, d\bar{x}_o/I_b$$

$$I_b = \ell^3 \int_0^1 m\,\bar{x}_o^2 \, d\bar{x}_o$$

Structural damping is represented by

$$g_{SF} = 2\,\Omega\,\bar{\omega}_{Fi}\,\eta_{SF_i} \quad ; \quad g_{SL} = 2\,\Omega\,\bar{\omega}_{Li}\,\eta_{SL_i}$$

The elastic coupling effect is represented by

$$E_{C1} = [(EI)_z-(EI)_y]\sin^2\theta; \quad E_{C2} = [(EI)_z-(EI)_y]\sin\theta\cos\theta$$

$$\int_0^1 E_{C1}\eta_k''\,\eta_i''\,d\bar{x}_o = \overline{\overline{E}}_{ik}^{s}\, I_b\Omega^2\ell$$

$$\int_0^1 E_{C2}\gamma_m''\,\eta_i''\,d\bar{x}_o = \overline{\overline{E}}_{im}^{cs}\, I_b\Omega^2\ell$$

$$\int_0^1 \gamma_i''\,\gamma_m''\,E_{C1}d\bar{x}_o = \overline{\overline{E}}_{im}^{s}\, I_b\Omega^2\ell$$

$$\int_0^1 \gamma_i''\,\eta_k''\,E_{C2}d\bar{x}_o = \overline{\overline{E}}_{ik}^{cs}\, I_b\Omega^2\ell$$

When using these expressions in a one mode analysis for each degree of freedom the lower indices are deleted for these expressions and the expressions for the generalized aerodynamic integrals. The generalized aerodynamic integrals F^i, L^i can be found in References 12,13 and 14. For this study some additional expressions had to be defined, only these are given below.

$$F_{im}^{21} = \int_{\bar{A}}^{\bar{B}} \bar{x}_o\eta_i\gamma_m'd\bar{x}_o \quad ; \quad F_{im}^{22} = \int_{\bar{A}}^{\bar{B}} \eta_i\gamma_m' \, d\bar{x}_o$$

$$F_{ikm}^{23} = \int_{\bar{A}}^{\bar{B}} \eta_i\eta_k'\gamma_m'd\bar{x}_o \quad ; \quad F_{ikm}^{24} = \int_{\bar{A}}^{\bar{B}} \eta_i\eta_k\gamma_m'd\bar{x}_o$$

$$L_{im}^{20} = \int_{\bar{A}}^{\bar{B}} \gamma_i\gamma_m'd\bar{x}_o \quad ; \quad L_{ikm}^{21} = \int_{\bar{A}}^{\bar{B}} \gamma_i\eta_k'\gamma_m'd\bar{x}_o$$

$$L_{ikm}^{22} = \int_{\bar{A}}^{\bar{B}} \gamma_i\eta_k\gamma_m'd\bar{x}_o \quad ; \quad L_{im}^{23} = \int_{\bar{A}}^{\bar{B}} \gamma_i\gamma_m'\bar{x}\, d\bar{x}_o$$

$$L_{ik\ell}^{24} = \int_{\bar{A}}^{\bar{B}} \gamma_i\eta_k'\eta' \, d\bar{x}_o$$

Appendix B. Elements of the $\underset{\sim}{A}$ - Matrix

The elements of the $\underset{\sim}{A}$ - matrix, which defines the equations of motion when written as first order differential equations, are given below:

$$A_{21} = 1; \quad A_{22} = A_{23} = A_{24} = 0$$

$$A_{43} = 1; \quad A_{41} = A_{42} = A_{44} = 0$$

$$A_{11} = -\bar{g}_{D1} + \frac{\gamma}{2}\left(\frac{\ell}{R}\right)^3 \mu(-F^9\sin\psi + F^{24}h_1^o\cos\psi)$$

$$A_{12} = -\left(\bar{\omega}_{F1}^2 + \frac{\bar{E}^s}{\bar{M}_{F1}}\right) + \frac{\gamma}{2}\left(\frac{\ell}{R}\right)^2\left[-\left(\frac{\mu^2}{2}F^7\sin 2\psi + \mu F^6\cos\psi\right) + \frac{\mu^2}{2}F^{23}h_1^o(1+\cos 2\psi)\right]$$

$$A_{13} = X_H + \frac{\gamma}{2}\left(\frac{\ell}{R}\right)^3\left[-2\theta\mu F^{11}\sin\psi + \mu(\beta_p+\beta_D)F^{11}\cos\psi + F^{14}g_1^o\mu\cos\psi\right]$$

$$A_{14} = \frac{\overline{\overline{E}}^{cs}}{\bar{M}_{F1}} + \frac{\gamma}{2}\left(\frac{\ell}{R}\right)^2\left\{\theta(-2F^{21}\mu\cos\psi - \mu^2\sin 2\psi F^{22}) + \lambda\mu F^{22}\cos\psi + \frac{\mu^2}{2}(1+\cos 2\psi)[F^{23}g_1^o + F^{22}(\beta_p+\beta_D)]\right\}$$

$$A_{31} = Y_G + \frac{\gamma}{2}\left(\frac{\ell}{R}\right)^3[\theta L^8\mu\sin\psi - 2\mu L^{17}g_1^o\cos\psi - \theta\mu L^{22}h_1^o\cos\psi - 2\mu(\beta_p+\beta_D)L^8\cos\psi]$$

$$A_{32} = \frac{\overline{\overline{E}}_{cs}}{\bar{M}_{L1}} + \frac{\gamma}{2}\left(\frac{\ell}{R}\right)^2\left[\theta\left(\frac{\mu^2}{2}L^{11}\sin 2\psi + L^{10}\mu\cos\psi\right) - 2\lambda L^{11}\mu\cos\psi - \theta\frac{\mu^2}{2}(1+\cos 2\psi)L^{21}h_1^o - \mu^2(\beta_p+\beta_D)L^{11}(1+\cos 2\psi) - L^{24}\mu^2 g_1^o(1+\cos 2\psi)\right]$$

$$A_{33} = -\bar{g}_{D2} + \frac{\gamma}{2}\left(\frac{\ell}{R}\right)^3[-\theta\mu L^{16}g_1^o\cos\psi - 2\,\frac{C_{Do}}{a}\,\mu L^{13}\sin\psi \quad \theta\mu(\beta_p+\beta_D)L^{13}\cos\psi]$$

$$A_{34} = -\left(\bar{\omega}_{L1}^2 - \frac{\overline{\overline{E}^s}}{\bar{M}_{L1}}\right) + \frac{\gamma}{2}\left(\frac{\ell}{R}\right)^2\left\{-\theta\lambda\mu L^{20}\cos\psi + \frac{\mu^2}{2}(1+\cos 2\psi)[-L^{21}g_1^o - (\beta_p+\beta_D)L^{20}]\theta + \frac{C_{Do}}{a}(-\mu^2 L^{20}\sin 2\psi - 2\mu L^{23}\cos\psi)\right\}$$

where

$$X_H = \frac{2\bar{P}_{111}g_1^o}{\bar{M}_{F1}} - \frac{\gamma}{2\bar{M}_{F1}}\left(\frac{\ell}{R}\right)^3[2\theta F^{10} - F^{11}\lambda] + \frac{\bar{B}^3}{\bar{M}_{F1}}2(\beta_P+\beta_D)$$

$$Y_G = -\frac{2(M_\eta)_{111}g_1^o}{\bar{M}_{L1}} + \frac{\gamma}{2\bar{M}_{L1}}\left(\frac{\ell}{R}\right)^3[L^7\theta - 2\lambda L^8] - \frac{\bar{B}^7}{\bar{M}_{L1}}2(\beta_P+\beta_D)$$

Appendix C. Approximate Reverse Flow Model and the Associated Aerodynamic Loads

The circular region of reversed flow, which exists over the retreating blade, is quite well known. In past treatments of reversed flow it has been customary[3] to define three separate regions: (a) normal flow, (b) reversed flow, (c) mixed flow, and evaluate the appropriate aerodynamic expressions for each region. When this model is used together with a modal representation of the blade the evaluation of the generalized aerodynamic expressions F^i, L^i becomes quite cumbersome, and a more convenient procedure had to be devised.

The approximate reverse flow model developed for the present study consists of replacing the circular region, by an approximate region which is a circular sector as shown in Figure 1. The approximation is based on the assumption that the area contained in the circular sector must be equal to the area contained in the approximate region. Two separate cases must be considered: (1) $\mu < 1$, (2) $\mu \geq 1$.

Case (1). For $\mu < 1$, the radius of the circular part is taken as μ. Simple geometric considerations show that the angle α is always a constant.

given by $\alpha = \pi/2$

Case (2). For $\mu \geq 1$ simple geometric considerations show that

$$\alpha = \pi - 2\sin^{-1}\left(\frac{1}{\mu}\right) + \mu^2\sin^{-1}\left(\frac{1}{\mu}\right) - \sqrt{\mu^2-1}$$

Thus, for $\mu < 1$ the generalized aerodynamic loads are calculated from

$$\bar{A}_{Fi} = \frac{\ell^2}{\Omega^2 I_b}\left[-\int_{\bar{A}}^{\mu} L_z\eta_i\, d\bar{x}_o + \int_{\mu}^{\bar{B}} L_z\eta_i\, d\bar{x}_o\right]$$

$$\bar{A}_{Li} = -\frac{\ell^2}{\Omega^2 I_b}\left[-\int_{\bar{A}}^{\mu} L_y\gamma_i\, d\bar{x}_o + \int_{\mu}^{\bar{B}} L_y\gamma_i\, d\bar{x}_o\right]$$

while for $\mu \geq 1.0$

$$\bar{A}_{Fi} = -A_{Fi} \text{ and } \bar{A}_{Li} = -A_{Li}$$

These expressions are based on the assumption that the lift curve slope in the reversed flow region is equal to the negative value of the lift curve slope in normal flow.

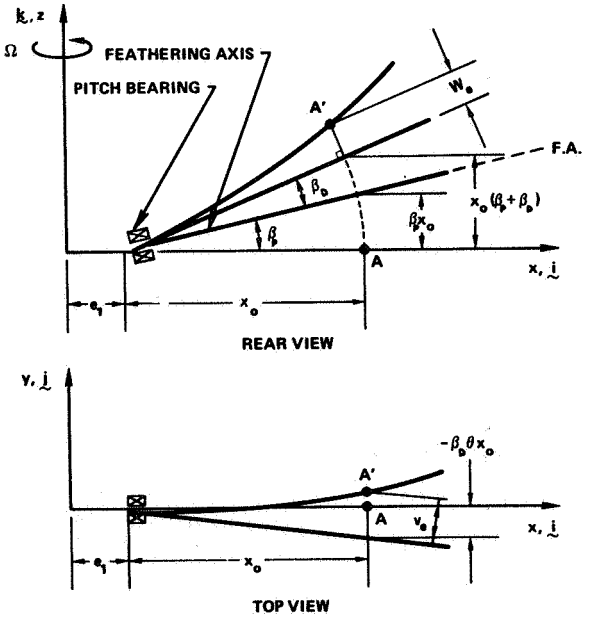

Figure 1. Displacement Field of a Torsionally Rigid Cantilevered Blade with Droop and Preconing.

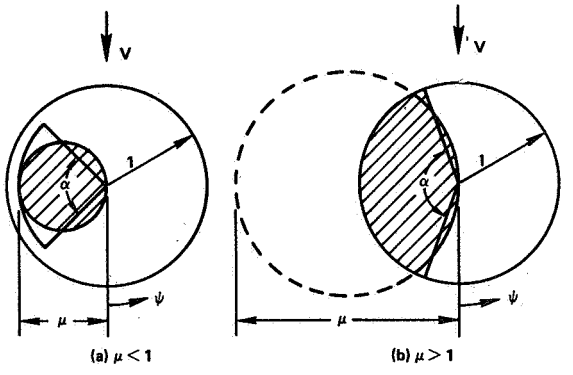

Figure 2. Geometry of Approximate and Exact Reverse Flow Regions.

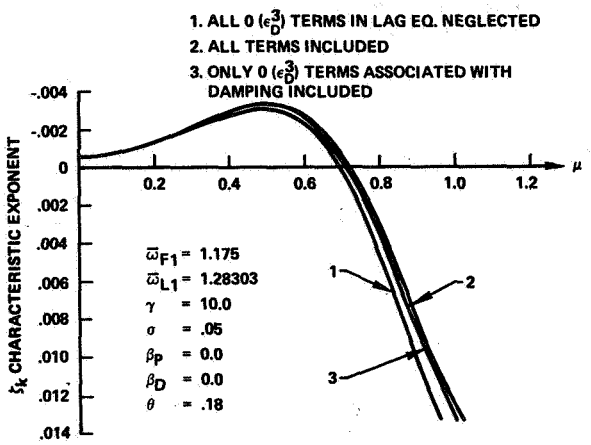

Figure 3. Effect of Third Order Terms in the Lag Equation on Characteristic Exponent for Lag.

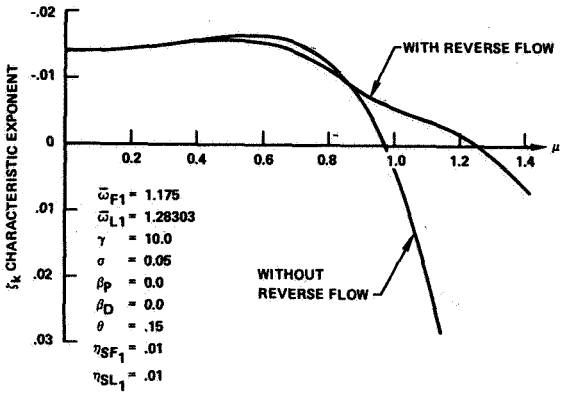

Figure 4. Effect of Reversed Flow on Characteristic Exponent for Lag.

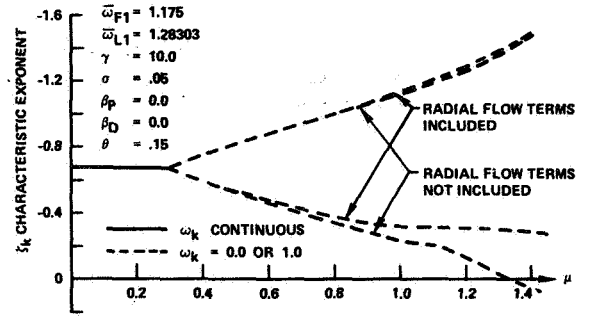

Figure 5. Effect of Radial Flow Terms on Characteristic Exponent for Flap.

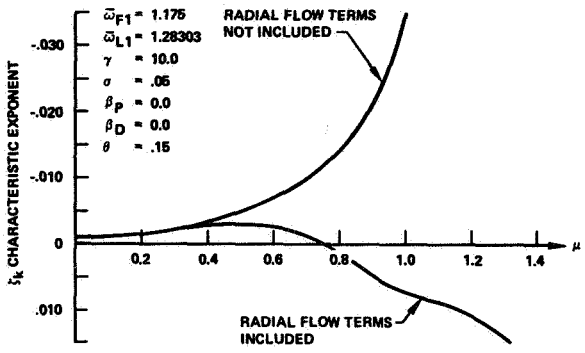

Figure 6. Effect of Radial Flow Terms on Characteristic Exponent for Lag.

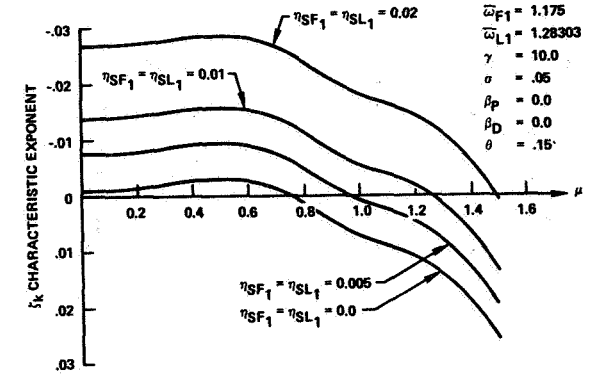

Figure 7. Effect of Viscous Structural Damping on Characteristic Exponent for Lag.

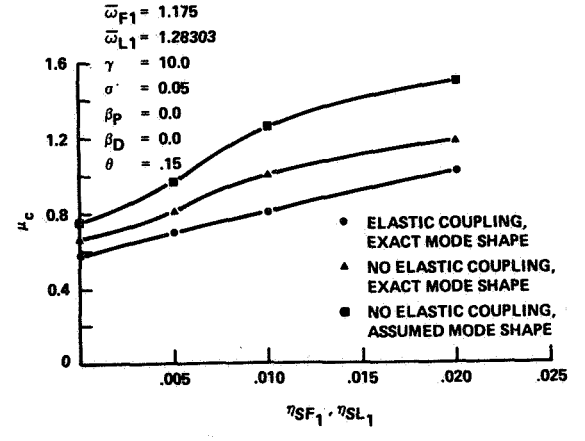

Figure 8. Critical Advance Ratio μ_c vs Structural Damping Coefficients η_{SF_1}, η_{SL_1}.

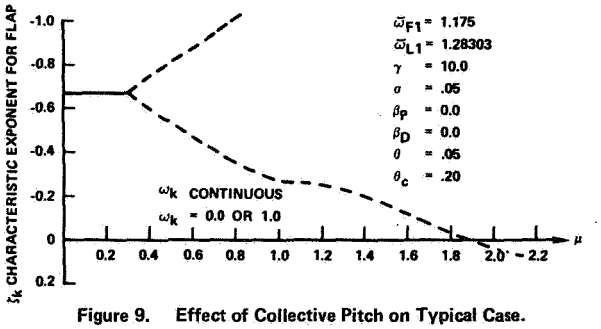

Figure 9. Effect of Collective Pitch on Typical Case.

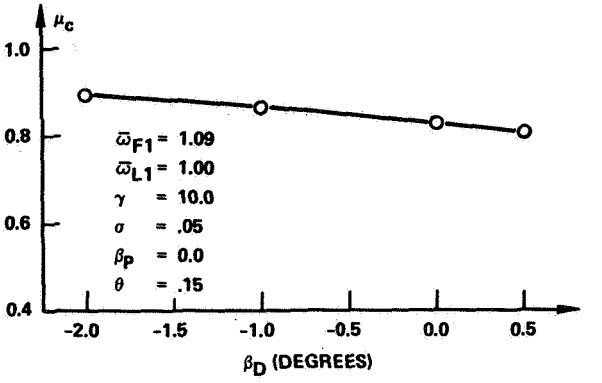

Figure 10. Effect of Droop on μ_c.

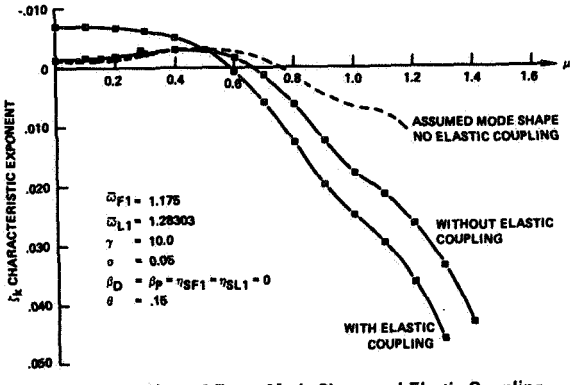

Figure 11. Effect of Exact Mode Shape and Elastic Coupling on Characteristic Exponent for Lag.

CORRELATION OF FINITE-ELEMENT STRUCTURAL DYNAMIC ANALYSIS WITH MEASURED FREE VIBRATION CHARACTERISTICS FOR A FULL-SCALE HELICOPTER FUSELAGE

Irwin J. Kenigsberg
Supervisor - Airframe Dynamics
Sikorsky Aircraft
Stratford, Connecticut

Michael W. Dean
Dynamics Engineer
Sikorsky Aircraft
Stratford, Connecticut

Ray Malatino
Helicopter Loads and Dynamics Engineer
Naval Air Systems Command
Washington, D. C.

Abstract

Both the Sikorsky Finite-Element Airframe Vibration Analysis Program (FRAN/Vibration Analysis) and the NASA Structural Analysis Program (NASTRAN) have been correlated with data taken in full-scale vibration tests of a modified CH-53A helicopter. With these programs the frequencies of fundamental fuselage bending and transmission modes can be predicted to an average accuracy of three percent with corresponding accuracy in system mode shapes.

The correlation achieved with each program provides the material for a discussion of modeling techniques developed for general application to finite-element dynamic analyses of helicopter airframes. Included are the selection of static and dynamic degrees of freedom, cockpit structural modeling, and the extent of flexible-frame modeling in the transmission support region and in the vicinity of large cut-outs. The sensitivity of predicted results to these modeling assumptions is discussed.

Introduction

Helicopter vibration and resulting aircraft vibratory stress can lead to costly schedule slippages as well as to problems in field service maintenance and aircraft availability. At the core of vibration control technology is the requirement to design the helicopter structure to minimize structural response to rotor excitations. Both the complexity of the structure and the increasingly stringent mission and vibration control specifications demand development of airframe structural vibration analyses that can be used rapidly and economically to evaluate and eliminate vibration problems during the preliminary design phase of helicopters.

The complex helicopter structure consists of sections that differ considerably in structural arrangement and load carrying requirements. These sections include the cockpit, cabin, tail cone, and tail rotor pylon. In addition, large fuselage cut-outs and concentrated masses such as the transmission, main rotor, and tail rotor, which are unique to helicopters, play a major role in controlling vibrations.

Although advanced analytical methods based on finite-element techniques have been developed for studying the vibration characteristics of complex structures, a detailed correlation of such methods with test data is not available in the general literature. Further, little information is available on the accuracy of various modeling assumptions that might be made to reduce the cost and time of applying these vibration analyses.

As a result a research project was established by Naval Air Systems Command with Sikorsky Aircraft to:

a) Determine the accuracy of the Sikorsky Finite-Element Airframe Vibration Analysis in predicting the vibration characteristics of complex helicopter airframe structures.

and

b) Develop and evaluate general helicopter dynamic modeling techniques that could be used to provide accurate estimates of vehicle dynamic characteristics while at the same time minimizing the complexity and cost of the analysis.

Due to the increased usage of NASTRAN throughout the industry as well as the efficiency resulting from employing a single analytical system for both static and dynamic analyses, a parallel correlation study using NASTRAN has been performed. The results of these correlation studies are the subject of this paper.

Phase I - Stripped Vehicle

Test Vehicle

At the initiation of this effort, the philosophy guiding the development of modeling techniques was based upon the concept of gradually increasing the complexity of the analytical representation. It was decided that the first

Presented at the AHS/NASA-Ames Specialists' Meeting on Rotorcraft Dynamics, February 13-15,1974

correlation study would be conducted on an aircraft stripped of all appendages. It was believed that the modeling techniques for representing airframe response characteristics could be identified and developed most easily in this manner. Then, as various appendages were added to the basic vehicle, only the modeling techniques required for the structure or masses added need be developed.

The vehicle used in this test and correlation study was the CH-53A Tie Down Aircraft, Vehicle designation number 613. A general arrangement of the structure is illustrated in Figure 1. For initial correlation, all appendages were removed. These included the nose gear, main landing gear, main landing gear sponsons, fuel sponsons, tail pylon aft of the fold hinge, tail rotor and associated gear boxes, engines, cargo ramp door, horizontal stabilizer, and all remaining electrical and hydraulic systems. The main rotor shaft and all gears were removed from the main transmission housing and only the housing itself was retained for the test configuration.

Testing

The ground test facility employed to establish the dynamic characteristics of the test vehicle was a bungee suspension system that simulates a free-free condition, a rotorhead-mounted unidirectional shaker, and the Sikorsky shake test instrumentation console. Instrumentation consisted of 14 fixed and 10 roving accelerometers. A complete description of the test apparatus and the instrumentation is provided in Reference 1.

All accelerometer signals and the reference shaker contactor signal were transmitted to the console. The signals were processed automatically by the console resulting in a calculation of the in-phase and quadrature components of the accelerations. The accelerations were then normalized to the magnitude of the shaker force at the particular frequency. As frequency was varied, the resulting response of each accelerometer was recorded on a XYY' plotter, Figure 2, as g's/1000 lbs. versus frequency.

Ideally, a fuselage mode can be identified by a peak in the quadrature response and a simultaneous zero crossing of the in-phase response. Once a mode is located, all quadrature responses at this frequency can be recorded to define the mode shape. The modes defined in this manner from the shake tests are listed in the left-hand column of Table I. It should be noted that this technique is applied more easily at lower frequencies, where sufficient modal separation exists so that the forced response in the vicinity of a resonance is dominated by a single mode. As shown in Figure 2, the mode shapes at higher frequencies must be extracted from the coupled response of many modes.

Analysis and Correlation

The shake test data indicated that the natural modes of vibration of a helicopter can be categorized as beam-like modes controlled by overall fuselage characteristics (e.g., length, depth, overall bending stiffness, mass distribution, etc.) and those controlled by the transmission support structure. Therefore, the overall helicopter structure was modeled utilizing three modules:

1) center section including the transmission support region

2) forward fuselage and cockpit

and

3) aft fuselage and tail.

The center section was modeled in greatest detail by applying finite-element techniques. The structural characteristics of the forward and aft fuselage were derived from beam theory. These equivalent beams were located at the neutral axis of the airframe section and were assigned the bending and torsional properties of the total section. The beam models of the forward and aft fuselage were cantilevered from rigid frames at the respective forward and aft ends of the center section, Figure 3. The influence coefficients of these beams with respect to their cantilevered ends were then combined with the influence coefficient matrix of the remaining structure.

The Phase I correlation was performed using the Sikorsky Finite-Element Airframe Vibration Analysis (FRAN/Vibration Analysis). This analysis consists of two programs: PPFRAN and a 200 dynamic-degree-of-freedom eigenvalue/eigenvector extraction procedure. PPFRAN is derived from the IBM/MIT Frame Structural Analysis Program, FRAN (Reference 2), a stiffness method, finite-element analysis limited to two types of elements, namely bending elements (bars) and axial elements (rods). This limitation necessitated further development of FRAN for application to stressed skin structures. This development consists of the addition of pre- and post-operative procedures linked to FRAN. In the pre-operative procedure (Pre-FRAN), the fuselage skin is transformed into equivalent rod elements. This transformation is developed by satisfying the criterion that the internal energy of the skin structure under an arbitrary set of loads be the same as that of the transformed structure under the same set of loads. The post-operative procedure (Post-FRAN) extracts the influence coefficient matrix corresponding to the selected dynamic degrees of freedom. A detailed description of the FRAN/Vibration Analysis is provided in Reference 1.

The elements used to represent the airframe structure are:

1) bending (bar) elements for fuselage frames and for the nose and tail beams

2) axial (rod) elements for the stringers

and

3) equivalent, diagonal rod elements for skin panels.

For dynamic analysis, the structure is assumed to be unbuckled, so that all skin panels are considered fully effective in resisting axial loads. Thus, the total axial area of each skin panel is lumped with the areas of adjacent stringers.

During Phase I correlation, three modeling parameters were varied: the number of bays over which the finite-element (flexible-frame) model extends (Figure 4), the number of nodes per frame (number of stringers), and the number of dynamic degrees of freedom assigned to each frame (Figure 5). The results of the correlation are presented in Table I, which shows the sensitivity of the analysis to each of the above parameters and the accuracy of the predicted frequencies and mode shapes. The criteria for establishing the level of mode shape correlation are:

E (Excellent) - Correct number of nodes, nodes less than 2.5 percent of fuselage length from measured location, local modal amplitudes within 20 percent of test values.

G (Good) - Correct number of nodes, nodes less than 2.5 percent of fuselage length from measured location, difference between actual and predicted local modal amplitudes exceeds ±20 percent of test values.

F (Fair) - Correct number of nodes, nodes more than 2.5 percent of fuselage length from measured location, difference between actual and predicted local modal amplitudes exceeds ±20 percent of test values.

P (Poor) - Incorrect number of nodes, nodes located improperly, difference between actual and predicted local modal amplitudes exceeds ±20 percent of test values.

A comparison of the 30- and 60-stringer analyses indicates that there is no change in the results when modeling the structure with half the number of actual stringers. In addition a comparison of results obtained with the basic and reduced dynamic degree of freedom allocation indicates that no more than 16 dynamic degrees of freedom per frame are required for dynamic modeling.

Although mode shape correlation resulting from the analysis in the frequency range of interest (below 1500 cpm) is encouraging, see Table I, the absence of a representative mass distribution made the analysis overly sensitive to certain modeling assumptions. This sensitivity appears to account for the less than satisfactory frequency correlation. For example, the frequency of the transmission pitch mode is normally controlled by the mass of the fully assembled transmission and the properties of the structure in the transmission support region. In the absence of a mass distribution representative of a fully assembled vehicle, however, any element of the structure and any lumped mass can contribute significantly to the control of the dynamic characteristics. In this case, the analytical representation appears to be too stiff because of the beam model used for the fuselage forward of F.S. 262, which constrains the upper and lower decks to deform equally. This constraint is not imposed by the actual structure. A comparison of the results of the 9- and 18-bay analyses indicates that due to the local nature of the transmission pitch mode, extension of the flexible-frame model aft beyond the limit of the 9-bay model has no significant effect on the prediction of this mode.

The poor frequency correlation for the first lateral bending mode persisted throughout this phase of correlation. This mode was characterized by differential shearing of the upper and lower decks of the aft cabin, Figure 7. The 6-bay and 9-bay flexible-frame model represented most of this structure experienceing the differential shearing as a beam capable of only bending and torsion. This overly constrained model resulted in predicted frequencies substantially higher than test values. Extending the flexible-frame representation to 18-bays appears to be the solution. However, size limitations in PPFRAN required that the 18-bay flexible-frame model be generated in two 9-bay substructures, married at a rigid intermediate frame at F.S. 442, Figure 3. Although the extended model improved the correlation of the first lateral bending mode, absence of a representative mass distribution again appears to make the model overly sensitive to the presence of the rigid frame at F.S. 442. This accounted for the remaining difference between test and analysis.

Many of the higher frequency modes are controlled by the structure in the area of the rear cargo ramp. This accounts for the failure to predict the Transmission Vertical mode until the flexible-frame model was extended into the ramp area, see Table I. Although this extension of the model improved correlation, the high frequency modes above 1500 cpm are difficult to identify analytically due to the coupling of overall fuselage modes with local frame modes. This difficulty is compounded in this investigation, because the frequencies of the basic fuselage modes are raised due to the stripped condition of the vehicle, while frequencies of the local frame modes are lowered due to the lumped-mass modeling used to represent each frame. Tests of a more representatively loaded fuselage can be expected to minimize the problem of mode identification.

From the results of this phase of the correlation, it is concluded:

1) The selection of static degrees of freedom in the flexible frame model can be based on a structural model that contains stringers numbering one half the number of actual stringers.

2) No more than sixteen dynamic degrees of freedom on each flexible frame are required for dynamic analysis. The typical location of

these degrees of freedom is illustrated in Figure 5.

3) Transmission modes can be predicted by a flexible-frame representation of the transmission support region extending about 1.5 transmission lengths forward and aft of the corresponding transmission supports, about 9 bays. If the vehicle contains large cutouts, such as the cargo ramp of the test vehicle, the flexible-frame model should extend through this region as well.

PHASE II - BALLASTED VEHICLE

Testing

Shake tests were performed after adding ballast to provide a more realistic representation of a helicopter mass distribution, Figure 6. At the transmission mounting plate, two lead blocks having a total weight of 4570 pounds were mounted so that the mass and pitching moment of inertia of the simulated transmission and rotor head approximated that of the actual CH-53A. At the tail, a 1500-pound block was mounted to simulate the removed tail pylon, stabilizer, and tail rotor. At the nose, a 3000-pound block was mounted on the nose gear trunnion fitting to balance the vehicle.

The natural modes of vibration identified by shake tests are listed in Table II along with the frequencies measured during Phase I. Not only did the ballast succeed in lowering the fuselage modes into a frequency range more representative of that encountered on a fully assembled aircraft, but additional modes were also identified that are strongly controlled by the ballast. In fact, these modes were identified as local modes of the ballast blocks themselves. Due to the complex structural nature of the ballast, Figure 6, these appendages did not lend themselves to simple analytical representations. Therefore, the flexibility of each ballast block was measured by instrumenting both the block and the adjacent airframe structure and then measuring the accelerations occurring at both locations near the modal frequencies of interest. The mass of each ballast block and its absolute acceleration resulted in a force which produced the relative motion between the two instrumented parts. The empirically defined flexibilities of the ballast were then used in the dynamic model.

Analysis and Correlation

The modeling techniques developed in Phase I of this study were applied to both the FRAN/Vibration Analysis and NASTRAN.

The finite-element model analyzed in Phase II was identical to the 18-bay model analyzed in Phase I, except for adding the mass and structural characteristics of the ballast blocks. The FRAN model was formed with rod and bar elements, as discussed previously, while the NASTRAN model used CROD, CBAR, and CSHEAR elements (Reference 3). As before, all skin panels were assumed fully effective in reacting axial load and this effective area was lumped into the adjacent stringers.

Including ballast to replace removed appendages resulted in a substantial improvement in the correlation, particularly in frequency prediction as shown in Table III. Significantly, ballast eliminated the difficulties identified as sensitivity to modeling assumptions and local frame modes in the absence of representative mass distributions. The average error in predicting the frequencies of fundamental fuselage bending modes and the transmission pitch mode was 3-4% for both the FRAN/Vibration Analysis and NASTRAN. In addition the shape correlation for these modes varied from good to excellent. The analyses also were able to predict accurately the significant changes in the characteristics of the fuselage and transmission modes resulting from the addition of the ballast, Figures 7, 8 and 9. To achieve this degree of correlation, modeling of the ballast flexibilities was required. This modeling was successfully accomplished in the vertical/pitch direction, Figure 10, but did not prove successful in the lateral/torsion direction, Figure 11. The contrast between these two results establishes the ability of finite-element analyses to predict accurately the characteristics of fuselage and transmission modes when the structural data base is defined with sufficient accuracy. Further improvement in the correlation could have been achieved if a more detailed definition of the ballast flexibilities had been acquired from measurements of static deflections.

Reasonable success has been achieved in predicting higher frequency, ramp-controlled modes, Figures 12 and 13. However, some margin does exist for further improvements in shape and frequency prediction. From the standpoint of modeling, it appears that the 200 dynamic degree of freedom limit established in this study is inadequate for predicting the shell-type modes of the cargo ramp structure. In addition, the test procedure employed, namely the use of a single rotorhead shaker, does not provide a means of uncoupling the forced response characteristics of modes at the higher frequencies, Figure 2.

Conclusions

1. Finite element analyses can predict accurately the frequencies and mode shapes of complex helicopter structures, provided the structural data base is defined accurately.

2. Complete stripping of a vehicle for correlation purposes may make the analysis overly sensitive to normally minor modeling assumptions.

3. Significant changes can be predicted accurately in the character and frequency of fuselage and transmission modes due to changes in mass distributions and structural characteristics.

4. The modeling techniques established by this study can be used during aircraft design regardless of the finite-element analytical system being used.

Recommendations

1) A full-scale shake test correlation should be performed on a fully assembled flight vehicle to establish and validate modeling techniques for those appendages removed during this study.

2) Appendages not amenable to accurate or economical structural analysis should be tested statically to determine flexibility data required for dynamic analysis.

3) Integrated structural design systems should be developed to couple static and dynamic analyses and thus provide the accurate structural data required for defining vibratory response characteristics as early as possible during aircraft design.

4) Use of additional shaker locations should be incorporated in the test procedure to provide a means of uncoupling higher frequency modes. Alternatively, more sophisticated means of processing shake test data (e.g., system identification techniques described in Reference 4) should be employed.

References

1) Kenigsberg, I. J., CH-53A FLEXIBLE FRAME VIBRATION ANALYSIS/TEST CORRELATION, Sikorsky Engineering Report SER 651195, March 28, 1973.

2) IBM 7090/7094 FRAN FRAME STRUCTURE ANALYSIS PROGRAM (7090-EC-01X).

3) McCormick, C. W., ed., THE NASTRAN USER'S MANUAL, (level 15), NASA SP-222(01), June 1972.

4) Flannelly, W. G., Berman, A., and Barnsby, R. M., THEORY OF STRUCTURAL DYNAMIC TESTING USING IMPEDANCE TECHNIQUES, USAAVLABS TR 70-6A,B, June 1970.

5) Willis, T., FRAN CORRELATION STUDY, Sikorsky Report SYTR-M-36, July 1969.

Illustrations

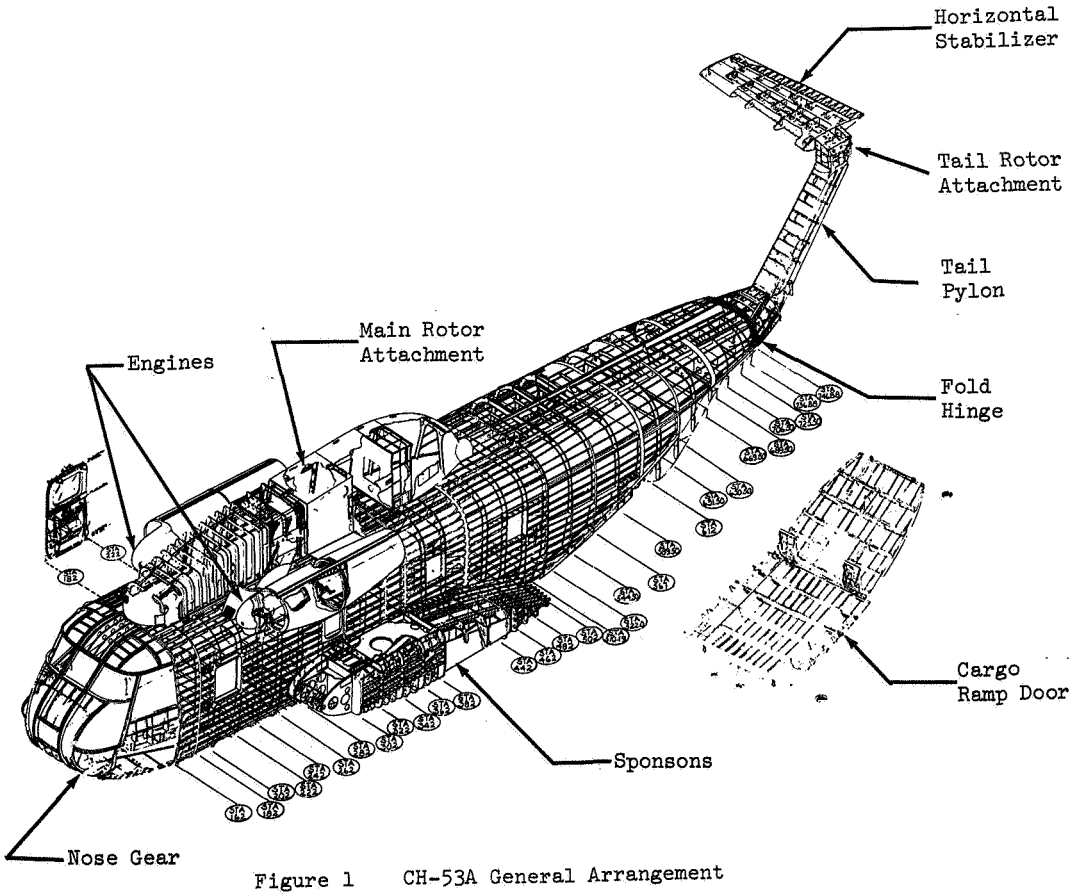

Figure 1 CH-53A General Arrangement

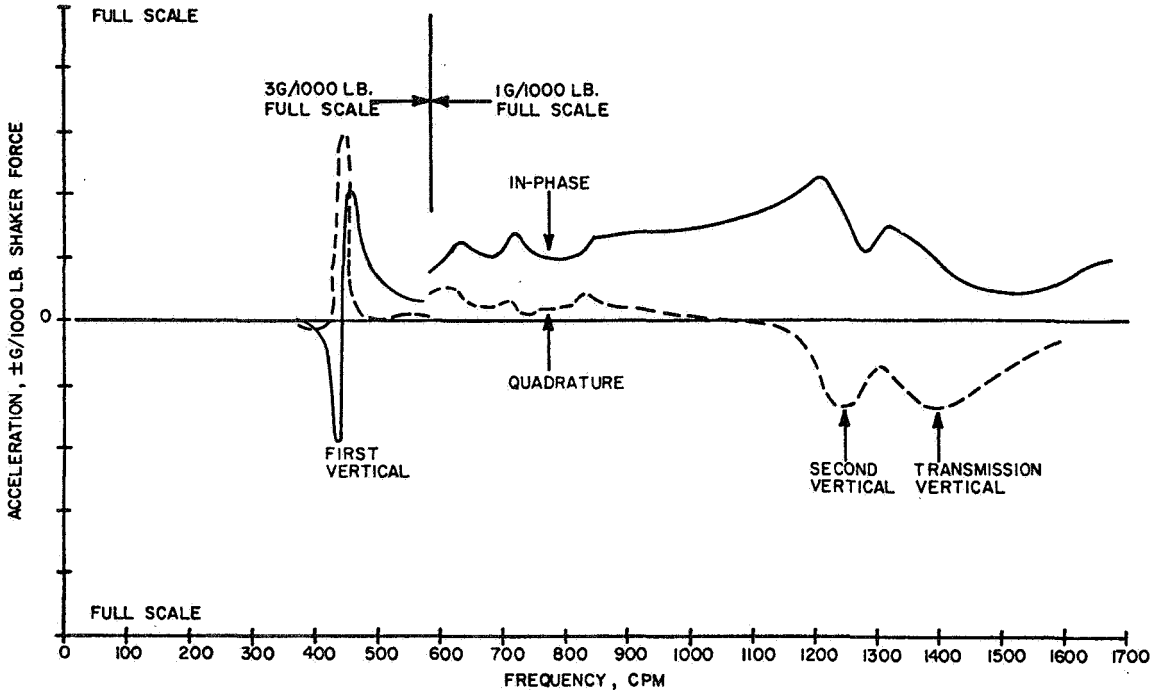

Figure 2 Typical Vertical Response to Vertical Excitation

TABLE I

PHASE I SHAKE TEST CORRELATION SUMMARY

TEST		ANALYSIS											
		18 Bay 30 Stringer Reduced DOF			9 Bay 30 Stringer Reduced DOF			6 Bay 30 Stringer Reduced DOF			6 Bay 30 Stringer and 60 Stringer Basic DOF		
Mode	Freq. (CPM)	Freq.	Error	Shape	Freq.	Error	Shape	Freq.	Error	Shape	Freq.	Error	Shape
1st Lateral	910	1207	33%	G	1466	60%	P	1435	58%	P	1440	58%	P
1st Vertical	1155	1175	2%	E	1282	11%	E	1242	8%	E	1241	8%	E
XSSN Pitch	1490	1709	13%	E	1710	13%	E	1748	17%	E	1758	17%	E
2nd Vertical	1950	2150	10%	G	2390	22%	F	2505	28%	F	2577	32%	F
XSSN Roll	2000	2405	20%	P	2870	43%	P	2900	45%	P	2894	45%	P
XSSN Vertical	2150	2250	4%	F									
Torsion	2300	2763	20%	F	2428	6%	P/F	2422	6%	P/F	2445	6%	P/F

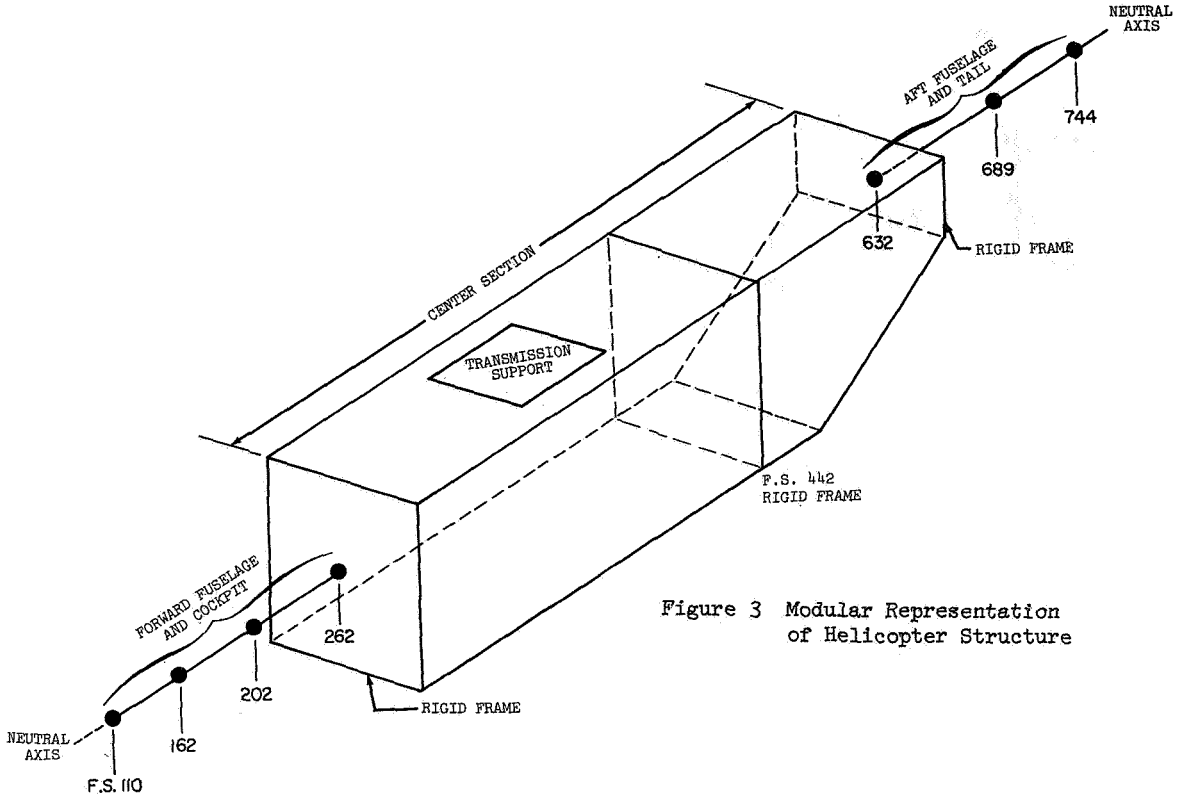

Figure 3 Modular Representation of Helicopter Structure

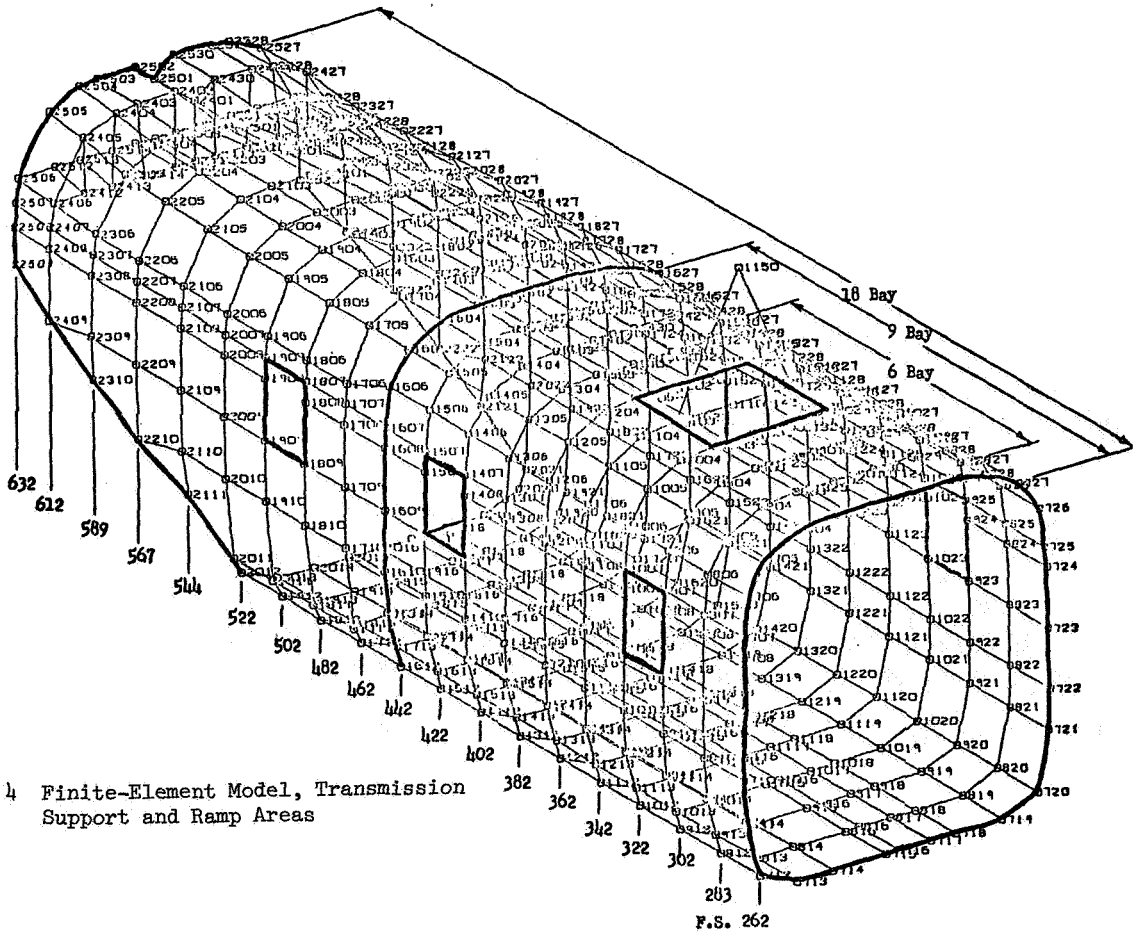

Figure 4 Finite-Element Model, Transmission Support and Ramp Areas

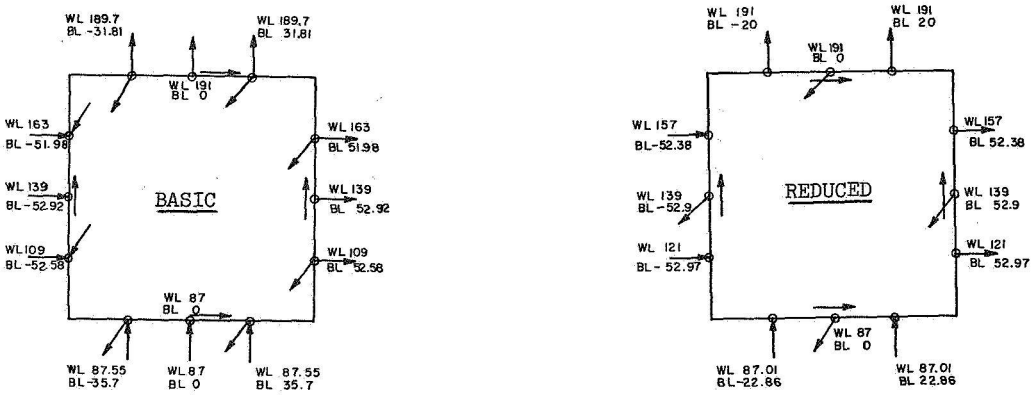

Figure 5 Degree of Freedom Locations for Basic and Reduced Dynamic Degree of Freedom Models

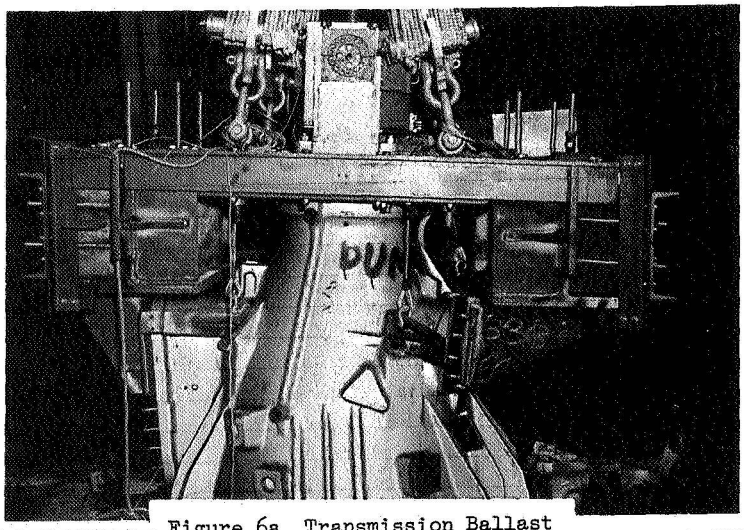

Figure 6a Transmission Ballast Installation

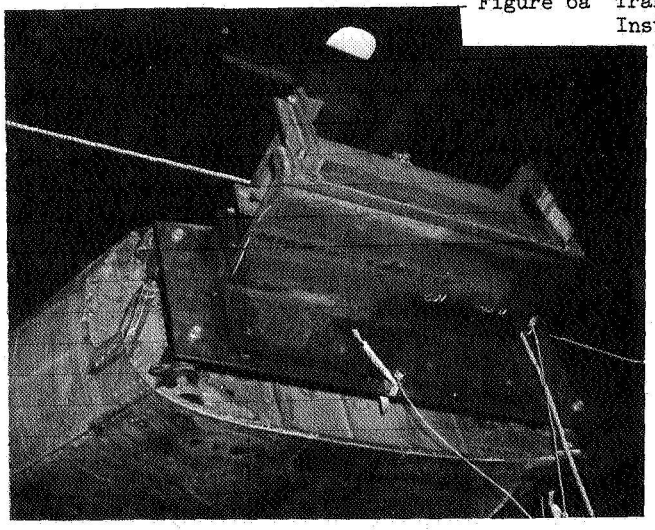

Figure 6b Tail Ballast Installation

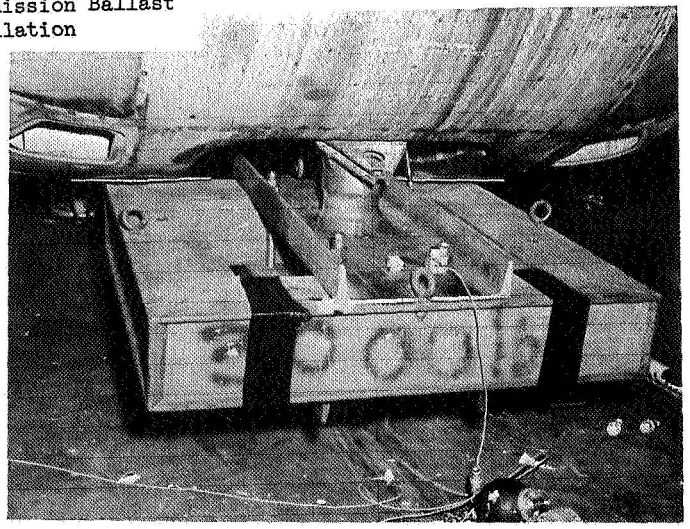

Figure 6c Nose Ballast Installation

Figure 6 Phase II Ballast Installations

TABLE II - SHAKE TEST FREQUENCIES

MODE	PHASE II TEST FREQUENCY CPM	PHASE I TEST FREQUENCY
1st Vertical Bending	440	1155
1st Lateral Bending	615	910
Transmission Pitch	740	1490
Nose Block Lateral/Roll	930	—
Nose Block Vertical/Coupled	970	—
Forward Cabin/Nose Block Lateral	990	—
Nose Block Vertical	1050	—
Second Vertical Bending	1290	1950
Torsion	1310	2300
Transmission/Ramp Vertical Bending	1425	2150
Ramp Vertical Bending	1640	—

TABLE III

PHASE II CORRELATION SUMMARY

VERTICAL/PITCH MODES

MODE	Frequency Test	FRAN	Error	Shape	NASTRAN	Error	Shape
1st Vertical Bending	440	438	0%	E	453	3%	E
Transmission Pitch	740	751	1.5%	G	785	6%	G
Nose Block Vertical/ Transmission Pitch	970	933	4%	G	956	1.5%	G
Nose Block Vertical	1050	1043	1%	F	1063	1%	F
Second Vertical	1290	1523	18%	F	1608	25%	F
Transmission Vertical/ Ramp Vertical	1425	1563	10%	F/G	1843	29%	F/G
Ramp Vertical	1640	1394	15%	P/F	1355	17%	P/F

LATERAL/TORSION MODES

1st Lateral Bending	615	659	7%	G	595	3%	G
Nose Block Lateral/Roll	930	735	21%	P	812	13%	P
Forward Cabin Lateral/ Nose Block Lateral	990	858	13%	P	970	2%	P
Torsion	1310	1601	22%	P	1325	1%	P

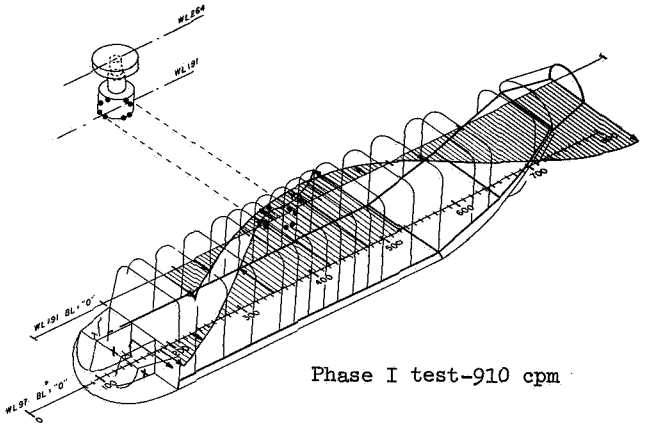

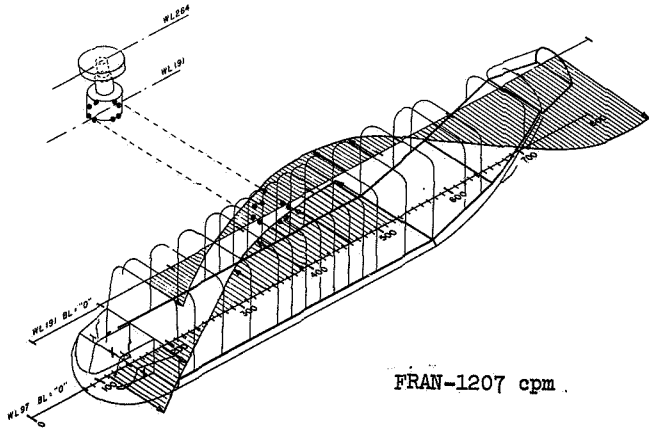

Figure 7a Correlation of First Lateral Bending Mode, Phase I - Stripped

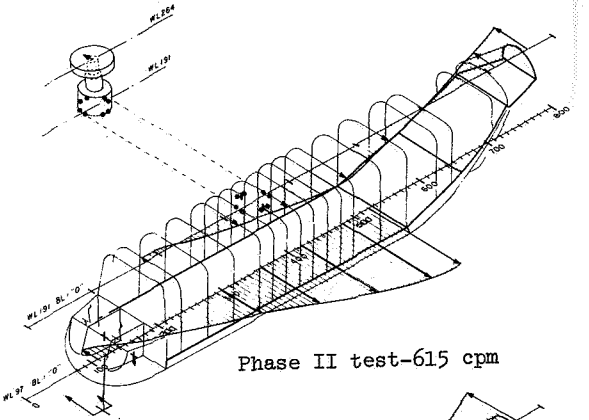

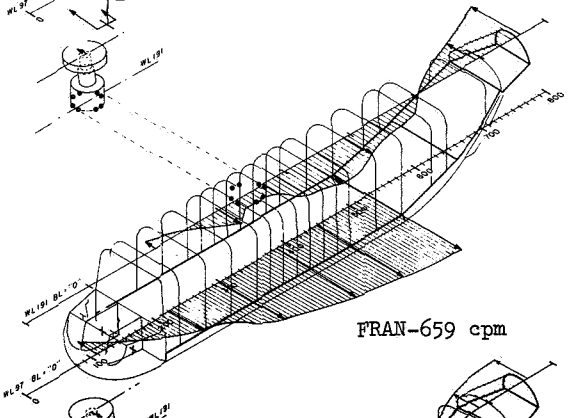

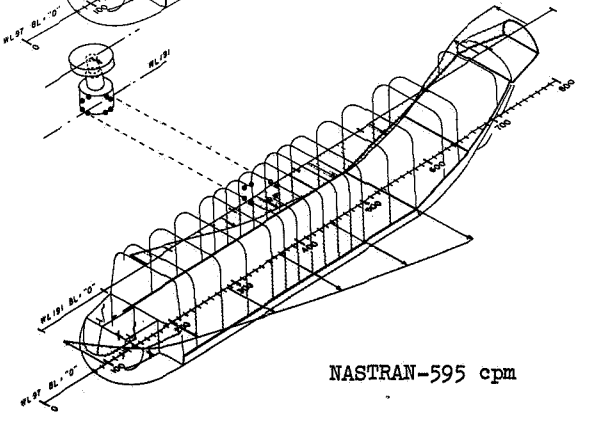

Figure 7b Correlation of First Lateral Bending Mode, Phase II - Ballasted

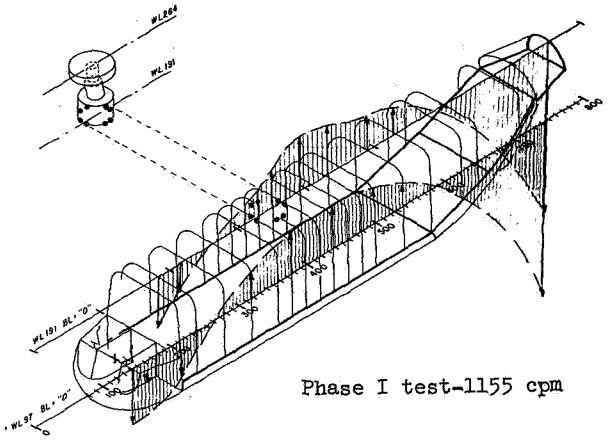

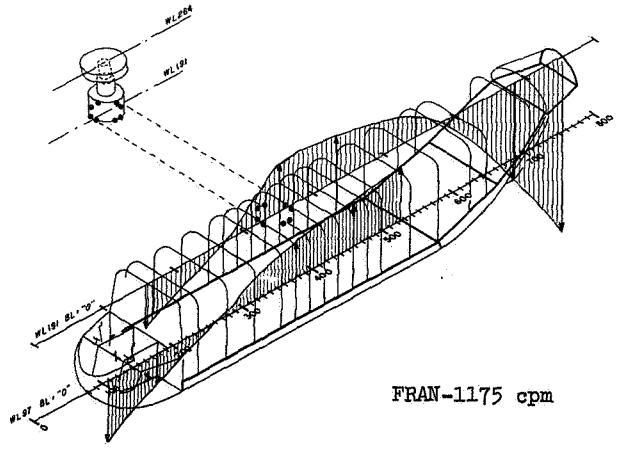

Figure 8a Correlation of First Vertical Bending Mode, Phase I - Stripped

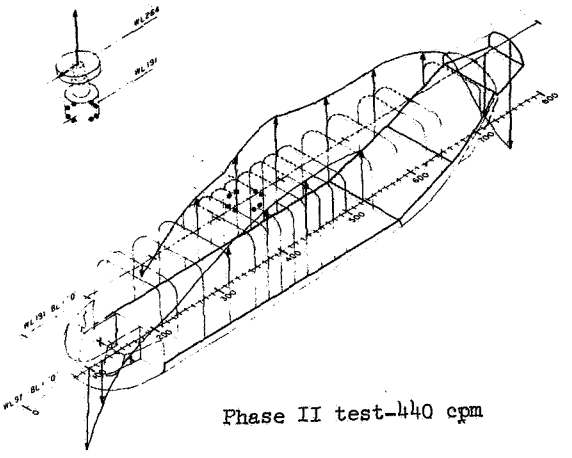

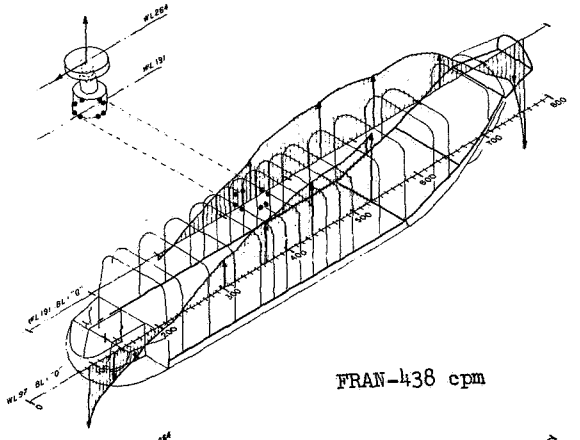

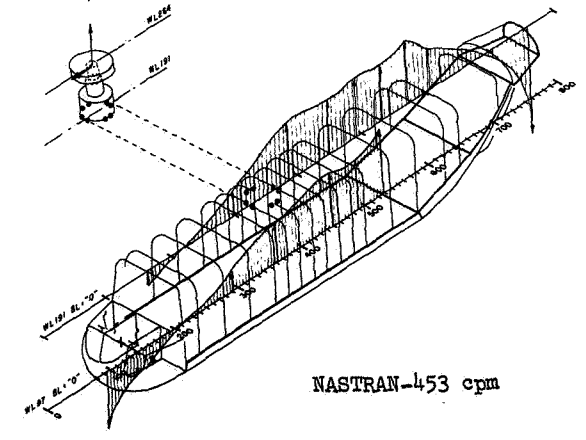

Figure 8b Correlation of First Vertical Bending Mode, Phase II - Ballasted

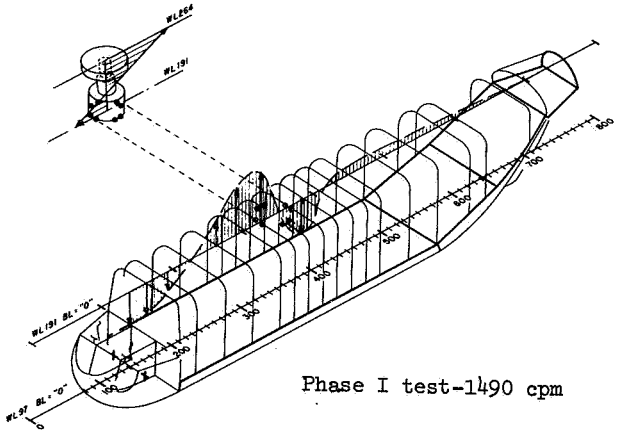

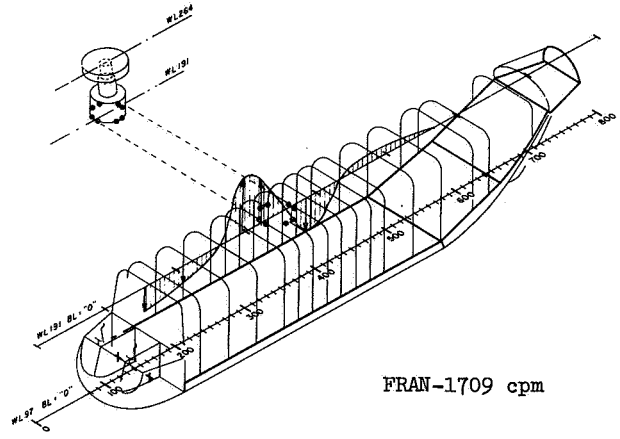

Figure 9a Correlation of Transmission Pitch Mode, Phase I - Stripped

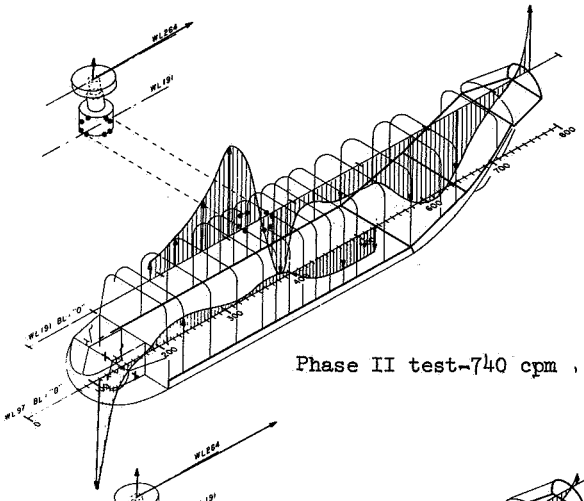

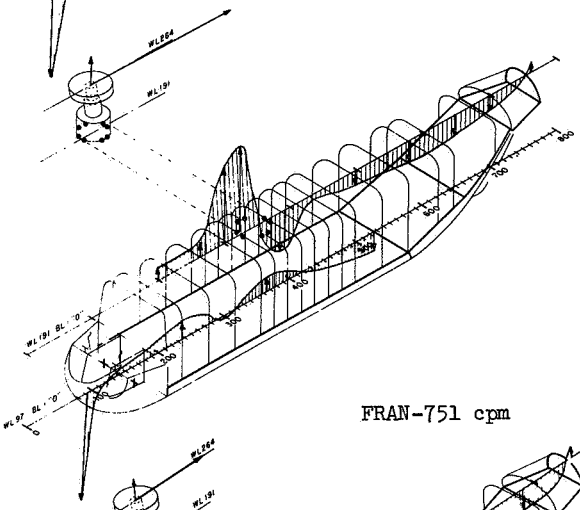

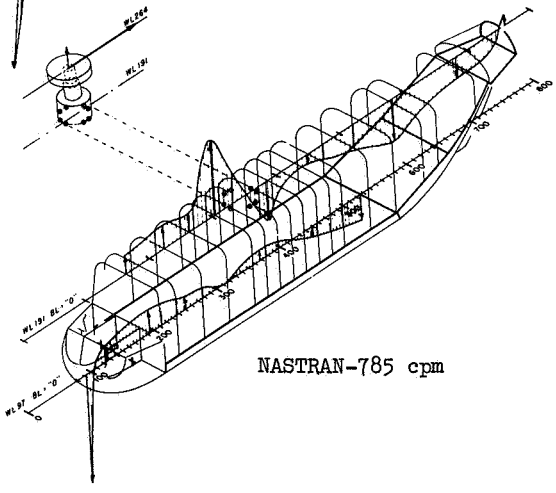

Figure 9b Correlation of Transmission Pitch Mode, Phase II - Ballasted

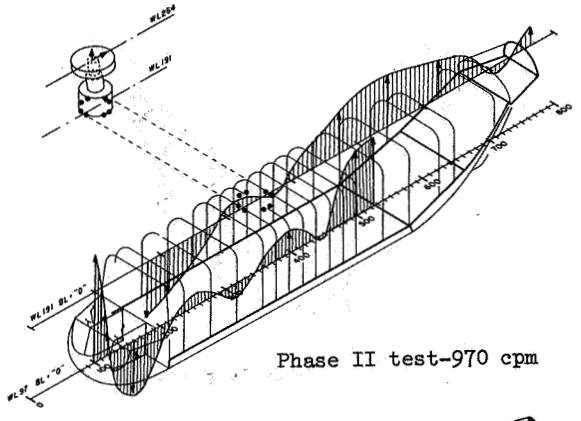

Phase II test-970 cpm

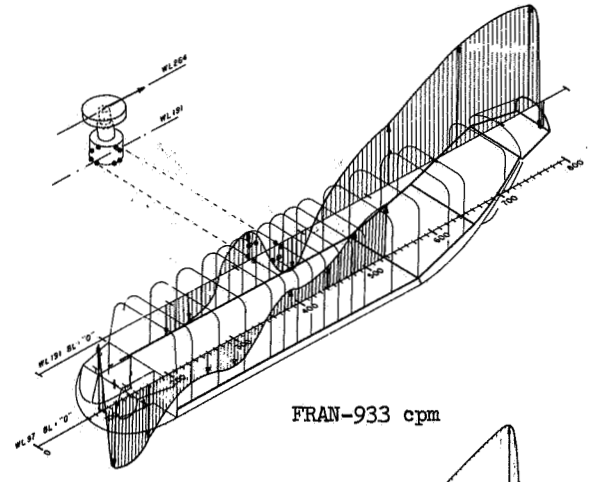

FRAN-933 cpm

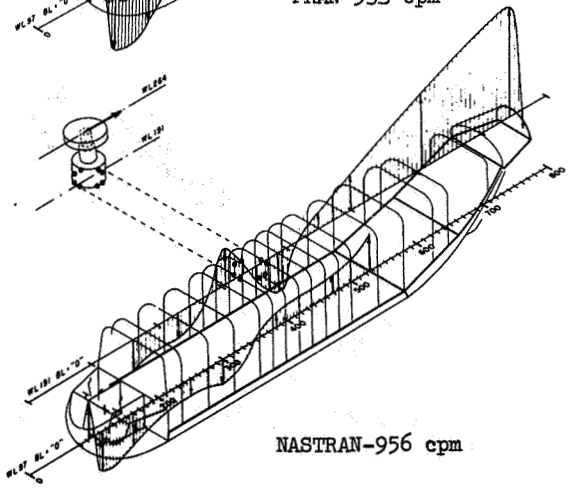

NASTRAN-956 cpm

Figure 10 Correlation Nose Block Vertical/Transmission Pitch Mode, Phase II - Ballasted

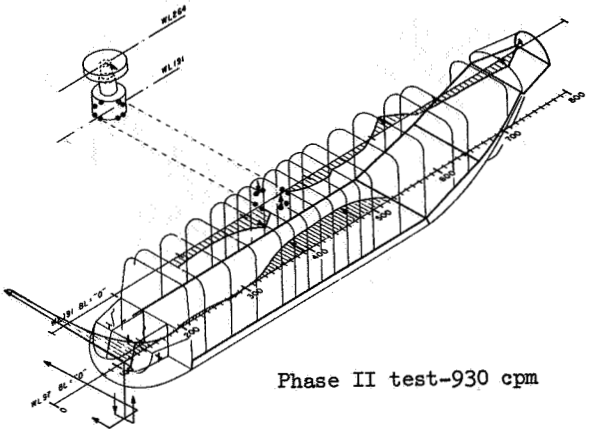

Phase II test-930 cpm

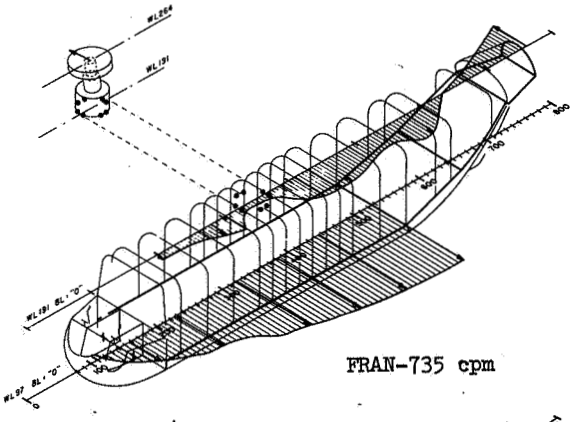

FRAN-735 cpm

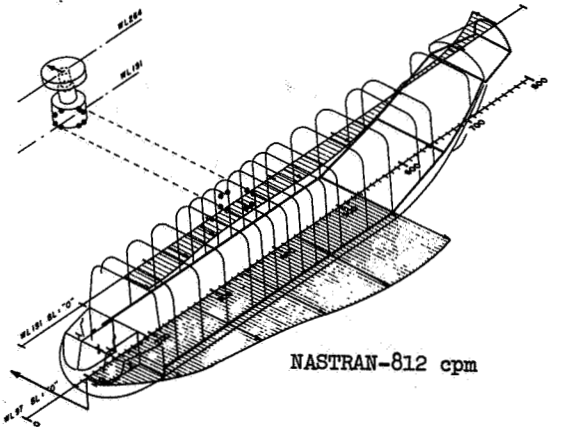

NASTRAN-812 cpm

Figure 11 Correlation of Nose Block Lateral/Roll Mode, Phase II - Ballasted

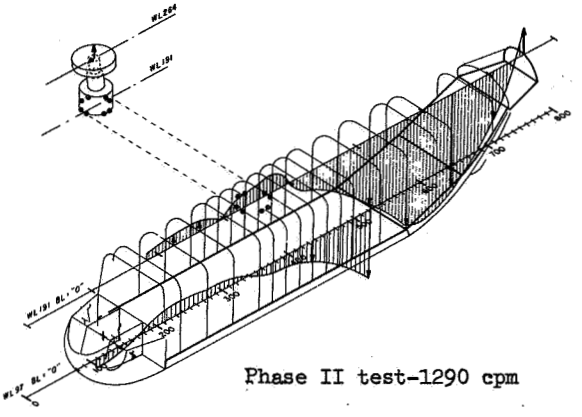

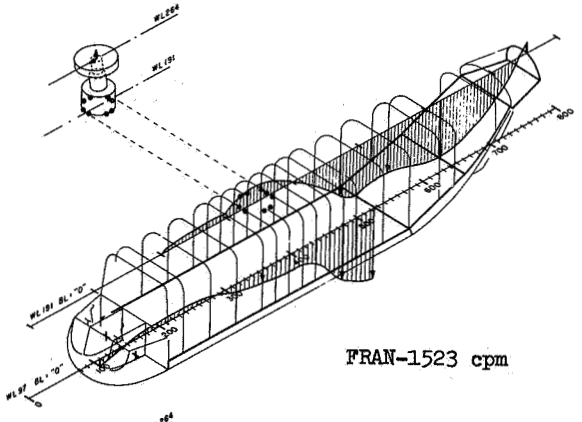

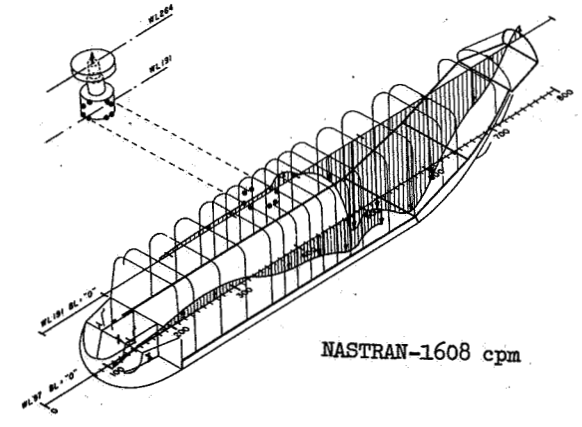

Figure 12 Correlation of Second Vertical Bending Mode, Phase II - Ballasted

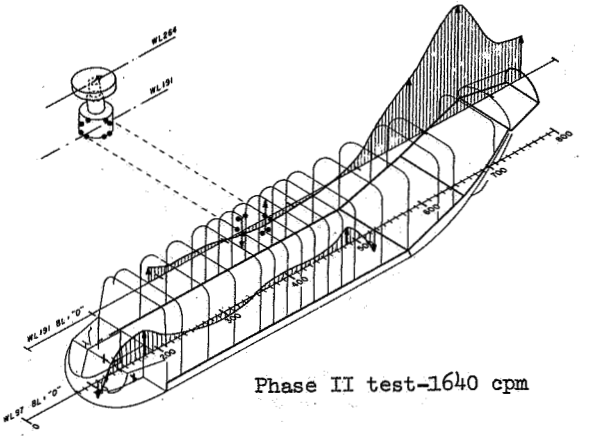

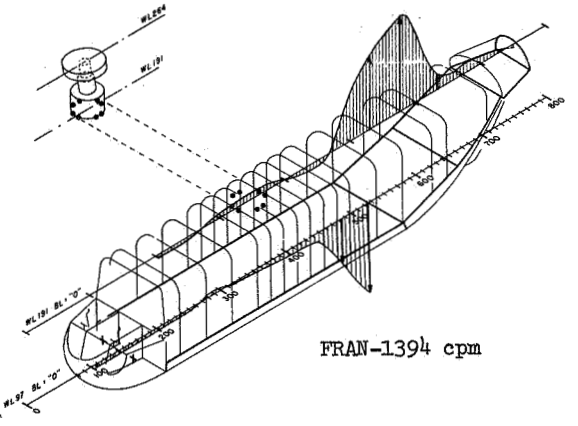

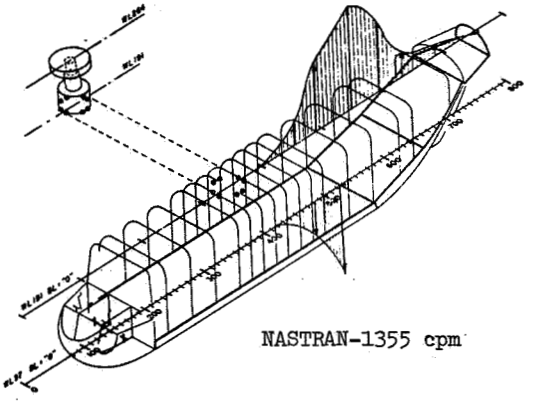

Figure 13 Correlation of Ramp Vertical Bending Mode, Phase II - Ballasted

COUPLED ROTOR/AIRFRAME VIBRATION PREDICTION METHODS

J. A. Staley
Senior Dynamics Engineer

J. J. Sciarra
Senior Structures Engineer

Boeing Vertol Company
Philadelphia, Pa.

Abstract

The problems of airframe structural dynamic representation and effects of coupled rotor/airframe vibration are discussed. Several finite element computer programs (including NASTRAN) and methods for idealization and computation of airframe natural modes and frequencies and forced response are reviewed. Methods for obtaining a simultaneous rotor and fuselage vibratory response, determining effectiveness of vibration control devices, and energy methods for structural optimization are also discussed. Application of these methods is shown for the vibration prediction of the Model 347 helicopter.

Notation

A - airframe mobility matrix
B - rotor impedance matrix
EI - blade bending rigidity
F - force
GJ - blade torsional rigidity
I - identity matrix
k - rotor frequency multiple, 1, 2, etc.
K - stiffness matrix
M - mass matrix
q - airframe mode generalized coordinate
X - airframe displacements
m - airframe mode generalized mass
ω - airframe mode natural frequency
ϕ - airframe mode shape (eigen vector)
Ω - rotor frequency
[] - matrix
{} - column vector

Subscripts

A - absorber, airframe
c - cosine component amplitude
H - hub
k - rotor frequency multiple, 1, 2, etc.
n - airframe mode number
o - zero hub motion
R - rotor
s - sine component

Superscripts

. - velocity
.. - acceleration
T - transpose

Presented at the AHS/NASA-Ames Specialists' Meeting on Rotorcraft Dynamics, February 13-15, 1971.

Part of the work presented in this paper was funded by the U.S. Army Research Office - Durham, North Carolina under Contract DAHC04-71-C-0048.

Prediction of helicopter airframe vibration involves two major problem areas:

- Prediction of rotor vibratory hub loads
- Prediction of airframe dynamic characteristics.

The effects of vibratory hub motion on vibratory hub loads and effects of vibration control devices and resulting airframe fatigue stresses must also be considered.

Methods for independent prediction of vibratory hub loads and airframe dynamic characteristics have been developed previously and are discussed briefly below. Independent determination of rotor vibratory loads and airframe vibratory response to these loads does not account for any interaction between airframe vibratory motion on rotor vibratory loads. One approximate method for accounting for these interactions is to assume that an effective rotor mass is attached to the airframe at the rotor hub. A more direct method is to compute (or measure) the rotor hub impedance and determine compatible vibratory hub loads and hub motions. This method is discussed below. A simple example of compatible rotor load-hub motion is given for a single rotor helicopter with vertical hub motion. In addition, flight test results for the Model 347 helicopter are compared with vibration predictions obtained using a coupled rotor/airframe vibration computer program.

Rotor Vibratory Hub Loads

Methods and digital computer programs have been developed for prediction of rotor vibratory hub loads for constant speed level flight conditions [1,2,3]. Rotor blades are represented by lumped parameter analytical models as indicated

in Figure 1. Iteration techniques are used to compute individual blade deflections and aerodynamic and inertia load distributions at integer multiples of the rotor rotating frequency. The total rotating and fixed system rotor vibratory hub loads are obtained by summing individual blade root shears and moments. The vibratory hub loads may be computed assuming no hub motion. If the vibratory hub motions are known, effects of these motions may be included when computing blade aerodynamic and inertia loads.

Airframe Dynamics

Structural Model, Natural Modes and Frequencies, and Forced Response

Finite element methods have been used in the helicopter industry for some time for prediction of airframe dynamic characteristics[4]. As indicated in Figure 2, developing a finite element airframe model consists of:

- Defining nodal data
- Defining elastic properties of members connecting nodes
- Defining mass properties associated with each node.

Nodal data and properties of structural members are used to develop stiffness matrices for individual members. These matrices relate forces at each node to nodal displacements. The stiffness matrices for individual members are superimposed to obtain the stiffness matrix for the entire airframe.

Most of the degrees of freedom are reduced from the airframe gross stiffness matrix. Mass properties are concentrated at the remaining (retained) degrees of freedom. Equations (1) are the airframe equations of motion with the gross stiffness matrix. Equations (3) are the airframe equations of motion, in terms of the reduced stiffness matrix.

$$\begin{bmatrix} M & 0 \\ 0 & 0 \end{bmatrix} \begin{Bmatrix} \ddot{X}_1 \\ \ddot{X}_2 \end{Bmatrix} + \begin{bmatrix} K_{11} & K_{12} \\ K_{21} & K_{22} \end{bmatrix} \begin{Bmatrix} X_1 \\ X_2 \end{Bmatrix} = \begin{Bmatrix} F_R \\ 0 \end{Bmatrix} \quad (1)$$

$$\left[\bar{K}_{11}\right] = \left[K_{11}\right] - \left[K_{12}\right]\left[K_{22}\right]^{-1}\left[K_{21}\right] \quad (2)$$

$$\left[M\right]\left\{\ddot{X}_1\right\} + \left[\bar{K}_{11}\right]\left\{X_1\right\} = \left\{F_R\right\} \quad (3)$$

The solution for natural modes and frequencies is made using the reduced stiffness matrix and the mass matrix associated with the retained degrees of freedom.

The airframe motions are expressed in terms of natural modes:

$$\left\{X_1\right\} = \left[\phi\right]\left\{q\right\} \quad (4)$$

and, after assuming sinusoidal motion with no external forces, Equation (3) becomes:

$$\omega_n^2\left\{\phi_n\right\} = \left[M\right]^{-1}\left[\bar{K}_{11}\right]\left\{\phi_n\right\} \quad (5)$$

The modal generalized mass is then computed. A value of modal damping is assumed for each mode, and these modal properties are used to compute airframe response to vibratory hub loads:

$$m_n = \left\{\phi_n\right\}^T\left[M\right]\left\{\phi_n\right\} \quad (6)$$

$$\ddot{q}_n + 2\zeta_n\omega_n\dot{q}_n + \omega_n^2 q_n = \left\{\phi_{Rn}\right\}^T\left\{F_R\right\}/m_n \quad (7)$$

Substructures Method

A large saving in computer time can be realized by performing the matrix reduction process on several smaller substructure stiffness matrices instead of on the large stiffness matrix for the entire airframe. In one application, use of the substructures method reduced computer running time from about ten to two hours on an IBM 360/65 computer.

The airframe is divided into several substructures, and all but mass and boundary degrees of freedom are reduced from the stiffness matrix of each substructure. The stiffness matrices of the substructures are then merged (superimposed or added just as they are for individual members) to form a stiffness matrix for the entire airframe. Any degree of freedom on the boundaries may be reduced after merging the substructure matrices (Figure 3).

NASTRAN

New developments in finite element analysis have been occurring on a continuous basis. New programs and new structural elements, both dynamic and stress analysis capability, FORTRAN programming capability by the engineer within the finite element program, and greater problem size

capability have been developed[5]. NASTRAN (NASA Structural Analysis)[6] is a government developed, maintained, and continually updated finite element program which has apparently provided a solution to the difficulties of developing and maintaining finite element programs by private contractors. NASTRAN is similar to other finite element computer programs except that it generally provides additional capability:

- More types of structural elements
- Common deck for stress and dynamic analysis
- User programming capability
- Transient vibration analysis, buckling, non-linear, and static capability
- Unlimited size capability for mass and stiffness matrices.

For a nominal fee, this program and manuals describing the program and its use are available. NASTRAN provides a standard for airframe dynamic analysis and relieves contractors of some of the problems of maintaining the most up-to-date methods for airframe structural analysis.

Energy Methods for Structural Optimization

One further development related to airframe dynamics is the Damped Forced Response Method[7,8]. The airframe forced response is computed, and structural members with significant strain energy are identified. These members are changed to reduce vibration response for modes with frequencies above and below the rotor exciting frequency. This method is outlined in Figure 4.

Vibration Control Devices

Vibration control devices such as absorbers are often used to reduce vibration in local areas of the airframe. The force output for an absorber may be computed by expressing the vibration as the sum of vibration due to rotor forces and the vibration due to the force output by the absorber.

$$\begin{Bmatrix} X_A \\ X_R \end{Bmatrix} = \begin{bmatrix} A_{AA} & A_{AR} \\ A_{RA} & A_{RR} \end{bmatrix} \begin{Bmatrix} F_A \\ F_R \end{Bmatrix} \qquad (8)$$

The absorber force output required to null vibration at the absorber attachment point is

$$\{F_A\} = -[A_{AA}]^{-1}[A_{AR}]\{F_R\} \qquad (9)$$

The corresponding motions at the rotor hub are

$$\{X_R\} = [A_{RR} - A_{RA} A_{AA}^{-1} A_{AR}]\{F_F\} \qquad (10)$$

The mobility matrices in the above equations may be obtained analytically using computed modal properties (Equations (1) through (7)) or by applying unit vibratory loads to the airframe in a series of shake tests.

This method was applied to prediction of cockpit vibration with a vertical cockpit absorber for the Model 347 helicopter[8]. Analytical and flight test results are compared in Figure 5.

Coupled Rotor/Airframe Analysis

Theory

Any vibratory motion of the rotor hub will change the rotor blade vibratory aerodynamic and inertia forces which are summed to obtain vibratory hub loads. Changes in hub loads will in turn cause changes in vibratory hub motions[9,10].

Airframe Motion is assumed to be related to vibratory hub loads by a mobility matrix for a particular exciting frequency:

$$\begin{Bmatrix} X_{ks} \\ X_{kc} \end{Bmatrix} = \begin{bmatrix} A_{k11} A_{k12} \\ A_{k21} A_{k22} \end{bmatrix} \begin{Bmatrix} F_{ks} \\ F_{kc} \end{Bmatrix} = [A_k] \begin{Bmatrix} F_{ks} \\ F_{kc} \end{Bmatrix} \qquad (11)$$

where

$$\{X_k\} = \{X_{ks}\} \sin k\Omega t + \{X_{kc}\} \cos k\Omega t$$

$$\{F_k\} = \{F_{ks}\} \sin k\Omega t + \{F_{kc}\} \cos k\Omega t$$

The airframe mobility data are airframe responses to unit vibratory hub loads; these data may be obtained analytically by using theoretical modal properties (Equation (4) through (7)), or by conducting an airframe shake test. It is emphasized that these are airframe response characteristics for no blade mass attached to the airframe at the rotor hub. All blade inertia effects will be included in the rotor vibratory hub loads as modified by vibratory hub motion.

In general, six sine and six cosine components of shaking forces and moments exist at each rotor hub; a tandem rotor helicopter would have a total of 24

components of vibratory forces. If only the rotor hub motions are considered, the relationship between hub motion and hub forces is:

$$\underset{24x1}{\begin{Bmatrix} X_{Hks} \\ X_{Hkc} \end{Bmatrix}} = \underset{24x24}{\begin{bmatrix} A_{Hk} \end{bmatrix}} \underset{24x1}{\begin{Bmatrix} F_{ks} \\ F_{kc} \end{Bmatrix}} \qquad (12)$$

The vibratory hub loads are assumed to be loads with no hub motion plus an increment of hub loads proportional to hub motion:

$$\underset{24x1}{\begin{Bmatrix} F_{ks} \\ F_{kc} \end{Bmatrix}} = \underset{24x1}{\begin{Bmatrix} F_{kso} \\ F_{kco} \end{Bmatrix}} + \underset{24x24}{\begin{bmatrix} B_{k11} & B_{k12} \\ B_{k21} & B_{k22} \end{bmatrix}} \underset{24x1}{\begin{Bmatrix} X_{Hks} \\ X_{Hkc} \end{Bmatrix}} \qquad (13)$$

$$= \begin{Bmatrix} F_{kso} \\ F_{kco} \end{Bmatrix} + \begin{bmatrix} B_k \end{bmatrix} \begin{Bmatrix} X_{Hks} \\ X_{Hkc} \end{Bmatrix}$$

The coefficients of the B matrix are obtained by making several computations of vibratory hub loads:

- Components of vibratory hub loads are computed assuming no hub motion
- Components of vibratory hub loads are computed assuming a small vibratory hub motion at the frequency for each degree of freedom of hub motion at each rotor
- Changes in sine and cosine components of vibratory hub forces per unit vibratory hub motion in each rotor hub degree of freedom are then computed.

The coupled rotor/airframe solution for compatible rotor hub motions and rotor hub loads is obtained by substituting Equation (13) in Equation (12) and solving for vibratory hub motions:

$$\begin{Bmatrix} X_{Hks} \\ X_{Hkc} \end{Bmatrix} = \left[[I] - [A][B] \right]^{-1} [A] \begin{Bmatrix} F_{kso} \\ F_{kco} \end{Bmatrix} \qquad (14)$$

Once a solution for Equation (14) is obtained, the total vibratory hub loads may be computed using Equation (13) and the vibration for the entire airframe may be computed using Equation (11).

Single Rotor Example

Figure 6 shows a simple example of the coupled rotor airframe method applied to a single rotor helicopter vertical vibration analysis. Hub vertical vibration response and the vertical vibratory hub loads are computed at a frequency of four times rotor speed (4/rev). The airframe is represented by its rigid body vertical mode and one flexible mode. Figure 6b shows airframe mobilities vs flexible mode natural frequency for 4/rev vertical hub forces. Hub vertical shaking forces vs hub vertical motion are shown in Figure 6c. The vibratory hub loads are seen to vary approximately linearly at least up to .005 inches of motion at the 4/rev frequency. Figures 6d and 6e show compatible rotor hub vertical vibration amplitudes and rotor hub shaking forces vs flexible mode natural frequency.

For this example, the rotor vibratory hub motions and forces both peak when the flexible mode natural frequency is just above the rotor hub force exciting frequency. This is not a general result, but depends upon the relationships between hub shaking forces and hub motions.

Coupled Rotor/Airframe Analysis Computer Program (D-65)

Figure 7 shows the flow-diagram for the Boeing Vertol D-65 Coupled Rotor/Airframe Analysis computer program. This program links three major computer programs[10]:

- Trim analysis program A-97
- Rotor vibratory hub loads analysis program D-88
- Airframe forced response analysis program D-96.

Compatible fuselage motions and vibratory hub loads are obtained using this program with the method discussed above. In its current state, the D-65 program computes three vibratory rotor forces and three vibratory rotor moments at each rotor for either single or tandem rotor helicopters. Response to translational and rotational vibratory hub forces is computed for the airframe, but compatibility of hub forces and motions is satisfied for hub translational degrees of freedom only in the current version of the program. The program will be modified in the near future to provide compatibility for hub rotational degrees of freedom.

Analysis vs Test Results for the Model 347 Helicopter

The D-65 coupled rotor/airframe program was used to predict Model 347 flight vibration levels. Figure 8 shows the model used to predict airframe dynamic characteristics. Figure 9 compares predicted vertical and lateral cockpit vibration levels vs vibration levels measured in flight. Vertical vibration levels are in reasonably good agreement at high airspeeds where vibration levels may become significant. Lateral vibration levels are higher than predicted.

Conclusions

Methods have been developed independently for prediction of rotor vibratory hub loads and airframe dynamic characteristics. Methods are available for including effects of vibration control devices on airframe vibration and for optimizing the airframe structure. The substructure method is available for minimizing computer running time in analysis of airframe structures, and NASTRAN now provides a common finite element structural analysis program available to all aerospace contractors. Rotor hub vibratory motions can modify rotor hub vibratory forces acting on the airframe. A linear coupled rotor/airframe analysis method provides an approach for determing compatible hub motions and hub shaking forces. This method should be studied further to determine its validity. A method of this type should be considered in applications of NASTRAN for prediction of helicopter vibration; the user programming feature in NASTRAN should permit a coupled rotor/airframe solution of this type within NASTRAN.

Figure 10 shows a scheme for solving for rotor trim, rotor forces with no hub motion, and the rotor impedance matrix using a rotor analysis program. NASTRAN would be programmed to use these mobilities and the rotor analysis results to solve for compatible rotor/airframe loads and motions. The NASTRAN airframe analysis could include airframe installed vibration control devices either in the initial airframe analysis or in the coupled rotor/airframe solution. Finally, results of these analyses could be used to determine optimum changes to the airframe structural elements for minimizing airframe vibration.

References

1. Leone, P. F., THEORY OF ROTOR BLADE UNCOUPLED FLAP BENDING OF AEROELASTIC VIBRATIONS, 10th American Helicopter Society Forum, Washington, D.C., 1954.
2. Boeing Vertol Company, D8-0614, AEROELASTIC ROTOR ANALYSIS, D-95, Thomas, E., and Tarzanin, F., 1967.
3. Boeing Vertol Company, D210-10378-1, & -2, AEROELASTIC ROTOR ANALYSIS, C-60, Tarzanin F. J., Ranieri, J. (to be published).
4. Sciarra, J. J., DYNAMIC UNIFIED STRUCTURAL ANALYSIS METHOD USING STIFFNESS MATRICES, AIAA/ASME 7th Structures and Materials Conference, April 1966.
5. The Boeing Company, D2-125179-5, THE ASTRA SYSTEM--ADVANCED STRUCTURAL ANALYSIS, Vol. 5, User's Manual.
6. NASA SP-222 (01), NASTRAN USER'S MANUAL, McCormick, Caleb W., National Aeronautics and Space Administration, Washington, D.C., 1972.
7. Sciarra, J. J., and Ricks, R. G., USE OF THE FINITE ELEMENT DAMPED FORCED RESPONSE STRAIN ENERGY DISTRIBUTION FOR VIBRATION REDUCTION, ARO-D Military Theme Review, Moffett Field, California, U.S. Army Research Office, September 1972.
8. Sciarra, J. J., APPLICATION OF IMPEDANCE METHODS TO HELICOPTER VIBRATION REDUCTION, Imperial College of Science and Technology, London, England, July 1973.
9. Gerstenberger, W., and Wood, E. R., ANALYSIS OF HELICOPTER CHARACTERISTICS IN HIGH SPEED FLIGHT, American Institute of Aeronautics and Astronautics Journal, Vol. 1, No. 10, October 1963, pp 2366-2381.
10. Novak, M. E.,ROTATING ELEMENTS IN THE DIRECT STIFFNESS METHOD OF DYNAMIC ANALYSIS WITH EXTENSIONS TO COMPUTER GRAPHICS,40th Symposium on Shock and Vibration, Hampton, Virginia, October 1969.

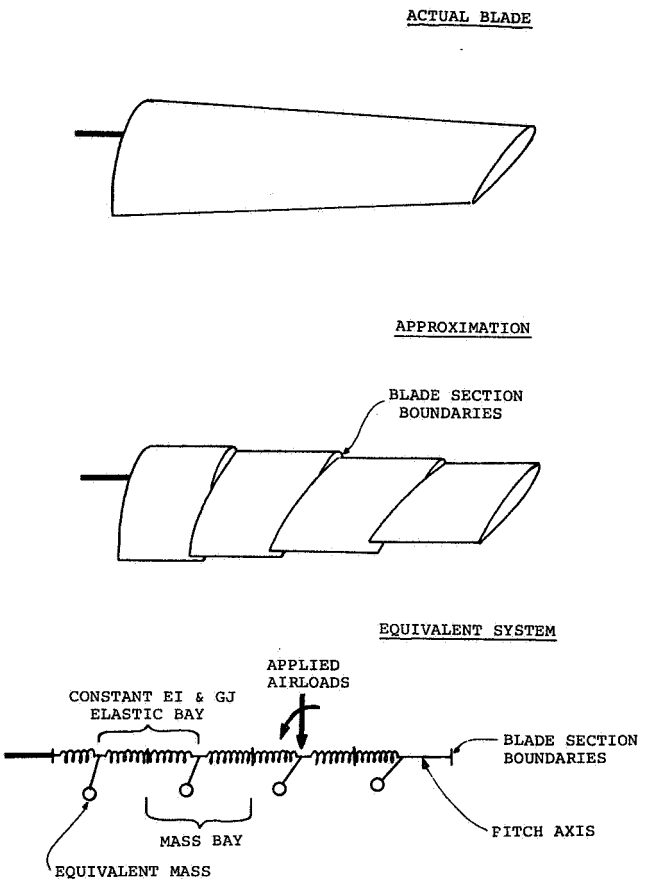

Figure 1. Rotor Blade Analytical Model

- AIRFRAME INPUT DATA
  - -NODAL COORDINATES AND CONSTRAINTS
  - -STRUCTURAL ALEMENT PROPERTIES
  - -MASS AND INERTIA PROPERTIES
- STRUCTURAL ANALYSIS
  - -FORM MEMBER STIFFNESS MATRICES AND ADD TO OBTAIN THE AIRFRAME GROSS STIFFNESS MATRIX
  - -REDUCE NON-MASS DEGREES OF FREEDOM FROM GROSS STIFFNESS MATRIX
- COMPUTE AIRFRAME NATURAL MODES AND FREQUENCIES AND GENERALIZED MASSES
- ROTOR VIBRATORY FORCES
- COMPUTE AIRFRAME FORCED RESPONSE

Figure 2. Uncoupled Airframe Dynamic Analysis

INPUT

- NODE NUMBERS, CONSTRAINTS RETAINED, REDUCED DEGREES OF FREEDOM
- STRUCTURAL PROPERTIES OF MEMBERS CONNECTING NODES
- MASSES AND INERTIAS TO BE CONCENTRATED AT RETAINED DEGREES OF FREEDOM FOR MASS MATRIX

ELEMENTS

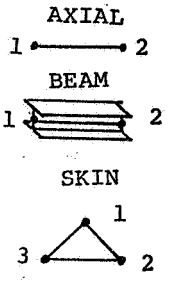

GENERATE STIFFNESS MATRIX, $\bar{K}$

- GENERATE MEMBER STIFFNESS MATRICES AND ADD TO OBTAIN AIRFRAME GROSS STIFFNESS MATRIX
- REDUCE GROSS STIFFNESS MATRIX TO RETAINED DEGREES OF FREEDOM

$$\left[K_G\right] = \begin{bmatrix} K_{11} & K_{12} \\ K_{21} & K_{22} \end{bmatrix} \sim 2000 \times 2000$$

$$\left[\bar{K}_{11}\right] = \left[K_{11} - K_{12}K_{22}^{-1}K_{21}\right] \sim 200 \times 200$$

- LARGEST COMPUTER TIME ASSOCIATED WITH REDUCTION PROCESS

COMPUTE NATURAL MODES, ϕ_n AND FREQUENCIES, ω_n

$$\omega_n^2 \left\{\phi_n\right\} = \left[M\right]^{-1}\left[K\right]\left\{\phi_n\right\}$$

INPUT

ROTOR FORCES, F_R

COMPUTE FORCED RESPONSE, $\{X\}$

$$\{X\} = [\phi]\{q\}$$

$$\ddot{q}_n + 2\zeta_n\omega_n\dot{q}_n + \omega_n^2 q_n = \frac{\{\phi_{nR}\}^T\{F_R\}}{\{\phi_n\}^T[M]\{\phi_n\}} = \frac{\mathcal{F}_n}{\mathcal{M}_n}$$

- COMPUTE RESPONSE OF EACH MODE; ADD TO OBTAIN TOTAL RESPONSE

q_n = MODE GENERALIZED COORDINATE

Figure 2. Continued

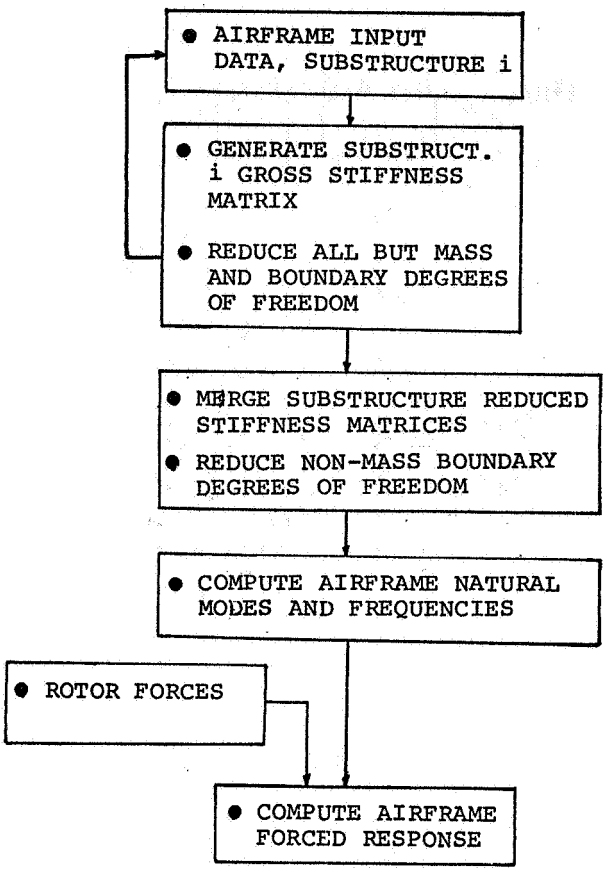

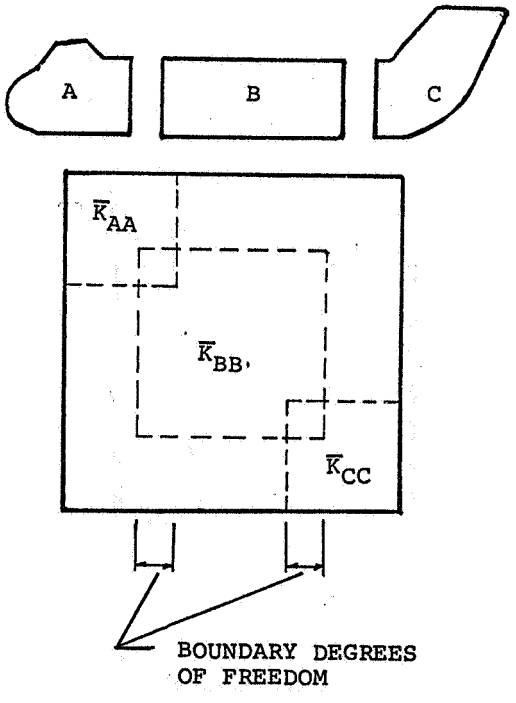

Figure 3. Substructure Method for Generating Airframe Reduced Stiffness Matrix

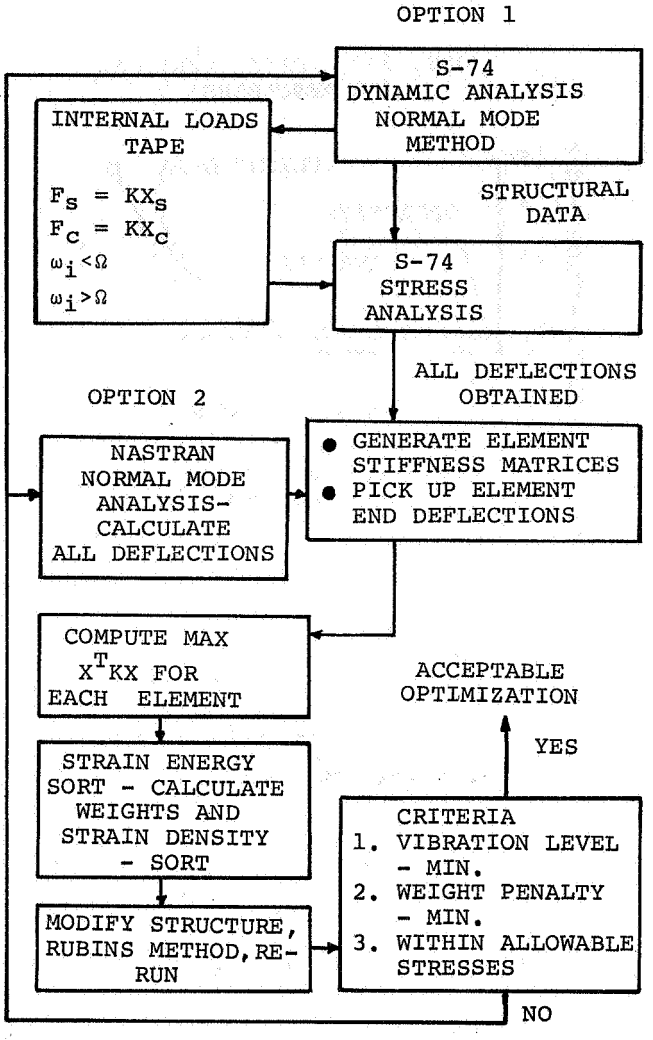

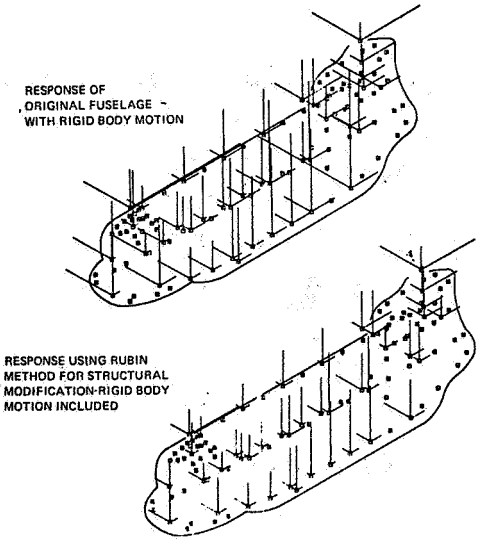

Figure 4. Damped Forced Response Method for Airframe Optimization

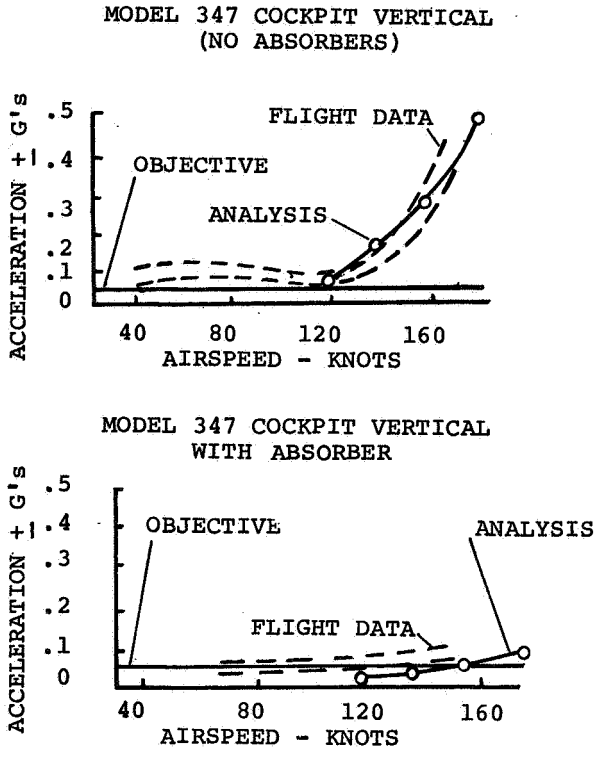

Figure 5. Predicted Vs. Measured Cockpit vibration Reduction with a Vertical Cockpit Absorber

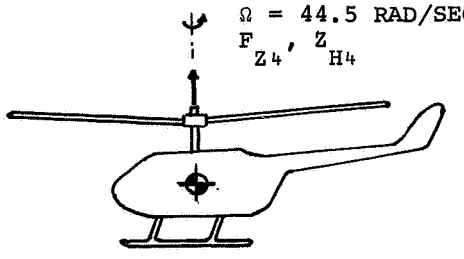

(a) Single Rotor Helicopter Vertical Vibration

$$\begin{Bmatrix} Z_{H4s} \\ Z_{H4c} \end{Bmatrix} = \begin{bmatrix} A_{11} & A_{12} \\ A_{21} & A_{22} \end{bmatrix} \begin{Bmatrix} F_{Z4s} \\ F_{Z4c} \end{Bmatrix} \qquad A_{22} = A_{11} \qquad A_{21} = -A_{12}$$

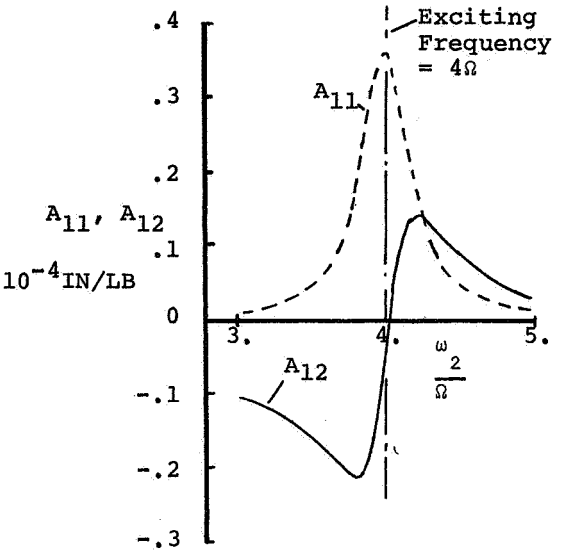

(b) Airframe-Hub Mobilities

$$F_{Z4} = F_{Z4c} \cos 4\Omega t + F_{Z4s} \sin 4\Omega t$$

$$Z_{H4} = Z_{H4c} \cos 4\Omega t + Z_{H4s} \sin 4\Omega t$$

$$\begin{Bmatrix} F_{Z4s} \\ F_{Z4c} \end{Bmatrix} = \begin{Bmatrix} 19.6 \\ -16.5 \end{Bmatrix} + \begin{bmatrix} 20.77 & 1.33 \\ -1.33 & 20.77 \end{bmatrix} \times 10^3 \begin{Bmatrix} Z_{H4s} \\ Z_{H4c} \end{Bmatrix}$$

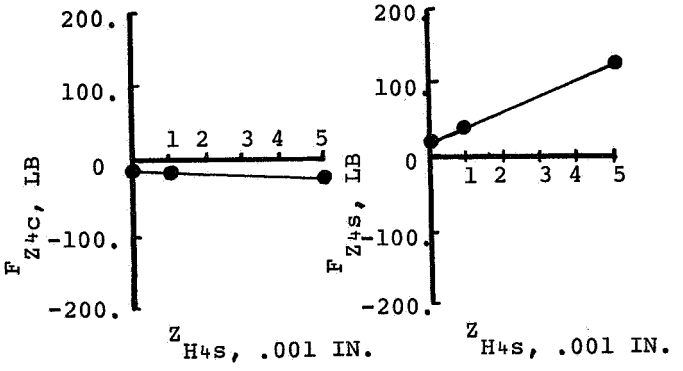

(c) Hub Forces Vs. Hub Motion

Figure 6. Continued

Figure 6. Coupled Rotor/Airframe Analysis for a Single Rotor Helicopter Vertical Vibration

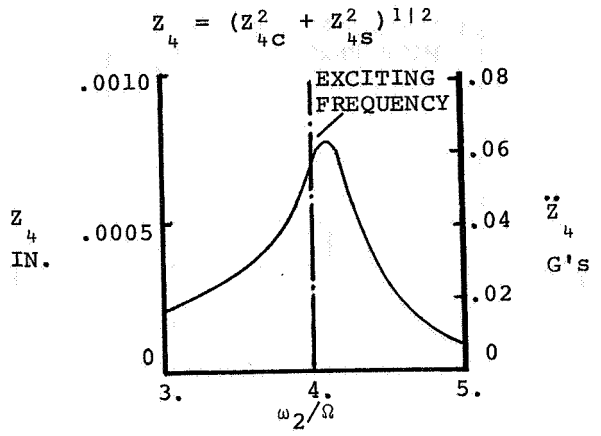

(d) Vibratory Hub Motion

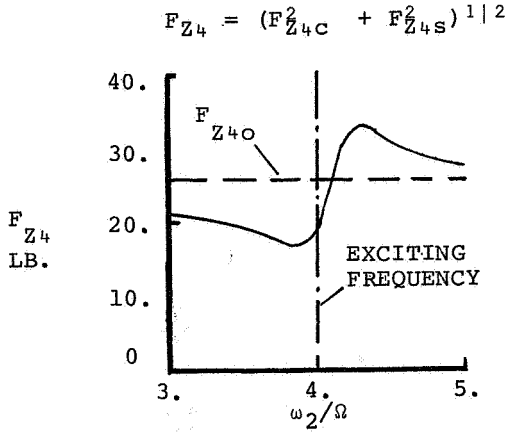

(e) Vibratory Hub Force

Figure 6. Continued

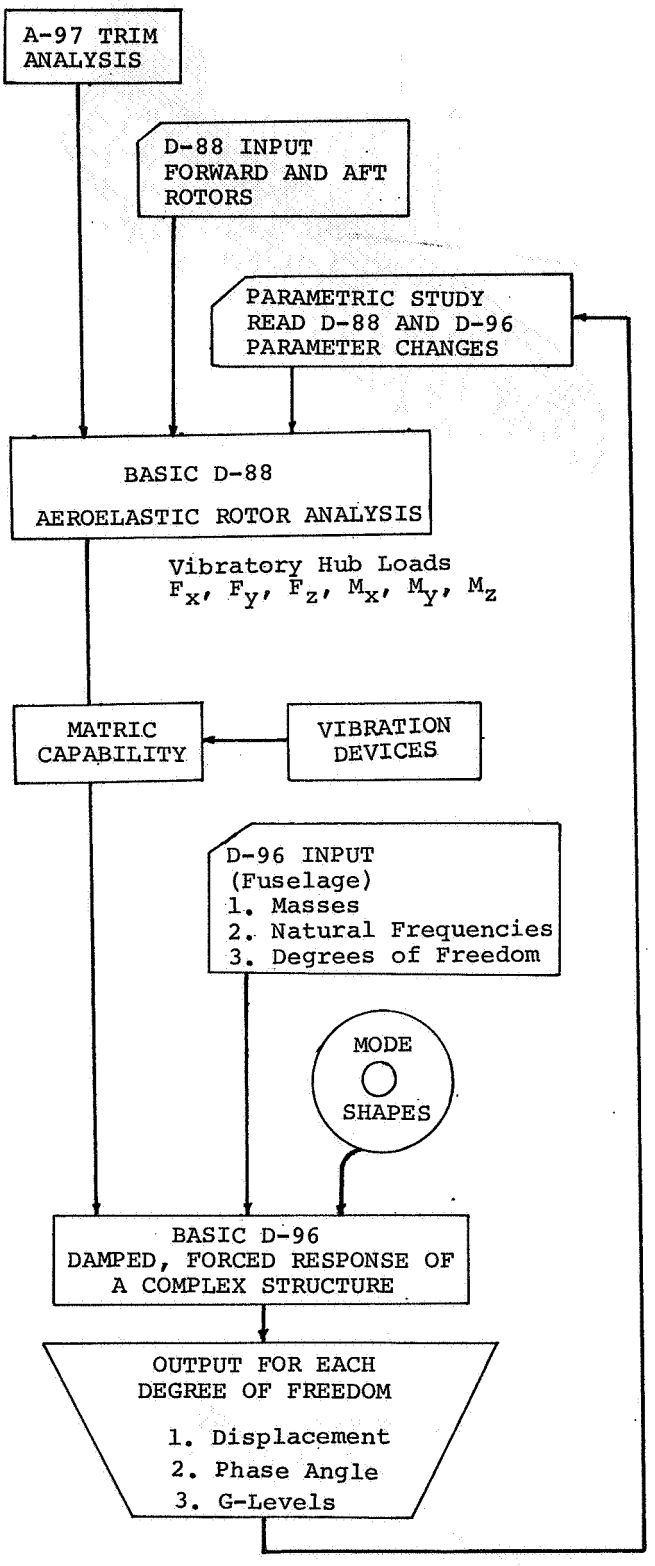

Figure 7. D-65 Coupled Rotor/Airframe Program Flow Diagram

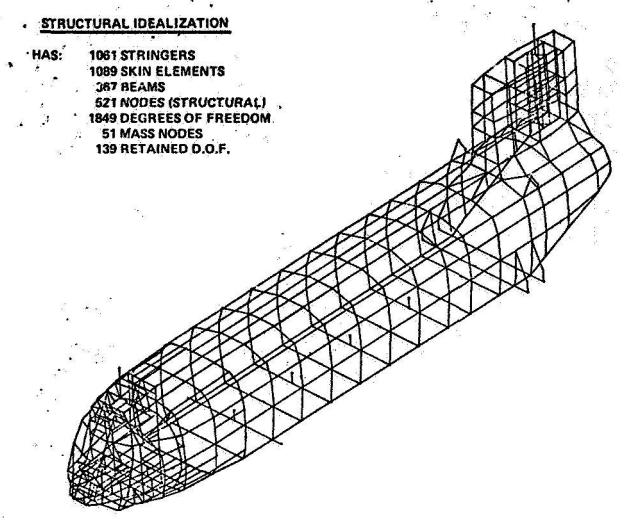

Figure 8. Model 347 Airframe Dynamic Model

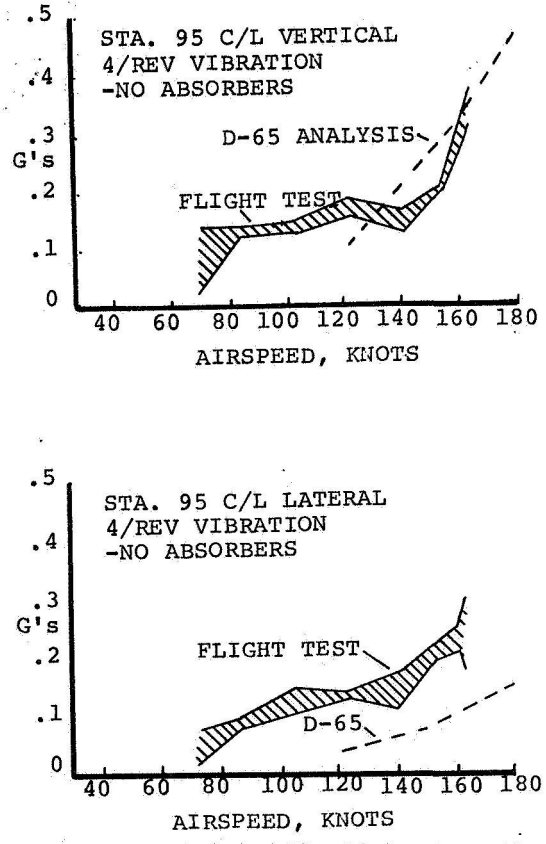

Figure 9. Model 347 Flight Data Vs. D-65 Coupled Rotor/Airframe Analysis Results

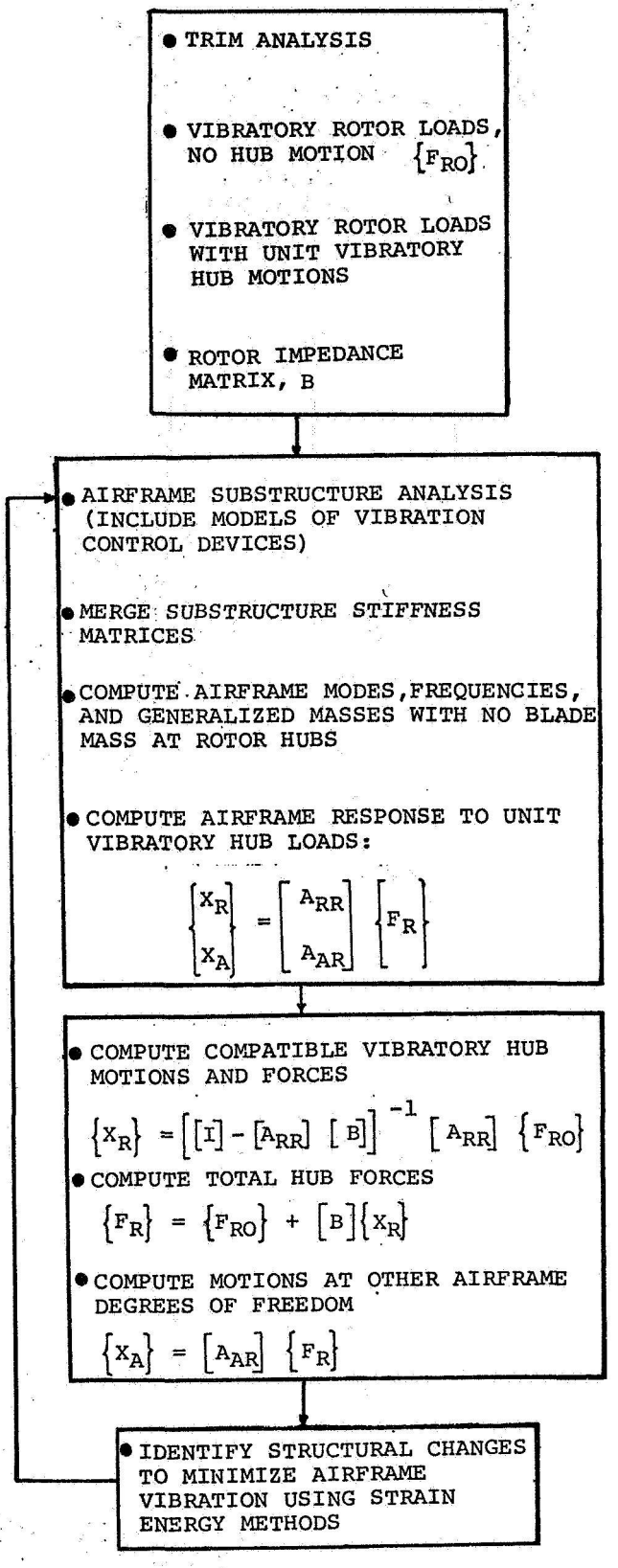

Figure 10. Coupled Rotor/Airframe/NASTRAN Analysis

HELICOPTER GUST RESPONSE CHARACTERISTICS INCLUDING UNSTEADY AERODYNAMIC STALL EFFECTS

Peter J. Arcidiacono
Chief Dynamics
Sikorsky Aircraft Division of United Aircraft Corporation
Stratford, Connecticut

Russell R. Bergquist
Senior Dynamics Engineer
Sikorsky Aircraft Division of United Aircraft Corporation
Stratford, Connecticut

W. T. Alexander, Jr.
Aerospace Engineer
U. S. Army Air Mobility Research and Development Laboratory
Eustis Directorate
Fort Eustis, Virginia

Abstract

The results of an analytical study to evaluate the general response characteristics of a helicopter subjected to various types of discrete gust encounters are presented. The analysis employed was a nonlinear coupled, multi-blade rotor-fuselage analysis including the effects of blade flexibility and unsteady aerodynamic stall. Only the controls-fixed response of the basic aircraft without any aircraft stability augmentation was considered. A discussion of the basic differences between gust sensitivity of fixed and rotary wing aircraft is presented. The effects of several rotor configuration and aircraft operating parameters on initial gust-induced load factor and blade vibratory stress and pushrod loads are discussed. The results are used to assess the accuracy of the gust alleviation factor given by MIL-S-8698. Finally, a brief assessment of the relative importance of possible assumptions in gust response analyses is made and a brief comparison of gust and maneuver load experiences in Southeast Asia is presented.

The results confirm that current gust alleviation factors are too conservative and that the inclusion of unsteady stall effects result in higher initial load factors than predicted using a steady stall aerodynamic analysis.

Notation

A_g gust alleviation factor; see Equation (1) and (3)

a two-dimensional lift curve slope of rotor blade section

b number of blades

B tip loss factor

c blade chord, ft

C_T vertical force coefficient, Thrust/$\pi\rho\Omega^2R^4$

GW gross weight, lbs

Presented at the AHS/NASA-Ames Specialists' Meeting on Rotorcraft Dynamics, February 13-15, 1974.

I_B blade mass moment of inertia about flapping hinge, slug - ft^2

R blade radius, ft

S fixed wing area, ft^2

$t_{3,1}$ partial derivative $\frac{2}{a}\frac{\partial(C_T/\sigma)}{\partial\lambda}$

V forward velocity, knots or ft/sec

V_{avg} average characteristic velocity for helicopter rotor

V_g maximum vertical velocity of gust, positive up, ft/sec

α angle between shaft and relative wind, positive tilted aft, radians

γ blade lock number, $\rho a c R^4/I_B$

Δn incremental rotor load factor; $\frac{\text{MAX THRUST}}{GW} - 1$

Δn_s incremental rotor load factor predicted by linear steady theory for sharp edge gust instantaneously applied to entire lifting device.

λ inflow ratio, $(V\sin\alpha - v)/\Omega R$

μ advance ratio, $V\cos\alpha/\Omega R$

v rotor induced velocity, positive up, ft/sec

ρ air density, slugs/cubic foot

σ rotor solidity, $bc/\pi R$

Ω rotor angular rotational velocity, radians/second

$\frac{\partial C_L}{\partial\alpha}$ three dimensional lift curve slope for fixed wing

Subscripts

FW denotes fixed wing

H denotes helicopter

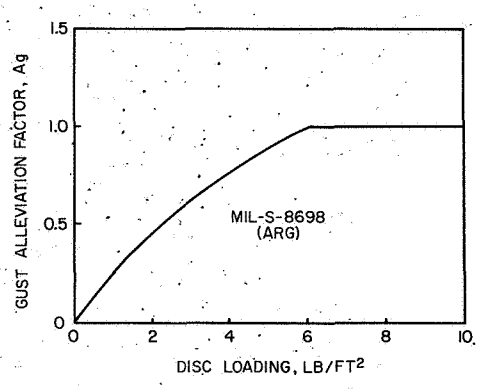

Figure 1. Current Gust Alleviation Factor.

Current procedures for predicting helicopter gust-induced loads involve computing rotor loads by means of a simplified linear theory and modifying these loads by a gust alleviation factor defined in Specification MIL-S-8698 (ARG). The alleviation factor is shown in Figure 1 and is a function of rotor disc loading alone. Further, no alleviation is allowed for disc loadings greater than 6.0 - a value exceeded by many modern helicopters. Attempts to verify the accuracy of this approach through flight test have been complicated by uncertainties regarding the gust profiles. This has led to side-by-side flight tests of fixed and rotary-wing aircraft (Reference 1) in order to build a semi-empirical bridge between the relatively straight forward fixed wing situation and the more complex situation associated with rotary wings. Limited qualitative results on aircraft of comparable gross weight indicated that the helicopter was less gust sensitive than the fixed wing aircraft, but extensive quantitative data from this type of test are, obviously expensive and difficult to obtain. Analytical confirmation of the MIL-S-8698 (ARG) gust alleviation factor has been hampered by the lack of an analysis which can handle both the transient response of the helicopter and the aeroelastic response of the rotor blades, while, simultaneously, providing a reasonably complete modeling of the rotor aerodynamic environment. An improved gust response analysis (described in Reference 2) has indicated that current procedures are too conservative. The primary objectives of this investigation were (1) to develop a similar computerized analysis based on the rotor aeroelastic and unsteady stall aerodynamic techniques developed at Sikorsky Aircraft and the United Aircraft Research Laboratories and (2) to apply the analysis to predict rotor gust alleviation factors for comparison with those given in Specification MIL-S-8698 (ARG) and in Reference 2. The principal contribution of this analysis relative to that of Reference 2 is the inclusion unsteady stall aerodynamics. The resulting computer program was designed to function on the CDC 6600 computer and is catalogued at both the Langley Research Center and the Eustis Directorate.

Comparison of Helicopter and Fixed Wing Gust Response

Before proceeding with a detailed analysis of the helicopter gust response characteristics, it is instructive to compare fixed wing and helicopter characteristics in relatively simple terms. Such a comparison follows.

In analyzing the response of fixed wing aircraft to discrete sharp edge gusts, (eg. Reference 3) the concept of a gust alleviation factor is employed. The gust alleviation factor is simply the ratio of the "actual" incremental load factor produced by the gust to the incremental load factor computed from simple steady-state theory. The "actual" load factor may represent a measurement or may be computed from some more rigorous theory applicable to the unsteady gust encounter situation. Thus, if Ag is defined as the gust alleviation factor, we have

$$A_g = \frac{\Delta n}{\Delta n_s} \tag{1}$$

for fixed wing aircraft we have

$$\frac{(\Delta n)_{FW}}{V_g} = \frac{\frac{1}{2}\rho \left(V \frac{\partial C_L}{\partial \alpha} A_g\right)_{FW}}{GW/S} \tag{2}$$

Following the same approach for a helicopter having a rotor as its sole lifting element, we can write:

$$(\Delta n)_H = (\Delta n_s)_H (A_g)_H \tag{3}$$

Using steady, linear rotor theory results from Reference 4, and assuming a sharp edge gust instantaneously applied to the entire rotor, is given by:

$$(\Delta n_s)_H = \rho \frac{b c R}{GW} \Omega R \frac{a}{2} t_{3,i} V_g \tag{4}$$

$$(\Delta n_s)_H = \frac{\frac{1}{2}\rho (t_{3,i} \Omega R) a V_g}{GW/bcR} \tag{5}$$

$$(\Delta n_s)_H = \frac{\frac{1}{2}\rho (V_{avg}) a}{GW/bcR} V_g \tag{6}$$

Hence, the actual load factor is given by

$$\frac{(\Delta n)_H}{V_g} = \frac{(\Delta n_s)_H (A_g)_H}{V_g} = \frac{\frac{1}{2}\rho (V_{avg}\, a\, A_g)_H}{GW/bcR} \qquad (7)$$

Equation (7) is of similar form to the corresponding fixed wing equation (Equation 2). Further, by comparing the two equations, it is clear that the characteristic or average velocity for the rotor is given by $t_{3/4}\,\Omega R$ and that the characteristic area for the rotor is the total blade area. The characteristic velocity V_{avg}, of the rotor is presented in Figure 2. A typical value of V_{avg} is about $0.5\Omega R$ and the effect of advance ratio (or forward speed) is seen to be small. This contrasts with the fixed wing case where the characteristic velocity is equal to the aircraft's forward velocity.

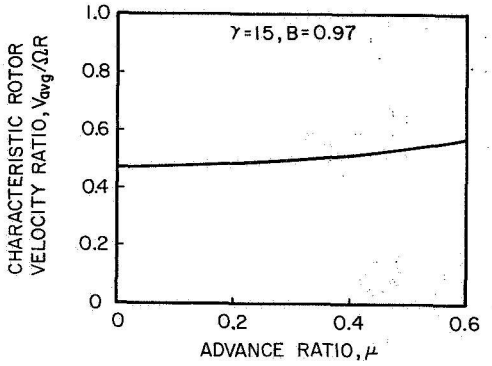

Figure 2. Rotor Characteristic Velocity Ratio.

Now, attempts have been made to measure the gust alleviation factors of helicopters through side-by-side flights with fixed wing aircraft. However, the relative alleviation factors so determined are only meaningful if the Gust Response Parameter for the two aircraft are equal. This equality of Gust Response Parameters is shown in Equation 8:

$$\left(\frac{\frac{1}{2}\rho V_{avg}\, a}{GW/bcR}\right)_H = \left(\frac{\frac{1}{2}\rho V \frac{\partial C_L}{\partial \alpha}}{GW/S}\right)_{FW} \qquad (8)$$

If the relation above is satisfied, Equations (2) and (7) indicate that the following equality also holds:

$$\frac{(\Delta n)_{FW}}{(V_g A_g)_{FW}} = \frac{(\Delta n)_H}{(V_g A_g)_H} \qquad (9)$$

Assuming the two aircraft encounter the same gust velocity profile, Equation (9) reduces to

$$\frac{(\Delta n)_H}{(\Delta n)_{FW}} = \frac{(A_g)_H}{(A_g)_{FW}} \qquad (10)$$

Thus, the ratio of the gust alleviation factors will be in proportion to the measured load factors for the two aircraft. If the fixed wing gust alleviation factor is known, $(Ag)_H$ can then be determined.

If Equation (8) is not satisfied, then the gust alleviation factor for the helicopter can be determined from the following relation:

$$\frac{(A_g)_H}{(A_g)_{FW}} = \frac{(\Delta n)_H}{(\Delta n)_{FW}} \left(\frac{\frac{\rho}{2} V \frac{\partial C_L}{\partial \alpha}}{GW/S}\right)_{FW} \left(\frac{GW/bcR}{\frac{\rho}{2} V_{avg}\, a}\right)_H \qquad (11)$$

Typical values of the Gust Response Parameters of Equation (8) are presented in Figure 3. The results of Figure 3 indicate that a helicopter having a blade loading of 100 lb/ft^2 and operating at a forward speed of 250 fps will exhibit approximately the same sensitivity to a gust as a fixed wing aircraft having a wing loading of about 60 lb/ft^2, provided, of course, that the gust alleviation factors for both aircraft are equal. In practice, for this example, the gust alleviation factor for the fixed wing will be significantly higher (meaning higher acceleration) than that for the helicopter.

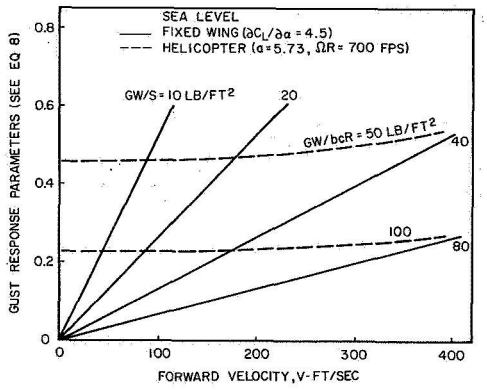

Figure 3. Fixed Wing and Helicopter Gust Response Parameters.

Factors Influencing Helicopter Gust Response

The computation of gust induced loads for helicopters is a difficult analytical task because the rotary wing lifting system is a complex aeroelastic mechanism operating in complicated aerodynamic environment. Principal factors which can be expected to influence the gust response of a helicopter are described briefly below.

a. Rotor blade response - Helicopter rotors differ from fixed wings in that the blades (wings) of the rotor are relatively flexible and, in many cases, are articulated relative to the fuselage. The blades, therefore, are much more responsive to gust loads than is the aircraft as a whole and react in such a way as to reduce or isolate (at least temporarily) the fuselage from the impact of the gust. Thus, while the blades are responding to the gust, the fuselage has time to build up vertical velocity which, in turn, reduces the effective velocity seen by the rotor. A simple example illustrating

the magnitude of the various forces contributing to the fuselage acceleration is shown in Figure 4 for a sharp edge gust applied instantaneously to a rotor having nonelastic flapping blades and operating in hover. In this extreme case, because of the overshoot of the blade flapping response, the peak acceleration experienced by the body is about the same as it would have been had the blades been completely rigid (i.e. equal to the acceleration given by the gust term alone). As seen in Figure 4, the forces associated with the blade dynamic response are large; hence any factor influencing the blade is potentially important.

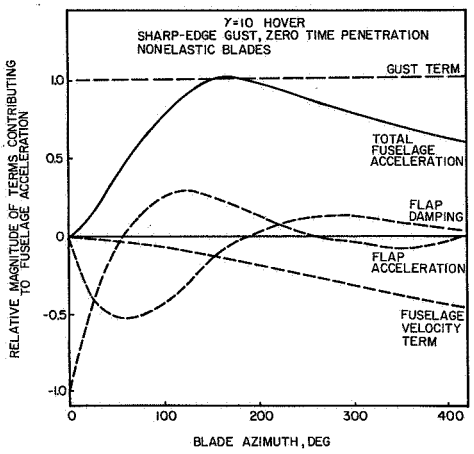

Figure 4. Comparison of Terms Contributing to Fuselage Acceleration.

b. Fixed wing response - If the helicopter is fitted with fixed wings (compound configuration), additional gust loads are, of course, generated. These can be treated using available fixed-wing techniques and are not of primary concern in this study.

c. Rotor Aerodynamic Modeling - The ability of a rotor to generate load factor during a gust encounter will depend on the proximity of the blade trim angle of attack distribution to stall. A rotor operating on the verge of stall prior to a gust encounter can be expected to generate less additional lift due to the gust than can a rotor initially operating further away from stall. The modeling of stall aerodynamics is important; therefore, the impact of unsteady aerodynamics on rotor stall was investigated in this study.

d. Gust Characteristics - Gust profile and amplitude are, of course, potentially important factors. In addition, the speed of the helicopter as it penetrates a given gust front can be expected to be significant. Figure 4 indicated the fuselage acceleration for a gust applied instantaneously to the entire disc. With a finite-time penetration of the gust front, the contribution of each blade to the fuselage loading will not be identical (as in Figure 4) but rather will be phased so that the peak loads for each blade occur at different times (see Figure 5). As a result, finite-time penetration of the gust reduces the peak fuselage accelerations produced by a given gust profile.

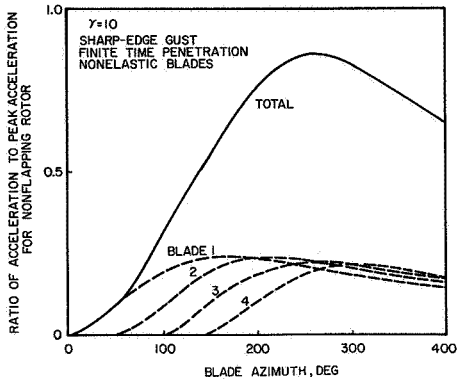

Figure 5. Finite-Time Penetration Causes Peak Blade Forces to be out of Phase.

e. Control system inputs - The ultimate effect of gust on the helicopter must be influenced by any reaction of the pilot or stability augmentation system to the initial loads produced by the gust. It is possible (but unlikely with a properly designed system) that the largest loads produced by the gust will not be the initial loads but, rather, those associated with the longer term response of the coupled system represented by the aircraft, pilot, and stability augmentation system (See Schematic in Figure 6). These longer term effects depend on the specific design characteristics of the aircraft system and no attempt was made to model them in the present study. Hence, the gust-induced loads considered are the initial loads caused by the gust for a controls-fixed rotor operating condition.

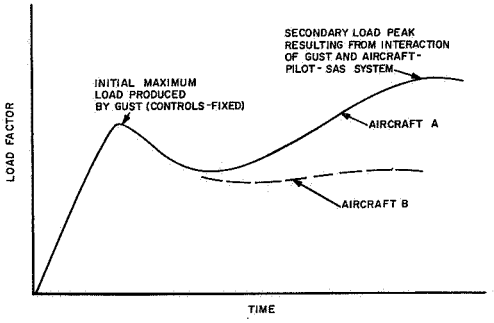

Figure 6. Schematic of Possible Load Factor Time Histories.

Brief Description of the Analysis

Complete documentation of the equations used in the analysis is given in Reference 5, while procedures for running the associated computer program may be found in Reference 6. Both of these references can be obtained from the Eustis Directorate of USAAMRDL.

Briefly, the analysis is essentially a digital flight simulator that can be used to determine the fully coupled rotor - airframe response of a helicopter in free flight. This is accomplished by the numerical integration of the blade - airframe equations of motion on a digital computer. The principal technical assumptions and features of the analysis are listed below.

1. The blade elastic response is determined using a modal approach based on the equations defined in References 7 and 8. The number of modes used consisted of three flatwise, two chordwise and one torsion for each blade.

2. The aerodynamic modeling of the blade includes unsteady aerodynamic effects based on the equations and tabulations defined in Reference 8 which assume that the lift and moment coefficients can be expressed as as functions of instantaneous angle of attack and its first two time derivatives. Steady-state drag was used, however, because of a lack of data on unsteady drag in stall.

3. Rotor inflow is assumed constant for this study although provision for time-varying induces velocities is available. The constant value is determined from classical momentum theory and was invariant with either position on the disc or with time. In view of the short times required for peak loads to be achieved, this assumption is considered reasonable.

4. The response of each individual blade is considered.

5. The fuselage is a rigid (nonelastic) body having six degrees of freedom. Provisions for fixed wings are included. The aerodynamic forces on the wings are computed using simple, finite-span wing theory, neglecting stall and unsteady effects.

6. Fuselage aerodynamic forces and moments are determined using steady-state nonlinear, empirical data.

7. The gust is assumed to be both two dimensional (i.e. does not vary along the lateral axis of the rotor) and deterministic in nature. Although three dimensional and random gust effects may prove important, their inclusion was beyond the scope of this study.

Simple Linear Gust Theory

As stated earlier, it was desired to cast the results obtained in this investigation in terms of correction factors (gust alleviation factors) that could be applied to results obtained from a simple specification eventually evolved.

The simple theory used is that defined in Reference 4, in which blade stall and compressibility effects are neglected. In addition, it is assumed here that the gust is sharp-edged and is instantaneously applied to the entire rotor. The increment in rotor load factor produced by the gust is then given by Equation (5). Using the relation,

$$GW = \rho \pi R^2 (\Omega R)^2 \left(\frac{C_T}{\sigma}\right)\sigma \qquad (12)$$

the incremental rotor load factor given by simple theory is

$$(\Delta n_s)_H = \frac{a}{2} t_{3,1} \frac{1}{(C_T/\sigma)} \frac{V_d}{\Omega R} \qquad (13)$$

The ratio of the $(\Delta n)_H$ computed by the more complete analysis described herein to the value given by Equation (13) represents a gust alleviation factor which can be used to correct the load factors results given by Equation (13). Thus:

$$(A_g)_H = \frac{(\Delta n)_H}{(\Delta n_s)_H} \qquad (14)$$

Values of Ag presented in this paper are based on a rotor blade lift curve slope, a, of 5.73. Hopefully, if Ag shows reasonably consistent trends, it can be used with some confidence to rapidly predict rotor load factors for combinations of parameters other than those considered in this study.

Scope of Study

Gust load factors, blade bending moments, vibratory hub loads, and rotor control loads were calculated for a range of values for rotor thrust coefficient-solidity ratio, blade Lock number, advance ratio, and blade flatwise and torsional stiffness. The effect of adding a wing was also investigated. The responses associated with three types of vertical gusts were investigated: sine-squared, ramp, and sharp-edged. The sine-squared gust and the ramp gust reached a maximum value of fifty feet per second at a penetration distance of ninety feet. The gust profiles are displayed in Figure 7. Three types of rotor systems were evaluated: articulated, nonarticulated (hingeless), and gimbaled. Emphasis in this paper is placed on the results for the reference articulated rotor. The reader is referred to Reference 10 for details of the other configurations studied. The articulated rotor properties can be found in Table I, together with the natural frequencies of the blades. As indicated, the number of modes used

consisted of three flatwise, two chordwise, and one torsional modes.

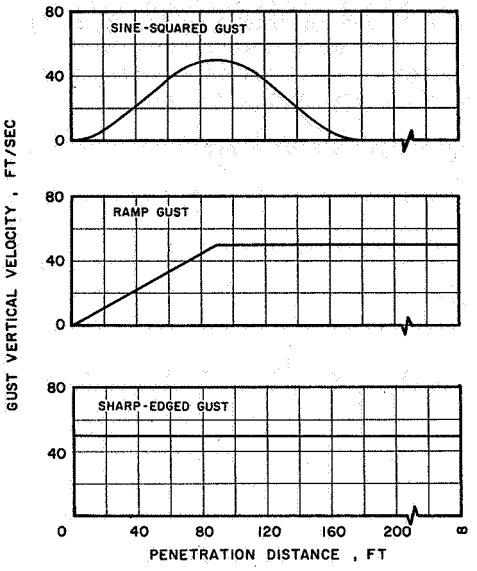

Figure 7. Gust Profiles.

Discussion of Results

Effect of Gust Profile

The effect of gust profile on incremental rotor thrust force for the reference articulated rotor was evaluated by the penetration of three gusts with profiles as shown in Figure 7. The helicopter was assumed to penetrate a stationary gust with a velocity of 350 feet per second. This corresponds to an advance ratio of 0.5.

The time history of the rotor thrust associated with each of the gust profiles is shown in Figure 8. It may be seen from this figure that while the actual gust wave form has little impact on maximum rotor force and consequently on rotor load factor, the particular time histories behave differently, although in an expected manner. Initially, the sine-squared and the ramp gust shapes result in similar peak rotor loads at approximately the same time. The sharp-edge gust induces a greater peak load with a faster build up. As the penetration distance increases, the loads produced by the sharp-edge gust and the ramp gust tend to merge since their respective velocities are both 50 fps while the value of the sine-squared gust velocity has dropped back towards zero.

Analysis of the computed results forming the basis for Figure 8 indicates that at the time the maximum rotor vertical force and load factor is reached, the helicopter fuselage has had time to develop only a modest amount of vertical velocity. The vertical velocities at the peak load points of the helicopter associated with the sine-squared and sharp-edged gusts are 6fps, and 3 fps, 3 fps, respectively. These compare to the 50 fps gust velocity, indicating that little gust alleviation

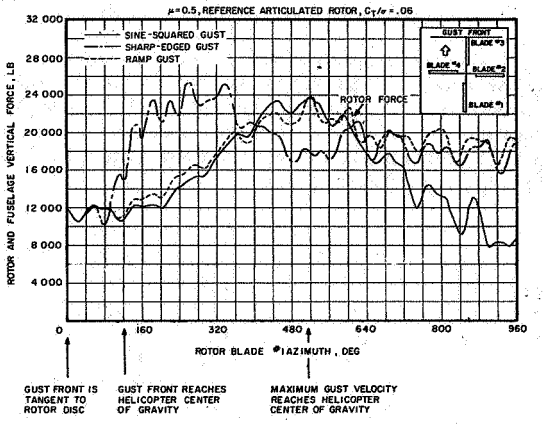

Figure 8. Rotor Force Time Histories.

is being produced by fuselage motion for the condition analyzed.

The three types of gust profiles evaluated did not produce greatly different peak rotor loads. While the sharp-edge gust does produce the largest loads, it is probably the least realistic of the three profiles. Since other studies, such as Reference 2, have used a sine-squared gust, the remainder of the results presented are based on this profile.

Effect of Rotor and Flight Condition Variables

The variation of gust alleviation factor, (as computed from Equation 14), with initial rotor loading is shown in Figure 9 for the three types

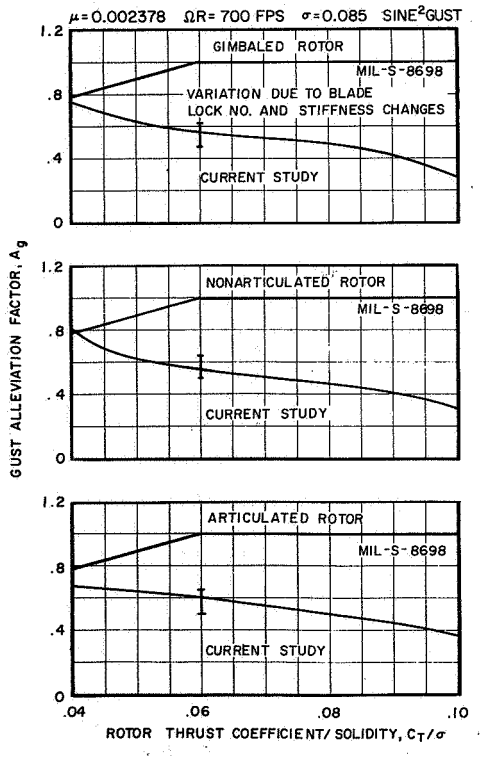

Figure 9. Gust Alleviation Factors for Different Rotors.

types of rotors analyzed. Rotor loading in this figure has been expressed both in terms of rotor thrust coefficient solidity ratio and rotor disc loading. It should be remembered that disc loading is not a unique function of C_T/σ but rather depends on the value of density, tip speed and solidity of the rotor. Values for these quantities are noted on the figure.

The results of Figure 9 indicate that increasing C_T/σ leads to a large reduction of gust alleviation factor, This is similar to the trend noted in Reference 2 and is believed to be related to the loss in average additional lift capability at the higher C_T/σ due to the occurrence of stall. The influence of rotor configuration is seen to be of rather secondary importance. Rotor configuration would be expected to influence fuselage motion through the transmittal of differing rotor pitching moments to the airframe, depending on the degree of rotor articulation. The relative insensitivity of the results to configuration is believed to be due to the short time in which the initial, controls-fixed load factor is generated. As a result, the fuselage response to the differing moments is not large and the load factor tends to be dominated by the rotor blade dynamic response, which is roughly the same for all rotors. This result is also similar to that observed in Reference 2.

It is also evident from Figure 9 that the gust alleviation factors defined in MIL-S-8698 (ARG) are too high (i.e. result in loads which are too high). The conservatism of the current specification is particularly evident at the high thrust coefficient-solidity ratios where rotor stall becomes a factor limiting gust-induced thrust generating capability. On this basis, one would expect the gust alleviation factor for upward gusts to be different from those for downward gusts (i.e. gusts which unload the rotor). While downgusts are not critical from a structural loads viewpoint, they could prove more important from a passenger - comfort point of view.

The results of Figure 9 are for typical reference rotor configurations (see Reference 10 and Table I herein). As part of this study, calculations were made to examine the sensitivity of the computed gust alleviation factors to separate variations in blade Lock Number, bending stiffness and torsional stiffness. Ranges of the parameters considered are noted below:

Lock Number: reference, 0.7 ref. 1.3 ref.

Bending stiffness: reference, 0.5 ref.

Torsional stiffness: reference, 0.5 ref.

The parameter variations listed above were made at an advance ratio of 0.3 and 0.5 for a C_T/σ of 0.06. The range of results is also shown in Figure 9 and as can be seen, the effect of blade Lock number and stiffness is relatively small. Lock number and advance ratio account for most of the small variation shown, with the lower advance ratios and higher Lock numbers being associated with the lower gust alleviation factors. The relatively small effect of blade stiffness variations is perhaps not surprising inasmuch as the total blade stiffness tends to be dominated by centrifugal stiffening effects. The variations shown for C_T/σ of 0.06 are believed to be representative of those at other C_T/σ values; however, this should be verified.

Articulated rotor load factors predicted using the results of Figure 9 are presented in Figure 10 where they are also compared to the results of Reference 2. Load factors predicted by the current study are seen to be higher than those of Reference 2. This increase appears to be due to the use of unsteady aerodynamics in the current study.

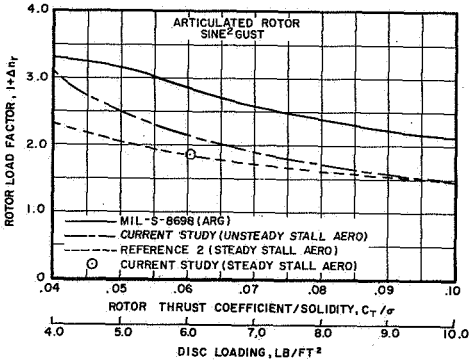

Figure 10. Comparison of Results with Reference 2

Gust-Induced Blade Stresses, Control Loads and Vibration

The effects of a gust encounter on other quantities of interest to the designer such as blade stresses, control loads, and aircraft vibration were briefly examined. In examining these effects, an attempt was made to generalize the results to a limited degree by relating the maximum values produced by the gust to the initial trim values. Results are based on the trim condition of $C_T/\sigma = 0.06$ and an advance ratio of 0.3 are presented in Figure 11. Detailed analysis of the trends shown were beyond the scope of this paper. The reader is referred to Reference 2 for a more detailed discussion.

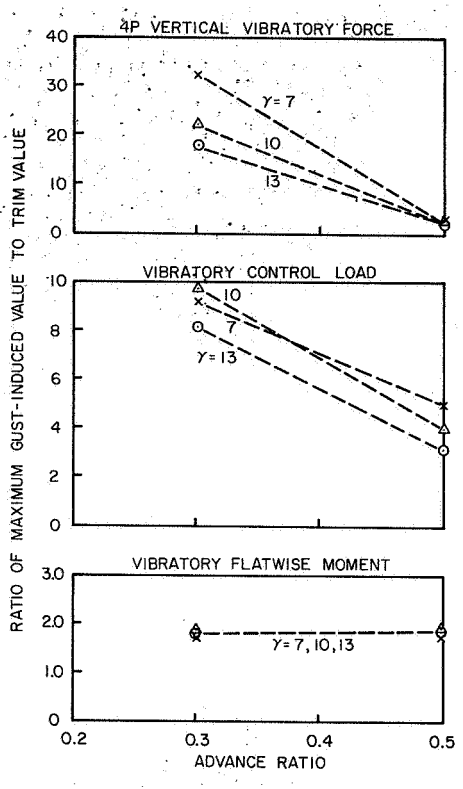

Figure 11. Effect of Gust on Vibration, Control Load and Flatwise Moment, $\frac{C_T}{\sigma}$ = 0.06, 50 fps SINE^2 Gust

Sensitivity of Results to Assumptions

As discussed in an earlier section of this report, many factors could potentially influence rotor gust response characteristics. To account for all of these factors leads to a time consuming, complex, digital analysis. In the following paragraphs, the results of a brief examination of the importance of some of these factors are discussed. Only the reference articulated rotor at one operating condition is considered. Any conclusions drawn from these results must, therefore, be considered preliminary and should be substantiated by further investigation. A summary of the results obtained is presented in Figure 12. Shown is the percentage change in the predicted gust alleviation factor resulting from the separate elimination of fuselage motion, blade elastic torsion, finite time penetration, and unsteady stall effects in the analysis. The baseline value corresponds to value for the complete analysis. A positive change in Ag means that the effect eliminated causes an increase in predicted loading. It is evident that the unsteady stall aerodynamic and finite-time gust penetration effects are most important. Excluding unsteady aerodynamics reduces the predicted value of Ag by about 29%. This is because the maximum lift capability of the rotor based on steady aerodynamic stall characteristics is lower than that based on unsteady characteristics (see Reference 9). The reduction is consistent with the observed lower values of predicted load factors obtained in Reference 2 and previously presented in Figure 10.

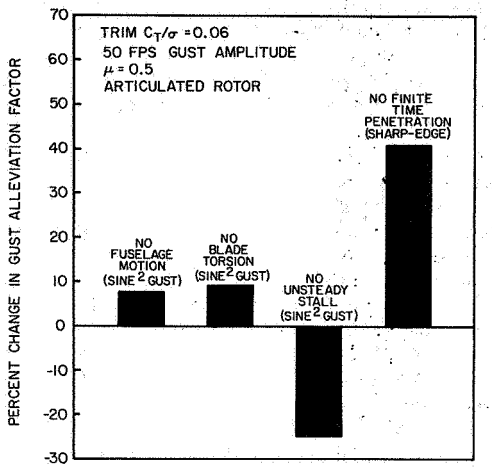

Figure 12. Sensitivity of Gust Alleviation to Analytical Assumptions.

The largest change in predicted gust alleviation factor was produced by the elimination of the finite time penetration of the gust front. As might be expected, when the gust is assumed to affect all blades simultaneously, the blade forces are all in phase and large values of Ag (and hence loading) result.

It should be emphasized that the results presented in Figure 12 were determined for only one reference trim condition. Further work is required to substantiate the generality of the results.

Gust Load Factor Experience in SEA

The earlier portions of this paper have been devoted to analytical techniques appropriate for determining the effects of gust encounters on helicopter response variables. One point which has been made is that rotor blades, because of their flexibility, tend to reduce the impact of the gust on the fuselage. Resulting gust alleviation factors have been found to be low and, hence, one would expect that gust-induced loads on the fuselage could be reduced in importance. Experimental evidence supporting this contention has been acquired by the U. S. Army in SEA. A brief discussion of that data is presented below.

The U. S. Army has been acquiring usage data on its combat operational helicopters in Vietnam since early 1966. Beginning with both the cargo and armored versions of the CH-47A, the CH-54A, AH-1G, nd UH-6A helicopters were instrumented to record the history of their actual combat usage.

Since control positions and c.g. accelerations were among the parameters measured and the data were recorded in analog format, occurrences of gust-induced loads were identified and isolated from pilot-induced (maneuver) accelerations by analyzing those particular trace recordings. Gust-induced acceleration peaks, therefore, were identified as those accelerations occurring when both

the cyclic and collective stick traces were steady or, if stick activity was present, the sense of the peaking acceleration had to be in opposition to that expected from the stick control motion.

A total of 1477 hours of flight data were acquired during the measurement programs for the cited aircraft (References 11-13). The conclusive finding in each of these programs was that normal loads attributed to gust encounters were of much lesser magnitude and frequency than maneuver loads. Further, when the total load factor experience was statistically examined for each aircraft, the loads directly attributed to gust encounters were found to be only a small percentage of the total experience. These points are graphically illustrated in Figure 13. The maneuver load scatter band was obtained from References 14 and 15.

It should be pointed out that while gust-induced load factors are smaller than typical maneuver load factors for military aircraft, gust loadings can be an important consideration from a ride comfort standpoint in commercial applications.

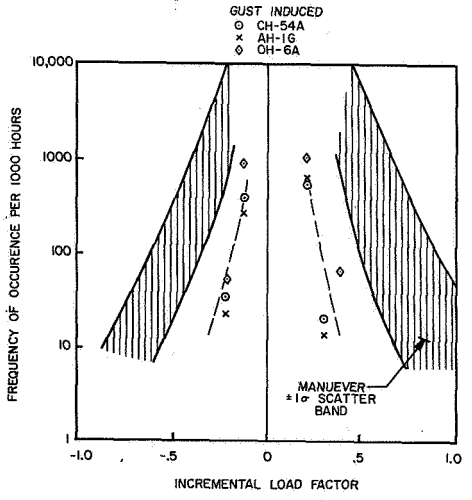

Figure 13. Gust-Induced Loads are Significantly Less than Maneuver Loads.

Conclusions

The following conclusions were reached as a result of this study. It should be noted that Conclusions 1-3 are based on the computation of initial gust-induced load factors for various rotor systems mounted on a single fuselage and operating with the controls fixed throughout the gust encounters.

1. The results of this study generally confirm those of Reference 2, indicating that the current method for computing gust-induced load factors for helicopter rotors (Specification MIL-S-8698 (ARG)) results in realistically high values and should be revised.

2. If the gust amplitude is sufficient to cause retreating blade angles of attack greater than the two-dimensional, steady-state stall angle, the inclusion of unsteady aerodynamic effects based on the model of Reference 8 results in gust-induced load factors which are higher than those based on a steady aerodynamic model such as that used in Reference 2.

3. Principal parameters influencing gust-induced load factor appear to be nondimensional blade loading, proximity of the rotor trim point to blade stall, and rate of penetration of the rotor into the gust.

4. Gust loadings on military helicopters appear to be significantly lower than those due to maneuvers.

References

1. Crim, Almer D., GUST EXPERIENCE OF HELICOPTER AND AN AIRPLANE IN FORMATION FLIGHT, NACA Technical Note 3354, NACA, 1954.

2. Harvey, K. W., Blankenship, B. L. Drees, J. M., ANALYTICAL STUDY OF HELICOPTER GUST RESPONSE AT HIGH FORWARD SPEEDS. USAAVLABS Technical Report 69-1, September 1969.

3. Bisplingoff, R. L., H. Ashley and R. L. Halfman, AEROELASTICITY, Addison-Wesley Publishing Company, Inc., Cambridge, Mass. 1955.

4. Bailey, F. J., Jr., A SIMPLIFIED THEORETICAL METHOD OF DETERMINING THE CHARACTERISTICS OF A LIFTING ROTOR IN FORWARD FLIGHT. NACA Report No. 716.

5. Bergquist, R. R., Thomas G. C. TECHNICAL MANUAL FOR NORMAL MODES AEROELASTIC COMPUTER PROGRAM, July 1972.

6. Bergquist, R. R., Thomas, G. C. USER'S MANUAL FOR NORMAL MODE BLADE AEROELASTIC COMPUTER PROGRAM, July 1972.

7. Arcidiacono, P. J., PREDICTION OF ROTOR INSTABILITY AT HIGH FORWARD SPEEDS, VOLUME 1. STEADY FLIGHT DIFFERENTIAL EQUATIONS OF MOTION FOR A FLEXIBLE HELICOPTER BLADE WITH CHORDWISE MASS UNBALANCE. USAAVLABS Technical Report 68-18A, February 1969.

8. Arcidiacono, P. J., Carta, F. O., Cassellini, L. M., and Elman, H. L., INVESTIGATION OF HELICOPTER CONTROL LOADS INDUCED BY STALL FLUTTER. USAAVLABS Technical Report 70-2, March 1970.

9. Bellinger, E. D., ANALYTICAL INVESTIGATION OF THE EFFECTS OF UNSTEADY AERODYNAMICS VARIABLE INFLOW AND BLADE FLEXIBILITY ON HELICOPTER ROTOR STALL CHARACTERISTICS. NASA CR-1769.

10. Bergquist, R. R., HELICOPTER GUST RESPONSE INCLUDING UNSTEADY STALL AERODYNAMIC EFFECTS. USAAVLABS Technical Report 72-68, May 1973.

11. Giessler, F. Joseph; Nash, John F.; and Rockafellow, Ronald I., FLIGHT LOADS INVESTIGATION OF AH-1H HELICOPTERS OPERATING IN SOUTHEAST ASIA, Technology, Inc., Dayton, Ohio; USAAVLABS Technical Report 70-51, U. S. Army Aviation Materiel Laboratories, Fort Eustis, Virginia, September 1970, AD 878039.

12. Giessler, F. Joseph; Nash John F.; and Rockafellow, Ronald I., FLIGHT LOADS INVESTIGATION OF CH-54A HELICOPTER OPERATING IN SOUTHEAST ASIA, Technology, Inc., Dayton, Ohio; USAAVLABS Technical Report 70-73, Eustis Directorate, U. S. Army Air Mobility Research and Development Laboratory, Fort Eustis, Virginia, January 1971, AD 881238.

13. Giessler, F. Joseph; Clay, Larry E.; and Nash, John F., FLIGHT LOADS INVESTIGATION OF OH-6A HELICOPTERS OPERATING IN SOUTHEAST ASIA, Technology, Inc., Dayton, Ohip; USAAMRDL Technical Report 71-60, Eustis Directorate, U. S. Army Air Mobility Research and Development Laboratory, Fort Eustis, Virginia, October 1971, AD 7308202.

14. Porterfield, John D., and Maloney, Paul F., EVALUATION OF HELICOPTER FLIGHT SPECTRUM DATA, Kaman Aircraft Division, Kaman Corporation, Bloomfield, Connecticut; USAAVLABS Technical Report 68-68, U. S. Army Aviation Materiel Laboratories, Fort Eustis, Virginia, October 1968, AD 680280.

15. Porterfield, John D., Smyth, William A. and Maloney, Paul F., THE CORRELATION AND EVALUATION OF AH-1G, CH-54A, and OH-6A FLIGHT SPECTRA DATA FROM SOUTHEAST ASIA OPERATIONS, Kaman Aircraft Division, Kaman Corporation, Bloomfield, Connecticut; USAAVLABS Technical Report 72-56, Eustis Directorate, U. S. Army Air Mobility Research and Development Laboratory, Fort Eustis, Virginia, October 1972, AD 755554.

TABLE I. Reference Articulated Rotor Characteristics

Density Slugs/ft^2	.002378
Tip speed, ft/sec	700.
Radius, ft	25
No. of blades	4.
Blade Chord, ft	1.67
Flap hinge off set ratio	0.04
Twist, deg	-8.0
Young's Modulus, psi	10^7
Mass per unit length at 0.75R slugs/ft	0.18
Lock Number	10.0
Rigid body flatwise frequency	1.03P
First bending flatwise frequency	2.66P
Second bending flatwise frequency	5.06P
Third bending flatwise frequency	8.50P
Rigid body chordwise frequency	0.25P
First bending chordwise frequency	3.68P
Second bending chordwise	10.20P
First bending torsional frequency	5.72P

APPLICATION OF ANTIRESONANCE THEORY TO HELICOPTERS

Felton D. Bartlett, Jr.
Research Engineer

William G. Flannelly
Senior Staff Engineer

Kaman Aerospace Corporation
Bloomfield, Connecticut

Abstract

Antiresonance theory is the principle underlying nonresonant nodes in a structure and covers both nonresonant nodes occurring naturally and those introduced by devices such as dynamic absorbers and antiresonant isolators. The Dynamic Antiresonant Vibration Isolator (DAVI) developed by Kaman Aerospace Corporation and the Nodal Module developed by the Bell Helicopter Company are specific examples of the applications of transfer antiresonances. A new and convenient technique is presented to numerically calculate antiresonant frequencies. It is shown that antiresonances are eigenvalues and that they can be determined by matrix iteration.

Novel applications of antiresonance theory to helicopter engineering problems, using the antiresonant eigenvalue equation introduced in this paper, are suggested.

Notation

f	force vector
K	stiffness matrix
M	mass matrix
y	response vector
Z	impedance matrix
θ	antiresonant eigenvector
ω	forcing frequency
ω_r	antiresonant frequency

In forced vibrations an antiresonance or "off-resonance node", is that frequency for which a system has zero motion at one or more points. A nodal point in a normal mode is a special case of an antiresonance. Driving point antiresonances have a readily grasped physical interpretation since they are the resonances of the system when it is restrained at the driving point. However, transfer antiresonances are not all real and, in general, have not been susceptible to analysis except in special cases. The eigenvalue equation for antiresonances used in this paper renders them as amenable to analysis as are resonances. The mathematics for analyzing resonances are conventional and well-known[1].

Although general analytical methods for transfer antiresonances were not heretofore commonly used, the existence of both driving point and transfer antiresonances in the forced vibration of a string were described by Lord Rayleigh[2]. The invention of the dynamic vibration absorber in 1909 gave antiresonances some practical engineering importance[3]. The absorber is an appendant dynamic system which has a driving point antiresonance at its fixed base natural frequency and it therefore reacts the forces at its base in the direction in which it acts. Isolating devices based on transfer antiresonances were not invented until this decade[4]. Sometimes natural fuselage transfer antiresonances for major hub excitations occurred near a critical point and at the proper frequency (e.g., the pilot's seat at blade passage frequency) by fortuity of helicopter design. Occasionally, engineers have manipulated transfer antiresonance frequencies and positions in design through lengthy trial-and-error response analyses. However, the industry has not used a direct analytical method for calculating the positions and frequencies of natural antiresonances.

Presented at the AHS/NASA-Ames Specialists' Meeting on Rotorcraft Dynamics, February 13-15, 1974.

Structures have antiresonances as an intrinsic "natural" property much as they have "natural" resonant frequencies. Natural transfer, or "off-diagonal", antiresonances are as important to structural dynamics engineering as are resonances. Unfortunately, many of the theorems which underly conventional analyses do not apply to transfer antiresonances. The antiresonant dynamical matrix is in general nonsymmetrical and therefore not positive definite. This results in both left-handed and right-handed eigenvectors which are unequal and require a new orthogonality condition for the calculation of successive eigenvectors. The antiresonant frequencies of the transfer antiresonance determinants are not necessarily real and the imaginary roots do not have a simple physical interpretation. These matters, along with the lack of an engineering eigenvalue formulation for antiresonances, may, in part, account for the relatively little attention given to natural antiresonances over the years.

Theory

The steady-state equations of motion for an undamped spring-mass system vibrating in the vicinity of equilibrium are:

$$(K - \omega^2 M)y = f \tag{1}$$

where the impedance matrix is defined as

$$Z = [\partial f_i / \partial y_j] = (K - \omega^2 M) \tag{2}$$

Let all the forces be zero except the force acting at the k-th generalized coordinate and further impose the restraint of zero motion for the j-th generalized coordinate. The resulting eigenvalues are jk antiresonances of Equation (1). Since Z is real and symmetric the antiresonance eigenvectors are real and the jk and kj antiresonance eigenvalues are real (positive or negative) and equal.

Partition Equation (1) so that the kj-th element of the impedance matrix appears in the lower right-hand corner.

$$\left[\begin{array}{cc|c} Z_{mn} & \begin{matrix} m \neq k \\ n \neq j \end{matrix} & \begin{matrix} Z_{mj} \\ m \neq k \end{matrix} \\ \hline Z_{kn} & n \neq j & Z_{kj} \end{array}\right] \left\{\begin{array}{c} y_\ell \\ \ell \neq j \\ \hline 0 \end{array}\right\} = \left\{\begin{array}{c} 0 \\ \hline f_k \end{array}\right\} \tag{3}$$

where

$$\left[\begin{array}{cc|c} Z_{mn} & \begin{matrix} m \neq k \\ n \neq j \end{matrix} & \begin{matrix} Z_{mj} \\ m \neq k \end{matrix} \\ \hline Z_{kn} & n \neq j & Z_{kj} \end{array}\right] \equiv \left[\begin{array}{c|c} Z_A & Z_C \\ \hline Z_R & Z_{kj} \end{array}\right] \tag{4}$$

If the impedance matrix is similarly partitioned so that the upper left-hand matrix does not contain the j-th row or the k-th column, then

$$Z = \left[\begin{array}{c|c} \tilde{Z}_A & \tilde{Z}_C \\ \hline \tilde{Z}_R & Z_{jk} \end{array}\right] \tag{5}$$

It follows from Equations (4) and (5) that

$$Z_A = \tilde{Z}_A^T \tag{6}$$

From Equation (3) we obtain

$$Z_A y = 0 \tag{7}$$

A kj antiresonance is defined such that for a force at k alone, the response at j is zero. Normalizing y and substituting for Z_A in Equation (7) results in the antiresonance eigenvalue equation.

$$M_A \theta_r = \frac{1}{\omega_r^2} K_A \theta_r \tag{8}$$

A jk antiresonance eigenvalue equation is similarly defined by considering Equation (5) and making use of Equation (6).

$$\tilde{\theta}_s^T M_A = \frac{1}{\omega_s^2} \tilde{\theta}_s^T K_A \tag{9}$$

Equations (8) and (9) constitute a set of right-handed and left-handed eigenvectors. Since Z_A is not symmetrical, the jk eigenvectors are not orthogonal but instead are biorthogonal with the kj eigenvectors[1]. Premultiply Equation (8) by $\tilde{\theta}_s^T$, postmultiply Equation (9) by θ_r, and subtract to obtain

$$\left(\frac{1}{\omega_r^2} - \frac{1}{\omega_s^2}\right) \tilde{\theta}_s^T K_A \theta_r = 0 \tag{10}$$

when $s \neq r$ we have

$$\tilde{\theta}_s^T K_A \theta_r = 0 \tag{11}$$

Thus, the kj antiresonance eigenvector is biorthogonal to the jk antiresonance eigenvector.

When s = r the corresponding generalized mass and stiffness are defined as

$$\tilde{\theta}_r^T M_A \theta_r = M_r \qquad (12)$$

$$\tilde{\theta}_r^T K_A \theta_r = K_r \qquad (13)$$

Successive antiresonance eigenvectors are found by applying the biorthogonality condition and using classical matrix iteration techniques. The (n + 1)st jk. antiresonant eigenvector is obtained from Equation (14),

$$(K_A^{-1} - \sum_{i=1}^{n} \frac{\theta_i \tilde{\theta}_i^T}{K_i}) M_A \theta_{n+1} = \frac{1}{\omega_{n+1}^2} \theta_{n+1} \qquad (14)$$

which establishes the method of sweeping.[5]

Discussion of Theory

Each antiresonant eigenvector consists of a pair which is biorthogonal with respect to both mass and stiffness. For driving point antiresonances (j = k), the two eigenvectors are, obviously, the same. An N-degree-of-freedom system has N^2 possible antiresonant eigenvectors corresponding to all possible forcing and response coordinates.

Since the mass and stiffness matrices are nonsymmetric in the antiresonance eigenvalue problem and consequently not positive definite when $j \neq k$, the antiresonant generalized masses and stiffnesses may be either positive or negative. In other words, the antiresonance frequencies are not necessarily real. When j = k the antiresonant mass and stiffness matrices are symmetrical and positive definite, resulting in at least N-1 positive real antiresonances. As shown in Reference 6 the driving point antiresonances lie between the natural resonant frequencies.

Applications of Antiresonance Theory

To illustrate the practical potential of antiresonance theory, consider a ten-degree-of-freedom beam specimen with springs to ground at stations 3 and 9 and mass and stiffness parameters simulating a 9000 pound helicopter. Antiresonances are continuous functions of frequency and position and Figure 1 presents a typical position spectrum plot of the specimen forcing at station 3 alone. The dashed vertical lines are the natural resonant frequencies determined conventionally. When an antiresonance line crosses a natural frequency line there is a nodal point in the "natural mode".

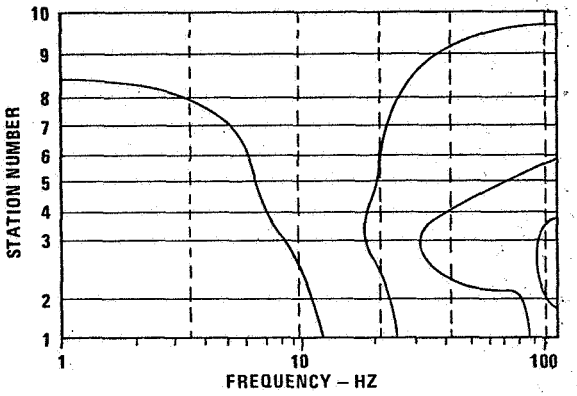

Figure 1. Antiresonance Lines Forcing at Station 3

With the same techniques of altering masses and stiffnesses to avoid undesirable natural resonances, the engineer can manipulate natural antiresonances. The stiffness between stations 2 and 3 was increased by 11.8% in the K_{23} term of the stiffness matrix and Figure 2 illustrates this effect in the natural frequencies and antiresonance lines. Similar changes in the mass of the structure have a similar effect. This possibility for response control indicates a profitable area for further exploration.

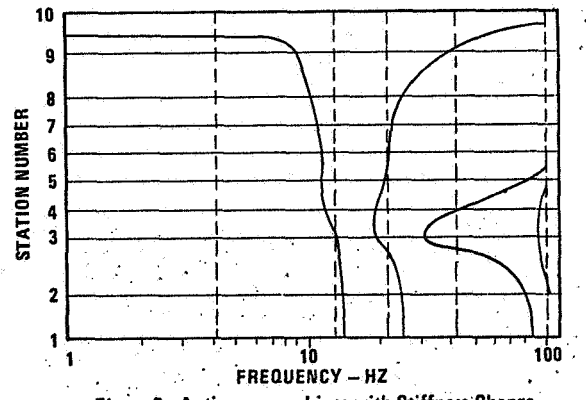

Figure 2. Antiresonance Lines with Stiffness Change Forcing at Station 3

Conventional Use of the Dynamic Absorber

A dynamic absorber is an appendant dynamic system attached to a helicopter, usually at a point, as shown in Figure 3. When we eliminate the i-th row and column, corresponding to the attachment point (see Figure 3) we obtain two uncoupled systems.

$$\begin{bmatrix} Z_{ff} & 0 \\ 0 & Z_{aa} \end{bmatrix} \begin{Bmatrix} y_f \\ y_a \end{Bmatrix} = \begin{Bmatrix} f \\ 0 \end{Bmatrix} \qquad (15)$$

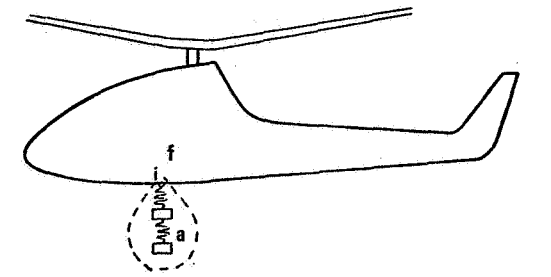

$$\begin{bmatrix} Z_{ff} & Z_{fi} & 0 \\ Z_{if} & Z_{ii} & Z_{ia} \\ 0 & Z_{ai} & Z_{aa} \end{bmatrix} \begin{Bmatrix} Y_f \\ Y_i \\ Y_a \end{Bmatrix} = \begin{Bmatrix} f \\ 0 \\ 0 \end{Bmatrix}$$

Figure 3. Conventional Absorber

The antiresonant eigenvalue equation is obtained from Equation (15) as

$$[K_{aa}^{-1} M_{aa}]\theta_r = \frac{1}{\omega_r^2}\theta_r \qquad (16)$$

which is of the form of Equation (7).

If the absorber system were attached at I points, instead of one, we would eliminate the I rows and columns corresponding to the attachments and find the simultaneous antiresonant frequencies of all I points.

Unconventional Use of the Dynamic Absorber

In some instances there may be only one significant unreacted force on the helicopter as, for example, when an in-plane isolation system or in-plane hub or flapping absorbers leave small hub moments but a relatively large vertical oscillatory force. We can use a dynamic absorber in the fuselage at some point i as a "resonator" to shift antiresonance lines so that there exists an antiresonance at another point j (e.g., the pilot's seat) for the one remaining large force or moment along the k-th generalized coordinate. This is creating a jk antiresonance by manipulation of a "resonator" at point i. The jk antiresonant frequency is not at the tuned frequency of the "resonator" and does not necessarily produce an antiresonance at j for excitations along generalized coordinates other than k.

The aforementioned system and equations of motion are shown in Figure 4. To obtain an antiresonance at j for a force at k we eliminate the k-th row and j-th column from the equations of motions. This results in the antiresonant eigenvalue equation,

$$\begin{bmatrix} Z_{ff'} \; {}_{f\neq k}^{f'\neq j} & Z_{fi} \; {}_{f\neq k} & 0 \\ Z_{if'} \; {}^{f'\neq j} & Z_{ii} & Z_{ia} \\ 0 & Z_{ai} & Z_{aa} \end{bmatrix} \begin{Bmatrix} \\ \theta \\ \\ \end{Bmatrix} = \begin{Bmatrix} \\ 0 \\ \\ \end{Bmatrix} \qquad (17)$$

which is of the form of Equation (7).

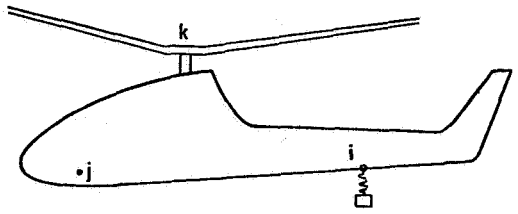

$$\begin{bmatrix} Z_{ff'} \; {}_{f\neq k}^{f'\neq j} & Z_{fj} \; {}_{f\neq k} & Z_{fi} \; {}_{f\neq k} & 0 \\ Z_{kf'} \; {}^{f'\neq j} & Z_{kj} & Z_{ki} & 0 \\ Z_{if'} \; {}^{f'\neq j} & Z_{ij} & Z_{ii} & Z_{ia} \\ 0 & 0 & Z_{ai} & Z_{aa} \end{bmatrix} \begin{Bmatrix} Y_{f'} \\ Y_j \\ Y_i \\ Y_a \end{Bmatrix} = \begin{Bmatrix} 0 \\ f_k \\ 0 \\ 0 \end{Bmatrix}$$

Figure 4. Antiresonance at Station j from a Resonator at Station i

This technique of using a remote dynamic absorber as a "resonator" allows the engineer to obtain an antiresonance, to a given excitation, at points where structural limitations prevent installation of an absorber. When the new resonant frequency introduced by the "resonator" cuts across a natural antiresonance line, the shifts are dramatic as shown in Figure 5. Figure 5 illustrates the antiresonance lines in the specimen, forcing at station 3, when an absorber of 77.2 pounds tuned to 7.7 Hz is added to station 2. The natural frequency introduced by the absorber intersects the antiresonance line of Figure 1 and produces new antiresonances at all stations,

forcing at station 3.

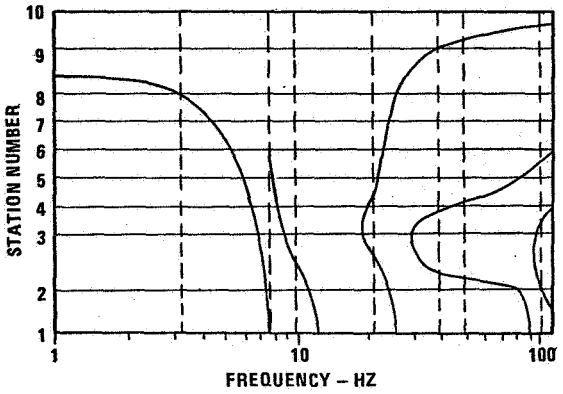

Figure 5. Antiresonance Lines with Dynamic Absorber at Station 2, Forcing at Station 3

The effect at station 5 of the 77.2 pound absorber located at station 2 and tuned to 7.7 Hz, in terms of both antiresonant frequency and bandwidth, is the same as the effect produced by a 193 pound absorber located at station 5 itself and tuned to 8.0 Hz. Bandwidth is here defined as the difference between the antiresonance frequency and the nearest natural frequency. This comparison is presented in Figure 6. The approximately two to one reduction in absorber weight does not imply that such savings are always obtainable.

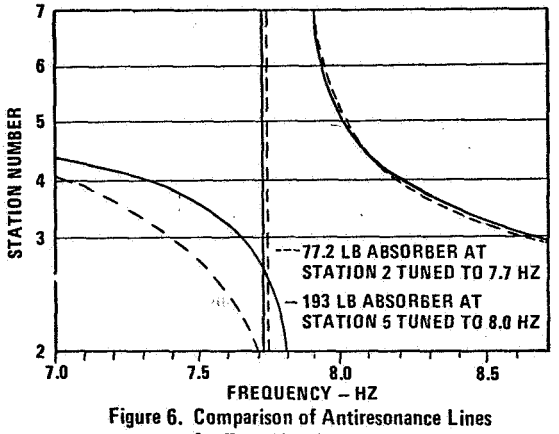

Figure 6. Comparison of Antiresonance Lines for Two Absorbers

Antiresonant Isolators

Passive antiresonant isolation devices have received considerable attention from the industry in recent years. Notable among these are Bell Helicopter's Nodal Module, Kaman's DAVI series, and the Kaman COZID.

Figure 7 illustrates the antiresonant isolation system and corresponding equations of motion. The excited structure

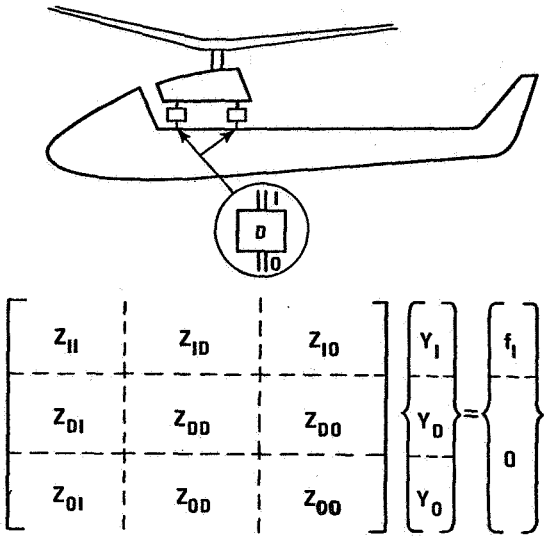

$$\begin{bmatrix} Z_{II} & Z_{ID} & Z_{IO} \\ Z_{DI} & Z_{DD} & Z_{DO} \\ Z_{OI} & Z_{OD} & Z_{OO} \end{bmatrix} \begin{Bmatrix} Y_I \\ Y_D \\ Y_O \end{Bmatrix} = \begin{Bmatrix} f_I \\ 0 \end{Bmatrix}$$

Figure 7. Antiresonance Isolation

is coupled to another structure through, and only through, the antiresonant isolation system which has inertial and elastic elements. Any isolator with a single input and single output, or a symmetrical arrangement having the same effect, has antiresonant frequencies given by the eigenvalues of

$$\begin{bmatrix} K_{DI} & K_{DD} \\ K_{OI} & K_{OD} \end{bmatrix}^{-1} \begin{bmatrix} M_{DI} & M_{DD} \\ M_{OI} & M_{OD} \end{bmatrix} \begin{Bmatrix} \theta \end{Bmatrix} = \frac{1}{\omega_A^2} \begin{Bmatrix} \theta \end{Bmatrix} \quad (18)$$

where I, O, and D represent the input, output and internal isolator degrees-of-freedom, respectively. The two-dimensional and three-dimensional DAVIs have, respectively, each two and three uncoupled equations of the form of Equation (18). Two outputs displaced with dynamic symmetry from a given input, or the converse, are also described by Equation (18) because the roots are not changed by transposing a matrix.

It is possible to solve for simultaneous antiresonances on arbitrarily placed multiple outputs for an equal number of arbitrarily placed multiple inputs by letting I and O be greater than one in Equation (18). However, such simultaneous antiresonances will, in the general case, occur only for those distributions of input forces given by the product of the rectangular impedance matrix of rows corresponding to the forced degrees of freedom and the vector of displacements. This is the reason why multiple input-output antiresonant isolators are not used in engineering. It is observed that the impedance matrix of

Figure 7, is, in general, nonsymmetric while the impedance matrix of Figure 3 is necessarily symmetric. That is the mathematically distinguishing feature between absorbers and antiresonant isolators.

It is obvious from Equation (18) that an infinite number of mechanical systems exist which will produce antiresonant transmissibilities at more than one frequency. Such systems can be analytically synthesized using desired antiresonant frequencies, the biorthogonality condition, and the methods of Reference 7. However, not all such synthesized systems will be physically realizable and not all of the physically realizable synthesized systems will be practical from an engineering standpoint.

An immediately practical application of Equation (18) would be the investigation of physical multi-input antiresonant isolators with internal coupling using simpler engineering arrangements for multi-harmonic antiresonances than has yet been achieved.

Conclusion

This paper has presented a solution to the antiresonant eigenvalue problem. It has been shown that antiresonances can be determined by matrix iteration techniques. Antiresonant nodes introduced by dynamic absorbers and antiresonant isolators have been discussed to illustrate the novel application of the theory to helicopter engineering problems.

References

1. Meirovitch, L., ANALYTICAL METHODS IN VIBRATIONS, McGraw-Hill Book Co., New York, 1967.

2. Strutt, J.W., Baron, Rayleigh, THE THEORY OF SOUND, 2nd Edition, Volume 1, Sec. 142a, Dover Publications, New York, 1945.

3. Den Hartog, J.P., MECHANICAL VIBRATIONS, 4th Edition, McGraw-Hill Publishing Co., New York, 1956.

4. Kaman Aircraft Report RN 63-1, DYNAMIC ANTIRESONANT VIBRATION ISOLATOR (DAVI), Flannelly, W.G., Kaman Aircraft Corporation, Bloomfield, Connecticut, November 1963.

5. Rehfield, L.W., HIGHER VIBRATION MODES BY MATRIX ITERATION, Journal of Aircraft, Vol. 9, No. 7, July 1972, p. 505.

6. Biot, M.A., COUPLED OSCILLATIONS OF AIRCRAFT ENGINE-PROPELLER SYSTEMS, Journal of Aeronautical Society, Vol. 7, No. 9, July 1940, p. 376.

7. USAAMRDL Technical Report 72-63B, RESEARCH ON STRUCTURAL DYNAMIC TESTING BY IMPEDANCE METHODS, Giansante, N., Flannelly, W.G., Berman, A., U. S. Army Air Mobility Research and Development Laboratory, Fort Eustis, Virginia, November 1972.

THE EFFECT OF CYCLIC FEATHERING MOTIONS ON DYNAMIC ROTOR LOADS

Keith W. Harvey
Research Engineer
Bell Helicopter Company
Fort Worth, Texas

Abstract

The dynamic loads of a helicopter rotor in forward flight are influenced significantly by the geometric pitch angles between the structural axes of the hub and blade sections and the plane of rotation.

The analytical study presented includes elastic coupling between inplane and out-of-plane deflections as a function of geometric pitch between the plane of rotation and the principal axes of inertia of each blade. In addition to a mean collective-pitch angle, the pitch of each blade is increased and decreased at a one-per-rev frequency to evaluate the dynamic coupling effects of cyclic feathering motions. The difference in pitch between opposed blades gives periodical coupling terms that vary at frequencies of one- and two-per-rev. Thus, an external aerodynamic force at n-per-rev gives forced responses at n, n±1, and n±2 per rev.

The numerical evaluation is based on a transient analysis using lumped masses and elastic substructure techniques. A comparison of cases with and without cyclic feathering motion shows the effect on computed dynamic rotor loads. The magnitude of the effect depends on the radial location of the pitch change bearings.

Introduction

For a stiff-in-plane rotor system, the blade chordwise stiffness may be 20 to 50 times greater than the blade beamwise stiffness. The elastic structure tends to bend in the direction of least stiffness, resulting in dynamic coupling between out-of-plane and inplane motions as a function of the geometric pitch angles due to collective pitch, built-in twist, forced cyclic feathering motions of the torsionally-rigid structure, and elastic deformation of the blade and control system in the torsional mode.

Typical cruise conditions for a modern helicopter require collective pitch angles of 14 to 16 degrees at the root, depending on the amount of built-in twist. Cyclic feathering motions of 6 to 7 degrees are required to balance the one-per-rev aerodynamic flapping moments. In current design practice, elastic torsional deflections of the blade and control system of a stiff-in-plane rotor are generally less than one degree. The largest part of the angular motion in the blade-torsion degree of freedom, therefore, is the forced feathering motion due to cyclic pitch.

Periodic variations of the inplane/out-of-plane elastic coupling terms are caused when the geometric pitch angle of each blade is increased and decreased at a frequency of one cycle per rotor revolution. When one blade is at high pitch and the opposed blade is at low pitch, an asymmetrical physical condition exists with respect to a reference system oriented either to the mast axis or to the plane of rotation. One-half revolution later, the reference blade is at low pitch and the opposed blade is at high pitch. Thus, periodic dynamic coupling occurs at the principal frequency of one-per-rev with respect to a rotating coordinate system. The coupling terms are nonlinear functions of blade pitch; hence, these terms also have 2-per-rev content.

Both the steady and periodic coupling terms have been treated in an analytical study of the effects of one-per-rev cyclic feathering motions on dynamic rotor loads. Equations have been derived and programmed for a digital computer solution of the transient response of an elastic two-bladed rotor.

The rotor is modeled by elastic substructure elements and lumped masses, for which the accelerations and velocities are integrated over small time increments to determine time histories of deflections, inertia loads, bending moments, etc. The time-variant analysis includes the capability to calculate rotor instabilities. The present computer program has been tested for this capability, but further discussion of instabilities is beyond the intent of the paper.

Dynamic rotor loads have been calculated for a parametric series of rotors, where the coupled natural frequencies were tuned over the range of contemporary design practice for teetering rotors. A description of the analysis and a summary of computed results is presented.

Objective

A primary consideration in the design of a helicopter rotor is to minimize oscillatory bending loads, or at least to reduce the loads to a level that will ensure satisfactory fatigue life. During early stages of design, the principal method of evaluating the dynamics of a proposed rotor is to calculate its coupled rotating natural frequencies. If required, design changes are made to achieve sufficient separation between the natural frequencies and harmonics of the rotor operating speed.

Current practice at Bell Helicopter Company is to require a separation of 0.3 per rev for all flight combinations of rotor speed and collective pitch. One purpose of the present analytical development is to determine whether the separation rule may be relaxed due to beneficial effects of cyclic feathering motions on rotor dynamic response.

Collective and Cyclic Modes

The calculation of natural frequencies for semi-rigid rotors uses a coordinate system that is based on the plane of rotation. The orientation of the centrifugal force field, the angular motion allowed by the flapping hinge(s), and the constraints of opposing blades lead to the segregation of natural frequencies into collective modes, cyclic modes, and (for four-bladed rotors) scissor or reactionless modes. This procedure allows the use of continuous-beam theory for a single blade, where the centerline boundary constraints are imposed from conditions of symmetry or asymmetry to match deflections, slopes, shears, and moments for the other blades.

The centerline boundary conditions for the collective mode (Figure 1) are:

- zero vertical (out-of-plane) slope change,
- vertical deflection constrained by mast tension/compression,
- inplane slope constrained by mast torsion, and
- zero inplane translation.

The centerline boundary conditions for the cyclic mode (Figure 2) are:

- vertical slope change unrestrained (except with flapping springs),
- zero vertical deflection,
- zero inplane slope change, and
- inplane deflection constrained by mast shear.

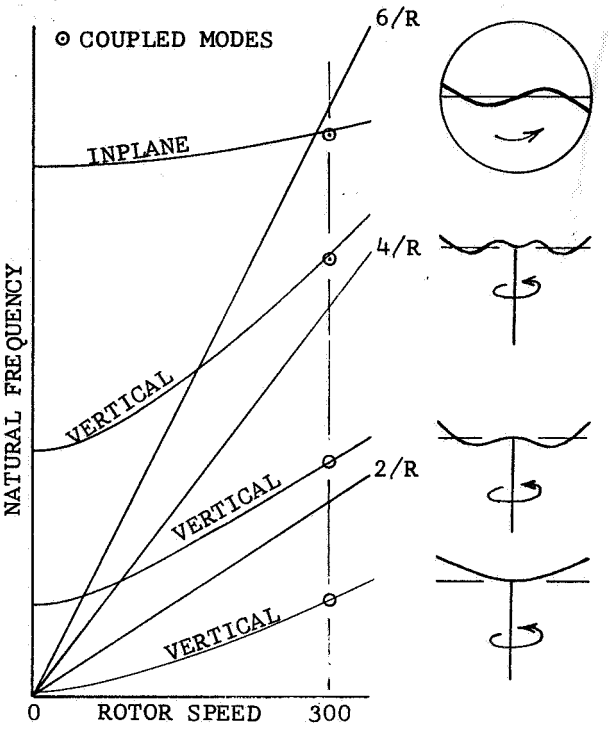

FIGURE 1. TYPICAL COLLECTIVE MODE FREQUENCIES AND MODE SHAPES.

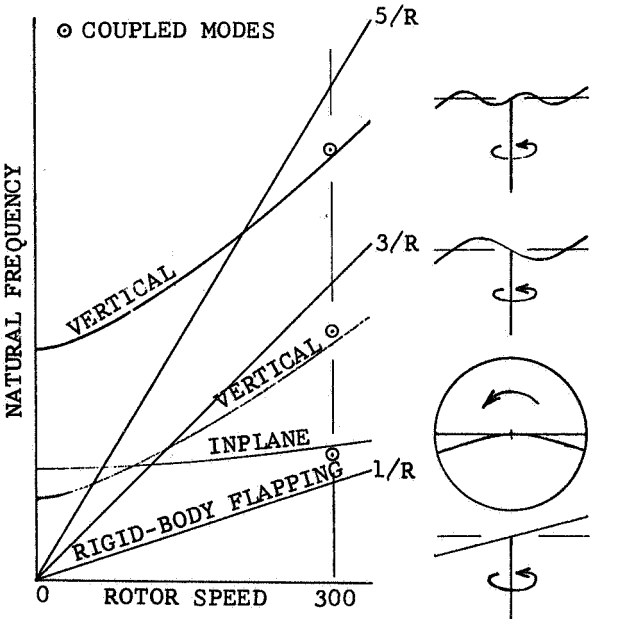

FIGURE 2. TYPICAL CYCLIC MODE FREQUENCIES AND MODE SHAPES.

For the reactionless modes, the centerline boundary conditions are:

- zero slope change and zero translation in both the inplane and vertical directions.

Uncoupled frequencies are determined by setting the geometric pitch angle of each elastic element to zero. The uncoupled frequencies are shown in Figures 1 and 2 by the labeled curves. Note that the frequencies of the vertical (out-of-plane) modes are highly dependent on rotor speed, and that the frequencies of the inplane modes are only slightly dependent on rotor speed.

Coupled natural frequencies are shown as small circles in the figures. Typical collective modes have very small frequency shifts as a function of collective pitch. However, the cyclic modes (Figure 2) couple significantly with collective pitch. Note that the inplane frequency decreases and the vertical frequencies increase with collective pitch. The method of determining these coupling effects is given in Reference 1.

By using only one blade plus appropriate boundary conditions, this method of calculating rotor natural frequencies is based on one explicit assumption, i.e., all other blades are at the same geometric pitch angle as the reference blade. If the blades are at different pitch angles, then the conditions of symmetry or asymmetry are not present. The inclusion of cyclic feathering motion, therefore, requires that the analysis treat separately each blade of the rotor and provide a means of matching the centerline slopes and deflections.

Elastic Substructured Rotor Analysis

A digital computer program has been developed to study the effects of cyclic feathering motions on dynamic rotor loads. The Bell Helicopter computer program is identified by the mnemonic ESRA for Elastic Substructured Rotor Analysis.

The analysis is a transient solution of elastic rotor blade motions, where the coupling terms for each blade are treated separately and the necessary constraints are imposed on each blade to insure slope and deflection continuity at the rotor centerline. Each blade is considered as being divided into a discrete number of segments, with uniform weight and stiffness properties over the length of a segment. The geometric pitch angle of each segment is a function of rotor azimuth position and input values of fore/aft and lateral cyclic pitch. To represent the hub structure that is inboard of the pitch-change bearings, the inboard elastic element may be specified as an uncoupled element (geometric pitch equals zero).

All forces are applied at the ends of the elastic elements. Slope and deflection changes over the length of a segment are based on linear moment distributions versus span. For compatibility, shear over the segment length must be constant, which requires concentrated forces for both internal and external forces. In its simplest form, the analysis follows a lumped-mass approach. All of the important rotor dynamic characteristics may be retained with this method, however, by using the concepts of equivalent structural segments.

The dynamic response equations are solved by a step-by-step iterative method in order to include transient conditions. If the initial deflections and velocities are specified (spanwise distributions for each blade), then the internal bending moment distributions are found with respect to the rotating reference system. Internal shear distributions are obtained from the moment distributions, and summed with applied airload forces and inertial components of the centrifugal force field to determine spanwise distributions of accelerations.

The first estimates of deflection and velocity changes are calculated for constant acceleration during the integration time step. Then bending moments, shears, and accelerations are calculated for the end of the time step. Subsequent deflection and velocity estimates are based on accelerations changing linearly with time, and the iterations continue until a prescribed error limit is satisfied for the entire set of accelerations, or until a limit is reached on the number of iterations.

In recognition of the problems inherent with this type of numerical integration, the initial development of the ESRA computer program has been limited to a qualitative study of cyclic feathering effects. The current program represents each blade with four elements, each with beamwise and chordwise bending elasticity. Only the forced rigid-body motion is allowed in the blade-pitch degree of freedom, i.e., elastic blade torsion is not considered.

The current computer program is limited to two-bladed rotors, and the torsional impedance of the drive system is assumed to be zero. In practice, the rotor senses a two-per-rev torque from the mast that is proportional to the drive-system impedance times the Hooke's-joint angular oscillation, which is a function of rotor flapping. The rotor is the predominant inertia component of the drive system, and a good approximation for two-bladed rotors is to assume

that the true axis of rotation remains perpendicular to the tip-path plane even when the tip path plane is not perpendicular to the mast. Thus, Coriolis accelerations equal to the product of coning times flapping are not appropriate in a two-bladed rotor analysis.

Bending deflections of the elastic elements are linearized; therefore, Coriolis accelerations from radial foreshortening are excluded also. Vertical and inplane translational motions of the rotor center are not included in the current version of the program.

Referring to the description above, the formulation of the analysis allows the removal of these limiting assumptions. For instance, nonlinear bending deflections and Coriolis accelerations may be included by a direct addition to the inertial forces acting on each mass. Translation of the rotor centerline, additional blades, control system flexibility, elastic blade torsion, and nonlinear hub and control kinematics also may be added within the existing computational method.

With the limitation of four elastic elements for each blade, plus provisions for slope and deflection continuity at the rotor centerline, the current ESRA program allows 15 distinct vibration modes for the rotor:

- 3 rigid-body modes (flapping, mast torsion, blade pitch)
- 6 coupled elastic collective modes (3 vertical, 3 inplane)
- 6 coupled elastic cyclic modes (3 vertical, 3 inplane)

In attempts to predict rotor loads for two-bladed rotors, emphasis is placed on response components at least up to the third harmonic of rotor speed. Three-per-rev airloads excite the cyclic mode that derives from the first elastic asymmetric mode in the out-of-plane direction. Four elastic elements for each blade should provide a very satisfactory dynamic representation for this frequency range. At a frequency of five-per-rev, the second elastic mode would be excited and computed loads may be marginally valid. Current design practice is to minimize higher frequency loads by proper tuning of the rotor natural frequencies, as discussed earlier.

Numerical Evaluation

A parametric computer study was accomplished to resolve a basic question:

> With respect to the natural frequency of the first coupled vertical elastic cyclic mode at or near 3 per rev, how much does cyclic feathering motion affect 3-per-rev dynamic rotor loads?

Selection of Rotor Dynamic Characteristics

Corresponding to a Huey main rotor, the computer study was based on a 48-foot diameter 2-bladed semi-rigid rotor, operating at 300 RPM. Two basic design approaches were selected as end points for the evaluation.

1. A constant blade weight distribution of 1.20 lb/in. with no dynamic tuning weights was picked to simulate the early production Huey rotors. Uniform beamwise and chordwise stiffness values were determined to locate the two lowest coupled cyclic mode frequencies at 1.40/rev (inplane) and 2.60/rev (vertical) for a collective pitch of 14.75 degrees. The fan plot of cyclic mode natural frequencies for this rotor is shown in Figure 3.

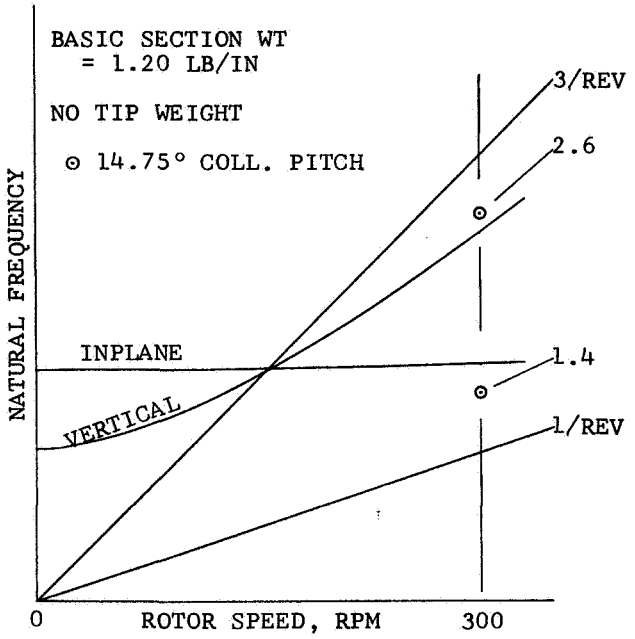

FIGURE 3. CYCLIC MODE, TUNED BELOW 3/REV.

2. A very recent rotor development at Bell (the Model 645 rotor) was simulated by a configuration with a constant blade weight distribution of 1.00 lb/in plus a dynamic tuning weight of 100 pounds located at the blade tip. Uniform beamwise and chordwise stiffness values were determined to locate the coupled cyclic mode frequencies at 1.40/rev (inplane) and 3.40/rev (vertical), as shown in Figure 4, again for 14.75 degrees of collective pitch.

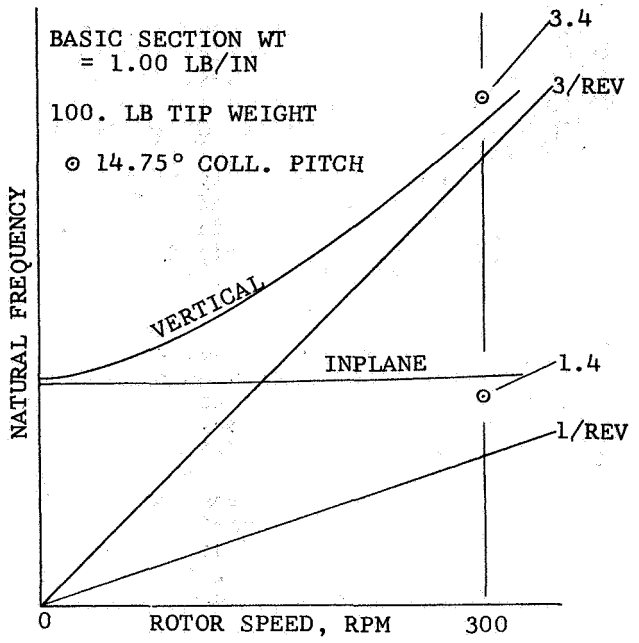

FIGURE 4. CYCLIC MODE, TUNED ABOVE 3/REV.

Between the two basic configurations, a series of intermediate rotor parameters was established by stepping the uniform blade weight from 1.20 down to 1.00 by increments of 0.025 lb/in., while increasing the tip weight from 0. to 100. by increments of 12.5 pounds. Beamwise and chordwise stiffnesses were varied to hold the coupled inplane frequency at 1.40/rev while tuning the coupled vertical frequencies from 2.60/rev to 3.40/rev in increments of 0.10/rev. Thus, to compensate for the program restriction of no hub motion, proper placement of the coupled inplane frequency was maintained by the selection of rotor stiffness. This approach affects the spanwise distribution of inplane bending moments, but is entirely adequate for a qualitative evaluation.

All of the above frequencies were tuned with the first segment uncoupled (hub structure to .25 radius), which maximized the coupling of the vertical mode near 3/rev and minimized the coupling of the inplane mode near 1/rev.

Additional input data was taken directly from the Bell Helicopter Rotorcraft Flight Simulation, program C81-68 (References 2, 3), for a Model 309 King-Cobra flying at 150 knots. Data used in the present computer evaluation included a collective pitch setting at the root of 14.75 degrees, a total cyclic pitch of 6.30 degrees, and the spanwise distributed airloads up to and including the third harmonic components.

The study results presented below are based, therefore, on full-scale parameters that are realistic with regard to current helicopter design practice. Although direct correlation with measured loads is not possible because of the simplifying assumptions, it may be noted that the magnitude of calculated bending moments is well within the expected range.

Computed Results

The forced response was computed for the series of nine parametric rotor configurations, where the inplane coupled frequency was held at 1.40/rev and the vertical coupled frequency was varied from 2.60/rev to 3.40/rev. The dynamic rotor loads for each configuration were calculated twice, once with cyclic feathering and once without cyclic feathering.

Figure 5 shows the 2/rev vertical bending moment at the rotor centerline as a function of natural frequency of the vertical elastic cyclic mode. The 1/rev variation in structural coupling due to cyclic pitch, and the 3/rev applied airloads produce a 2/rev component of bending moment. This additional component peaks and changes sign as the vertical mode is tuned through 3/rev. For the two-bladed rotor, 1/rev and 3/rev vertical bending moments at the centerline are negligible.

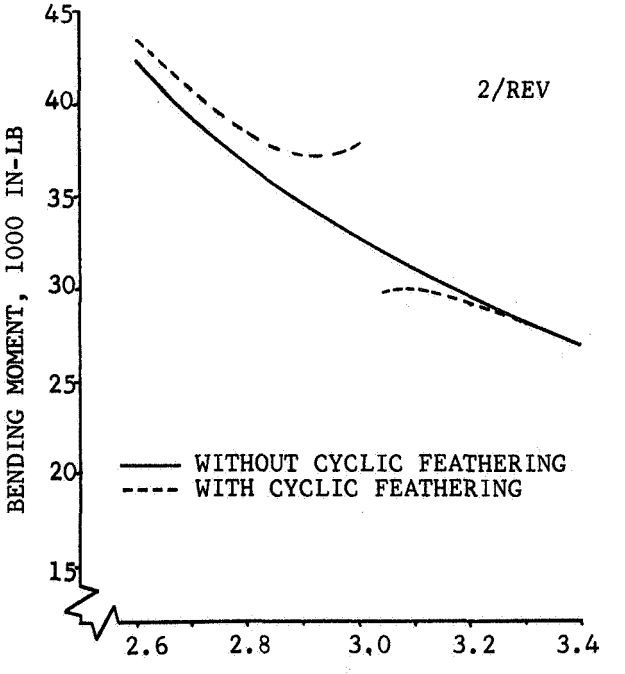

FIGURE 5. VERTICAL MOMENT AT CENTERLINE

Inplane bending moments at the rotor centerline are shown in Figure 6. The large peak in the overall oscillatory moment occurs as the coupled vertical mode is tuned through resonance at 3/rev. Note that the coupling associated with cyclic feathering increases the 1/rev response by about 5 percent for the vertical frequency tuned to 2.6/rev. In other respects, the effect of cyclic feathering appears to be minimal.

Beamwise moments and chordwise moments at midspan are shown in Figures 7 and 8, respectively. Two-per-rev moment components are not shown in the figures because of their small magnitudes. The significance of the cyclic feathering effects at midspan is consistent with that indicated in earlier figures for the rotor centerline.

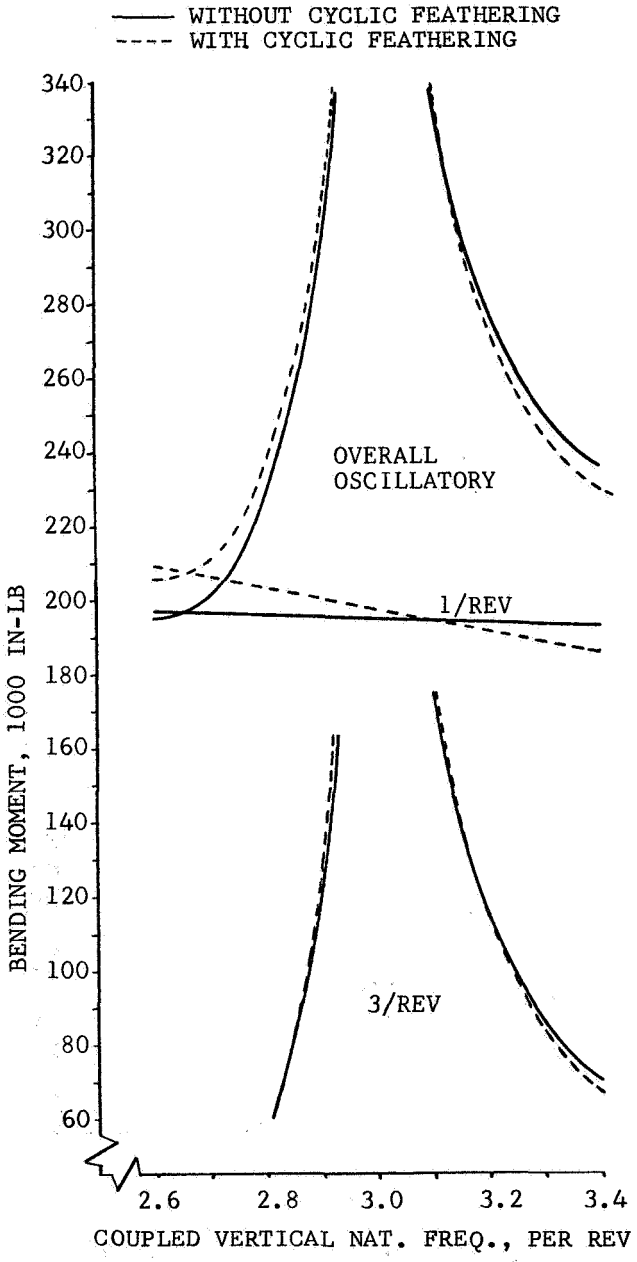

FIGURE 6. INPLANE MOMENT AT CENTERLINE

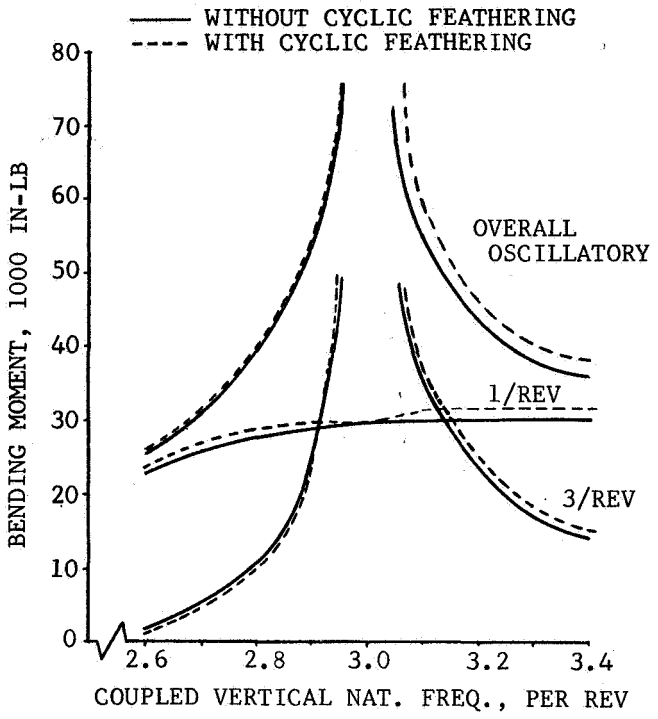

FIGURE 7. BEAMWISE MOMENT AT MID SPAN

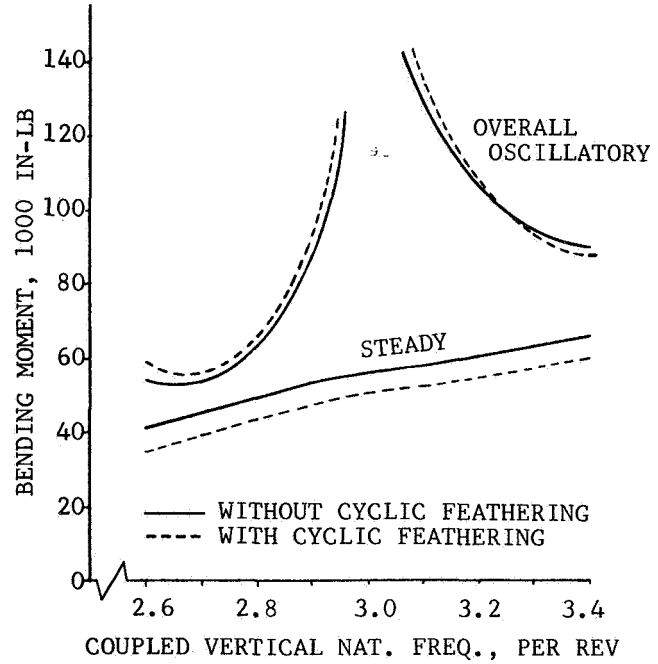

FIGURE 8 . CHORDWISE MOMENT AT MID SPAN

As discussed in a previous section, the aeroelastic effect of blade bending velocity was excluded from this study by basing the response calculations on a prescribed set of airloads. No inference is intended regarding the magnitude of aerodynamic damping that may be associated with elastic bending velocities. Conversely, the procedure was selected so that the time-variant structural couplings could be studied in an analytical environment that does not include other sources of damping.

The computed responses appear as undamped resonances centered at 3/rev, from which it follows that cyclic feathering motions do not provide any significant amount of equivalent damping to suppress 3/rev dynamic loads. Regarding the vertical cyclic mode near 3/rev, in particular, the effect of cyclic feathering motion does not provide relief for the design rule that requires 0.3/rev separation of coupled frequencies from excitation harmonics of rotor speed.

The results presented above are all based on rotor structural simulations with the inboard 25 percent radius treated as non-feathering hub structure. This option of the program was selected to maximize the coupling (as a function of collective pitch) of the vertical cyclic mode near 3 per rev. As noted, the largest change in rotor loads due to the inclusion of cyclic feathering motions was a 5 percent increase in inplane bending moments at the rotor centerline.

The pitch-change or feathering bearings of production two-bladed main rotors are located typically at about 10 percent radius. In this respect at least, the above results are based on a dynamic model that is not representative of actual design practice.

To evaluate the importance of the radial location of the bearings, another set of rotor loads was computed for a case where the entire radius is in the feathering system.

A constant blade weight distribution of 1.20 lb/in with no dynamic tuning weights was selected, as before, to simulate the early production Huey rotors. The structural properties of the rotor were modified to maintain a 1.40/rev natural frequency for the coupled inplane cyclic mode. For the modified parameters, the natural frequency of the coupled vertical cyclic mode is 2.87/rev.

The computed results are shown in Figures 9 through 12 for the case in which the feathering bearings are located at zero percent radius. The bar graphs show first, second, and third harmonics plus overall levels of oscillatory bending moments. The open bars are for the condition of no cyclic pitch, i.e., the geometric pitch of the elastic elements held fixed at the specified value of collective pitch. The closed bars are for the condition that the geometric pitch of the elastic structure is a function of both collective pitch and cyclic pitch.

Vertical and inplane oscillatory bending moments at the rotor centerline are shown in Figures 9 and 10, respectively. The vertical moments are not changed

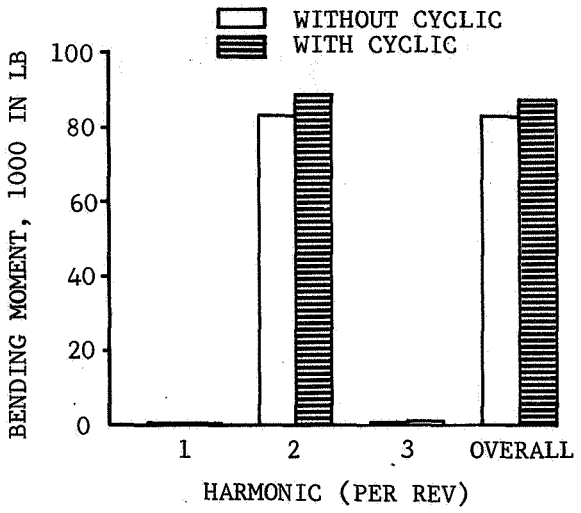

FIGURE 9. VERTICAL MOMENT AT CENTERLINE

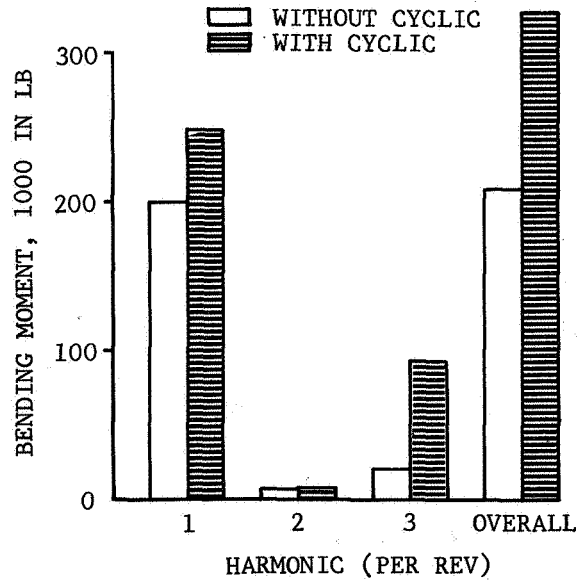

FIGURE 10. INPLANE MOMENT AT CENTERLINE

significantly by the inclusion of cyclic pitch. However, the inplane centerline moments increase by 57 percent, with both the first and third harmonics contributing to the increase.

Beamwise and chordwise oscillatory bending moments at 50 percent radius are shown in Figures 11 and 12. Most of the increase in the overall oscillatory moments at mid-span is due to an increase in 3/rev response.

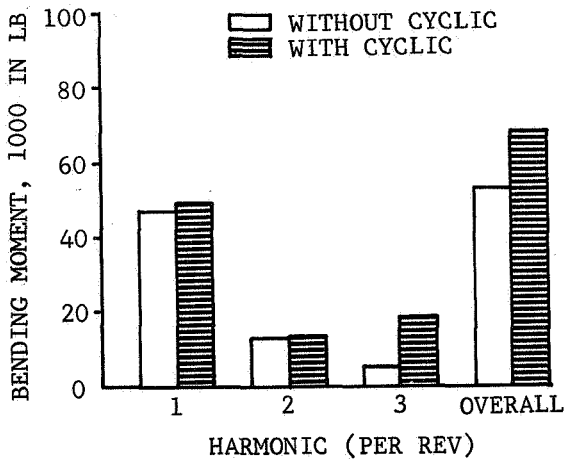

FIGURE 11. BEAMWISE MOMENT AT MID-SPAN

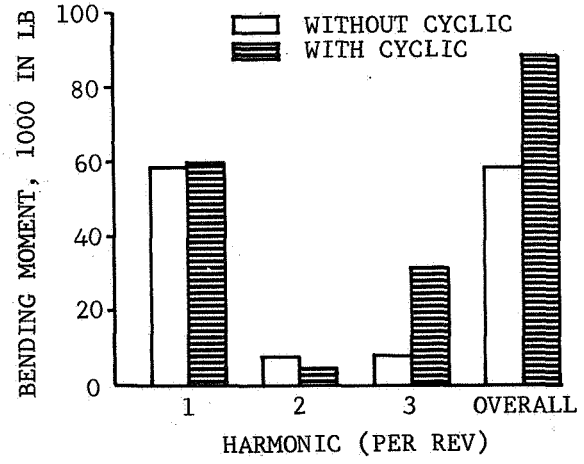

FIGURE 12. CHORDWISE MOMENT AT MID-SPAN

Due to cyclic feathering motions, a significant increase (57 percent) in rotor loads is indicated with the feathering bearings at zero percent radius; a minimal increase (5 percent) is indicated with the feathering bearings at 25 percent radius. This suggests that the radial location of the feathering bearings may have a controlling influence on the magnitude of the cyclic-feathering effect. Further study of this relationship is in progress.

Conclusions

1. The cyclic feathering motions of a helicopter rotor cause time-dependent elastic coupling due to asymmetrical pitch on opposed blades. The effect of these motions on dynamic loads may be calculated by modeling the rotor with elastic substructure elements, by providing individual treatment of each blade, and by matching slopes and moments at the rotor centerline.

2. Cyclic feathering motion of the elastic blade structure does not cause any significant damping effect on the 3-per-rev dynamic loads of a two-bladed semi-rigid rotor. The design rule requiring 0.3/rev separation between coupled natural frequencies and aerodynamic excitation frequencies should not be relaxed on the expectation of beneficial effects from cyclic feathering.

3. The inplane one-per-rev rotor loads of a stiff-in-plane rotor are affected significantly by cyclic feathering of the elastic structure. The magnitude of the effect is decreased as the feathering bearings are moved radially away from the rotor centerline.

References

1. Blankenship, B. L. and Harvey, K. W., A DIGITAL ANALYSIS FOR HELICOPTER PERFORMANCE AND ROTOR BLADE BENDING MOMENTS, Journal of the American Helicopter Society, Vol. 7, No. 4, October 1962, pp 55-69.

2. Duhon, J. M., Harvey, K. W., and Blankenship, B. L., COMPUTER FLIGHT TESTING OF ROTORCRAFT, Journal of the American Helicopter Society, Vol. 10, No. 4, October 1965, pp 36-48.

3. USAAVLABS Technical Report 69-1, ANALYTICAL STUDY OF HELICOPTER GUST RESPONSE AT HIGH FORWARD SPEEDS, Harvey, K. W., Blankenship, B. L., and Drees, J. M., U.S. Army Aviation Materiel Laboratories, Ft. Eustis, Virginia, September 1969.

CONTROL LOAD ENVELOPE SHAPING BY LIVE TWIST

F. J. Tarzanin, Jr.
Senior Engineer, Boeing Vertol Company, Philadelphia, PA

P. H. Mirick
Aerospace Engineer, Eustis Directorate, USAAMRDL, Ft. Eustis, VA

Abstract

For flight conditions at high blade loadings or airspeeds, the rotor control system experiences a rapid load growth, resulting from retreating blade stall. These loads frequently grow so large that the aircraft flight envelope is restricted long before the aircraft power limit is reached. A theoretical study of one flight condition and a limited model test have shown that blade torsional flexibility plays a major role in determining the magnitude of these large, stall-induced control loads. Recently, an extensive analytical investigation* was undertaken to determine the effect of changing blade torsional properties over the rotor flight envelope. The results of this study showed that reducing the blade stiffness to introduce more blade live twist** could significantly reduce the large retreating blade control loads. Too much live twist, however, may increase the control loads by introducing a large nose-down advancing blade torsional moment. Still, significant control load reductions can be achieved and the flight envelope can be expanded by increasing live twist to reduce retreating blade stall loads, but not enough to greatly increase advancing blade loads.

Introduction

For any practical helicopter design, the level-flight, steady-state loads should be below the endurance limit (infinite life load) so that sufficient life will be available to absorb the larger maneuver loads. A major design objective is to produce an aircraft with a flight envelope limited by aircraft power and not by structural limits Frequently, however, the operational flight envelope is limited by a rapid growth of stall-induced control loads that exceed the endurance limit. Therefore, the flight envelope is limited by control loads, and the available power cannot be fully utilized.

The rapid control load growth is attributed to stall flutter which is a consequence of high angles of attack and resulting blade stall. Visual confirmation of the large stall loads can be found in pitchlink or blade torsional gage waveforms on which characteristic stall spikes appear in the fourth quadrant of the blade azimuth. These high loads result from an aeroelastic, self-excited pitch motion in conjunction with repeated submersion of a large portion of the rotor blade in and out of stall.

An aeroelastic rotor analysis program[1] was developed, using unsteady aerodynamic theory that could preduct the large stall-induced control loads. Limited analytical studies of a single flight condition, using this program[2] and another study by Sikorsky Aircraft[3], indicated that modifications to the blade torsional properties could significantly reduce the stall-induced control loads. These encouraging theoretical results led to a model test[3] to verify the control load reduction. The test results showed that, by reducing the blade torsional natural frequency from 5.65 to 3 per rev, the model stall flutter torsion spike was reduced 73 percent, giving a first verification of the analytical trend.

Next, an extensive study was undertaken to explore the impact of modified blade torsional properties on blade torsional loads over the flight envelope. The study had two major parts--the first part compared model test results of blades with different torsional properties with analytical results to evaluate the analysis; while the second part analytically explored the variation of control loads for flight conditions of hover and 125, 150, and 175 knots with blade loadings (C_T/σ) from 0.05 to 0.18. This paper summarizes the results of this study.

Theory and Test Comparison

For useful analytical results, confidence in the theory must be established to show that the fundamental phenomena are properly accounted for. The aeroelastic rotor analysis has been successfully correlated with control loads obtained from full-scale CH-47C flight data for both stalled and unstalled conditions. Additional correlation with the model rotors

* Work performed under Contract DAAJ02-72-C-0093, Investigation of Torsional Natural Frequency on Stall-Induced Dynamic Loading, by The Boeing Vertol Company, U. S. Army Air Mobility Researc and Development Laboratory (USAAMRDL).

** Live twist is the steady and vibratory elastic pitch deflection that results from blade torsional loads.

test was performed to further evaluate the analysis.

The model test used three six-foot diameter rotor sets. Each rotor set had three articulated blades with identical airfoil and planform, but each set had a different torsional natural frequency. The first set of blades had a torsional natural frequency of 4.25 per rev and was constructed of fiberglass, using conventional crossply torsion wrap. The second set of blades had mass properties similar to the first blade set, but had a torsional natural frequency of 3.0 per rev. These blades were constructed with fiberglass, using a uniply torsion wrap which substantially reduced the blade torsional stiffness. The third set of blades had a torsional natural frequency of 5.65 per rev and was constructed of carbon composite. Although the carbon blades were not significantly stiffer than the first set of blades, they had significantly lower torsional inertia which accounted for the higher torsional natural frequency.

A number of runs were made for each rotor set at full-scale tip speeds and an advance ratio of 0.3. Due to the difference in torsional properties, the blade live twist of each rotor set was different, resulting in propulsive force and thrust differences for identical collective, cyclic, and shaft angle. One run for each rotor set was selected such that the rotors would have similar propulsive force variations with thrust. From each of these runs, five test points were selected which covered the range of available blade loading (C_T/σ) and which provided at least one flight condition below stall, one condition in transition, and two stalled conditions. A detailed description of the test conditions and all the model blade physical properties are given in Reference 4.

The variation of test and analytical blade torsion amplitude with blade loading (C_T/σ) is shown in Figures 1, 2, and 3 for the low stiffness, standard reference, and carbon blades, respectively. Each blade was instrumented to record blade torsion data. Due to gauge failures, only two gauges on the standard reference blades and only one gauge on the carbon blades were operational. In general, the analysis correctly predicts the trend of blade torsional load amplitude with blade loading for both stalled and unstalled flight conditions. The predicted stall inception agrees well with test for the low stiffness blade. For the standard reference blade and the carbon blade, stall inception is predicted about 0.01 C_T/σ too early (see Figures 2 and 3). The analysis predicts approximately the correct torsional load growth rate in stall; but, because the stall inception is predicted early, the

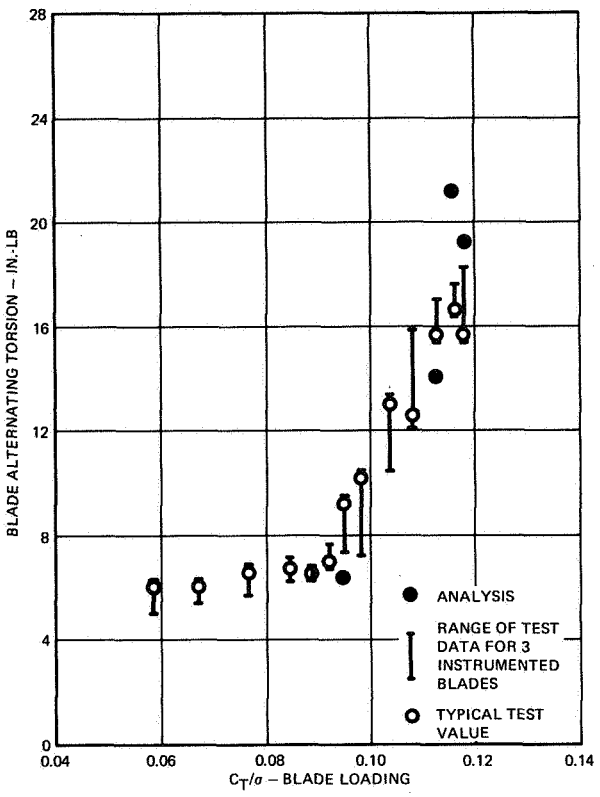

Figure 1. Comparison of Measured and Calculated Blade Torsion Amplitude for the Low Stiffness Blade (3 per rev).

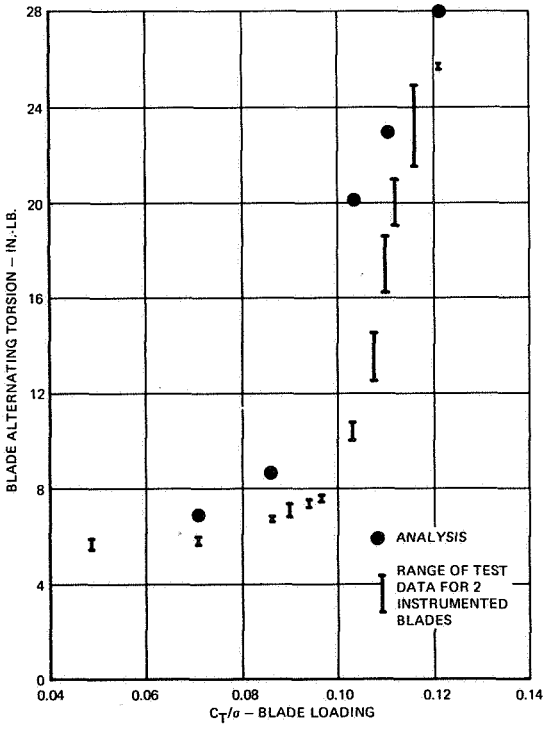

Figure 2. Comparison of Measured and Calculated Blade Torsion Amplitude for the Standard Blade (4.25 per rev).

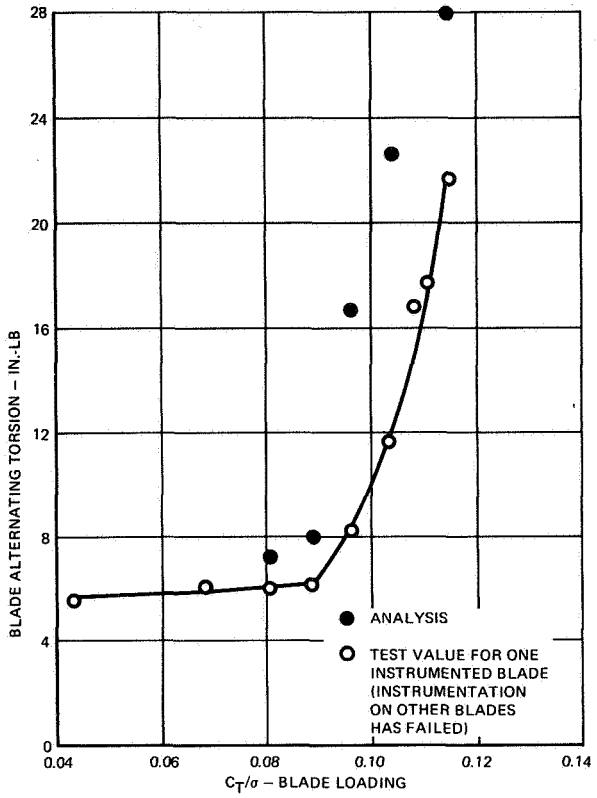

Figure 3. Comparison of Measured and Calculated Blade Torsion Amplitude for the Carbon Blade (5.65 per rev).

stall loads are overpredicted for the two stiffer blades.

A number of possible explanations for the analytical overprediction are discussed in Reference 4. The two most likely explanations are first, questionable model blade physical properties (possible 0.02 chord error in the carbon blade center of gravity, 0.06 chord error in the standard blade shear center, and -0.07 chord error in the carbon blade shear center) secondly, the unsteady aerodynamic plunging representation is inadequate (a lack of cyclic pitch led to model blade flapping of 12 , the theory may be overly sensitive to these large plunging velocities).

Even though correlation is not as good as desired, it is clear that the analysis predicts the large stall-induced control load increase (stall flutter), approximates the control load increase with increasing rotor thrust, and defines the proper load trend for changes in blade torsional properties. These results are sufficient to provide a degree of confidence in the theoretical trends, indicating that the qualitative results of the flight envelope investigation are meaningful.

Analytical Investigation of Stall-Induced Dynamic Loading

The analysis and test of Reference 2 showed that changes in blade torsional property can change the stall-induced control loads. For this discovery to have a practical application, it must be shown that realistic changes in the blade torsional properties will lead to a significant reduction in the large stall-induced control loads throughout the flight envelope. To determine the variation of control loads over the flight envelope, an extensive analytical study was performed. The aircraft used for this study was a single-rotor helicopter with CH-47C blades. A 20.1 square-foot frontal area was assumed for the fuselage and a tail rotor sufficient for trim purposes was added. The main rotor consisted of three articulated 30-foot radius blades with a constant chord of 25.25 inches. The blade cross-section is a cambered 23010 airfoil with 9.137 degrees of linear twist along the blade span.

To perform this study, blade torsional properties were modified by changing blade torsional stiffness (GJ), changing control system stiffness, and changing blade pitch inertia. Using the CH-47C blade's torsional natural frequency of 5.2 per rev as a baseline, the frequencies were adjusted from 3 per rev to 7 per rev.

Natural frequencies of 3 rev, 4 rev, and 7 rev were obtained by multiplying the torsional stiffness distributions by 0.25, 0.5 and 3.3, respectively. A control system stiffness of 1650 pounds per inch generated a frequency of 3 per rev; 11,850 pounds per inch was used for the basic blade, and an infinite stiffness produced a 6 per rev frequency. Pitch inertia changes resulted in blades with frequencies of 3, 4 and 7 per rev due to scaling the pitch inertia by factors of 3.08, 1.7 and 0.55, respectively. All changes were made by only varying the blade properties indicated, while holding all other parameters at the nominal CH-47C values.

Figure 4 shows the relationship between pitch-link load amplitude and torsional frequency (3 per rev to 7 per rev) at an airspeed of 125 knots and a blade loading of 0.115 for the three methods of varying frequency. Each method produced approximately the same trend of increasing pitch-link loads with increasing torsional natural frequency. Figure 5 illustrates the variation of pitchlink load amplitude with natural frequency at 150 knots airspeed and blade loadings of 0.115. For both airspeeds, the variation in torsional stiffness leads to larger changes in pitch-link loads, than do changes in control stiffness or pitch inertia.

Since blade torsional stiffness changes resulted in the largest change in control load and the lowest loads, the effect of blade torsional stiffness changes will be

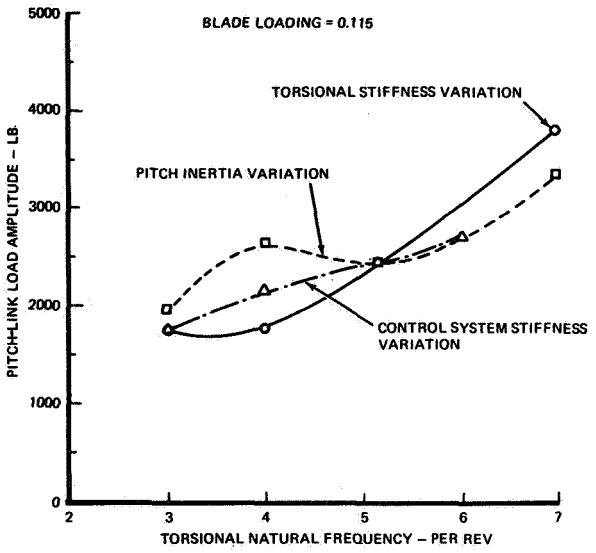

Figure 4. Variation of Pitch-Link Load Amplitude with Natural Frequency at 125 Knots.

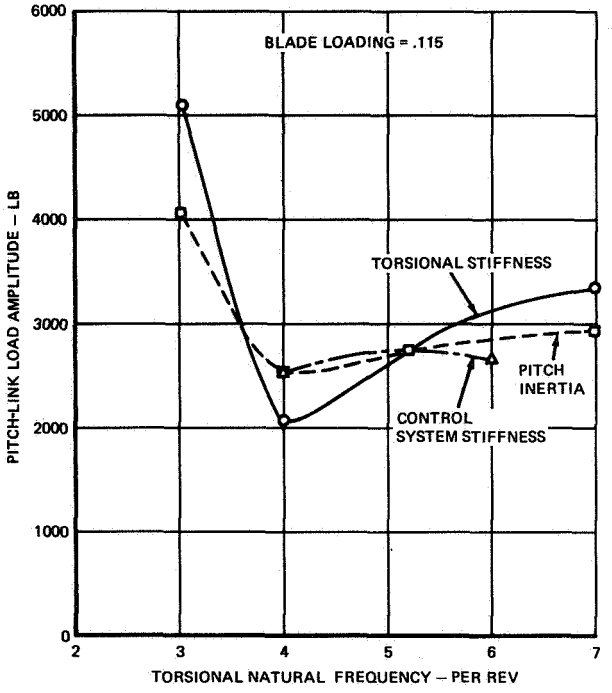

Figure 5. Variation of Pitch-Link Load Amplitude with Natural Frequency at 150 Knots.

explored in greater depth. It is apparent from these results that it is not the reduced torsional frequency alone that reduces pitch-link loads, but also the increase in blade live twist, resulting from reduced torsional stiffness.

Four blades with different torsional natural frequencies (i.e., 3 per rev, 4 per rev, 5.17 per rev and 7 per rev) were analyzed for 24 flight conditions to investigate the interactive effects of torsional stiffness, blade loading (C_T/σ), and airspeed. The airspeeds ranged from hover to 175 knots and blade loading from 0.05 to 0.018.

Hover

Figure 6 shows the variation of pitch-link load amplitude with blade loading for four sets of rotor blades. One degree of cyclic pitch was used to provide some means of introducing a cyclic load variation. If this were not done, the analysis would predict only steady loads. At blade loadings of 0.115 and 0.12 the pitch-link load has a 1-per-rev waveform with an amplitude of about 100 pounds for all four blades. These loads represent an unstalled condition, and there is virtually no load variation with blade loading or torsional natural frequency. At a blade loading of 0.15, the loads increase to between 200 pounds and 300 pounds, with the 3 per rev and 4 per rev blades having the lowest load. At this condition, the rotor power is around 4000 horsepower which is well beyond the available rotor power.

At a blade loading of 0.165, the pitch-link load for the 3 per rev blade increases sharply to 1000 pounds. The major portion of this load is a 950 pound, 8-per-rev component. Since the blade torsional natural frequency is 3 per rev, it was surprising to observe that there was little 3-per-rev load and a very large 8-per-rev load. Further examination revealed that the blade second torsional natural frequency is almost exactly 8 per rev, explaining the source of the large load. It is not known why the torsionally soft blade prefers to oscillate in its second mode. Further investigation is necessary.

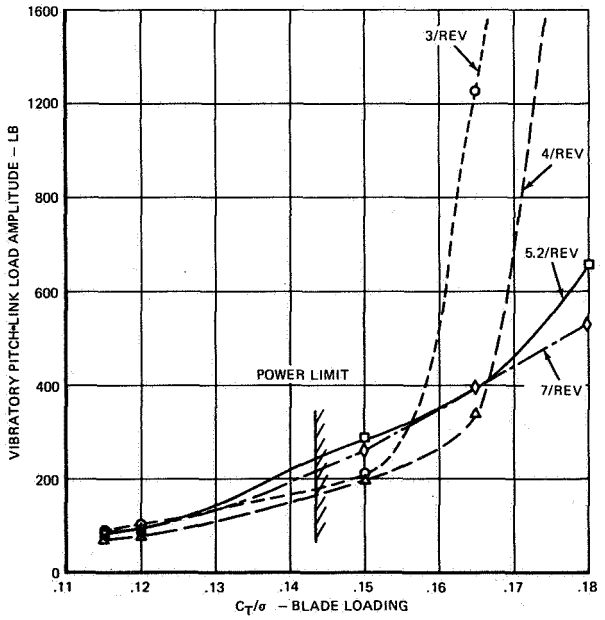

Figure 6. Variation of Pitch-Link Load Amplitude with Blade Loading in Hover for One Degree of Cyclic Pitch.

The 4-per-rev blade, at the same flight condition, has a pitch-link load of 340 pounds which is the lowest of the four blades. The 5.2-per-rev and 7-per-rev blades had approximately the same load at about 400 pounds. The required rotor power for all blades is approximately 5000 horsepower which is 66-percent more than the available rotor power of a CH-47C rotor. Since the required power is so high, results at this (0.165) and higher blade loadings probably have no practical application.

At a blade loading of 0.18, the 3 per rev blade pitch-link load increases to 4500 pounds, with the 8-per-rev component again providing the largest load. The 4-per-rev blade also shows a large load increase, reaching a load of about 4000 pounds. However, this blade's large torsional loads occurred at the first torsional natural frequency (3600 pounds at 4 per rev). The 5.2-per-rev blade has a load of 650 pounds and the 7-per-rev blade load is 540 pounds. At this condition, the loads reduce with increasing torsional frequency. The required rotor power for this flight condition is over twice the available power, indicating that rotor stall has reached a larger portion of the blade.

These results indicate that in hover, increased torsional frequency (i.e., torsional stiffness) delays the inception of stall flutter. This conclusion generally agrees with propeller experience. However, the large power required at a blade loading of 0.16 (i.e., 50 percent above available power) implies that this flight condition and higher blade loadings do not apply to current aircraft. If current power to rotor solidity ratios are therefore used, there is very little difference between the torsional loads of the four blades up to reasonable blade loadings (for this discussion, approximately 0.15 blade loading).

125 Knots

The variations of pitch-link loads with blade loading for each of the four different torsional frequency blades are shown in Figure 7 for an airspeed of 125 knots. The basic blade (with a torsional natural frequency of 5.2 per rev) pitch-link load increases slowly with increasing blade loading up to a value of 0.10. In this region, the pitch-link load waveform is predominantly 1 per rev (see Figure 8) and the loads are classified as unstalled (even though some stall is present). Stall inception occurs at a blade loading of about 0.103. The stall inception represents the flight condition in which the control loads begin to exhibit the rapid increase, due to blade stall. In this region, the pitch-link load waveform has a large, high-frequency torsional load component which generally appears between an azimuth position of 270 degrees to 60 degrees and usually determines the load amplitude as shown in Figure 9. The stalled pitch-link load continues to rise to 2650 pounds at a blade loading of 0.11. Increasing the blade loading beyond this point results in a load reduction. This reversal of the load trend may at first appear surprising, but it has been observed in model data (see Figure 1) and full-scale results (see Figure 10).

The 7-per-rev blade has generally the same pitch-link load trend, with blade loading as the basic blade. There is an unstalled load region up to a blade loading of 0.09 (with a typical waveform given in Figure 8), a stalled load region typified by a large load increase with blade loading (with a typical stalled waveform at a blade loading of 0.10 as shown in Figure 8), and a load reversal at a blade loading of 0.11. However, as far as control loads are concerned, the 7-per-rev blade is significantly worse than the basic blade. In the unstalled region, the loads are about the same; in stall the 7-per-rev blade loads are 65-percent larger. Stall inception occurs at a blade loading of about 0.095 which is 0.008 before the basic blade.

The 4-per-rev blade has a significantly different pitch-link load trend with increasing blade loading than the two blades

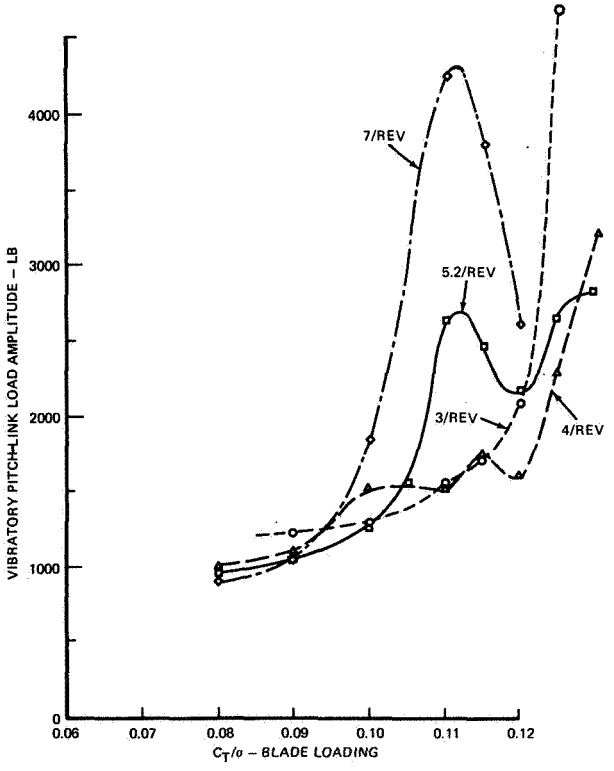

Figure 7. Variation of Pitch-Link Load Amplitude with Blade Loading at 125 Knots.

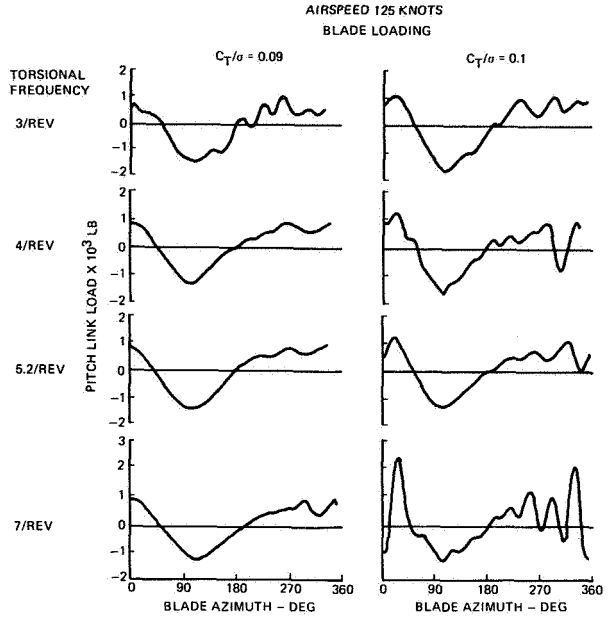

Figure 8. Pitch-Link Load Waveforms for 125 Knots, at Blade Loadings of 0.09 and 0.10.

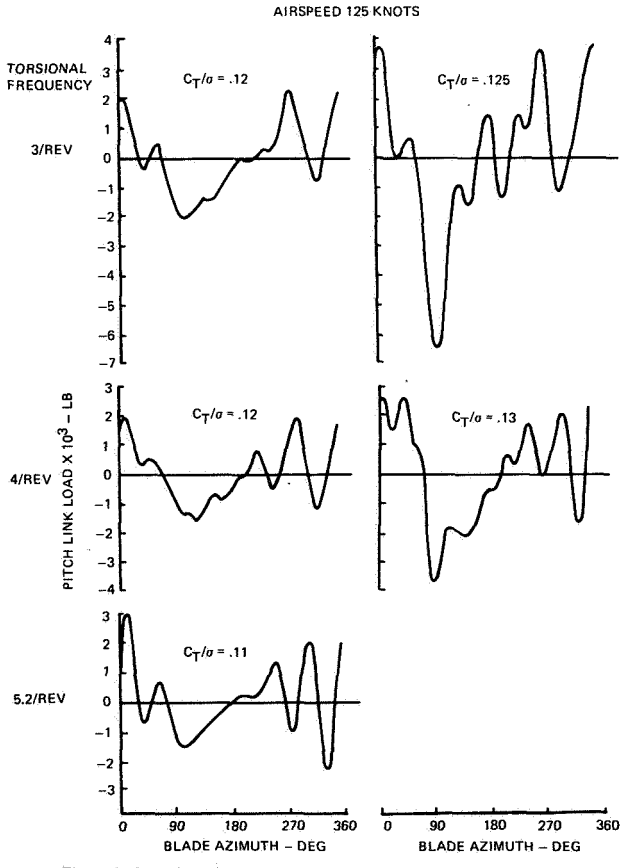

Figure 9. Pitch-Link Load Waveforms for 125-Knots at High Blade Loadings.

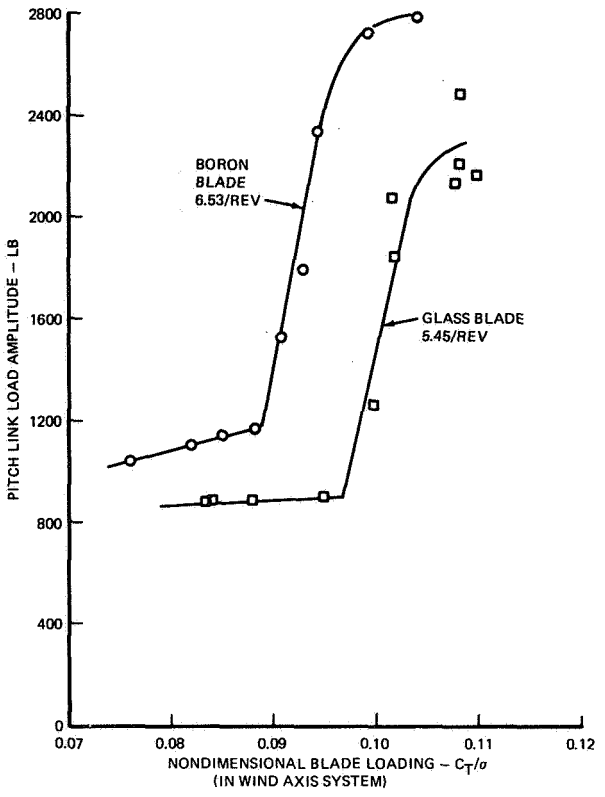

Figure 10. CH-47C Advanced-Geometry Blade Flight Test Data at an Advance Ratio of 0.2.

previously discussed. While there is the typical unstalled region with little load growth up to a blade loading of 0.09 (a typical unstalled waveform is given in Figure 8), there is an irregular, but moderate, load growth between 0.09 and 0.12. At a blade loading of 0.12, the torsion load is only 1641 pounds and the waveform just attains a fully stalled characteristic (see Figure 9). There is a large load increase (1360 in-lbs) as the blade loading increases from 0.12 to 0.13. Examining the 0.13 pitch-link load waveform (see Figure 9) shows that the large load is not caused by stall flutter; instead, it is due to a large nose-down moment generated by the advancing blade combined with moderate stall spikes.

The 3-per-rev blade has a load trend similar to the 4-per-rev blade. The unstalled load region extends to a blade loading of 0.115, and a typical unstalled waveform is given in Figure 8. Even at a blade loading of 0.12, the pitch-link load waveform does not show a fully stalled waveform (see Figure 9). However, at 0.125, the pitch-link load increases by 150 percent to 5273 pounds, by far the largest load of any blade. The waveform at 0.125 (see Figure 9) shows large stall spikes with an amplitude of 2500 pounds; however, the large load increase is due to

a 5000 pound load at 90° azimuth which results from a large nose-down pitching moment. The load growth is so large at this condition that it may represent the lower boundary of an instability.

It is clear from these results that stall inception occurs earlier as the blade torsional frequency is increased. Further, the maximum retreating blade stall-induced pitch-link loads are larger for blades with higher torsional frequencies (i.e., the 7-per-rev blade has the largest stall-induced loads).

The CH-47C flight test data substantiating the conclusion that stall inception occurs at higher blade loadings as blade frequency is decreased. Figure 10 shows the results of a CH-47C advanced-geometry blade flight test for aft rotor blades with a boron filament spar and a fiberglass spar at an advance ratio of 0.2. The glass blade has a stall inception delay of 0.0085, due to reducing the torsional frequency from 6.53 per rev to 5.45 per rev. The single-rotor study results show a stall delay of 0.008 for reducing the torsional frequency from 7 per rev to 5.2 per rev at an advance ratio of 0.3.

The large advancing blade loads experienced by the 3-per-rev and 4-per-rev blades, beyond a blade loading of 0.12, are not due to the stall-flutter phenomenon which results from retreating blade stall and unstall cycles. This load is associated with the negative lift on the advancing blade tip and appears to be a divergence-like phenomenon. Large, negative tip lift causes the blade to bend tip down; the high tip drag coupled with the flap deflection causes a nose-down moment. The moment causes elastic nose-down pitch which leads to more negative lift, resulting eventually in even larger loads.

150 Knots

At 150 knots (see Figure 11), the basic CH-47C blade has an unstalled load region up to about 0.08 which is typified by a slow increase of pitch-link load with blade loading and a predominantly 1-per-rev waveform. In the region between 0.08 and 0.1, a different load trend is observed. The load increases gradually from 1500 to 2000 pounds, but at a faster rate than the sub-stall load growth, and the waveforms show significant evidence of stall spikes for the retreating blade (see Figure 12). Stall inception (i.e., rapid load growth) appears to occur around 0.103, reaching maximum load near 0.11 (see Figure 12). The load drops at a blade loading of 0.115, showing a load reversal as observed at 125 knots.

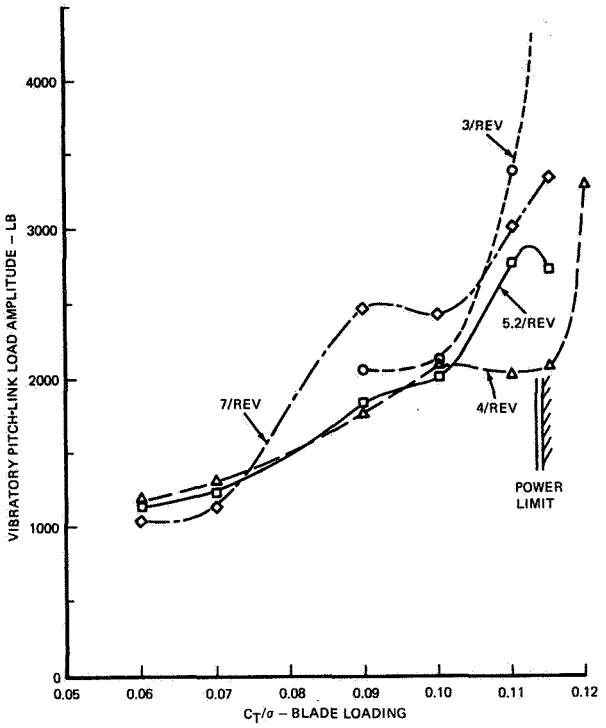

Figure 11. Variation of Pitch-Link Load Amplitude with Blade Loading at 150 Knots.

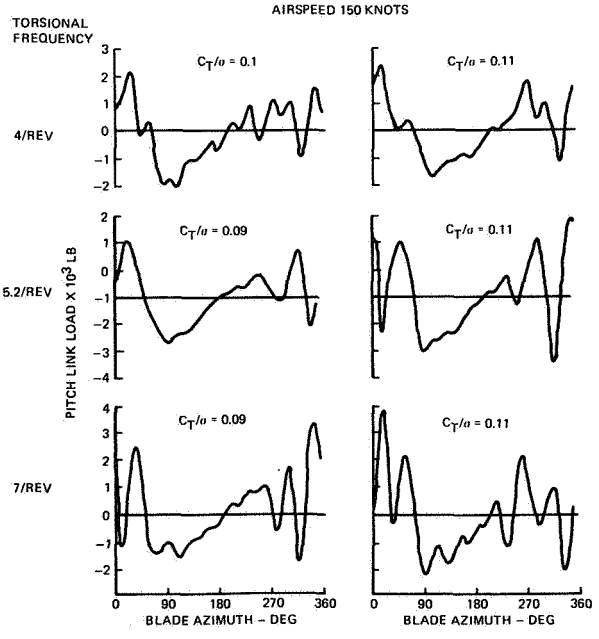

Figure 12. Pitch-Link Load Waveforms at 150 Knots for Blade Loadings of 0.09 to 0.11.

The 7-per-rev blade shows a similar load trend with blade loading as the basic blade, but with significantly larger stall loads. The unstall loads occur up to 0.07. Stall inception occurs at approximately 0.075, reaching a fully stalled waveform at 0.09 (see Figure 12). The loads level out at 0.10, reach a second stall inception near 0.105, and the load begins to grow again. Examining the pitch-link load waveform at 0.11 (see Figure 12) shows that the load increase is due to a large stall spike occurring in the 0 to 50-degree azimuth region, not to retreating blade stall spikes.

With an expected unstalled waveform the 4-per-rev blade has a typical unstalled control load growth up to a blade loading of about 0.09. Between 0.09 and 0.115, there is an irregular load growth. In this region, the waveforms show evidence of retreating blade stall (see Figure 12), but no large load increase. At a blade loading of 0.11, the torsion load is 2100 pounds and the waveform just attains a fully stalled characteristic (see Figure 12). There is a 1230-pound load increase as the blade loading increases from 0.115 to 0.12. Examining the 0.12 pitch-link load waveform (see Figure 13) shows that the large load increase is caused by a large, advancing-blade nose-down spike combined with retreating blade stall spikes.

The 3-per-rev blade shows a reasonable pitch-link load through a blade loading of 0.11. However, at 0.115, the blade is apparently unstable since the loads have grown so large that the blade would probably fail. The pitch-link load waveform at 0.11 (see Figure 13) contains relatively small retreating-blade, stall-induced spikes. There is, however, a large compression load for the advancing blade at 90 degrees blade azimuth. By examining the pitch link load waveform for the unstable flight condition, it appears that the blade divergence involves a large advancing blade compression load that continually increases with each rotor revolution.

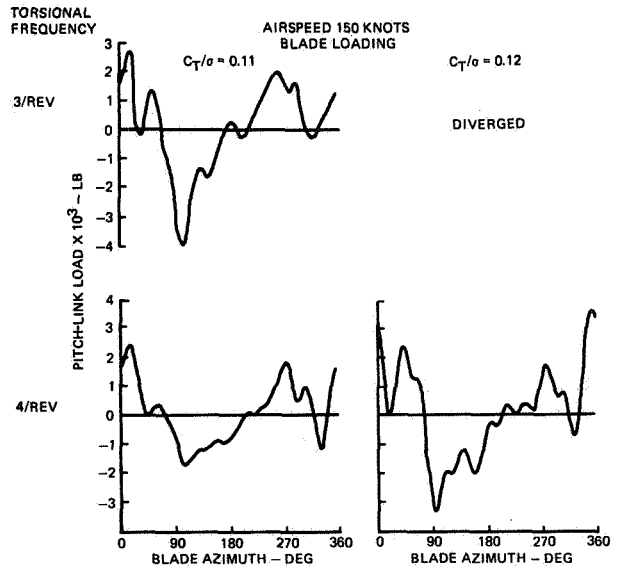

Figure 13. Pitch-Link Load Waveforms at 150 Knots for the 3-per-rev and 4-per-rev Blades at High Blade Loadings.

The 3-per-rev blade is experiencing an additional problem which is not apparent by simply observing the load trend. For all the load conditions calculated at 150 knots, the required power exceeds the available power. Apparently, the blade is experiencing so much live twist that there is a significant increase in rotor drag. The other blades, by contrast, exceed the available power only at a blade loading of 0.115. It is, therefore, obvious that the 3-per-rev blade is not an acceptable configuration for the 150-knot flight condition.

175 Knots

At 175 knots (see Figure 14), the basic blade pitch-link load trend shows unstalled loads continuing to a blade loading of 0.07 and stall inception occurring about 0.075. The stalled load increases with a moderate growth rate up to 0.09. Figure 15 illustrates the pitch-link load waveform at 0.09, showing the retreating blade stall spikes and a large nose-down load at 90 degrees azimuth. Beyond a blade loading of 0.09, the load does not reverse as it does for previous airspeeds (even though the retreating blade stall spike is significantly reduced at a blade loading of 0.11 as shown in Figure 15). Instead, the load continues to increase at about one half the previous growth rate, due to an increasingly large nose-down load at 90 degrees azimuth.

The 7-per-rev blade pitch-link load trend is almost identical with the basic blade trend up to 0.09. As Figure 15 shows, the waveform exhibits typical high-frequency stall spikes. The torsion load shows a slight load reversal beyond 0.09, but then resumes the load increase at the typical stalled load growth rate. The load growth at 0.11 is due to a combination of a large stall spike at around 30 degrees azimuth and an increasing nose-down load at 90 degrees azimuth (see Figure 15).

The 4-per-rev blade has a typical substall load growth up to 0.07 and generally follows the load trend of the 7-per-rev blade and the basic blade up to 0.08. Beyond this point, the load growth rate drops significantly. At a blade loading of 0.09, the pitch link load is 500 pounds

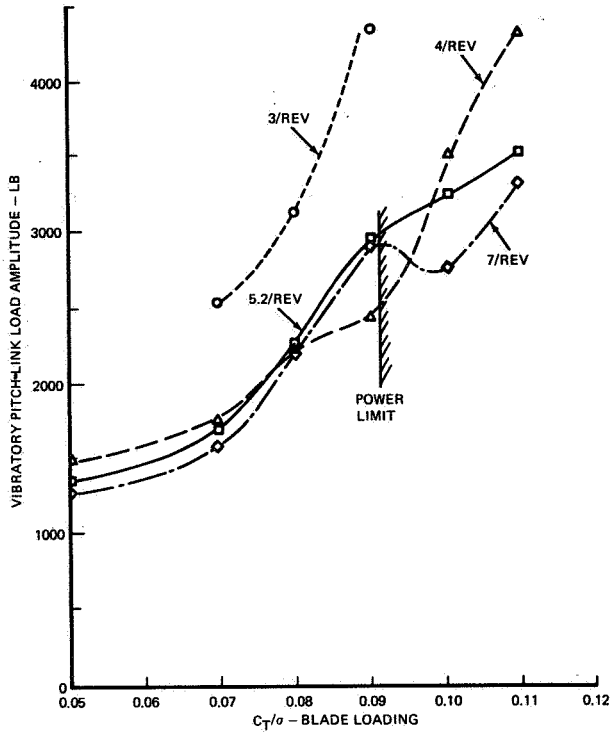

Figure 14. Variation of Pitch-Link Load Amplitude with Blade Loading at 175 Knots.

below the other two blades. Also 0.09, the pitch-link load waveform shows little evidence of retreating blade stall (see Figure 15), but does show that the major component of the load results from a nose-down moment at 90 degrees blade azimuth. Beyond this point, the load growth rate increases sharply from 2500 pounds at 0.09 to 4200 pounds at 0.11.

The 3-per-rev blade is not seriously considered at this airspeed. The loads are 1500 pounds beyond any of the other blades, and an advancing blade instability is apparent at a blade loading of 0.09. Further, the required rotor power exceeds the available CH-47C power for all 175-knot flight conditions examined.

Examining the 175-knot pitch-link load waveforms at a blade loading of 0.11 clearly shows that all four blades experience increased advancing-blade compression loads when compared to the 150-knot waveforms (compare Figures 12 and 14). The 7-per-rev blade shows a 1300-pound advancing-blade load increase for the 25-knot airspeed increase. The basic 5.2-per-rev blade load increase is 2200 pounds, the 4-per-rev blade load increase is 3500 pounds, and the 3-per-rev blade has diverged. Therefore, the blades experience advancing blade load problems which are intensified as airspeed is increased and blade torsional stiffness is reduced.

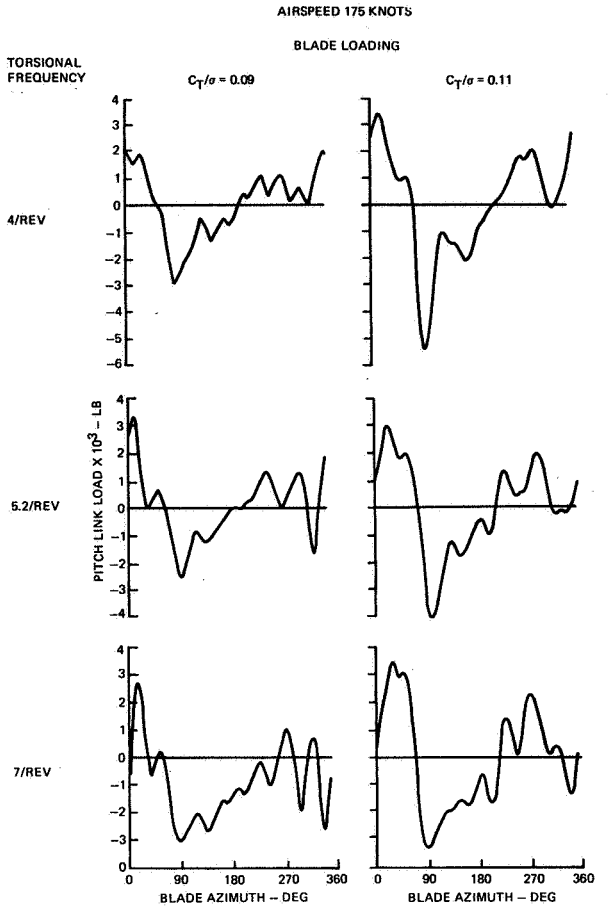

Figure 15. Pitch-Link Load Waveforms for 175 Knots at Blade Loadings of 0.09 and 0.11.

When comparing the 175-knot results for the 4-per-rev, 5.2-per-rev and 7-per-rev blades, it should be noted that the rotor power limit for a single CH-47C rotor is reached just beyond a blade loading of 0.09. For conditions below lthe power limit, the 4-per-rev blade is slightly better than the others, since the maximum pitch-link load is 500 pounds lower. The three blades appear to have adequate maneuver margin, although the 4-per-rev blade may experience larger maneuver loads.

These results show that a significant reduction of the basic blade control loads can be realized over a considerable range of advance ratios and blade loading and that these reductions lead to a significant extension of the control load-limiting aircraft flight envelope. These results can be summarized by obtaining the flight condition (as a function of C_T/σ and μ) that first experiences a 2500-pound pitch-link load. The 2500-pound load approximates the original pitch-link endurance limit load for the CH-47C control system. These flight conditions lead to a blade loading versus advance ratio envelope for the 2500-pound

pitch-link load or an endurance-limit flight envelope. Figure 16 compares the endurance limit flight envelopes for each of the four different frequency blades investigated.

As Figure 16 shows, the blade with a torsional natural frequency of 4 per rev (dashed line) has the best flight envelope and represents a significant improvement over the basic blade configuration. The 4-per-rev flight envelope has essentially the same shape as the basic blade, but it occurs at a higher blade loading. The basic blade envelope occurs at a blade loading of 0.016 below the 4-per-rev blade at an advance ratio of 0.29. At an advance ratio of 0.38, the basic and 4-per-rev blades are approximately equal; but at an advance ratio of 0.4, the 4-per-rev blade envelope is expanded beyond the basic blade by a blade loading of 0.005.

The 3-per-rev blade (short dashes) shows a different flight envelope. At an advance ratio below 0.29, the 3-per-rev blade reaches the endurance limit at a blade loading of 0.123. However, the 3-per-rev envelope drops sharply with increasing advance ratio and eventually falls below the three other blades at a 0.375 advance ratio. The sharp boundary reduction of this blade at the higher advance ratios is due to the large advancing-blade load growth which eventually becomes an instability.* These instabilities show that the 3-per-rev blade is clearly unacceptable, at least for the current pitch-link-controlled configuration.

The 7-per-rev blade clearly has the poorest flight envelope up to an advance ratio of about 0.37. At the higher advance ratios above 0.35, the 7-per-rev blade has the smallest reduction of blade-loading capability with increasing advance ratio. In this region, the 7-per-rev blade surpasses the 3-per-rev blade at an advance ratio of 0.37, surpasses the basic blade at 0.40, and will probably surpass the 4-per-rev blade around 0.44. Therefore, a torsionally stiff blade may be required to attain a reasonable flight envelope beyond advance ratios of 0.44.

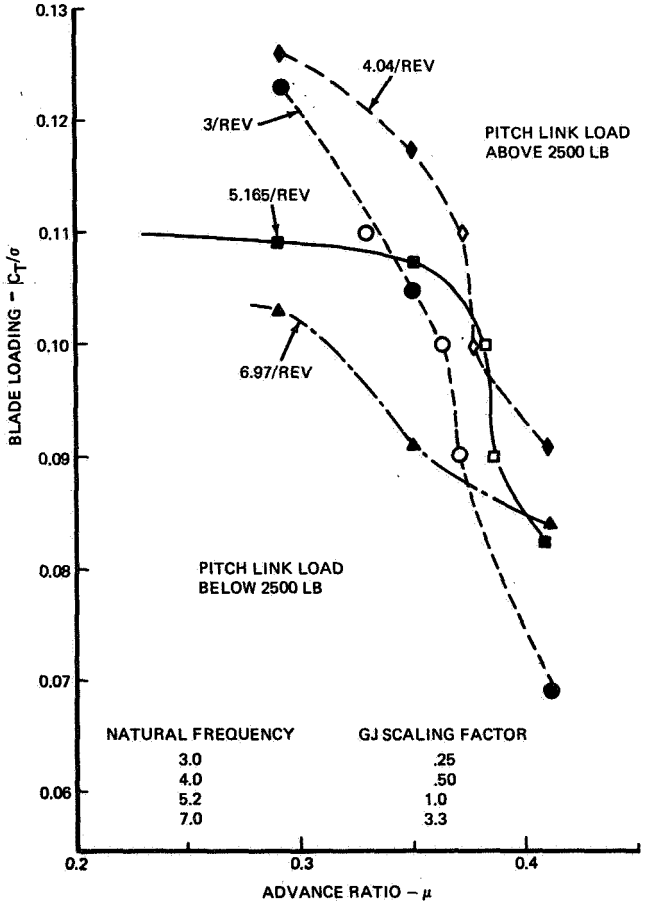

Figure 16. Control Load Endurance Limit Boundaries for Blades with Torsional Natural Frequencies of 3, 4, 5.2 and 7 Per Rev.

Conclusions and Recommendations

The results of the theory-test comparison performed for the 6-foot-diameter model blades and the study of varying torsional properties for the full-scale CH47C size blades have lead to:

1. The theory-test comparison with the 6-foot-diameter model data indicates that the aerolastic rotor analysis reasonably represents the large stall induced control loads, the control load change with blade loading, and the load variation with changes in blade torsional properties. Therefore, the analytical study of the CH47C size blades should provide at least a qualitative evaluation of the control load variation.

2. Changes in control system stiffness, pitch inertia, and blade torsional stiffness vary the large, stall-induced control loads. However, the control load change is not a simple function of torsional natural frequency as previously suspected, since torsional frequency changes, due to varying the blade torsional stiffness, produce control load changes larger than

* It may not be possible for an actual rotor to experience blade divergence. Before large divergence loads result, there is a significant increase in required rotor power. Therefore, a real rotor may simply run out of power and be unable to attain a flight condition for which divergence would occur.

other methods of changing torsional frequency.

3. A blade with a torsional natural frequency of 4 per rev represents a compromise between significantly reducing stall flutter loads, while allowing moderate increases in the advancing blade loads at high speeds. This compromise provides the best endurance limit flight envelope up to an advance ratio of 0.45. Beyond this advance ratio it appears that a torsionally stiff blade will provide a better endurance limit flight envelope.

4. Additional work is required in the following areas.

- A model test program is needed to validate the analytical results over a wide range of flight conditions with remote collective and cyclic pitch to insure trimmed flight.
- Theory improvements are needed to eliminate deficiencies discovered in the theory-test comparison.
- Continue analytical studies to investigate mechanisms of the load generation, maneuver and high-speed load trends and other means for expanding the endurance limit flight envelope.

References

1. F. J. Tarzanin, Jr., PREDICTION OF CONTROL LOADS DUE TO BLADE STALL, 27th Annual National V/STOL Forum of the AHS, Preprint No. 513, May 1971.
2. F. J. Tarzanin, Jr. and R. Gabel, BLADE TORSIONAL TUNING TO MANAGE ROTOR STALL FLUTTER, Presented at the AIAA 2nd Atmospheric Flight Mechanics Conference, AIAA Paper No. 72-958, September 1972.
3. F. O. Carta, L. M. Casellini, P. J. Arcidiacono, H. L. Elman, ANALYTICAL STUDY OF HELICOPTER ROTOR STALL FLUTTER, 26th Annual Forum of the AHS, June 1970. the AHS, June 1970.
4. F. J. Tarzanin, Jr. and J. Ranieri, INVESTIGATION OF TORSIONAL NATURAL FREQUENCY ON STALL-INDUCED DYNAMIC LOADING. Performed under contract DAAJ02-72-C-0092, USAAVLABS TR- (Not yet released).

APPLICATION TO ROTARY WINGS OF A SIMPLIFIED AERODYNAMIC LIFTING SURFACE THEORY FOR UNSTEADY COMPRESSIBLE FLOW

B. M. Rao* and W. P. Jones**
Department of Aerospace Engineering
Texas A&M University, College Station, Texas

Abstract

In a recent paper, Jones and Moore have developed a simple numerical lifting surface technique for calculating the aerodynamic coefficients on oscillating wings in subsonic flight. The method is based on the use of the full lifting surface theory and is not restricted in any way as to frequency, mode of oscillation or aspect ratio when $M < 1$. In this study, this simple but general method of predicting airloads is applied to helicopter rotor blades on a full three-dimensional basis. The general theory is developed for a rotor blade at the $\psi = \pi/2$ position where flutter is most likely to occur. Calculations of aerodynamic coefficients for use in flutter analysis are made for forward and hovering flight with low inflow for Mach numbers 0 and 0.8 and frequency ratios p/Ω=1 and 4. The results are compared with values given by two-dimensional strip theory for a rigid rotor hinged at its root. The comparisons indicate the inadequacies of strip theory for airload prediction. One important conclusion drawn from this study is that the curved wake has a substantial effect on the chordwise load distribution. The pitching moment aerodynamic coefficients differ appreciably from the results given by strip theory.

Introduction

In a survey paper, Ref. 1, Jones' et al. give a detailed account of significant developments in the field of unsteady aerodynamics of helicopter rotor blades. One of the problem areas surveyed was that of blade flutter as it has been found that under certain operating conditions, rotor blades can flutter in both hovering and forward flight. This phenomenon has been investigated by several researchers in Refs. 2, 3, 4, and 5 and the results of their studies have improved our understanding of the problem. For the case of hovering flight, J. P. Jones in Ref. 2 applied a method developed by W. P. Jones in Ref. 6 to derive the approximate aerodynamic coefficients for an oscillating single rotor blade for use in his flutter analysis. He approximated the actual flow conditions by neglecting curvature effects and assuming a simple two-dimensional mathematical model cosisting of a reference blade and an infinite number of wakes lying beneath the reference blade extending from $-\infty$ to ∞. He considered flapping and pitching motions and compared his results with those obtained experimentally by Daughaday and Kline in Ref. 3. On the basis of this work it was concluded that the wake is primarily responsible for some of the vibratory phenomena found on helicopters in practice. For low inflow conditions, Loewy in Ref. 4 used a similar mathematical model to that of J. P. Jones and investigated the variation in the pitching moment damping coefficient of a particular blade section as p/Ω varied for specified positions of axis of oscillation and a range of values of wake spacing. He found that the damping coefficient became negative whenever p/Ω was slightly greater than an integer for axis of oscillation forward of quarter-chord. Similarly he found that the damping coefficient for a flapping oscillation dropped sharply at integral values of p/Ω but did not actually become negative. Timman and Van de Vooren in Ref. 5, on the other hand, assumed that there was no inflow through the rotor disk and developed a theory for calculating the aerodynamic forces on a blade rotating through its own wake. Their results agree with those obtained in Refs. 2 and 4 in the limit when zero spacing between the wakes is assumed. All this theoretical work confirms the conclusion that the proximity of the wake is a contributing factor to rotor blade flutter.

All the theoretical work described above is based on the assumption that the flow is incompressible. However, with the advent of helicopters capable of flying with blade tip speeds ranging up to and in excess of the speed of sound, compressibility effects need to be taken into account when determining coefficients for use in flutter analysis. Jones and Rao in Ref. 7 were able to do this on the basis of two-dimensional theory and have derived coefficients for a range of Mach numbers, reduced frequencies, and wake spacing. Their analysis is based on the use of Loewy's model, Ref. 4, of the helical wake and the application of a theory developed earlier by Jones in Ref.8 for an oscillating airfoil in compressible flow. The values of the coefficients given in Ref. 7 agree with those obtained in Refs. 2 and 4 for zero Mach number but differ appreciably when the Mach number is varied. Hammond in Ref. 9 also developed a theory for determining compressibilty effects by using a different model of flow from that used in Ref. 7. In his model, the wake of the qth blade of a Q bladed rotor after n revolutions extends from $-2\pi(n+q/Q)$ to ∞; in Jones and Rao's model it extends from $-\infty$ to ∞. His aerodynamic coefficients for several Mach numbers and inflow ratios are in general agreement with the results of Jones and Rao in Ref. 7.

While the aerodynamic derivatives predicted by two-dimensional strip theory are widely used in predicting the flutter speeds of helicopter rotor blades, the method does not allow for curvature and finite aspect ratio effects. For incompressible flow, Ashley, Moser, and Dugundji in Ref. 10 developed a three-dimensional model in which they

Presented at the AHS/NASA-Ames Specialists' Meeting on Rotorcraft Dynamics, February 13-15, 1974. The funds for computation were provided by the U. S. Army Research Office, Durham.

* Associate Professor
** Distinguished Professor

modified Reissner's theory, Ref. 11, for oscillating wings in rectilinear flow by including the free stream velocity variations along the span. Their results indicate a negligible difference between two and three-dimensional solutions up to 95% of the span. Jones and Rao in Ref. 12 similarly studied tip vortex effects in compressible flow and they also concluded that such effects are negligible except in regions close to the tip. In some of his earlier work, Miller in Refs. 13, 14, and 15, developed a helical wake model in which the rotor wake was divided into a "near" wake and a "far" wake. The near wake included the portion attached to the blade that extend approximately one-quarter of a revolution from the blade trailing edge. The effects of the near wake include an induced chordwise variation in downwash and were formulated using an adoptation of Loewy's strip theory. The chordwise variation in the velocity over the airfoil induced by the far wake was neglected. Miller extended his model to study the forward flight case and found that the nonuniform downwash induced at the rotor disk by the wake vortex system could account for the higher harmonic airloads encountered on rotor blades in forward flight. He also showed that under certain conditions of low inflow and low speed transition flight the returning wake could be sucked up into the leading edge of the rotor which would account for some of the vibration and noise. Piziali in Ref. 16 has developed an alternative numerical method in which the wake of a rotor blade is represented by discrete straight line shed and trailing vortex elements. He satisfied the chordwise boundary conditions, but the rotor blade was limited to one degree of freedom in flapping. Sadler in Ref. 17, using a model similar to Piziali's, developed a method for predicting the helicopter wake geometry at a "start up" configuration. He represented the wake by a fine mesh of transverse and trailing vortices starting with the first movement of the rotor blade generating a bound vortex, and, to preserve zero total vorticity, a corresponding shed vortex in the wake. Integrating the mutual interference of the trailing and shed vortices upon each other over small intervals of time, Sadler was able to predict a wake geometry. Although his model showed fair agreement with the available experimental data for advance ratios above one-tenth, Sadler's method is limited due to the large computational time required to represent the wake by a finite mesh.

Though many forms of flutter can occur on rotor blades, attention in this report is concentrated on the determination of appropriate aerodynamic coefficients for use in the analysis of blade flutter of the classical bending-torsion type. Shipman and Wood in Ref. 20 have considered this problem but they did not take compressibilty and finite span effects into account. The two-dimensional mathematical model used is similar to that employed by other authors except that they assumed that flutter would first occur when the relative velocity over the rotor blade reaches its critical value when $\psi \simeq \pi/2$. For greater or lower values of ψ, the relative speed would be reduced below the critical speed for flutter and any incipient growing flutter oscillation would be damped. This reasoning led them to represent the blade motion by a series of oscillatory pulses, where each disturbance occurs over the range, $\frac{\pi}{2} - \Delta\psi_1 < \psi < \frac{\pi}{2} + \Delta\psi_2$. Corresponding to each burst of oscillation, packets of vorticity are assumed to be shed into the wake. With increasing forward speed, the spacing between the packets of vorticity also increases and it was found that the flutter speed became constant when μ, the advance ratio, was above 0.2. The approach used in the present study differs from that adopted by Shipman and Wood in that continuous high frequency small oscillations are assumed to be superimposed on the normal periodic motion of the blade. The airloads and aerodynamic derivatives associated with the perturbed oscillation of the rotor blade can then be calculated by the method described in this paper. Since the rotor blade will first attain its critical speed for classical flutter at $\psi = \pi/2$, the aerodynamic derivatives corresponding to this value of ψ only have been calculated. The method takes finite aspect ratio and subsonic compressibility effects fully into account. Typical results for a rotor blade hinged at its root describing flapping and twisting oscillations are given for a range of Mach numbers and frequency values.

Basic Equations

In the development of the analysis of the Jones-Moore theory, Ref. 18, for oscillating wings in rectilinear flight, the space variables x, y, z, and t are replaced by X, Y, Z, and T, respectively, so that

$$x = \ell X, \quad y = \frac{\ell Y}{\beta}, \quad z = \frac{\ell Z}{\beta}, \quad t = \frac{\ell T}{U} \tag{1}$$

where ℓ is a convenient reference length, U is the uniform velocity, M is the Mach number and $\beta = (1-M^2)^{1/2}$. The velocity potential of the flow around a surface oscillating at a frequency p can then be expressed as

$$\phi(x,y,z,t) = U\ell\Phi(X,Y,Z)e^{i(\lambda X + \omega T)} \tag{2}$$

where $\omega = p\ell/U$, $\lambda = M^2\omega/\beta^2$. The function Φ may be regarded as a modified velocity potential. Furthermore, it can be shown that it satisfies the wave equation

$$\frac{\partial^2\Phi}{\partial X^2} + \frac{\partial^2\Phi}{\partial Y^2} + \frac{\partial^2\Phi}{\partial Z^2} + \kappa^2\Phi = 0 \tag{3}$$

where $\kappa = M\omega/\beta^2$.

Since in this problem the motion of the surface is assumed to be prescribed, the downwash velocity at any point on it must be the same as the downwash induced by the velocity (or doublet) distribution over the surface and its wake. This condition must be satisfied in order to ensure tangential flow over the surface at all points. It is also assumed that the rotor blade is a thin surface oscillating about its equilibrium position in the plane $z = 0$. If $\zeta = \zeta' e^{ipt}$ defines the downwash displacement at any point (x,y) at time t, this boundary condition requires that the downward velocity and $\partial\phi/\partial z$ must be equal. In the transformed coordinates, this implies that

$$W = \frac{\partial \Phi}{\partial Z} = \frac{we^{-i(\lambda X + \omega T)}}{U\beta} \tag{4}$$

where $w = \frac{\partial \zeta}{\partial t} + U\frac{\partial \zeta}{\partial x}$ is known.

A further condition that must be imposed on any solution is that it leads to zero pressure difference across the wake created by the oscillating surface. From the general equations of flow it can be established that the local lift $\tilde{\ell}(x,y,t)$ at any point is given by

$$\tilde{\ell}(x,y,t) = \rho(\frac{\partial k}{\partial t} + U\frac{\partial k}{\partial x}) \tag{5}$$

where $k = \phi_u - \phi_\ell$, the discontinuity in the velocity potential. From Eq. (5), it immediately follows that on the surface

$$\tilde{\ell}(x,y,t) = \rho U^2(i\nu K + \frac{\partial K}{\partial X})\, e^{i(\lambda X + \omega T)} \tag{6}$$

where $\nu = \omega/\beta^2$ and $K = \Phi_u - \Phi_\ell$. This yields

$$i\nu K + \frac{\partial K}{\partial X} = 0 \tag{7}$$

everywhere in the wake since the lift must then be zero. From Eq. (7), it can be deduced that at any point in the wake

$$K(X,Y) = K(X_t,Y)\, e^{-i\nu(X-X_t)} \tag{8}$$

where $X = X_t$ denotes the position of the trailing edge of the section at Y.

As shown in Ref. 19, the solution of Eq. (3) may then be derived from the integral equation

$$4\pi W(X_p,Y_p,0) = \iint_{Z\to 0} K(X,Y)\frac{\partial^2}{\partial Z^2}(\frac{e^{-i\kappa\xi}}{\xi})dXdY \tag{9}$$

where W is the modified downwash at the point X_p,Y_p given by Eq. (4), K has to take the form specified by Eq. (8) at points in the wake and $\xi = [(X-X_p)^2 + (Y-Y_p)^2 + Z^2]^{1/2}$.

The double integral in Eq. (9) must be taken over the area of the oscillating surface and its wake. It should be remembered, however, that K = 0 along the leading edge and the sides of the area of integration.

In the numerical technique developed in Ref. 18 for calculating the airloads on oscillating wings in rectilinear flight, the wing is divided into a number of conveniently shaped boxes and K is assumed to be constant over each box. The wake, on the other hand, is divided into a number of chordwise strips and K over each strip is defined by Eq. (8). The contribution of the wake to the downwash $W(X_p,Y_p)$ is then derived by direct numerical integration.

The application of the method outlined above to determine the airloads on rotor blades presents certain difficulties, the principal one being that the flow velocity over the rotor blades is not constant as assumed in the derivation of Eqs. (3) and (8) for wings in straight flight. To overcome this difficulty, it is assumed that the rotor blade can be represented by a number of spanwise segments over every one of which the flow is taken to have its average value and appropriate Mach number. On this basis the above analysis can be modified for application to rotor blades as outlined in the next section.

Rotor Blade Theory

In the present analysis, the rotor blade is taken to be fixed at the $\psi = \pi/2$ position and its helical wake is assumed to extend rearwards as indicated in Fig. 1. Normally, one would expect the vorticity shed by the perturbed blade to be carried downstream by the distorted wake of the loaded rotor blade. However, in the present preliminary study, uniform inflow is assumed and any distortion of the wake due to blade-tip vortex interference is ignored. The aerodynamic coefficients corresponding to any prescribed motion can then be calculated for forward and hovering flight by the method described below.

a) Forward Flight (Rotor Blade at $\psi = \pi/2$)

Let R denote the tip radius of the blade and assume $x = Rx'$, $y = Ry'$, and $z = Rz'$. For forward flight with velocity V, the relative local velocity at section y will be denoted by $U(=V+\Omega Ry')$ and $U'(=\mu+y')$, where Ω is the angular rotation and $\mu(=V/\Omega R)$ is the advance ratio. It then follows that at the section y'_p, the downwash $w(x'_p,y'_p)$ is given by

$$w(x'_p,y'_p) = \Omega R(i\frac{p}{\Omega}\zeta' + U'_p\frac{\partial \zeta'}{\partial x'})\, e^{ipt} \tag{10}$$

where $\zeta = R\zeta' e^{ipt}$ is the displacement of the blade at the point, (x'_p,y'_p). When the blade is describing flapping and twisting motions, ζ' may be expressed as

$$\zeta' = \gamma' f(y') + x'\alpha' F(y') \tag{11}$$

where γ' and α' are the amplitudes at the reference section and f(y') and F(y') are the modes of flapping and twisting oscillations, respectively. If the blade is assumed to be rigid and hinged at the root, f(y') = y', and F(y') = 1 in the above equation. For convenience, the reference section is taken to be at the tip but, in actual flutter calculations, the section at 0.8R would be a better choice.

To obtain the distribution of K corresponding to the motion prescribed by Eq. (10), Eq. (9) is first expressed in terms of the original variables and K is replaced by $Rk'e^{ipt}$. It may then be written as

$$\frac{4\pi w' e^{-i\lambda' x'_p}}{\beta_p} = \iint k'(x',y')e^{-i\lambda' x'}\frac{\partial^2}{\partial z'^2}(\frac{e^{-i\kappa' r'}}{r'})\frac{dx'dy'}{\beta} \tag{12}$$

where $\kappa' = \frac{Mp}{\beta^2\Omega U'}$, $\lambda' = M\kappa'$, $w = w'e^{ipt}$, $\beta^2 = 1-M^2$, and $r' = [(x'-x'_p)^2 + \beta^2(y'-y'_p)^2 + \beta^2 z'^2]^{1/2}$.

The above equation can be used to obtain the solution to the problem of determining the flow over a rotor blade with a rectilinear wake. Since

the wake can withstand no lift, the condition, $\frac{\partial k}{\partial t} + U\frac{\partial k}{\partial x} = 0$, must be satisfied. For a rectilinear wake, this yields

$$k'(x',y') = k'_t(y')e^{-i\frac{p(x'-x'_t)}{\Omega U'}} . \quad (13)$$

However, if the wake originating from a blade strip is assumed to be curved

$$k'(s',y') = k'_t(y')e^{-i\frac{p(s'-s'_t)}{\Omega q'}} , \quad (14)$$

where $q' = (\mu^2 + y'^2 + 2\mu y'\sin\psi)^{1/2}$, $s = Rs'$ is the distance along the vortex path and y' specifies the spanwise location of the blade strip.

For computational purposes, Eq. (12) may be conveniently expressed as

$$4\pi\bar{W}(x'_p,y'_p) = \int\int \bar{K}(x',y')\frac{G}{\beta}\,dx'dy', \quad (15)$$

where $\bar{W}(x'_p,y'_p) = \frac{w(x'_p,y'_p)}{\beta_p} e^{-i\lambda'_p x'_p}$,

$\bar{K}(x',y') = k'(x',y')\, e^{-i\lambda' x'}$, and

$$G = \frac{\partial^2}{\partial z'^2}\left(\frac{e^{-i\kappa' r'}}{r'}\right) = -\beta^2\left(\frac{e^{-i\kappa' r'}}{r'}\right)\left[\,(1+i\kappa' r')\left(1-\frac{3\beta^2 z'^2}{r'^2}\right) + \kappa'^2\beta^2 z'^2\,\right].$$

It should be noted that in the wake

$$\bar{K}(x',y') = \bar{K}_t(y')\, e^{-i\frac{\nu'(s'-s'_t)}{q'}} , \quad (16)$$

where $\nu' = \frac{p}{\Omega\beta^2}$.

b) Hovering Flight

For the simplest case of hovering flight, $\mu = 0$ and $s' = y'\theta$. Hence Eqs. (10), (11), (12), (13), and (15) can be simply modified by replacing μ with zero. Eqs. (14) and (16) then become

$$k'(\theta,y') = k'_t(y')\, e^{-i\frac{p}{\Omega}(\theta-\theta_t)} \quad (17)$$

and $$\bar{K}(\theta,y') = \bar{K}'_t(y')\, e^{-i\nu'(\theta-\theta_t)} , \quad (18)$$

where y' defines the location of the blade strip from which the wake originates.

Method Of Solution

The schematic diagram of the oscillating rotor blade is shown in Fig. 1. Eqs. (15) and (16) are combined and expressed as

$$4\pi\bar{W}(x'_p,y'_p) = -\int\int_{\text{blade surface}} \bar{K}(x',y')\beta\left(\frac{e^{-i\kappa' r'_s}}{r'^3_s}\right)(1+i\kappa' r'_s)\,dx'dy' - \int\int_{\text{wake}} \bar{K}_t(y')e^{-i\frac{\nu'(s'-s'_t)}{q'}}\beta\left(\frac{e^{-i\kappa' r'_w}}{r'^3_w}\right)$$

$$\left[\,(1+i\kappa' r'_w)\left(1-\frac{3\beta^2 z'^2}{r'^2_w}\right) + \kappa'^2\beta^2 z'^2\,\right] ds'dn', \quad (19)$$

where $r'_s = [\,(x'-x'_p)^2 + \beta^2(y'-y'_p)^2\,]^{1/2}$

$r'_w = [\,(x'-x'_p)^2 + \beta^2(y'-y'_p)^2 + \beta^2 z'^2\,]^{1/2}$

$ds' = (dx'^2+dy'^2)^{1/2}$

and dn' is perpendicular to ds' and approximately equal to dy' on blade. The rotor blade is divided into a number of rectangular boxes (M x N) on which the doublet strengths are assumed to be constant as in Ref. 18. Based on this assumption, Eq. (19) can be expressed as

$$4\pi\bar{W}_{mn} = \sum_{i=1}^{\Sigma}\sum_{j=1}^{\Sigma} S_{ij}\bar{K}_{ij} + \sum_{j=1}^{\Sigma} T_j\bar{K}_{tj} \quad (20)$$

In Eq. (20) S_{ij} and T_j may be interpreted as the aerodynamic influence coefficients and the actual expressions are given later in this section. S_{ij} T_j are the downwash velocities induced at the box mn due to the unit strength doublets located at the box ij and the wake strip j respectively. $\bar{K}_{ij}$ and $\bar{K}_{tj}$ are the doublet strengths at the box ij and the trailing edge of the wake strip j, respectively. With the use of the wake boundary condition, $\bar{K}_{tj}$ can be expressed as

$$\bar{K}_{tj} = \bar{K}_{Mj}/[e^{-i\frac{\nu'(x'_{tj}-x'_{Mj})}{U'_j}} + 2i\frac{\nu'(x'_{tj}-x'_{Mj})}{U'_j}] \quad (21)$$

Eqs. (20) and (21), then yield

$$4\pi\bar{W}_{mn} = \sum_{i=1}^{\Sigma}\sum_{j=1}^{\Sigma} A_{ij}\bar{K}_{ij} \quad (22)$$

where $A_{ij} = S_{ij}$ for $i \neq M$

and $A_{ij} = S_{ij} + T_j/[e^{-i\frac{\nu'(x'_{tj}-x'_{Mj})}{U'_j}} + 2i\frac{\nu'(x'_{tj}-x'_{Mj})}{U'_j}]$

for $i = M$.

For a given mode shape ($\bar{W}_{mn}$'s are known), Eq. (22) represents a system of M x N linear algebraic equations, the solution of which yields the values for $\bar{K}_{mn}$'s. M and N denote the total number of chordwise and spanwise stations respectively.

Once the appropriate $\bar{K}$ distribution has been found, it is then relatively easy to determine the aerodynamic forces per unit span acting on the rotor blade. If, in Eq. (5), $k = Rk'e^{ipt} = R\bar{K}e^{ipt}e^{i\lambda' x'}$, it then follows that the local lift $L(y) = L'(y)\, e^{ipt}$ and the nose-up pitching moment, $M(y) = M'(y)\, e^{ipt}$, referred to the mid-point of the chordwise section at y are given by

$$\frac{L'(y)}{\rho(U_R)^2(c/2)} = (L_1+iL_2)\left(\frac{2z'_f}{c}\right) + (L_3+iL_4)\alpha'$$

$$= \left(\frac{\Omega R}{U_R^2}\right)\left(\frac{2R}{c}\right)\left(i\frac{p}{\Omega}\int_{x'_\ell}^{x'_t} k'dx' + U'k'_t\right) \quad (23)$$

$$\frac{M'(y)}{\rho(U_R)^2(c/2)} = (M_1+iM_2)\left(\frac{2z'_f}{c}\right) + (M_3+iM_4)\alpha'$$

$$= \left(\frac{\Omega R}{U_R^2}\right)\left(\frac{2R}{c}\right)^2\left[U'\left(\int_{x'_\ell}^{x'_t} k'dx' - k'_t x'_t\right) - i\frac{p}{\Omega}\int_{x'_\ell}^{x'_t} k'x'dx'\right] \quad (24)$$

where c is the local chord, U_R is a reference velocity, z'_f and α' are the local amplitudes of the flapping and twisting motions respectively, and L_1, L_3, M_1, M_3, and L_2, L_4, M_2, M_4, are the in phase and out of phase airload coefficients, respectively.

Expressions for Aerodynamic Influence Coefficients

Forward Flight (Rotor Blade at $\psi = \pi/2$)

The influence coefficients are calculated by the method outlined in Ref. 18. For a box not containing the collocation point

$$S_{ij} = -\int_{y'_j-d_2}^{y'_j+d_2}\int_{x'_i-d_1}^{x'_i+d_1}\left(\frac{e^{-i\kappa' r'_s}}{r'^3_s}\right)\beta(1+i\kappa' r'_s)dx'dy' \quad (25)$$

where $\kappa' = \frac{Mp}{\beta^2\Omega U'_j}$, $r'_s = [(x'-x'_m)^2 + \beta^2(y'-y'_n)^2]^{1/2}$, $d_i = \Delta x'/2$, $d_2 = \Delta y'/2$, and $\Delta x'$ and $\Delta y'$ are the chordwise and spanwise spacings of the rectangular grid on the surface of the rotor blade. When the collocation is inside the box considered, the value of S_{ij} must be calculated by the method of Ref. 18. For the curved wake

$$T_j = -\int_{n'_j-d_2}^{n'_j+d_2}\int_{s'_t}^{\infty} e^{-i\frac{\nu'(s'-s'_t)}{q'}}\left(\frac{e^{-i\kappa' r'_w}}{r'^3_w}\right)\beta[(1+i\kappa' r'_w)\left(1-\frac{3\beta^2 z'^2}{r'^2_w}\right) + \kappa'^2\beta^2 z'^2]\,ds'dn' \quad (26)$$

where $r'_w = [(x'-x'_m)^2 + \beta^2(y'-y'_n)^2 + \beta^2 z'^2]^{1/2}$, $x' = \mu\theta + y'_j \sin\theta$, $y' = y'_j\cos\theta$, $z' = d'\theta/2\pi$, $ds' = (dx'^2+dy'^2)^{1/2} = (\mu^2+y'^2_j+2\mu y'_j\cos\theta)^{1/2}d\theta$, and $d(=Rd')$, the downward displacement of the wake per revolution, is assumed to be small. T_j's are evaluated numerically at the j'th spanwise strip by taking small increments of θ and n.

Hovering Flight (Low Inflows)

For hovering flight, $\mu = 0$, $s' = y'_j\theta$, and $ds' = y'_j d\theta$. The expression for S_{ij}, Eq. (25), can be simply modified by replacing μ with zero and the wake integration for the j'th strip

$$T_j = -\int_{n'_j-d_2}^{n'_j+d_2}\int_{\theta_t}^{\infty} e^{-i\nu'(\theta-\theta_t)}\left(\frac{e^{-i\kappa' r'_w}}{r'^3_w}\right)\beta[(1+i\kappa' r'_w)\left(1-\frac{3\beta^2 z'^2}{r'^2_w}\right) + \kappa'^2\beta^2 z'^2]\,y'_j\,d\theta dn' \quad (27)$$

where $x' = y'_j \sin\theta$, $y' = y'_j\cos\theta$, and $z' = d'\theta/2\pi$.

The effect of the helical wake in hovering flight is estimated by two different methods. In the first method, a Helical Wake Model is used and the actual helical path is taken in evaluating the T_j coefficients. In the second method, a Circular Wake Model is employed and the helical wake is replaced by its near wake, which is assumed to extend over $\theta_t \le \theta \le \pi/2$, and a number of regularly spaced circular disks of vorticity below the reference plane. The formula for k' for the n'th disk at $z' = nd'$ is taken to be simply

$$k'(\theta, y', nd') = k'_t(y')e^{-i\frac{p}{\Omega}[(\theta-\theta_t)+2n\pi]}, \quad (28)$$

the actual spacing between consecutive disks being Rd'.

Results and Discussion

A rectangular rotor blade of R/c = 10 was chosen and the blade was assumed to extend from 0.1R to R. For the computation of the airload coefficients, a grid of thirty six rectangular boxes consisting of six chordwise and six spanwise stations were used. The convergence of the results was tested by taking grid sizes of 6x8 (chordwise x spanwise) and 8x6. Rigid mode shapes for flapping and twisting oscillations are assumed so that

$$\zeta = \gamma y' + \alpha x'$$

$$w'(x'_p, y'_p) = \Omega R[\alpha'(\mu+y'_p+i\frac{p}{\Omega}x'_p) + \gamma' i\frac{p}{\Omega}(\mu+y'_p)]$$

$$= \Omega R[(\mu+y'_p+i\frac{p}{\Omega}x'_p)\alpha' + i\frac{p}{\Omega}(\mu+y'_p)\left(\frac{c}{2R}\right)\left(\frac{2z'_f}{c}\right)]. \quad (29)$$

It should be noted that the above equation is valid only for the blade position at $\psi = \pi/2$. For hovering flight, $\mu = 0$ in Eq. (29).

The airload coefficients for Mach numbers 0 0.8 for several values of $\frac{p}{\Omega}$ and wake spacing of two chords were obtained with reference to the blade's quater-chord axis. In Figs. (2) thru (5), selected airload coefficients for slow forward flight (μ = 0.1) are compared with the results obtained for hovering flight using both a helical wake model and two-dimensional strip theory. For this particular comparison, the reference velocity in Eqs. (23) and (24) was taken as the relative local velocity, U, and the tip Mach number was 0.8. From these plots, one can conclude that strip theory predicts substantially larger values for the airload coefficients. One of the most important observations one can make is that the curved wake changes the chordwise load distribution in such a way that the center of pressure shifts forward of the quarter-chord axis position (see Fig. 4).

Figs. (6) and (7) compare the results by several mathematical models used for the hovering flight case. The airload coefficients are referred to the tip velocity (ΩR) and this choice was made to indicate the trends of spanwise load distribution. The Circular Wake model representation results in a substantial saving in computational time. For example, to obtain the airload coefficients for one set of geometric and flight conditions using 6x6 grid on the blade, the Circular Wake model took only 1.5 minutes of computing time on IBM 360/65 while the Helical Wake model took 2.5 minutes. Although the Circular Wake model seems to indicate the general trends of the airload coefficients, one should use the full helical wake to compute the airload coefficients accurately.

Some typical results for hovering flight using the Circular Wake representation, compared with the results of two-dimensional strip theory, Ref. 7, are shown in Figs. (8) thru (11). The results for the curved wake are in good agreement with the results for strip theory for the inner blade sections; however, the agreement is poor towards the tip. Figs. (12) and (13) show the variation with axis position of M_4, conveniently referred to as pitching moment damping airload coefficient, at spanwise stations of 0.475R and 0.925R, respectively. From these results, one can conclude that the agreement between the curved wake results and strip theory is good near the quarter-chord position for M = 0 and M = 0.8 but it becomes very poor as the axis is moved towards the trailing edge.

References

1. Jones, W. P., McCrosky, W. J., and Costes, J. J., "Unsteady Aerodynamics of Helicopter Rotor Blades," NATO AGARD Report No. 595, April 1972.
2. Jones, J. P., "The Influence of the Wake on the Flutter and Vibration of Rotor Blades," Aeronautical Quarterly, Vol. IX, August 1958.
3. Daughaday, H. and Kline, J., "An Investigation of the Effect of Virtual Delta-Three Angle and Blade Flexibility on Rotor Blade Flutter," Cornell Aeronautical Laboratory Report, SB-86 2-5-2, August 1954.
4. Loewy, R. G., "A Two-Dimensional Approximation to the Unsteady Aerodynamics of Rotary Wings," Journal of the Aeronautical Sciences, Vol. 24, No. 2, February 1957, pp. 81-92.
5. Timman, R. and Van de Vooren, A. I., "Flutter of a Helicopter Rotor Ratating in its Own Wake," Journal of the Aeronautical Sciences, Vol. 24, No. 9, September 1957, pp. 694-702.
6. Jones, W. P., "Aerodynamic Forces on Wings in Non-Uniform Motion," R&M No. 2117, 1945, British Aeronautical Research Council.
7. Jones, W. P. and Rao, B. M., "Compressibility Effects on Oscillating Rotor Blades in Hovering Flight," AIAA Journal, Vol. 8, No. 2, February 1970, pp. 321-329.
8. Jones, W. P., "The Oscillating Airfoil in Subsonic Flow," R&M No. 2921, 1956, British Aeronautical Research Council.
9. Hammond, C. E., "Compressibility Effects in Helicopter Rotor Blade Flutter," GITAER Report 69-4, December 1969, Georgia Institute of Technology, School of Aerospace Engineering.
10. Ashley, H., Moser, H. H., and Dugundji, J., "Investigation of Rotor Response to Vibratory Aerodynamic Inputs, Part III, Three-Dimensional Effects on Unsteady Flow Through a Helicopter Rotor," WADC TR 58-87, October 1958, AD203392, U. S. Air Force Air Research and Development Command.
11. Reissner, E., "Effects of Finite Span on the Airload Distributions for Oscillating Wings, Part I - Aerodynamic Theory of Oscillating Wings of Finite Span," NACA Technical Note No. 1194, 1947.
12. Jones, W. P. and Rao, B. M., "Tip Vortex Effects on Oscillating Rotor Blades in Hovering Flight," AIAA Journal, Vol. 9, No. 1, January 1971, pp. 106-113.
13. Miller, R. H., "On the Computation of Airloads Acting on Rotor Blades in Forward Flight," Journal of the American Helicopter Society, Vol. 7, No. 2, April 1962, pp. 55-66.
14. Miller, R. H., "Unsteady Airloads on Helicopter Rotor Blades," Journal of the Royal Aeronautical Society, Vol. 86, No. 640, April 1964, pp. 217-229.
15. Miller, R. H., "Rotor Blade Harmonic Air Loading," AIAA Journal, Vol. 2, No. 7, July 1964, pp. 1254-1269.
16. Piziali, R. A., "A Method for Predicting the Aerodynamic Loads and Dynamic Response of Rotor Blades," USAAV-LABS Technical Report 65-74, January 1966, AD 628583.
17. Sadler, S. G., "A Method for Predicting Helicopter Wake Geometry, Wake Induced Flow and Wake Effects on Blade Airloads," presented at the 27th Annual National V/STOL Forum of the American Helicopter Society, Washington, D. C., May 1972.
18. Jones, W. P. and Moore, J. A., "Simplified Aerodynamic Theory of Oscillating Thin Surfaces in Subsonic Flow," AIAA Journal, Vol. 11, No. 9, September 1973, pp. 1305-1309.
19. Jones, W. P., "Oscillating Wings in Compressible Subsonic Flow," R&M No. 2885, October 19 55, British Aeronautical Research Council.
20. Shipman, K. W. and Wood, E. R., "A Two-Dimensional Theory for Rotor Blade in Forward Flight," Journal of Aircraft, Vol. 8, No. 12, December 1971, pp. 1008-1015.

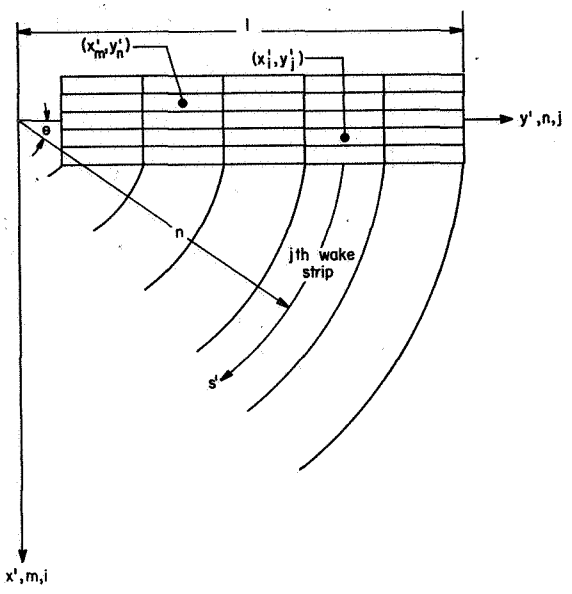

Fig. 1 Schematic Diagram of Rotor Blade and its Wake.

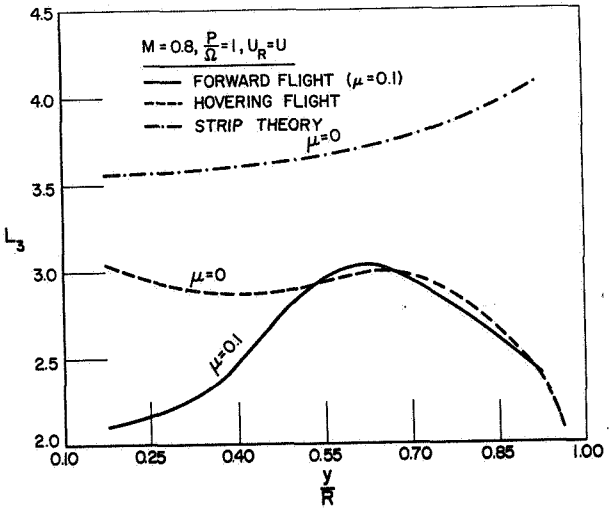

Fig. 2 Spanwise Variation of L_3.

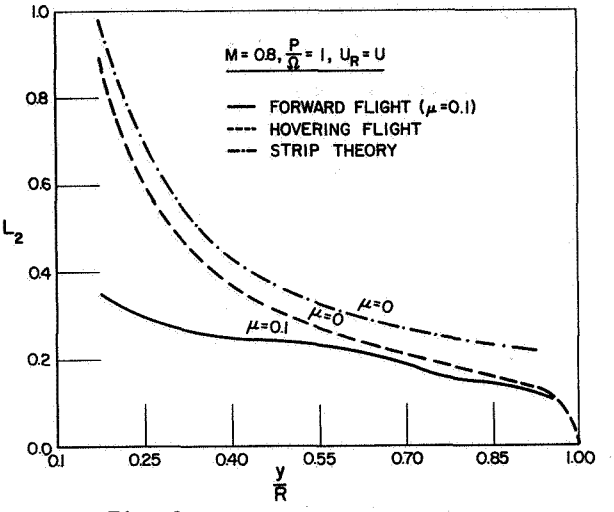

Fig. 3 Spanwise Variation of L_2.

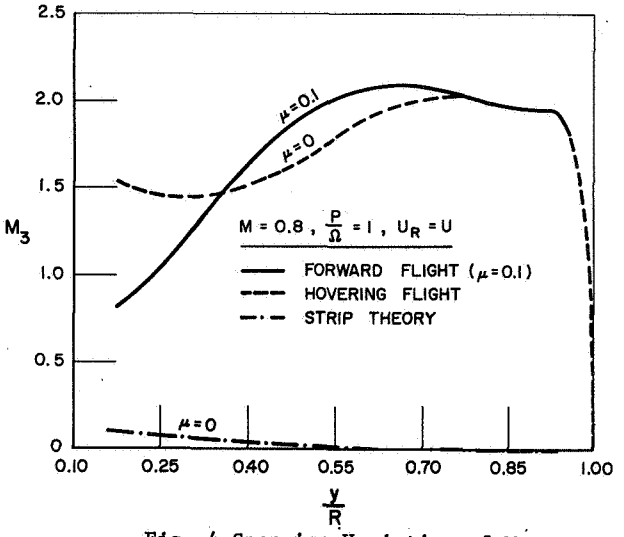

Fig. 4 Spanwise Variation of M_3.

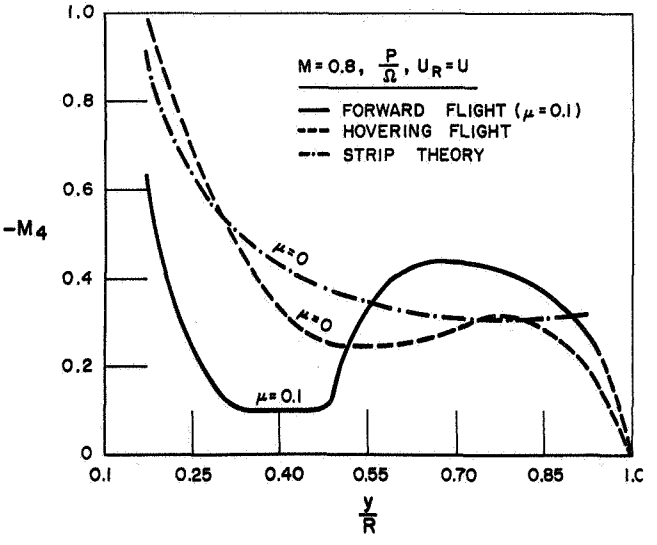

Fig. 5 Spanwise Variation of M_4.

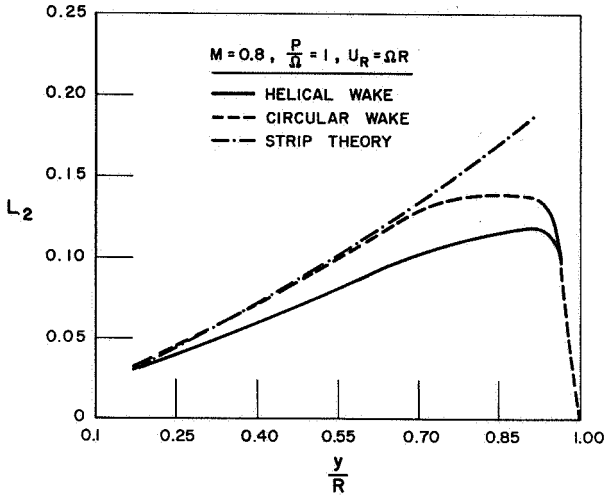

Fig. 6 Spanwise Variation of L_2 for Hovering Flight.

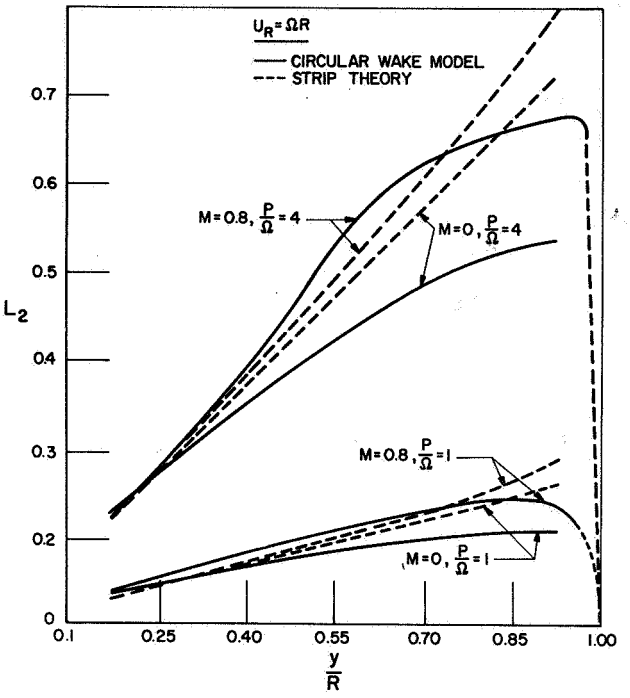

Fig. 8 Spanwise Variation of L_2 for Hovering Flight.

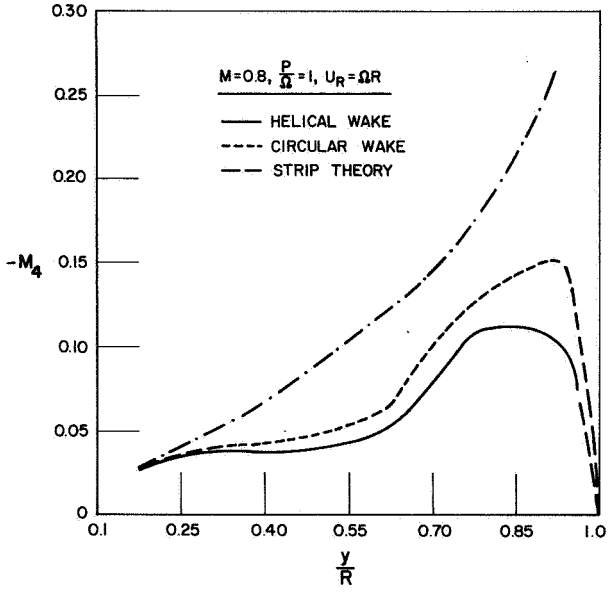

Fig. 7 Spanwise Variation of M_4 for Hovering Flight.

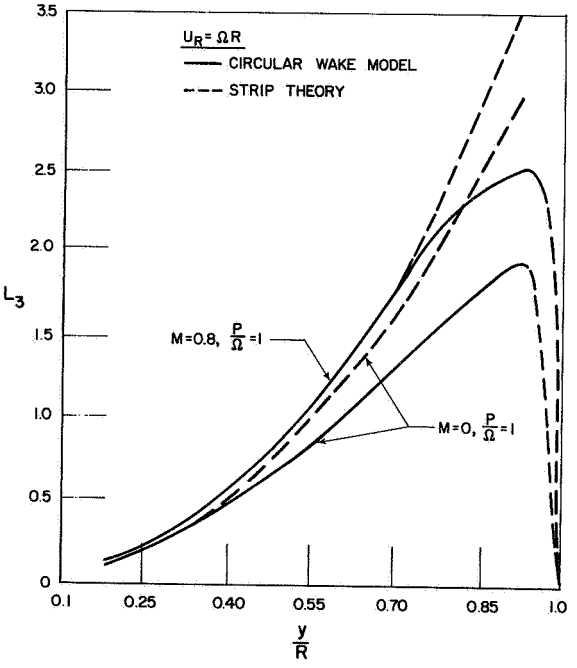

Fig. 9 Spanwise Variation of L_3 for Hovering Flight.

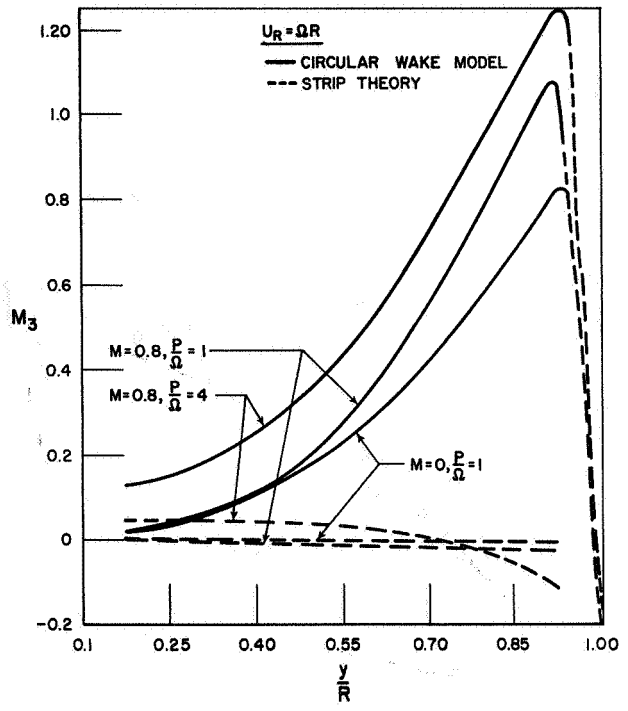

Fig. 10 Spanwise Variation of M_3 for Hovering Flight.

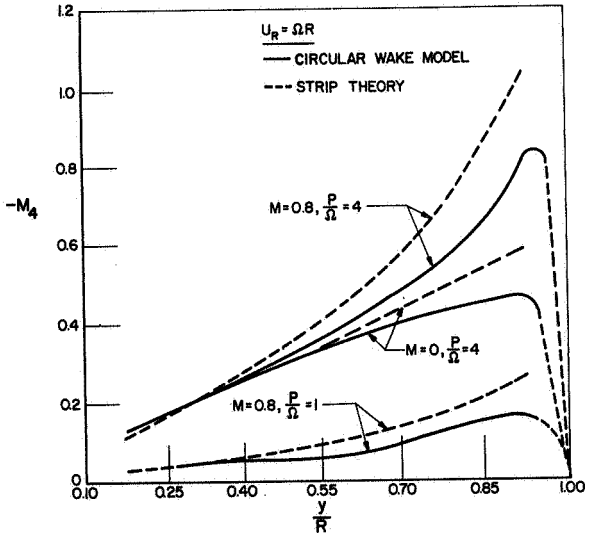

Fig. 11 Spanwise Variation of M_4 for Hovering Flight.

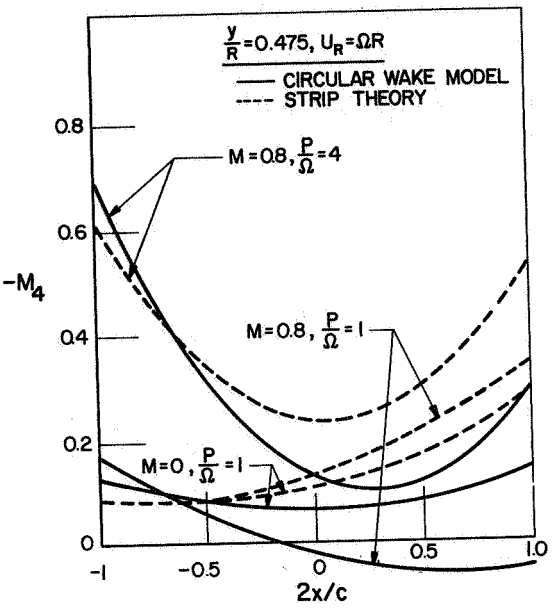

Fig. 12 Variation of M_4 With Reference Axis Position for Hovering Flight.

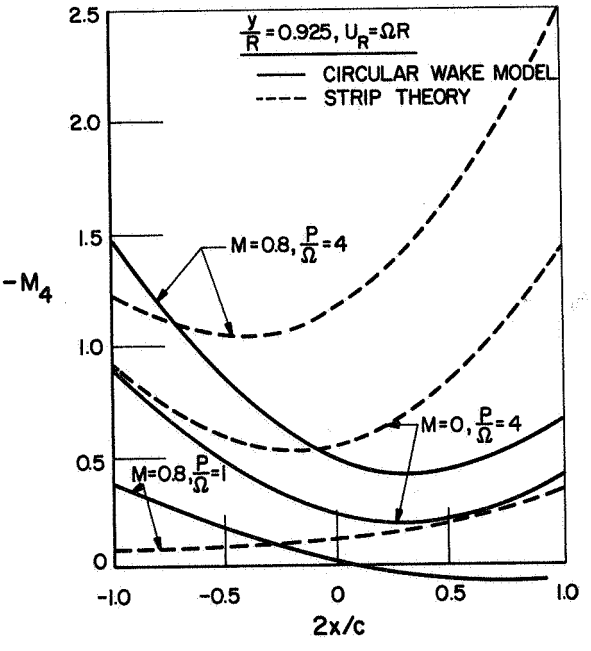

Fig. 13 Variation of M_4 With Reference Axis Position for Hovering Flight.

ROTOR AEROELASTIC STABILITY COUPLED WITH HELICOPTER BODY MOTION

Wen-Liu Miao
Boeing Vertol Company
Philadelphia, Pennsylvania

Helmut B. Huber
Messerschmitt-Boelkow-Blohm Gmbh
Ottobrun-Munich
Federal Republic of Germany

Abstract

A 5.5-foot-diameter, soft-in-plane, hingeless-rotor system was tested on a gimbal which allowed the helicopter rigid-body pitch and roll motions. With this model, coupled rotor/airframe aeroelastic stability boundaries were explored and the modal damping ratios were measured. The time histories were correlated with analysis with excellent agreement.

The effects of forward speed and some rotor design parameters on the coupled rotor/airframe stability were explored both by model and analysis. Some physical insights into the coupled stability phenomenon were suggested.

Introduction

The coupled rotor-airframe aeroelastic stability phenomenon of air resonance has received considerable attention in recent years. A scaled model of the BO-105 helicopter was built and tested to explore this phenomenon and its sensitivity to design parameters.[1] An extensive analytical study was performed and correlated with BO-105 flight test data.[2]

To further explore this coupled stability phenomenon, a large scale model having different resonance characteristics than the BO-105 was built and tested. Parameters that were influential to the stability[1, 2] were incorporated into the model and their effects were examined. An improved test technique enabled the determination of modal damping ratio at every test point, providing better data for correlation and better assessment of stability.

Description of Model

The model, shown in Figure 1, consisted of a Froude-scaled model rotor mounted on a rigid fuselage, which in turn was mounted on a two-axis gimbal having ±10 degrees travel in pitch and roll. The model had a 5.5-foot-diameter, soft-in-plane, hingeless rotor with pertinent hub parameters such as precone, sweep, and control system stiffness being variables to enable investigation of their effects on coupled rotor-airframe stability.

A proportional (closed-loop) control system equipped with a cyclic stick provided lateral and longitudinal control to fly the model in the pitch and roll degrees of freedom. In addition, a shaker system was installed in the longitudinal and lateral cyclic system

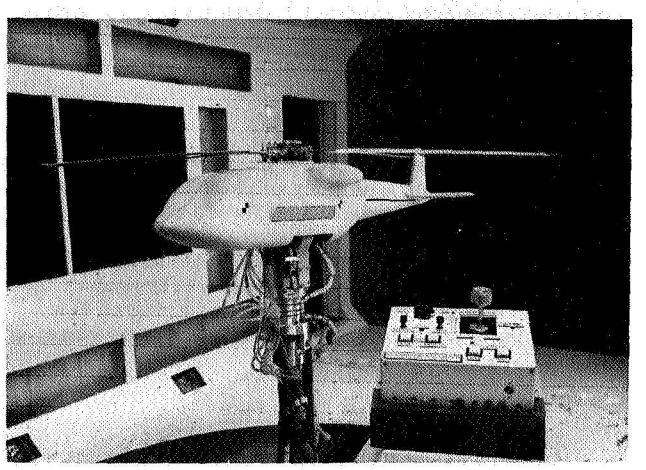

Figure 1. Dynamic Model Helicopter With 5.5-Foot-Diameter Single Rotor

(see Figure 2) to allow excitation of the model at the desired frequency. This enabled the measurement of the modal damping ratios at each test point. The measured modal damping permitted the precise determination of the stability boundaries and also showed the extent of stability when the model was stable.

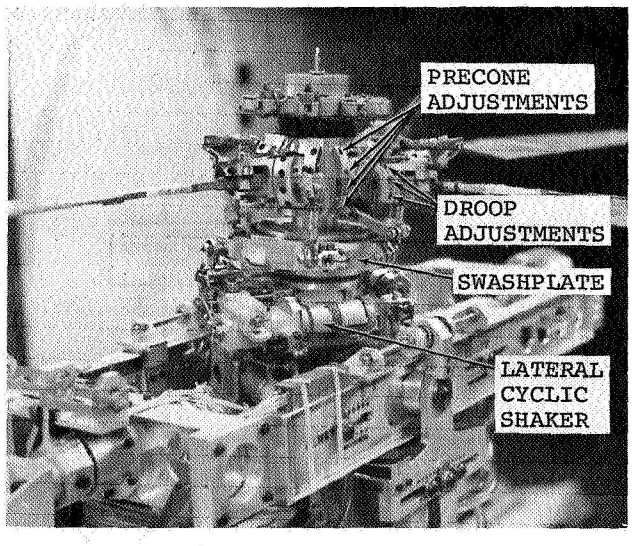

Figure 2. Details of Model Rotor Hub and Swashplate

Presented at the AHS/NASA-Ames Specialists Meeting on Rotorcraft Dynamics, February 13-15, 1974.

The stability and control augmentation system was based on position feedback. Position potentiometers on the helicopter gimbal axes provided position feedback signals which were amplified, filtered, and fed into the cyclic actuators for automatic stabilization of the model. The filter was designed to block any feedback at a frequency of $\Omega-\omega_\zeta$ and thus eliminated any control inputs that would tend to interact with the air-resonance mode.

Collective pitch was set by means of an open-loop control and a pitch-angle indicator. Other controls provided for the operator included mounting-pylon pitch attitude, stick trim, and quick-acting and slow-acting, self-centering snubbers to lock out the pitch and roll degrees of freedom. The horizontal stabilizer was manually trimmable and rotor speed was controlled by the wind tunnel operator.

Signals from the blade flap, torsion, and chord strain gages, along with body pitch and roll motion, cyclic stick position, and 1/rev, were recorded on oscillograph as well as on multiplex tape recorder. One of the chord-bending traces was filtered to display the chord bending at the critical lag natural frequency to allow quick determination of modal damping on line. Most of the testing was performed in the wind tunnel at the University of Maryland.

Test Technique

As discussed in References 1 and 2, the air-resonance mode stability is determined by the blade collective pitch as well as the rotor speed. Therefore, for every airspeed, a comprehensive variation of rpm and collective pitch was conducted.

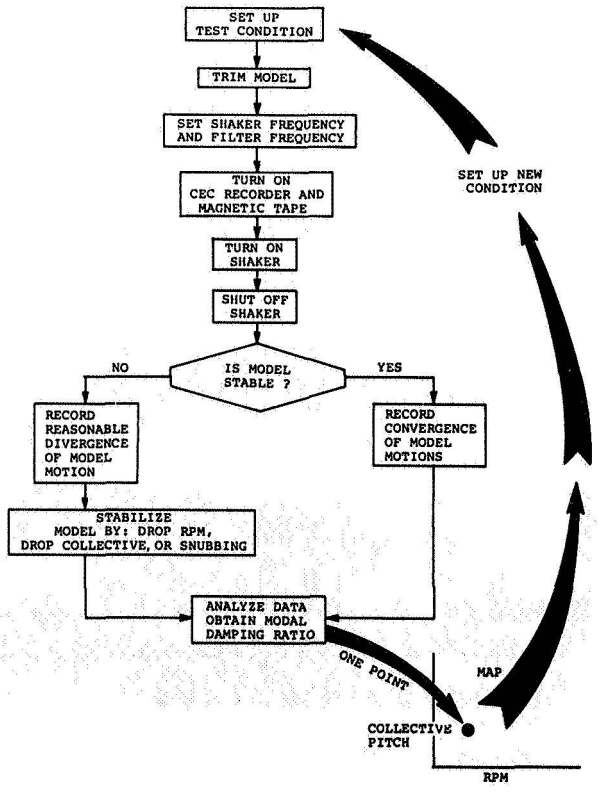

Figure 3. Flow Diagram of Test Technique

Figure 3 shows the test flow of events for each data point taken. After the test conditions had been set up (rpm, tunnel speed, and collective pitch), the model was trimmed and was held at the trim attitude with the stability and control augmentation system (SCAS). The shaker and the tracking filter frequencies were set to $\Omega-\omega_\zeta$ and ω_ζ respectively, with the absolute magnitudes dependent on the rotor speed. Both the multiplex tape recorder and the CEC recorders were turned on to record the steady-state response of the model. The swashplate was then oscillated in the lateral control direction. After the termination of the excitation, recording was continued until steady-state conditions were again reached, when practical. The decay of the filtered, in-plane, bending-moment trace was reduced to obtain the modal damping ratio.

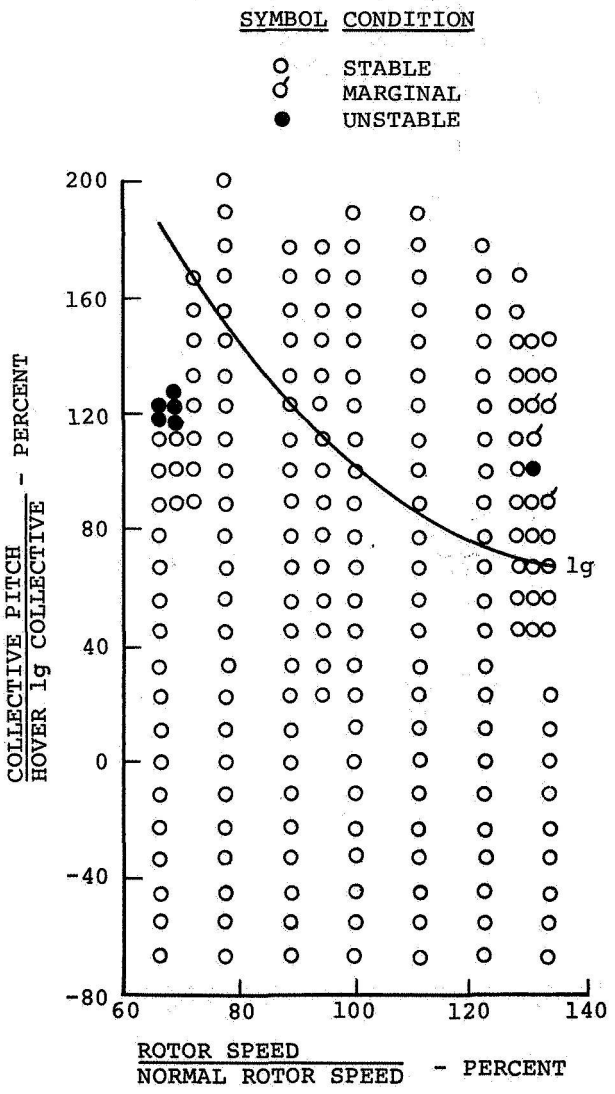

Figure 4. Typical Map of Test Points in Hover

Test Results

Figure 4 shows a typical map of test points taken at a constant tunnel speed, in this case in hover. Two

stability boundaries were present: one at about 70 percent of normal rotor speed and 120 percent of normal collective pitch and another at about 135 percent rpm and 100 percent collective. Examination of the coupled frequency variation with rotor speed while holding constant thrust, Figure 5, reveals that the low-rpm boundary corresponds to the resonance with the body-pitch-predominant mode and the high-rpm boundary with the body-roll-predominant mode.

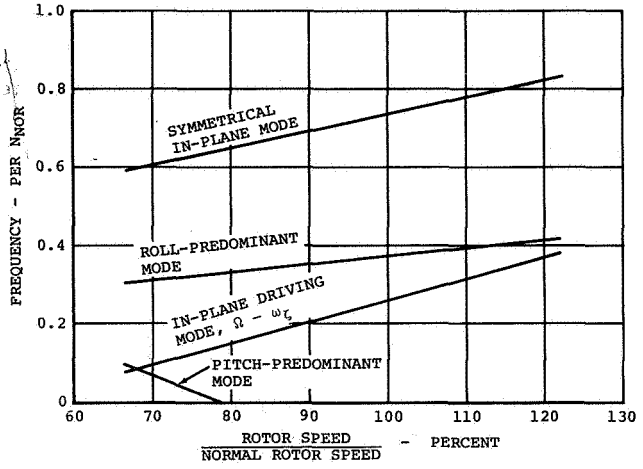

Figure 5. Coupled Resonance Characteristics

Figures 6, 7, and 8 show the time histories of three hover air-resonance points which are at constant collective pitch of 133 percent θ_{NOR} (1g hover collective at N_{NOR}) with rotor speeds of 100 percent, 72 percent, and 67 percent N_{NOR} respectively. At N_{NOR} the chord bending decayed after the excitation terminated, at a rate of approximately 1 percent of critical damping, and the body participation was barely detectable. Approaching the stability boundary at 72 percent rpm, the chord bending took longer to decay compared to the 100 percent rpm case. Body participation was quite pronounced in both pitch and roll. While the filtered chord-bending gage in the rotating system was indicating at the blade lag natural frequency, ω_ζ, the body pitch and roll motions responding in the same air-resonance mode were at the fixed-system frequency of $\Omega-\omega_\zeta$. It is of interest that these $\Omega-\omega_\zeta$ body motions are superimposed on some very low-frequency, flying-quality-type motions.

At 67 percent rpm, Figure 8, the air-resonance mode started to diverge after being excited; when the body was snubbed, the blade motion decayed and returned to the 1/rev forced response.

The response characteristics described here held true for all airspeeds tested up to a scaled test speed limit of 225 knots.

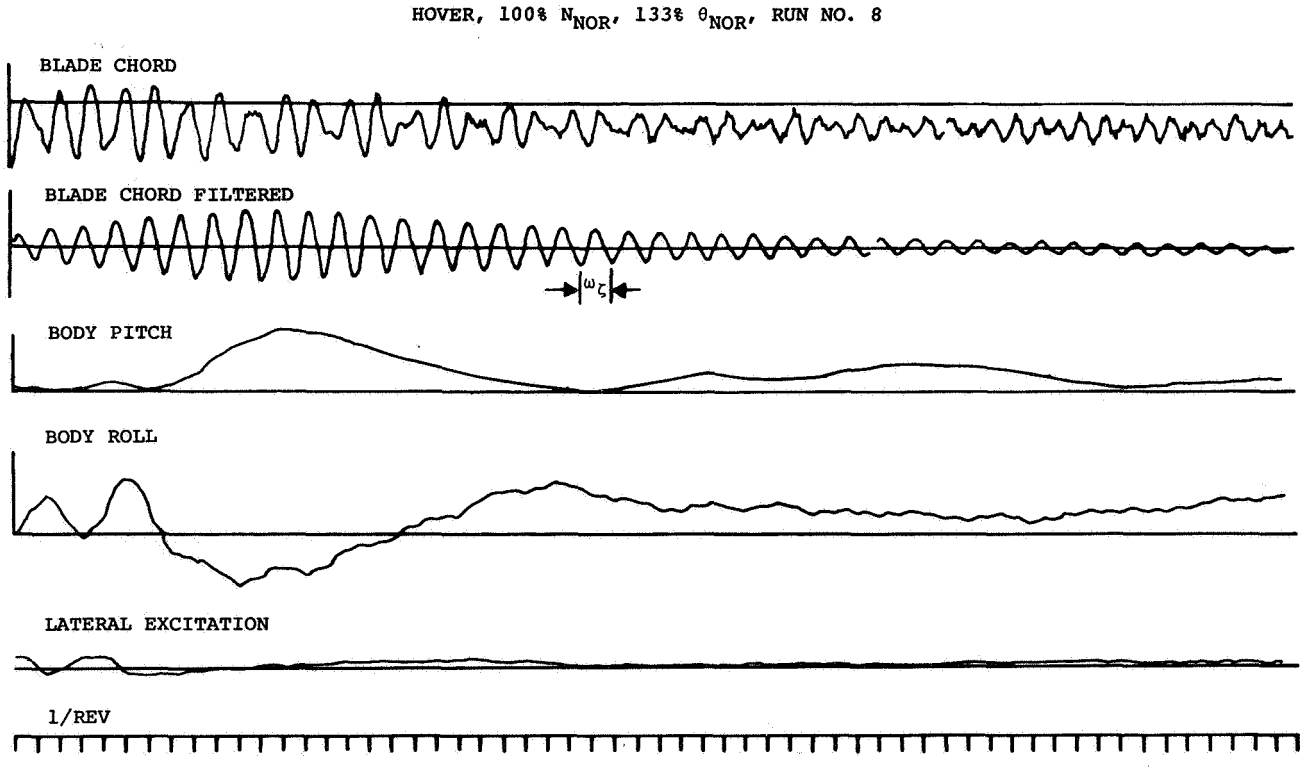

Figure 6. Response Time Histories in Hover at N_{NOR}

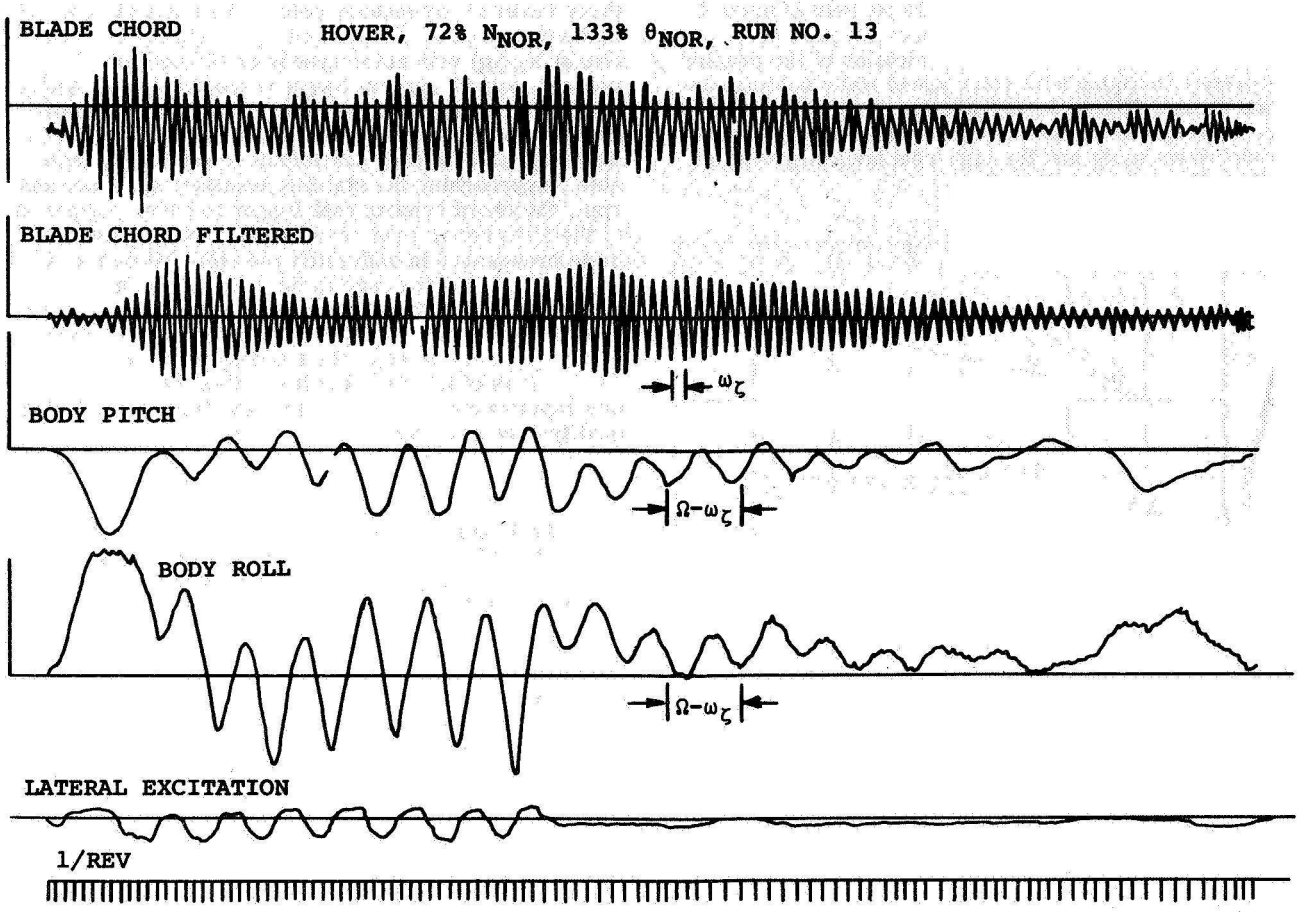

Figure 7. Response Time Histories in Hover at 72 Percent N_{NOR}

Analytical Model

To treat the dynamically and aerodynamically coupled rotor-airframe air-resonance problem, the analytical model shown in Figure 9 is used. In this model, the elastic cantilevered blade is represented by a spring-restrained, hinged rigid blade. Three hinges are used to simulate the first flap, first lag, and first torsion modes, in that order from inboard to outboard. In addition, a pitch degree of freedom is provided inboard of the flap hinge to facilitate the simulation of any torsional stiffness distribution relative to the flap and lag hinges. The blade model includes built-in pitch axis precone, blade sweep, kinematic pitch-flap and pitch-lag coupling, and a variable chordwise center-of-gravity distribution over the blade span.

The aerodynamic model is based on current blade-element theory and can handle all hover, forward flight, and maneuver flight conditions. It uses two-dimensional airfoil data with stall, reverse-flow, and compressibility effects.

The airframe has five rigid-body freedoms: longitudinal, lateral, vertical, pitch, and roll; and two flexible freedoms: pylon pitch and pylon roll. The equations of motion are nonlinear and are solved by a numerical time-history solution technique. The blade degrees of freedom are calculated for each individual blade.

To evaluate the aeroelastic stability, the aircraft can be perturbed from the trimmed state. For air-resonance investigations this is usually done by oscillatory stick excitations, which can be simulated in any frequency. The time history of each degree of freedom is then subjected to an oscillation analysis program to obtain the frequencies, amplitudes, phases, and damping coefficients. A more detailed discussion of this analytical procedure can be found in Reference 2.

Using a linear lift-curve slope, this coupled analysis in hover can be reduced to a set of second-order differential equations with constant coefficients by applying the quasi-normal coordinate transformation

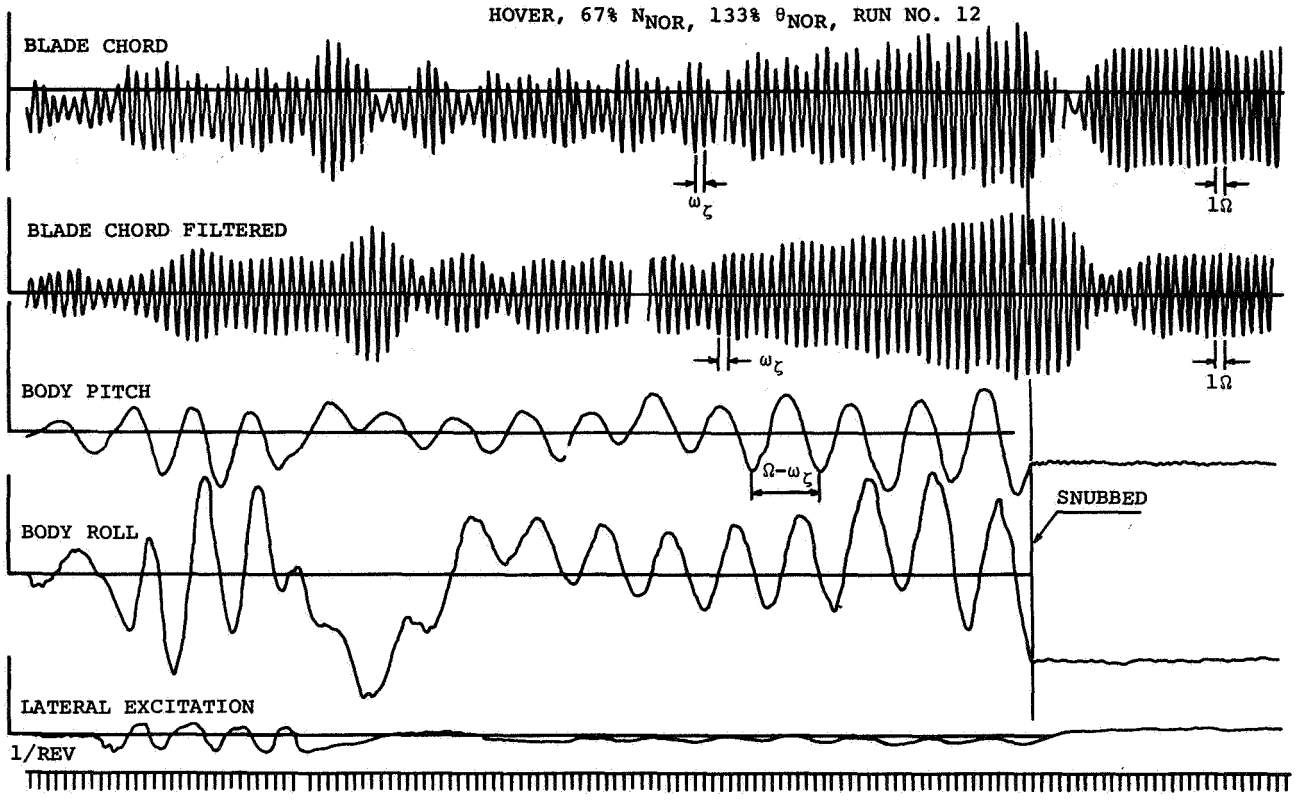

Figure 8. Response Time Histories in Hover at 67 Percent N_{NOR}

for the rotating coordinates[3]. This enables the closed-form solution. The eigenvalues and eigenvectors thus obtained yield the information on frequencies, damping, and mode shapes.

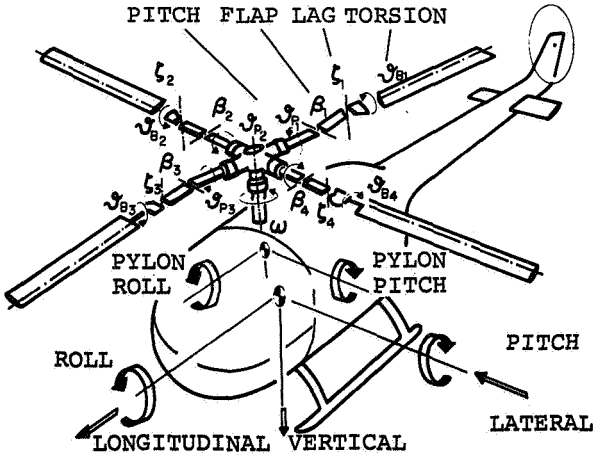

Figure 9. Coupled Rotor-Fuselage Analytical Model

Correlation

Rotor Thrust

Figure 10 shows the air-resonance mode modal damping ratio variations with thrust at N_{NOR} in hover. The agreement between test and analysis is quite good. The propitious trend with increasing collective pitch is due partly to the increase of aerodynamic damping, but is mainly a result of the favorable pitch-flap-lag coupling. A typical blade elastic coupling is shown in Figure 18 where the blade flap, lag, and pitch torsion responses to a cyclic-pitch input are indicated. The type of elastic coupling of this rotor system is discussed in more detail in a subsequent section.

Rotor Speed

Shown in Figure 11 are the test correlations of the air-resonance mode damping variation with rotor speed at constant collective pitch (133 percent θ_{NOR}) in hover. The analytical results are in good agreement with test points over the whole rotor speed range. The stability boundary corresponding to the resonance with the body-pitch-predominant mode at low rpm is predicted well by theory. The somewhat higher level of damping of the test points might indicate that the structural damping of the real model blade is higher than the 0.5 percent damping assumed in the analysis.

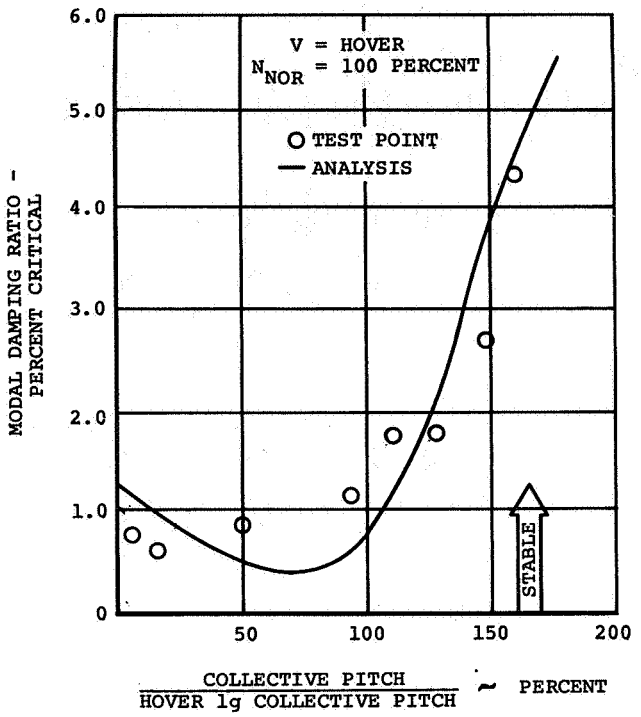

Figure 10. Effect of Thrust on Air-Resonance Stability

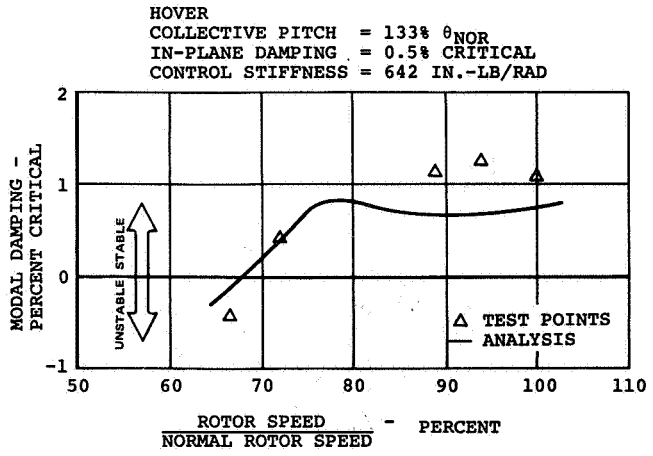

Figure 11. Effect of Rotor Speed on Air-Resonance Stability

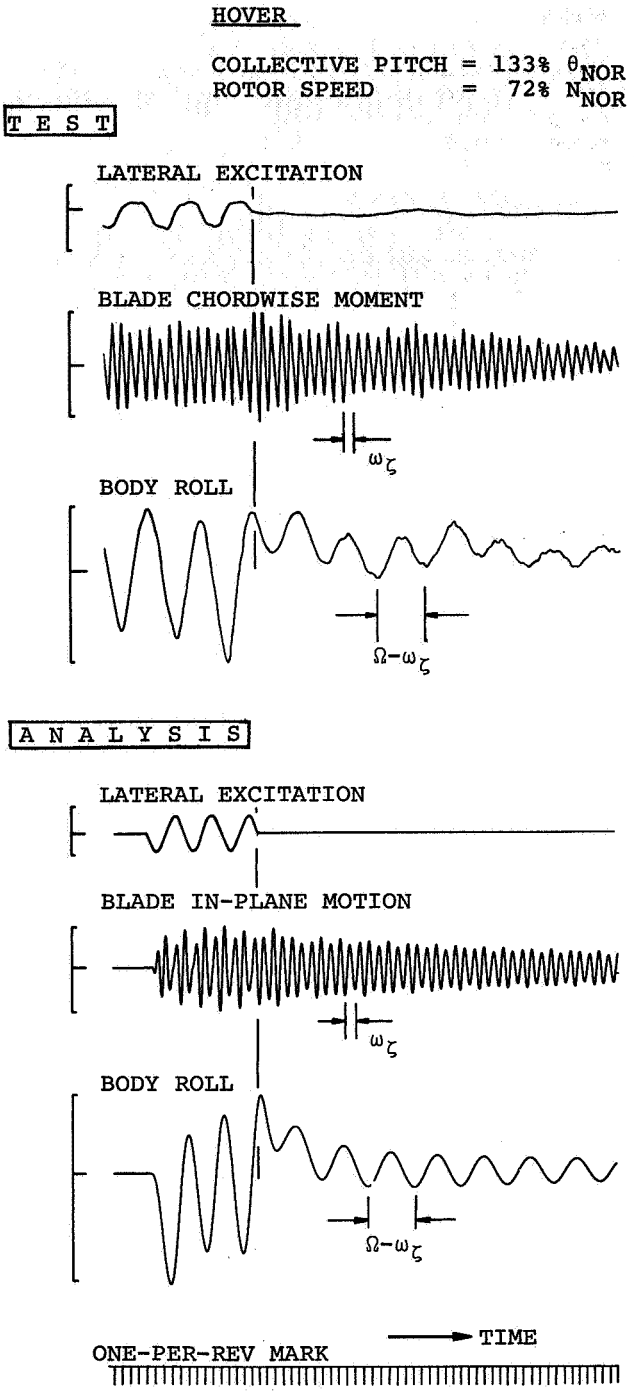

Figure 12. Correlation of Test and Analysis of Time Histories in Hover

The good agreement of Figure 11 is merely a reflection of the excellent correlation between test and analysis in the time-history waveform of blade and body motions. One example is shown in Figure 12. For this case the oscillation analysis program yields a damping coefficient of 0.39 percent at blade lag natural frequency for the rotating blade.

Forward Flight

The test trend of air-resonance mode damping with airspeed is also verified by analysis in Figure 13. Test points shown in this diagram were obtained with constant collective pitch, so that they do not correspond to a 1g-thrust/level-flight condition. The analysis was

performed under the same collective/shaft-angle settings to get an exact simulat ion of the test conditions. At 150 knots, the collective pitch is slightly reduced, from 133 percent to 111 percent, which produces a sharp decrease in rotor thrust. Therefore the air-resonance mode is less stable than for a normal 1g-thrust condition.

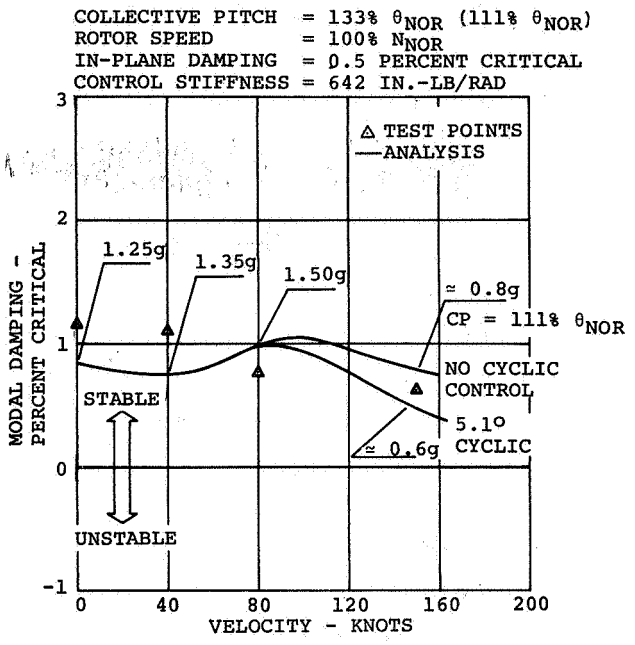

Figure 13. Effect of Forward Speed on Air-Resonance Stability at Constant Collective Pitch

Theory shows some influence of cyclic control on air-resonance stability at high speed. As longitudinal cyclic also controls rotor thrust in forward flight, this variation of air-resonance stability comes solely from the change in rotor thrust. With thrust held constant the stability is insensitive to steady 1/rev cyclic-pitch variation. This is shown in a later section.

In Figure 14 one example of a typical time history at a scaled airspeed of 80 knots is compared between test and analysis. When one considers the complex frequency modulations during this excited air-resonance case, the correlation can be said to be excellent. This should indicate that theory allows a definitive and reliable view of a helicopter's stability characteristics.

Additional test results of air-resonance stability in forward flight are illustrated in Figure 15. This trend, which was obtained for a 1g/level-flight condition, follows the rotor power curve quite well. As shown in Figure 10, for a moderate range of thrust variation, say around 1g, the air-resonance mode becomes more stable with increasing thrust and less stable with decreasing thrust. The forward-speed trend here simply reflects this thrust (and aerodynamic coning angle) dependency. This trend, which shows that the air-resonance mode stability improves significantly at high forward speeds, is also apparent in the BO-105 flight test data[2].

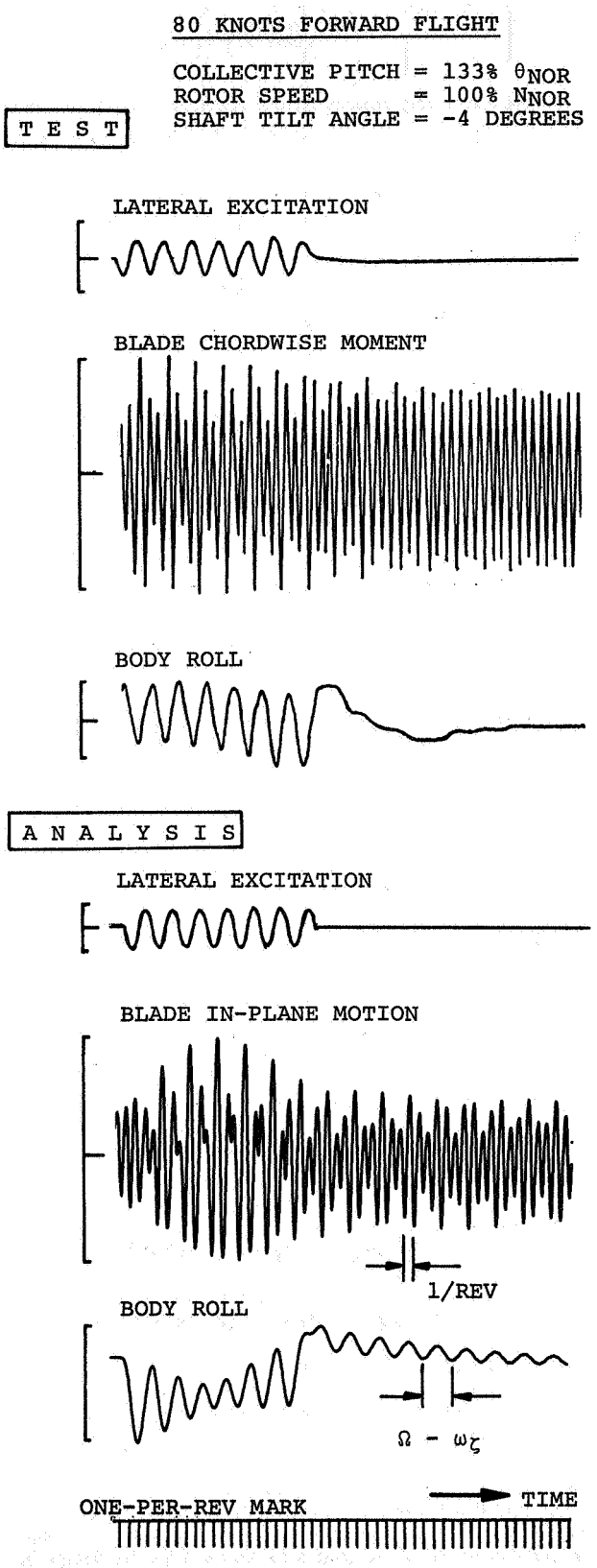

Figure 14. Correlation of Test and Analysis of Time Histories in Forward Flight

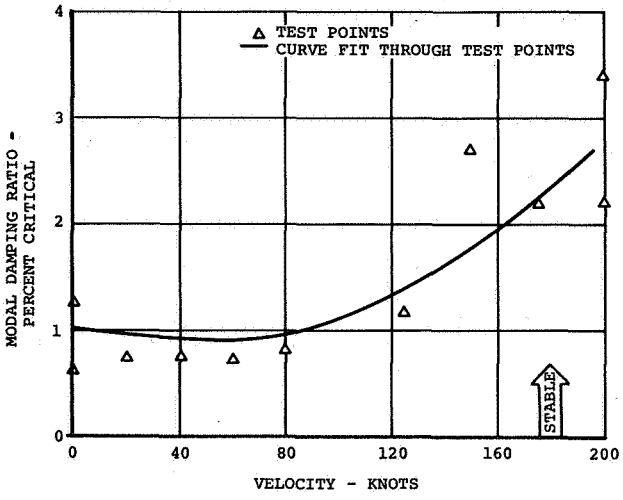

Figure 15. Effect of Forward Speed on Air-Resonance Stability in 1g Level Flight

Physics of Air Resonance

General

The mechanism and the stability characteristics of air resonance have been well described in numerous papers.[1,2,4,5,6] It suffices to say here that the soft-in-plane hingeless-rotor system derives its inherent stability mainly from the powerful flap damping. While rotors with untwisted blades may have substantial reduction in the flap damping near zero thrust, the damping available remains essentially unchanged for blades with nominal twist. Figure 16 shows the test data for various blades of different twist. Above a thrust coefficient of 0.005, the twisted blade and the untwisted blade both have the same thrust-per-collective slope. While the untwisted blade has a drastic reduction in slope with reduction in thrust in both theory and test, that of the twisted blade remains the same.

Let us examine the coupling terms that are inherent in the hingeless rotor system with an equivalent hinge sequence of pitch-flap-lag from inboard to outboard. One term that stands out is the perturbation pitch moment produced by the induced drag (steady force) acting through a moment arm of vertical-flapping displacement (perturbation deflection). This flap-pitch coupling term due to the induced drag has the sense of flap up/pitch noseup. Figure 17 compares the air-resonance mode damping of the same rotor system with this particular coupling term suppressed. With the induced-drag term suppressed, the air-resonance mode does not become unstable at high collective where the induced drag dominates.

By the same consideration, the air-resonance mode should become more stable in descent since during descent, the induced drag acts toward the leading edge producing a flap-pitch coupling of flap-up/pitch-nose-down sense, which is stabilizing.

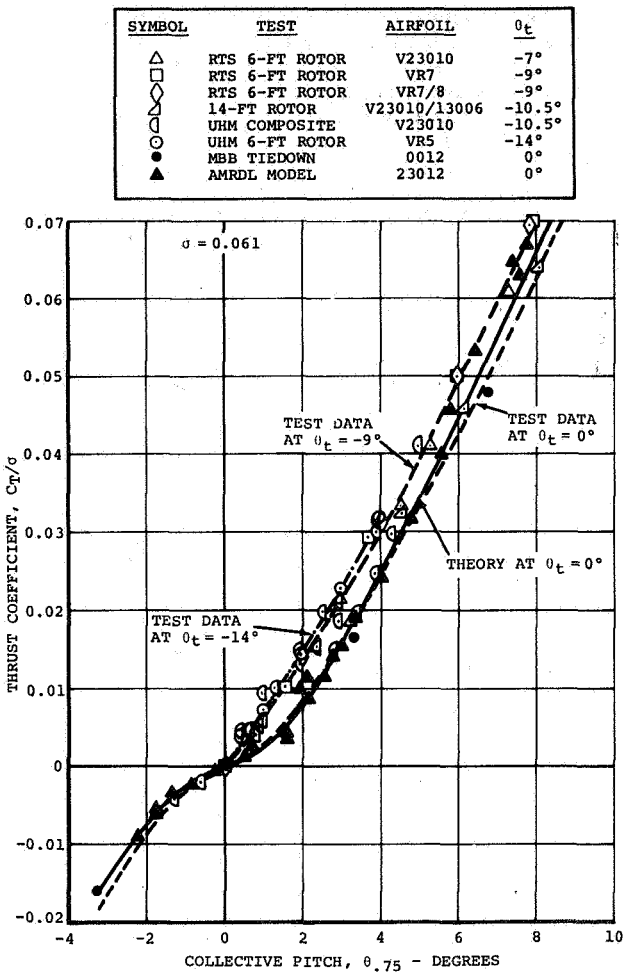

Figure 16. Effect of Blade Twist on Thrust Coefficient

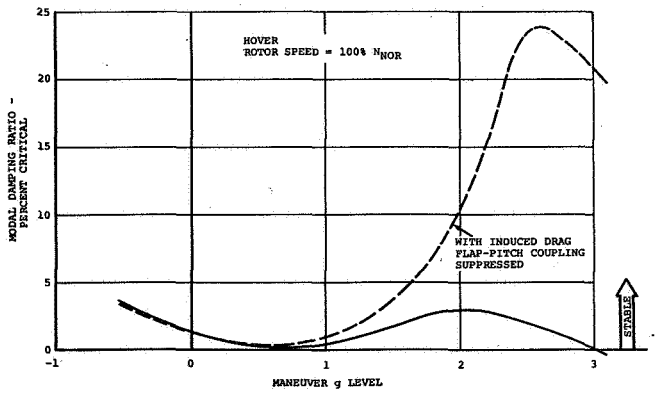

Figure 17. Stability Characteristics With Suppression of Flap-Pitch Coupling Term Due to Induced Drag

Pitch-Flap-Lag Coupling Characteristics

For a complete understanding of the elastic-coupling characteristics of a hingeless rotor with a pitch-flap-lag sequence of hinges, all blade motions must be considered together. For this purpose it is instructive to analyze a simple cyclic-pitch case in hover. In Figure 18 the elastic flap, lead-lag, and pitch motions are shown over one rotor revolution. It can be seen clearly that the flap and lag motions are accompanied by an elastic pitch torsion, the resultant coupling being in the sense of flap up/lead forward/pitch nosedown. For a clear understanding this complex coupling can be divided into two distinct coupling phenomena: the one equivalent to a negative pitch-flap coupling (flap up/pitch nosedown), the other equivalent to a positive pitch-lag coupling (lead forward/pitch nosedown). The coupling factors are 0.4 degree pitch per degree flap and 0.6 degree pitch per degree lag.

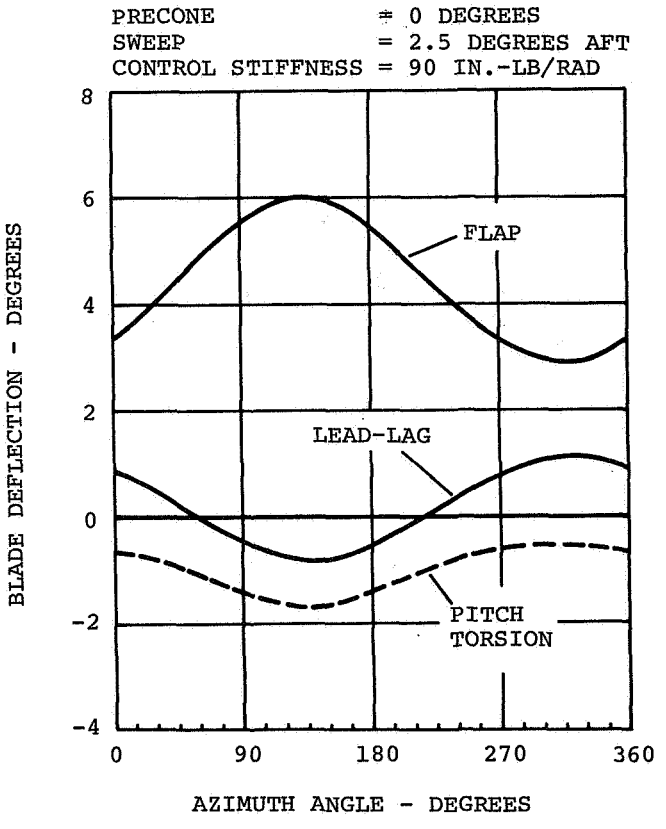

Figure 18. Blade Elastic Coupling

Besides the well-known stabilizing effect of pitch-flap coupling, the pitch-lag part of the total coupling is of utmost importance for the in-plane motions of the blade. Positive pitch-lag coupling (decrease of pitch as the blade leads forward, increase of pitch as the blade lags back) has a highly stabilizing effect on the lead-lag oscillations. Recent investigations[1,2] have shown that these coupling characteristics can be influenced by several hub and blade parameters, for example, by feathering axis precone, blade sweep, and control system flexibility. Some of these design rules have already been applied to this model rotor design (low precone, aft sweep, soft control systems).

Parametric Sensitivities

The following paragraphs describe the air-resonance mode stability sensitivities obtained from the model test.

Climb and Descent

Figure 19 shows the sensitivity with 1g climb and descent at a scaled airspeed of 80 knots. With normal control system stiffness (90 in.-lb/rad), descent stabilizes the mode as discussed in the previous section; conversely, climb has a destabilizing effect.

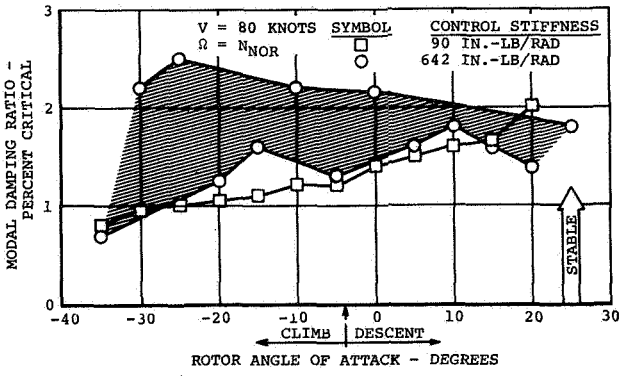

Figure 19. Effects of Climb, Descent, and Control System Stiffness on Air-Resonance Stability

Control System Stiffness

Also shown in Figure 19 are the test data obtained with the control system stiffness seven times stiffer than normal. The effect of climb and descent almost disappeared. Since the stability is affected by the pitch-flap-lag coupling, a stiff control system minimizes the coupling effect, be it favorable or unfavorable.

Precone

Precone of the pitch axis directly alters the pitch-flap-lag coupling. The beneficial effect of lower precone has been evaluated many times.[1,2,7] Figure 20 shows the test confirmation of the favorable effect of the low precone.

Cyclic Trim

An evaluation of the cyclic trim on the air-resonance stability was accomplished by varying the angle of incidence of the tail. The tail incidence angle was varied from 2 degrees through 45 degrees. As shown in Figure 21, the stability is insensitive to the range of cyclic-trim variation at constant thrust. This suggests that the steady 1/rev cyclic-pitch variation in forward flight can be ignored with respect to the air resonance.

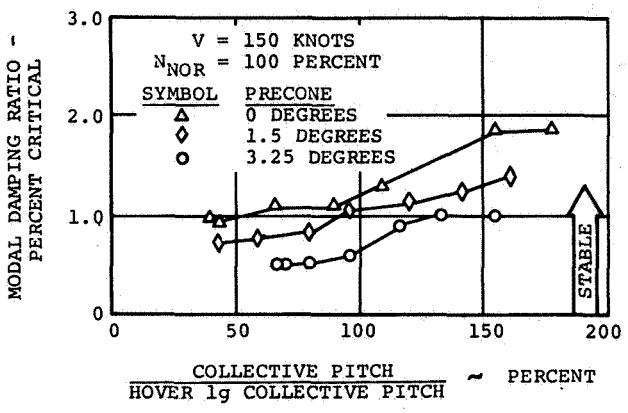

Figure 20. Effect of Blade Precone on Air-Resonance Stability

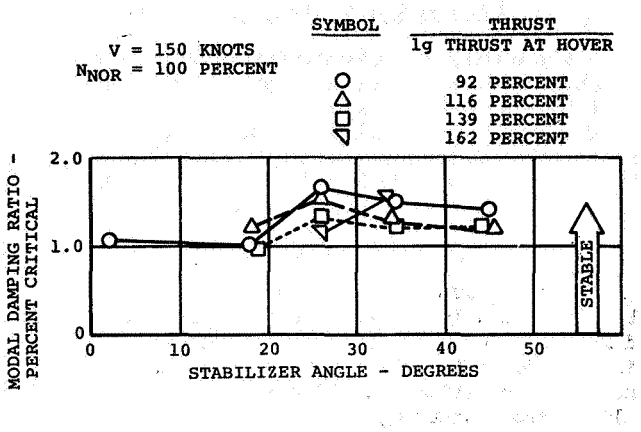

Figure 21. Effect of the Incidence Angle of the Horizontal Tail on Air-Resonance Stability

Conclusions

1. The air-resonance mode stability is sensitive to collective pitch (thrust).

2. Air-resonance mode stability is also sensitive to climb and descent; that is, descent is stabilizing while climb is destabilizing.

3. The prime coupling term in the rotor system which causes the degradation of stability at high thrust is the induced drag. This coupling also provides the trend versus climb and descent.

4. Air-resonance mode stability in 1g level flight shows the rotor-power-curve trend with highly stable characteristics at high speed.

5. The elastic-coupling behavior of the model rotor with normal control system stiffness is characterized by a pitch-flap coupling (0.4 degree pitch per degree flap) and a pitch-lag coupling (0.6 degree pitch per degree lag).

6. High control system stiffness minimizes the flap-pitch coupling effectiveness and reduces the sensitivity of the air-resonance stability to design parameters which are otherwise influential.

7. Less precone is stabilizing for a soft-in-plane hingeless-rotor system with an equivalent hinge sequence of pitch-flap-lag from inboard to outboard.

8. Variation in cyclic trim does not affect air-resonance stability.

9. The testing technique to define air-resonance modal damping discretely at many operational conditions proved highly successful. Use of these methods to define modal damping, rather than defining only the boundaries, allows for a more definitive view of an aircraft's stability characteristics.

References

1. Burkam, J.E., and Miao, W., EXPLORATION OF AEROELASTIC STABILITY BOUNDARIES WITH A SOFT-IN-PLANE HINGELESS-ROTOR MODEL, Preprint No. 610, 28th Annual National Forum of the American Helicopter Society, Washington, D.C., May 1972.

2. Huber, H.B., EFFECT OF TORSION-FLAP-LAG COUPLING ON HINGELESS ROTOR STABILITY, Preprint No. 731, 29th Annual National Forum of the American Helicopter Society, Washington, D.C., May 1973.

3. Gabel, R., and Capurso, V., EXACT MECHANICAL INSTABILITY BOUNDARIES AS DETERMINED FROM THE COLEMAN EQUATION, Journal of the American Helicopter Society, January 1962.

4. Lytwyn, R.T., Miao, W., and Woitsch, W., AIRBORNE AND GROUND RESONANCE OF HINGELESS ROTORS, Preprint No. 414, 26th Annual National Forum of the American Helicopter Society, Washington, D.C., June 1970.

5. Donham, R.E., Cardinale, S.V., and Sachs, I.B., GROUND AND AIR RESONANCE CHARACTERISTICS OF A SOFT INPLANE RIGID ROTOR SYSTEM, Journal of the American Helicopter Society, October 1969.

6. Woitsch, W., and Weiss, H., DYNAMIC BEHAVIOR OF A HINGELESS FIBERGLASS ROTOR, AIAA/AHS VTOL Research, Design, and Operations Meeting, Atlanta, Georgia, February 1969.

7. Hodges, D.H., and Ormiston, R.A., STABILITY OF ELASTIC BENDING AND TORSION OF UNIFORM CANTILEVERED ROTOR BLADES IN HOVER, AIAA/ASME/SAE 14th Structures, Structural Dynamics, and Materials Conference, Williamsburg, Virginia, March 1973.

AN APPLICATION OF FLOQUET THEORY TO PREDICTION OF MECHANICAL INSTABILITY

C. E. Hammond
Langley Directorate
U.S. Army Air Mobility R&D Laboratory
NASA Langley Research Center
Hampton, Virginia

Abstract

The problem of helicopter mechanical instability is considered for the case where one blade damper is inoperative. It is shown that if the hub is considered to be nonisotropic the equations of motion have periodic coefficients which cannot be eliminated. However, if the hub is isotropic the equations can be transformed to a rotating frame of reference and the periodic coefficients eliminated. The Floquet Transition Matrix method is shown to be an effective way of dealing with the nonisotropic hub and nonisotropic rotor situation. Time history calculations are examined and shown to be inferior to the Floquet technique for determining system stability. A smearing technique used in the past for treating the one damper inoperative case is examined and shown to yield unconservative results. It is shown that instabilities which occur when one blade damper is inoperative may consist of nearly pure blade motion or they may be similar to the classical mechanical instability.

Notation

c_i	lag damping rate
c_x	effective hub damping in x-direction
c_y	effective hub damping in y-direction
e	lag hinge offset
I_b	second mass moment of blade about lag hinge
k_i	lag spring rate
k_x	effective hub stiffness in x-direction
k_y	effective hub stiffness in y-direction
m_b	blade mass
m_x	effective hub mass in x-direction
m_y	effective hub mass in y-direction
N	number of blades in rotor
p_j	characteristic exponent corresponding to jth eigenvalue of the Floquet Transition Matrix
P_x	force acting on hub in x-direction
P_y	force acting on hub in y-direction
S_b	first mass moment of blade about lag hinge
T	period of the periodic coefficients, $T = 2\pi/\Omega$
$\bar{x}$, $\bar{y}$	coordinates of hub in rotating reference frame
x_c, y_c	coordinates of rotor center of mass in fixed reference frame
x_h, y_h	coordinates of hub in fixed reference frame
x_i, y_i	coordinates of elemental blade mass dm in fixed reference frame
ζ_i	lag deflection of ith blade
η_h	defined by Equations (18)
η_i	defined by Equations (7)
Λ_j	jth eigenvalue of the Floquet Transition Matrix
ν_h	defined by Equations (18)
ν_o	defined by Equations (7)
ρ	distance from lag hinge to elemental blade mass dm
ψ_i	azimuthal location of ith blade
Ω	rotor speed
ω_h	defined by Equations (18)
ω_{o_i}	defined by Equations (7)
[A(t)]	characteristic matrix, periodic with period T
[D(t)]	state matrix, periodic with period T
[Q]	Floquet Transition Matrix
$[\phi(t)]$	state transition matrix
$\{z(t)\}$	state vector

Presented at the AHS/NASA Ames Specialists' Meeting on Rotorcraft Dynamics, February 13-15, 1974.

The problem of mechanical instability of helicopters on the ground has been recognized and understood for many years. The analysis by Coleman and Feingold[1] has become the standard reference on this phenomenon although it was not published until many years after the first incidents of mechanical instability, or ground resonance as it is commonly known, were encountered on the early autogyros. The mechanical instability phenomenon is most commonly associated with helicopters having articulated rotors; however, helicopters using the soft-inplane hingeless rotors which have become popular in recent years are also susceptible to this problem. Machines employing these soft-inplane hingeless rotors are also known to experience a similar problem, commonly known as air resonance, which occurs in flight rather than on the ground. The air resonance problem has received much attention in recent years (see, e.g., Refs. 2 and 3).

From the analysis of Reference 1 and others it is known that the ground resonance problem is due primarily to a coupling of the blade inplane motion with the rigid body degrees of freedom of the helicopter on its landing gear. These analyses have shown that with the proper selection of blade lag dampers and landing gear characteristics the problem of mechanical instability can be eliminated within the operating rotor speed range. All of the mechanical instability analyses conducted to date have one assumption in common - all blades are assumed to have identical properties. This is a reasonable assumption under ordinary circumstances; however, the U.S. Army has a requirement on new helicopters which invalidates this assumption. The requirement is that the helicopter be free from ground resonance with one blade damper inoperative. As will be shown later, this one blade damper inoperative requirement has a serious impact on the classical method of analyzing a helicopter for mechanical instability. Further, there is at present no published method available for treating the case where each of the blades is permitted to have different properties. Thus the designer is faced with the dilemma of trying to satisfy the requirement with an analysis method in which one of the basic assumptions is severely violated.

Two methods have been used to circumvent this difficulty. The first of these involves a physical approximation so that the classical analysis becomes applicable. In this approach all blades are still assumed to have identical lag dampers even when one blade damper is removed, but the value of each of the dampers is reduced by the amount c_i/N where N is the number of blades and c_i is the original lag damper rate. As can be seen, with this approach a system is analyzed which is quite different from the actual situation of a rotor with no damping on one blade. The second method which has been used is to reformulate the equations of motion allowing for differing blade characteristics and to obtain the stability characteristics of the system using a time history integration of the equations. This second approach has the drawback that interpretation of stability characteristics from time history calculations is often difficult and open to question. The method will yield correct results, however, provided the equations are integrated over a sufficiently long time period.

The purpose of this paper is to present a method of obtaining the mechanical stability characteristics directly for a helicopter operating on the ground with one blade damper inoperative. As will be shown later, the equations governing the motion of this system have periodic coefficients. This fact suggests the use of Floquet theory as the means for determining the stability characteristics of the system. In the following, the one-damper-inoperative problem is formulated and the resulting equations are solved using the Floquet Transition Matrix method described by Peters and Hohenemser.[4] Results obtained using this method are compared with results obtained from the two previously used methods and recommendations are made concerning the future use of the three methods described.

Equations of Motion

The equations of motion for the mechanical instability problem will be formulated using an Eulerian approach. It will be assumed, as is done in Reference 1, that the helicopter on its landing gear can be represented by effective parameters applied at the rotor hub. It will be further assumed that only inplane motions of the hub and blades are important in determining the ground resonance characteristics of the helicopter. Thus the degrees of freedom to be considered consist of two inplane hub degrees of freedom and a lead-lag degree of freedom for each blade in the rotor. The mathematical model to be used in the analysis is shown in Figure 1. Note that in the figure only a typical blade is shown. The analysis will be formulated for a rotor having N blades, and each blade is assumed to have a rotational spring and damper which act about the lag hinge.

The blade equations are developed by summing moments about the lag hinge. The coordinates of the elemental mass dm in the fixed system are

$$\left.\begin{aligned} x_i &= x_h + e\cos\psi_i + \rho\cos(\psi_i + \zeta_i) \\ y_i &= y_h + e\sin\psi_i + \rho\sin(\psi_i + \zeta_i) \end{aligned}\right\} \qquad (1)$$

where

$$\psi_i = \Omega t + 2\pi(i-1)/N \qquad i = 1,2,\ldots,N$$

These expressions can be differentiated twice with respect to time to yield the accelerations experienced by the differential mass

$$\left.\begin{aligned} \ddot{x}_i &= \ddot{x}_h - e\Omega^2\cos\psi_i - \rho(\Omega + \dot{\zeta}_i)^2\cos(\psi_i + \zeta_i) \\ &\quad - \rho\ddot{\zeta}_i\sin(\psi_i + \zeta_i) \\ \ddot{y}_i &= \ddot{y}_h - e\Omega^2\sin\psi_i - \rho(\Omega + \dot{\zeta}_i)^2\sin(\psi_i + \zeta_i) \\ &\quad + \rho\ddot{\zeta}_i\cos(\psi_i + \zeta_i) \end{aligned}\right\} \qquad (2)$$

Using D'Alembert's principle the summation of moments about the lag hinge can be written as

$$\int \rho \sin(\psi_i + \zeta_i)\ddot{x}_i dm - \int \rho \cos(\psi_i + \zeta_i)\ddot{y}_i dm - k_i\zeta_i - c_i\dot{\zeta}_i = 0 \qquad i = 1,2,\ldots,N \qquad (3)$$

where the integrals are evaluated over the length of the blade. Introducing the expressions for $\ddot{x}_i$ and $\ddot{y}_i$ and defining the following

$$\left.\begin{aligned} S_b &= \int \rho \, dm \\ I_b &= \int \rho^2 \, dm \end{aligned}\right\} \qquad (4)$$

the blade equations become

$$I_b\ddot{\zeta}_i + e\Omega^2 S_b \sin\zeta_i - S_b[\ddot{x}_h \sin(\psi_i + \zeta_i) - \ddot{y}_h \cos(\psi_i + \zeta_i)] + k_i\zeta_i + c_i\dot{\zeta}_i = 0 \qquad (5)$$

$$i = 1,2,\ldots,N$$

If small displacements are now assumed the blade equations may be linearized to obtain

$$\ddot{\zeta}_i + \eta_i\dot{\zeta}_i + (\omega_{o_i}^2 + \Omega^2\nu_o^2)\zeta_i = (\nu_o^2/e)[\ddot{x}_h \sin\psi_i - \ddot{y}_h \cos\psi_i] \qquad i = 1,2,\ldots,N \qquad (6)$$

where the following parameters have been introduced

$$\left.\begin{aligned} \nu_o^2 &= eS_b/I_b \\ \omega_{o_i}^2 &= k_i/I_b \\ \eta_i &= c_i/I_b \end{aligned}\right\} \qquad (7)$$

Under the assumptions stated earlier the hub equations of motion can be written directly as

$$\left.\begin{aligned} m_x\ddot{x}_h + c_x\dot{x}_h + k_x x_h &= P_x \\ m_y\ddot{y}_h + c_y\dot{y}_h + k_y y_h &= P_y \end{aligned}\right\} \qquad (8)$$

where the coefficients on the left side of these equations are the effective hub properties in the x- and y-directions, respectively. The determination of these properties depends on an extensive knowledge of the helicopter inertial characteristics and the stiffness, damping, and geometrical characteristics of the landing gear system. These properties may be determined either by ground shake tests of the helicopter, as suggested in Reference 1, or by direct calculations. The right-hand side of the above equations are the forces acting on the hub due to the fact that the rotor is experiencing accelerations in the x- and y-directions. If the accelerations of the rotor center of mass are $\ddot{x}_c$ and $\ddot{y}_c$, respectively, the P_x and P_y are given by

$$\left.\begin{aligned} P_x &= -Nm_b\ddot{x}_c \\ P_y &= -Nm_b\ddot{y}_c \end{aligned}\right\} \qquad (9)$$

The equations as written also indicate that in the absence of the rotor the hub degrees of freedom are uncoupled. This is an approximation, but it is an assumption made in Reference 1 and one generally used in helicopter mechanical stability analyses.

If all blades in the rotor are assumed to have the same mass distribution, the coordinates for the total rotor center of mass may be written as

$$\left.\begin{aligned} x_c &= x_h + \frac{1}{N}\sum_{i=1}^{N} x_{i_c} \\ y_c &= y_h + \frac{1}{N}\sum_{i=1}^{N} y_{i_c} \end{aligned}\right\} \qquad (10)$$

where x_{i_c} and y_{i_c} are the coordinates of the individual blade center of mass, measured with respect to the hub. If the center of mass of the ith blade is a radial distance ρ_c from the lag hinge

$$\left.\begin{aligned} x_{i_c} &= e\cos\psi_i + \rho_c\cos(\psi_i + \zeta_i) \\ y_{i_c} &= e\sin\psi_i + \rho_c\sin(\psi_i + \zeta_i) \end{aligned}\right\} \qquad (11)$$

Making the observation that, for $N > 1$

$$\sum_{k=1}^{N}\cos\psi_k = \sum_{k=1}^{N}\sin\psi_k = 0$$

the rotor center of mass coordinates become

$$\left.\begin{aligned} x_c &= x_h - (\rho_c/N)\sum_{i=1}^{N}\zeta_i\sin\psi_i \\ y_c &= y_h + (\rho_c/N)\sum_{i=1}^{N}\zeta_i\cos\psi_i \end{aligned}\right\} \qquad (12)$$

These expressions may now be differentiated twice with respect to time and the forces P_x and P_y obtained as

$$\left.\begin{aligned} P_x &= -Nm_b\ddot{x}_h + S_b\sum_{i=1}^{N}\left[(\ddot{\zeta}_i - \Omega^2\zeta_i)\sin\psi_i + 2\Omega\dot{\zeta}_i\cos\psi_i\right] \\ P_y &= -Nm_b\ddot{y}_h - S_b\sum_{i=1}^{N}\left[(\ddot{\zeta}_i - \Omega^2\zeta_i)\cos\psi_i - 2\Omega\dot{\zeta}_i\sin\psi_i\right] \end{aligned}\right\} \qquad (13)$$

The hub equations of motion thus become

$$\left.\begin{aligned} &(m_x + Nm_b)\ddot{x}_h + c_x\dot{x}_h + k_x x_h = \\ &S_b\sum_{i=1}^{N}\left[(\ddot{\zeta}_i - \Omega^2\zeta_i)\sin\psi_i + 2\Omega\dot{\zeta}_i\cos\psi_i\right] \\ &(m_y + Nm_b)\ddot{y}_h + c_y\dot{y}_h + k_y y_h = \\ &-S_b\sum_{i=1}^{N}\left[(\ddot{\zeta}_i - \Omega^2\zeta_i)\cos\psi_i - 2\Omega\dot{\zeta}_i\sin\psi_i\right] \end{aligned}\right\} \qquad (14)$$

The equations of motion for the system thus consist of (N + 2) coupled second-order differential

equations with the coupling terms having periodic coefficients. The periodic coefficients arise because the blade equations are written in a rotating reference system whereas the hub equations are in a fixed system. As is shown in the Appendix, if all the blades have identical lag springs and lag dampers, the periodic coefficients may be eliminated through the use of multiblade coordinates. The effect of these coordinates is to transform the blade equations from the rotating to the fixed system of reference. The resulting constant coefficient system of equations is the set normally solved in the classical ground resonance analysis. As is shown, however, if the blades are allowed to have different lag springs and dampers, the periodic coefficients cannot be eliminated in the usual manner.

An alternative does exist, however, for eliminating the periodic coefficients even when the blades are allowed to have differing characteristics. The alternative consists of transforming the hub equations into the rotating system of reference. In order to eliminate the periodic coefficients using this approach, the additional assumption must be made that the hub is isotropic. That is

$$m_x = m_y$$
$$c_x = c_y$$
$$k_x = k_y$$

This is the approach used in Reference 1 for treating the two-bladed rotor which is another case where the periodic coefficients in the equations of motion cannot be eliminated by transforming the blade equations to the fixed system.

The transformation from fixed to rotating coordinates is given by

$$\left.\begin{aligned} \bar{x} &= x_h \cos \Omega t + y_h \sin \Omega t \\ \bar{y} &= -x_h \sin \Omega t + y_h \cos \Omega t \end{aligned}\right\} \qquad (15)$$

Differentiating these expressions allows the following identities to be established

$$\dot{x}_h \cos \Omega t + \dot{y}_h \sin \Omega t = \dot{\bar{x}} - \Omega \bar{y}$$
$$-\dot{x}_h \sin \Omega t + \dot{y}_h \cos \Omega t = \dot{\bar{y}} + \Omega \bar{x}$$
$$\ddot{x}_h \cos \Omega t + \ddot{y}_h \sin \Omega t = \ddot{\bar{x}} - \Omega^2 \bar{x} - 2\Omega \dot{\bar{y}}$$
$$-\ddot{x}_h \sin \Omega t + \ddot{y}_h \cos \Omega t = \ddot{\bar{y}} - \Omega^2 \bar{y} + 2\Omega \dot{\bar{x}}$$

The hub equations in the rotating system are then obtained by appropriate combinations of the x_h and y_h equations, Equations (14). The resulting equations are given below

$$\ddot{\bar{x}} + \eta_h \dot{\bar{x}} + (\omega_h^2 - \Omega^2)\bar{x} - 2\Omega \dot{\bar{y}} - \Omega \eta_h \bar{y}$$
$$= \nu_h^2 \sum_{j=1}^{N} \left[(\ddot{\zeta}_j - \Omega^2 \zeta_j) \sin \frac{2\pi}{N}(j-1) + 2\Omega \dot{\zeta}_j \cos \frac{2\pi}{N}(j-1) \right] \qquad (16)$$

$$\ddot{\bar{y}} + \eta_h \dot{\bar{y}} + (\omega_h^2 - \Omega^2)\bar{y} + 2\Omega \dot{\bar{x}} + \Omega \eta_h \bar{x}$$
$$= -\nu_h^2 \sum_{j=1}^{N} \left[(\ddot{\zeta}_j - \Omega^2 \zeta_j) \cos \frac{2\pi}{N}(j-1) - 2\Omega \dot{\zeta}_j \sin \frac{2\pi}{N}(j-1) \right] \qquad (17)$$

where the following parameters have been introduced

$$\left.\begin{aligned} \nu_h^2 &= S_b/(m_x + N m_b) \\ \omega_h^2 &= k_x/(m_x + N m_b) \\ \eta_h &= c_x/(m_x + N m_b) \end{aligned}\right\} \qquad (18)$$

Introducing the rotating coordinates into the blade equations, Equations (6), results in

$$\ddot{\zeta}_j + \eta_j \dot{\zeta}_j + (\omega_{o_j}^2 + \Omega^2 \nu_o^2)\zeta_j$$
$$= (\nu_o^2/e)\left[(\ddot{\bar{x}} - \Omega^2 \bar{x} - 2\Omega \dot{\bar{y}}) \sin \frac{2\pi}{N}(j-1) - (\ddot{\bar{y}} - \Omega^2 \bar{y} + 2\Omega \dot{\bar{x}}) \cos \frac{2\pi}{N}(j-1) \right] \qquad (19)$$
$$j = 1,2,\ldots,N$$

Since modern helicopters do not in general have isotropic hubs, the above equations can only be used to approximate the effects of a nonisotropic rotor. They are, however, easily solved for the stability characteristics of the system and thus they might be used to obtain a first approximation to the mechanical stability boundary for a helicopter with one blade damper inoperative.

From the foregoing discussion it can be seen that if either the rotor or the hub is isotropic, the mechanical stability characteristics of the system may be obtained using conventional techniques. If both the rotor and hub are nonisotropic the equations of motion of the system contain periodic coefficients and thus the standard eigenvalue techniques cannot be used to determine whether the system is stable or unstable. It is the purpose of this paper to demonstrate that Floquet theory can be used to analyze this general situation of a nonisotropic rotor coupled with a nonisotropic hub.

Solution of the Equations

If the periodic coefficients in the equations of motion are eliminated by assuming either an isotropic rotor or an isotropic hub, the stability of the system can be determined using standard eigenvalue techniques. The general case of a nonisotropic rotor coupled with a nonisotropic hub will be treated using Floquet techniques as described by Peters and Hohenemser,[4] and Hohenemser and Yin.[5] A brief description of the technique will be presented here for the sake of completeness.

In state vector rotation the free motions of the system may be written as

$$\{\dot{z}\} = [D(t)]\{z\} \qquad (20)$$

where the state variables for the problem being considered consist of

$$\zeta_1, \zeta_2, \ldots, \zeta_N, x_h, y_h, \dot{\zeta}_1, \dot{\zeta}_2, \ldots, \dot{\zeta}_N, \dot{x}_h, \dot{y}_h$$

and the equations which describe the motions of the system are Equations (6) and (14). The matrix $[D(t)]$ is periodic with period T and for the mechanical stability problem $T = 2\pi/\Omega$.

Floquet's theorem states that the solution to the above system of equations has the form

$$\{z\} = [A(t)]\{\alpha e^{(\lambda+i\omega)t}\} \tag{21}$$

where $[A(t)]$ is the characteristic matrix and is also periodic with period T. The column of initial conditions $\{z(0)\}$ is used in determining $\{\alpha\}$ as

$$\{\alpha\} = [A(0)]^{-1}\{z(0)\} \tag{22}$$

The matrix $[A(0)]$, the modal damping λ, and the modal frequency ω are determined from the Floquet Transition Matrix $[Q]$ which is defined by the equation

$$\{z(T)\} = [Q]\{z(0)\} \tag{23}$$

for all sets of initial conditions $\{z(0)\}$. It is shown in References 4 and 5 that the eigenvalues Λ_j of the matrix $[Q]$ can be used to determine λ_j and ω_j since

$$\Lambda_j = e^{(\lambda_j+i\omega_j)T} \tag{24}$$

and the modal matrix of $[Q]$ is just $[A(0)]$. The characteristic matrix $[A(t)]$ is then shown to be given by

$$[A(t)] = [\phi(t)][A(0)]\left[e^{-(\lambda+i\omega)t}\right] \tag{25}$$

where the state transition matrix $[\phi(t)]$ is defined by

$$\{z(t)\} = [\phi(t)]\{z(0)\} \tag{26}$$

The characteristic multipliers Λ_j of the system are uniquely defined since the matrix $[Q]$ is real; however, only the real parts of the characteristic exponents $p_j = \lambda_j + i\omega_j$ are defined uniquely since

$$p_j = \frac{1}{T}\left(\ln|\Lambda_j| + i \arg \Lambda_j\right) \tag{27}$$

The imaginary part can only be determined within an integer multiple of $2\pi/T$. This indeterminacy of the ω_j causes no particular difficulty if one is only interested in the stability of the system. However, if one is interested in understanding the mechanism involved in any instability which might be found, this indeterminacy can be quite troublesome.

The Floquet Transition Matrix which is the basic element needed in the stability analysis is easily determined by a numerical integration of the equations of motion over one period T. If one desires to compute the characteristic functions $[A(t)]$ the matrix $[\phi(t)]$ is saved at each time point in the numerical integration to obtain $[Q]$. For the calculations of this paper, the fourth order Runge-Kutta method with Gill coefficients[6] was used for the numerical integration.

A comment is in order concerning the characteristic functions $[A(t)]$. The matrix $[A(t)]$ is a complex valued matrix and is determined at as many time points as desired. The computation of these functions can be relatively expensive and intepretation can be difficult. The interpretation is made easier by the procedure outlined in Reference 5 for converting the complex functions into real functions which may be plotted as functions of time. The scheme used is essentially the same as that used when it is desired to plot as a function of time the modes of a system having constant coefficients. That is, for a conjugate pair of characteristic exponents

$$p_j = \lambda_j + i\omega_j$$
$$\bar{p}_j = \lambda_j - i\omega_j$$

the characteristic functions are also conjugate pairs. Thus the real modal function column for this conjugate pair of characteristic exponents will be given by

$$\{z_j(t)\} = \{A_j(t)\}e^{(\lambda_j+i\omega_j)t} + \{\bar{A}_j(t)\}e^{(\lambda_j-i\omega_j)t} \tag{28}$$

where $\{A_j(t)\}$ is the jth column of $[A(t)]$ and $\{\bar{A}_j(t)\}$ is the complex conjugate of this column. The purpose in performing these manipulations is to be able to plot the modal functions to determine the relative magnitudes and phases of the various degrees of freedom in each mode. A discussion of this technique as it applies to constant coefficient systems is given by Meirovitch.[7] In this paper the $\exp(\lambda_j t)$ is omitted from the above equation since it is simply a constant which multiplies each component of the mode and causes each component to damp at the same rate. Thus the plots of the characteristic functions which are presented later in the paper will appear to be neutrally damped.

In making the calculations for this paper it was found that the output from the calculation of the modal functions became so voluminous and these calculations became so expensive that the modal functions were only computed for selected points. Generally a sweep of rotor speed was made and the results examined. If an unstable region was indicated the rotor speed corresponding to the maximum positive λ_j was rerun and the modal functions calculated.

Discussion of Results

In order to demonstrate the application of the above-mentioned techniques and to obtain a general understanding of the effect of one blade damper inoperative on mechanical stability, a set of parameters were chosen. The parameters in the

mechanical stability analysis were chosen so as to be in the general range of interest for a single rotor helicopter and were such that the system was stable with all dampers functioning up to a rotor speed of 400 rpm. The parameter values chosen for the calculations are shown in Table 1.

The parameters presented in Table 1 correspond to an isotropic rotor and a nonisotropic hub. In the following discussion results are presented for the case of an isotropic hub coupled with a nonisotropic rotor and a nonisotropic hub coupled with an isotropic rotor as well as the case of interest which involves a nonisotropic hub coupled with a nonisotrpic rotor. When an isotropic hub is mentioned, this means that the hub parameters in both the x- and y-directions were assigned the values shown in Table 1 for the x-direction. An isotropic rotor implies that all dampers are operational and a nonisotropic rotor is meant to indicate that the lag damper has been removed from blade number 1. The analysis has been formulated in such a way that any number of blade lag dampers or lag springs may be removed to make the rotor nonisotropic. The results presented here, however, only involve the removal of the lag damper from one blade.

The case of an isotropic hub was first run in an effort to become familiar with the nonisotropic rotor results before proceeding with the more complicated Floquet analysis. The isotropic hub permits the equations to be transformed into the rotating reference frame and results in a system of equations with constant coefficients, Equations (16), (17), and (19), even with a nonisotropic rotor.

Figure 2 shows the results of the calculations for the isotropic hub with all blade dampers working. Note that since the equations were solved in the rotating system, the frequencies in the lower portion of Figure 2 are plotted in the rotating system. The numbers attached to the different modes in Figure 2 and in subsequent similar figures have no significance other than to provide a label for the various modes. In Figure 2 the dashed lines represent the uncoupled hub modes. The uncoupled rotor modes follow along the curves labeled 1,2 which also represent, in the terminology of Reference 5, the rotor collective modes. Note that the uncoupled blade frequencies are zero for rotor speeds less than about 65 rpm. This is due to the fact that the blades are critically damped for these low rotor speeds. At the higher rotor speeds modes 3 and 4 are essentially rotor modes and modes 5 and 6 are essentially hub modes. At the lower speeds, however, due to the coupling between rotor and hub, mode 4 changes to a hub mode and mode 5 changes to a blade mode. Note from the damping plot that all the modes indicate stability over the entire rotor speed range.

The results for one blade damper inoperative and an isotropic hub are plotted in Figure 3. Note that the removal of a blade damper has caused the appearance of a mode which was not present in Figure 2, namely the mode labeled 3 in Figure 3, and that this mode exhibits a mild instability between 160 and 200 rpm. At rotor speeds below about 100 rpm this mode has a frequency which corresponds to the uncoupled frequency of the blade which has no damper. At rotor speeds above 100 rpm this mode begins to deviate in frequency from the uncoupled frequency. Another interesting point is that mode 1 in Figure 3 is precisely the same as the collective modes of Figure 2, and in Figure 3 there is only one such mode. Thus it appears that the unstable mode in Figure 3 has evolved from one of the two collective modes shown in Figure 2 because of the removal of one of the blade dampers.

A time history calculation was made for the point of maximum instability in Figure 3 which occurs at approximately 175 rpm. The results of the time history calculation are shown in Figure 4. These results were obtained using the same integration scheme as that used for generating the Floquet Transition Matrix. The top portion of the figure represents the individual blade lag motions whereas the lower portion represents the hub response in the x- and y-directions. Note from the figure that each of the degrees of freedom was given an initial displacement but the initial velocities were zero. The equations were integrated for 17 rotor revolutions. The figure indicates the blades which have lag dampers are well damped, but the blade on which the damper is inoperative experiences large lag excursions. Also, the hub motions, although not large, do not appear to have a high degree of damping. From the time history one would conclude that the system is stable since the motions of the various degrees of freedom do not appear to be increasing in amplitude with increasing time. The eigenvalue analysis has shown, however, that an instability exists. The problem with the time history calculations is, of course, that the equations of motion have not been integrated over a sufficiently long time period for the initial conditions chosen. Herein lies the difficulty with using the time history approach for calculating the stability characteristics of systems. One can never be sure if a sufficiently long integration period has been used, and the choice of initial conditions which will minimize the integration time required is a trial and error process. It has been observed on an analog computer that for the ground resonance problem the choice of initial conditions has a strong bearing on the conclusion inferred from the time history traces. The time history integration is also much more time consuming on the digital computer than the eigenvalue analysis. The time to generate Figure 4 which is for only one rotor speed was much greater than the time required to generate the eigenvalue results for all of Figure 3. It is thus concluded that whenever it is at all possible the eigenvalue approach to stability calculation is to be desired over the time history approach.

Having examined the case of one blade damper inoperative an an isotropic hub, the next logical step is to examine the more realistic situation of a nonisotropic hub. Before examining the one damper inoperative situation it was first desired

to confirm that the system was stable with all dampers working. The modal damping and frequency of the various modes with all dampers working and a nonisotropic hub are shown in Figure 5. As can be seen from the damping plot, all the modes are stable. In this case the equations of motion are solved in the fixed frame of reference and hence the frequencies are plotted in this frame. The dashed lines on the frequency plot represent the uncoupled system: the horizontal dashed lines being the hub modes and the slanted dashed lines being the rotor modes. Note that because the rotor modes become critically damped at low rotor speeds the two uncoupled rotor frequencies come together before reaching the origin. The uncoupled rotor lines also represent the collective modes for the rotor. These modes are completely uncoupled from the other modes and hence are not included in the eigenvalue analysis of the nonisotropic hub coupled with an isotropic rotor. The damping for the collective modes is exactly the same as that shown for modes 1,2 in Figure 2.

The validity of the Floquet analysis was verified by comparing results from this analysis with results from both the rotating system analysis (isotropic hub) and from the fixed system analysis (isotropic rotor). In each case the results from the Floquet analysis were identical to results from the other analyses.

Having thus established the validity of the Floquet analysis, results were obtained for the nonisotropic hub and one blade damper inoperative. These results are shown in Figure 6. Note that these results are very much similar to those shown in Figure 5 except that, as was the case with the isotropic hub and one blade damper inoperative, there are additional modes introduced. Also indicated is a relatively strong instability between 210 and 305 rpm. The frequencies of the additional modes which are introduced correspond, at low rotor speeds, to the frequencies of the uncoupled blade which has no damper. In the rotor speed range where the instability occurs, however, the frequency deviates from the uncoupled value as indicated by the mode labeled 3. In this range and at higher rotor speeds the mode labeled 5 is nearer the uncoupled blade frequency. It thus appears that for this case the instability is more a coupled rotor hub mode than a pure blade mode as was indicated for the isotropic hub.

This conjecture is further strengthened by an examination of the modal functions. The modal functions for a rotor speed of 255 rpm, which is the point of maximum instability, are shown in Figure 7. The functions are plotted over a time period corresponding to one rotor revolution. Note from this figure that blade 1, the blade without a damper, has a significantly higher contribution to the mode than the other blades. Also from the plot of hub response it can be seen that the participation of the lateral hub degree of freedom, which has the higher of the uncoupled hub frequencies shown on Figure 6, is considerable. It is thus concluded from Figures 5 and 6 that the one damper inoperative situation can lead to a classical mechanical instability.

Time history traces for this same condition are shown in Figure 8. These traces show the same general trends as observed in the case of the isotropic hub, that is, a large response of the blade having no damper and moderate responses from the other blades and the hub degrees of freedom. Again the time history traces are inconclusive regarding the stability of the system.

One of the methods used in the past for treating the one blade damper inoperative case involves a smearing of the total blade damping. The reasoning for this approach is as follows. If the rotor has N blades then the total damping available in the rotor is Nc_i where c_i is the damping on one blade. If one damper is removed, the total damping becomes $(N - 1)c_i$. Thus, using this approach, each blade in the rotor would be treated as if it had a lag damper equal to $c_i(N - 1)/N$.

After an examination of the preceding one damper inoperative results it would be expected that this approach would lead to unconservative results. This is due to the fact that the instabilities encountered in the previous results involved large motions of the blade which had no damper. The smearing technique results in damping, which is not greatly different from the original value, being applied to each blade and thus the true situation is not adequately modeled.

To illustrate this method, the nonisotropic hub case was analyzed using the smearing approach. The results from these calculations are shown in Figure 9. Note that although mode 3 becomes lightly damped the system remains stable throughout the rotor speed range considered. The fact that mode 3 approaches instability is attributable to the fact that this mode was not heavily damped in the original calculations. A run of the isotropic hub case, where all the modes were originally well damped, indicated that the smearing technique resulted in well damped modes for one blade damper removed. The smearing technique is thus not recommended for treating the one blade damper inoperative situation since it leads to unconservative results.

Since one way for eliminating the classical mechanical instability is to increase the blade damping, it was decided to attempt this approach on the instability indicated in Figure 6. The approach was to leave the damping identically zero on one blade and increase the damping on the remaining three blades. The results of this series of calculations are shown in Figure 10 where the region of instability is presented as a function of blade lag damping and rotor speed. As can be seen from the figure, increasing the blade damping on three of the blades has very little effect on the stability boundaries when one blade has zero damping. This result was somewhat expected since from the previous calculations it was observed

that the blade with zero damping responds more or less independently of the other blades in the rotor.

During the increased damping calculations no attempt was made to determine whether or not the nature of the instability had changed. That is, whether the instability had changed from one involving both blade and hub motion to one consisting of primarily blade motion with only small amounts of hub motion. Further delving into possible corrective actions for the instability which occurs with one blade damper inoperative was beyond the scope of this paper and thus more research is needed to determine how the instability may be eliminated.

Conclusions

There are several conclusions which may be inferred from the preceding results. First of all, the fact that a helicopter is free from mechanical instability with all blade dampers working does not guarantee that it will be free of instabilities with one blade damper inoperative. The instability encountered with one blade damper inoperative may be a blade mode instability or it may be the classical mechanical instability.

The Floquet Transition Matrix method can be used effectively in examining the mechanical stability characteristics of helicopters with one blade damper inoperative. When both the hub and rotor are considered to be nonisotropic, the equations of motion contain periodic coefficients and the Floquet approach provides an efficient means for dealing with this situation. Since the Floquet approach yields the stability characteristics directly, it furnishes a more desirable approach to stability problems than time history calculations.

Time history calculations can lead to erroneous conclusions relative to the determination of system stability. The erroneous conclusions stem primarily from the fact that the time history calculations require considerable computer time and the tendency is to integrate over as short a time period as possible. Thus, if the initial conditions are not chosen properly, the time history traces may still contain transients when the integration is terminated. The time history approach to stability problems is thus recommended only when no other recourse is available, and then several different combinations of initial conditions and integration periods should be examined before making a conclusion regarding stability.

The smearing approach which has been used in the past for treating the one blade damper inoperative situation leads to unconservative results. Therefore, this method is considered to be an unacceptable means for determining stability under these conditions.

References

1. Coleman, R. P., and Feingold, A. M., THEORY OF SELF-EXCITED MECHANICAL OSCILLATIONS OF HELICOPTER ROTORS WITH HINGED BLADES, NACA Report 1351, 1958.

2. Donham, R. E., Cardinale, S. V., and Sachs, I. B., GROUND AND AIR RESONANCE CHARACTERISTICS OF A SOFT IN-PLANE RIGID-ROTOR SYSTEM, Journal of the American Helicopter Society, Vol. 14, No. 4, October 1969, pp. 33-41.

3. Lytwyn, R. T., Miao, W., and Woitsch, W., AIRBORNE AND GROUND RESONANCE OF HINGELESS ROTORS, Journal of the American Helicopter Society, Vol. 16, No. 2, April 1971, pp. 2-9.

4. Peters, D. A., and Hohenemser, K. H., APPLICATION OF THE FLOQUET TRANSITION MATRIX TO PROBLEMS OF LIFTING ROTOR STABILITY, Journal of the American Helicopter Society, Vol. 16, No. 2, April 1971, pp. 25-33.

5. Hohenemser, K. H., and Yin, S. K., SOME APPLICATIONS OF THE METHOD OF MULTIBLADE COORDINATES, Journal of the American Helicopter Society, Vol. 17, No. 3, July 1972, pp. 3-12.

6. Carnahan, B., Luther, H. A., and Wilkes, J. O., Applied Numerical Methods, John Wiley & Sons, Inc., New York, 1969.

7. Meirovitch, L., Analytical Methods in Vibrations, The Macmillan Company, New York, 1967, p. 411.

Appendix

If the rotor is considered to be isotropic the periodic coefficients appearing in the equations of motion can be eliminated through the use of multiblade coordinates similar to those described in Reference 1. These coordinates essentially transform the blade degrees of freedom into a fixed reference frame. The transformations are given by

$$\left.\begin{aligned} \xi_I &= \sum_{i=1}^{N} \zeta_i \sin \psi_i \\ \xi_{II} &= \sum_{i=1}^{N} \zeta_i \cos \psi_i \end{aligned}\right\} \qquad \text{(A1)}$$

Differentiating these expressions leads to the establishment of the following identities

$$\left.\begin{aligned} \sum_{i=1}^{N} \dot{\zeta}_i \sin \psi_i &= \dot{\xi}_I - \Omega \xi_{II} \\ \sum_{i=1}^{N} \dot{\zeta}_i \cos \psi_i &= \dot{\xi}_{II} + \Omega \xi_I \end{aligned}\right\} \qquad \text{(A2)}$$

$$\left.\begin{aligned}\sum_{i=1}^{N} \ddot{\zeta}_i \sin\psi_i &= \ddot{\xi}_I - \Omega^2\xi_I - 2\Omega\dot{\xi}_{II} \\ \sum_{i=1}^{N} \ddot{\zeta}_i \cos\psi_i &= \ddot{\xi}_{II} - \Omega^2\xi_{II} + 2\Omega\dot{\xi}_I\end{aligned}\right\}$$

It can be seen from these identities that the transformation is made by multiplying the blade equations, Equations (6), by either $\sin\psi_i$ or $\cos\psi_i$ and adding the equations. Crucial to this operation is the ability to remove the η_i and $\omega_{o_i}^2$ from the summations. This can only be done if all the blades have identical lag springs and lag dampers. If one or more of the blades have differing characteristics, the η_i and/or $\omega_{o_i}^2$ cannot be factored from the summation and hence the identities above cannot be applied. Thus, if one or more of the blades are permitted to have different lag springs or lag dampers, the periodic coefficients cannot be eliminated using the procedure described in this Appendix.

If Equations (6) are first multiplied by $\cos\psi_i$ and summed and then multiplied by $\sin\psi_i$ and summed, the following equations are obtained after introduction of the identities (A2)

$$\begin{aligned}&\ddot{\xi}_{II} + \eta_i\dot{\xi}_{II} - \left[\Omega^2(1-\nu_o^2) - \omega_{o_i}^2\right]\xi_{II} + 2\Omega\dot{\xi}_I \\ &\quad + \Omega\eta_i\xi_I = (\nu_o^2/e)\left[\ddot{x}_h \sum_{i=1}^{N} \sin\psi_i \cos\psi_i \right. \\ &\quad \left. - \ddot{y}_h \sum_{i=1}^{N} \cos^2\psi_i\right]\end{aligned} \tag{A3}$$

$$\begin{aligned}&\ddot{\xi}_I + \eta_i\dot{\xi}_I - \left[\Omega^2(1-\nu_o^2) - \omega_{o_i}^2\right]\xi_I - 2\Omega\dot{\xi}_{II} \\ &\quad - \Omega\eta_i\xi_{II} = (\nu_o^2/e)\left[\ddot{x}_h \sum_{i=1}^{N} \sin^2\psi_i \right. \\ &\quad \left. - \ddot{y}_h \sum_{i=1}^{N} \sin\psi_i \cos\psi_i\right]\end{aligned}$$

Making the following observations that for $N > 2$

$$\sum_{i=1}^{N} \sin\psi_i \cos\psi_i = 0$$

$$\sum_{i=1}^{N} \cos^2\psi_i = \sum_{i=1}^{N} \sin^2\psi_i = N/2$$

the equations become

$$\left.\begin{aligned}&\ddot{\xi}_{II} + \eta_i\dot{\xi}_{II} - \left[\Omega^2(1-\nu_o^2) - \omega_{o_i}^2\right]\xi_{II} + 2\Omega\dot{\xi}_I \\ &\quad + \Omega\eta_i\xi_I = -(N\nu_o^2/2e)\ddot{y}_h \\ &\ddot{\xi}_I + \eta_i\dot{\xi}_I - \left[\Omega^2(1-\nu_o^2) - \omega_{o_i}^2\right]\xi_I - 2\Omega\dot{\xi}_{II} \\ &\quad - \Omega\eta_i\xi_{II} = (N\nu_o^2/2e)\ddot{x}_h\end{aligned}\right\} \tag{A4}$$

These two equations describe the rotor motions in the fixed frame of reference. In terms of the variables described by Equations (A1) the hub equations, Equations (14), become

$$\left.\begin{aligned}(m_x + Nm_b)\ddot{x}_h + c_x\dot{x}_h + k_x x_h &= S_b\ddot{\xi}_I \\ (m_y + Nm_b)\ddot{y}_h + c_y\dot{y}_h + k_y y_h &= -S_b\ddot{\xi}_{II}\end{aligned}\right\} \tag{A5}$$

The stability of the rotor-hub system can now be determined using Equations (A4) and (A5) which have constant coefficients. This set of equations or a set similar to it is the one normally used in helicopter mechanical stability analyses.

As a final observation, note that if the blade equations, Equations (6), are simply summed, the following equation

$$\ddot{\xi}_o + \eta_i\dot{\xi}_o + (\omega_{o_i}^2 + \Omega^2\nu_o^2)\xi_o = 0 \tag{A6}$$

is obtained, where

$$\xi_o = \sum_{i=1}^{N} \zeta_i \tag{A7}$$

This equation represents the rotor collective mode and it may be observed that this equation is completely decoupled from the hub degrees of freedom. Hence, the collective mode cannot influence the stability of the system and it is therefore not normally included in the mechanical stability analysis.

TABLE 1. PARAMETERS USED IN THE SAMPLE CALCULATIONS

Number of blades	4
Blade mass, m_b	6.5 slugs (94.9 kg)
Blade mass moment, S_b	65.0 slug-ft (289.1 kg-m)
Blade mass moment of inertia, I_b	800.0 slug-ft^2 (1084.7 kg-m^2)
Lag hinge offset, e	1.0 ft (0.3048 m)
Lag spring, k_i	0.0 ft-lb/rad (0.0 m-N/rad)
Lag damper, c_i	3000.0 ft-lb-sec/rad (4067.5 m-N-s/rad)
Hub mass, m_x	550.0 slugs (8026.6 kg)
Hub mass, m_y	225.0 slugs (3283.6 kg)
Hub spring, k_x	85000.0 lb/ft (1240481.8 N/m)
Hub spring, k_y	85000.0 lb/ft (1240481.8 N/m)
Hub damper, c_x	3500.0 lb-sec/ft (51078.7 N-s/m)
Hub damper, c_y	1750.0 lb-sec/ft (25539.3 N-s/m)

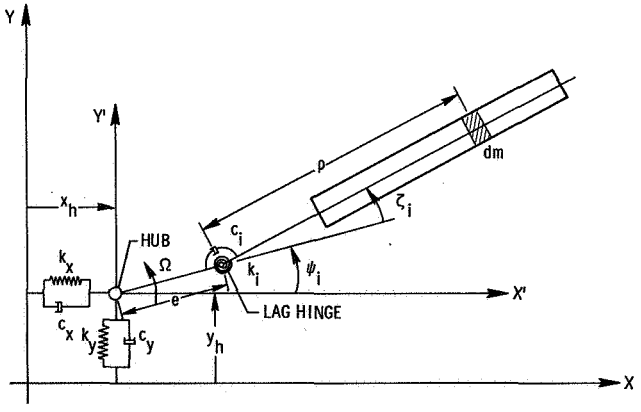

Figure 1. Mathematical representation of the rotor and hub.

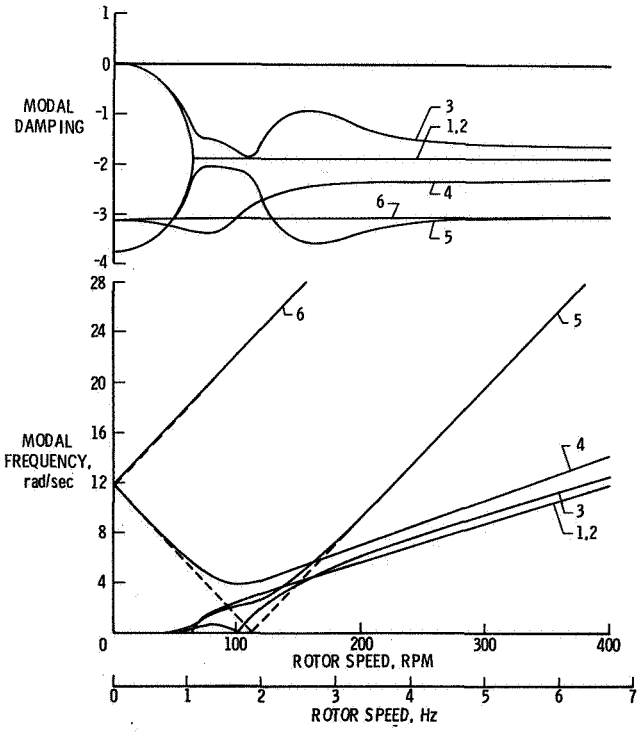

Figure 2. Modal damping and frequencies for isotropic hub, all blade dampers working. Frequencies plotted in the rotating system.

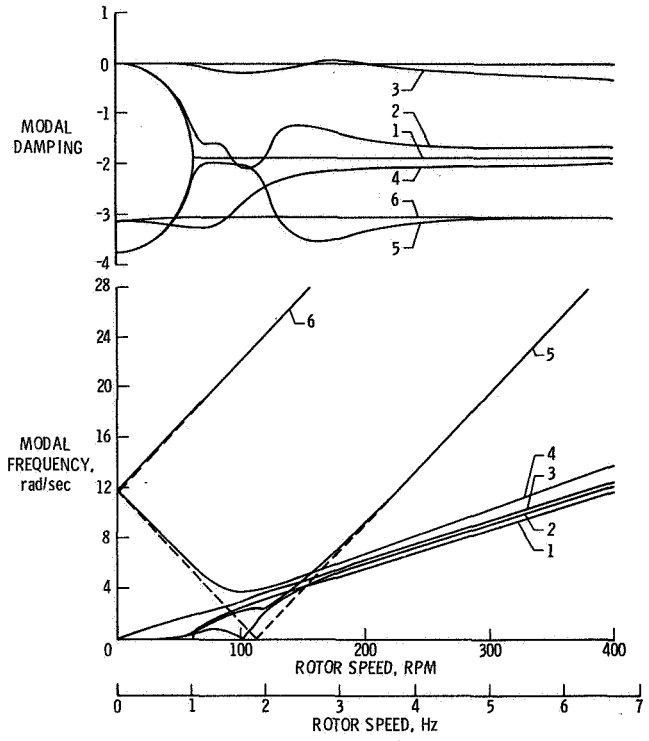

Figure 3. Modal damping and frequencies for isotropic hub, one blade damper inoperative. Frequencies plotted in the rotating system.

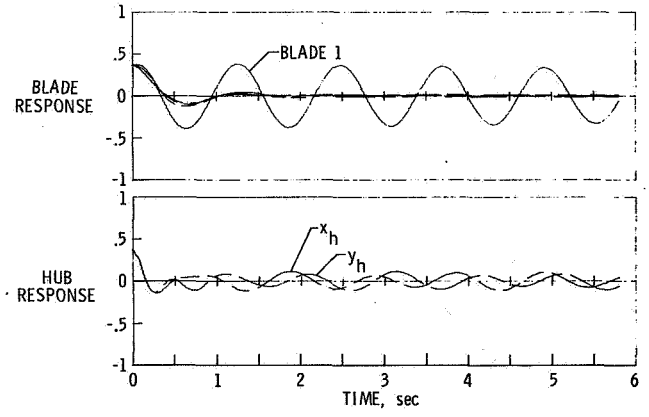

Figure 4. Time history calculations for isotropic hub, one blade damper inoperative, Ω = 175 rpm.

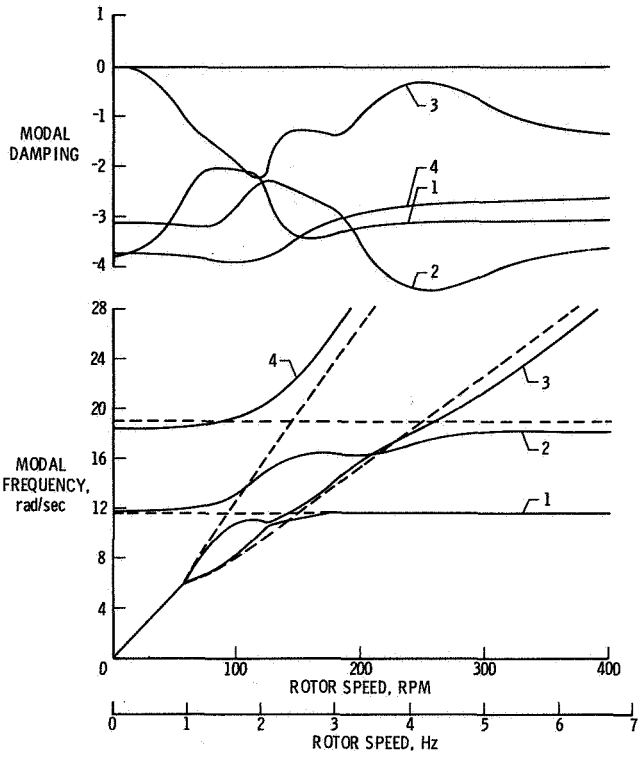

Figure 5. Modal damping and frequencies for non-isotropic hub, all blade dampers working. Frequencies plotted in the fixed system.

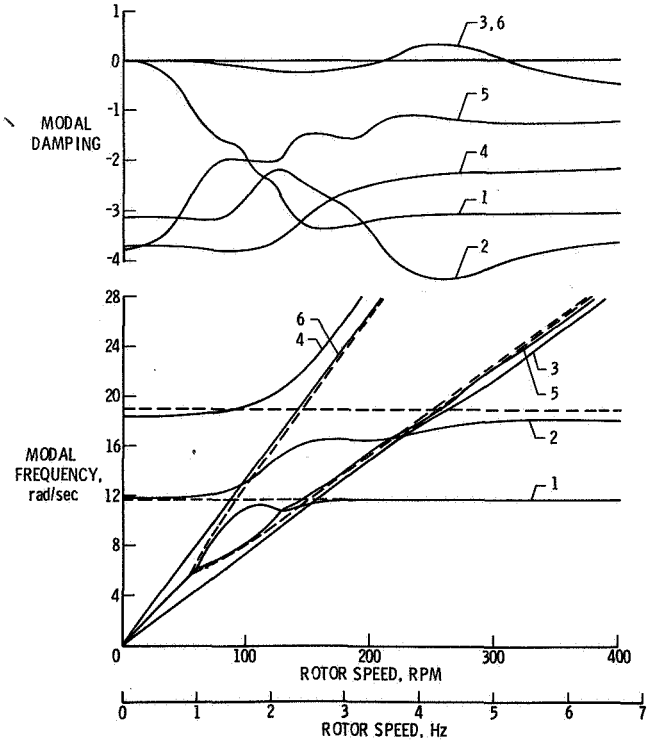

Figure 6. Modal damping and frequencies for non-isotropic hub, one blade damper inoperative. Frequencies plotted in the fixed system.

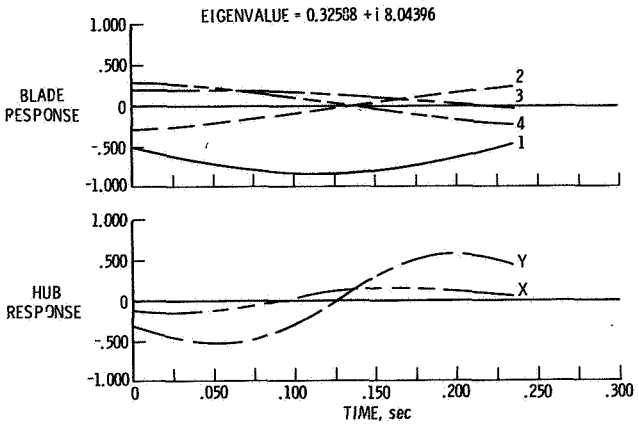

Figure 7. Modal functions for nonisotropic hub, one blade damper inoperative, Ω = 255 rpm.

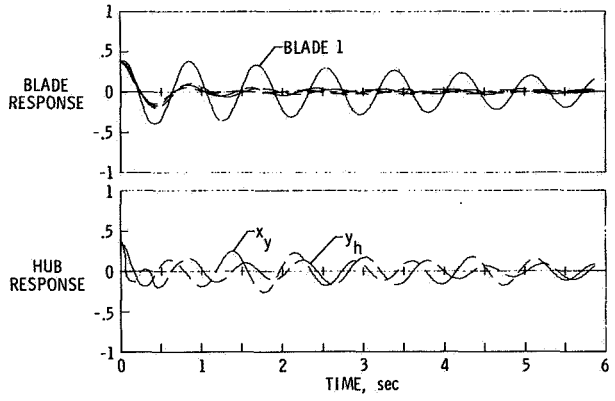

Figure 8. Time history calculations for nonisotropic hub, one blade damper inoperative, Ω = 255 rpm.

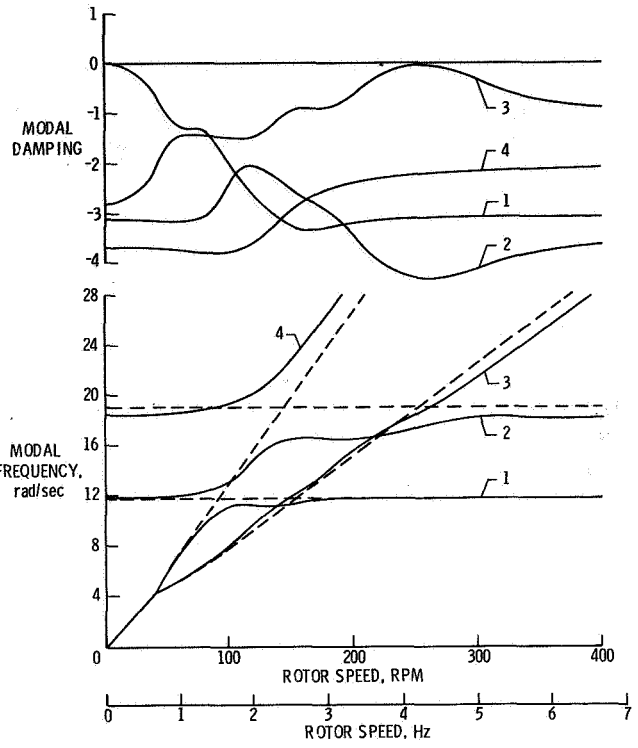

Figure 9. Modal damping and frequencies obtained for nonisotropic hub, one blade damper inoperative, using the smearing technique.

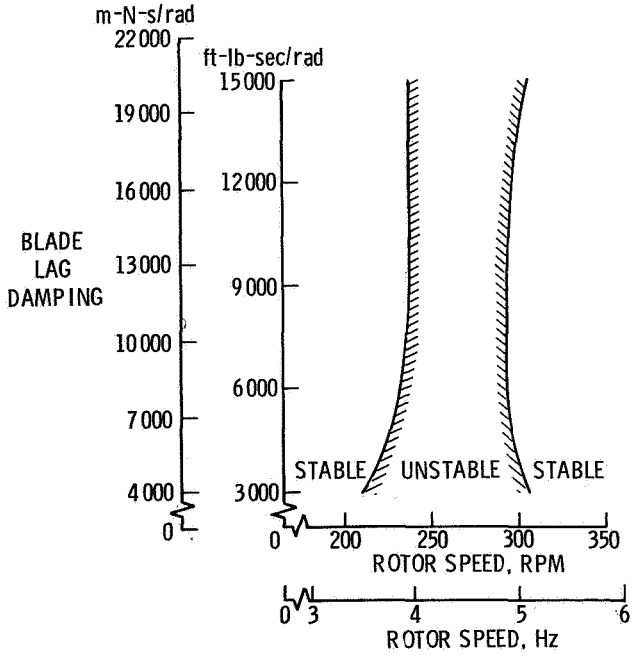

Figure 10. Instability region as a function of blade lag damping for the nonisotropic hub and one blade damper inoperative.

THEORY AND COMPARISON WITH TESTS OF TWO FULL-SCALE PROPROTORS

Wayne Johnson
Research Scientist
Large-Scale Aerodynamics Branch
Ames Research Center, NASA
and
U.S. Army Air Mobility R & D Laboratory
Moffett Field, California

Abstract

A nine degrees-of-freedom theoretical model has been developed for investigations of the dynamics of a proprotor operating in high inflow axial flight on a cantilever wing. The theory is described, and the results of the analysis are presented for two proprotor configurations: a gimballed, stiff-inplane rotor, and a hingeless, soft-inplane rotor. The influence of various elements of the theory is discussed, including the modeling used for the blade and wing aerodynamics and the influence of the rotor lag degree of freedom. The results from full-scale tests of these two proprotors are presented and compared with the theoretical results.

Notation

c_{ℓ_α}	blade lift-curve slope
p	wing torsion degree of freedom
q_1	wing vertical bending degree of freedom
q_2	wing chordwise bending degree of freedom
R	rotor radius
V	forward velocity
β	blade flap degree of freedom
β_0	rotor coning degree of freedom
β_{1c}	rotor tip path plane pitch degree of freedom
β_{1s}	rotor tip path plane yaw degree of freedom
γ	blade Lock number
δ_3	pitch/flap coupling
ζ	damping ratio of eigenvalue, $-\mathrm{Re}\lambda/\lvert\lambda\rvert$
ζ	blade lag degree of freedom
ζ_0	rotor collective lag degree of freedom
$\dot{\zeta}_0$	time derivative of ζ_0; rotor speed perturbation degree of freedom for autorotation case
ζ_{1c}	rotor vertical cyclic lag degree of freedom
ζ_{1s}	rotor lateral cyclic lag degree of freedom
λ	eigenvalue or root
ν_β	rotating natural frequency of blade flap motion
ν_ζ	rotating natural frequency of blade lag motion
ω	frequency of eigenvalue, $\mathrm{Im}\lambda$
Ω	rotor rotational speed

The tilting proprotor aircraft is a promising concept for short haul, V/STOL missions. This aircraft uses low disk loading rotors located on the wing tips to provide lift and control in hover and low speed flight; it also uses the same rotors to provide propulsive force in high speed cruise, the lift then being supplied by a conventional wing. Such operation requires a ninety degree change in the rotor thrust direction, which is accomplished by mechanically tilting the rotor shaft axis. Thus the aircraft combines the efficient VTOL capability of the helicopter with the efficient, high speed cruise capability of a turboprop aircraft. With the flexible blades of low disk loading rotors, the blade motion is as important an aspect of tilt rotor dynamics as it is for helicopters. When operated in cruise mode (axial flight at high forward speed), the rotor is operating at a high inflow ratio (the ratio of axial velocity to the rotor tip speed); such operation introduces aerodynamic phenomena not encountered with the helicopter rotor, which is characterized by low inflow. The combination of flapping rotors operating at a high inflow ratio on the tips of flexible wings leads to dynamic and aerodynamic characteristics that are in many ways unique to this configuration. The combination of efficient VTOL and high speed cruise capabilities is very attractive; it is therefore important to establish a clear understanding of the behavior of this aircraft and adequate methods to predict it, to enable a confident design of the aircraft. Experimental and theoretical investigations have been conducted over several years to provide this capability. However, much remains to be studied, both in the fundamental behavior and in the more sophisticated areas such as the design and development of automatic control systems for the vehicle. This paper presents the results of a theoretical model for a proprotor on a cantilever wing, including application to two proprotor designs: a gimballed, stiff-inplane rotor and a hingeless, soft-inplane rotor. Using these two cases, the influence on the system dynamics of several elements of the analysis was examined, including the effects of the rotor blade lag motion and the rotor and wing aerodynamic models. The predicted stability characteristics are then compared with the results of full-scale tests of these two proprotor designs. The development of this theory is presented in detail in Reference 1, together with some additional applications to the analysis of proprotor aeroelastic behavior.

Presented at the AHS/NASA-Ames Specialists' Meeting on Rotorcraft Dynamics, February 13-15, 1974.

Analytical Model

Figure 1 shows the proprotor configuration considered for the theory and for the full-scale tests. The rotor is operating in high inflow axial flight on a cantilever wing. For the tests, the rotor was unpowered, hence operating in autorotation (really in the windmill brake state). This configuration incorporates the features of greatest importance to the aircraft: the high inflow aerodynamics of a flapping rotor in axial flow and the coupled dynamics of the rotor/pylon/wing aeroelastic system. Many features of the aircraft-coupled wing and rotor motion may be studied with such a model, theoretically and experimentally, with the understanding that the model must eventually incorporate the entire aircraft.

The theoretical model of the proprotor developed in Reference 1 consists of nine degrees of freedom: the first mode flap (out of disk plane) and lag (inplane) motion for each of three blades; and vertical bending, chordwise bending, and torsion for the cantilever wing. The degrees of freedom of the individual rotor blades are combined into degrees of freedom representing the motion of the rotor as a whole in the nonrotating frame. Thus the rotor flap motion is represented by tip path plane pitch and yaw (β_{1c} and β_{1s}) and coning (β_0) degrees of freedom. The rotor lag motion is represented by cyclic lag ζ_{1c} and ζ_{1s} (lateral and vertical shift of the rotor net center of gravity) and collective lag ζ_0. Wing vertical and chordwise bending of the elastic axis (q_1 and q_2) and torsion about the elastic axis (p) complete the set of nine degrees of freedom.

The rotor blade motion is represented by first mode flap and lag motion, which are assumed to be respectively pure out-of-plane and pure inplane deflection of the blade spar. For the gimballed and hingeless rotor blades considered here (except for the flap mode of the gimballed rotor), there is, in fact, some elastic coupling of the flap and lag modes, so that there is actually participation of both out-of-plane and inplane motion in each mode. In the coefficients giving the aerodynamic forces on the rotor, it is further assumed that the mode shapes are proportional to the radial distance from the hub, i.e., equivalent to rigid body rotation about a central hinge. The model based on these two assumptions, which considerably simplify the aerodynamic and structural terms of the rotor equations, proves to be an adequate representation of the proprotor dynamics.

The theoretical results presented here will usually be for the rotor operating unpowered, i.e., windmilling or autorotation operation. An important element of autorotation dynamic behavior is the rotor speed perturbation. With no restraint of the rotor shaft rotation, this degree of freedom has considerable influence on the aeroelastic behavior of the proprotor and wing. The rotor speed perturbation is modeled by using the collective lag mode ζ_0. By setting the rotating natural frequency of this mode to zero, i.e., zero spring restraint, ζ_0 becomes equivalent to the rotor speed perturbation. (The natural frequency for the cyclic lag modes, ζ_{1c} and ζ_{1s}, is not set to zero in the representation.) The other extreme case is that of the hub operating at constant angular velocity (Ω) with no speed perturbation, with ζ_0 then the elastic inplane deflection of the blade with respect to the hub. This case will be considered to represent powered operation of the rotor, although it is really the limit of operation with a perfect governor on rotor speed.

The proprotor operating in high inflow has simpler aerodynamics than the low inflow rotor in forward flight. As for the case of low inflow (i.e., the hovering helicopter rotor), the symmetry of axial flow results in a corresponding symmetry in the equations of motion; it also means that the differential equations of motion have constant coefficients. In high inflow there is the additional fact that both out-of-plane and inplane motions of the blade produce significant angle-of-attack changes at the sections, and the resulting lift increment has significant components both normal to and in the disk plane. Hence the rotor aerodynamic forces are primarily due to the lift changes produced by angle-of-attack changes, i.e., the c_{ℓ_α} terms in the aerodynamic coefficients. This is in contrast to low inflow, where, for example, the inplane blade motion produces significant contributions to the forces by the lift and drag increments due to the dynamic pressure changes, i.e., the c_ℓ and c_d terms in the aerodynamic coefficients. As a result, high inflow rotor aerodynamics are well represented by considering only the c_{ℓ_α} forces. If, in addition, the lift curve slope is assumed constant, then the aerodynamic coefficients depend on only two parameters, the Lock number γ and the inflow ratio $V/\Omega R$. Reference 1 presents the aerodynamic coefficients also for a more complete theoretical model of the rotor aerodynamics, namely a perturbation about the local trim state, including the c_{ℓ_α}, c_ℓ, c_d, and c_{d_α} terms (and also derivatives with respect to the Mach number). Such a model is in fact little more difficult to derive than with the c_{ℓ_α} terms alone. The influence of its use in the theory is examined below.

This nine degrees-of-freedom model will have nine roots or eigenvalues (really nine pairs of complex roots) and correspondingly nine eigenvectors or modes. Of course, each mode involves motion of all nine degrees of freedom. The modes are identifiable by their frequencies (which will be near the uncoupled natural frequencies, nonrotating for the rotor modes), and also by the participation of the degrees of freedom in the eigenvector. The nine modes will be denoted as follows (the approximate uncoupled, nonrotating natural frequency of the mode is given in parentheses):

p	wing torsion (ω_p)
q_1	wing vertical bending (ω_{q_1})
q_2	wing chordwise bending (ω_{q_2})
β	coning (ν_β)
$\beta + 1$	high frequency flap ($\nu_\beta + \Omega$)
$\beta - 1$	low-frequency flap ($\nu_\beta - \Omega$)
ζ	collective lag (ν_ζ)
$\zeta + 1$	high-frequency lag ($\nu_\zeta + \Omega$)
$\zeta - 1$	low-frequency lag ($\nu_\zeta - \Omega$)

The basic theoretical model will consist of all nine degrees of freedom, autorotation operation, and just the c_{ℓ_α} rotor aerodynamic forces. The wing aerodynamic forces are also included (based on a strip theory calculation). The dynamic stability of the system, specifically the frequency and damping ratio of the modes, will be examined for variations of the forward velocity V and the rotor rotational speed Ω. Both V and Ω sweeps change the inflow ratio $V/\Omega R$, and hence the rotor and wing aerodynamic forces. A variation of the rotor speed Ω also changes the values of the wing and rotor blade nondimensional (per rev) natural frequencies. The rotor frequencies may also vary with $V/\Omega R$ due to the change in the rotor collective pitch angle. Several elements of the theoretical model will be examined to determine their influence on the predicted proprotor dynamics: the influence of the blade lag motion (by dropping the ζ_{1c} and ζ_{1s} degrees of freedom), the wing aerodynamics (by dropping the wing aerodynamic coefficients), the rotor speed perturbation (i.e., the autorotation and powered cases), and the more complete model of the rotor aerodynamics (compared to just the c_{ℓ_α} terms).

Two Full-Scale Proprotors

The theory described above will be applied to two full-scale proprotors. The first is a 25-ft diameter gimballed, stiff-inplane proprotor, designed and constructed by the Bell Helicopter Company, and tested in the Ames 40- by 80-ft wind tunnel in July 1970. The second is a 26-ft diameter hingeless, soft-inplane

proprotor, designed and constructed by the Boeing Vertol Company, and tested in the Ames 40- by 80-ft wind tunnel in August 1972. The configuration for the dynamics tests consisted of the windmilling rotor operating in high inflow axial flow on the tip of a cantilever wing, as shown in figure 1. As far as their dynamic characteristics are concerned, the two rotors differ primarily in the placement of the rotating natural frequencies of the blade flap and lag motions. The Bell rotor has a gimballed hub and stiff-inplane cantilever blade attachment to the hub, hence $\nu_\beta = 1/\text{rev}$ (nearly, for it does have a weak hub spring) and $\nu_\zeta > 1/\text{rev}$; it also incorporates positive pitch/flap coupling ($\delta_3 < 0$) to increase the blade flap/lag stability. The Boeing rotor has a cantilever or hingeless hub with soft-inplane blade attachment, hence $\nu_\beta > 1/\text{rev}$ and $\nu_\zeta < 1/\text{rev}$. The different placement of the blade frequencies, at the opposing extremes of the possible choices, results in quite different dynamic characteristics for the two aircraft.

The rotors are described in References 2 to 5. Table I gives the major parameters of the rotor, and of the cantilever wing used in the full-scale tests (a more complete description of the parameters required by the theory is given in Reference 1). The wing frequencies in the theory were match to the experimentally measured values by adjusting the spring constants. The typical wing frequencies given in table I are for the coupled motion of the system (including the rotor) at 100 knots and design Ω. The blade rotating natural frequencies are shown in figures 2 and 3 for the Bell and Boeing rotors, respectively. The variation of the Bell lag frequency (fig. 2b) with $V/\Omega R$ is due to the collective pitch change. The Boeing rotor blade frequencies vary little with collective pitch ($V/\Omega R$) since the blade has nearly isotropic stiffness at the root.

The damping ratio of the wing modes was measured in the full-scale tests by the following technique. The wing motion was excited by oscillating an aerodynamic shaker vane on the wing tip (visible in fig. 1) at the wing natural frequency. After a sufficient amplitude was achieved, the vane was stopped. Then the frequency and damping ratio were determined from the decay of the subsequent transient motion of the wing.

Results and Discussion

Gimballed, Stiff-Inplane Rotor

The effects of several elements of the theoretical model will be examined for a gimballed, stiff-inplane rotor (the Bell rotor). The theoretical results will then be compared with the results of full-scale tests. The test results and results from the Bell theories are from Reference 2. The predicted variation of the system stability with forward speed V at the normal airplane mode rotor speed ($\Omega = 458$ rpm) is shown in figure 4, in terms of the frequency and damping ratio of the eigenvalues. The wing vertical bending mode (q_1) becomes unstable at 495 knots. The damping of that mode first increases with speed; the peak is due to coupling between the wing vertical bending (q_1) and low-frequency rotor lag ($\zeta - 1$) modes (it occurs at the resonance of the frequencies of these two modes). Figure 5 shows the influence of the rotor lag motion, comparing the damping of the wing modes with and without the ζ_{1c} and ζ_{1s} degrees of freedom. The rotor low-frequency lag mode has an important influence on the motion, particularly on the wing vertical bending mode; the q_1 damping is increased when its frequency is below that of the $\zeta - 1$ mode (low V), and decreased when its frequency is above that value. The high speed instability is relatively unaffected, however, indicating that the mechanism of that instability involves primarily the rotor flap motion. Therefore, the net effect of the reduced damping at high speed due to the lag motion is a reduction of the rate at which the damping decreases, which is beneficial since the instability is then less severe.

Figure 6 shows the influence of powered operation (stabilizing) and of omitting the wing aerodynamics (destabilizing). The powered state effect is the influence of dropping the rotor speed perturbation degree of freedom. The wing aerodynamics effect is mainly the loss of the aerodynamic damping of the wing modes due to the angle-of-attack changes during the motion. Figure 7 shows the influence of the more complete theoretical model for the blade aerodynamics, compared with the results using only the $c\ell_\alpha$ terms. The basic behavior remains the same, but the better aerodynamic model reduces slightly the level of the predicted damping ratio. The predicted speed at the stability boundary is significantly reduced, however, because of the gradual variation of the damping with speed. It is therefore concluded that for the prediction of the characteristics of an actual aircraft, the best model available for the rotor aerodynamics should be used.

Figure 8 shows the variation of the dynamic stability with velocity at the normal rotor speed ($\Omega = 458$ rpm), in terms of the frequency and damping ratio of the wing modes; the full-scale test results for the Bell rotor are compared with the predicted stability. Also shown are predictions from the Bell linear and nonlinear theories, from Reference 2. Figure 8 shows reasonable correlation between the predicted and full-scale test stability results. Additional comparisons with the full-scale test data are given in Reference 1.

Figure 9 shows the influence of the rotor lag motion. The predicted and measured stability is shown for the Bell rotor on the full-stiffness wing, and on a quarter-stiffness wing. (By operating on a quarter-stiffness wing at one-half design rotor speed, $\Omega = 229$ rpm; the wing frequencies and inflow ratio are modeled for an equivalent speed twice the actual tunnel speed.) Also shown is the predicted stability for the rotor on the full-stiffness wing, but without the ζ_{1c} and ζ_{1s} degrees of freedom. Figure 9a shows the variation of the wing vertical bending mode damping. The full-scale experimental data show a definite trend to higher damping levels with the full-stiffness wing, and this trend correlates well with the results of the present theory. Figures 9b and 9c show the predicted stability of all the wing modes. The difference in damping at the same inflow ratio is due to the rotor lag motion. Figure 9d shows the frequencies of the $\zeta - 1$, q_1, and p modes for the full-stiffness and quarter-stiffness wings. The full-stiffness wing has a resonance of the $\zeta - 1$ and q_1 modes which produces the peak in the damping. Slowing the rotor on the quarter-stiffness wing greatly increases the lag frequency (per rev), removing it from resonance with the q_1 mode. Another way to remove the influence of the rotor lag motion, in the theory, is simply to drop the ζ_{1c} and ζ_{1s} degrees of freedom from the full-stiffness wing case. When these degrees of freedom are dropped, the predicted wing vertical bending damping is almost identical to that for the quarter-stiffness wing (figs. 9a and 9b). Figure 10 examines further the influence of the rotor lag motion on the wing vertical bending mode damping. Predicted stability with and without the ζ_{1c} and ζ_{1s} degrees of freedom is compared with experimental results from tests of a 0.1333-scale model of a

gimballed, stiff-inplane proprotor. The test results are from Reference 6; this rotor is a model of the Bell M266, similar in design to the full-scale rotor considered here. The experimental data correlates well with the predictions, including the influence of the rotor lag motion.

Hingeless, Soft-Inplane Rotor

The effects of several elements of the theoretical model will be examined for a hingeless, soft-inplane rotor (the Boeing rotor). Then the theoretical results will be compared with the results of full-scale tests, and with results from the Boeing theory (the latter are from Reference 3). The predicted variation of the system stability with forward velocity at normal rotor speed ($\Omega = 386$ rpm) is shown in figure 11. The low-frequency flap ($\beta - 1$) mode becomes unstable at 480 knots. By the time this instability occurs, the mode has assumed the character of a wing vertical bending mode (i.e., the q_1 motion, and the associated p, ζ_{1c}, ζ_{1s}, and ζ_0 motions); hence this instability has the same mechanism as does the Bell rotor. With the soft-inplane rotor, $\nu_\zeta < 1$/rev, the proximity of the $\zeta - 1$ and q_1 mode frequencies significantly reduces the wing mode damping at low speeds; this effect is the air resonance phenomenon. A similar influence occurs with the resonance of the $\zeta - 1$ and q_2 modes, leading to an instability of the wing chord mode (this instability can occur because the wing chord mode aerodynamic damping remains low even at high speed). At higher Ω, this q_2 mode instability is, in fact, the critical instability. The influence of the rotor lag motion is shown in figure 12. The substantial decrease in the damping of the wing vertical and chordwise bending modes due to the rotor lag motion is the air resonance effect. Figure 13 shows the influence of powered operation and of omitting the wing aerodynamics, and figure 14 shows the influence of the better theoretical model for the rotor aerodynamics on the predicted stability. The effects, and hence the conclusions from figures 13 and 14 are similar to those for the Bell rotor.

Figure 15 shows the variation of the predicted stability of the Boeing rotor with rotor speed at 50 knots. At this low speed, the resonance of the $\zeta - 1$ and q_1 mode frequencies actually results in an instability of the wing vertical bending mode. Figure 16 shows the stability variation with rotor speed at 192 knots. The reduction in wing vertical bending mode damping due to air resonance is still present, but the increase in the rotor lag aerodynamic damping and wing vertical bending aerodynamic damping with flight speed has been sufficient to stabilize the motion even at resonance. Figure 17 summarizes the air resonance behavior of the Boeing rotor.

Figure 18 compares the predicted and full-scale results for the stability of the wing modes for a velocity sweep of the Boeing rotor at $\Omega = 386$ rpm. Figure 19 shows the variation of the wing vertical bending mode damping with rotor speed at V = 50 to 192 knots. These runs were conducted to investigate the air resonance behavior of this configuration, i.e., the influence of the rotor lag motion. Reasonable correlation is shown between the predicted and measured stability, except at the higher speeds where tunnel turbulence made extraction of the damping ratio from the experimental transient wing motion difficult. Also shown are predictions from the Boeing theory, from Reference 3. Additional comparisons with the full-scale test data are given in Reference 1.

Concluding Remarks

This paper has presented theoretical results for the stability of a proprotor operating in high inflow on a cantilever wing. Some experimental results from full-scale tests have been presented, showing reasonable correlation with the predicted stability. The nine degrees-of-freedom theoretical model has been established as a useful and accurate representation of the basic dynamic characteristics of the proprotor and cantilever wing system. The significant influence of the rotor speed perturbation degree of freedom (i.e., windmilling or powered operation), the wing aerodynamics, and the rotor aerodynamic model on the predicted stability have been shown, indicating the importance of including these elements accurately in the theoretical model. From a comparison of the behavior of the gimballed, stiff-inplane rotor and the hingeless, soft-inplane rotor, it is concluded that the placement of the natural frequencies of the rotor blade first mode bending – i.e., the flap frequency ν_β and the lag frequency ν_ζ – has a great influence on the dynamics of the proprotor and wing. Moreover, the theoretical and experimental results have demonstrated that the rotor lag degree of freedom has a very important role in the proprotor dynamics, for both the soft-inplane ($\nu_\zeta < 1$/rev) and stiff-inplane ($\nu_\zeta > 1$/rev) configurations.

References

1. NASA TN-D (in preparation), THE DYNAMICS OF TILTING PROPROTOR AIRCRAFT IN CRUISE FLIGHT, Johnson, Wayne, 1974.

2. NASA CR 114363, ADVANCEMENT OF PROPROTOR TECHNOLOGY TASK II – WIND TUNNEL TEST RESULTS, Bell Helicopter Company, September 1971.

3. Boeing Vertol Company Report No. D222-10059-1, WIND TUNNEL TESTS OF A FULL SCALE HINGELESS PROP–ROTOR DESIGNED FOR THE BOEING MODEL 222 TILT ROTOR AIRCRAFT, Magee, John P., and Alexander, H. R., July 1973.

4. NASA CR 114442, V/STOL TILT–ROTOR STUDY TASK II – RESEARCH AIRCRAFT DESIGN, Bell Helicopter Company, March 1972.

5. NASA CR 114438, V/STOL TILT–ROTOR AIRCRAFT STUDY VOLUME II – PRELIMINARY DESIGN OF RESEARCH AIRCRAFT, Boeing Vertol Company, March 1972.

6. Kvaternik, Raymond G., STUDIES IN TILT–ROTOR VTOL AIRCRAFT AEROELASTICITY, Ph.D. Thesis, Case Western Reserve University, June 1973.

TABLE I – DESCRIPTION OF THE FULL-SCALE PROPROTORS, AS TESTED IN THE AMES 40- BY 80-FT WIND TUNNEL.

	Bell	Boeing
Rotor		
Type	gimballed, stiff-inplane	hingeless, soft-inplane
Number of blades	3	3
Radius, R	3.81 m (12.5 ft)	3.96 m (13 ft)
Lock number, γ	3.83	4.04
Solidity ratio	0.089	0.115
Pitch/flap coupling, δ_3	-15 deg	0
Rotor rotation direction, on right wing	clockwise	counterclockwise
Tip speed, ΩR (cruise mode)	183 m/sec (600 ft/sec)	160 m/sec (525 ft/sec)
Rotation speed, (cruise mode)	458 rpm	386 rpm
Wing		
Semispan, y_w/R	1.333	1.281
Mast height, h/R	0.342	0.354
Typical frequencies		
Vertical bending	3.2 Hz 0.42/rev	2.3 Hz 0.36/rev
Chordwise bending	5.35 0.70	4.0 0.62
Torsion	9.95 1.30	9.2 1.48

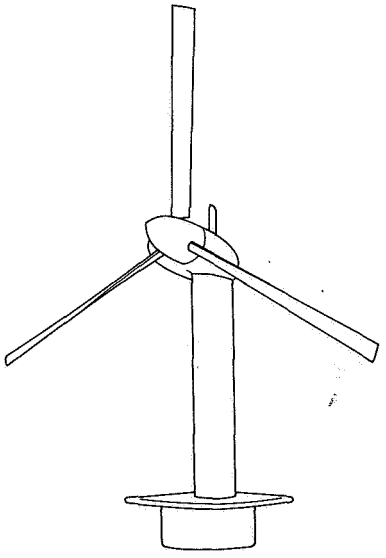

Figure 1. Configuration of analytical model, and for full-scale tests: proprotor operating in high inflow axial flight on a cantilever wing.

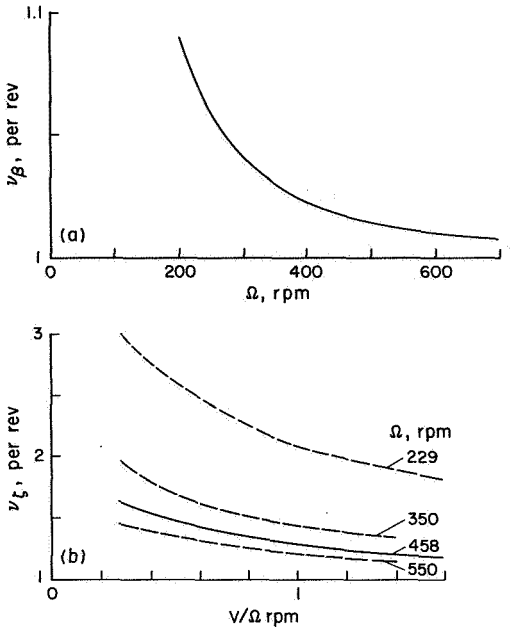

Figure 2. Blade rotating natural frequencies for the Bell rotor. (a) flap frequency ν_β (normal $\Omega = 458$ rpm), (b) lag frequency ν_ζ (V/ΩR = 1 at 355 knots and normal Ω).

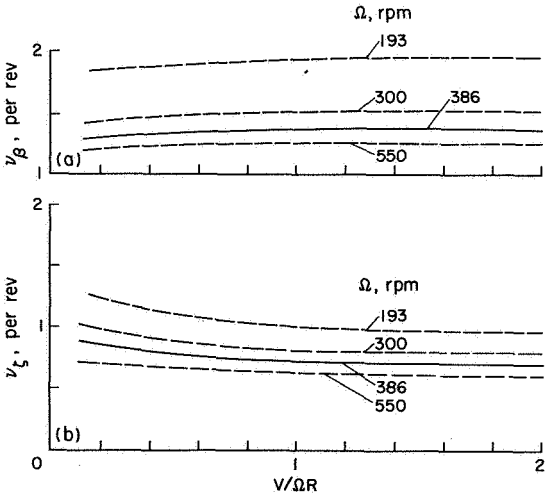

Figure 3. Blade rotating natural frequencies for the Boeing rotor (V/ΩR = 1 at 311 knots and normal Ω, 386 rpm). (a) flap frequency ν_β, (b) lag frequency ν_ζ.

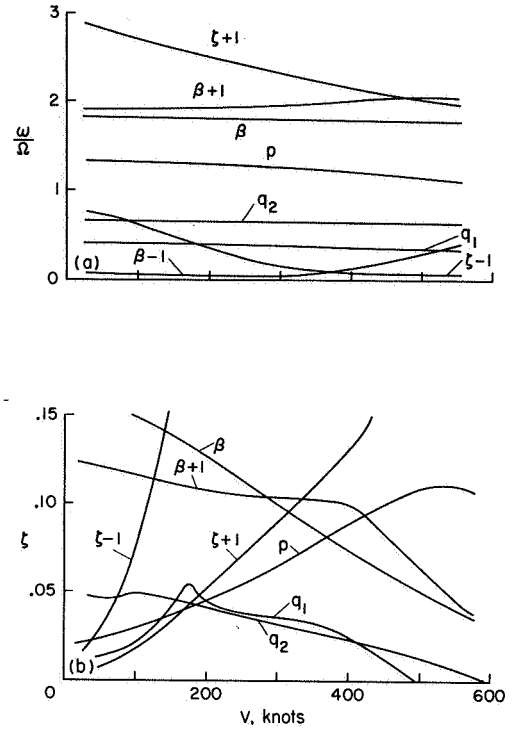

Figure 4. Predicted stability of Bell rotor, velocity sweep at $\Omega = 458$ rpm. (a) frequency of the modes, (b) damping ratio of the modes, (c) root locus.

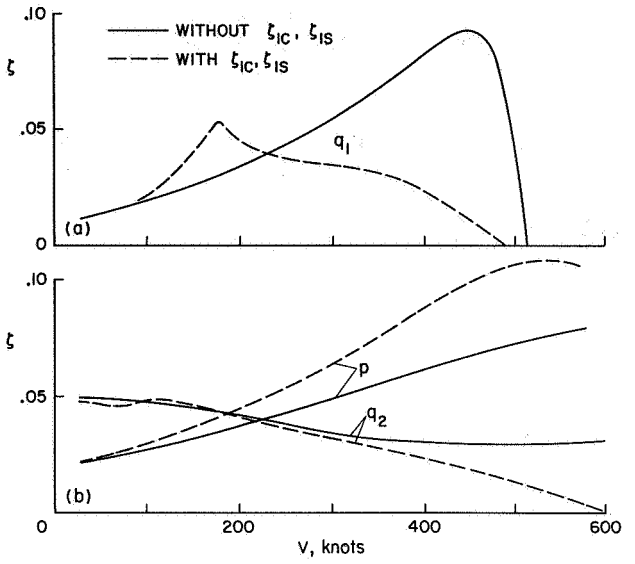

Figure 5. Effect of deleting the rotor lag degrees of freedom (ζ_{1c} and ζ_{1s}), Bell rotor velocity sweep at $\Omega = 458$ rpm. (a) damping of wing vertical bending mode (q_1), (b) damping of chordwise bending (q_2) and torsion (p) modes.

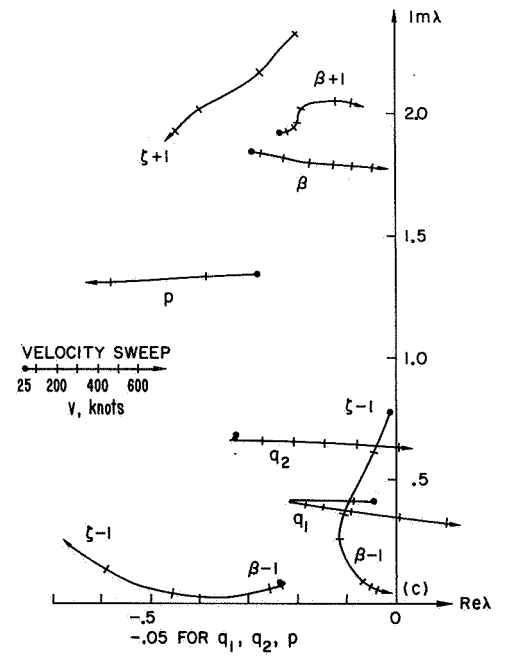

Figure 6. Influence of powered operation, and wing aerodynamic forces, Bell rotor velocity sweep at $\Omega = 458$ rpm. (a) damping of wing vertical bending mode (q_1), (b) damping of chordwise bending (q_2) and torsion (p) modes.

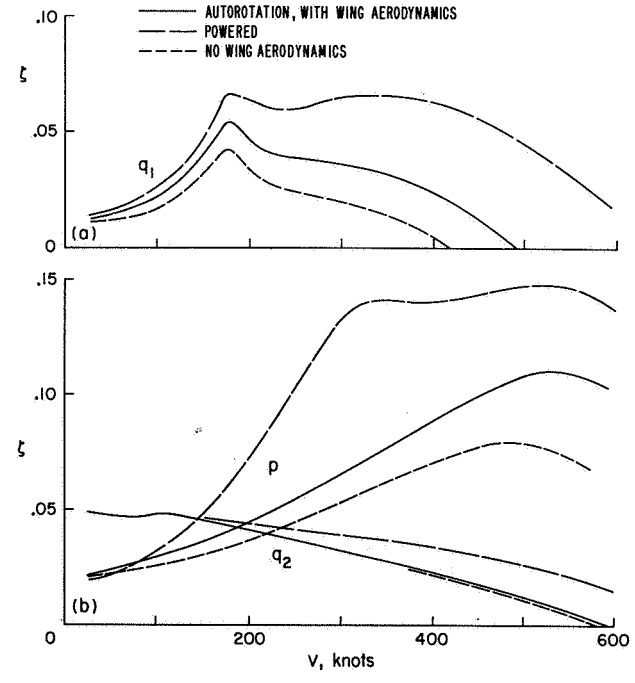

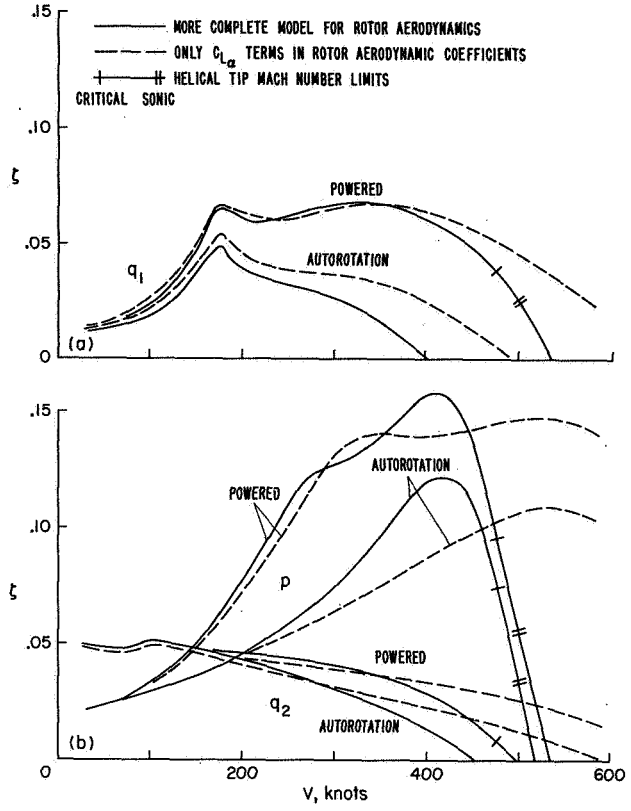

Figure 7. Influence of a more complete model for the rotor aerodynamics, Bell rotor velocity sweep at $\Omega = 458$ rpm. (a) damping of wing vertical bending mode (q_1), (b) damping of chordwise bending (q_2) and torsion (p) modes.

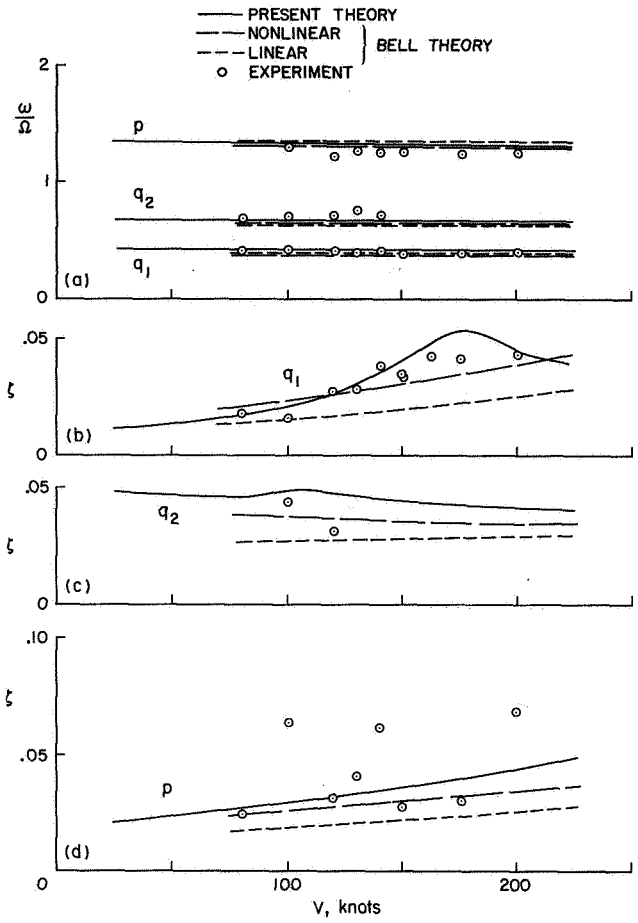

Figure 8. Comparison with full-scale experimental data, Bell rotor velocity sweep at $\Omega = 458$ rpm. (a) frequency of the modes, (b) damping of the wing vertical bending mode (q_1), (c) damping of wing chordwise bending mode (q_2), (d) damping of wing torsion mode (p).

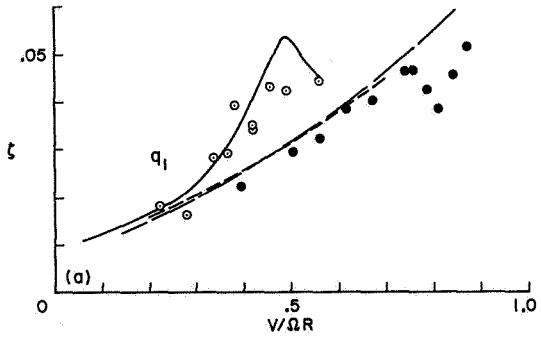

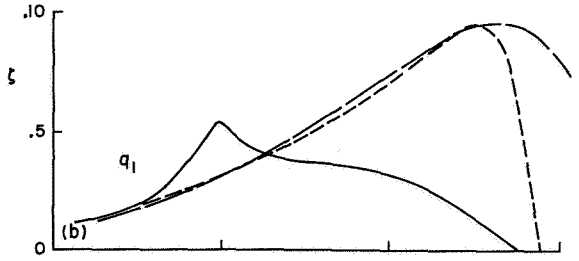

Figure 9. Influence of the rotor lag motion, Bell rotor velocity sweeps on the full-stiffness wing, on a quarter-stiffness wing, and on the full-stiffness wing without the ζ_{1c} and ζ_{1s} degrees of freedom (theory only). (a) damping of the wing vertical bending mode (q_1), comparison with full-scale experimental data, (b) damping of wing vertical bending mode (q_1), (c) damping of wing chordwise bending (q_2) and torsion (p) modes, (d) frequency of the modes.

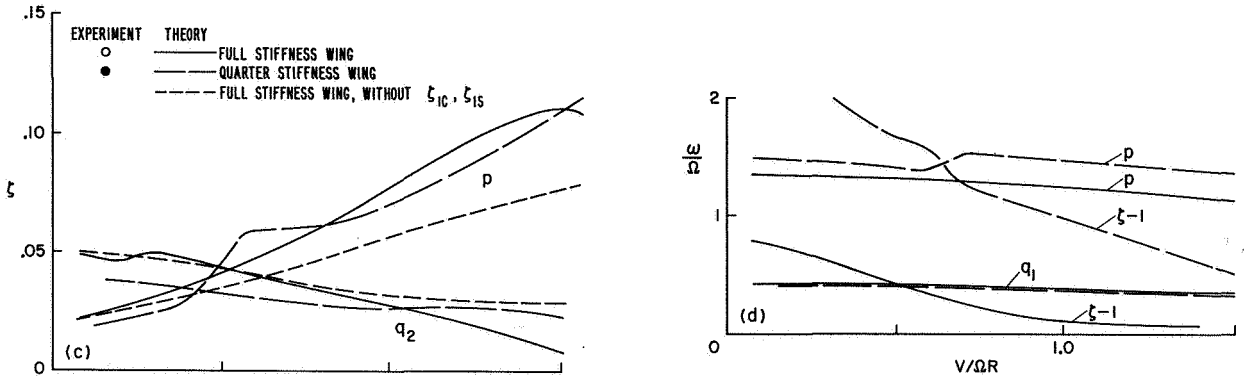

Figure 9. Concluded.

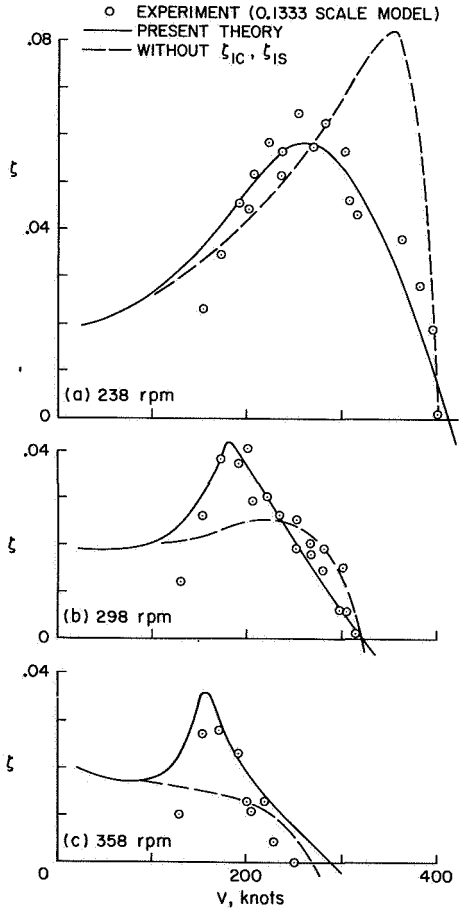

Figure 10. Comparison with experimental data from tests of a 0.1333-scale rotor and cantilever wing model of Bell M266 aircraft (experimental points from Reference 6), velocity sweeps at (a) Ω = 238 rpm, (b) Ω = 298 rpm, (c) Ω = 358 rpm (equivalent full-scale V and Ω).

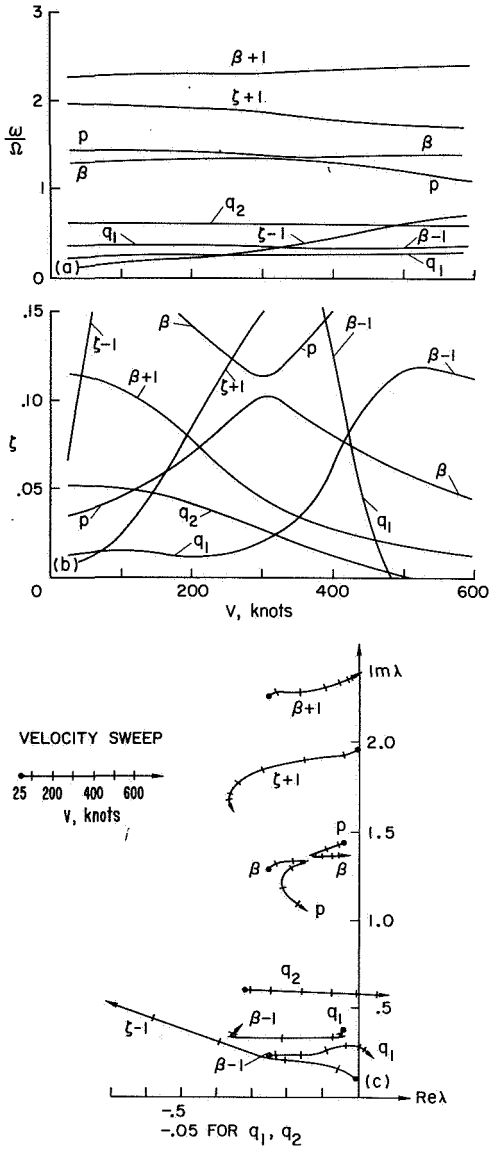

Figure 11. Predicted stability of Boeing rotor, velocity sweep at Ω = 386 rpm. (a) frequency of the modes, (b) damping ratio of the modes, (c) root locus.

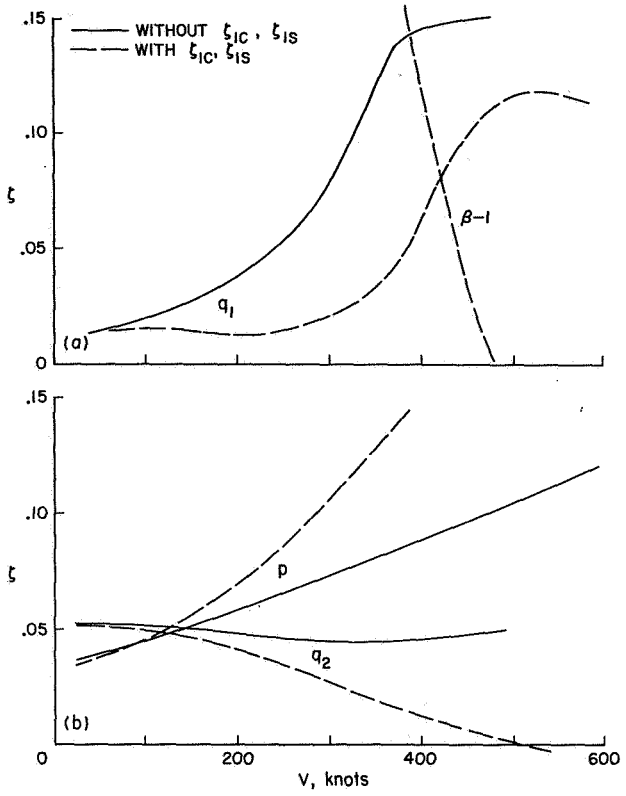

Figure 12. Effect of deleting the rotor lag degree of freedom (ζ_{1C} and ζ_{1S}), Boeing rotor velocity sweep at $\Omega = 386$ rpm (a) damping of wing vertical bending (q_1) and flap ($\beta - 1$) modes (the $\beta - 1$ mode is shifted by 250-300 knots to higher speed by the removal of the lag influence, beyond the scale shown), (b) damping of wing chordwise bending (q_2) and torsion (p) modes.

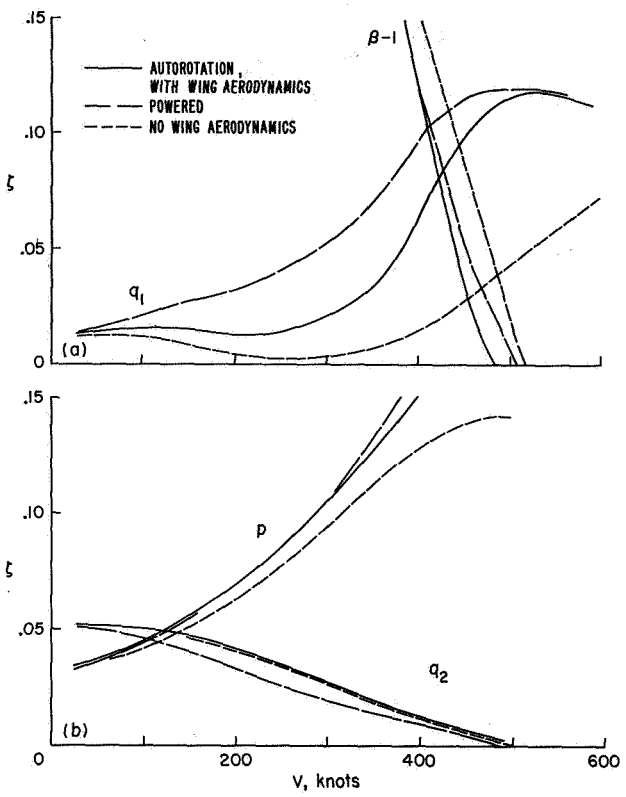

Figure 13. Influence of powered operation, and wing aerodynamic forces, Boeing rotor velocity sweep at $\Omega = 386$ rpm. (a) damping of wing vertical bending (q_1) and rotor flap ($\beta - 1$) modes, (b) damping of wing chordwise bending (q_2) and torsion (p) modes.

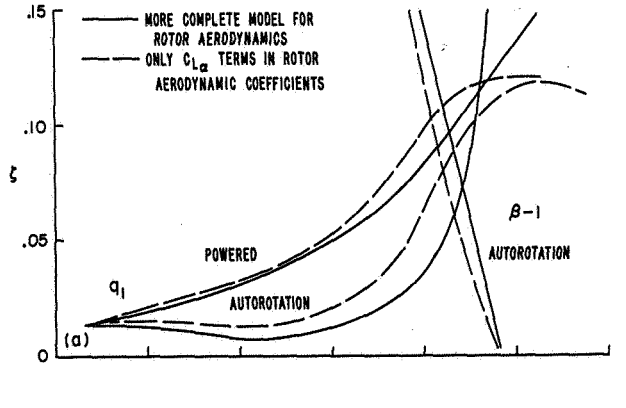

Figure 14. Influence of a more complete model for the rotor aerodynamics. Boeing rotor velocity sweep at $\Omega = 386$ rpm (a) damping of wing vertical bending (q_1) and rotor flap ($\beta - 1$) modes, (b) damping of wing chordwise bending (q_2) and torsion (p) modes.

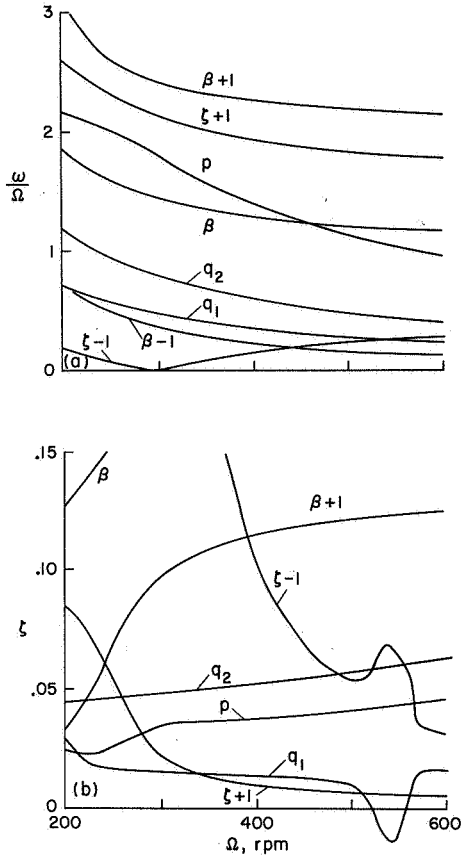

Figure 15. Predicted stability of Boeing rotor, rpm sweep at 50 knots. (a) frequency of the modes, (b) damping ratio of the modes.

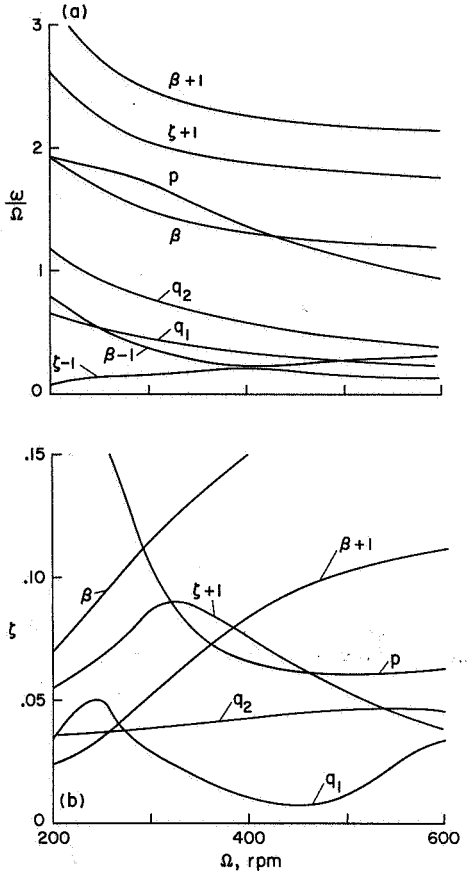

Figure 16. Predicted stability of Boeing rotor, rpm sweep at 192 knots. (a) frequency of the modes, (b) damping ratio of the modes.

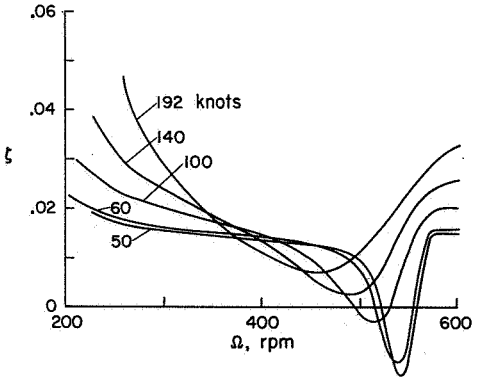

Figure 17. Air resonance behavior of soft-inplane hingeless rotor. Boeing rotor at 50 to 192 knots, variation of damping of wing vertical bending mode (q_1) with rotor speed.

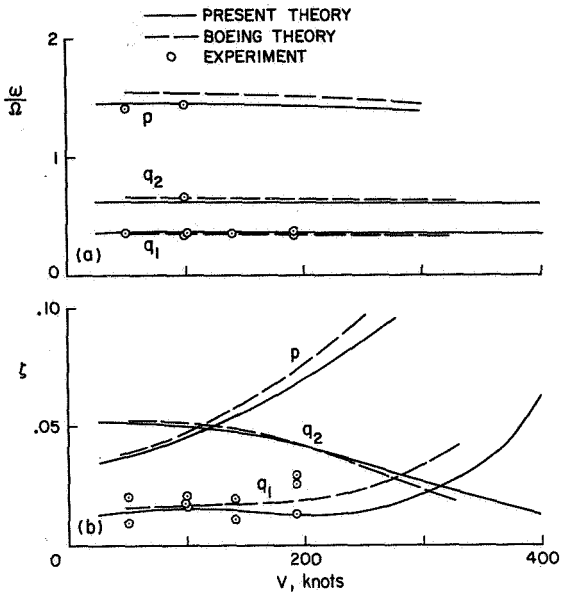

Figure 18. Comparison with full-scale experimental data, Boeing rotor velocity sweep at $\Omega = 386$ rpm. (a) frequency of the modes, (b) damping of the wing vertical bending (q_1), chord bending (q_2), and torsion (p) modes; the experimental data is for q_1 only.

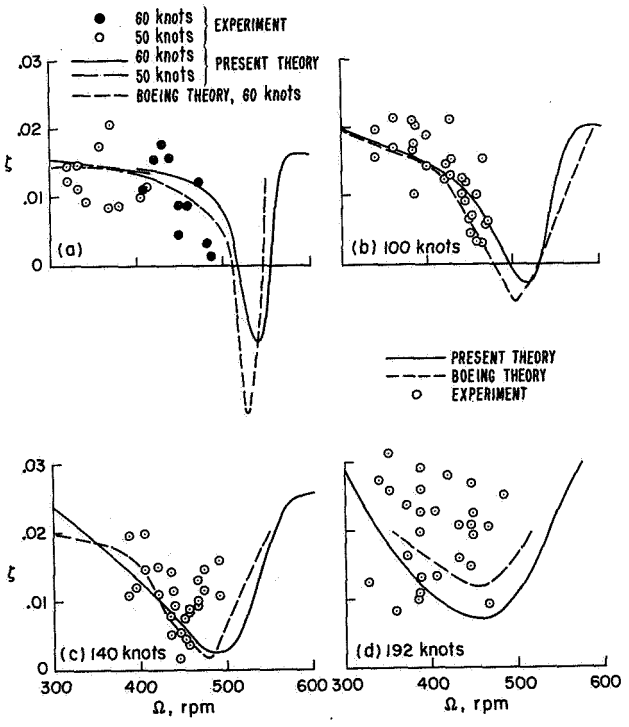

Figure 19. Comparison with full-scale experimental data, Boeing rotor rpm sweeps, damping of wing vertical bending mode at (a) 50-60 knots, (b) 100 knots, (c) 140 knots, (d) 192 knots.

EXPERIMENTAL AND ANALYTICAL STUDIES IN TILT-ROTOR AEROELASTICITY

Raymond G. Kvaternik
Aerospace Technologist
NASA Langley Research Center
Hampton, Virginia

Abstract

An overview of an experimental and analytical research program underway within the Aeroelasticity Branch of the NASA Langley Research Center for studying the aeroelastic and dynamic characteristics of tilt-rotor VTOL aircraft is presented. Selected results from several joint NASA/contractor investigations of scaled models in the Langley transonic dynamics tunnel as well as some results from a test of a flight-worthy proprotor in the NASA Ames full-scale wind tunnel are shown and discussed with a view toward delineating various aspects of dynamic behavior peculiar to proprotor aircraft. Included are such items as proprotor/pylon stability, whirl flutter, gust response, and blade flapping. Theoretical predictions, based on analyses developed at Langley, are shown to be in agreement with the measured stability and response behavior.

Notation

e	Blade flapping hinge offset
H	Rotor normal shear force
$\partial H/\partial \alpha_m$	Rotor normal shear force component in phase with pitch angle
$\partial H/\partial q$	Rotor normal shear force component in phase with pitch rate
R	Blade radius
$\bar{R}$	0.75 blade radius
ΔT	Rotor perturbation thrust
V	Airspeed
$V_F/\Omega R$	Flutter advance ratio
w_g	Vertical component of gust velocity
α_m	Mast angle of attack
α_o	Oscillation amplitude of airstream oscillator
β	Blade flapping angle
$\partial\beta/\partial\alpha_m$	Blade flapping derivative
δ_3	Pitch-flap coupling angle
ϵ_g	Gust-induced angle of attack
ζ_R	Hub damping ratio
$\dot{\psi}$	Aircraft yaw rate
Ω	Rotor rotational speed
ω	Frequency
ω_β	Blade flapping natural frequency
ω_θ	Pylon pitch frequency
ω_ψ	Pylon yaw frequency

Presented at the AHS/NASA Ames Specialists' Meeting on Rotorcraft Dynamics, February 13-15, 1974.

The feasibility of the tilt-proprotor composite aircraft concept was established in the mid 1950's on the basis of the successful flight demonstrations of the Bell XV-3 and Transcendental Model 1-G and Model 2 convertiplanes. Flight research conducted with the XV-3 identified several dynamic deficiencies in the airplane mode as technical problems requiring further attention.[1] A more serious proprotor dynamic problem was identified in a 1962 wind-tunnel test of the XV-3. In that test, conducted in the Ames full-scale tunnel, a proprotor/pylon instability similar in nature to propeller whirl flutter was encountered. Clearly, to maintain the viability of the tilt-proprotor concept it remained to demonstrate that neither the whirl flutter anomaly nor the major flight deficiencies were endemic to the design principle. An analytical and experimental research program having this objective was undertaken by Bell in 1962. Results of this research, which defined the instability mechanism and established several basic design solutions, were reported by Hall.[2] Edenborough[3] presented results of subsequent full-scale tests at Ames in 1966 which verified the analytical prediction techniques, the proposed design solutions, and demonstrated stability of the XV-3 through the maximum wind-tunnel speed of 100 m/s (195 kts).

In 1965 the U.S. Army inaugurated the Composite Aircraft Program which had the goal of producing a rotary-wing research aircraft combining the hovering capability of the helicopter with the high-speed cruise efficiency and range of a fixed-wing aircraft. Bell Helicopter Company, with a tilt-proprotor design proposal, was awarded one of two exploratory definition contracts in 1967. The Model 266 was the design resulting from their work (Fig. 1). The research aircraft program which was to have been initiated subsequent to the exploratory definition phase was never begun, however, primarily due to lack of funding.

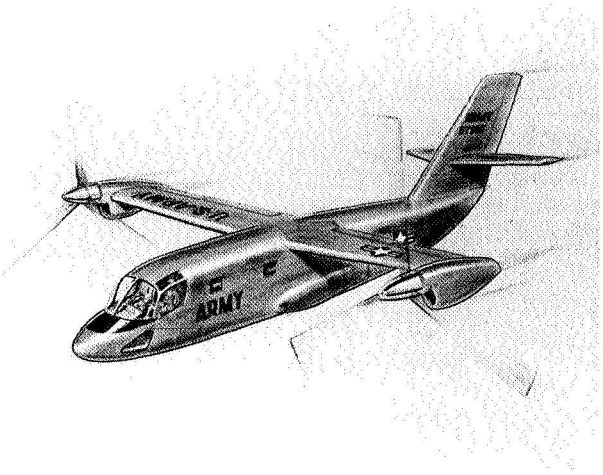

Figure 1. Artist's conception of Bell Model 266 tilt-proprotor design evolved during the Army Composite Aircraft Program.

Concurrent with the developments described above, various VTOL concepts based on the use of propellers having independently hinged blades were proposed with several reaching flight-test status. These included the Grumman proposal in the Tri-Service VTOL Transport competition, the Vertol VZ-2 built for the Army, and the Kaman K-16 amphibian built for the Navy. A vigorous investigation of the whirl flutter phenomenon peculiar to conventional propellers had been initiated in 1960 as a result of the loss of two Lockheed Electra aircraft in fatal accidents. The possibility that hinged blades could adversely affect the whirl flutter behavior of a propeller undoubtedly contributed considerable impetus to examine the whirl flutter characteristics of these flapping propellers. Work related to these efforts was reviewed by Reed.[4]

The foregoing constitutes a résumé of proprotor-related experience through 1967. This paper will present an overview of a research program initiated within the Aeroelasticity Branch of the NASA Langley Research Center. Included in this program are joint NASA/contractor wind-tunnel investigations of scaled models in the transonic dynamics tunnel and the in-house development of supporting analyses. For completeness, motivating factors leading to the work and the scope of the investigation are outlined below.

A 0.133-scale semispan dynamic and aeroelastic model of the Model 266 tilt rotor built by Bell in support of their work pertaining to the Composite Aircraft Program was given to Langley by the Army in 1968. The availability of this model and the interest of both government and industry in the tilt-rotor VTOL aircraft concept suggested the usefulness of continuing the experimental work initiated by Bell with the model to further define the aeroelastic characteristics of proprotor-type aircraft. Because both the XV-3 experience and studies conducted during the Composite Aircraft Program identified certain high-risk areas associated with operation in the airplane mode of flight, specifically proprotor/pylon stability (whirl flutter), blade flapping, and flight mode stability, it was judged that the research effort would be primarily directed to these areas.

The experimental portion of the research program was initiated in September 1968 in a joint NASA/Bell study of proprotor stability, dynamics, and loads employing the 0.133-scale semispan model of the Model 266. Several other cooperative experimental studies followed this investigation. The models employed in these studies are positioned in chronological order in the composite photo given in Figure 2. Briefly, these other studies included: (1) A study of a folding proprotor version of the tilt-rotor model used in the first study, (2) a parametric investigation of proprotor whirl flutter, (3) a stability and control investigation employing an aerodynamic model, and (4) a "free-flight" investigation of a complete tilt-rotor model.

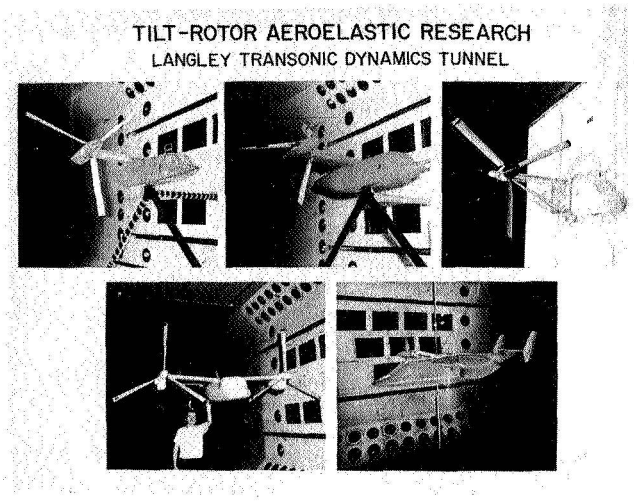

Figure 2. Tilt-rotor models tested in the Langley transonic dynamics tunnel.

The results pertaining to the above-mentioned studies are quite extensive. The particular results to be presented herein have been selected with a view toward highlighting some of the dynamic aspects of proprotor behavior, delineating the effects of various design parameters on proprotor/pylon stability and response, and providing validation of analyses developed at Langley. The results pertaining to investigations conducted in the Langley transonic dynamics tunnel are presented first. These are arranged in chronological order according to Figure 2. To provide additional data for correlation, some experimental results obtained by Bell in tests of a semispan model and a full-scale flight-worthy proprotor are also included. In each case both experimental and analytical results are for the pylon fully converted forward into the airplane mode of operation and the rotors in a windmilling condition. Equivalent full-scale values are given unless noted otherwise.

Model Tests in Langley Transonic Dynamics Tunnel

Bell Model 266
(a) September 1968

Although the 0.133-scale semispan model of the Bell Model 266 was not designed to permit extensive parametric variations, in that it represented a specific design, it did permit a fairly diversified test program. The principal findings of this investigation have been published and are available in the literature.[5,6] Some results adapted from Reference 6 pertaining to stability and gust response are discussed below.

Proprotor/Pylon Stability. To provide an indication of the relative degree to which stability could be affected, and to provide a wide range of configurations for correlation with analysis, several system parameters were varied either individually or in combination with other parameters and the level of stability established.

A baseline stability boundary, based on a reference configuration, was first established. The degree to which stability could be affected was then ascertained by varying selected system parameters (or flight conditions). Stability data were obtained by holding rpm constant as tunnel speed was incrementally increased, transiently exciting the model by means of lightweight cables attached to the model, and analyzing the resulting time histories to determine the damping. The reference configuration consisted of the basic Model 266 parameters with the pylon yaw degree of freedom locked out and the wing aerodynamic fairings removed. A 100% fuel weight distribution was maintained by appropriately distributing lead weights along the wing spar. The hub flapping restraint was set to zero and the δ_3 angle to -0.393 radian (-22.5°). The reference stability boundary as well as changes in this boundary due to several parameter variations are shown in Figure 3.

For the reference configuration instability occurred in the coupled pylon/wing mode in which the pylon pitching angular displacement is in phase with the wing vertical bending displacement. A characteristic feature of this coupled mode is the predominance of wing bending (relative to pylon pitch) and the frequency of oscillation, which is near the fundamental wing vertical bending natural frequency. For descriptive purposes this flutter mode is termed the "wing beam" mode herein. Negligible wing chordwise bending or rotor flapping (relative to space) was observed. The pylon/rotor combination also exhibited a forward whirl precessional motion, the hub tracing out an elliptical path in space. However, because of the large ratio of pylon yaw to pylon pitch stiffness the pylon angular displacement was primarily in the pitch direction. The flutter mode of the model in each of its perturbations from the reference configuration was essentially the same as for the reference configuration.

The proprotor/pylon instability described above is similar in nature to classical propeller

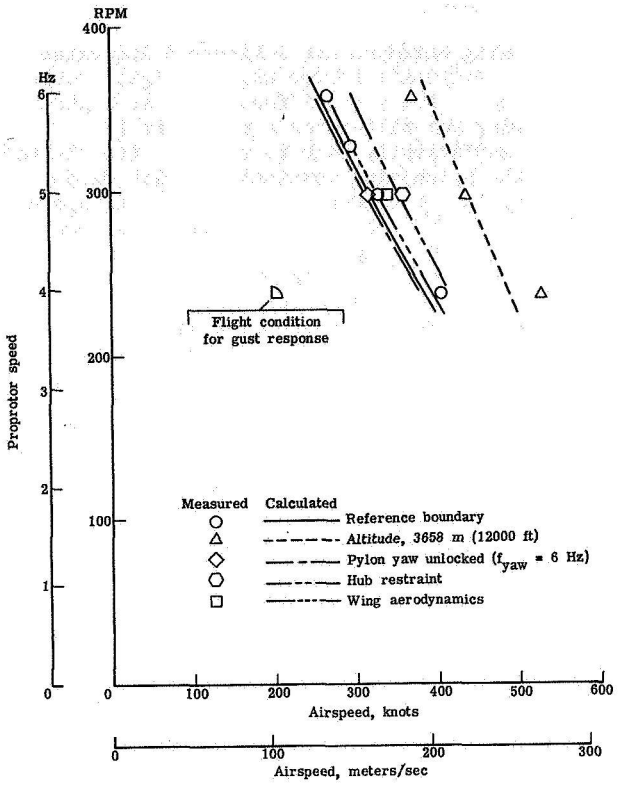

Figure 3. Effect of several system parameters on proprotor/pylon stability.

whirl flutter. However, because of the additional flapping degrees of freedom of the proprotor the manner in which the precession generated aerodynamic forces act on the pylon is significantly different.[6] Specifically, while aerodynamic cross-stiffness moments are the cause of propeller whirl flutter, the basic destabilizing factors on proprotor/pylon motion are aerodynamic in plane shear forces which are phased with the pylon motion such that they tend to increase its pitching or yawing velocity and, hence, constitute negative damping on the pylon motions.

(1) Altitude – Altitude has a highly beneficial effect on proprotor/pylon stability. This increased stability is a consequence of the fact that the destabilizing rotor normal shear forces decrease with altitude for pylon pitch frequencies near the fundamental wing elastic mode frequencies. This means that a given level of these destabilizing shear forces is attained at progressively higher airspeeds as altitude increases.

(2) Hub Flapping Restraint – A stabilizing effect due to moderate flapping restraint is also indicated in Figure 3. Increasing the flapping restraint increased the flapping natural frequency from its nominal value of about 0.80/rev bringing it closer to the "optimum" flapping frequency in the sense of Young and Lytwyn.[7] They showed that this increased stability because the pylon support

stiffness requirements were reduced as the optimum flapping frequency was approached.

(3) Wing Aerodynamics – Figure 3 indicates that wing aerodynamic forces have a slight stabilizing effect. Now the stiffness of a strength-designed wing for tilt-rotor application is generally sufficiently high to relegate the flutter speed of the pylon/wing combination (with blades replaced by lumped concentrated weights) to speeds well beyond the proprotor mode flight envelope. This suggests that wing aerodynamics will contribute primarily to the damping of any coupled rotor/pylon motions. This is substantiated in Figure 4, which shows the variation of the wing beam mode damping with airspeed through the flutter point for the reference configuration and the corresponding configuration with the wing airfoil segments installed. The damping of the mode is increased; however, the magnitude of the increase is small indicating that proprotor aerodynamic forces are predominant in the ultimate balance of forces at flutter. This provides some justification for neglecting, in this flutter mode at least, wing aerodynamics as a first approximation.

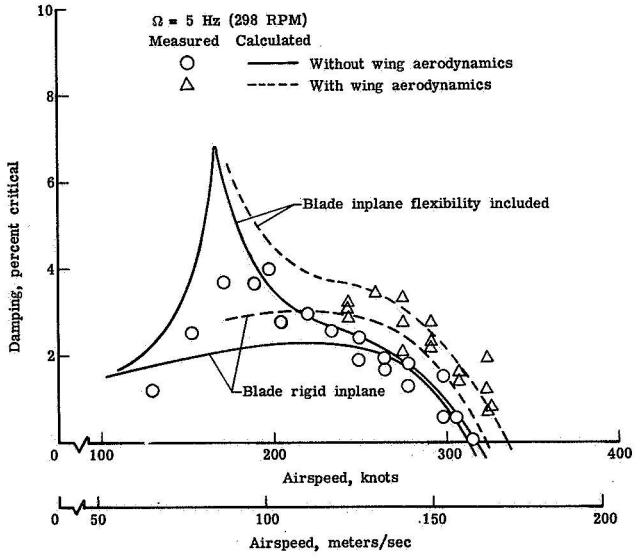

Figure 4. Comparison of measured and calculated wing beam mode damping for reference configuration.

The initial increase in the stability of the wing beam mode before instability occurs is associated with the fact that $\partial H/\partial q$, the component of the normal shear force associated with pylon pitch rate, initially becomes more stabilizing with increasing airspeed until $\partial H/\partial \alpha_m$, the component of the normal shear force in phase with pylon pitch angle, becomes sufficiently large to lower the coupled pylon pitch frequency to a level where $\partial H/\partial q$ becomes increasingly destabilizing with increasing airspeed.[6] The increased damping response at about 103 m/s (200 kts) is due to coupling of the blade first inplane cyclic mode with the wing beam mode. Note, however, that the predicted flutter speed is not sensitive to blade inplane flexibility for the Model 266.

(4) Pylon Restraint – When the pylon yaw stiffness was reduced by unlocking the pylon yaw degree of freedom and soft-mounting the pylon in yaw relative to the wing tip the stability decreased slightly (Fig. 3). The particular yaw flexibility employed in this variation effectively produced a more nearly isotropic arrangement of the pylon support spring rates. Since the region of instability in a plot of critical pylon yaw stiffness against critical pitch stiffness is extended along the line representing a stiffness ratio of unity, the configuration approaching isotropy in the pylon supports is more prone to experience an instability than one in which one of the stiffnesses is significantly less than the other.

The general trend of decreasing stability with increasing rotor speed shown in Figure 3 was found for all values of the adjustable parameters of the model. In each case the predicted flutter mode and frequency were in agreement with the corresponding measured mode and frequency.

Gust Response. Analytical methods for determining aircraft response to turbulence are usually based on power spectral analysis techniques which require the definition of the aircraft frequency response function, that is, the response to sinusoidal gust excitation. A study to assess the feasibility of determining these frequency response functions for fixed-wing aircraft utilizing models in a semi-free-flight condition using a unique airstream oscillator system in the transonic dynamics tunnel has been underway within the Aeroelasticity Branch for several years.[8] This system (Fig. 5) consists of two sets of biplane vanes located on the sidewalls of the tunnel entrance section. The

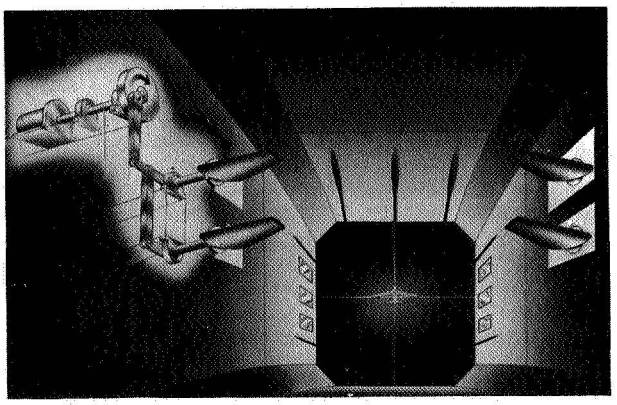

Figure 5. Langley transonic dynamics tunnel airstream oscillator showing cutaway of driving mechanism.

vanes can be oscillated in phase or 180° out of phase to produce nominally sinusoidal vertical or rolling gusts, respectively, over the central portion of the tunnel. The gusts are generated by the cross-stream flow components induced by the trailing vortices from the tips of the vanes. With a

view toward the possible application of this technique to rotary-wing aircraft the airstream oscillator was employed to excite the model for several "flight" conditions below the proprotor stability boundary. Although the model was not "free" the data so obtained did give an indication of the frequency response characteristics of the cantilevered model and permitted the evaluation of the effects of airspeed, rotor speed, and rotor and wing aerodynamics on the overall dynamic response.

A measure of the gust-induced angle of attack (or stream angle) was provided by means of a small balsa vane flow direction transmitter (see Fig. 6) which gave readings proportional to the stream angle. The variation of the vertical component of

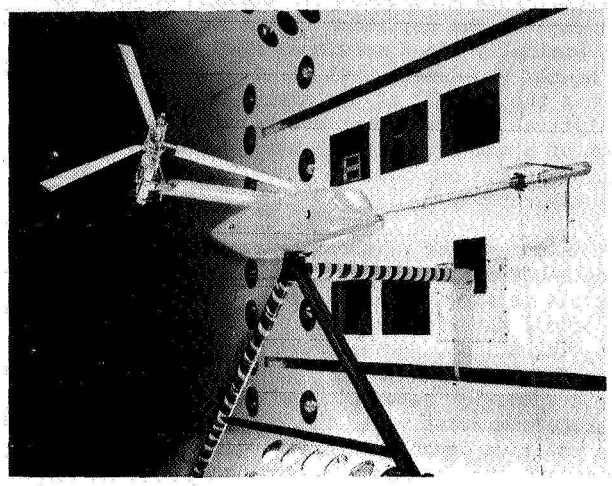

Figure 6. 0.133-scale semispan tilt-rotor model in simulated conversion mode showing boom-mounted flow direction transmitter.

the stream angle for in phase (symmetrical) oscillation of the biplane vanes is shown in Figure 7. The curve shown is actually an average of data obtained from runs at several tunnel speeds and air densities. The amplitude of the stream angle has been normalized on the maximum amplitude of oscillation of the biplane vanes and plotted against the frequency parameter ω/V, where ω is the frequency of oscillation of the biplane vanes in rad/sec and V is the tunnel speed in m/s (ft/sec). This parameter is proportional to the reciprocal of the wavelength (spacing) between vortices shed from the tips of the oscillating vanes.

The frequency response of wing vertical bending moment was taken as one measure of system response to vertical gust excitation. To ascertain the relative influence of rotor and wing aerodynamics, three model configurations were employed: wing only, with the rotor blade weight replaced by an equivalent lumped weight; rotor only, with the wing aerodynamic fairings removed; wing and rotor combined. For the "flight" condition indicated in Figure 3 the relative effects of rotor and wing aerodynamics are displayed in Figures 8 and 9. In each of these figures the wing bending moment has been normalized by the maximum amplitude of the stream angle using the curve of Figure 7.

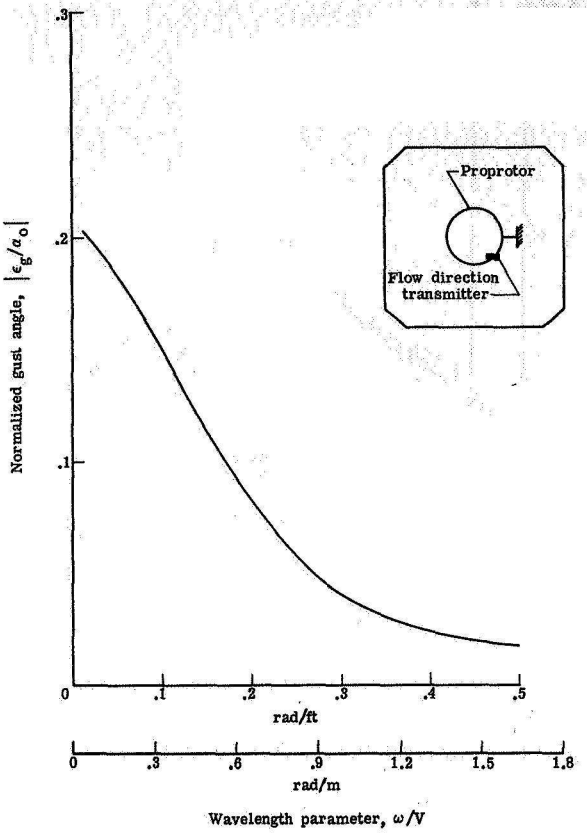

Figure 7. Measured variation of vertical component of gust angle with frequency parameter for vanes oscillating in phase.

Comparison of the rotor-on and rotor-off response curves for the wing panels on configuration is shown in Figure 8. Two proprotor-related effects are indicated: first, the significant contribution of the rotor inplane normal force (H-force) to wing bending response, as indicated by the relative magnitudes of the bending moments; and second, the rotor contribution to wing beam mode damping,* as indicated by the relative sharpness of the resonance peaks. The peak amplitudes occur when the gust frequency is in resonance with the wing beam mode frequency. The peak for the blades-off condition is shifted to the higher frequency side of the rotor-on peak because the rotor H-force decreases the frequency of the wing beam mode. For the rotor-on case the bending moment is considerably larger than for the rotor-off case throughout the range of gust frequencies investigated. The wing chord mode frequency (about 2.8 Hz) is within the gust frequency range but is absent from the response curves because the gust excitation is

*At this particular airspeed, the rotor was still contributing positive damping to the wing beam mode.

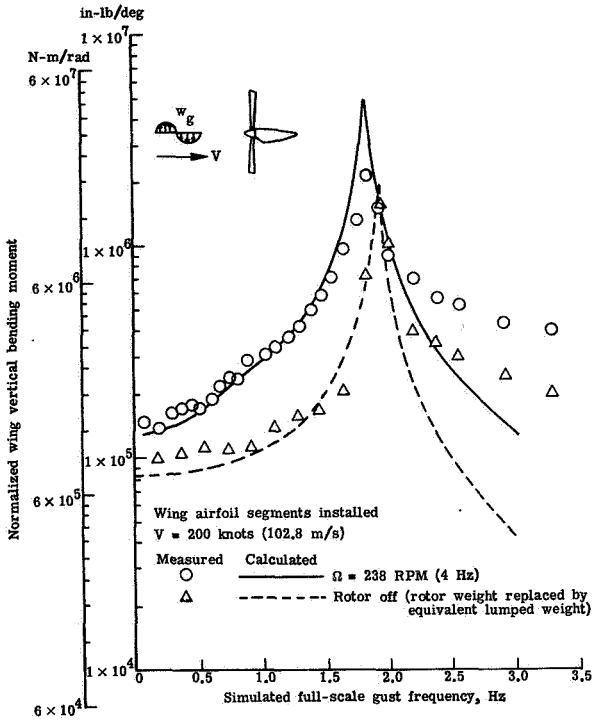

Figure 8. Effect of proprotor aerodynamics on wing root bending moment amplitude response function.

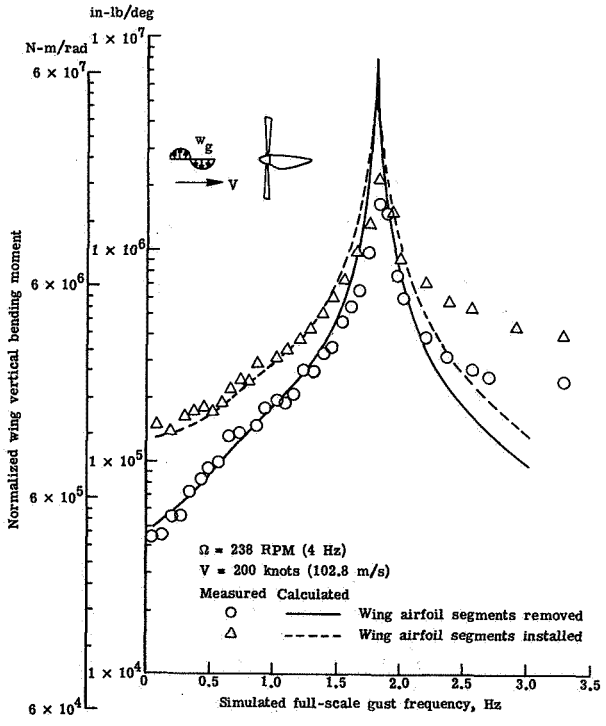

Figure 9. Effect of wing aerodynamics on wing root bending moment amplitude response function.

primarily vertical and there is very little coupling between the wing beam and chord modes.

Figures 8 and 9 quite clearly illustrate that proprotors operating at inflow ratios typical of tilt-rotor operation in the airplane mode of flight are quite sensitive to vertical gusts. This sensitivity is due to the fact that the proprotors, being lightly loaded in the airplane mode of flight, operate at low blade mean angles of attack ($\bar{\alpha}$) and any gust-induced angle of attack is a significant fraction of $\bar{\alpha}$.

Note that good correlation is achieved for frequencies up to about 2 Hz beyond which the calculated responses are much lower than the measured values. This discrepancy is thought to be a consequence of the deviation of the induced gust from its nominally one-dimensional nature to one which is highly two-dimensional (i.e., varies laterally across the tunnel) at the higher frequencies. The analytical results shown are based on the assumption of a one-dimensional gust. Unsteady aerodynamic effects may also be a contributing factor to the discrepancy.

A comparison of the wing panels-on and wing panels-off response curves for the rotor-on configuration is given in Figure 9. As might be expected, the wing response for the case in which the wing airfoil segments are installed is higher than for the rotor alone. The reduced magnitude of the response at resonance for the rotor-plus-wing combination relative to the rotor alone is due to the positive damping contributed by the wing aerodynamics. This increased damping is evident by comparing the widths of the resonance peaks.

Close examination of Figures 8 and 9 reveals a very heavily damped, low amplitude resonance "peak" at a gust frequency of about 0.8 Hz. This resonance is a manifestation of the low-frequency (i.e., $\Omega - \omega_\beta$) flapping mode. Analyses have indicated that the flapping modes are generally well damped for moderate or zero values of flapping restraint.[6] These results constitute an experimental verification.

These results indicate that "free-flight" tilt-rotor models could be used to measure the frequency response functions needed in gust response analyses. This would be a fruitful area for future analytical and experimental research.

(b) January 1970

A joint NASA/Bell/Air Force test program was conducted in the transonic dynamics tunnel in January 1970 for the purpose of investigating any potential problem areas associated with the folding proprotor variant of the tilt-rotor concept. The model used in this study was the same model employed in the first investigation but modified to permit rapid feathering and unfeathering of the proprotor and to include a blade fold-hinge. The main objectives were to investigate stability at low (including zero) rotor rotational speeds,

during rotor stopping and starting, and during blade folding. All objectives of the test program were met. No aeroelastic instabilities were encountered during the blade folding sequence of transition, the blade loads and/or the feathering axis loads inboard of the fold hinge being identified as the critical considerations from a design point of view. The stop-start portion of the test indicated that additional flapping restraint would be required to minimize flapping during rotor stopping.* Stability investigations conducted over a wide range of rotor speed identified an apparently new form of proprotor instability involving the rotor at low and zero rotational speeds. The influence of several system parameters on this instability was established both experimentally and analytically.[6]

Proprotor/Pylon Stability. For the stability investigation a reference configuration was again established. This consisted of the basic Model 266 configuration with the pylon locked to the wing tip in both pitch and yaw, a hub restraint of 117,683 N-m/rad (86,800 ft-lb/rad), δ_3 = -0.393 rad (-22.5°), a simulated wing fuel weight distribution of 15%, and the wing aerodynamic fairings installed. The flutter boundary obtained for this configuration and that for δ_3 = -0.558 rad (-32°), are shown in Figure 10 as a function of rotor speed. Open symbols denote flutter points. Excessive vibration resulting from operation near resonances with the pylon/wing or blade modal frequencies often limited the maximum attainable airspeed. These points are indicated by the solid symbols. The annotation to the right of the flutter boundaries indicates that the model experienced several modes of flutter. The predicted flutter modes and frequencies were in agreement with the experimental results. The nature of these flutter modes is discussed below.

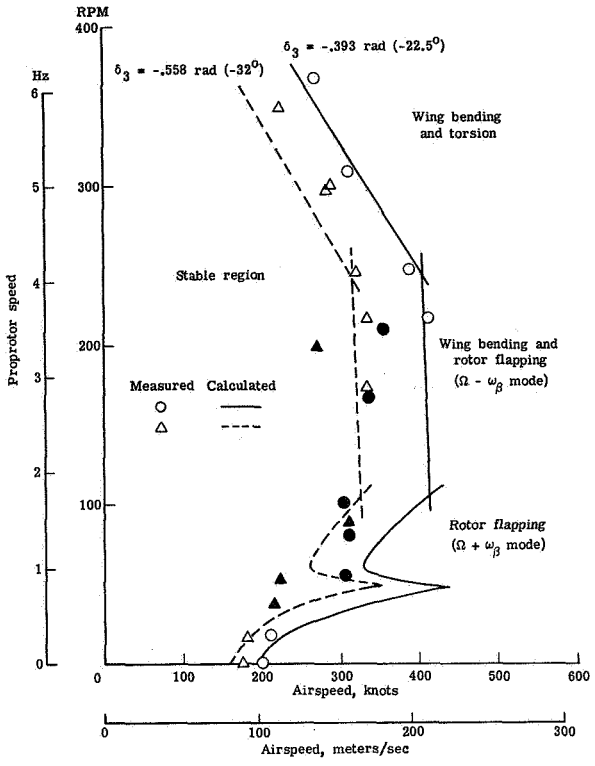

Figure 10. Model 266 flutter boundaries showing variation in character of flutter mode as rpm is reduced to zero.

For Ω greater than about 4 Hz (240 rpm) instability occurred in the wing beam mode and had the characteristics described earlier for the September 1968 test. For Ω between about 2 Hz (120 rpm) and 4 Hz (240 rpm) the motion at flutter was predominantly wing vertical bending and rotor flapping with the hub precessing in the forward whirl direction. Examination of the root loci indicated that this instability was associated with the low-frequency (i.e., $\Omega - \omega_\beta$) flapping mode root becoming unstable. The subcritical response through flutter for δ_3 = -0.558 rad (-32°) and Ω = 2.86 Hz (172 rpm) is shown in Figure 11 where, in addition to the measured wing beam mode damping and frequency, the calculated variation of both the wing beam and low-frequency flapping modes is shown. These results illustrate an interesting modal response behavior similar to that described by Hall.[2] The wing beam mode, being least stable at low airspeeds, is at first dominant. As airspeed increases, however, its damping continually increases. The damping of the $\Omega - \omega_\beta$ flapping mode meanwhile is continually decreasing. Crossover occurs analytically at 144 m/s (280 kts) at a damping of 17% of critical. Beyond 280 knots, the $\Omega - \omega_\beta$ flapping mode is the dominant mode and very abruptly becomes unstable as airspeed is increased. Hence, a transition from a dominant wing beam mode to a dominant flapping mode with an accompanying change in frequency. Since the flapping mode frequency is only slightly less than the wing beam mode in the vicinity of flutter there is only a gradual, albeit distinct, transition in the frequency of the wing beam mode as the flapping mode begins to predominate over the wing mode. Examination of the $\Omega - \omega_\beta$ flapping mode eigenvector indicated that a larger amount of wing vertical motion was evident in this mode than in the wing beam mode eigenvector. This implies that the predominant motion in the flutter mode is not necessarily determined by the root which analytically goes unstable as airspeed is increased but the frequency at which a root goes unstable.

Below about 2 Hz (120 rpm) instability is in the high-frequency (i.e., $\Omega + \omega_\beta$) flapping mode and is characterized by large amplitude flapping, the rotor tip-path-plane exhibiting a precessional motion in the forward whirl direction. The modes of instability at zero rotational speed were similar in character to those at low rotor speeds but with larger amplitudes of flapping. Although the rotor was not turning, the flapping behavior of the blades

*These aspects of this investigation are given detailed treatment in Reference 9.

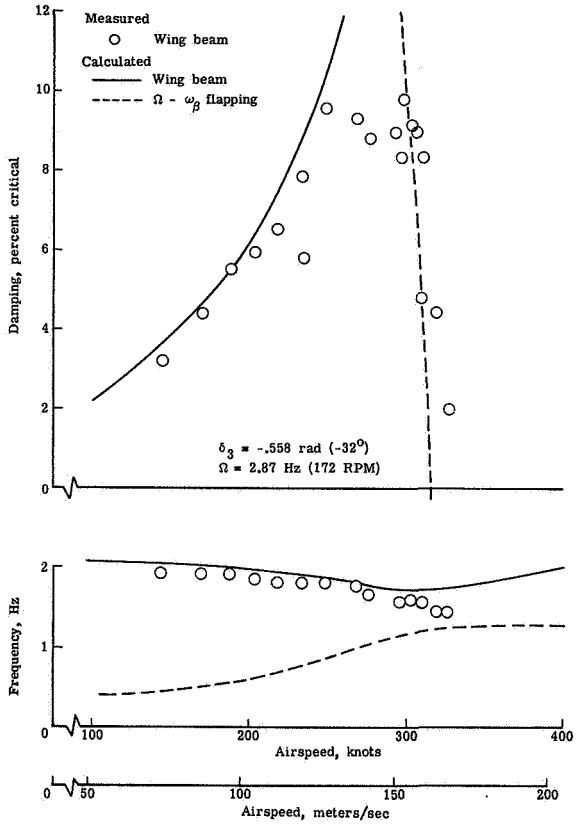

Figure 11. System response characteristics for flutter at Ω = 172 rpm and δ_3 = -32°.

was patterned such that the tip-path-plane appeared to be wobbling or whirling in the forward direction. Negligible wing motions accompanied the flapping motion. Figure 12 shows the variation of flap damping with airspeed. A hub damping of ζ_R = 0.015 was originally used in calculating the stability boundaries, leading to very conservative values for the flutter speed at the low rotor speeds. Based on the results of Figure 12, which indicate that the rotor hub structural damping is closer to ζ_R = 0.025, the stability boundaries were recalculated using ζ_R = 0.025. The predicted boundaries in Figure 10 reflect this change.

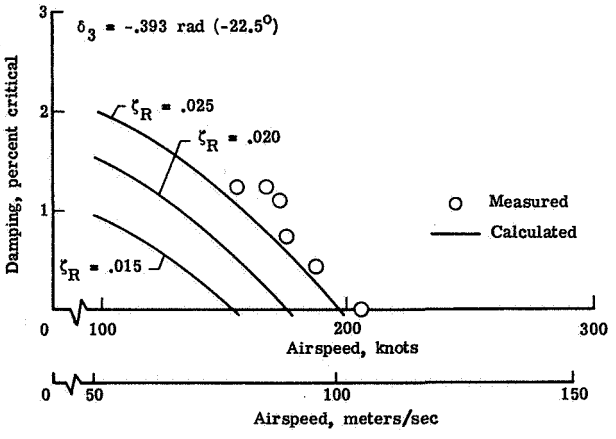

Figure 12. Variation of $\Omega + \omega_\beta$ flapping mode damping with airspeed for zero rpm.

The small region of increased stability in the region of 0.8 Hz (48 rpm) is due to a favorable coupling of the flapping mode with wing vertical bending.

The instabilities encountered at low and zero values of rotational speed were quite mild and had a relatively long time to double amplitude. The necessity of limiting the flapping amplitude during the feathering sequence of transition dictates that significantly increased values of hub restraint are needed as rotor rotational speed is reduced to zero. Since increased flapping restraint was found to stabilize this mode[6] this instability is probably only of academic interest, at least for the configuration tested. However, since it was a new phenomenon and was not understood at the time of the test, attention was directed to assessing the effect of the variation of several system parameters on the flutter speed. Both experimental and analytical trend studies were conducted for this purpose.[6] Based on these studies it was concluded that rotor precone was the primary cause of the instability.

Blade Flapping. In the feathering sequence of transition flapping sensitivity to a given mast angle of attack varies with rotor rotational speed. A typical variation of steady-state one-per-rev flapping response is given in Figure 13. These data were taken to establish a steady-state flapping response baseline for evaluating the transient

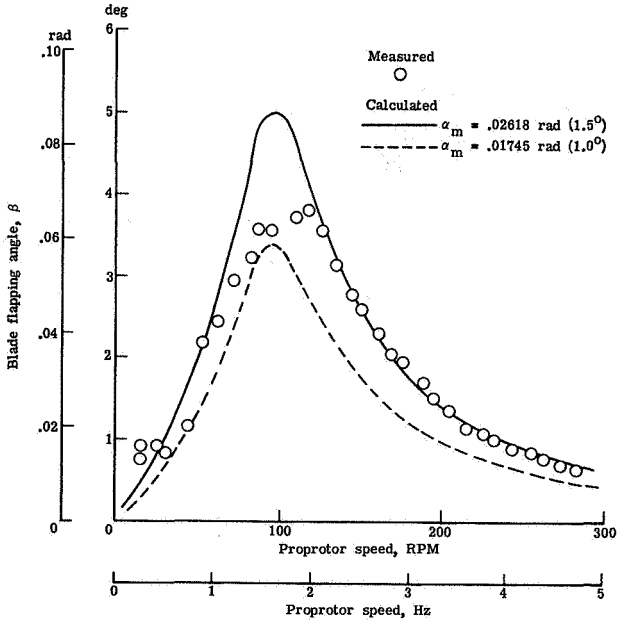

Figure 13. Variation of blade flapping with rotor rpm.

flapping response during the feathering portion of the test. Since the proprotor mast was not affixed to a rigid backup structure the wind-on mast angle of attack was not known (it was nominally 1°). The important conclusion following from Figure 13 is that the measured trend is predicted correctly. The peak in the flapping response occurs when the rotor rotational speed is in resonance with the flapping natural frequency in the rotating system.

Grumman Helicat (March 1971)

A wide variety of technical considerations confront the structural dynamicist in the design of a proprotor VTOL aircraft. Perhaps the most celebrated consideration has been that of proprotor/pylon whirl flutter, having been the concern of many investigators in both government and industry. Several years ago Baird[10] raised the question of whether proprotor whirl flutter, in particular forward whirl flutter, could be predicted with confidence. His skepticism was prompted by the lack of agreement between the experimental results obtained with several small models of flapping-blade propellers and the corresponding theoretical predictions.[4] To provide a large data base from which to assess the predictability of proprotor whirl flutter, a joint NASA/Grumman investigation was conducted in the transonic dynamics tunnel employing an off-design research configuration of a 1/4.5-scale semispan model of a Grumman tilt-rotor design designated "Helicat" (Fig. 14). This design is characterized

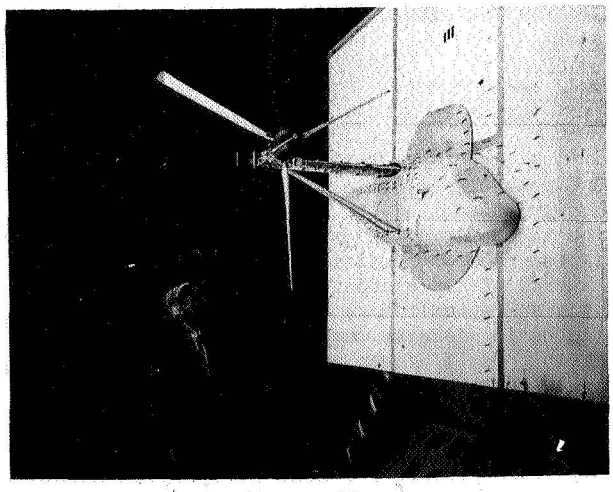

Figure 14. Grumman "Helicat" tilt-rotor model in whirl flutter research configuration.

by a rotor which incorporates offset flapping hinges in contrast to the Bell rotor in which the blades are rigidly attached to the hub which is in turn mounted on the drive shaft by a gimbal or universal joint housed in the hub assembly. The Helicat model was specifically designed to permit rather extensive parametric changes in order to provide a wide range of configurations. These variations included pylon pitch and yaw stiffness and damping, hinge offset, and pitch-flap coupling. To obtain flutter at low tunnel speeds, a reduced-stiffness pylon-to-wing-tip restraint mechanism which permitted independent variations in pitch and yaw stiffness was employed. The resulting pylon-to-wing attachment was sufficiently soft to insure that the wing was effectively a rigid backup structure. Details concerning this model as well as a summary of results are contained in Reference 11.

Some whirl flutter results are given in Figures 15 to 17, where flutter advance ratio $V_F/\Omega R$ is plotted versus pylon frequency nondimensionalized by the rotor speed. The effect of δ_3 on stability

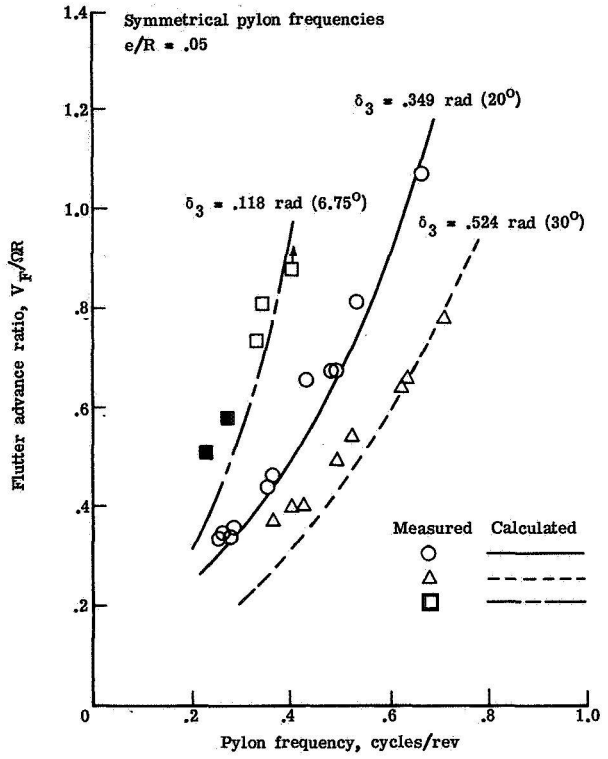

Figure 15. Effect of pitch-flap coupling on whirl flutter.

is shown in Figure 15 for the case in which the pylon pitch and yaw frequencies are identical and e/R set to 0.05. Many of the configurations were not exactly symmetrical in the frequencies. These data were adjusted to reflect a symmetric frequency support condition using Figure 18 of Reference 11. The results show a strong increase in flutter advance ratio (and hence flutter speed for a fixed rpm) with increasing pylon support stiffness and decreasing δ_3. All flutter was in the forward whirl mode except for the two points denoted by the solid symbols, which were in the backward mode. The analytical results shown assumed a symmetric frequency configuration and, since the structural damping varied somewhat, an average value of damping of $\zeta = 0.01$ in pitch and $\zeta = 0.02$ in yaw. The analytical results shown were obtained using the theory of Reference 6 which is based on the assumption of a gimbaled rotor. For analysis purposes the restoring centrifugal force moment from the offset flapping hinge was represented by introducing an

equivalent hub spring which preserved the blade in-vacuum flapping natural frequency in the manner indicated in Appendix B of Reference 6.

The beneficial effect of increased hinge offset is demonstrated in Figure 16. The results for the 13% hinge offset are particularly noteworthy

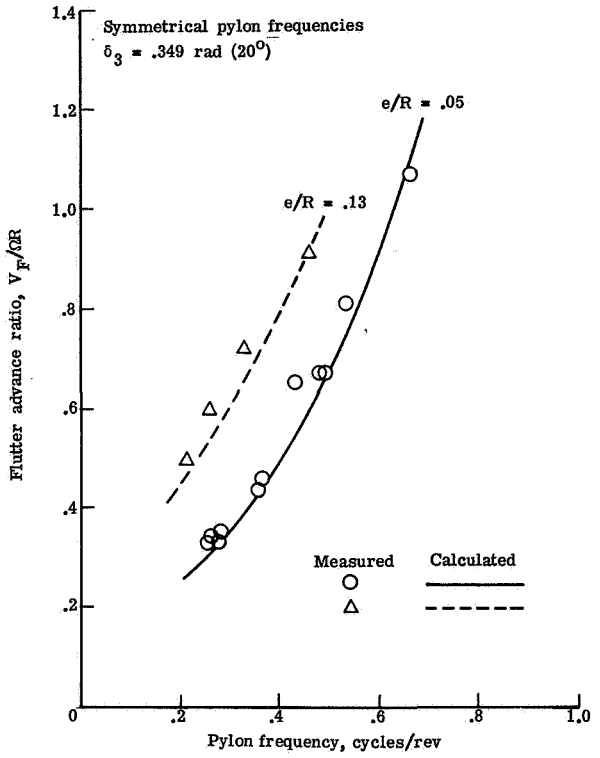

Figure 16. Effect of hinge offset on whirl flutter.

in that both forward and backward whirl motions were found to occur simultaneously; in effect, the flutter was bimodal. Theory also predicted this bimodal behavior, the forward and backward whirl modes being within a few knots of each other analytically.

The effect of asymmetry in the pylon support stiffness is shown in Figure 17. Again the symmetric frequency data reflect adjustments to true symmetry for configurations which were nearly, but not exactly, symmetric. The nonsymmetric results reflect actual measured values, the lower of either the pitch or yaw frequencies being plotted. It was analytically shown[6] that for sufficient asymmetry in the pylon support stiffness increasing the asymmetry more does not increase the flutter speed. The data for the nonsymmetric frequencies are an experimental demonstration of this fact. Flutter in all the asymmetric conditions was in the backward whirl mode.

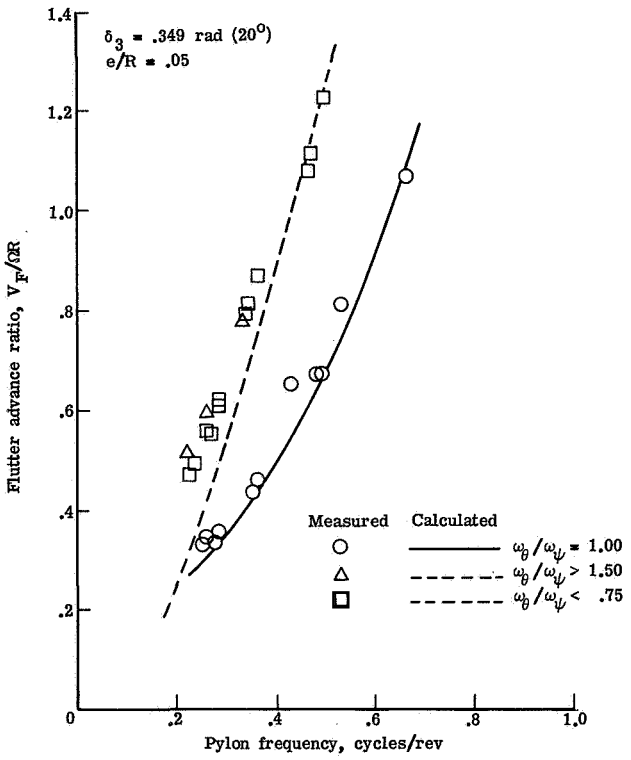

Figure 17. Effect of pylon support stiffness on whirl flutter.

Bell Model 300
(a) August 1971

A joint NASA/Bell investigation employing a 1/5-scale aerodynamic model of a Bell tilt-rotor design designated the Model 300 was conducted in the transonic dynamics tunnel in August 1971 for the purpose of providing the longitudinal and lateral static stability and control characteristics and establishing the effect of proprotors on the basic airframe characteristics in both air and freon. Use of freon permitted testing at full-scale Mach numbers and near full-scale Reynolds numbers. Flapping was measured in both air and freon for several values of tunnel speed over a range of sting pitch angles. The resultant flapping derivatives, obtained by evaluating the slopes of the flapping amplitude versus pitch angle curves, are shown in Figure 18. Since the range of inflow ratios over which the derivatives were measured was the same in air and freon and the test medium densities at the simulated conditions were about the same, an indication of the effects of Mach number on the flapping derivatives can be obtained by comparing the air and freon results. The speed of sound in freon is approximately half that in air so that for a given tunnel speed (or inflow ratio) the Mach number in freon is about twice that in air. The calculated results reflect the

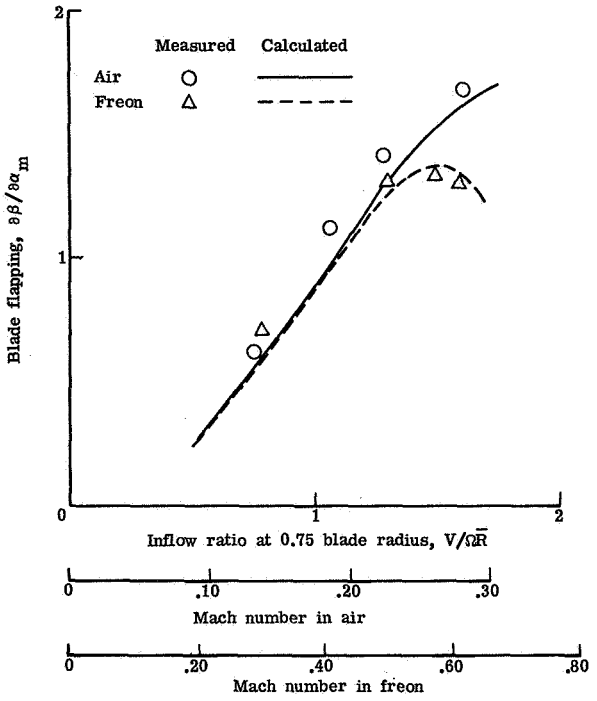

Figure 18. Effect of Mach number on proprotor flapping.

variation of δ_3 with blade pitch. Drag was neglected in the calculated results shown for air but was accounted for, in an approximate manner, in the results shown for freon.[6] The drag rise associated with operation at high Mach numbers is seen to reduce flapping as Mach number is increased and suggests that calculations based on the neglect of blade drag will predict conservative values of flapping at Mach numbers where drag is important.

These data are believed to be the first which provide an indication of the effects of Mach number on blade flapping.

(b) March 1972

The most recent investigation conducted in the transonic dynamics tunnel utilized a 1/5-scale dynamic and aeroelastic "free-flight" model of the Bell Model 300 tilt rotor for the purpose of demonstrating the required flutter margin of safety and to confirm that the aircraft rigid-body flight modes are adequately damped.[12] During this test the importance of rotor thrust damping on stability of the Dutch roll mode was investigated. This damping is associated with rotor perturbation thrust changes which can be generated during axial oscillations of the rotor shaft and constitutes a positive damping force on aircraft yawing motions.

The rotors of tilt-rotor aircraft are generally designed to have an interconnecting shaft between the two rotor/engine systems to provide synchronization of the rotor speeds and to insure that in the event of an engine failure either engine may drive both rotors. Interconnect shafting is also employed in wind-tunnel models. The availability of thrust damping to provide a stabilizing force for yawing motion is dependent on the structural integrity of this cross-shafting and has implications which are pertinent to both full-scale flight and model testing. Consider the case of a windmilling "free-flight" model. A fully effective interconnect maintains synchronization of the rotor speeds during any motions. A yawing motion of the model to the left, say, as might occur during a disturbance, generates blade angle-of-attack changes which decrease the lift of blade elements on the right rotor and increase the lift of blade elements on the left rotor. This produces resultant perturbation thrust changes which tend to damp the yawing motion, as depicted in the sketch in the right-hand portion of Figure 19. If the

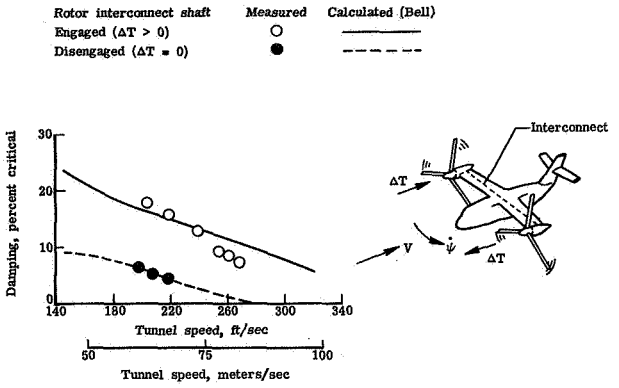

Figure 19. Thrust damping effects on tilt-rotor Dutch roll mode stability.

interconnect is absent, the rotors are able to maintain their inflow angle and, hence, angle of attack by increasing or decreasing rotor speed. The perturbation thrust changes thus go to zero and the stabilizing contribution of this damping to the aircraft yawing motion is lost. The effects of thrust damping on the stability of the Dutch roll mode was investigated by measuring the Dutch roll mode damping as a function of tunnel speed for the cases in which the model interconnect was engaged and disengaged. Some typical results are shown at the left of Figure 19 along with the damping levels predicted by Bell. The substantial contribution of thrust damping to total damping is quite apparent. It is of interest to point out that for the rotors contrarotating in the direction indicated in the sketch at the right of Figure 19 (inboard up) the perturbation thrust changes accompanying an aircraft rolling angular velocity are destabilizing on Dutch roll motion. For contrarotating rotors turning in the opposite direction (inboard down) the ΔT due to both yawing and rolling motion are stabilizing on Dutch roll motion.

Rotor rpm governors of the type which maintain rpm by blade collective pitch changes while maintaining constant torque are being considered for use on full-scale tilt-rotor aircraft. With the interconnect engaged, full thrust damping is available (assuming a perfect governor). However, in the event of an interconnect failure, the governors

would respond to any rpm changes by varying blade collective pitch in a manner which tends to maintain the original blade angle-of-attack distribution and hence torque. This is aerodynamically equivalent to the windmilling case with no interconnect. It is axiomatic that tilt-rotor aircraft must be designed to have stable Dutch roll characteristics should an interconnect failure occur anywhere within the flight envelope.

Some Additional Results Applicable to the Bell Model 300 Tilt Rotor

A dynamic test of a flight-worthy proprotor for the Bell Model 300 tilt-rotor aircraft was conducted in the NASA Ames full-scale wind tunnel in July 1970 (Fig. 20). Two different test stands

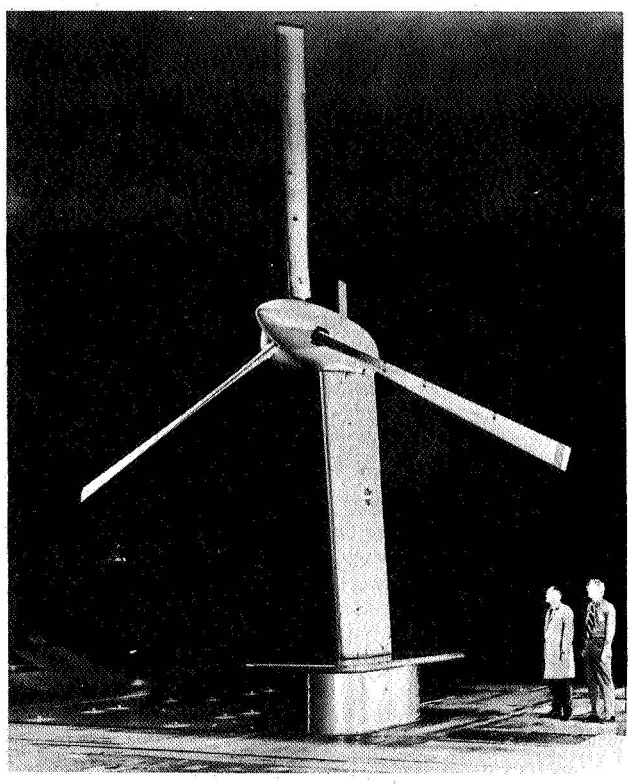

Figure 20. Bell 25-foot flight-worthy proprotor in NASA Ames full-scale tunnel for dynamic testing.

were used. One duplicated the actual stiffness characteristics of the Model 300 wing; the other was one-fourth as stiff. By using the reduced stiffness spar and operating the proprotor at one-half its design rotational speed it was possible to preserve the per-rev natural frequencies of the wing and simulate, at any given tunnel speed, the inflow of flight at twice that speed. This expedient did not, however, maintain the blade per-rev elastic mode frequencies or simulate compressibility effects on rotor aerodynamics.

Some results from the full-scale test are compared with data obtained from a test of a 1/5-scale model and theory in Figure 21. Note that

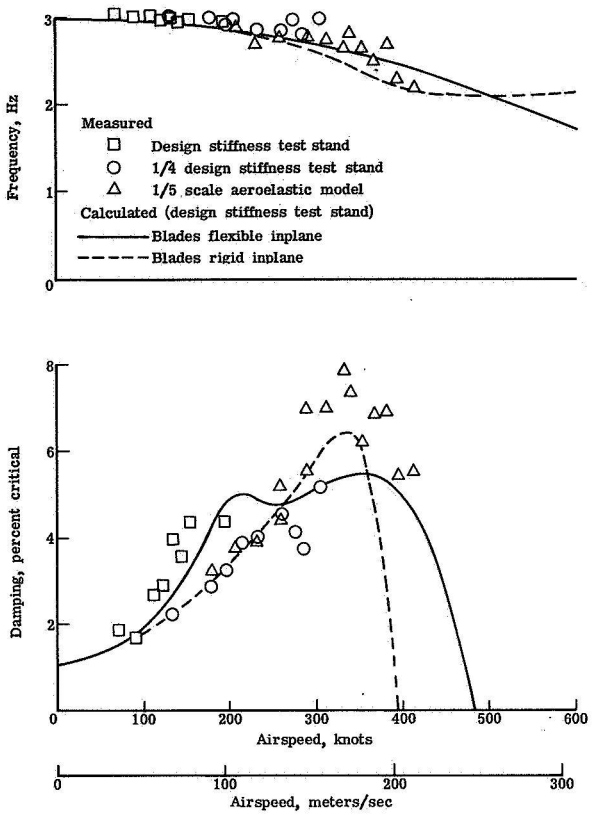

Figure 21. Model/full-scale comparisons of wing beam mode damping and frequency variation with airspeed for Bell Model 300.

the calculated results are based on the use of the design stiffness test stand characteristics. To provide for an indication of the effect of blade inplane flexibility on stability, the predicted results for the case in which the blades are assumed to be rigid inplane are also shown. The predicted increase in damping at about 103 m/sec (200 kts) for the case in which blade inplane flexibility is included is associated with coupling of the blade first inplane cyclic mode with wing vertical bending. For the range of tunnel speed over which full stiffness test stand data are available, the results are in good agreement with theory assuming flexible blades. Note that a significant stabilizing effect is predicted for the Model 300 as a consequence of blade inplane flexibility. This trend is in contrast to that predicted for the Model 266. The data for the quarter-stiffness test stand are in agreement with theory assuming rigid blades because operation at half the design rpm has effectively stiffened the blades by a factor of 4. The 1/5-scale model data are also seen to be in better agreement with analysis based on the assumption of rigid blades. This is because the model hub employed at the time the data were obtained was too stiff. If this increased stiffness is taken into account the predicted damping is in agreement with theory (Fig. 22). The model/full-scale comparisons shown in Figure 21 indicate that assessment of full-scale stability can be made on the basis of results of small-scale model tests.

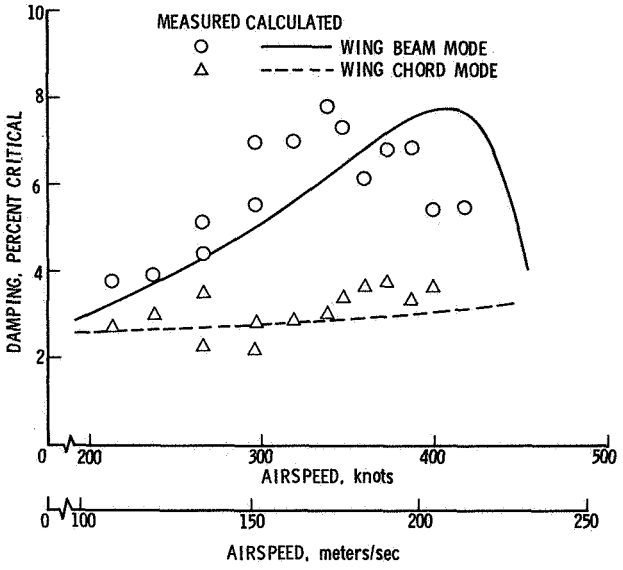

Figure 22. Variation of wing beam and chord mode damping with airspeed for 1/5-scale aeroelastic model of Bell Model 300.

Conclusions

An overview of an experimental and analytical proprotor research program being conducted within the Aeroelasticity Branch of the NASA Langley Research Center has been presented. On the basis of the particular results shown herein the following basic conclusions can be drawn:

(1) A proprotor/pylon/wing system can exhibit a wide variety of flutter modes depending on the degree of fixity of the pylon to the wing, rotor characteristics, and rotor rotational speed. In particular, for pylons which are rigidly affixed to the wing tip, the instability can occur in coupled pylon/wing, pylon/wing/rotor, or rotor modes; for pylons which are soft-mounted to the wing, a true whirl instability akin to classical propeller whirl flutter can occur.

(2) Lightly loaded proprotors operating at inflow ratios typical of tilt-rotor operation in the airplane mode of flight exhibit a marked sensitivity to gust excitation.

(3) Blade inplane flexibility can have a significant effect on stability.

(4) A significant contribution to aircraft lateral-directional (Dutch roll) stability arises from rotor thrust damping. Since the availability of this thrust damping is dependent on the integrity of the rotor interconnect shaft, tilt-rotor aircraft must be designed to have acceptable lateral-directional response characteristics should an interconnect failure occur anywhere within the operating envelope.

(5) Proprotor whirl flutter, both backward and forward, can be predicted with simple linearized perturbation analyses using quasi-steady rotor aerodynamics.

(6) For strength designed wings, wing aerodynamics have only a slight stabilizing effect on proprotor flutter speeds.

(7) The drag rise associated with proprotor operation at high Mach numbers reduces blade flapping and suggests that calculations based on the neglect of blade drag will predict conservative values of flapping at Mach numbers where drag is important.

The analytical portion of this research program is continuing. Attention is presently being directed toward refining the existing stability and response analyses and extending them by including additional degrees of freedom.

Acknowledgments

The author acknowledges the assistance provided by Bell and Grumman in preparing and testing the models employed in the investigations conducted in the transonic dynamics tunnel. Particular thanks are extended to Troy Gaffey of Bell for his general advice and assistance since the initiation of this research program and to Jerry Kohn of Grumman for performing the correlations with the data obtained during the whirl flutter investigation using the Helicat model.

References

1. Deckert, W. H., and Ferry, R. G., LIMITED FLIGHT EVALUATION OF THE XV-3 AIRCRAFT, Air Force Flight Test Center, Report TR-60-4, May 1960.

2. Hall, W. E., PROP-ROTOR STABILITY AT HIGH ADVANCE RATIOS, Journal of the American Helicopter Society, June 1966.

3. Edenborough, H. K., INVESTIGATION OF TILT-ROTOR VTOL AIRCRAFT ROTOR-PYLON STABILITY, Journal of Aircraft, Vol. 5, March-April 1968.

4. Reed, W. H., III., REVIEW OF PROPELLER-ROTOR WHIRL FLUTTER, NASA TR R-264, July 1967.

5. Gaffey, T. M., Yen, J. G., and Kvaternik, R. G., ANALYSIS AND MODEL TESTS OF THE PROPROTOR DYNAMICS OF A TILT-PROPROTOR VTOL AIRCRAFT, presented at the Air Force V/STOL Technology and Planning Conference, Las Vegas, Nevada, September 1969.

6. Kvaternik, R. G., STUDIES IN TILT-ROTOR VTOL AIRCRAFT AEROELASTICITY, Ph. D. Dissertation, Case Western Reserve University, June 1973.

7. Young, M. I., and Lytwyn, R. T., THE INFLUENCE OF BLADE FLAPPING RESTRAINT ON THE DYNAMIC STABILITY OF LOW DISK LOADING PROPELLER-ROTORS, Journal of the American Helicopter Society, October 1967.

8. Gilman, J., Jr., and Bennett, R. M., A WIND-TUNNEL TECHNIQUE FOR MEASURING FREQUENCY-RESPONSE FUNCTIONS FOR GUST LOAD ANALYSIS, Journal of Aircraft, Vol. 3, November-December 1966.

9. Yen, J. G., Weber, G. E., and Gaffey, T. M., A STUDY OF FOLDING PROPROTOR VTOL AIRCRAFT DYNAMICS, AFFDL-TR-71-7 (Vol. I), September 1971.

10. Baird, E. F., CAN PROP-ROTOR STABILITY BE PREDICTED?, presented at the Aerospace Flutter and Dynamics Council Meeting, San Francisco, California, November 12-14, 1969.

11. Baird, E. F., Bauer, E. M., and Kohn, J. S., MODEL TESTS AND ANALYSIS OF PROP-ROTOR DYNAMICS FOR TILT-ROTOR AIRCRAFT, presented at the Mideast Region Symposium of the American Helicopter Society, Philadelphia, Pennsylvania, October 1972.

12. Marr, R. L., and Neal, G. T., ASSESSMENT OF MODEL TESTING OF A TILT-PROPROTOR VTOL AIRCRAFT, presented at the Mideast Region Symposium of the American Helicopter Society, Philadelphia, Pennsylvania, October 1972.

COMPARISON OF FLIGHT DATA AND ANALYSIS FOR HINGELESS ROTOR REGRESSIVE INPLANE MODE STABILITY

by

W. D. Anderson
and
J. F. Johnston
Lockheed California Co.
Burbank, California

Abstract

During the development of the AH-56A, a considerable amount of analytical and experimental data was obtained on the stability of the regressive inplane mode, including coupling with other modes such as body roll and rotor plunge. The data were obtained on two distinctly different control systems; both gyro controlled, but one with feathering moment feedback and the other with direct flapping feedback. The paper presents a review of the analytical procedures employed in investigating the stability of this mode, a comparison of analytical and experimental data, a review of the effect of certain parameters, including blade droop, sweep, δ_3, α_1, vehicle roll inertia, inplane frequency, rpm and forward speed. It is shown that the stability of this mode is treatable by analysis and that adequate stability is achievable without recourse to auxiliary inplane damping devices.

Notation

B subscript referring to blade feathering

$C_{1/2}$ measure of damping, cycles to half amplitude

F subscript referring to fuselage

g structural damping ratio

I imaginary part of root, rad/sec

K_{θ_o} collective feathering stiffness, ft-lb/rad/blade

K_β root flapping moment per unit of blade flapping, ft-lb/rad

L rotor lift, pounds

M moment, ft-lb

M_{xy} blade product of inertia about feathering axis, slug-ft^2

N_R normal rotor speed

R real part of root, per second, subscript referring to rotor, or rotor radius, ft

V airspeed, knots

X_F airframe longitudinal motion, ft

Y_F airframe lateral motion, ft

Z_F airframe vertical motion, ft

α_1 pitch lag coupling - positive nose up feather due to lag aft of blade

β_o rotor blade collective flapping or coning, radians

δ_3 pitch flap coupling angle - $\tan^{-1}(-\theta/\beta)$

∂ to indicate partial differentiation

ϵ_x rotor blade cyclic inplane motion sine component, positive forward, radians

ϵ_y rotor blade cyclic inplane motion cosine component, positive to the right, radians

ζ fraction of critical damping

θ pitch motion, radians

θ_0 blade collective feathering, radians

λ blade effective sweep angle, radians

τ_s servo time constant, sec

ϕ roll motion, radians

ω frequency, rad/sec

ω_{nip} inplane natural frequency, rad/sec

Ω rotor rotational speed, rad/sec

Presented at the AHS/NASA-Ames Specialists' Meeting on Rotorcraft Dynamics, February 13-15, 1974.

In hingeless rotors two fundamental types of coupled rotor body inplane mode stability problems exist. One is associated with a soft inplane system having the inplane frequency less than rotational speed, and the other with a stiff inplane system where the inplane frequency is above rotational speed. The soft inplane system when coupled with a basic body mode is unstable in the absence of aerodynamics, and therefore its stability must be provided by aerodynamic or auxiliary damping. This type of system is discussed in References 1, 2, and 3. In contrast, the stiff inplane system does not exhibit this inherent mechanical instability, and so its stability is less dependent upon aerodynamic or auxiliary damping.

Both types of modes, however, are subject to aeroelastic phenomena which can be stabilizing or destabilizing. Also, both types can exhibit response characteristics caused by pilot and/or gust inputs which are undesirable. The critical inplane mode in the soft inplane system is advancing in the stationary system, whereas for the stiff inplane system, the mode is regressive. The frequency of the mode in each case is the magnitude of ($\omega_{nip} - \Omega$) or ($\Omega - \omega_{nip}$).

This paper deals specifically with the stiff inplane system. The various types of coupled rotor body regressive inplane stability/response problems associated with this type of system are discussed. The paper deals with both a feathering moment feedback gyro-controlled system and a direct flapping moment feedback gyro-controlled system.

These two types are described in more detail in Reference 4. The inplane mode characteristics of the direct flapping moment feedback type system would be more characteristic of any direct control hingeless rotor system employing a stiff inplane rotor.

The stiff inplane hingeless rotor system is worthy of serious consideration because of its inherent characteristics of being free from ground/air resonance mechanical instability type phenomena and its ability to provide a stable, highly maneuverable, rotary wing vehicle.

The absolute level of the stability of the inplane mode is not the only consideration in establishing design criteria. An equal or even more important criterion is that of response of the mode as a result of pilot or gust disturbances. The stability of the mode can appear adequate, but if it is easily excited by either pilot or gust inputs, the mode can be unsatisfactory. Conversely, the mode may exhibit very low damping characteristics, but not be easily excited by either pilot and or gust excitations, and be quite satisfactory because no high loads or undesirable body motions occur.

Besides the basic stability considerations of the regressive inplane mode, certain other basic types of coupled rotor body regressive inplane mode stability/response problems may be encountered. Some of these may be either low or high airspeed phenomena or virtually independent of airspeed.

It is not intended here to go into a complete theoretical treatise describing each of these types of phenomena, but the effects of some parameters and flight conditions on stability/response characteristics for particular rotor vehicle configurations are presented. Because stability and response characteristics depend on considerations of the detail design, generalized conclusions cannot always be drawn as to the effect of each parameter discussed.

The fundamental types of regressive inplane mode stability/response problems discussed include those associated with:

- The basic regressive inplane mode.
- The coupled regressive inplane body roll mode.
- A coupled regressive inplane-roll-rotor plunge mode.

The first type can exhibit itself to the pilot as an apparent rotor weaving or rotor disc fuzziness with very little body response. The second type appears to the pilot as rotor tip path plane response and body roll or just body roll oscillation. Depending on the frequency of this mode, and the gain of the feed forward loop of the control system, this mode may be subject to pilot-induced or pilot-coupled oscillations. The last type basically exhibits itself to the pilot as a rotor umbrella mode and a vertical plunge of the vehicle. This mode can exist in the absence of the inplane mode but can be seriously affected by its presence. The mode has been characterized as a "Hop" mode because of the plunge response of the airframe.

Analytical Method

The analytical method employed in the study consists of a fundamental 13-degree-of-freedom representation of the coupled rotor body control system. The body is characterized by 5 degrees of freedom – yaw being ignored. Likewise, the rotor is represented by eight multiblade coordinates including rotor disc plunge, pitch and roll; lateral and longitudinal inplane; and pitch, roll, and collective elastic feathering/torsion. The model is shown schematically in Figure 1. The equations are solved as linear constant coefficient equations, modified as required to represent the control system being considered.

For the solutions shown, certain simplifying assumptions were made. These include neglecting the effects of retreating blade stall, reverse flow, and advancing tip Mach number.

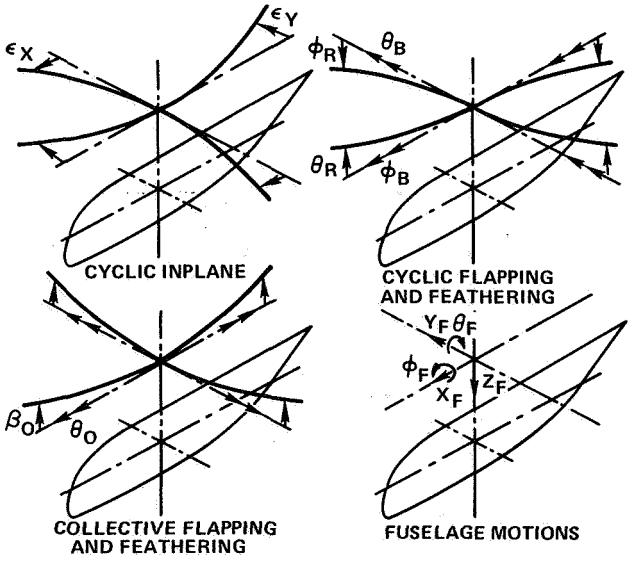

Figure 1. Description of Analytical Model.

The model includes the effects of elastic coupling phenomena of inplane moments times flapping deflections causing feathering moments. A simplified inflow model is used which characterizes the induced velocity from low transition speed to high speed as a trapezoidal distribution with upwash at the front of the rotor and downwash at the back of the rotor, for positive rotor lift.

To gain a fairly comprehensive understanding of such modes as the regressive inplane mode as well as the other coupled rotor body fundamental aeroelastic modes, it is felt this type of model is a necessity.

Effect of Parameters

Following is a discussion of each type of mode and the relevant parameters which affect the stability/response of the mode together with some parametric effects.

Basic Regressive Inplane Mode

The basic regressive inplane bending mode can be lightly damped without any problem, provided it is not easily excited by the pilot or by gusts. The mode if its frequency is well separated from any other rotor body control mode frequencies, behaves very much as a single blade would behave.

Figure 2 shows a complex plane plot of a typical mode of response of the regressive inplane mode. It is noted that motions of all other degrees of freedom are small compared with the response of the blade inplane ϵ_x and ϵ_y. This would be for a case where the inplane mode frequency is well separated from other rotor-body control mode frequencies, and the inter-coupling with these modes is not large. In this case the inplane mode is reasonably above the body roll mode, with a frequency ratio of 1.32 in nonrotating coordinates.

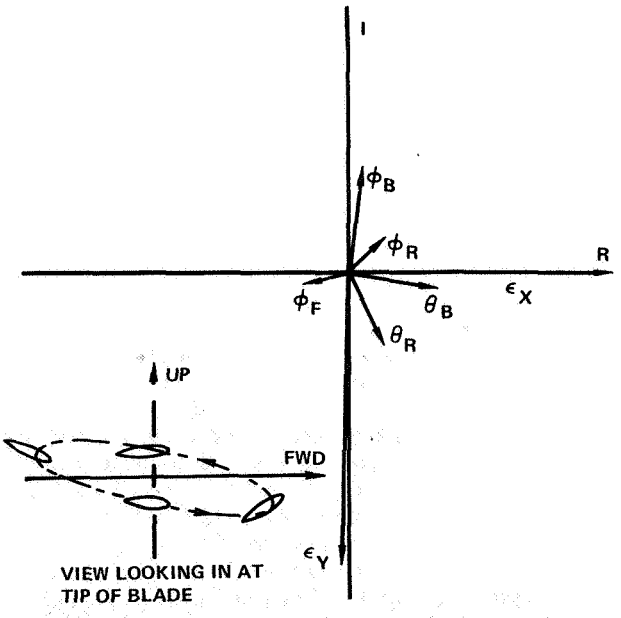

Figure 2. Complex Plane Plot of Typical Regressive Inplane Mode, V = 20 KN, $\omega_\epsilon/\omega_{Roll} = 1.32$.

For this case, the effect of several parameters is examined. The stability/response of the mode is largely controlled by such parameters as discussed in Reference 4 and 5. That is, parameters such as blade kinematic and elastic pitch-flap-lag couplings are extremely important. Also, such items as precone, feather bearing location, hub/blade stiffness distributions and control system flexibility play important roles in the stability of the mode. A discussion of each of several parameters affecting the stability of the mode follows.

Inplane Damping. Figure 3 shows a locus of roots as a function of equivalent structural damping in the inplane mode. Identified on this figure are lines of constant damping in terms of one over cycles to half amplitude, $1/C_{1/2}$. This figure shows the expected results. That is, computing the approximate change in fraction of critical damping from the root locus plot by taking an increment of change in the real part of the root due to the change in modal structural damping, g_{ST}, and dividing it by the sum of the imaginary part of the root and rotational speed results in a value of damping roughly half the change in equivalent structural damping. This is consistent with the well known relationship of $g \simeq 2\zeta$ where $g << 1$.

Since some centrifugal stiffening effect is existant in the inplane mode, the actual change in damping, 2ζ, is less than the change in equivalent structural damping in the mode.

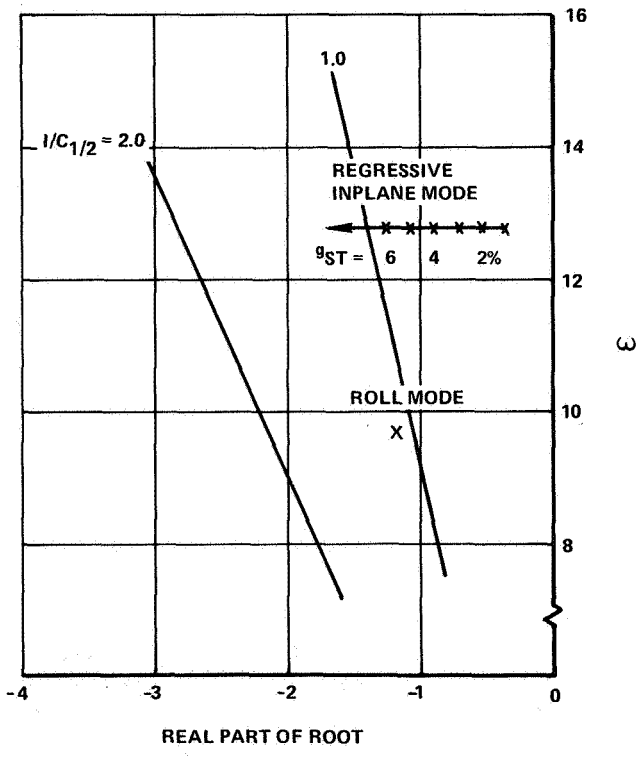

Figure 3. Locus of Roots – Effect of Structural Damping, V = 20 KN.

Kinematic Pitch Lag Coupling. Figure 4 shows the change in damping due to a variation in pitch lag coupling. The indicated sense of this coupling for improved stability is nose down feathering due to lag aft of the blade for the stiff inplane system whereas Reference 6 showed that the opposite coupling is stabilizing for articulated or soft inplane system. The effect of this parameter on the stability of the regressive cyclic inplane mode is similar to the effect on the stability of the reactionless inplane mode as indicated in Reference 5. The fundamental mechanism of the α_1 coupling is to cause blade flapping to couple through coriolis forces to damp the inplane mode. This can be deduced by examining Figure 2.

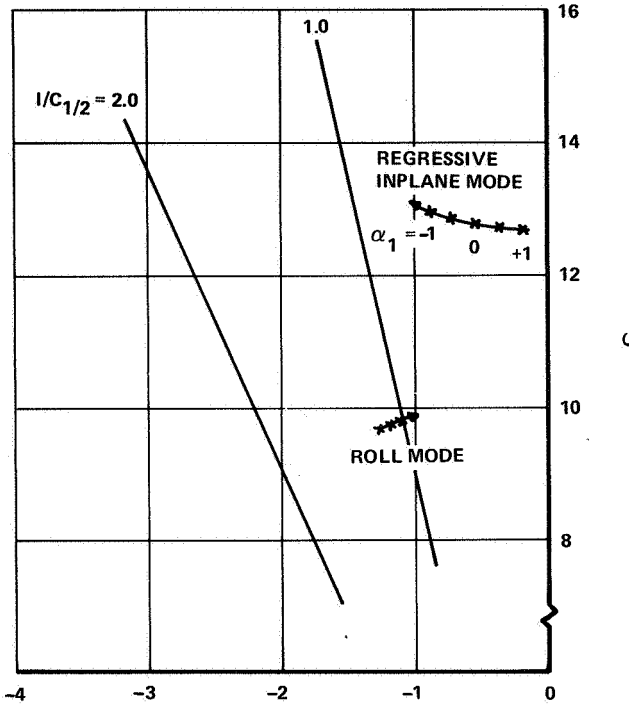

Figure 4. Locus of Roots – Effect of Pitch Lag (α_1) coupling, V = 20 KN.

A schematic of the response of a single blade for this mode looking in at the blade tip is shown in the lower left corner of Figure 2. The response shown is a stable response. With the inplane frequency above the basic flapping frequency, nose up blade feathering when the blade is forward, positive α_1, will cause the blade to flap up as the blade is going aft. The up flapping velocity of the blade generates a Coriolis force which reduces the inplane motion.

Blade Droop. Blade droop is the built in vertical angular offset of the blade below the feathering axis (see Reference 5) and causes an elastic pitch lag coupling which is similar in effect to stabilizing α_1 coupling. The droop effect though is somewhat more effective in stabilizing this particular mode since some additional phase lag results in the response of the elastic blade feathering which improves the amount of flap induced Coriolis damping in the mode. This is accomplished through an increment of up flapping velocity at the time the blade is moving aft, causing a Coriolis force forward to reduce the inplane motion. The effect of blade droop on the regressive inplane mode is shown in Figure 5.

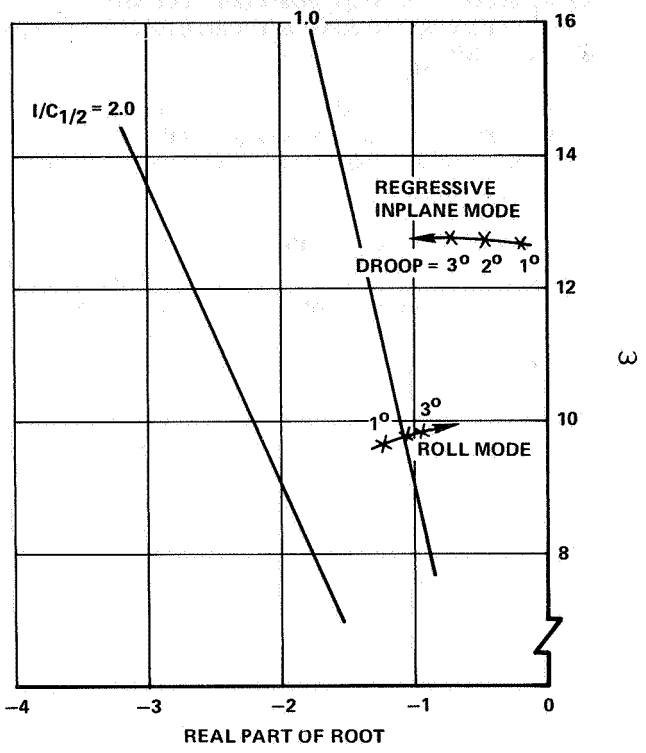

Figure 5. Locus of Roots – Effect of Blade Droop Angle, V = 20 KN.

An additional insight into the effect of droop on the characteristics of the system is shown in Figure 6. Shown is a predicted frequency response of inplane response and of vehicle roll rate response due to lateral stick excitation as a function of excitation frequency. It is noted that the inplane becomes quite responsive at low values of blade droop. It is also noted that even with the fairly large separation of the roll mode and inplane mode frequency, an influence of blade droop is seen on the roll mode. This influence is seen to make an increase in the peak response of roll rate at its peak response frequency with increasing blade droop.

Other Parameters. Other parameters such as built in blade sweep forward or aft of the feathering axis, δ_3 coupling, control system flexibility, stiffness distribution of the blade and hub and location of the feather bearings influence the stability of this mode. Again, it is pointed out that the influence of each parameter depends to a large part on the detail design. However, in general, for a stiff inplane hingeless rotor, couplings which result in nose down feathering due to lag aft of the blade add damping to the regressive inplane mode. Also, with the inplane mode frequency above the flapping mode frequency, couplings which act as a negative spring increment to the flapping mode or a positive spring increment to the inplane mode are stabilizing to the inplane mode. These couplings may, however, influence the stability/response characteristics of other modes, in particular the roll mode.

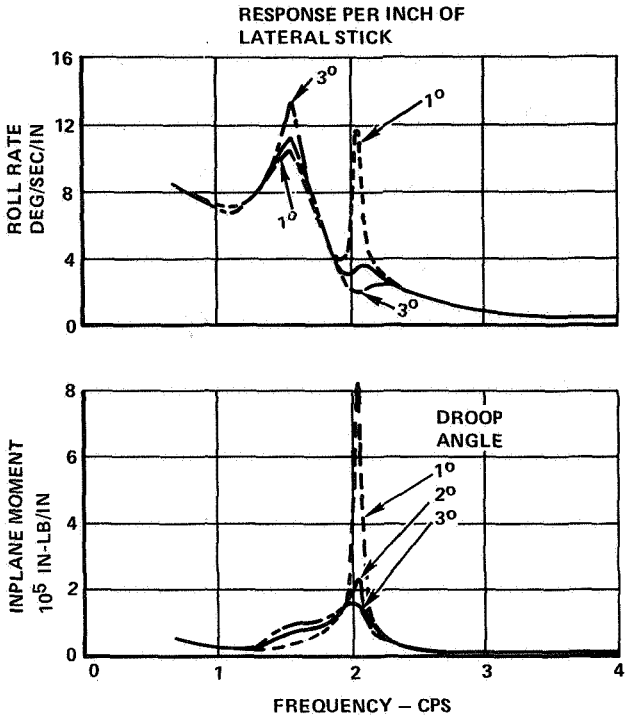

Figure 6. Effect of Blade Droop on Inplane and Vehicle Roll Frequency Response Characteristics, V = 20 KN.

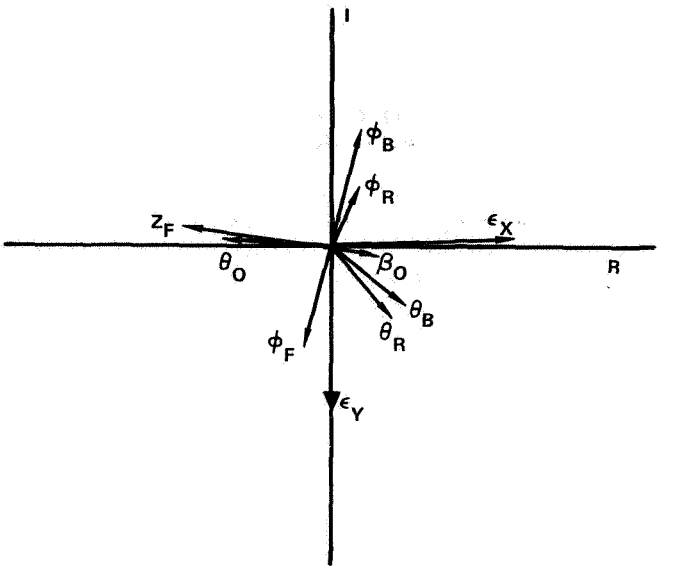

Figure 7. Complex Plane Plot of Typical Coupled Regressive Inplane Roll Mode, V = 160 KEAS, $\omega_\epsilon/\omega_{Roll} = 1.1$.

Coupled Regressive Inplane Body Roll Mode

Next is considered the coupled regressive inplane bending-body roll mode where the frequency of the inplane mode and of the roll mode are nearly coalescent. Figure 7 is a complex plane plot of a typical coupled regressive inplane-roll mode for a direct flapping moment gyro control type system where the inplane to roll mode frequency ratio is 1.1. Comparing this figure with Figure 2, it is noted that the roll response of the airframe relative to the inplane is significantly larger in this mode. In this case, the phase relationships between inplane, the rotor pitch and roll, and the cyclic blade angle are still in a damping phase for the inplane but the rotor roll-airframe roll phasing is such as to provide a slight driving to the airframe roll motion. For this particular case, the net damping of the regressive inplane mode would be somewhat reduced. Again, a discussion on the effect of significant parameters which influence the characteristics of this mode follows.

Inplane Frequency. Figure 8 shows the influence of inplane frequency on coupled regressive inplane bending-roll mode damping. Data are shown for a low-speed, 20-knot case and a high-speed, 235-knot condition (compound helicopter flight mode). It is interesting to note that at low speed, the roll mode loses damping due to frequency coalescence whereas at the high-speed condition, it is the inplane mode that tends to lose stability.

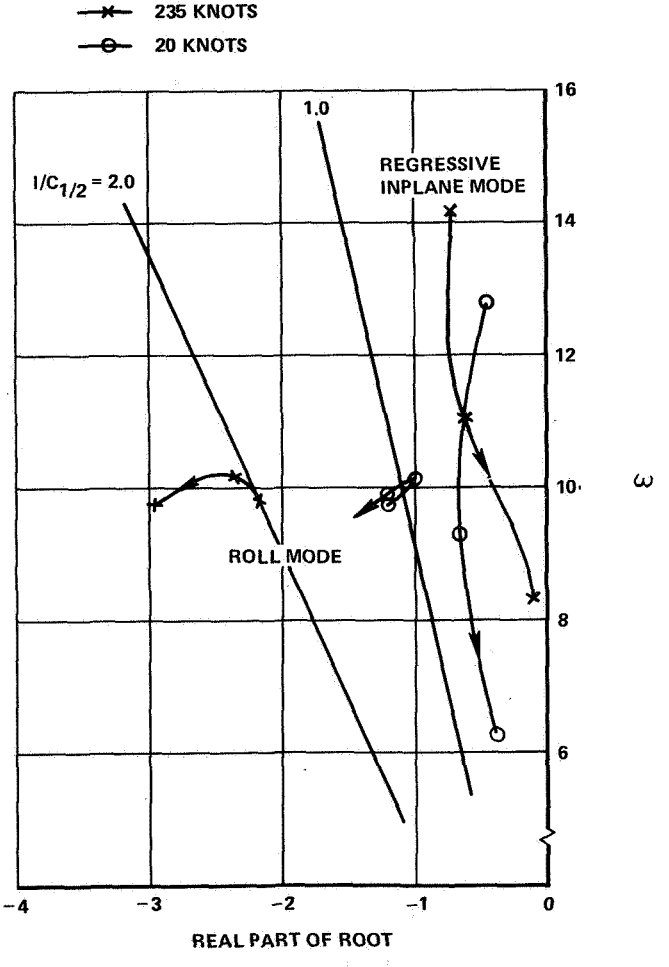

Figure 8. Locus of Roots – Effect of Inplane Frequency.

Blade Droop. The influence of blade droop, where the inplane mode and roll mode frequencies are close, is shown in Figure 9. These data show a significant effect of droop on the tradeoff of damping between the two modes. It is noted that increasing droop has a significant effect in increasing the damping of the inplane mode, but an equally significant effect in reducing the damping of the roll mode.

Vehicle Roll Inertia. Figure 10 shows the influence of vehicle roll inertia. In the case shown, a small reduction in damping of the regressive inplane mode and a significant improvement in damping of the roll mode result from increasing the roll inertia. A reduction in roll frequency is also seen. Ordinarily, a roll mode in the 0.6 to 1.3 Hz frequency region, with the damping sufficiently low, can be subject to pilot-coupled oscillations. As can be seen from Figure 10, this problem is avoided by the corresponding large increase in damping of the roll mode as the frequency decreases into this range with the increasing roll inertia.

Pitch Flap (δ_3) Coupling. The influence of pitch-flap coupling on coupled regressive inplane-roll mode stability is shown in Figure 11. This figure shows the inplane mode to be little affected by δ_3 coupling with flap-up, pitch-down coupling being slightly stabilizing. The effect on the roll mode is to increase its frequency with positive coupling and also to improve its damping. The inplane mode frequency is decreased as was expected, but the damping increase was not expected. For a case (not shown) where the inplane frequency was considerably above the roll mode frequency, the influence of the more positive pitch flap coupling was to destabilize the inplane mode slightly with a more significant effect of improving the stability of the roll mode.

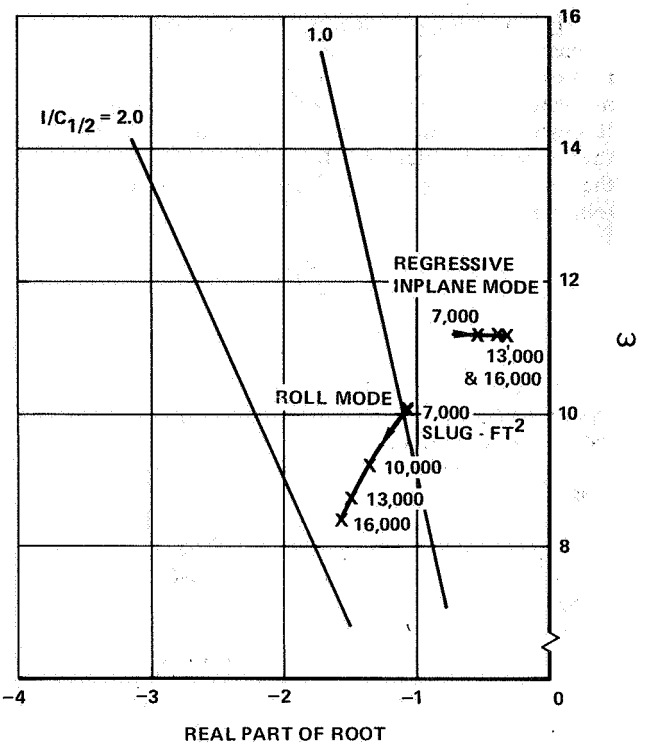

Figure 10. Locus of Roots – Effect of Airframe Roll Inertia, V = 20 KN.

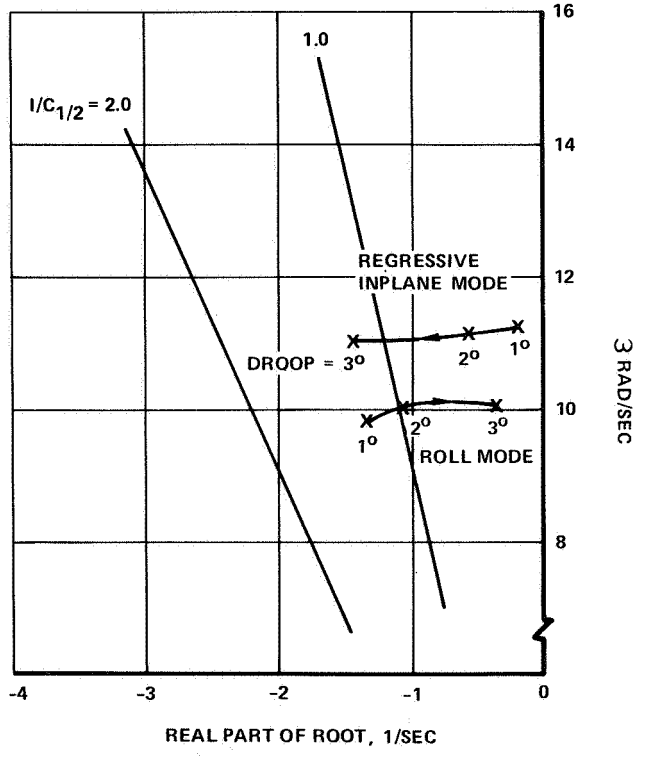

Figure 9. Locus of Roots – Effect of Blade Droop Angle, V = 20 KN.

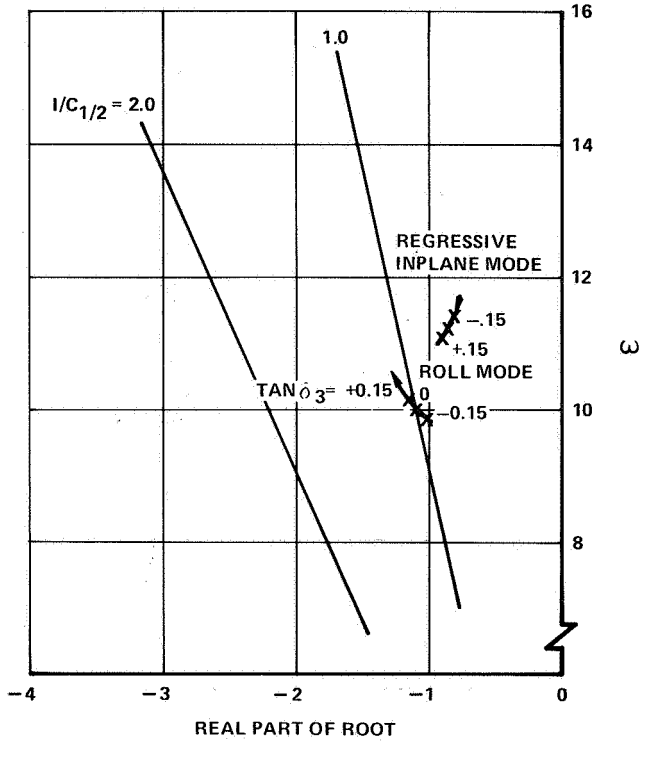

Figure 11. Locus of Roots – Effect of Pitch Flap (δ_3) Coupling, V = 20 KN.

Feedback Ratio. Feedback ratio, λ, is the ratio of the moment applied to the control gyro by rotor cyclic flapping moment or shaft moment to the corresponding rotor shaft moment. This parameter is described in detail in Reference 4. It is used both to prevent excessive rotor shaft moments while the vehicle is in contact with the ground, and to aid in tailoring the vehicle handling qualities. This ratio is defined by the following equation:

$$\lambda = \frac{M_{gyro}}{M_{shaft}}$$

The influence of this parameter on coupled roll regressive inplane mode stability is fundamentally on the roll mode. As shown in Figure 12, increasing the magnitude of this parameter increases the frequency of the roll mode and reduces its damping while increasing the damping of the inplane mode.

Servo Time Constant. For the configuration being discussed, the blade cyclic feathering is obtained through irreversible servo actuators which are slaved to the control gyro. The lag in the servos then causes a lag in the response of the cyclic blade feathering as commanded by the control gyro. The influence of the cyclic servo time constant is shown in Figure 13. It is noted that the effect of increasing servo time constant is to reduce the frequency and damping of the roll mode and the damping of the inplane mode. The effect of the cyclic servo time constant becomes increasingly important with increasing speed in determining the damping of the third type of mode, discussed below.

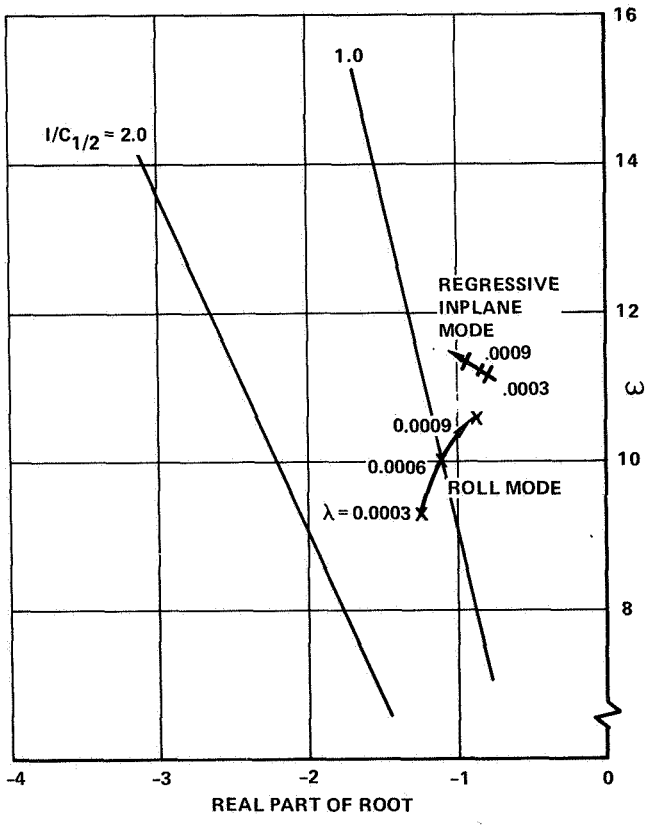

Figure 12. Locus of Roots – Effect of Feedback Ratio, V = 20 KN.

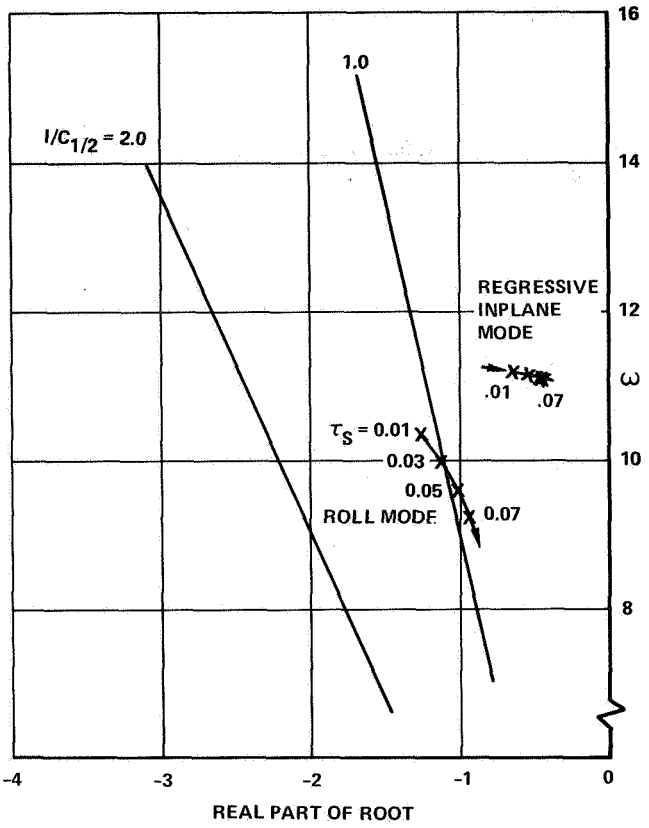

Figure 13. Locus of Roots – Effect of Cyclic Servo Time Constant, V = 20 KN.

Coupled Regressive Inplane-Roll-Rotor Plunge Mode

This mode is most critical in high-speed flight. It has been characterized as a Hop mode because plunging of the rotor disc results in a vertical bounce of the airframe. The parameters strongly influencing the stability of this mode in a feathering moment feedback system are inplane frequency, collective control stiffness, pitch-flap coupling, blade product of inertia relative to the feathering axis and blade sweep. A typical mode shape for this type of mode is shown in Figure 14. It is noted that a considerable amount of rotor inplane pitching, rolling and plunging, and airframe vertical and rolling motion occurs. The mode may become critical with increasing speed if the rotor plunge mode and coupled roll inplane mode are allowed to approach coalescence.

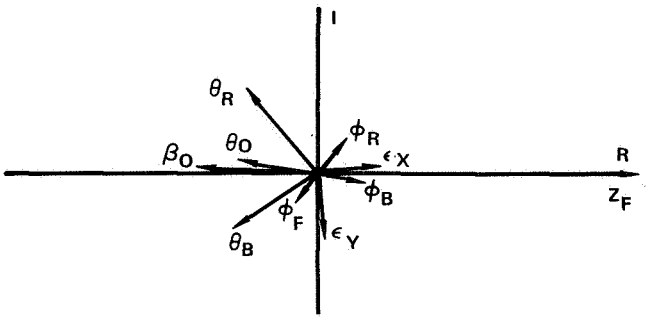

Figure 14. Typical Mode Shape of Coupled Regressive Inplane Bending – Roll – Rotor Plunge Mode, V = 180 KEAS.

This coalescence can be caused by the influence of several factors. First, any couplings that cause the rotor plunged mode to decrease in frequency with increasing forward speed may cause coalescence. This can be due principally to collective control system flexibility, blade sweep, adverse pitch-flap coupling and blade product of inertia effects; all affecting the collective pitch response to vehicle normal acceleration or rotor coning. On a first-order basis, a negative or positive aerodynamic spring on the collective plunge or coning mode of the rotor can be expressed by the following equation:

$$\frac{\partial L}{\partial \theta_o} = \frac{1}{K_{\theta_o}} \left(K_{\theta_o}\ \delta_3 - \Omega^2 \Sigma\, Mxy - \lambda K_\beta \right) \frac{\partial L}{\partial \Theta_o}$$

where $\frac{\partial L}{\partial \Theta_o}$ approximately doubles between hover and 120 knots.

Another source of coalescence or near coalescence can be due to the coupled roll-inplane mode increasing in frequency with increasing speed. As the lift due to collective blade angle increases with speed, so do the aerodynamic derivatives associated with the cyclic motions of the rotor disc, and the aerodynamic coupling terms between cyclic and collective rotor disc motions. Any kinematic or aeroelastic couplings that phase these aerodynamics to act to stiffen the coupled roll inplane mode with increasing speed will cause an increase in the frequency of this mode with speed.

Absolute coalescence of these two modes is not necessary for instability to occur. Both coupling between the modes and frequency proximity are key to stability. Couplings which cause cyclic aerodynamic forces or moments due to lift or plunge response of the rotor, which in turn result in cyclic response of the rotor disc which cause rotor disc lift or plunge driving forces, can be destabilizing. When these couplings are sufficiently strong and properly phased, the system will be unstable.

The significant aerodynamic coupling terms between these two modes, which are strongly affected by forward speed, are a rolling moment on the rotor due to change in collective blade angle, a pitching moment on the rotor due to change in coning of the rotor, and lift or plunge aerodynamic loadings due to roll velocity of the rotor or to change in longitudinal cyclic blade angle. These are direct aerodynamic couplings between these two modes.

Indirect aerodynamic couplings exist through the inplane response of the rotor system. This is particularly true in a feathering moment feedback system, because relatively high inplane exciting forces are generated as a result of changes in rotor lift. The resulting inplane responses can couple through blade static and elastic coning relative to the feather axis and cause perturbational cyclic feathering responses. These cyclic featherings result in aerodynamic forces which can be either stabilizing or destabilizing.

Again Figure 14 shows a typical mode shape or eigenvector for this type of coupled roll-regressive inplane bending rotor plunge mode. In this case, which happens to be stable but lightly damped, the collective feathering is at an amplitude and phase with respect to β_o, collective coning of the rotor, to act as a negative aerodynamic spring on the coning mode. Likewise, θ_o, collective blade angle, acts in conjunction with longitudinal cyclic blade angle in causing the rotor to pitch up. As can be seen from this figure, the rotor pitch response is lagging the collective blade angle response by approximately 45 degrees, whereas the coning response is actually leading the collective blade feathering response by a small phase angle.

Further examination of Figure 14 shows that the coning response, in addition to the rotor pitch response, is also being driven by longitudinal cyclic blade angle. It is interesting to note that the lateral inplane response is leading the rotor coning response by approximately 90°. Positive lift on the rotor combined with lateral cyclic blade angle causes a lateral inplane excitation. Positive lift results in an increase in lateral inplane bending to the left, which is aft bending on the aft blade and forward bending on the forward blade. The fact that the lateral inplane response is lagging its excitation by approximately 90° and the response is virtually pure regressive indicates that the inplane mode is very close to being in resonance. The inplane response, in coupling through the feathering axis, is a prime source of the longitudinal cyclic blade angle.

Even though the mode shown in Figure 14 is stable, one can see the potential for the mode to lose damping, which it does for the case shown, with increasing air speed. Lift and rotor disc rolling moment due to θ_o and longitudinal cyclic both increase with air speed, as well as rotor disc pitching moment, due to coning of the rotor. These aerodynamic terms in conjunction with the inplane aerodynamics due to rotor coning are the principal coupling terms between rotor disc plunge and coupled roll regressive inplane response. It is through these terms and the choice of rotor/control system parameters that the coupled rotor vehicle system can be made to have adequate damping at high speed.

Figure 15 shows the effect of pitch flap coupling, blade product of inertia, control system collective stiffness, and blade sweep which, as indicated earlier, are key parameters in influencing the stability of this mode.

Studies are also presented for the stability characteristics of this type mode, for the direct flapping moment feedback type control system. In this system, one other parameter was intro-

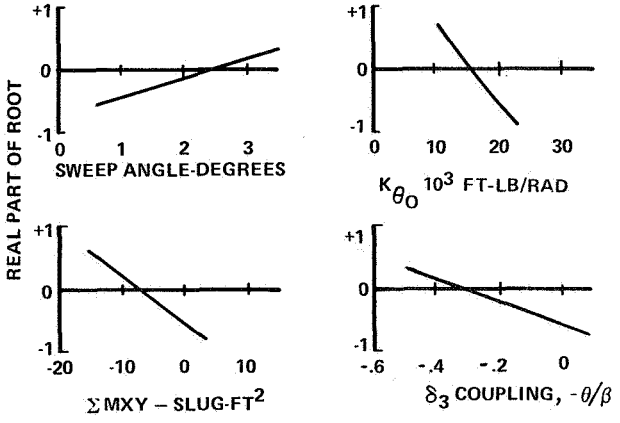

Figure 15. Effect of Parameters on Stability of Coupled Regressive Inplane Bending – Roll – Rotor Plunge Mode, V = 180 KEAS.

duced which has a significant effect on this mode. The parameter is the time constant or frequency response characteristic of the main power cyclic actuators. It is through these actuators that the control gyro commands cyclic blade feathering. As indicated earlier, a lag in the servo response results in a lag in the cyclic blade feathering, which can have an adverse effect on the stability of the hop mode. Inasmuch as the hingeless rotor depends on corrective control such as by stabilizing gyro to prevent pitchup at high speed, it is recognized that lag in the corrective control may lead to dynamic instability. This influence or effect is shown in Figure 16.

Figure 16 shows also the effect of δ_3 coupling as well as collective control system stiffness and inplane frequency.

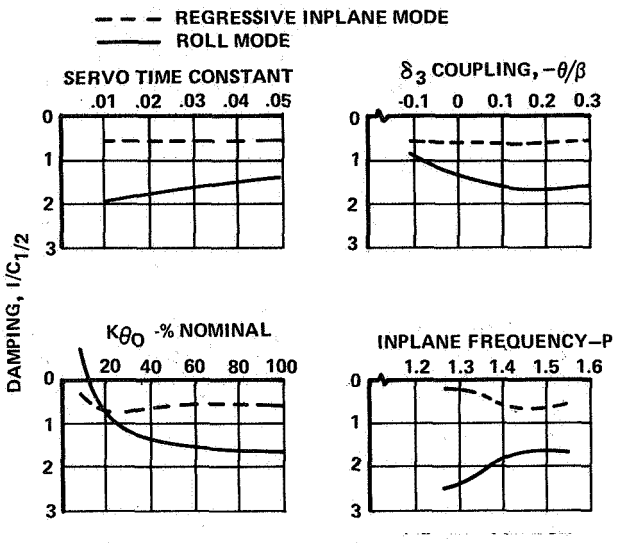

Figure 16. Effect of Parameters on Rotor Vehicle High Speed Dynamic Stability – Direct Flapping Moment Feedback Control System, V = 280 KEAS.

Experimental and Analytical Comparison

The experimental and analytical comparison is based upon data obtained during the development of the AH-56A. Early in the development of the AH-56A, a vehicle equipped with an experimental rotor system in which the blades had been modified by adding torsional doublers encountered a dynamic Hop phenomenon. The principal effect of the torsional doublers on this mode was to lower the inplane frequency and cause it to become more critically coupled with the rotor plunge/body roll mode. An analytical study was undertaken to define this phenomenon which extended the coupled rotor body linear analysis method available at that time and led to the development of the linear math model discussed earlier.

Figure 17 shows a comparison of the experimental and analytical data obtained for the vehicle configuration which initially encountered the Hop or coupled roll-regressive inplane bending-rotor plunge mode phenomenon. Additionally, the following table summarizes the normalized roll rate, chord moment and collective control load comparison obtained for this condition. In both the experimental and analytical data, the responses are due to a roll doublet excitation and are normalized on vehicle c.g. vertical acceleration.

	95% N_R		100% N_R	
	Test	Analysis	Test	Analysis
Roll Rate, deg/sec/g	20	19.1	15.5	9.2
Collective Control Load, lb/g	2700	2820	2370	2610
Inplane Moment, in. lb/g	424K	420K	770K	670K
Frequency Ratio, ω/Ω	0.52	0.51	0.54	0.54
Speed, KEAS	190	180	178	180

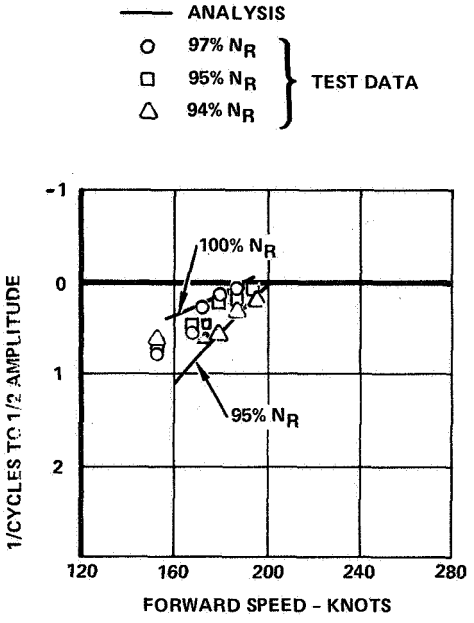

Figure 17. Comparison of Theory and Test Damping vs Speed For Initial Encounter With Hop on Early AH-56A Development Configuration.

The loss in damping was caused by a coalescing of the rotor body roll mode, the inplane mode (with both modes exciting blade cyclic feathering), and the rotor plunge mode. The terms discussed in the equation for $\partial L/\partial\theta_0$ previously given were such as to cause the rotor coning or plunge mode to decrease in frequency with increasing speed. In hover, the frequency of this mode was close to 1P. With increasing speed, the frequency dropped into the 0.5 to 0.6P frequency range in the 200-knot speed regime and coalesced with the lower-frequency body roll, regressive inplane modes. This resulted in the observed reduction in damping of the Hop mode with increasing forward speed.

A modification was made to the system which included approximately doubling the collective control system stiffness, reducing the pitch-flap coupling from a value of 0.27 to a value of 0.05 at a collective blade angle of 5 degrees, increasing the blade sweep from 2.5 to 4 degrees sweep forward, and reducing the inplane frequency from approximately 1.55P to 1.4P. The

reduction in pitch-flap coupling and the increase in collective control system stiffness were done specifcally to eliminate the Hop phenomenon within the flight envelope. The increase in sweep and reduction in inplane frequency were done to improve certain handling quality characteristics. These changes resulted in the frequency of the collective coning mode remaining virtually constant with increasing forward speed. The changes also resulted in the coupled roll regressive inplane mode remaining at nearly a constant frequency with speed. The resultant effect was to increase significantly the speed at which the predicted coupling between these modes became critical.

Figure 18 shows a comparison of the predicted damping of the coupled roll-regressive inplane bending mode with test results for this modified configuration as a function of speed. This figure indicates fairly good agreement between the measured and predicted values. Figure 19 shows a comparison between the predicted and measured chord-bending response due to a lateral stick doublet at 170 knots. As can be seen, good agreement between the two responses was obtained.

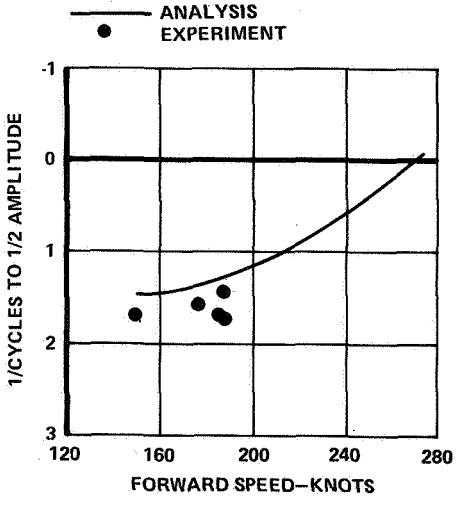

Figure 18. Comparison of Theory and Test Damping vs Speed For Modified Rotor – Control Configuration.

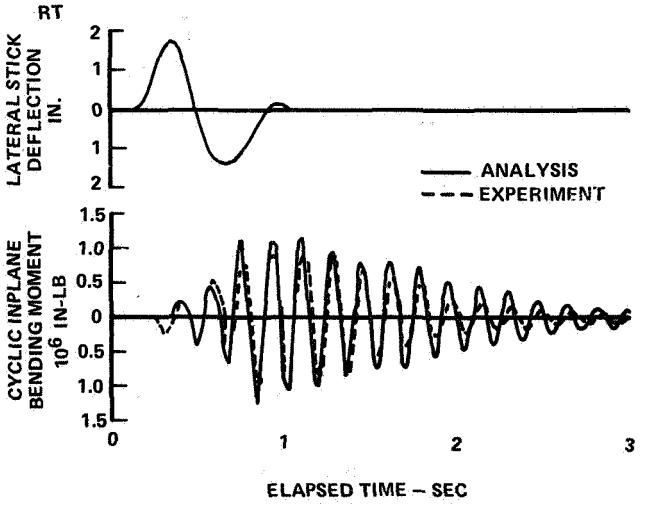

Figure 19. Comparison of Experimental and Analytical Transient Chord Bending Response Due to Lateral Stick Doublet, V = 175 KN.

The rotor system was then modified to increase the blade droop from $2^{o}20'$ to $3^{o}10'$ (Reference 5). This configuration change had little effect on the high-speed coupled roll-regressive inplane mode stability characteristics, and the vehicle was subsequently flown to 240 knots' true airspeed with no indication of a high-speed dynamic stability problem.

This latter configuration change however, did, lower the damping of the coupled roll regressive inplane mode in hover and low-speed flight because of the increase in blade droop. The mode was characterized by roll oscillation and inplane response due to pilot lateral stick inputs. The frequency of the mode was approximately 1 Hz. This, coupled with the roll oscillation of the airframe, made the mode susceptible to pilot coupled oscillation.

Figure 20 shows a comparison of the experimentally determined and predicted roots of the coupled roll-regressive inplane mode for the two different blade-droop configurations. Again, fairly good agreement is seen between experimental and analytical results.

A major revision was then made to the control system which replaced the feathering-moment feedback system with a direct flapping-moment feedback system. This change necessitated placing the main cyclic power actuators between the control gyro and blade feathering instead of between the pilot and the gyro.

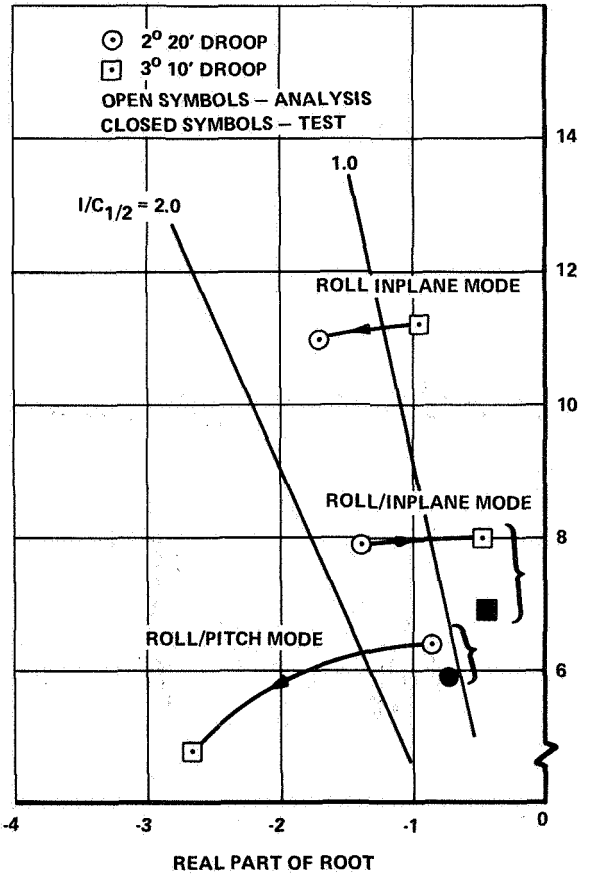

Figure 20. Effect of Droop Angle on Low Speed Roll Mode Stability – Comparison of Experiment and Analysis, V = 20 KN.

The rotor and control system parameters were selected to provide a system that was completely free of either the undesirable Hop or roll mode characteristics discussed earlier. The various parameters, which were established to be critical by extensive parametric studies, using the linear analysis method adapted to computer graphics, were established and controlled very carefully. These parameters included both cyclic and collective pitch flap coupling, inplane frequency, main cyclic power actuator time constant, gyro to blade-feathering gear ratio and phasing, blade sweep and droop, and shaft-moment to gyro-moment feedback ratio.

The initial configuration, when tested on the whirl tower, was determined to have met all criteria except that the inplane frequency was below the criteria value by about 0.05P, or 0.21 Hz. Some limited flight testing was performed with this configuration to validate the criterion, after which the final configuration, conforming to the original criteria, was reached by removing 6.8 pounds tip weight from each blade. The results with both configurations,are discussed in the following.

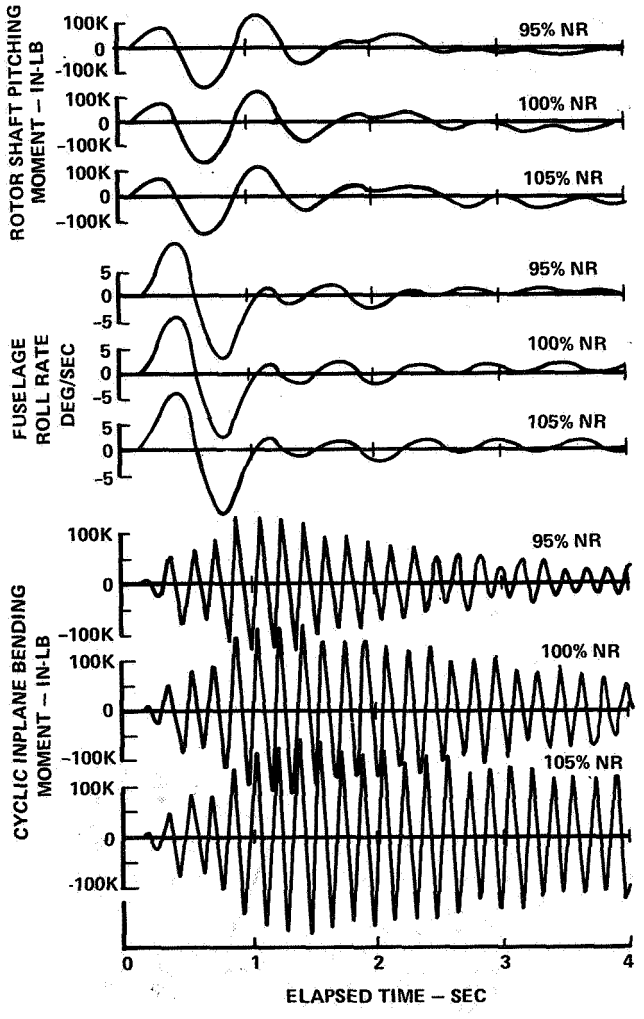

Figure 21. Rotor Speed Effect on Transient Response Due to Lateral Stick Doublet, V = 160 KEAS.

Figure 21 shows the effect of predicted rotor vehicle responses as a function of rotor speed for a lg, 160-knot flight condition with the degraded inplane frequency. The excitation in each case is a lateral stick doublet at 1.5 Hz which is the technique used in flight test for exciting coupled rotor-body dynamic modes to determine their stability characteristics.

It is noted that with increasing rotor speed, the damping of all responses decreases, and the magnitude of the pitch response of the rotor disc in the mode increases. This was noted by the pilot as a characteristic of the mode in that, with similar excitations, the rotor disc tip path oscillations would be imperceptible at lower rotor speeds but would become increasingly responsive at higher rotor speeds.

Figure 22 shows a comparison between the calculated roots and the experimentally determined damping and frequency for this configuration at 160 knot airspeed. The actual vehicle responses contain a varying mix of the two roots, increasing in inplane content with increasing rpm.

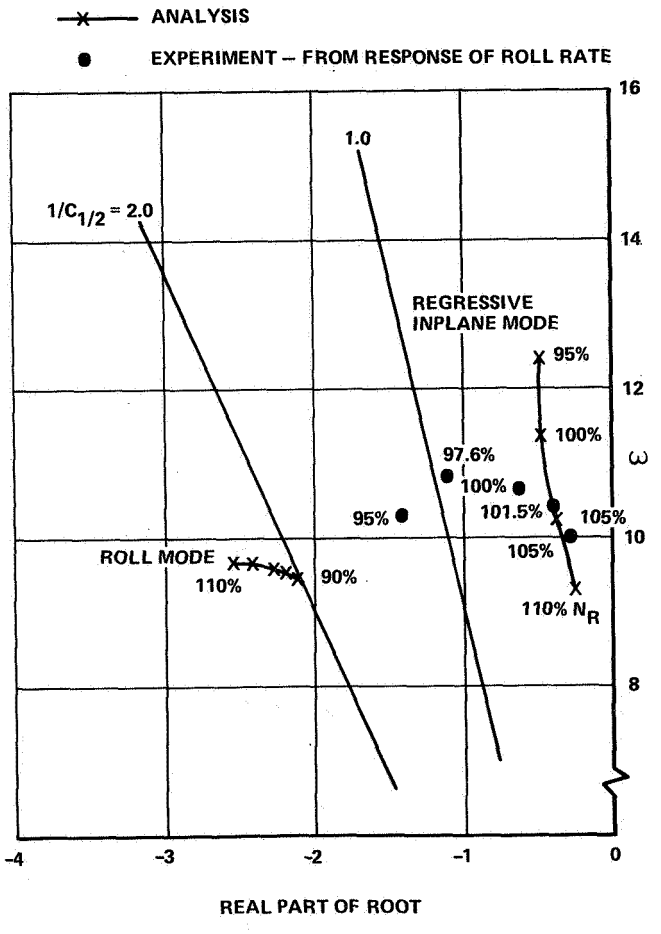

Figure 22. Locus of Roots – Comparison of Test and Analysis – Reduced Inplane Frequency, V = 160 KN.

Figure 23 shows the predicted effect of increasing the inplane frequency by removal of tip weight on the frequency and damping of the coupled roll-regressive inplane modes. Figure 24 shows the corresponding predicted transient response at 105 percent of normal rotor speed with the tip weight removed. The comparison in roots shown on Figure 23 and the comparison of the 105 percent rpm transient response in Figure 24 with the 95 and 105 percent rpm cases in Figure 22 show a significant improvement in the damping and transient response characteristics at rotor overspeed for the configuration with the tip weight removed to give the desired inplane frequency placement.

For the final configuration, Figure 25 shows a comparison of the measured and predicted damping as a function of forward speed. The data show good agreement in measured and predicted damping levels from hover through transition and in higher-speed flight. Experimental data on damping of the regressive inplane mode consist of only one point because even though the mode was not excessively damped, it was extremely difficult to excite by the pilot with lateral stick doublet type excitations to amplitudes sufficiently large to obtain a reliable determination of its stability. This final configuration was tested over a very large flight envelope covering speeds to 220 knots true airspeed and maneuvering load factors from -0.2g to 2.6g in the 180 to 200-knot true airspeed flight regime. The pilot reported "excellent" to "deadbeat" damping and minimal responses to air turbulence in high-speed flight.

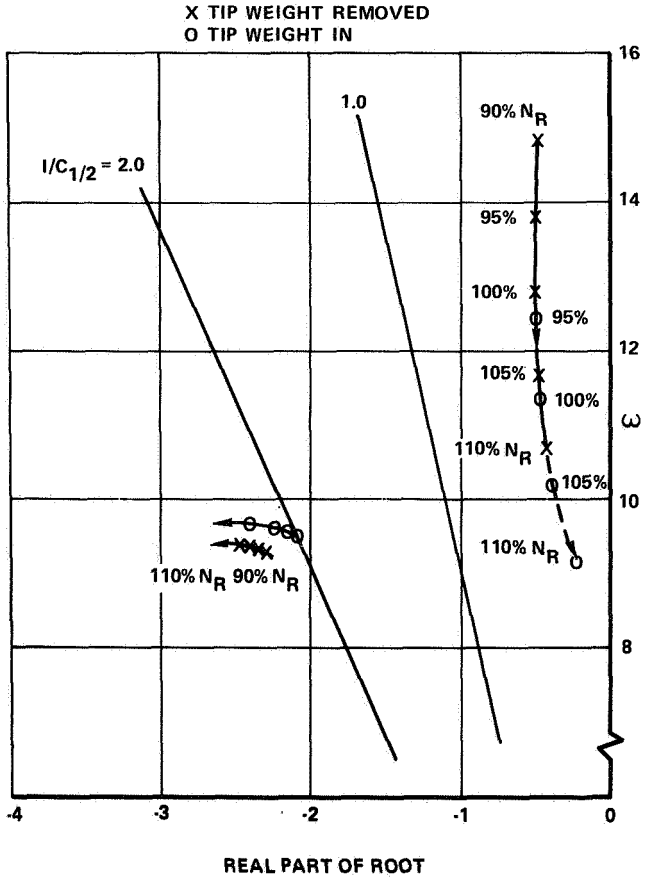

Figure 23. Locus of Roots – Effect of Tip Weight, V = 160 KEAS.

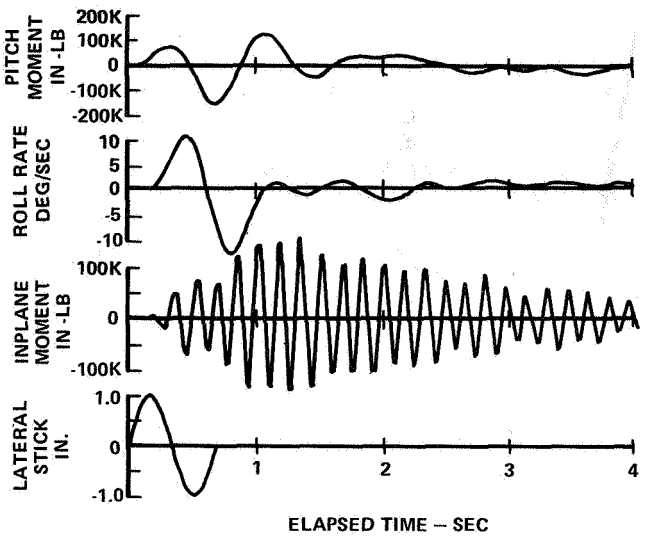

Figure 24. Transient Response Due to Lateral Stick Doublet – Tip Weight Removed, V = 160 KEAS.

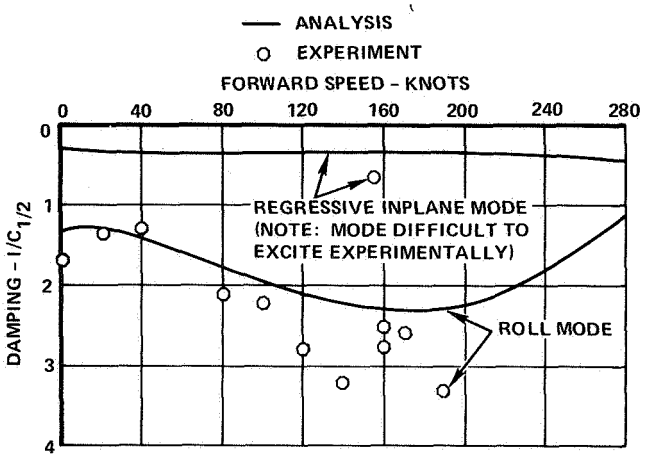

Figure 25. Damping vs Forward Speed – Comparison of Test and Analysis For Final AH-56A (AMCS) Configuration.

Conclusions

Several types of modes can exist in a stiff inplane hingeless rotor which involve coupling with the regressive inplane mode. These include phenomena where the inplane mode is not well coupled with the rest of the system, phenomena where the inplane mode and body roll mode are the primary participants, and even phenomena where the rotor plunge mode is heavily involved in the total system dynamic behavior. These phenomena, particularly the first two types, are not limited to any particular flight regime but can be critical in either stability or response in either low- or high-speed flight or can exhibit characteristics which are virtually independent of speed. Each of the modes is treatable by analysis, and certain parameters such as blade droop, control system stiffness, pitch-flap and pitch-lag couplings, blade sweep, blade product of inertia, inplane frequency and control system parameters are influential in controlling the stability and response characteristics of these modes. Additionally, a totally satisfactory system can be achieved without recourse to auxiliary damping devices.

References

1. Burkam, J.E.; Miao, Wen-Liu; EXPLORATION OF AEROELASTIC STABILITY BOUNDARIES WITH A SOFT-IN-PLANE HINGELESS-ROTOR MODEL, Journal of the American Helicopter Society, Volume 17, Number 4, October 1972

2. Huber, H.; EFFECT OF TORSION-FLAP-LAG COUPLING ON HINGELESS ROTOR STABILITY; Preprint No. 731, Presented at the 29th Annual National Forum, Washington, D.C., May 1973

3. Donham, R.E.; Cardinal, S.V.; Sachs, I.B.; GROUND AND AIR RESONANCE CHARACTERISTICS OF A SOFT IN-INPLANE RIGID-ROTOR SYSTEM, Journal of the American Helicopter Society, Volume 14, Number 4, October 1969

4. Potthast, A.J.; Blaha, J.T.; HANDLING QUALITIES COMPARISON OF TWO HINGELESS ROTOR CONTROL SYSTEM DESIGNS, Preprint No. 741, Presented at the AHS 29th Annual National Forum, Washington, D.C., May 1973

5. Anderson, W.D.; INVESTIGATION OF REACTIONLESS MODE STABILITY CHARACTERISTICS OF A STIFF INPLANE HINGELESS ROTOR SYSTEM, Preprint No. 734, Presented at the AHS 29th Annual National Forum, Washington, D.C., May 1973

6. Chou, P.C.; PITCH-LAG INSTABILITY OF HELICOPTER ROTORS, Journal of the American Helicopter Society, Volume 3, Number 1, July 1958.

HUB MOMENT SPRINGS ON TWO-BLADED TEETERING ROTORS

Walter Sonneborn
Grp. Eng. Mechanical Systems Analysis

Jing Yen
Grp. Eng. VTOL Technology
Bell Helicopter Company
Fort Worth, Texas

Two-bladed teetering rotors with elastic flapping hinge restraint are shown to be suitable for zero-g flight. The alternating moment component introduced into the fuselage by the hinge spring can be balanced about the aircraft center of gravity by alternating hub shears. Such shears can be produced in proper magnitude, frequency, and phase by additional underslinging of the hub and by judicious choice of the location of the first inplane cantilevered natural frequency. Trends of theoretical results agree with test results from a small scale model and a modified OH-58A helicopter.

Centrally hinged rotors have traditionally relied upon thrust vector tilt for generating control moments about the helicopter cg. All present production two-bladed rotors have central teetering (flapping) hinges. Such rotors, without hub restraint, have no control power in zero-g flight.

Recent military specifications for transport and attack helicopters call for the ability to sustain zero-g flight for several seconds. Helicopter control under this condition of no rotor thrust requires hub moments which in two-bladed rotors can be generated by springs restraining the flapping hinge. The resulting flapping-dependent hub moment, when observed in the fixed system, has a mean value in the direction of and proportional to the maximum flapping relative to the shaft. A 2/rev oscillatory moment with an amplitude equal to this mean value results in both the fore and aft and lateral directions. This paper discusses methods for producing 2/rev hub shears for balancing the oscillatory component of the spring moment about the helicopter center of gravity. Practical magnitudes of hub moments are defined by minimum control power requirements for zero-g flight, and maximum values are limited by a variety of factors. Test results from a 1/12-scale Froude model and flight test results from an OH-58A helicopter with variable hub restraint are presented.

MAGNITUDE OF HUB MOMENT

The basic benefits of hub moment are better aircraft rate damping and positive control power in zero-g flight. Minimum hub moment requirements have been investigated by analysis and testing of an OH-58A helicopter. Zero-g flight was demonstrated with this helicopter using only stiff elastomeric bearings in the see-saw hinge for hub restraint increasing the 1-g control power by 10%. Figure 1 shows a record of the maneuver. Only small

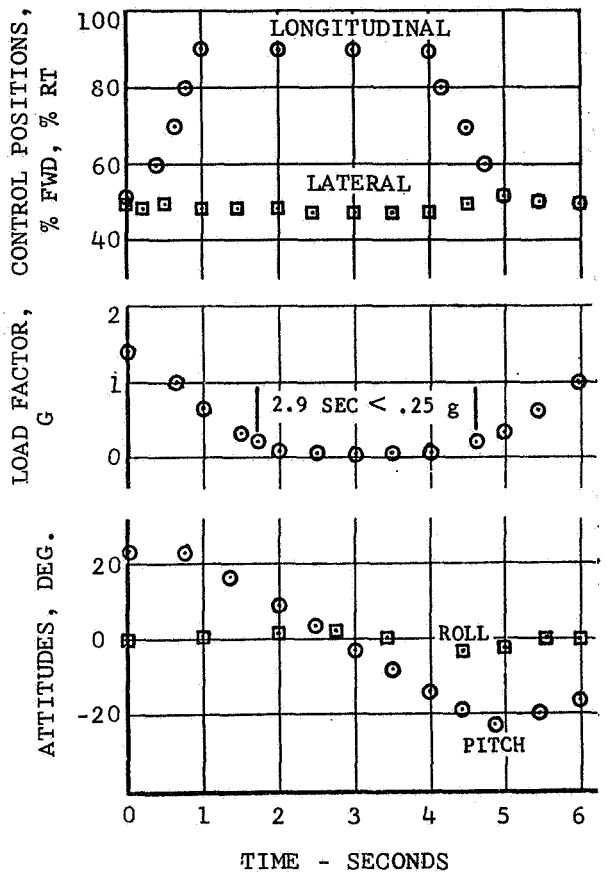

FIGURE 1. Model OH-58A pushover with elastomeric flapping bearings.

lateral inputs were made during the maneuver, and the roll angle did not exceed ±5 degrees. The lateral SCAS was engaged and contributed significantly to roll stabilization. This test and analysis indicated that some 25% of the 1-g control power is adequate for zero-g flight. The OH-58A helicopter was subsequently fitted with ground-adjustable hub torsion springs which added 23% or 37% to the 1-g control power (see Figure 2). The pilot's reactions were favorable with regard to the lower spring value, but the stiffer spring made roll control power excessive and also increased the gust sensitivity noticeably.

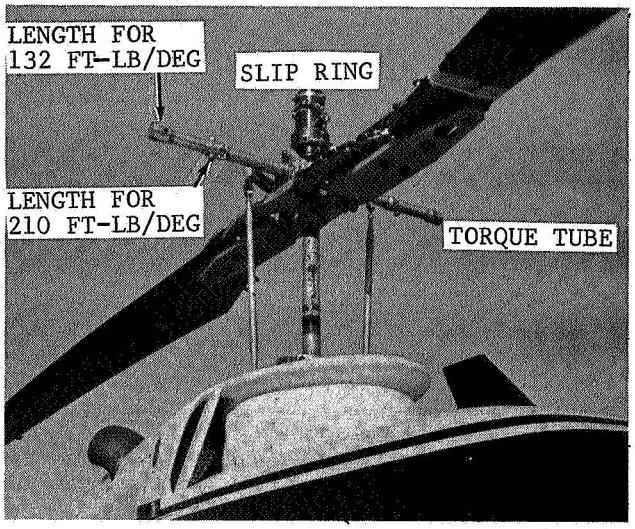

FIGURE 2. Experimental Model 640 rotor with ground-adjustable torsion tube flapping restraint.

Other considerations limiting the hub restraint of two-bladed rotors are:

- Fuselage vibration caused by oscillatory hub moment at 2/rev.
- Increase in beamwise bending of flexure.
- A weight penalty of about 90 pounds per 1000 ft-lb/deg of effective control moment.
- Instability of the coupled pylon/rotor system at extreme spring stiffnesses.[1]

These tend to discourage the designer from introducing significantly more hub moment than that equivalent to 25% of the 1-g control power from thrust vector tilt.

EFFECT OF UNDERSLINGING AND CHORDWISE FREQUENCY

The effects of underslinging on 2/rev hub shears and of hub restraint on 2/rev hub moments are shown by an analysis of the simple rigid body model shown in Figure 3. The kinematics of an underslung,

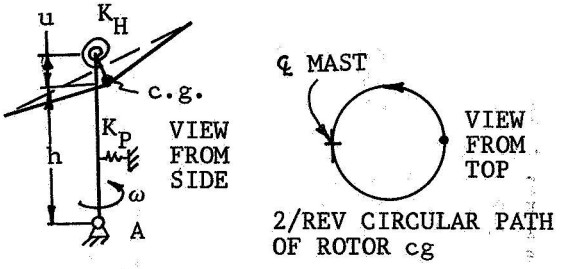

FIGURE 3. Simple rigid body math model of two-bladed rotor.

flapping, two-bladed rotor with a teetering hinge cause the center of mass of this rotor to travel in a circular path at 2/rev if the mast does not oscillate about point A (this assumption will be partly justified below). The resulting centrifugal forces introduce hub shears S for fore and aft (F/A) flapping:

$$S_{F/A}=2a_1\omega^2\ u\ m\ \cos 2\omega t \quad (1a)$$

$$S_{LAT}=2a_1\omega^2\ u\ m\ \sin 2\omega t \quad (1b)$$

where

a_1 = F/A flapping angle

m = rotor mass

ωt = rotor azimuth

The moments M from the hub spring are:

$$M_{F/A}=-0.5a_1K_H(1+\cos 2\omega t) \quad (1c)$$

$$M_{LAT}=-0.5a_1K_H\ \sin 2\omega t \quad (1d)$$

Now taking moments about point A below the rotor ($M_A = M + Sh$), it is evident that all oscillatory components can be cancelled in both the fore and aft and lateral direction if

$$\frac{1}{2}\ a_1K_H = (2a_1\omega^2\ u\ m)\ h \quad (2a)$$

and $\frac{du}{dK_H} = \frac{1}{4\omega^2 hm}$ (2b)

When this condition is met a rigid mast will not oscillate, but merely experience a steady tilt, the amount of which is determined by the mean value of the hub spring moment and the stiffness K_p of the pylon spring.

The dynamic analysis was extended to include the effects of the first inplane mode and the rotor coning mode. Also included were aerodynamic calculations at the 3/4 blade radius and a modal representation of the pylon support system. The set of five differential equations was solved on a hybrid computer (Bell program ARHB2). The solution showed that the location of the first inplane cantilevered blade natural frequency ω_{ζ_c} has a prounounced effect on hub shears. Figure 4 shows how the requirement for underslinging u of the cg changes with ω_{ζ_c}.

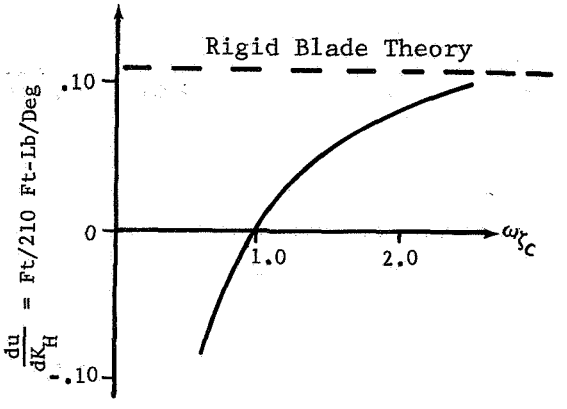

FIGURE 4. Underslinging requirement versus blade cantilevered first inplane natural frequency.

The blades act like a dynamic absorber whenever alternating hub spring moments begin to induce pylon motion. They retain this absorber function over a large range of blade frequencies because of the relatively large absorber (blade) mass. The chordwise bending moments induced at the blade root in this manner have been computed for the experimental Model 640 rotor. (see Figure 5. The pylon parameters used are representative of an OH-58A helicopter). This rotor has a cantilevered blade natural frequency of 0.94/rev. (This frequency is raised to 1.4/rev in the coupled rotor/pylon system.)

Since the loads induced by spring restraint are not in phase with the loads of the unrestrained rotor, small amounts of hub restraint can reduce chordloads (see Figure 5). In general, the spring induced loads are small when compared with the ± 7000-inch-pounds loads occurring in the unrestrained rotor at V_H in level flight.

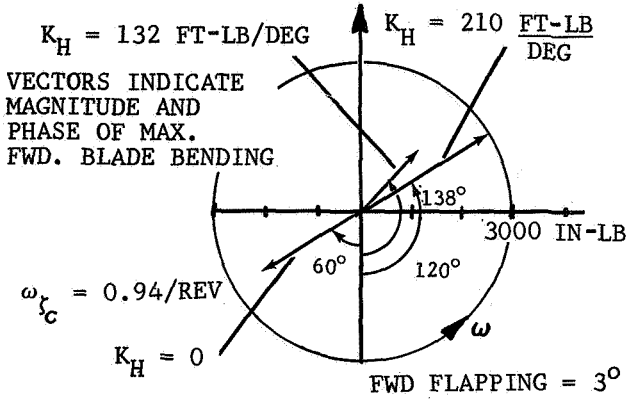

FIGURE 5. Blade root chord loads as a function of hub moment spring rate.

The ideal moment balance about point A, as suggested by equation (2a) and the above discussion, is actually not fully achieved. When the underslinging on a flapping hub-restrained rotor is varied, the complete calculations show a residual pylon oscillation remaining and the phase of the pylon response changing in a continuous manner (see Figure 6). The reason

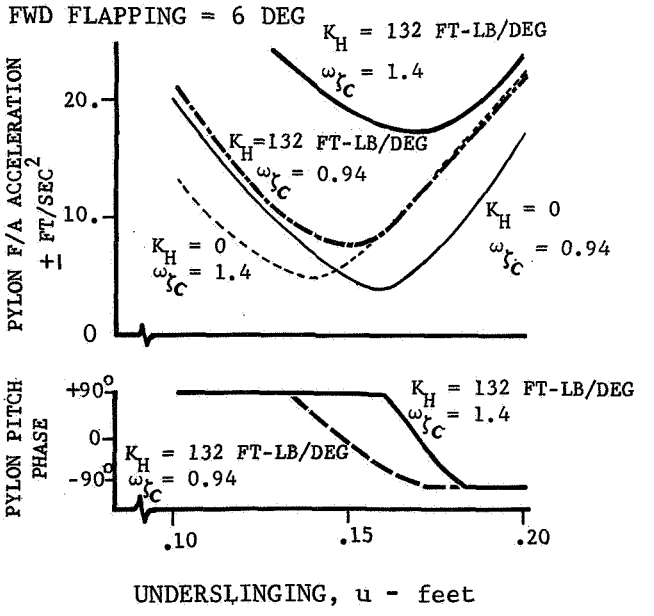

FIGURE 6. Pylon response versus underslinging.

for this is that the airloads of the free-flapping rotor are slightly modified when the airload moment due to hub spring is considered. Figure 7 shows the lift and drag increments on a lifting rotor resulting from this, and it is evident that an inplane shear 90 degrees out of phase from the desired shear results. (If the rotor were not producing any

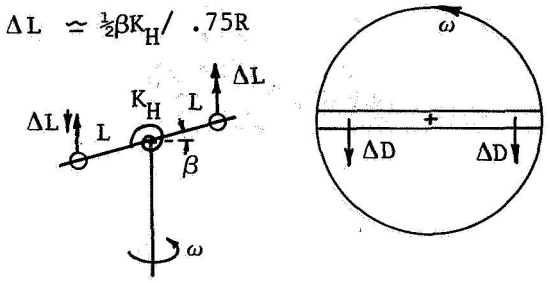

FIGURE 7. Change ΔL in blade lift to balance hub moment, and resulting drag components.

net lift then both blades would experience a drag increase, leaving no net hub shear). Figure 8 shows records of computed pylon responses with and without consideration of the inplane shears due to airloads.

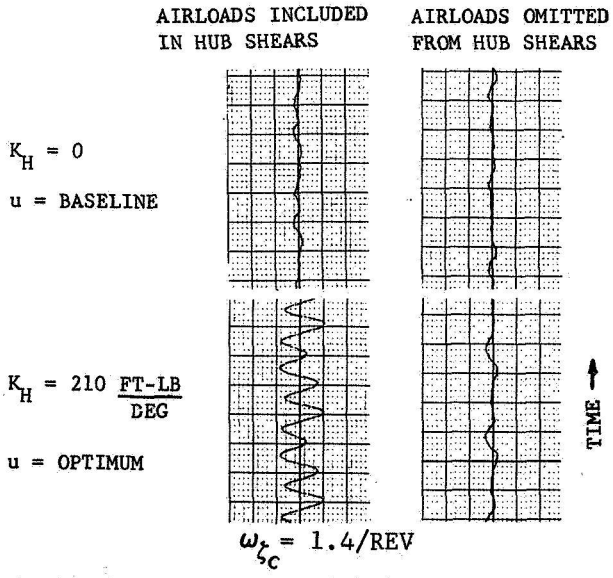

FIGURE 8. Comparison of hub acceleration responses.

EXPERIMENTAL RESULTS

Model Tests

A test was conducted on a 1/12-scale Froude model. Figure 9 shows the apparatus also shown schematically in Figure 3. The model was operated at a fixed cyclic and collective pitch and at 900 rpm. The mahogany blades were heavier than typical for helicopter design practice, hence little coning took place, and even at the smallest possible amount of underslinging (determined by the bearing diameter of the see-saw hinge) some hub spring was required for smooth running of the model. Accelerometers above and below the planes of the pylon gimbal support detected this smooth condition. The amplitude of the 2/rev acceleration was a function of the hub spring rate and the amount of underslinging, as shown in Figure 10. The data scatter near the equilibrium position is indicative of the residual oscillation. The phase change of the pylon response occurred in the gradual manner found in the analysis. However, it was noted that additional underslinging was only about half as effective as anticipated in balancing hub moments. (The cantilevered blade frequency is 1.5/rev). A partial explanation is in the different mast bending due to a shear and a moment (see Figure 11a).

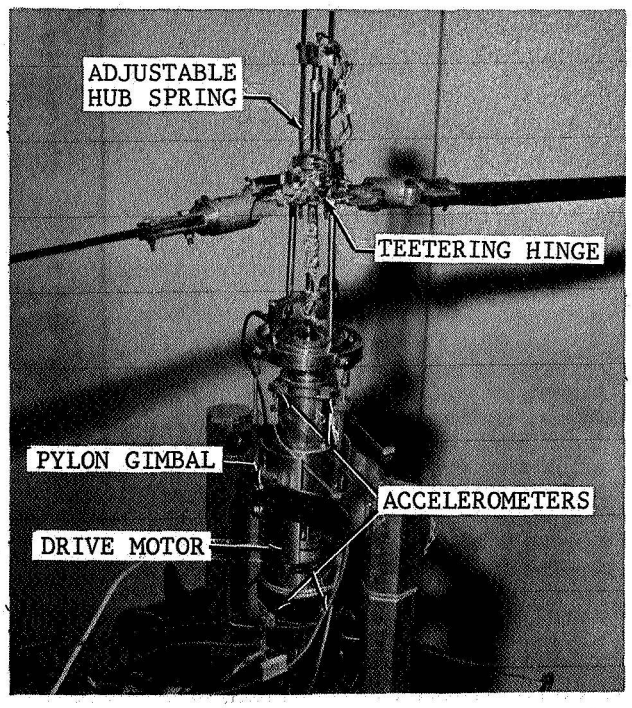

FIGURE 9. (Model (1/12 Froude Scale) with variable underslinging and hub restraint.

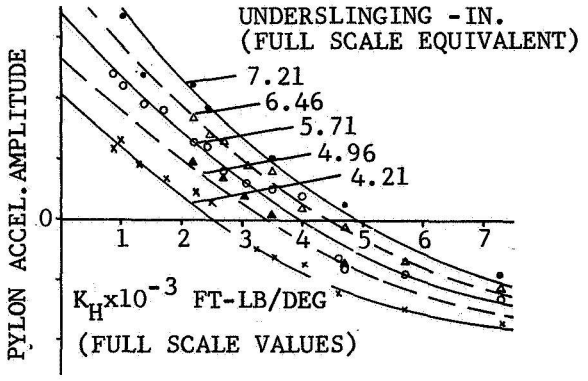

FIGURE 10. Model pylon accelerations versus hub spring.

The mast deflection of the tip of the mast under an applied moment is greater than that resulting from the balancing shear force by an amount equal to 20% of the radius of the circle described by the cg of the underslung rotor. In addition, the excursions of the rotor's center of mass are reduced when part of the total disk flapping occurs in blade flexures. The magnitude of this effect is dependent on rotor coning (see Figure 11b). Both of the above effects were omitted from the analysis.

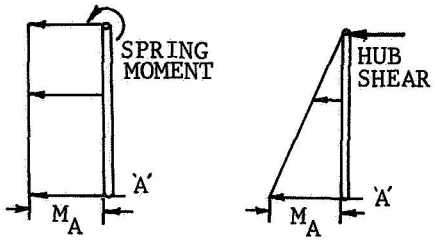

(a) Moment Diagrams

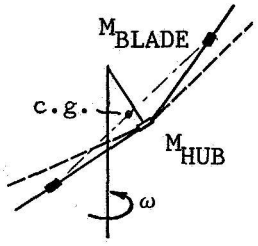

(b) Shift of Rotor C.G. Due to Flexure Bending

FIGURE 11. Factors reducing the effect of underslinging.

Flight Test Results

The OH-58A helicopter shown in Figures 2 and 12 was flown at 3250 pounds gross weight with hub restraints of 0, 132, and

FIGURE 12. Modified OH-58A helicopter with restrained flapping hinge.

210 foot pounds per degree. The cg was varied from station 106.1 to 111.8 Figure 13 shows the 2/rev vibration measurements at the pilot's seat.

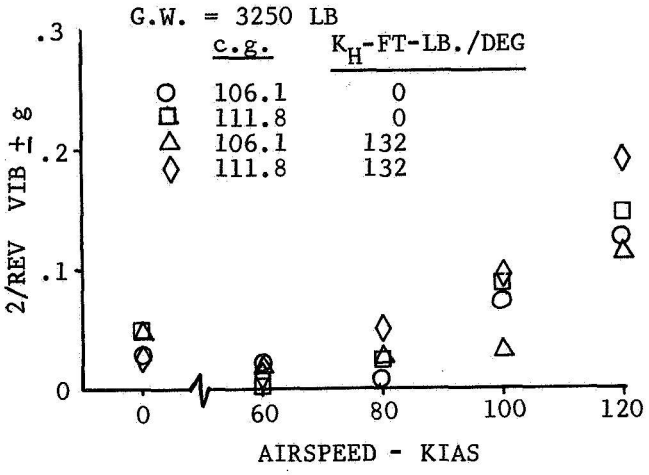

FIGURE 13. Vertical vibration of pilot's seat.

The influence of hub restraint (132 ft-lb/deg) is negligible compared with the increase in vibrations with forward speed. There are several reasons for this. The helicopter has a focused pylon isolation system[2] which is effective for isolating inplane hub shears and hub moments. (There is no vertical isolation). In addition to the moment and horizontal shear isolation, the predicted dynamic absorber effect appears to take place. The first cantilevered inplane natural frequency of the test blade is located at 0.94/rev and it was shown in Figure 4 that for this frequency placement nearly no additional underslinging is required. The dynamic absorber effect of the blade is reflected in the oscillatory chordwise

loads. The measured change in these loads in hover as a function of hub restraint and flapping is similar to the computed values:

K_H FT-LB/DEG	AFT FLAPPING	OSC. CHORD MOMENT @ STA 7.8-IN.LB MEASURED	COMPUTED
0	4.1°	2900	2175
132	3.4°	900	2000
210	2.6°	3000	3000

No computations were made for the forward flight case. It is helpful, however, to compare the oscillatory moments introduced by the hub spring with the moments about the aircraft cg due to the 1/rev hub shears from airloads. These shears are estimated from the modal shear coefficient of the first inplane cyclic mode. The ± 7000-inch-pound chordwise moment at V_H corresponds to a hub shear of ± 80 pounds per blade, which is equivalent to a 2/rev moment about the helicopter cg of ± 450 ft-lb. The maximum oscillatory spring moment was only 50% of this value when flapping reached 3.3 degrees in hover at the forward cg and with the 132 ft-lb/deg hub spring. (This amount of flapping is usually not exceeded in normal maneuvers). This comparison shows that the vibratory excitation introduced by the hub spring is relatively small to begin with.

The pylon isolation system and the placement of the blade first cantilevered inplant frequency near 1/rev made additional underslinging unnecessary in this aircraft for vibration isolation. (The baseline underslinging for the experimental Model 640 rotor was 2.375 inches).

CONCLUSION

(1) Two bladed rotors with hub restraint are suitable for zero-g flight.

(2) Hub restraint which added some 27% to the one-g control power of an OH-58A helicopter with a Bell Model 640 rotor caused a negligible increase in 2/rev vibrations during hover and level flight.

(3) The 2/rev oscillatory moment component due to hub restraint in a two-bladed rotor can be balanced about a point below the rotor hub by additional rotor underslinging. The amount of this underslinging depends on the location of the natural frequency of the first cantilevered inplane blade mode.

REFERENCES

1. Gladwell, G.M.L. and Stammers, C. W., On the Stability of an Unsymmetrical Rigid Rotor Supported in Unsymmetrical Bearings, Journal of Sound and Vibrations, 3,(3), (1966), pp. 221-232.

2. Balke, R. W., Development of the Kinematic Focal Pylon Isolation System for Helicopter Rotors, The Shock and Vibration Bulletin, 38,(3), November (1968), p. 263.

OPEN AND CLOSED LOOP STABILITY OF HINGELESS ROTOR HELICOPTER AIR AND GROUND RESONANCE

Maurice I. Young*, David J. Bailey**,† and Murray S. Hirschbein**
The University of Delaware
Newark, Delaware

Abstract

The air and ground resonance instabilities of hingeless rotor helicopters are examined on a relatively broad parametric basis including the effects of blade tuning, virtual hinge locations, and blade hysteresis damping, as well as size and scale effects in the gross weight range from 5,000 to 48,000 pounds. A special case of a 72,000 pound helicopter air resonance instability is also included. An evolutionary approach to closed loop stabilization of both the air and ground resonance instabilities is considered by utilizing a conventional helicopter swashplate-blade cyclic pitch control system in conjunction with roll, roll rate, pitch and pitch rate sensing and control action. The study shows that nominal to moderate and readily achieved levels of blade internal hysteresis damping in conjunction with a variety of tuning and/or feedback conditions are highly effective in dealing with these instabilities. Tip weights and reductions in pre-coning angles are also shown to be effective means for improving the air resonance instability.

Notation

C_e = landing gear equivalent viscous damping coefficient, lb/ft/sec
C_s = pneumatic shock strut viscous damping coefficient, lb/ft/sec
C_t = tire viscous damping coefficient, lb/ft/sec
CG = helicopter center of gravity
I_x = moment of inertia about x axis, slug-ft2
K_e = landing gear equivalent spring rate, lb/ft
K_s = non-linear, pneumatic shock strut spring rate, lb/ft
K_t = tire spring rate, lb/ft
M = mass of helicopter
M_1 = control moment acting in lateral swashplate equation of motion, ft-lb
M_2 = control moment acting in longitudinal swashplate equation of motion, ft-lb
N = number of blades
T/W = thrust to weight ratio
XYZ = inertial coordinate system
db = decibels
e_1 = offset of virtual flapping hinge, ft
e_2 = offset of virtual lead-lag hinge, ft
h = distance between center of mass of helicopter and coordinate system axis, ft
t = lateral and roll coupling parameter
x, y, z = helicopter longitudinal, lateral and vertical displacements, ft
α_1, α_2 = helicopter pitch and roll angular displacements, rad
$\dot{\alpha}_1, \dot{\alpha}_2$ = helicopter pitch and roll rate, rad/sec
β_K = flapping angular displacement of k^{th} blade, rad
γ_k = lead-lag angular displacement of k^{th} blade, rad
δ = logarithmic decrement
ζ_1 = non-dimensionalized (by rotor radius) displacement of virtual flapping hinge from rotor center of rotation, ft/ft
η_j = generalized fuselage and rotor system degrees of freedom
θ_i = constrained swashplate-blade pitch degrees of freedom
$\lambda_{\alpha 2}$ = percent of uncoupled critical roll damping
$\lambda_{\ell\ell}$ = percent of uncoupled blade lead-lag damping
Ψ_k = azimuthal coordinate of the k^{th} blade, rad
ω_β = out-of-plane or flapping frequency ratio, cycles/revolution
$\omega_{\ell\ell}$ = in-plane or lead-lag frequency ratio, cycles/revolution

Presented at the AHS/NASA-Ames Specialists' Meeting on Rotorcraft Dynamics, February 13-15, 1974.

Acknowledgement is made of the support of the U.S. Army Research Office, Durham, N. C. under Grant DA-ARO-D-1247G112.

*Professor of Mechanical and Aerospace Engineering. **Graduate student and research assistant. †Currently U.S. Army Transportation Engineering Agency, Fort Eustis, Virginia.

Introduction

In recent years an intensive research and development effort within government and industry has focused on hingeless rotor helicopters with a view towards mechanical simplification, improved flying qualities and greater aerodynamic cleanness. The approach being employed capitalizes on modern structural materials and technology which, in principle, permit the hingeless rotor blades to flap and lead-lag by flexing elastically, rather than by the use of mechanical hinges. In order to keep cyclic bending fatigue stress and

blade weight within bounds, the in-plane or lead-lag hingeless blade fundamental natural frequency ratio, as a practical matter, inevitably falls within the range .6-.9 cycles per revolution, although frequency ratios as small as .5 or as great as 1.2 are possible. As a consequence of this .6-.9 range of frequency ratios, both ground and air resonance instabilities can still occur which stem from this frequency ratio being less than unity.

There arises the added concern that slight amounts of internal blade structural damping to be expected in hingeless rotor blades can cause such instabilities to be much more severe and difficult to control than in an articulated rotor case, where mechanical lead-lag dampers would be a standard design feature. On the other hand, the elastic flapping of hingeless rotor blades and the presence of large blade structural moments which are aeroelastically coupled to the fuselage oscillations both in hovering and on its landing gear, and the aforementioned relatively high frequency ratio of hingeless blade lead-lag oscillations compared to those of conventional articulated rotors (.2-.4 cycles per revolution), present the favorable possibility of significant alterations in the ground and air resonance stability characteristics. This is in contrast to centrally hinged, articulated rotors, where flapping motion would be expected to have negligible effect on such instabilities. Several recent investigations[1,2,3] have contributed to increased understanding of hingeless rotor helicopter ground and air resonance characteristics, but in each case were directed principally at design and development of a particular machine with its unique size, structural and operational characteristics, rather than at broad development of parametric trends and general principles, as well as the possibilities for enhancing system stability by application of modern control engineering techniques in conjunction with existing conventional blade pitch control systems.

In this study, the effects of the various design and operating parameters which traditionally influence the ground and air resonance instabilities of articulated rotor helicopters have been considered, but with the addition of the unique hingeless rotor helicopter parameters such as blade internal damping and virtual hinge locations. The effect of scale on stability is investigated by considering aerodynamically similar designs which range in gross weight from 5,120 pounds to 48,000 pounds by keeping tip speed and mean rotor lift coefficient constant. Several other cases of general interest are also considered, such as off-loading, rpm reduction, increasing blade number, etc. In view of the enormous control power available with a hingeless rotor due to its structural characteristics and the possible need for or desirability of full artificial stabilization or stability augmentation of certain design configurations or operating conditions, a closed loop stabilization approach is also investigated. It is viewed as an evolutionary approach which would employ a conventional helicopter swashplate type of control system of blade collective and cyclic pitch. A variety of output variables and their derivatives are examined as possible sources of closed loop feedback information for control actuation. The roll and the roll rate variables are seen to be highly effective. The dynamics of cyclic and collective pitch change are also examined[4] as part of such a closed loop stabilization system for ground and air resonance where the control process is seen to be that of a multiple input-multiple output, interacting control system[5].

Detailed parametric studies of the ground and air resonance stability boundaries are carried out using a standard eigenvalue routine. The parameter combinations which can result in the instabilities are examined with a view towards comparing designs with inherent stability with those that are a result of artificial stabilization. Finally those combinations of design, operating and stability augmentation parameters yielding hingeless rotor type aircraft free of the ground and air resonance instabilities are obtained.

Analysis

The analysis is carried out with the objective of developing a broad understanding of the influence of the principal design and operating parameters on both the system air and ground resonance instabilities. Consequently the degrees of freedom chosen for the analytical model are those which can be expected to be common to all hingeless rotor helicopter designs in hovering and on the ground, irrespective of size and gross weight, operational requirements or specific structural design approaches.

The fuselage body degrees of freedom are taken as those which would represent both the hovering and ground oscillations of a single rotor helicopter either in the air or on a three point, conventional oleo-shock strut type of landing gear. These then follow as the lateral, longitudinal and vertical translational degrees of freedom and the angular roll and pitch degrees of freedom. A yawing degree of freedom is not included, since it is deemed an unnecessary and unproduc-

tive complication of marginal significance. This follows from the large yawing inertia of the body, the close proximity of the aircraft center of gravity to the two main landing gear and the rotor thrust line, the net effect of which is to virtually decouple the yawing freedom from the others, and thereby effectively eliminates its influence on the air and ground resonance instabilities.

The landing gear type and arrangement used in the analysis of ground resonance are viewed as typical, but by no means universal. However, the effective spring and viscous damping restraints which are arrived at in the landing gear analysis are sufficiently broad in character to be representative of the many different landing gear systems currently in use. The two most prevalent systems are the skid type, and pneumatic shock strut and tire type configurations. Since the skid-type landing gear represents a special case of the more general shock strut and tire formulation, an analytic model of the latter has been employed. This formulation has the added advantage of permitting various effects, such as the shock strut damping, the non-linear pneumatic spring rate and the combined spring rate of the tire and landing surface to be more easily studied and is developed in detail in Reference 6.

The hingeless rotor blades are flexible, cantilever structures which flap elastically in oscillations normal to the plane of rotation and lead-lag elastically in the plane of rotation. A generalized coordinate, normal mode type of analysis could be employed effectively for the structural dynamic aspects. However this does not lend itself well to a simple determination of the aerodynamic forces and moments which play a central role in the stabilization process because of the blade bending curvature during the oscillations. Consequently the concept of virtual springs and hinges[7,8] for the flapping and lead-lag oscillations of the blade is used, where quasi-rigid body blade motions are introduced to replace the continuous, elastic bending deformations of the real blades. These degrees of freedom are illustrated in Figure 1. An isometric view of the body degrees of freedom is also shown.

The blade pitch changes are treated as constrained degrees of freedom in the stability analysis. That is the blade pitch can be changed collectively or cyclically by displacement or tilting of a swashplate mechanism. In the open loop case this is done by the pilot displacing the collective or cyclic pitch control sticks. This results in a transient response of the aircraft either about its initial hovering state or on its landing gear by altering the aerodynamic forces and moments produced by the hingeless rotor. Since it takes the form of a reference input or external disturbance, it has no effect on the system stability as long as these disturbances are reasonably small. In the general closed loop case the aircraft roll position, roll rate, pitch position and pitch rate are sensed and used to drive a system of swashplate actuators with a view towards employing the enormous control power inherent in the cantilever blade design of hingeless rotor systems. This can yield full stabilization, if required, or it can augment the inherent stability of the system when design and operating conditions permit. The swashplate-blade pitch change arrangement and the system block diagram are shown schematically in Figure 2. More sophisticated closed loop control system arrangements offer the possibility of enhanced performance and optimization of the system at the expense of complexity or possible reduction in reliability. For example an inner control loop on rotor blade bending deflections by strain gage techniques, as well as sensing of body translational displacements and velocities offer interesting possibilities which are considered in Reference 9. Needless to say, departure of blade pitch from the settings called for by the control system complicates and may degrade the stability and controllability of the system. For example blade torsion which is not included in this study is an important factor considered in Reference 16.

The combination of the fuselage, landing gear (when applicable) and the rotor blade systems yields 5+3N freedoms in the closed loop case and 5+2N freedoms in the open loop case where the blade number N is at least four. The minimum number of four blades follows from the possibilities of a dynamic instability unique to two-blade systems[10] and resonant amplification of three blade aerodynamic loadings in the case of three blades[11] which must be avoided by using a minimum of four blades in a hingeless rotor system.

The number of blade freedoms is reduced by introduction of quasi-normal coordinates to describe the rotor motions[12,13]. This approach reduces the complexity of the analysis by eliminating all blade motions which do not couple with the body in a coherent manner during open and closed loop oscillations. These coordinates describe the various significant patterns of blade motion by five degrees of freedom in the open loop case. These are the rotor cone vertex angle, the lateral and longitudinal tilt of the rotor cone, and the lateral and longitudinal displacements of the blade system center of gravity with respect to the geometric center of the rotor (due to lead-lag motion in the rotating frame of reference). In the closed loop case three freedoms are added through the displacements of the swashplate for blade collective pitch changes and by the angular tilting of the swashplate for blade lateral and longitudinal cyclic pitch changes.

The analysis proceeds assuming that the rotor system has four blades. The single exception to this is the consideration of a very heavy helicopter (72,000 lbs.) air resonance behaviour. In this case a six blade design obtained by adding two blades to a four blade, 48,000 lb. design is examined. This leads to a final quasi-normal coordinate model which has ten degrees of freedom for the open loop case and thirteen for the closed loop case. These equations of motion are then reduced to a canonical form suitable for application of a standard digital computer routine for determining the complex eigenvalues and eigenvectors of the system. In effect twice the number of first order, linear differential equations with constant coefficients result. This is a twenty-sixth order system in the closed loop case, if ideal actuators are assumed. As more realistic models of the control hardware are employed (due to leakage across hydraulic seals, imperfect relays, amplifier frequency response characteristics, etc.) the order of the system would increase further. This is deemed to be a specialized design problem which needs attention on an *ad hoc* basis.

Discussion of Numerical Results

The discussion of the numerical results begins with the open loop stability or stability boundary characteristics of the hingeless rotor helicopter ground resonance problem and is then followed by an examination of the potential influence of closed loop, feedback control in system stability. This approach is then repeated for the air resonance problem. The discussion closes with an overview of the potential of closed loop control for both of these hingeless rotor helicopter instabilities.

Ground Resonance

In order to develop insight into the nature of the ground resonance instability as it might occur for a typical helicopter employing a hingeless rotor, a 12,000 pound reference case based on the S-58 helicopter[14] is considered first. The rotor is modelled as one with four hingeless blades with a flapping frequency ratio of 1.15 cycles per revolution, and a lead-lag frequency ratio of .70 cycles per revolution at a rotor tip speed of 650 ft/sec. The wheels are first assumed to be locked, preventing the aircraft from rolling freely in a longitudinal direction. The uncoupled lateral and longitudinal translation modes of the aircraft are assumed to have five percent and three percent of critical damping, respectively, as a result of tire hysteresis losses. As the thrust to weight ratio is varied from zero to unity the vertical loading on the landing gear decreases. The stability of the small, coupled oscillations about a series of initial steady states determined by the thrust to weight ratio (T/W) is then studied as a function of oleo-shock strut damping for several small, but typical values of blade hysteresis lead-lag damping. Both damping parameters are expressed in terms of percent of equivalent viscous critical damping.

The unstable mode of oscillation is found in all cases to be dominantly a fuselage rolling mode with a small amount of lateral translation coupling, and still lesser amounts of pitching and longitudinal motion. Release of the brakes, permitting the aircraft to move freely longitudinally, has a slightly stabilizing effect, but of minor importance compared to the influence of oleo-shock strut damping and blade internal damping. The numerical results of the study with brakes on are presented in Figure 3. Equivalent viscous damping of the uncoupled rolling mode expressed in percent of critical damping is taken as the abscissa, while thrust to weight ratio is the ordinate. The horizontal dash line at T/W = .9 is a visual reminder that this is an unrealistic condition and that the stability data beyond this value is probably unreliable, since the analytical modelling of the landing gear depends on the questionable assumption of an initial steady state for thrust to weight ratios greater than nine tenths. The aircraft is, of course, in the transient condition of landing or take-off.

It is seen that if blade hysteresis damping should be equivalent to one percent of critical lead-lag damping, then slight amounts of oleo-damping of the rolling mode produce stable oscillations. If the blade internal damping is as little as one quarter of a percent of critical, stability can still be achieved for all thrust to weight ratios, if roll damping is equivalent to fourteen percent of critical damping. Internal blade damping of one percent or greater is found to eliminate the instability entirely, if only slight amounts of landing gear damping are available, for example from tire hysteresis. Thus the ground resonance instability for the reference case is found to be quite mild and easily eliminated with the moderate amounts of blade and landing gear damping normally present.

In order to understand the influence of the tuning of a hingeless rotor on this desirable result, the lead-lag frequency ratio is varied about reference frequency ratio of .7 cycles per revolution as the

flapping frequency ratio is held constant at 1.15 cycles per revolution. Blade damping is taken at one-half percent of critical while roll damping is held fixed at eight percent of critical. Figure 4 shows the effect of this tuning on the unstable mode by plotting the log decrement of this mode versus thrust to weight ratio. It is seen that increasing the lead-lag frequency ratio above .7 makes the system stable, while decreasing it below this reference value makes it progressively more unstable. Figure 5 considers the effect of the offset of the virtual flapping hinge and tuning of the flapping frequency ratio on the instability with respect to the reference case. It is seen that a flapping frequency ratio of 1.0 corresponding to a conventional, articulated rotor is considerably more unstable than the reference case. It is seen that increasing the offset and frequency ratio to progressively higher values is beneficial and stabilizing although tending to reach a point of diminishing returns at a flapping frequency ratio of 1.20 cycles per revolution.

Size and scale effects are investigated by considering the coupling of the lateral and rolling motion as the distance between the rotor hub and the center of gravity of the aircraft is varied with respect to the reference case, where it was assumed to be at a distance of seven feet. As this distance is decreased to five feet, the instability is observed to change in relationship to the thrust to weight ratio, but not in general character. On the other hand as the coupling increases by increasing the distance to nine feet, there is a stabilizing effect. This is illustrated in Figure 6. This result can be understood in terms of the coupled rolling natural frequency, which tends to decrease as this distance increases. Thus if the lead-lag natural frequency ratio is held fixed at .7, stability can be improved by detuning the fuselage coupled rolling mode to a lower frequency. This result is typical of all helicopter ground resonance instabilities.

The influence of large size and scale changes is considered by studying the stability of two additional hingeless rotor helicopters of 5,120 and 48,000 pounds, respectively, which are obtained from the reference case by aerodynamic scaling. That is the rotor diameter and overall proportions of the aircraft were altered to accomodate the gross weight changes at the same mean rotor lift coefficient and tip speed. It is seen in Figure 7 that aircraft smaller than the reference case of 12,000 pounds tend toward inherent stability with the blade tuning and nominal amounts of damping assumed. On the other hand the relatively heavy machines tend to a more severe instability at slightly higher thrust to weight ratios than the reference case, but still well within the range of achieving inherent stability with moderate amounts of blade hysteresis damping and oleo-shock strut damping of the unstable, coupled rolling mode.

Ground Resonance with Feedback

As an alternative or as a supplement to parameter selection which results in stable oscillations, closed loop feedback control is considered. Since proportional control action (at least qualitatively) alters the frequency of oscillation of simple systems by adding or subtracting a virtual spring effect, depending on whether feedback is negative or positive, the reference case was used as a basis for investigating this possibility. Figure 8 shows the effect of proportional roll feedback and control action (in this case positive feedback is actually employed) in detuning an unstable coupling by depressing the critical fuselage roll mode frequency. It is seen that this is very effective in stabilizing the system. It should be noted that in the case of other design reference parameters, proportional feedback and control action of opposite sign might be beneficial, if the detuning of the critical fuselage roll frequency required increasing, rather than decreasing. The application of this control action is deemed beneficial, but is best decided on an *ad hoc* basis.

A more conventional use of feedback control is considered in Figure 9 which shows the effect of negative feedback with derivative or rate control action. This tends to augment the damping of the critical fuselage rolling mode. This is seen to be highly effective also, and, at least to a first approximation, is interchangeable with oleo-shock strut damping of the unstable roll mode.

A logical extension of the foregoing application of feedback control to the stability of ground resonance is the blending of both proportional and derivative control action. In this case the critical roll mode can be both detuned and damped to approach an optimum. This is shown to be the case in Figure 10. Here the system is made progressively more stable over the entire range of thrust to weight ratios. It is not the intention here to optimize the stability boundary, but to show that this is possible even with small values of blade internal hysteresis damping and the normal amounts of landing gear damping of the reference case. In view of the relatively unimportant influence of the pitching, and longitudinal

degrees of freedom for the reference case, pitch rate feedback and control action was not deemed effective. However, this remains a potentially useful and important tool in the event that special design or operational requirements modify the open loop system.

Air Resonance

The basic reference helicopter of 12,000 pounds gross weight is examined for its air resonance stability as a function of lead-lag frequency ratio for several values of flapping frequency ratio. It is seen in Figure 11 that lead-lag frequency ratios of .70 or less result in instability over the structurally feasible range of flapping frequency ratios between 1.10 and 1.20. It is also to be noted that in the neighborhood of neutral stability (for the assumed blade equivalent viscous internal damping of 1/2%), increasing flapping frequency ratio is stabilizing. This interaction effect between these two key blade natural frequency ratios is further illuminated in Figure 15. It can also be seen that the lighter blades (i.e. an overall mass fraction of 4½% rather than 6½%) require higher frequencies for neutral stability. It is shown in Reference 12 that in the stable range of lead-lag frequency ratios, an increasing helicopter blade mass fraction improves stability further. On the other hand, it is also shown that for an unstable configuration, increasing blade mass fractions can further degrade stability.

The critical effect of internal damping of the blade lead-lag motion is presented in Figure 13 for the reference case with a flapping frequency ratio of 1.10 (comparable results were obtained at frequency ratios of 1.15 and 1.20). It is seen that increased internal damping enhances air resonance stability and internal damping levels of 1% of critical virtually eliminate the air resonance instability for a lead-lag frequency ratio of .75 or greater (since hingeless rotor flapping frequency rates greater than 1.10 improve stability further).

Although the frequency ratios for lead-lag and flapping motions of hingeless rotor blades have a fundamental effect on the air resonance stability boundaries, design differences in structure, materials, and proportioning of such blades can result in differences in the virtual hinge locations and stiffness with important modifications in the stability boundaries. These effects are presented in Figure 14, which show that more outboard location of the virtual hinges for lead-lag motion tends to stabilize, although not by a substantial degree. This effect is believed to stem from a decrease in the relative energy level of the blade in-plane motion, just as in classical ground resonance.

Size effects as distinguished from gross weight are presented in Figure 15. It is seen that the reference helicopter air resonance stability is virtually unaffected by large changes in the body pitch and roll moments of inertia, provided that the lead-lag frequency ratio is sufficiently large for stability ($\omega_{\ell\ell} \geq .75$). However relatively large machines are seen to be less unstable, if an air resonance instability exists. The influence of gross weight changes through aerodynamic scaling is presented in Figure 16 for 5120, 12,000 and 48,000 pound machines which operate at the same mean rotor lift coefficient and tip speed. It is seen that very large increases in gross weight tend to be stabilizing with respect to the minimum lead-lag frequency ratio required for neutral stability, although gross weight effects for machines in the 5,000 to 12,000 pound class are not clear-cut because of the greater sensitivity to all the other system parameters. In fact, it may be difficult to obtain a rational trend when blade mass fraction is held constant, when in reality the very small machines will tend toward larger blade mass fractions. In contrast to this, if the gross weight of the reference machine is decreased by off-loading (cargo, for example), there is a clear-cut improvement in the air resonance stability. This is shown in Figure 17 and stems from the reduction in blade initial coning. The effect of coning is discussed further below.

Built-in pre-coning angles are normal in the design of hingeless rotors; to minimize steady bending stress is a routine consideration. Figure 18 shows the stability boundary for the reference case and the effect of deviating from the nominally ideal case of built-in pre-coning matching the coning that would result from a 1-g load of a centrally hinged, articulated rotor. It is seen immediately that "over-coning" destabilizes and "under-coning" stabilizes for the entire range of lead-lag frequency ratios. This suggests that a direct, profitable trade-off between steady bending stress and air resonance stability exists. That is reduce coning by structural action and enhance stability. Figure 19 continues this theme by showing the influence of a concentrated tip weight on the air resonance instability. In this case it is seen that tip weight is beneficial and stabilizing, providing the lead-lag frequency ratio is of the order of three-fourths or greater ($\omega_{\ell\ell} \geq .75$). Figure 20 shows the design effect of an RPM reduction at fixed gross weight. This

would increase coning and the data shows a consistent loss of stability for the various lead-lag frequency ratios.

Aerodynamic scaling for very large helicopters appears to be barred by the adverse trend of coning at constant mean rotor lift coefficient and tip speed, unless blade number is increased beyond four blades. For example increasing gross weight from 48,000 pounds to 72,000 pounds was considered by increasing disk loading and solidity by fifty percent - that is adding two blades to the original four-blade design. This yields the beneficial effect of no increase in coning angle and only a minor modification of the stability boundary. This is illustrated in Figure 21. The dash or ghost line on this figure represents a second mode of marginal stability at a high frequency. This is discussed at length in reference 15. The implication is that a high frequency air resonance instability might become a factor in very large hingeless rotor helicopters. However, the effect of including the additional rotor degrees of freedom suppressed by the "quasi-normal" or "multi-blade" coordinate transformations requires additional, careful study since the current analysis limits rotor flapping type motions to those which result in either collective or cyclic flapping of the individual blades.

Air Resonance with Feedback

Proportional feedback and control action proves to be a very effective means of stabilizing air resonance. Figure 22 shows the influence of proportional roll control action for the reference helicopter; roll corrections alone are found to be highly effective over the entire range of lead-lag frequency ratios, whereas aircraft pitching motion is found to be a relatively small component of the air resonance instability mode and not a productive avenue for closed loop stabilization.[15] Figure 23 examines the efficacy of proportional roll control for a case of maximum air resonance instability when $\omega_{\zeta\zeta}$=.60. It is seen to be very effective and virtually a linear influence on stability over the range of practical interest.

Sensing aircraft roll rate is also found to be highly effective in closed loop control, but less so for pitch rate because of the relatively small participation of pitch in the air resonance instability. However the complex phase relationships which exist in the mode of air resonance instability[15] make it very desirable that aircraft roll and pitch control actions be mixed (i.e. the interacting control actions referred to above[5]). This is illustrated in Figure 24 which shows the influence of pitch control action for several levels of roll control action (where both are based on roll rate feedback information). The linearity of this stabilization method is made evident by cross-plotting the influence of pitch control action for a magnitude of roll control action which results in (almost) neutral stability.

Closed Loop Stabilization

The foregoing data illustrates that an appropriate mix of aircraft roll and roll rate information, in conjunction with aircraft roll and pitch control action, permits straightforward artificial stabilization of both the air and ground resonance instabilities of hingeless rotor helicopters under very adverse design conditions. More importantly, perhaps, the data indicates that the marginally stable configurations resulting from the lead-lag frequency ratio being tuned to .70-.80 and/or internal damping levels for this oscillation being of the order of ½% of critical or less can be easily stabilized by utilizing existing, conventional control systems.

A significant difference between the ground resonance and air resonance modes of instability is the phase relationship between rotor cone tilting and fuselage rolling motion. Also the fact that a slight positive or regenerative roll feedback and control action can be beneficial in stabilizing ground resonance. The reverse is true for air resonance. The common, beneficial element for both instabilities is in sensing aircraft roll rate and utilizing this information for negative feedback to implement roll control action. This in effect is stability augmentation of the aircraft roll damping both on the ground and in the air. The additional control action for aircraft pitch has been found to be beneficial for stabilizing air resonance[15] and not detrimental for stabilizing ground resonance.[6] Thus the interacting, closed loop control system driven by roll rate information emerges as a simple, evolutionary approach to complete artificial stabilization, or stability augmentation of the hingeless rotor helicopter air and ground resonance instabilities.

Conclusions

1. The ground and air resonance instabilities of hingeless rotor helicopters are marginal ones, but they will persist as design considerations because of the natural tendency of the lead-lag frequency ratios to be less than unity (and conceivably as small as .60), while internal damp-

ing levels will be slight, unless special materials and design measures which increase internal damping can be found and which are acceptable with respect to other design and operating constraints.

2. The air resonance instability is very sensitive to blade coning, while ground resonance is not. Reductions in coning by a variety of means are beneficial, but the possibility of accepting a modest level of steady bending stress in lieu of other approaches (such as tip weights) is worthy of more consideration (since this would also reduce Coriolis-type fatigue loads in steady forward flight).

3. Completely artificial stabilization of both the air and ground resonance instabilities is possible, by utilizing the concept of interacting controls. This is not suggested as a serious approach to design, but as an indication that a modest stability augmentation approach, in conjunction with adherence to simple design criteria and objectives, can eliminate both the air and ground resonance instabilities.

4. The ground resonance instability which was studied exhaustively in Reference 6 is seen to be inherently the same, whether conventional oleo shock strut or skid type landing gear are used, providing the effective stiffness and damping are properly represented in the overall system design. On the other hand, failure or malfunction of a single element of the system which destroys the assumed symmetries (e.g. a single blade damper on an articulated rotor system) must be evaluated on an *ad hoc* basis since the system might then become unstable despite the stability of the normal system.

References

1. Donham, R. E., Cardinale, S. V., and Sachs, I. B., "Ground and Air Resonance Characteristics of a Soft In-Plane Rigid-Rotor System," AIAA/AHS VTOL Research, Design and Operations Meeting, Georgia Institute of Technology, Atlanta, Georgia, February 1969.

2. Woitsch, W. and Weiss, H., "Dynamic Behavior of a Fiberglass Rotor," AIAA/AHS VTOL Research, Design and Operations Meeting, Georgia Institute of Technology, Atlanta, Georgia, February 1969.

3. Lytwyn, R. T., Miao, W., and Woitsch, W., "Airborne and Ground Resonance of Hingeless Rotors," 26th Annual Forum of The American Helicopter Society, Washington, D.C., June 1970, Preprint No. 414.

4. Young, M. I., "The Dynamics of Blade Pitch Control," Journal of Aircraft, Vol. 10, No. 7, July 1973.

5. Ogata, K., Modern Control Engineering Prentice-Hall, Englewood Cliffs, N.J., 1970, pp. 377-396.

6. Bailey, D. J., "Automatic Stabilization of Helicopter Ground Instabilities," University of Delaware, Master of Mechanical and Aerospace Engineering Thesis, May 1973.

7. Young, M. I., "A Simplified Theory of Hingeless Rotor Helicopters," Proceedings of the Eighteenth Annual National Forum of The American Helicopter Society, Washington, D.C., May 1962, pp. 38-45.

8. Ward, J. F., "A Summary of Hingeless Rotor Structural Loads and Dynamics Research," Journal of Sound and Vibrations, 1966, Vol. 4, No. 3, pp.358-377.

9. Young, M. I., Hirschbein, M. S., and Bailey, D. J., "Servo-Aeroelastic Problems of Hingeless Rotor Helicopters," University of Delaware, Department of Mechanical and Aerospace Engineering, Technical Report No. 155, August 1972, (Revised October 1973).

10. Kelley, B., "Rigid Rotors vs. Hinged Rotors for Helicopters," Annals of The New York Academy of Sciences, Vol. 107, Article 1, 1964, pp. 40-48.

11. Marda, R. S., "Bending Vibrations of Hingeless Rotor Blades," University of Delaware, Master of Mechanical and Aerospace Engineering Thesis, April 1972.

12. Young, M. I. and Lytwyn, R. T., "The Influence of Blade Flapping Restraint on the Dynamic Stability of Low Disk Loading Propeller-Rotors," Journal of The American Helicopter Society, Vol. 12, No. 4, October 1967, pp. 38-54.

13. Hohenemser, K. H. and Sheng-Kuang, Y., "Some Applications of Multiblade Coordinates," Journal of The American Helicopter Society, Vol. 17, No. 3, July 1972, pp. 3-12.

14. Seckel, E., Stability and Control of Airplanes and Helicopters, Academic Press, 1964, pp. 456-457.

15. Hirschbein, M. S., "Flight Dynamic Stability and Control of Hovering Helicopters," University of Delaware, Master of Mechanical and Aerospace Engineering Thesis, October 1973.

16. Huber, H. B., "Effect of Torsion-Flap-Lag Coupling on Hingeless Rotor Stability," Preprint No. 731, 29th Annual National Forum of the American Helicopter Society, Washington, D. C., May 1973.

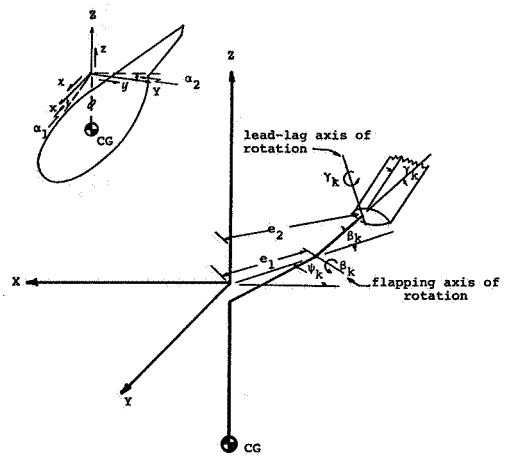

Fig. 1 XYZ - coordinate system, x, y, z, α_1, α_2 - displacements.

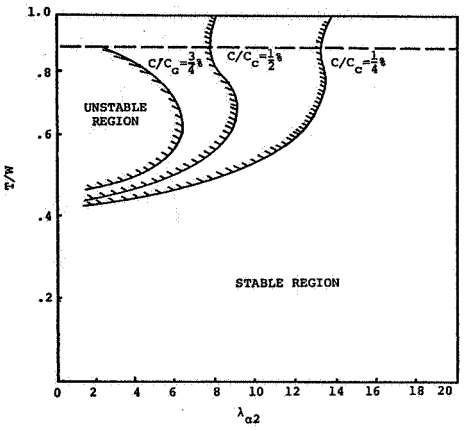

Fig. 3 Stability boundary as a function of roll damping.

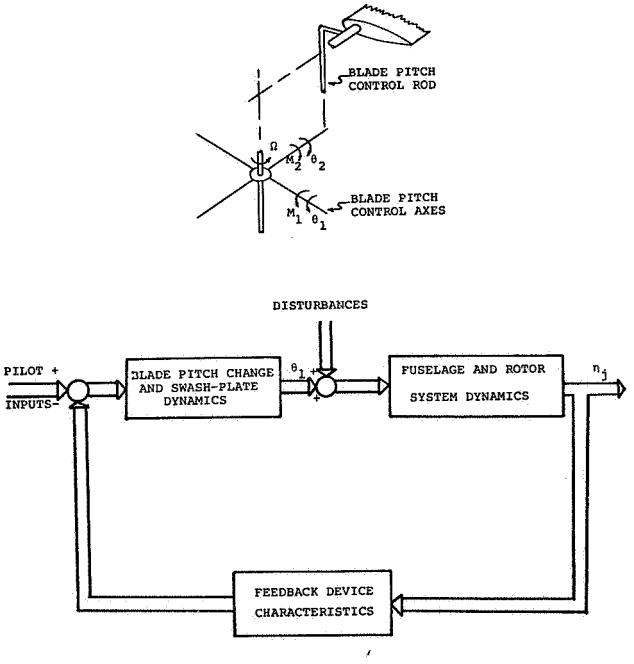

Fig. 2

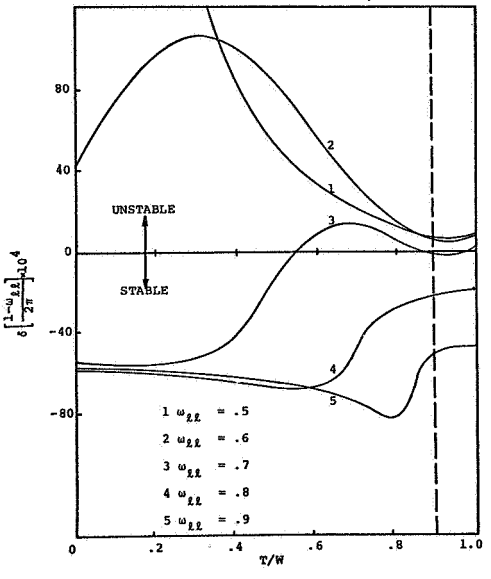

Fig. 4 The effect of lead-lag natural frequency ratio.

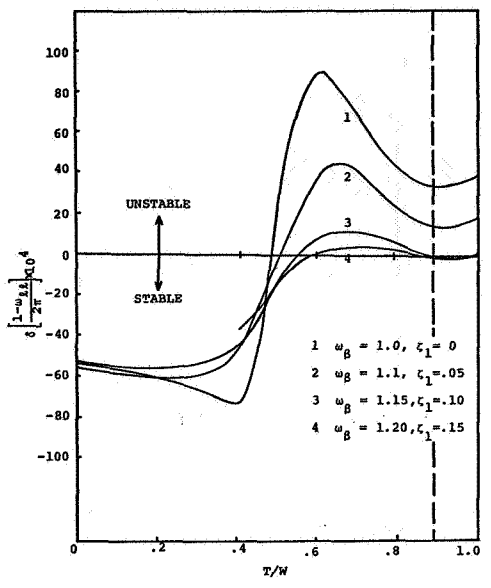

Fig. 5 The effect of flapping natural frequency ratio and virtual flapping hinge offset.

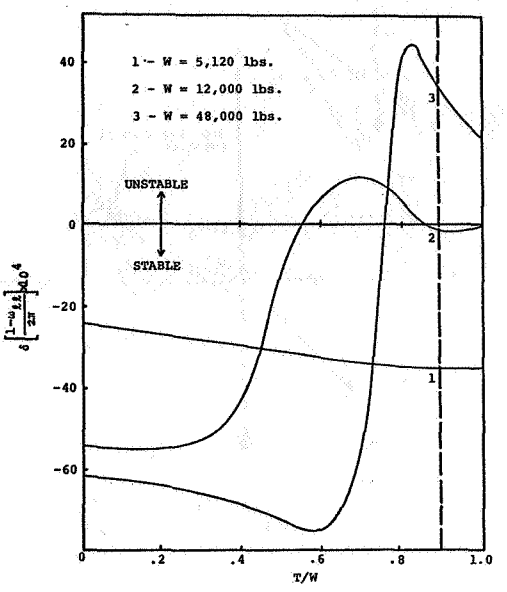

Fig. 7 Size effects.

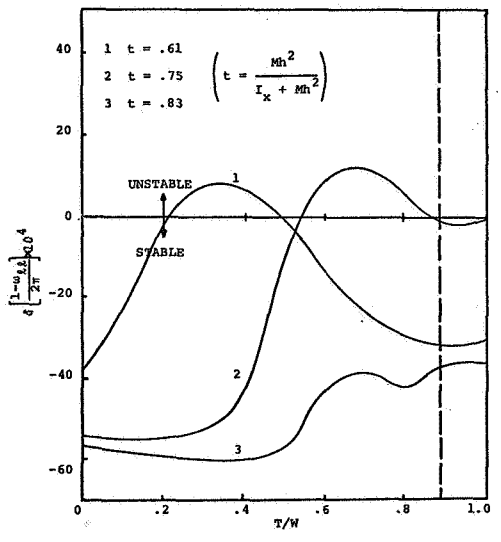

Fig. 6 The effect of coupling between lateral and rolling motion.

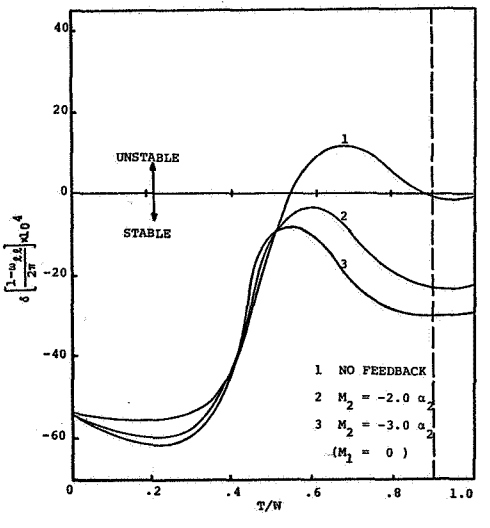

Fig. 8 The effect of roll position feedback control.

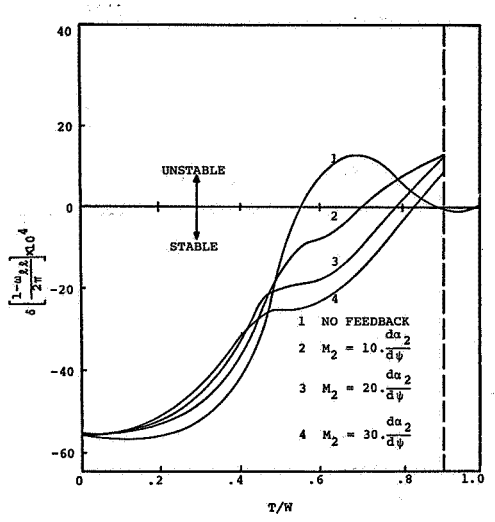

Fig. 9 The effect of roll rate feedback control.

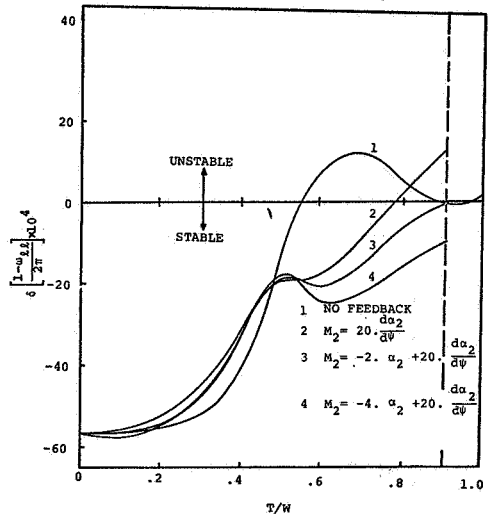

Fig. 10 The effect of roll position and roll rate feedback control.

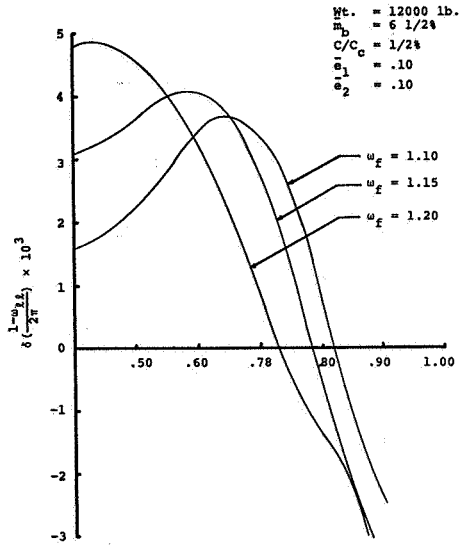

Fig. 11 The effects of lead-lag natural frequency ratio.

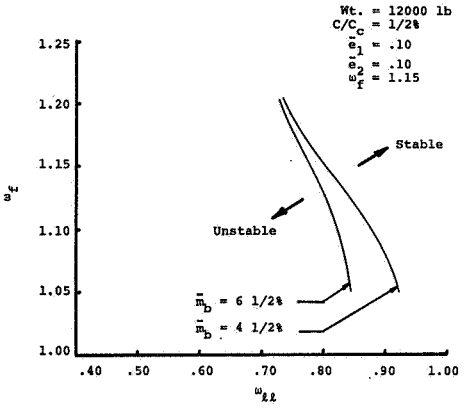

Fig. 12 Flapping-in-plane natural frequency ratio stability boundary.

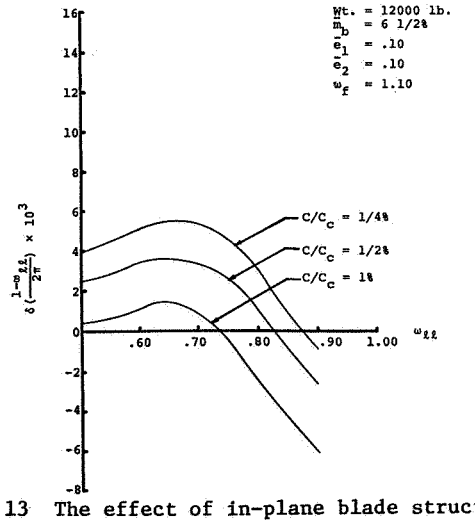

Fig. 13 The effect of in-plane blade structural damping.

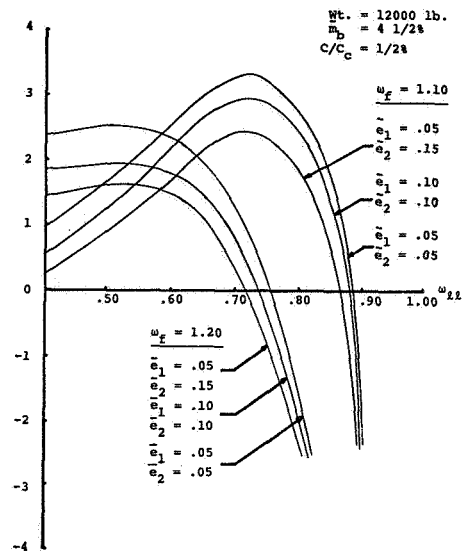

Fig. 14 The effect of virtual hinge offset.

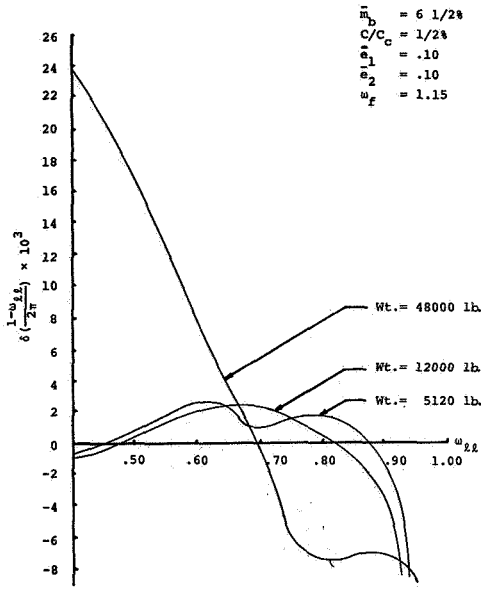

Fig. 16 The effect of scaling.

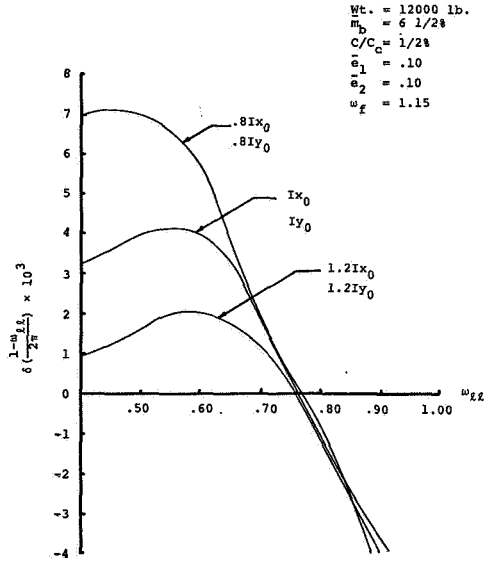

Fig. 15 The effect of changes in the body moments of inertia.

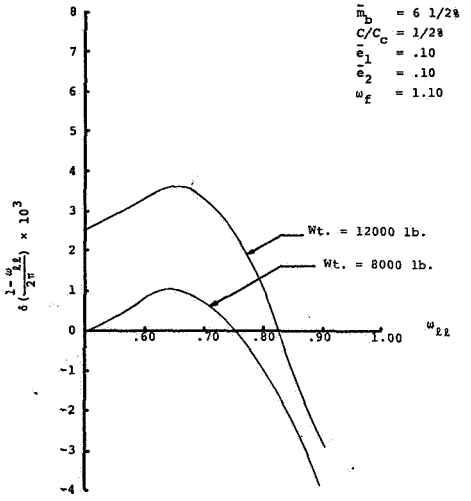

Fig. 17 The effect of off loading without changing Ix_0 and Iy_0.

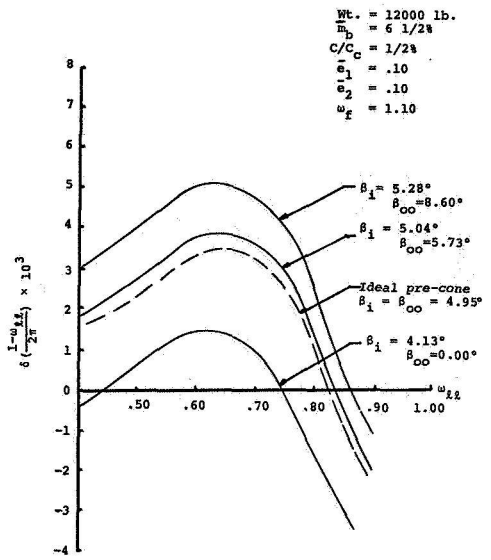

Fig. 18 The effects of pre-cone angle.

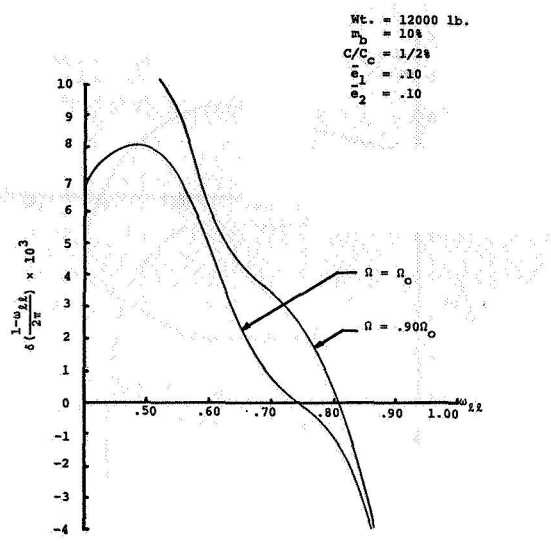

Fig. 20 The effects of a 10% RPM reduction.

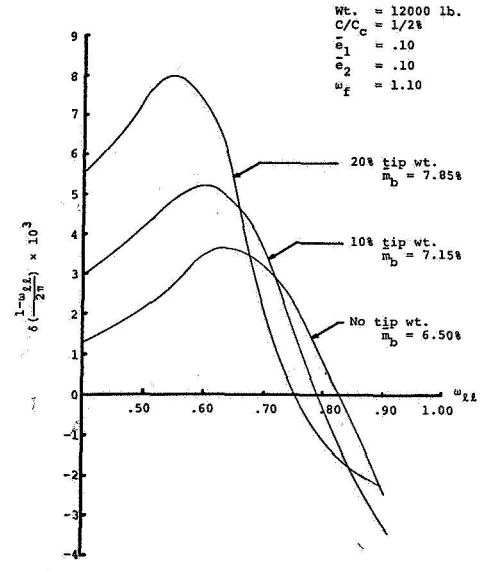

Fig. 19 The effect of tip weights.

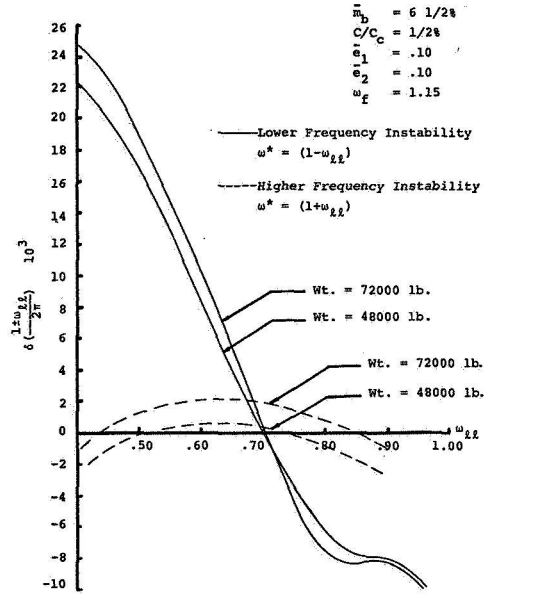

Fig. 21 Stability of heavy helicopters.

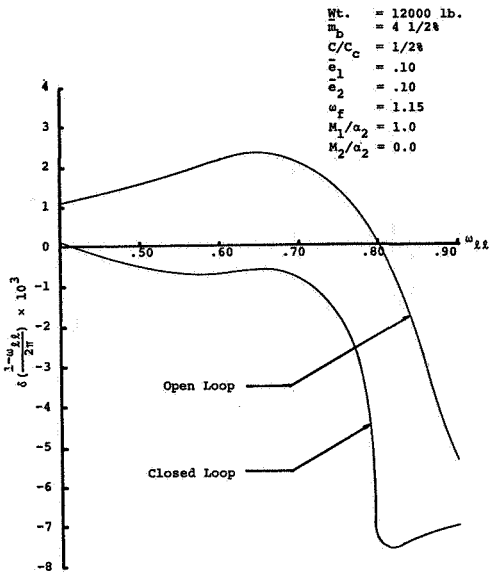

Fig. 22 Comparison of open loop stability to closed loop stability with roll position feedback.

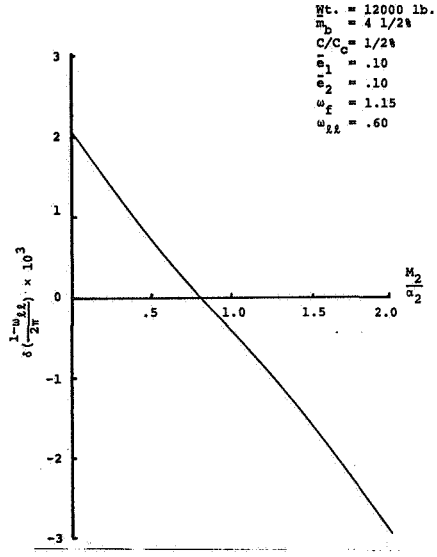

Fig. 23 The effect of roll position feedback control at maximum instability.

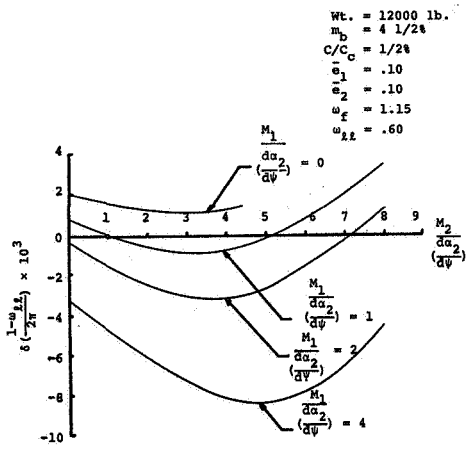

Fig. 24 The effect of roll rate feedback with pitch and roll interacting control actions.

VERTICAL-PLANE PENDULUM ABSORBERS FOR MINIMIZING HELICOPTER VIBRATORY LOADS

Kenneth B. Amer
Manager, Technical Department

James R. Neff
Chief, Dynamics Analysis

Hughes Helicopters
Culver City, California

Abstract

This paper discusses the use of pendulum dynamic absorbers mounted on the blade root and operating in the vertical plane to minimize helicopter vibratory loads.

The paper describes qualitatively the concept of the dynamic absorbers and presents results of analytical studies showing the degree of reduction in vibratory loads attainable. Operational experience of vertical plane dynamic absorbers on the OH-6A helicopter is also discussed.

Introduction

In a helicopter it is important to maintain a low level of vibration for two reasons; first for the comfort of the crew and passengers, and secondly to minimize maintenance problems. During early flight tests of the OH-6A helicopter (see Figure 1) in 1963, a high level of 4/rev fuselage vibration was encountered primarily during approach to hover and during high speed flight.

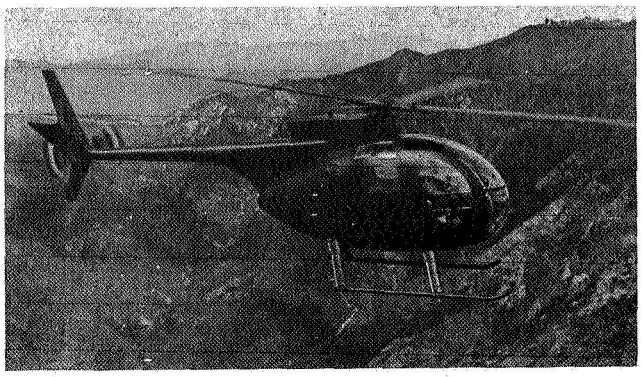

Figure 1. OH-6A Helicopter

Various analytical studies and experimental programs were conducted in an effort to alleviate this problem. The configuration finally adopted was vertical-plane pendulum absorbers mounted at the roots of the main rotor blades (see Figure 2). It is the purpose of this paper to describe the concept of the vertical-plane pendulum dynamic absorber and to present the results of analytical studies and flight tests showing the degree of reduction in vibratory loads attained.

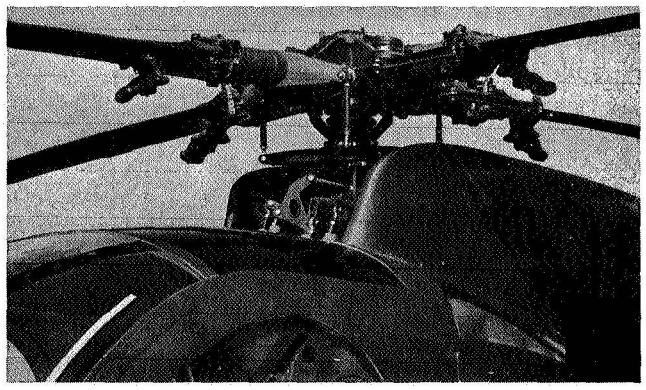

Figure 2. Pendulum Absorbers on OH-6A

Over 3 million flight hours of satisfactory experience have been obtained with the use of vertical-plane pendulum absorbers on the OH-6A helicopter and on its commercial counterpart, the Model 500 helicopter. This operational experience is also discussed in this paper.

Sources of Fuselage Vibration

The OH-6A helicopter has a 4-bladed main rotor. Table I summarizes the sources of 4/rev fuselage vibration from the main rotor. It can be seen from Table I that vertical shears at the blade root with frequencies of 3/rev, 4/rev, and 5/rev can induce 4/rev vibrations in the fuselage. The 3/rev and 5/rev blade root shears induce 4/rev fuselage vibrations by producing 4/rev hub moments. The 4/rev blade root shear produces a 4/rev hub vertical force. With regard to in-plane blade root shears, both the 3/rev and the 5/rev component of in-plane root shear produce a 4/rev hub horizontal force. A further discussion of the mechanism by which rotor blades induce vibration in the fuselage can be found in Chapter 12 of Reference 1, particularly the tables on pages 318 and 319.

Table I. Sources of 4/Rev Fuselage Vibration - 4-Bladed Rotor

Vertical Shear	Load Path	In-Plane Shear	Load Path
3/rev	Hub moment	3-rev	Hub horizontal force
4/rev	Hub vertical force	-	-
5/rev	Hub moment	5/rev	Hub horizontal force

Table I indicates that there are 5 possible sources of excessive fuselage 4/rev vibration in the OH-6A helicopter. The next step was to establish which of the 5 possible sources of vibration were the most important. Tables II and III provide an answer to this question.

Table II. OH-6A Main Rotor Blade Natural Frequencies (per rev) - 100% RPM - Pendulums Off

Flapwise	Chordwise (Cyclic Mode)
2.72	5.14
4.87	

In Table II are listed the main rotor blade flapwise and chordwise natural frequencies near the 3/rev through 5/rev frequency. It can be seen from Table II that the two frequencies most likely to cause a 4/rev vibration in the fuselage are the first and second mode flapwise bending frequencies which are very close to 3/rev and 5/rev. The blade chordwise natural frequency is also close to 5/rev (see Table II). However, Table III confirms that the blade flapwise first mode and second mode frequencies are the primary source of the vibration problem, in that the fuselage vibration is much more responsive to hub moments than it is to hub vertical or horizontal forces.

Table III. OH-6A Cockpit Response to Rotor Excitation, V = 100 Knots (No Pendulums Installed)

	4/Rev Vertical	4/Rev Pitching Moment	4/Rev Rolling Moment	4/Rev Longitudinal Shear	4/Rev Lateral Shear
Excitation Force, lb	130	*86	**112	10	35
Unit Response at Cockpit, in/sec/lb	.0012	.00265	.0106	.00193	.0077
Response at Cockpit, in/sec	.16	.23	1.19	.019	.27

* Blade vertical shear force causing pitching moment.
** Blade vertical shear force causing rolling moment.

Thus blade vertical bending at a frequency of 4/rev and blade chordwise bending at frequencies of 3/rev and 5/rev can be ignored and the primary sources of vibration can be concluded to be blade flapwise bending at 3/rev and at 5/rev.

Concept of Vertical-Plane Dynamic Absorbers

Based on the above evaluation, it was concluded that it was necessary to reduce the level of blade 3/rev and 5/rev flapwise bending. After investigating a number of possible approaches,* it was decided to pursue the concept of a dynamic vibration absorber which is discussed in Reference 2 in the section starting on page 87.

The concept of a dynamic vibration absorber consists of adding a small mass to a large mass. The uncoupled natural frequency of the small mass (vibration absorber) is chosen to be equal to the frequency of the disturbing force. Thus, for the OH-6 vibration problem, it was concluded that it would be necessary to incorporate two dynamic vibration absorbers; one tuned at 3/rev and the other tuned at 5/rev. Furthermore, inasmuch as rotor speed can vary somewhat, it was necessary that the vibration absorbers maintain the proper frequency relative to rotor speed. In order to accomplish this, it was decided to use the concept of a tuned centrifugal pendulum discussed on page 219 of Reference 2. This concept has been used for many years to minimize the torsional vibrations of piston engines. Thus, the final configuration that evolved consisted of two pendulums mounted at the roots of the main rotor blades; one tuned to a natural frequency of 3/rev, the other tuned to a natural frequency of 5/rev. Inasmuch as the shear force and blade motion which were to be minimized were in the vertical plane, the dynamic pendulums were oriented to oscillate in the vertical plane.

Figure 3 shows schematically the pendulum motion relative to the blade deflection for the case of response to 3/rev excitation. It is evident that the centrifugal force from the pendulums is directed such as to cancel most of the transverse shear due to blade modal response. The net result is a significant reduction in the 3/rev vertical shear force transmitted to the hub.

* Other approaches evaluated included providing control of blade first and second mode natural frequencies by means of anti-node weights and by use of preloaded internal cables. Flight tests did not show these methods to be sufficiently effective. Hub-mounted vertical plane pendulums were flown and proved to be effective, but considerations of drag and weight were unfavorable for this configuration. Fuselage-mounted non-rotating dampers were eliminated because of the difficulty of tuning to a sufficiently wide range of frequency. Fuselage-mounted centrifugal pendulum dampers were considered impractical from the standpoint of space requirements and mechanical complexity.

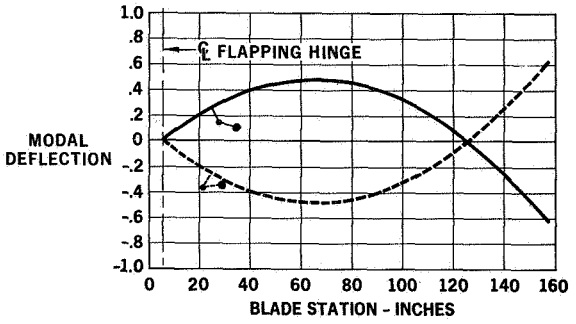

Figure 3. Pendulum Motion Schematic

Basic Physical Parameters

The pendulum configuration that was established, flight tested, and put into service has the following characteristics:

3/rev pendulum
weight: 1.8 lb
actual mass ratio: .048
modal mass ratio: .64

5/rev pendulum
weight: .7 lb
actual mass ratio: .019
modal mass ratio: .52

The pivot axis of both pendulums is located at 15% of the blade span from the center line of the rotor, and 29% of the chord from the leading edge. This location was chosen so that existing bolts in the blade root fitting could be used, thus preventing the introduction of stress concentration points into critical sections of the blade. Analysis indicates that a location further outboard would be more favorable, but this has not been confirmed by test, because of the structural considerations cited above.

Damping of the pendulums due to friction in the pivot bearings is estimated to be equivalent to 1% of the critical viscous damping ratio for the 3/rev pendulums at an amplitude of $\pm 16^{\circ}$. For the 5/rev pendulums at the same amplitude the damping ratio is 3% of critical.

The dampers are "bench" tuned, by means of shims, to the correct pendular frequency within 0.5% of the length of the 3/rev pendulums and to within 1% of the length of the 5/rev pendulums. The effect of mis-tuning has been investigated only to the extent of showing that $\pm$ one shim does not have a consistently observable effect on either qualitative or measured cockpit vibration.

Analytical Studies

Analytical studies were conducted to investigate the effectiveness of vertical plane pendulum absorbers in minimizing the blade vertical root shears and the fuselage vibration levels. The results of these analytical studies are presented in Table IV for the OH-6A at a forward speed of 100 knots. It can be seen from Table IV that the addition of the 3/rev pendulum dynamic absorber reduces the 3/rev vertical root shear by 75%. The addition of the 5/rev vertical dynamic absorber reduces the 5/rev vertical root shear by 85%. The net result is a 72% reduction in the vibration level in the crew compartment.

Table IV. Effect of Vertical-Plane Pendulum Absorbers on Root Shear and Cockpit Vibration - OH-6A

(Analytical Studies, 100 Knots)

Configuration	Root Shear 3/Rev	5/Rev	Cockpit Vibration, amp. in/sec
Undamped Blade	91	42	1.8
Damped Blade	23	6	.5

The analytical procedure used to achieve the results of Table IV is designated SADSAM. This analytical procedure is described in Reference 3 and was conducted in two steps. In the first step, SADSAM was used to calculate the blade root shears for a forward speed of 100 knots both without and with the pendulum absorbers. The analytical model of the blade used in this step was a ten station, fully coupled representation with aerodynamic excitation forces obtained from flight measured pressure distributions (Reference 4). In the second phase of the analysis, a 41 degree-of-freedom fuselage mathematical model, adjusted to agree with shake test results, was analyzed using SADSAM to obtain the effect of the resulting hub moments on the response in the crew compartment.

Flight Test Results

The favorable analytical results referred to above led to a decision to fabricate an experimental set of pendulum dynamic absorbers. These absorbers, similar to those shown in Figure 2, were installed on the flight test OH-6A helicopter. Tests were conducted measuring the vibration level in the crew compartment, both without and with the vertical-plane dynamic absorbers installed. The measured vibration levels at the pilot's seat are presented in Figure 4. It can be seen that the addition of the vertical-plane vibration absorbers reduces the vibration level at the pilot's seat approximately in half. The qualitative assessment by the pilot was also very favorable. Based on these results the decision was made to incorporate vertical-plane dynamic absorbers in the production OH-6A helicopter.

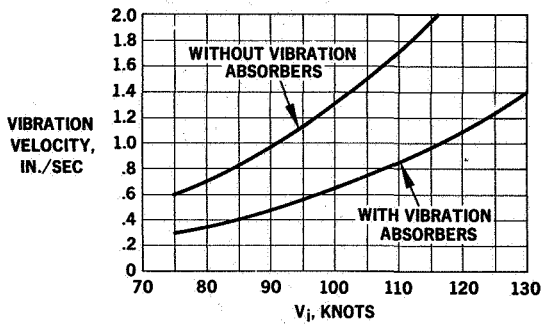

Figure 4. Measured Vibration Level of OH-6A Without and With Pendulum Absorbers

Operational Experience on OH-6A

The vertical plane pendulum absorbers were incorporated on all production OH-6A helicopters and on its commercial counterpart, the Model 500. Over 3,000,000 flight hours have been accumulated. Up to a service life of between 300 and 600 hours, the absorbers did a good job of controlling the vibration level of the helicopter. However, after approximately 300 to 600 hours of service, the bearings and shafts on which the absorbers are mounted exhibited excessive wear, resulting in increased vibration level in the helicopter. Replacement of the bearings and shafts generally returned the helicopter to an acceptable level of vibration. The premature wearing of the bearings and shafts was attributed to the high PV value.

Laboratory tests were conducted on various combinations of bearings and shaft types with the objective of selecting a combination that would have the desired service life of 1200 hours. It was also required that any new shaft and/or bearing materials be interchangeable with the initial production bearings and shafts. Thus no change in geometry was permitted.

The results of these laboratory tests showed that all combinations of shafts and bearings tests, with the exception of one, were inferior to the original configuration (which consisted of a bearing consisting of a stainless steel outer race with a bonded self-lubricating teflon liner, and a stainless steel shaft with an 8 RMS finish). The only improved configuration consisted of an Astro AM1282 bearing, which was specially made for the laboratory test operating on the original shaft. This Astro bearing is currently under consideration for retrofit.

Conclusions

This paper has demonstrated both analytically and by operational experience that the use of pendulum dynamic absorbers, mounted on the blade root and operating in the vertical plane, can successfully reduce helicopter vibratory loads. The specific application on an OH-6A helicopter was a 4-bladed rotor with the pendulums tuned to 3/rev and 5/rev. The pendulums reduced the vibration level in the cockpit to approximately one half of the level that existed prior to the installation of the pendulums.

References

1. Gessow, Alfred and Myers, Garry C., "Aerodynamics of the Helicopter," The MacMillan Company, New York, 1952.

2. Den Hartog, J. P., "Mechanical Vibrations," Fourth Edition, McGraw-Hill Book Co., New York, 1956.

3. Peterson, L., "SADSAM User's Manual," The MacNeal-Schwendler Corp., 7442 N. Figueroa St., Los Angeles, CA, Report MSR-10, December 1970.

4. Scheiman, James, "A Tabulation of Helicopter Rotor Blade Differential Pressures, Stresses, and Motions as Measured in Flight," NASA TMX-952, March 1964.

Acknowledgment

The contribution of R. A. Wagner and other Hughes personnel to the development of the vertical-plane pendulum absorbers is hereby acknowledged.

EVALUATION OF A STALL-FLUTTER SPRING-DAMPER PUSHROD IN THE ROTATING CONTROL SYSTEM OF A CH-54B HELICOPTER

William E. Nettles
U.S. Army Air Mobility Research & Development Lab.,
Eustis Directorate, Ft. Eustis, Va.

William F. Paul and David O. Adams
Sikorsky Aircraft, Division of United Aircraft Corp.
Stratford, Conn.

Abstract

This paper presents results of a design and flight test program conducted to define the effect of rotating pushrod damping on stall-flutter induced control loads. The CH-54B helicopter was chosen as the test aircraft because it exhibited stall-induced control loads. Damping was introduced into the CH-54B control system by replacing the standard pushrod with spring-damper assemblies.

Design features of the spring-damper are described and the results of a dynamic analysis is shown which defined the pushrod stiffness and damping requirements. Flight test measurements taken at 47,000 lb gross weight with and without the damper are presented.

The results indicate that the spring-damper pushrods reduced high-frequency, stall-induced rotating control loads by almost 50%. Fixed system control loads were reduced by 40%. Handling qualities in stall were unchanged, as expected.

The program proved that stall-induced high-frequency control loads can be reduced significantly by providing a rotating system spring-damper. However, further studies and tests are needed to define the independent contribution of damping and stiffness to the overall reduction in control loads. Furthermore, the effects of the spring-damper should be evaluated over a range of higher speeds and with lower-twist blades.

Notation

AOB	angle of bank
CAS	calibrated airspeed, kt
C	damping rate, lb-sec/in.
C_M	blade section pitching moment coefficient
C/C_C	damping ratio
ERITS	equivalent retreating indicated tip speed, kt.
GW	aircraft gross weight
I	torsional moment of inertia
K	spring constant
K_D	damper spring rate, lb/in.
N_R	rotor speed
α	blade section angle of attack
θ_{75}	blade angle at 75% rotor radius
ω	torsional natural frequency, cycles/sec
ω/Ω	ratio of natural frequency to rotor frequency

Presented at the AHS/NASA-Ames Specialists' Meeting on Rotorcraft Dynamics, February 13-15, 1974.

Introduction

Control system loads can limit the forward speed and maneuvering capability of high performance helicopters. The slope of the control load buildup is often so steep (Figure 1) that it represents a fundamental aeroelastic limit of the rotor system. This limit cannot be removed by strengthening the entire control system without incurring unacceptable weight penalties.

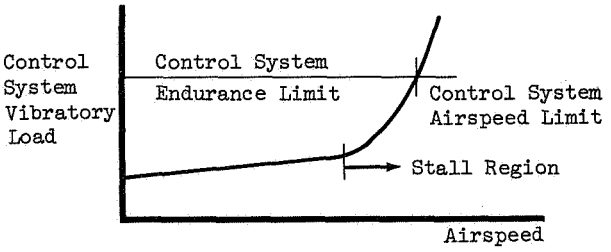

Figure 1. Control Load Characteristic

Studies of the problem reported in Reference 1-7 indicate that the abrupt increase in control loads is induced by high-frequency stall-induced dynamic loading. This loading is attributable to a stall-flutter phenomenon which occurs primarily on the retreating side of the rotor disc in high advance ratio and/or high load factor flight regimes. At the relatively high retreating blade angles of attack which occur under these conditions, the blade section experiences unsteady aerodynamic

stall and the moment coefficient varies with the time-varying angle of attack as shown in Figure 2. Inspection of the moment hysteresis loops exhibited in this figure indicate that positive work can be done on the system as the blade section oscillates in torsion. This aeroelastic mechanism, by which energy is added to the system, can be termed "negative damping" and produces pitch oscillations of increasing amplitude at the blade/control system natural frequency. The rotor system is therefore more responsive to rotor loading harmonics which are close to the blade torsional frequency, and the end result is a rapid buildup of higher harmonic control loads during maneuvers and high-speed flight.

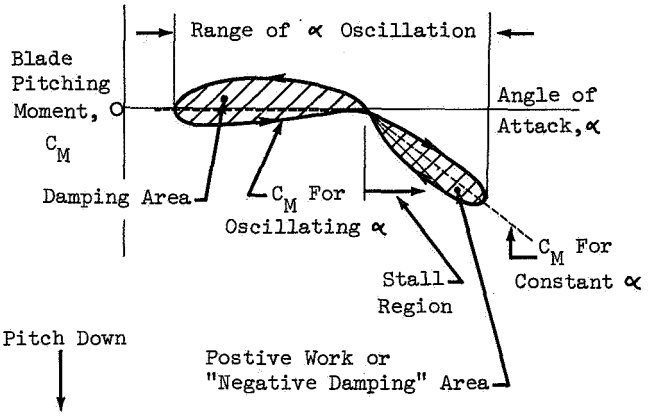

Figure 2. Pitching Moment Hysteresis Loops.

The response of the rotor system is usually stable, because the blades are moving into and out of the negative damping region once per revolution. However, during maneuvers in which a significant portion of the rotor disc is deeply stalled, very large oscillations can exist (Reference 7) and the negative damping region can increase to a point where blade oscillations can continue into the advancing portion of the rotor disc.

Efforts to understand the problem have centered on defining unsteady aerodynamic characteristics of the blades in stall (References 4 and 6) and on incorporating this data into blade aeroelastic computer analyses (References 6 and 9). Results of the studies are encouraging. The buildup of control loads and high-frequency stall-induced loads is predicted with reasonable accuracy.

Recognizing that the basic cause of the problem was insufficient pitch damping, the Eustis Directorate contracted with Sikorsky Aircraft to evaluate the effects of pushrod spring-dampers on control loads of the CH-54B helicopter. This helicopter was selected for the study since it exhibited high-frequency stall-induced control loads during maneuvers at maximum speeds and 48,000 pounds gross weight and was available to the program. Rotating pushrod dampers were used instead of fixed system dampers because they provided the required damping directly at the blade attachment. The program was limited in scope to an analytical and experimental feasibility study of the concept, and was conducted in four phases.

(1) Dynamic Analysis

(2) Functional Design

(3) Ground Tests

(4) Flight Test Evaluation

Dynamic Analysis

An aeroelastic analysis of the CH-54B rotor was performed to evaluate the effectiveness of spring-dampers in reducing the control loads associated with retreating blade stall-flutter and to evolve design criteria. The primary mathematical analysis used was the Normal Modes Rotor Aeroelastic Analysis Y200 Computer Program. This analysis, which is described in Reference 8, represents blade flatwise, edgewise, and torsional elastic deformation by a summation of normal mode responses and performs a time-wise integration of the modal equations of motion. This analysis can also be used to study blade transient response following a control input or disturbance. Aerodynamic blade loading is determined from airfoil data tabulated as a function of blade section angle of attack, Mach number, and first and second time derivatives of angle of attack. Unsteady aerodynamics and a nondistorted helical wake inflow were used throughout this investigation.

The version of the Y200 Program used for this study is a single-blade, fixed-hub analysis. The assumptions were made that all blades are identical and encounter the same loads at given azimuthal and radial positions and that blade forces and moments do not cause hub motion. Any phenomena which are related to nonuniformity between blades or to the effect of hub motion on blade response are not described by this analysis.

Free Vibration Characteristics

For a blade restrained at the root by a pushrod, the first step in the aeroelastic analysis is the calculation of the undamped natural frequencies and modes for a blade rotating in a vacuum. In order to analyze the spring-damper/blade system using the normal modes procedure, the damped free vibration modes and frequencies were calculated based on the model shown in Figure 3. The torsional system was represented by fifteen elastically-connected lumped inertias restrained in torsion by a spring-damper at the blade root. The eigenvalues and eigenvectors of the system response were calculated using a Lagrangian formulation of the damped free vibration equations. A radial mode

shape, natural frequency and modal damping were calculated and used in the Y200 Program.

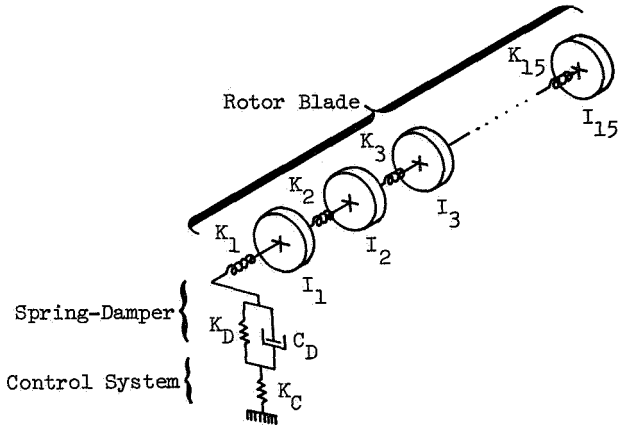

Figure 3. Schematic of the Spring-Damper Free Vibration Problem.

Spring-Damper Behavior

The behavior of the CH-54B spring-damper was determined by employing the free vibration analysis to determine the general relationship between the properties of the damper itself and those of the blade first torsional mode. Figure 4 shows the variation of blade first torsional natural frequency and percent critical damping with changes in the spring and damping constants of the spring-damper.

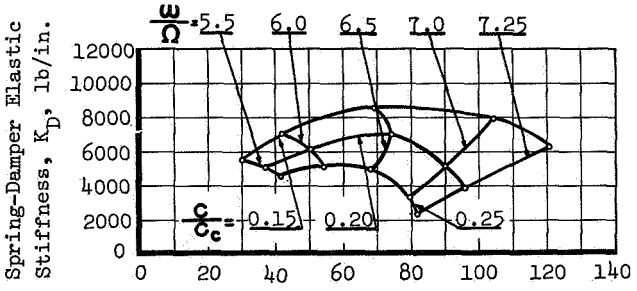

Figure 4. Effect of Spring-Damper Properties on First Torsional Mode Frequency and Damping.

Three trends are evident from this figure:

1. For a given damper spring constant, K_D, high levels of damping can increase the root dynamic stiffness enough to result in torsional natural frequencies which are close to those obtained with a rigid pushrod. It is clear from Figure 4 that as the damping constant, C_D, is increased, the damper spring is effectively bridged so that the torsional natural frequency approaches the standard pushrod value (7.4 per rev.)

2. For each spring constant, K_D, a specified value of the damping constant, C_D, maximizes the modal damping. Increasing or decreasing the damping constant decreased the percent critical damping ratio of the torsional vibration.

3. The variation in the percent critical damping parameter with damping constant is relatively gradual, so small manufacturing differences between the six production dampers will not cause great differences in first torsional mode damping.

Rotor System Analysis

For the initial analytical comparison of the control system loading with and without damping, prior to design of actual hardware, a representative flight condition was selected for which experimental data existed for the conventional system. This data was extracted from the structural substantiation flight tests of the CH-54B and represents a condition in which stall-induced dynamic loading was experienced. The specific flight condition used - gross weight 47,000 lb, 100% Rotor Speed (185 RPM), sea level standard, 30° angle of bank right turn- was selected because it was the condition which consistently produced stall-induced high-frequency loading. The plot of rotating pushrod load against azimuth for this condition is shown in Figure 5a.

The pushrod load resulting from the Y200 Normal Modes Program for the same flight condition is compared with flight test results in Figure 5b. To account for the increase in rotor lift experienced in the turn, a lift of about 60,000 lb and a propulsive force of 3,300 lb was calculated. Although the calculated pushrod load shows a significantly greater steady nose-down load, the vibratory amplitude and frequency content of the analytical result match the test reasonably well.

To study the effectiveness of the spring-damper in reducing vibratory control loads, the flight condition described above was simulated using several spring-damper configurations. Each of these cases was run with the same control settings as the standard case. The results are shown in Figure 6. As shown, the combination of 5000 lb/in. and damping between 50 and 90 lb-sec/in. was about optimum. Referring back to Figure 4, it is seen that a damping value of 90 lb-sec/in. would provide a frequency of 7P which was the same as the standard aircraft. This configuration was therefore selected because the test results could then be used to evaluate the spring-damper at the same torsional frequency as the

standard aircraft. Also it would provide an option to reduce the damping in follow-on programs to allow an evaluation at 5.5/rev and 20% critical damping.

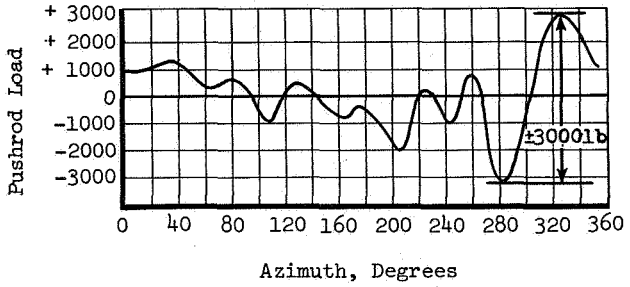

Figure 5a. Measured Flight Test Result.

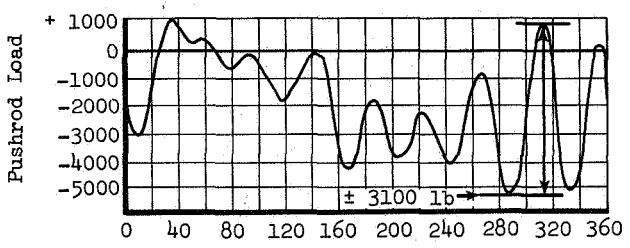

Figure 5b. Derived Result.

Figure 5. Comparison of Measured and Derived Conventional Pushrod Load - CH54B, 47000 lb G.W., Sea Level, 100 KT, 30° AOB Right Turn.

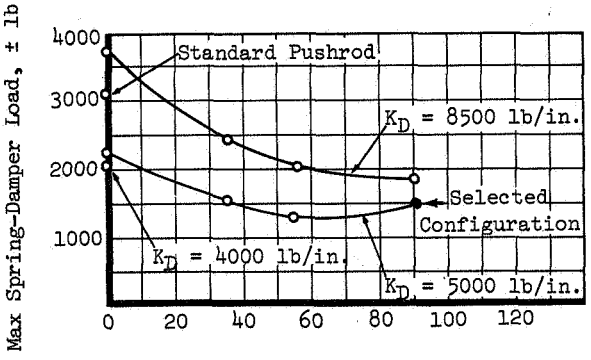

Figure 6. Effect of Spring-Damper Parameters on the Amplitude of Vibratory Control Loads

The plots of pushrod load against azimuth shown in Figure 7 compare a standard pushrod with a spring-damper having a spring rate of 5,000 lb/in. and a damping rate of 90 lb-sec/in. For this configuration the free vibration analysis gives a torsional frequency of 7 per rev and 0.20 critical damping ratio. The Figure shows approximately equal amounts of one-per-rev variation occurring in the control load time-histories since the pushrod spring-dampers do not affect the low-frequency torsional motion. As a result, the overall peak-to-peak control load is reduced by only 25%, while the high-frequency retreating blade control loads are reduced by more than 50%. It is these high-frequency loads that cause the 6 per rev control system loads in the fixed system.

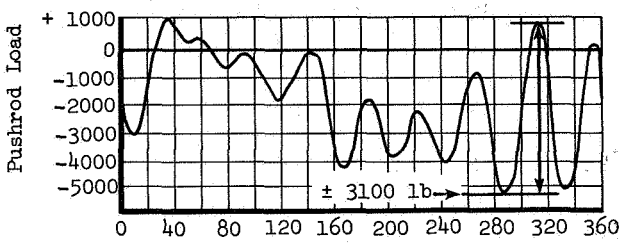

Figure 7a. Conventional Pushrod.

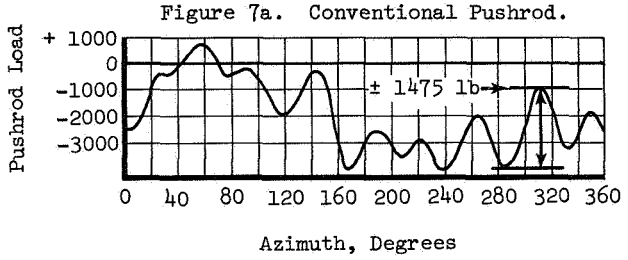

Figure 7b. Stall-Flutter Spring-Damper, K_D = 5000 lb/in., C_D = 90 lb-sec/in.

Figure 7. Comparison of Derived Conventional Pushrod Load and Spring-Damper Load - CH-54B, 47000 lb G.W., Sea Level, 100 KT, 30° AOB Right Turn.

It is clear from this analysis that (1) damping at the blade root is effective in reducing control loads for a given root stiffness and (2) reducing root stiffness tends to decrease the loads for a given damping constant (at least for the ranges investigated).

Functional Design

Design Requirements

The aeroelastic analysis indicated that spring and damping introduced at the blade root could significantly reduce stall-induced loads. The most favorable location for the test of a blade root spring-damper is at the pushrod connecting the rotating swashplate to the blade horn, since the existing pushrod may be replaced easily with the spring-damper. It was determined that a spring-damper device could be fabricated to replace the conventional pushrod, provided that the restrictive size limitations could be met. The use of an elastomer as the primary structural member met the size and spring rate requirements.

The design requirements, based on the aeroelastic analysis and the planned test programs, are summarized as follows:

- Replace Conventional Pushrod
- Life - 50 hr

- Load - ±5,000 lb
- Spring Rate - 5,000 lb/in.
- Damping Rate - 90 lb-sec/in.
- Maximum Elastic Deflection - ±1/2 in.
- Adjustable for Blade Tracking
- Fail-Safe Design

Principles of Operation

The final configuration of the stall-flutter spring-damper pushrod designed to meet the above requirements is shown in Figures 8 and 9.

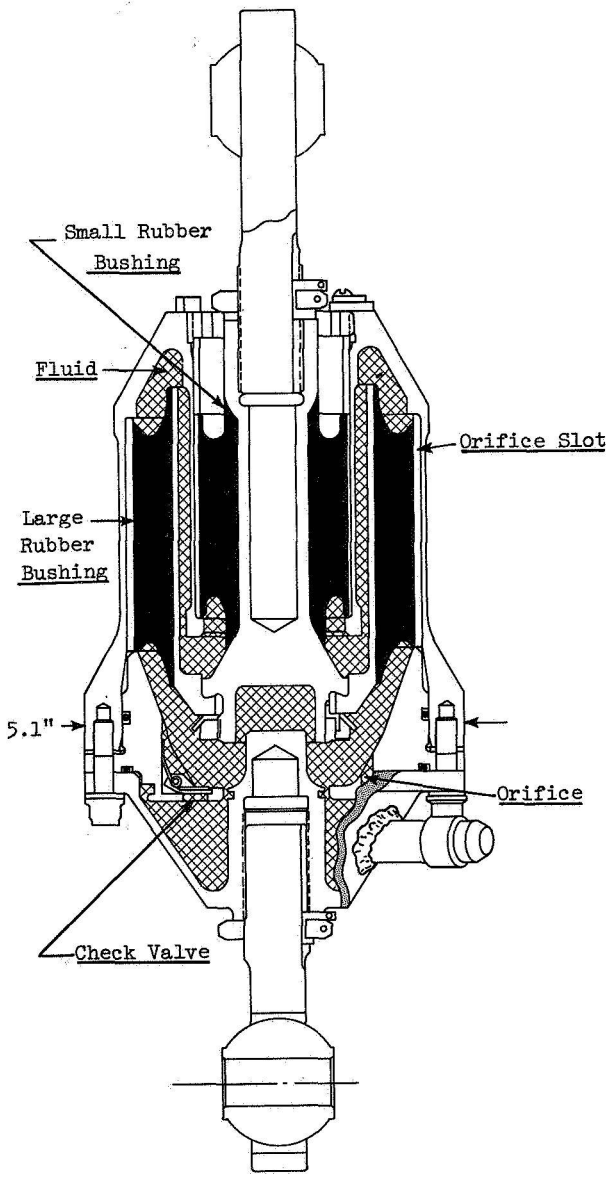

Figure 8. Stall-Flutter Spring-Damper Pushrod Assembly.

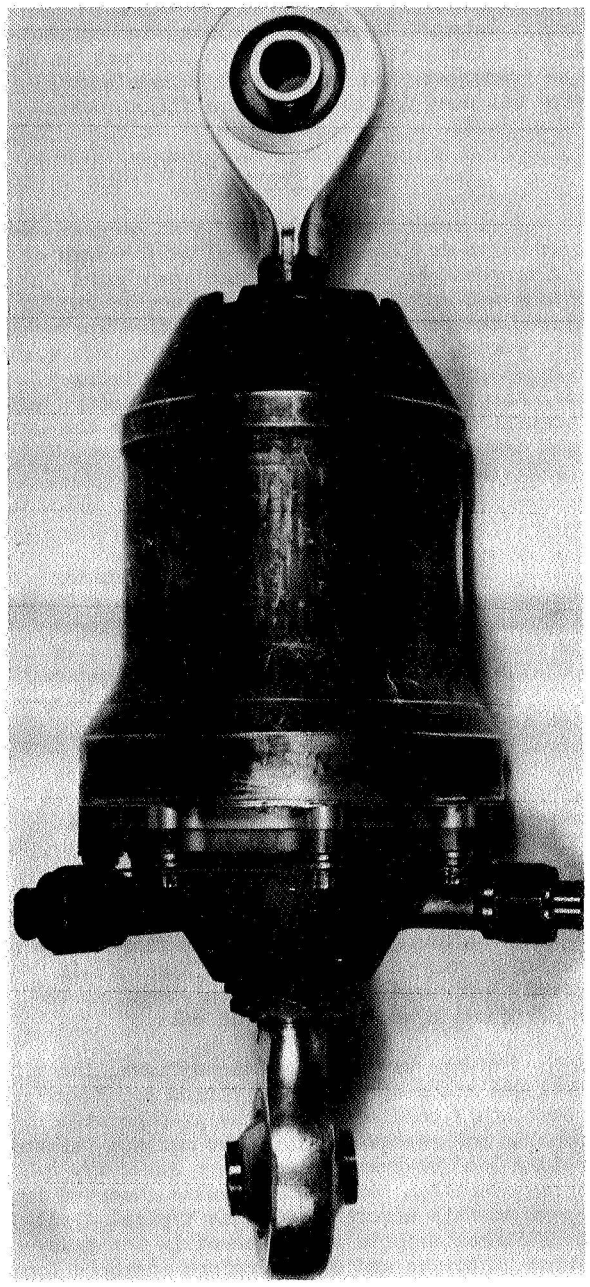

Figure 9. Stall-Flutter Spring-Damper Pushrod.

The concept consists basically of a piston restrained in a cylinder by two natural rubber elastomeric bushings which provide the required spring rate. Damping is obtained by displacement of fluid through orifices. The bushings are mounted in parallel, thereby providing a fail-safe design. In addition, physical stops are incorporated to limit spring-damper deflection to ± 1/2 inch in the event of overload or complete rubber failure. No sliding action takes place as the spring-damper is deflected. Elastomeric elements were chosen because of their high allowable

strains, integral hydraulic sealing, and compactness. An integral air-oil accumulator was found to be inadequate and an external accumulator system was used in the ground and flight tests.

Ground Tests

A comprehensive ground test program was conducted to develop the required performance of the spring-damper, to demonstrate structural adequacy and safety for the flight tests, and to evaluate the performance of an installed spring-damper system. This was accomplished by the means of single unit dynamic performance and fatigue tests, flight unit proof and operation tests, and an installed system whirl tests utilizing the flight test spring-dampers and rotor blades.

Flight Test Evaluation

The performance of the stall-flutter spring-damper pushrod system installed on a CH-54B helicopter was evaluated in a series of flight tests consisting of: (1) base-line flights of the CH-54B helicopter in standard configuration, and (2) comparison flights with the spring-damper system installed.

The investigation was limited to the feasibility of the damper and did not extend to an extensive evaluation of the overall effect on the CH-54B operating envelope.

Baseline Flights

A short series of baseline flights was conducted on the instrumented test aircraft in standard configuration in order to obtain up-to-date performance and control load data.

Of the several conditions flown, the 115 kt, 96% rotor speed, level flight point was the best stall condition from the standpoint of uniformity and repeatability. The maximum pushrod vibratory load observed was about ± 2,100 lb. This is lower than some stall results observed in the past on this aircraft, but the typical stall-flutter characteristic was observed in the pushrod time histories and was therefore adequate for baseline purposes.

Spring-Damper Pushrod Tests

The spring-damper pushrods were installed on the CH-54B rotor head as shown in Figure 10 and 11. Flight test time histories of rotating pushrod load for rigid pushrods and for the spring-damper pushrods at 47,000 lb gross weight are shown in Figures 12 and 13. These segments of data which depict the time history for approximately 1-1/2 revolutions were selected as representative samples from oscillograph traces in which the waveform was continuously repeated for more than 15 revolutions.

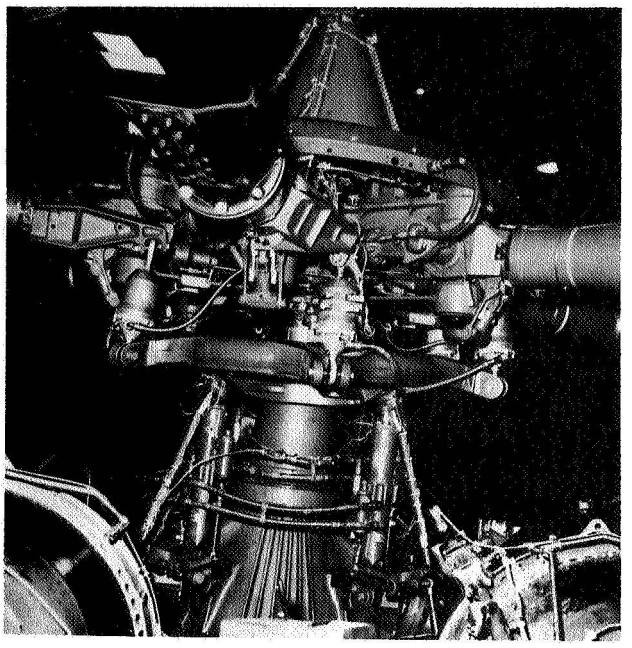

Figure 10. Spring-Damper System Flight Aircraft Installation.

Figure 11. First Flight of the Spring-Damper System, February 6, 1973.

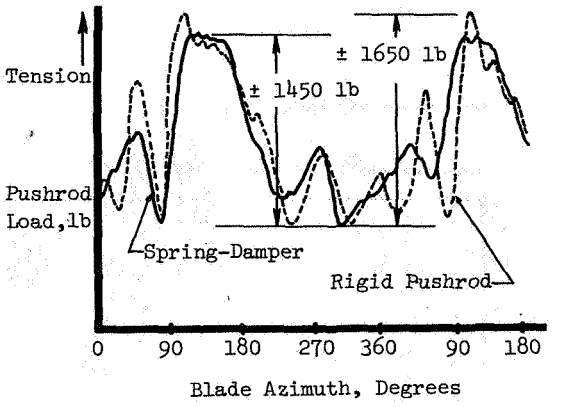

Figure 12. Rotating Pushrod Load Comparison 110 KT 96% N_R Level Flight, 4700 lb.

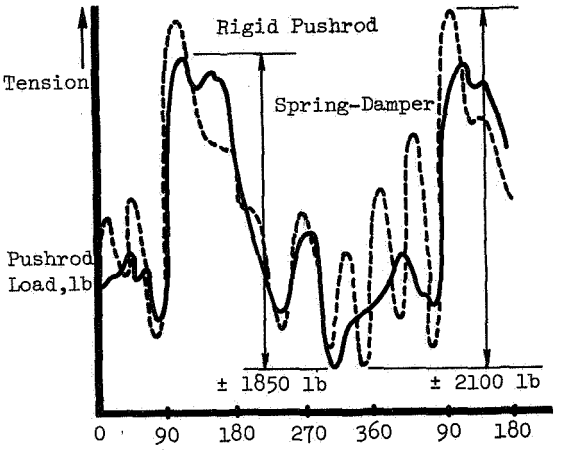

Figure 13. Rotating Pushrod Load Comparison 115 KT 96% N_R Level Flight, 47000 lb GW.

As shown, the rigid pushrod record exhibits the high-frequency oscillation beginning on the retreating side which is characteristic of the stall-flutter phenomenon. This frequency was between 7 and 8 per rev and compares well with the calculated system torsional natural frequency of 7.4 per rev. As seen, the high-frequency loads were significantly reduced with the spring-damper pushrods. The overall reduction was smaller because the low-frequency response was not reduced. This was expected because the high twist blades produce large 1p loads and the spring-damper was not designed to reduce these loads. As shown, the results demonstrate a reduction of almost 50% in high-frequency loads. A spectral analysis of the data burst which contains this cycle is shown in Figure 14.

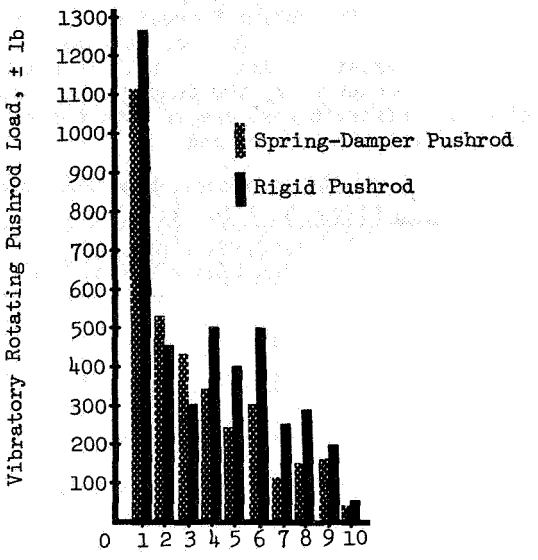

Figure 14. Comparison of Spectral Analyses - CH-54B, 47000 lb G.W., 115 KT 96% N_R Level Flight, 2000' Altitude.

Comparison of Stationary Control Loads

Flight test time-histories of right lateral stationary star load for rigid pushrods and for spring-damper pushrods are shown in Figure 15. These records show the expected dominance of the 6 per rev response in a 6-bladed rotor. As shown, stationary control loads were reduced by 40% for the spring-damper case.

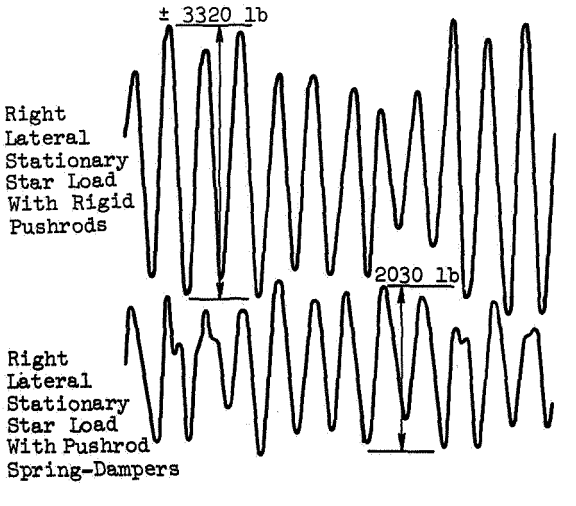

Figure 15. Comparison of Stationary Control Loads.

A plot of stationary control load against ERITS (Equivalent Retreating Indicated Tip Speed) is shown and defined in Figure 16. The sharp increase in load as stall is entered is seen to be unchanged by the damper installation, but as the aircraft goes deeper into the stall region, the loads are reduced.

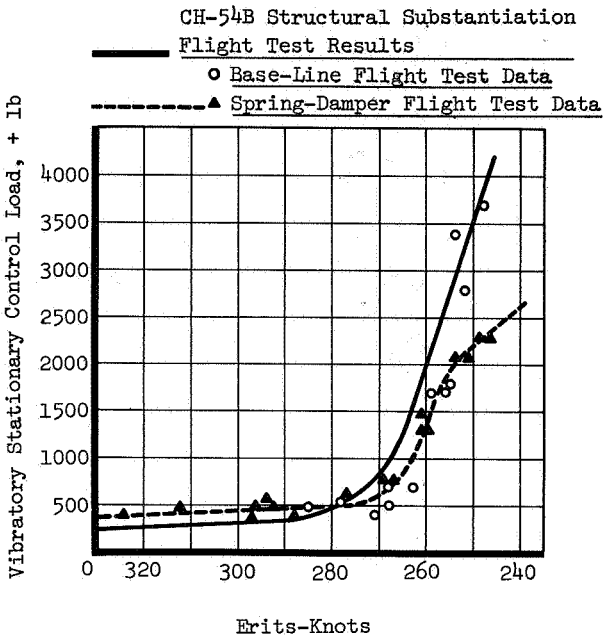

Figure 16. Stationary Control Load Against Erits

Note: Erits - Equivilent Retreating Indicated Tip Speed

$$= \frac{\text{Rotating Tip Speed} \times \sqrt{\text{Air Density Ratio}} - \text{CAS}}{\sqrt{\frac{\text{Load Factor} \times \text{Gross Weight}}{37{,}500}}}$$

Comparison of Aircraft Handling Qualities

The handling qualities of the aircraft were unchanged with the spring-dampers installed. Pilot's reports state that the aircraft exhibited the characteristic increase in vibration, difficulty in maintaining airspeed, and forward control motion required when approaching a stall condition in both the baseline and spring-damper flights. The stalled condition of the rotor appears unaffected by the installation of the spring-damper. Blade stresses and blade motions (except for the stall-flutter torsional oscillation) are virtually the same in each case. Cockpit vibration levels are unchanged. This was expected because the stall was not changed, just the local torsional response of the blade was changed.

The effect of the damper on the control system can be seen in plots of control positions against airspeed (Figure 17). The lateral control is unaffected, but as much as 10% more forward longitudinal control is required when flying at the 115 kt, 96% N_R reference stall condition.

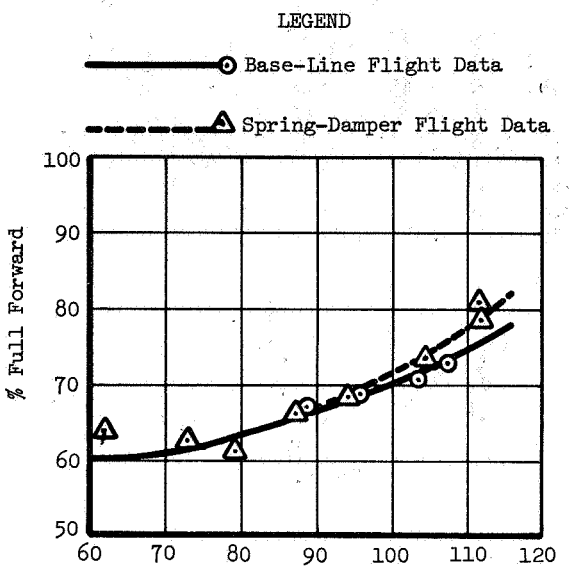

Figure 17a. 100% Rotor Speed.

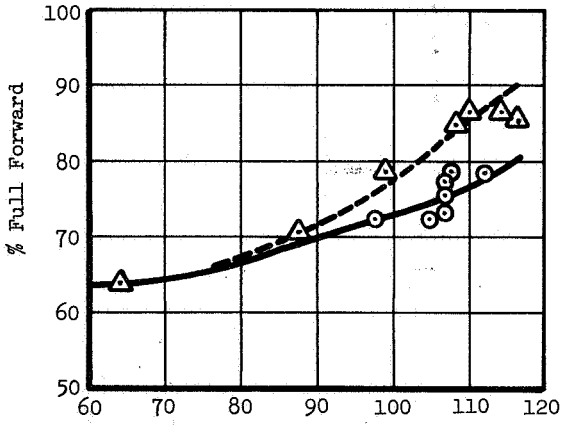

Figure 17b. 96% Rotor Speed

Figure 17. Longitudinal Control Positions.

Aeroelastic Analysis of Flight Test Data

Following completion of flight testing, three additional computer analysis conditions were run, using test conditions actually observed in the flight tests. The methods used were the same as described earlier with the exception that a calculated lift higher than the gross weight actually flown was used. The amplitudes of pushrod load predicted were much lower than observed using the correct lift, and since the comparison with and without the spring dampers was of primary interest, the calculated lift was increased. This shows that improvement in the

analysis is needed.

Figure 18 shows pushrod load vs azimuth for the 115 kt, 96% N_R reference condition for conventional pushrods as generated by the aeroelastic analysis and as observed in the baseline flight. The analysis again shows a good correlation in wave shape with test result. Based on analysis of force-displacement phase shifts seen in the flight test results, a damping rate of 70 lb-sec/in. was determined to be a likely value actually achieved. Figure 18 also compares the analytical result with the flight test result.

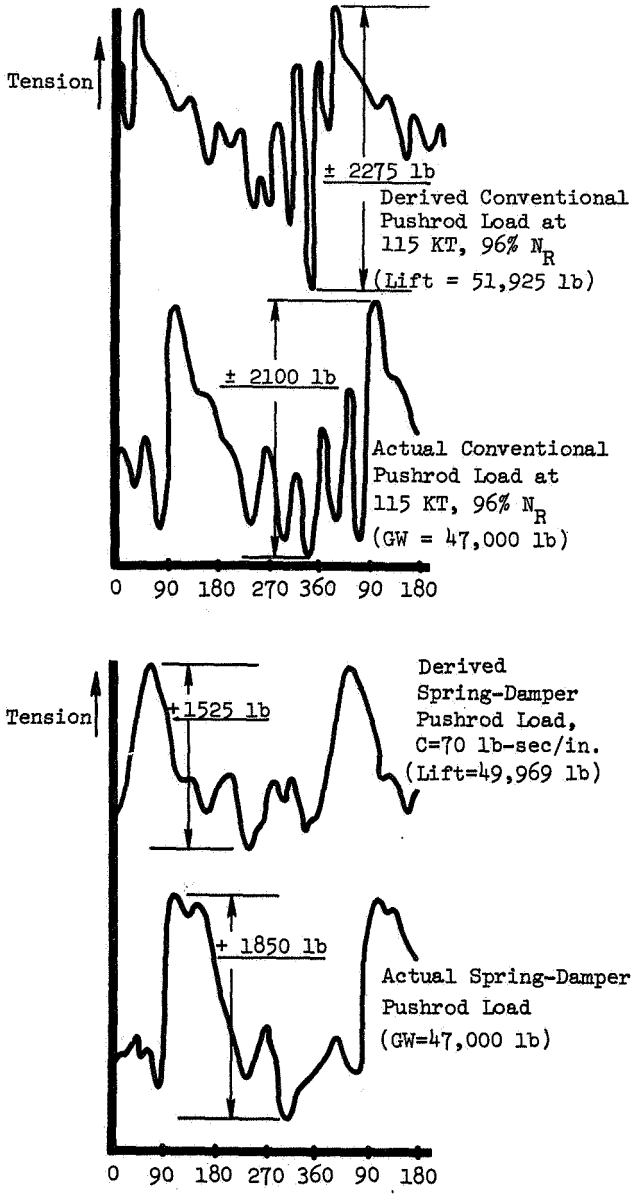

Figure 18. Comparison of Measured and Derived Pushrod and Spring-Damper Loads.

A good correlation in wave shape is obtained. However, the sharp reduction in peak-to-peak amplitude over the rigid pushrod case as predicted by the aeroelastic analysis is again not achieved in practice. It should be noted that the aeroelastic analysis assumes that all blades and spring-dampers are identical, which is known not to be case. Difference among spring-dampers would at least contribute to the dominant one-per-rev component and perhaps the harmonics as well.

Conclusions

It is concluded that:

1. Stall-flutter spring-damper pushrods located in the rotating control system effectively reduced stall-induced high-frequency rotating control loads on the CH-54B by almost 50% and overall stationary control loads by more than 40%.

2. The spring-damper pushrod system does not significantly alter the performance or handling qualities of the CH-54B helicopter.

Recommendations

The test results were very encouraging, but as usual raised more questions than it answered. Some of these are stated below:

1. The combination of a spring and damping worked well, but quantatively what was the contribution of each?

2. Would lower twist, higher mach number and lower frequency provide different results?

3. Would a high-speed aircraft show some improvement in performance in stall with the spring-damper?

To help answer these questions, the CH-54B rotor system could be installed on an H53 helicopter and flown to high speed. Damping, torsional frequency, and twist could easily be varied to qualify their effects. Plans to accomplish this are underway.

References

1. Harris, F. D., and Pruyn, R. R., BLADE STALL - HALF FACT, HALF FICTION, American Helicopter Society, 23rd Annual National Forum Proceedings, AHS Preprint No. 101, May, 1967.

2. Ham, N. D., and Garelick, M. S., DYNAMIC STALL CONSIDERATIONS IN HELICOPTER ROTORS, Journal of the American Helicopter Society, Vol. 13, No. 2, April 1968, pp. 49-55.

3. Ham, N. D., AERODYNAMIC LOADING ON A TWO-DIMENSIONAL AIRFOIL DURING DYNAMIC STALL, AIAA Journal, Vol. 6, No. 10, October 1968, pp 1927-1934.

4. Liiva, J., et al., TWO-DIMENSIONAL TESTS OF AIRFOILS OSCILLATING NEAR STALL, Vol. I, Summary and Evaluation of Results, The Boeing Company, Vertol Division; USAAVLABS TR 68-13A, U. S. Army Aviation Materiel Laboratories, Fort Eustis, Virginia, April 1968, AD 670957.

5. Carta, F. O., et al., ANALYTICAL STUDY OF HELICOPTER ROTOR STALL FLUTTER, American Helicopter Society, 26th Annual National Forum, AHS Preprint No. 413, June, 1970.

6. Arcidiacono, P. J., et al., INVESTIGATION OF HELICOPTER CONTROL LOADS INDUCED BY STALL FLUTTER, United Aircraft Corporation, Sikorsky Aircraft Division; USAAVLABS Technical Report 70-2, U. S. Army Aviation Materiel Laboratories, Fort Eustis, Virginia, March 1970, AD 869823.

7. Carta, F. O., and Niebanck, C. F., PREDICTION OF ROTOR INSTABILITY AT HIGH FORWARD SPEEDS, Vol. III, Stall Flutter, United Aircraft Corporation, Sikorsky Aircraft Division; USAAVLABS Technical Report 68-18C, U. S. Army Aviation Materiel Laboratories, Fort Eustis, Virginia, February 1969, AD 687322.

8. Arcidiacono, P. J., STEADY FLIGHT DIFFERENTIAL EQUATIONS OF MOTION FOR A FLEXIBLE HELICOPTER BLADE WITH CHORDWISE MASS UNBALANCE, USAAVLABS TR-68-18A, February 1969, AD 685860.

9. Carta, F. O., et al., INVESTIGATION OF AIRFOIL DYNAMIC STALL AND ITS INFLUENCE ON HELICOPTER CONTROL LOADS, USAAVLABS TR72-51, Eustis Directorate, U. S. Army Air Mobility Research and Development Laboratory, Fort Eustis, Virginia, September 1972, AD 752917.

MULTICYCLIC JET-FLAP CONTROL FOR ALLEVIATION OF HELICOPTER BLADE STRESSES AND FUSELAGE VIBRATION

John L. McCloud, III* and Marcel Kretz**
Ames Research Center, Moffett Field, California 94035

Abstract

Results of wind tunnel tests of a 12-meter-diameter rotor utilizing multicyclic jet-flap control deflection are presented. Analyses of these results are shown, and experimental transfer functions are determined by which optimal control vectors are developed. These vectors are calculated to eliminate specific harmonic bending stresses, minimize rms levels (a measure of the peak-to-peak stresses), or minimize vertical vibratory loads that would be transmitted to the fuselage.

Although the specific results and the ideal control vectors presented are for a specific jet-flap driven rotor, the method employed for the analyses is applicable to similar investigations. A discussion of possible alternative methods of multicyclic control by mechanical flaps or nonpropulsive jet-flaps is presented.

Notation

a, b, c, ...	matrix elements
b	number of blades
c	chord of blades
c_l	blade section lift coefficient
Δc_l	increment of blade section lift coefficient due to multicyclic jet-flap deflection
$\overline{C}_L$	rotor average lift coefficient $(6C_{LR}/\sigma)$
C_{LR}/σ	rotor lift coefficient $(L/\rho(\Omega R)^2 bcR)$
C_{XR}/σ	rotor propulsive force coefficient $(X/\rho(\Omega R)^2 bcR)$
C_{YR}/σ	rotor side-force coefficient $(Y/\rho(\Omega R)^2 bcR)$
F_1, F_2, F_3	forces measured below the rotor hub
L	rotor lift
R	rotor radius
T	transfer matrix
V	forward flight velocity
V_{n_c}	cosine component of the summation of forces F for the nth harmonic
V_{n_s}	sine component of the summation of forces F for the nth harmonic
X	rotor propulsive force
Y	rotor side force
α_s	rotor shaft axis inclination
δ	jet-flap deflection angle
$\theta_{3P} = \frac{1}{3}\tan^{-1}(\delta_{3s}/\delta_{3c})$ $\theta_{4P} = \frac{1}{4}\tan^{-1}(\delta_{4s}/\delta_{4c})$	azimuth angles for maximum deflection
σ	blade bending stress (or rotor solidity for rotor coefficient definitions)
ρ	air density
ψ	azimuth position
Ω	rotor rotational velocity

Subscripts

c	cosine
m	variable parts
p	primary control
s	sine
0, 1, 2, 3 . . .n	harmonic number

Superscript

T	transpose of matrix or vector

(Units are as noted, or such as to produce unitless coefficients.)

Introduction

To achieve its full potential as the most effective VTOL aircraft, the helicopter must drastically reduce its characteristic vibrations and attendant high maintenance costs. As shown in Reference 1, helicopter maintenance costs are twice those of fixed-wing aircraft of the same empty weight. With the same basic elements — engines, gear boxes, pumps, propellers, and avionics equipment — in both aircraft, this difference is assuredly traceable to the high vibration environment of helicopter components. Coping with this environment, helicopter designers are forced to provide heavier systems, which result in higher ratios of empty weight to payload. These ratios combine to yield maintenance costs per unit payload that are greater than twice those of fixed-wing aircraft. The relationship between oscillating loads — hence vibration — and maintenance costs has been dramatically demonstrated and reported in Reference 2. As shown in that report, the Sikorsky bifilar system reduced rotor-induced vibratory loads by 54.3%, which in turn reduced failure rates so that 48% fewer replacement parts were required, and overall maintenance costs were reduced by 38.5%.

Many vibration suppression systems are being investigated by various groups. These systems are characterized as either absorption, isolation, or active control. The multicyclic jet-flap control is an active control system, which controls or modulates the oscillating loads at their source, that is, on the blades themselves. That we can effectively change the loading distribution of a helicopter rotor in forward flight so as to reduce cyclic blade stress variations, or to reduce vibratory loads transmitted to the fuselage, has been demonstrated by large-scale wind tunnel tests of the Giravions Dorand jet-flap rotor at Ames Research Center. The rotor, its design, and performance characteristics have been reported on in References 3 and 4. Its supporting wind tunnel test equipment and some of the results of the multicyclic load alleviation tests were presented in Reference 5. Some of that multicyclic test data will be shown herein also.

*Research Scientist
Ames Research Center, Moffett Field, Calif. 94035

**Chief Engineer
Giravions Dorand, 92150 Suresnes, France

The main purpose of this paper is to show the method used to analyze the multivariable data, and how it is possible to develop several "ideal" control schedules or vectors to achieve specific blade stress and vibratory load reductions. A simplified analysis of the results is presented, indicating that multicyclic systems that do not employ propulsive jet-flaps may be feasible.

Rotor and Test Apparatus

The Dorand Rotor is two-bladed, with a teetering hub and offset blade coning hinges, but no feathering hinges. The rotor is driven in rotation by a jet-flap, of the blown mechanical flap type, on the outer 30% of the blade radius. The mechanical flaps are deflected by a swash-plate and cam system, which provided both collective and harmonic control. Swash-plate tilt provided the longitudinal and lateral control, whereas the cams introduced second, third and fourth harmonic variations. The rotor is shown, mounted in the NASA-Ames 40- by 80-ft wind tunnel, in Figure 1. Further details of the rotor and test apparatus are given in References 3, 4, 5, and 6.

Results and Analysis

The wind tunnel tests, their range and the modi operandi, are described in Reference 6. The tests simulated forward flight conditions at blade-loading coefficients C_{LR}/σ somewhat greater than conventional rotors employ.

Figures 2 and 3 (taken from Reference 5) show some typical results from the multicyclic tests. Figure 2 shows three sets of jet-flap deflection angle and blade-bending stresses with and without multicyclic control. Some control distortion is affecting the "without multicyclic control" in that the deflection is not purely sinusoidal. The basic bending stresses are predominantly three per revolution (3P), typical for a relatively stiff, heavy blade. The peak-to-peak stress reductions are 29, 21, and 36%. Figure 3 shows the effect of the multicyclic control on the forces below the hub in the nonrotating system: on the left, traces for three vertical force transducers for the condition of zero multicyclic control; on the right, traces for the same transducers for multicyclic control applied.

These tests produced data for a large number of flight conditions and multicyclic deflection combinations. More of these data are presented in Reference 6, which includes both time histories and harmonic coefficients of blade-bending stress, vertical forces, and jet-flap deflection.

Blade-Bending Stresses

As discussed in Reference 5, the relationships between the time histories of jet-flap deflections and the resulting blade-bending stresses can be expressed by a transfer matrix.* The time histories of jet-flap deflection and blade-bending stress are both expressed as harmonic series. If the harmonic coefficients of the stress variation (Eq. 1) are related to the jet-flap deflection harmonic coefficients (Eq. 2), as shown in Eq. 3, they can be expressed in the matrix form as in Eq. 4.

$$\sigma = \sigma_o + \sigma_{1_c} \cos\psi + \sigma_{1_s} \sin\psi + \sigma_{2_c} \cos 2\psi + \sigma_{2_s} \sin 2\psi + \ldots \quad (1)$$

$$\delta = \delta_o + \delta_{1_c} \cos\psi + \delta_{1_s} \sin\psi + \delta_{2_c} \cos 2\psi + \delta_{2_s} \sin 2\psi + \ldots \quad (2)$$

if

$$\sigma_{n_s} = (a_{n_s})(\delta_o) + (b_{n_s})(\delta_{1_c}) + (c_{n_s})(\delta_{1_s}) + (d_{n_s})(\delta_{2_c}) + \ldots (\sigma_{n_{s_0}}) \quad (3)$$

then

$$\begin{vmatrix} \sigma_o \\ \sigma_{1_c} \\ \sigma_{1_s} \\ \cdot \\ \cdot \\ \sigma_{n_s} \end{vmatrix} = \begin{vmatrix} a_o & b_o & c_o & d_o & \cdot & \cdot & \sigma_{o_0} \\ a_{1_c} & b_{1_c} & c_{1_c} & d_{1_c} & \cdot & \cdot & \sigma_{1_{c_0}} \\ a_{1_s} & b_{1_s} & c_{1_s} & d_{1_s} & \cdot & \cdot & \sigma_{1_{s_0}} \\ \cdot & \cdot & \cdot & \cdot & \cdot & \cdot & \cdot \\ \cdot & \cdot & \cdot & \cdot & \cdot & \cdot & \cdot \\ a_{n_s} & b_{n_s} & c_{n_s} & d_{n_s} & \cdot & \cdot & \sigma_{n_{s_0}} \end{vmatrix} \times \begin{vmatrix} \delta_o \\ \delta_{1_c} \\ \delta_{1_s} \\ \cdot \\ \delta_{n_s} \\ 1 \end{vmatrix} \quad (4)$$

The last term of Eq. 3 and the last column of the transfer matrix represent the harmonics of stress, which are due to the flight condition. With the column matrices or vectors of the harmonic contents of jet-flap deflection and blade stresses known for several conditions, computer routines can solve for the transfer matrix elements.

A sample result of this method was shown in Reference 5, together with correlation plots showing very good agreement between stresses calculated using the transfer matrix and measured stresses. The matrix, based on 15 flight conditions, showed large amounts of interharmonic coupling, particularly for the third and fourth harmonics of stress.

It is apparent from Eq. 4 that it is possible to determine multicyclic jet-flap deflection amplitudes that will eliminate the corresponding higher harmonic stress coefficients. These higher harmonic stress terms are set to zero and the equation is then solved for the required jet-flap deflection coefficients. These coefficients will be hereinafter called the "ideal harmonic control vector." Reference 6 presents some of these control vectors.

Although the objective of zero higher harmonic stresses was achieved, the requisite multicyclic jet-flap deflections produced different amounts of 1P stresses and, in some instances, the peak-to-peak stresses were increased. The changes in 1P stresses imply a change in the rotor's thrust and inplane forces. (Note that the ideal harmonic control vector as determined in Eq. 4 may be considered to be for "fixed stick" conditions as existed in the wind tunnel tests.) Therefore, a second transfer matrix (Eq. 5) was defined as shown below.

*This method of analysis was first suggested and developed by Dr. Jean-Noel Aubrun of Giravions Dorand.

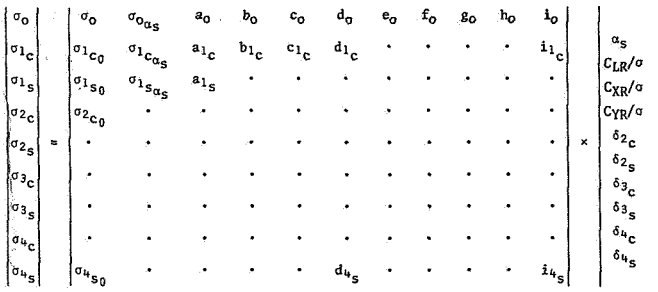

(5)

Notice that the columns of the transfer matrix and the elements of the control vector have been rearranged. The first column represents stress levels for the condition of zero rotor shaft inclination, zero rotor force coefficients, and no jet-flap deflections. The second through fourth columns represent the changes in stress level due to rotor angle of attack and the rotor's force coefficients. The remaining columns correspond to stress derivatives with respect to the multicyclic jet-flap deflections. The control vector has been realigned to reflect the column changes. Note that the matrix elements are no longer defined by Eq. 3, but by Eq. 5 itself, and the basic "collective" and "1P cyclic" terms have now been replaced by the rotor's force coefficients, C_{LR}/σ, C_{XR}/σ and C_{YR}/σ (multiplied by 10^3 for numerical convenience). This can be considered the transfer matrix for "fixed flight" conditions. Correlations for this matrix are not as good as those for the "fixed stick" conditions, probably because of the greater scatter in the force data. However, for 30 test conditions, the correlation is very good, comparable to the 15-test condition correlation shown in Reference 5.

The matrix, based on 30 flight conditions, is shown in Figure 4. Again, it is possible to determine multicyclic jet-flap deflections to produce zero higher harmonic stresses. These deflections also define an ideal harmonic control vector, this time for fixed flight conditions. Although the 1P stresses may still change, and the peak-to-peak stress increase, the rotor's force output is unchanged, at least to the accuracy of the basic methodology.

While elimination of a particular harmonic, or all higher harmonics of stress, may be beneficial, it may be more desirable to reduce other stress parameters, such as the root-mean-square, or the peak-to-peak values. It is difficult to relate peak-to-peak values to the harmonic coefficients, and the iterative algorithm necessary to affect peak-to-peak minimization would be considerably more complex, for example, than one to minimize the root-mean-square values. The rms value of the variable portion of the stresses will be minimized when the sum of the squares of the harmonic coefficients is also minimized. This sum is given by

$$\sigma_m{}^T\sigma_m = \sum_1^4 \left(\sigma_{n_c}{}^2 + \sigma_{n_s}{}^2\right) \qquad (6)$$

This product will be minimized when the multicyclic deflections are given by

$$\delta_{irms} = -(T_m{}^T T_m)^{-1}(T_m{}^T T_p)\ \delta_p \qquad (7)$$

where irms indicates an ideal root-mean-square, and the matrices and vectors are defined by partitioning Eq. 5, as shown below:

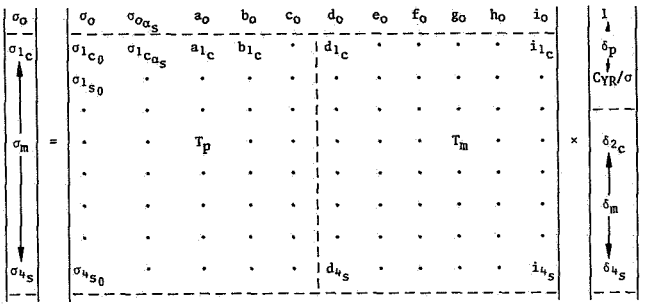

These ideal vectors have also been calculated for the 30 cases with resultant rms reductions between 40 and 66%. Figure 5 shows a few of these cases, with stress calculated for "zero" multicyclic. These stresses have been, in effect, extrapolated, whereas the data in Figure 2 were measured. As indicated on the figure, the ideal rms control also reduced peak-to-peak stresses. For the 30 cases investigated, the ideal rms control vectors reduced peak-to-peak stresses from 39 to 65%.

The ideal multicyclic vectors given by Eq. 7 are a function of the flight condition as defined by shaft axis inclination, advance ratio, and the rotor's lift, propulsive, and side-force coefficients. The elements of these ideal rms control vectors have been plotted against propulsive force coefficient in Figure 6. Different symbols denote the corresponding lift coefficient levels. The effects of C_{LR}/σ and C_{XR}/σ and shaft axis inclination are quite apparent. (The range of side-force coefficients was insufficient to deduce its effect.) The third and fourth harmonics were quite constant in phase; hence, only their amplitudes have been plotted. Note that these harmonics do not appear sensitive to rotor lift coefficient.

Transmitted Vibration Forces

The rotor suspension system for the wind tunnel tests incorporated a six-component balance and a parallelogram support discussed in References 4 and 5. The parallelogram support absorbed inplane vibratory loads very effectively, so that the vertical vibratory loads were the only ones of interest. These loads are due to thrustwise hub shears in combination with the motions of the hub due to the parallelogram support. For this two-bladed rotor, the transmitted loads contained only even-order harmonics as shown in Figure 3. These loads may also be related to the harmonics of the jet-flap deflection by a transfer matrix, as shown by Eq. 8.

With this transfer matrix it is possible to eliminate the second and fourth harmonics of the vertical vibratory loads by the same procedures used to eliminate the higher harmonic blade-bending stresses if two of the harmonic components of the control vector are specified. The resulting

$$\begin{vmatrix} V_o \\ V_{2_c} \\ V_{2_s} \\ V_{4_c} \\ V_{4_s} \end{vmatrix} = \begin{vmatrix} V_{o_0} & V_{o_{\alpha_s}} & p_o & q_o & r_o & \cdot & \cdot & \cdot \\ V_{2_{c_0}} & V_{2_{c_{\alpha_s}}} & p_{2_c} & q_{2_c} & r_{2_c} & \cdot & \cdot & \cdot \\ \cdot & \cdot & \cdot & \cdot & \cdot & \cdot & \cdot & \cdot \\ \cdot & \cdot & \cdot & \cdot & \cdot & \cdot & \cdot & \cdot \\ \cdot & \cdot & \cdot & \cdot & \cdot & \cdot & \cdot & \cdot \end{vmatrix} \times \begin{vmatrix} 1 \\ \alpha_s \\ C_{LR}/\sigma \\ C_{XR}/\sigma \\ C_{YR}/\sigma \\ \delta_{2_c} \\ \delta_{2_s} \\ \delta_{3_c} \\ \delta_{3_s} \\ \delta_{4_c} \\ \delta_{4_s} \end{vmatrix} \quad (8)$$

$$\begin{vmatrix} V_{2_c} \\ V_{2_s} \\ V_{4_c} \\ V_{4_s} \\ \sigma_{3_s} \\ \sigma_{4_s} \end{vmatrix} = \begin{vmatrix} V_{2_{c_0}} & V_{2_{c_{\alpha_s}}} & p_{2_c} & q_{2_c} & r_{2_c} & \cdot & \cdot & \cdot \\ V_{2_{s_0}} & V_{2_{s_{\alpha_s}}} & p_{2_s} & \cdot & \cdot & \cdot & \cdot & \cdot \\ V_{4_{c_0}} & V_{4_{c_{\alpha_s}}} & p_{4_c} & \cdot & \cdot & \cdot & \cdot & \cdot \\ V_{4_{s_0}} & V_{4_{s_{\alpha_s}}} & p_{4_s} & \cdot & \cdot & \cdot & \cdot & \cdot \\ \sigma_{3_{s_0}} & \sigma_{3_{s_{\alpha_s}}} & a_{3_s} & b_{3_s} & c_{3_s} & \cdot & \cdot & \cdot \\ \sigma_{4_{s_0}} & \sigma_{4_{s_{\alpha_s}}} & a_{4_s} & \cdot & \cdot & \cdot & \cdot & \cdot \end{vmatrix} \times \begin{vmatrix} 1 \\ \alpha_s \\ C_{LR}/\sigma \\ C_{XR}/\sigma \\ C_{YR}/\sigma \\ \delta_{2_c} \\ \delta_{2_s} \\ \delta_{3_c} \\ \delta_{3_s} \\ \delta_{4_c} \\ \delta_{4_s} \end{vmatrix} \quad (9)$$

where

$$V_{n_c} \triangleq (F_1 + F_2 + F_3)_{n_c}$$

$$V_{n_s} \triangleq (F_1 + F_2 + F_3)_{n_s}$$

deflection harmonic components would define ideal vibration control vectors whose elements would depend also on the flight condition. Such vectors have been calculated for the third harmonic jet-flap deflections set to zero and are shown in Reference 6. These vectors (calculated for 12 cases) show the second and fourth control components to be constant in phase, but they are significantly different in phase and magnitude from the ideal stress control vectors. As might be expected, the lack of third harmonic jet-flap deflection, and a large fourth harmonic requirement, resulted in very large third harmonic blade stresses, when these ideal vibration control vectors were input into Eq. 5.

When ideal rms (stress) control vectors are input into Eq. 8, the vibratory loads sometime increase. A sample case is shown in Figure 7. Shown are the stress and vibratory loads for "zero" multicyclic, the actual multicyclic used in the wind tunnel test, and the ideal rms control vector. The actual peak-to-peak stress reduction is 39% and the ideal stress reduction is 47%. The ideal rms control vector increased the vibratory loads 78%, while the actual control increased them by only 48%. The upper portion of the figure shows the actual and ideal multicyclic component amplitudes and phases. The actual phases are quite close to the ideal phases, but the actual third and fourth harmonics are too low. It is also apparent, however, that these third and fourth harmonics caused the increase in vibratory loads.

It is apparent from the foregoing that some sort of combined matrix is needed to effect reductions in both stress and vibratory loads. It would not be possible to eliminate all of the harmonic components since for this test rotor, we only have six elements in the control vector, δ_{2_c}, δ_{2_s} through δ_{4_s}. It is possible, however, to eliminate six of the response elements. For example, one may select both harmonics of vibratory loads and the third and fourth sine components of stress — the largest of the stress components — and construct a transfer matrix such as shown below. The multicyclic deflections required are determined by the solution of this equation for the condition that V_{2_c}, V_{2_s}, V_{4_c}, V_{4_s}, σ_{3_s} and σ_{4_s} are all equal to zero. The remainder of the stress coefficients and V_0 can be determined from Eqs. 5 and 8 after the multicyclic control vector has been evaluated.

Of course, other ideal control vectors are also possible, and these would depend quite obviously on the particular rotor and flap control system and the number of blades, etc. The blades' natural frequencies, the position and extent of the flaps will all affect the blade stress transfer matrix. The number of blades will have a definite effect on the harmonics of blade loads transmitted to the nonrotating system; hence, the compromise between loads and stress control would differ in each case. However, the basic method for analysis used herein can be applied to any such investigation, experimental or theoretical.

Multicyclic Lift Requirements

The results presented here correspond to a specific jet-flap driven rotor. The question arises to what extent other circulation control means would permit a similar reduction of stress levels in the blades and of vibratory loads. Such systems as mechanical flaps, servo flaps controlling the twist of the blades, low-powered jet-flaps, conventional rotor blades having multicyclic control in addition to swash-plate control may introduce multicyclic lift effects and are, at least conceptually, capable of producing some amount of stress and vibration alleviation. This capability being assumed, the problem then becomes one of degree rather than one of nature. The systems differ only by their unsteady flow characteristics but have to offer the similar capability of producing high frequency lift inputs up to at least the fourth harmonic of rotor frequency. The remaining question is "How much incremental lift is needed?"

There was no instrumentation on the blades to determine the local lift variations, and had there been, it would not be possible to determine the amount due to the multicyclic jet-flap deflection directly. However, knowing the jet-flap deflection and the average jet momentum coefficient, it is possible to calculate an incremental lift coefficient, assuming a nonvariant alpha. This has been done for several of the wind tunnel test cases and the Δc_l ranged from ±0.12 to ±0.68 for the higher harmonic components. Figure 8 shows the variation of the local blade element coefficient Δc_l for an ideal rms control vector. The corresponding stress reduction projected for this case would be 50%. (Note that Δc_l is approximately ±0.68.) The figure shows that the highest lift variation occurs on the retreating blade, a fact that proves favorable for the jet-flap, whose capability increases in low Mach-number flows.

It is believed that these magnitudes of Δc_l are obtainable with low powered jet-flaps. Assuming that somewhat lesser incremental lift variations would be necessary for softer conventional rotor blades, multicyclic mechanical and/or servo-flap control appears feasible. Two study contracts underway also support this contention.

The sensitivity of the blade stresses and vibration to multicyclic control and our present inability to predict harmonic loading, stresses, and and vibration, leads to the desirability of completely automating multicyclic control such as would be attained by feedback control systems. The Giravions Dorand firm is engaged in a basic research program to develop such a feedback system and early results are quite encouraging.

CONCLUDING REMARKS

Wind tunnel tests of a jet-flap rotor simulating forward flight have shown that it is possible to modulate the rotor's loading by means of a multicyclic control system so that rotor blade stresses and vibratory loads transmitted to the fuselage can be reduced. A method of analyzing the multivariable problem has been presented and several "ideal" control schedules are presented. The schedules themselves are applicable only to the specific jet-flap rotor tested, but the method of determining the schedules is applicable to similar systems. It was shown that it is not possible to eliminate all oscillatory blade-bending and vibratory loads with a system such as the test rotor, which had only three higher harmonics of azimuthal control. Such limited systems can, however, be used to eliminate specific selected harmonic component stress and vibration responses.

A simplified estimate of the incremental lift coefficient being generated multicyclically by the test rotor indicates that similar multicyclic mechanical or low-powered jet-flaps could also be sucessful in reducing blade stresses or vibratory loads.

References

1. Aronson, R. B. and Jines, R. H., "Helicopter Development Reliability Test Requirements, Vol. I - Study Results," USAAMRDL TR 71-18A, February 1972.

2. Veca, A. C., "Vibration Effects on Helicopter Reliability and Maintainability," USAAMRDL TR 73-11, April 1973.

3. Evans, William T. and McCloud, John L., III, "An Analytical Investigation of a Rotor Driven and Controlled by a Jet-Flap," NASA TN D-3028.

4. McCloud, John L., III, Evans, William T., and Biggers, James C., "Performance Characteristics of a Jet-Flap Rotor," in Conference on V/STOL and STOL Aircraft, Ames Research Center, NASA SP-116, 1966, pp. 29-40.

5. McCloud, John L., III, "Studies of a Large-Scale Jet-Flap Rotor in the 40- by 80-Foot Wind Tunnel," presented at Mideast Region Symposium A.H.S. Status of Testing and Modeling Techniques for V/STOL Aircraft, Philadelphia, PA, October 1972.

6. Kretz, M., Aubrun, J.-N., Larche, M., "March 1971 Wind-Tunnel Tests of the Dorand DH 2011 Jet-Flap Rotor" NASA CRs 114693 and 114694.

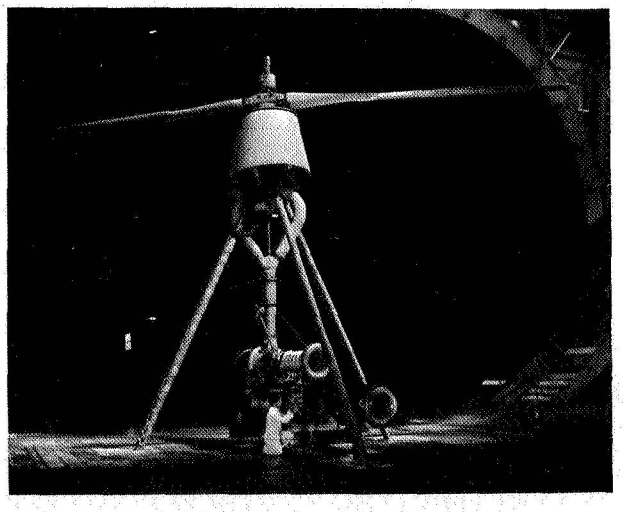

Figure 1. Jet-flap rotor in the Ames 40- by 80-Foot Wind Tunnel.

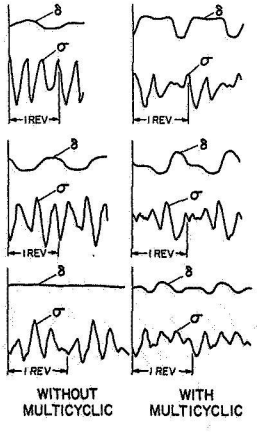

Figure 2. Effect of multicyclic jet-flap deflection on blade stresses.

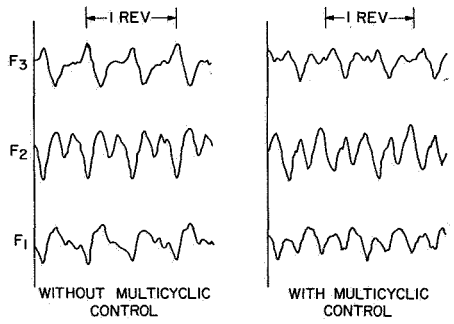

Figure 3. Effect of multicyclic jet-flap deflection on vertical forces below hub.

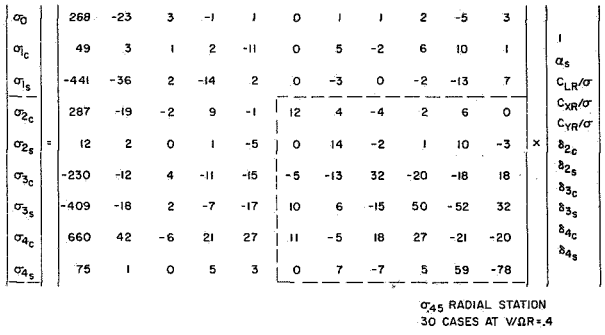

Figure 4. Transfer matrix for fixed flight conditions.

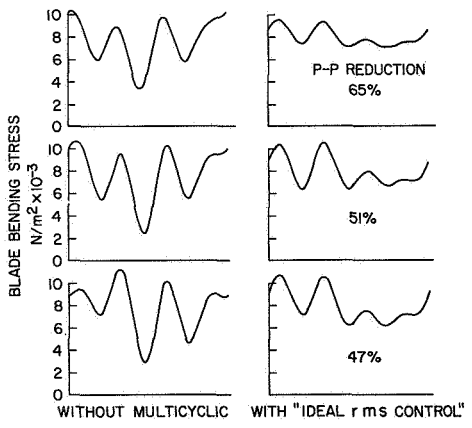

Figure 5. Calculated blade bending stresses using equations 5, 6, and 7.

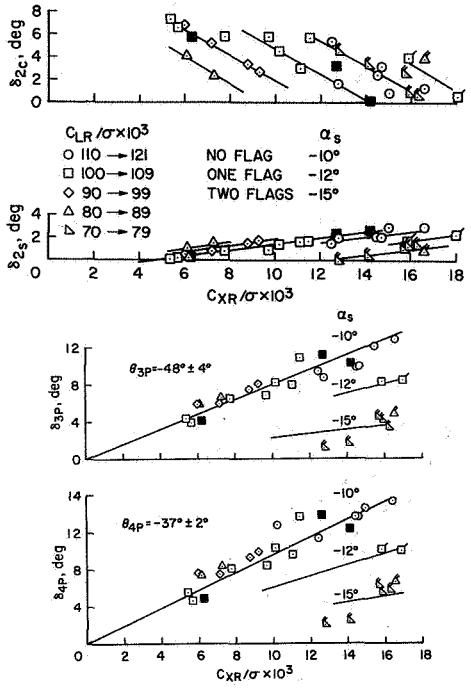

Figure 6. Ideal rms vector relations.

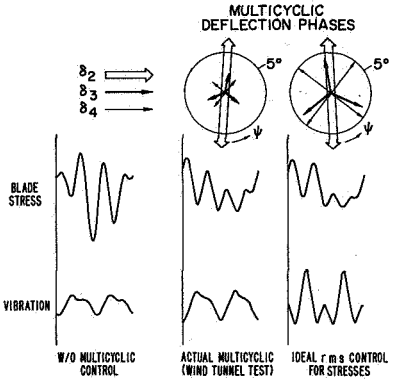

Figure 7. Calculated blade stresses and vibratory loads using equations 5, 6, 7 and 8.

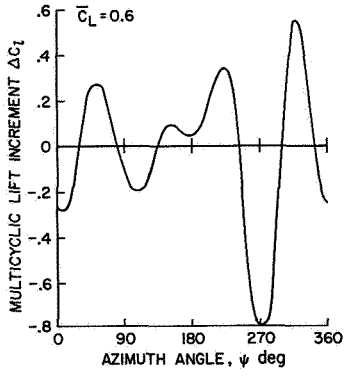

Figure 8. Variation of the estimated increment of blade section lift coefficient due to multicyclic jet-flap deflection.

IDENTIFICATION OF STRUCTURAL PARAMETERS FROM HELICOPTER DYNAMIC TEST DATA

Nicholas Giansante
Research Specialist

William G. Flannelly
Senior Staff Engineer

Kaman Aerospace Corporation
Bloomfield, Connecticut

Abstract

A method is presented for obtaining the mass, stiffness, and damping parameters of a linear mathematical model, having fewer degrees of freedom than the structure it represents, directly from dynamic response measurements on the actual helicopter without a priori knowledge of the physical characteristics of the fuselage. The only input information required in the formulation is the approximate natural frequency of each mode and mobility data measured proximate to these frequencies with sinusoidal force excitation applied at only one point on the vehicle. This dynamic response information acquired from impedance testing of the actual structure over the frequency range of interest yields the second order structurally damped linear equations of motion.

The practicality and numerical soundness of the theoretical development was demonstrated through a computer simulation of an experimental program. It was shown, through approximately 400 computer experiments, that accurate system identification can be achieved with presently available measurement techniques and equipment.

Notation

C	influence coefficient
d	damping
f	force
$\tilde{f}$	force phasor
g	structural damping coefficient
i	imaginary operator ($i = \sqrt{-1}$)
J	number of generalized coordinates
K	stiffness
m	mass
N	number of degrees of freedom
P	number of forcing frequencies
Q	number of modes
R	residual
S	modal mobility ratio
Y	displacement mobility, $\partial\tilde{y}/\partial\tilde{f}$
Ω	natural frequency
$[\Phi]$	matrix of modal vectors

Subscripts

i	modal index
j, k	degree of freedom index, generalized coordinate index
( )	a subscripted index in parentheses means the index is held constant

Superscripts

(q)	q-th iteration
*	modal parameter
R	real
I	imaginary
T	transpose
-1	inverse
-T	transpose of the inverse
+	pseudoinverse, generalized inverse

Brackets

[ ], ( )	matrix
⌈ ⌋	diagonal matrix
{ }	column or row vector

Presented at the AHS/NASA-Ames Specialists' Meeting on Rotorcraft Dynamics, February 13-15, 1974.

capital letters under matrices indicate the number of rows and columns, respectively

a dot over a quantity indicates differentiation with respect to time

The success of a helicopter structural design is highly dependent on the ability to predict and control the dynamic response of the fuselage and mechanical components. Conventionally, this involves the formulation of intuitively based equations of motion. Ideally, this process would reduce the physical structure to an analytical mathematical model which would predict accurately the dynamic response characteristics of the actual structure. Obviously, the creation of such an intuitive abstraction of a complicated real structure requires considerable expertise and inherently includes a high degree of uncertainty. Structural dynamic testing is required to substantiate the analytical results and the analysis is modified until successful correlation is obtained between the analytical predictions and the test results.

Until a prototype vehicle is available, intuitive methods are the only choice for describing an analytical model. However, once the helicopter is built, the method of structural dynamic testing using impedance techniques can be used to define directly a dynamic model which correlates with the test data. Such a model, synthesized from test data, succeeds in unifying theory and test, minimizing the intuitive foundation of conventional analyses.

System Identification has been defined as the process of obtaining the linear equations of motion of a structure directly from test data. In System Identification the objective is the extraction of the mass, stiffness and damping parameters of a simple mathematical model directly from dynamic response measurements on the actual helicopter without a priori knowledge of the physical characteristics of the fuselage. Figure 1 presents a pictorial representation of the System Identification process.

This paper describes the theory of System Identification using impedance techniques as applied to a mathematical model having fewer degrees of freedom than the structure it represents. The method yields the mass, stiffness and damping characteristics of the structure, the influence coefficient matrix, the orthogonal modes, the exact natural frequencies, the generalized parameters associated with each mode and dynamic response fidelity over the frequency range of interest. The only information necessary to implement the method is the approximate natural frequency of each mode and mobility data measured proximate to these frequencies with the excitation applied at a single point on the vehicle. This data can be readily obtained from impedance type testing of the helicopter over the frequency spectrum of interest.

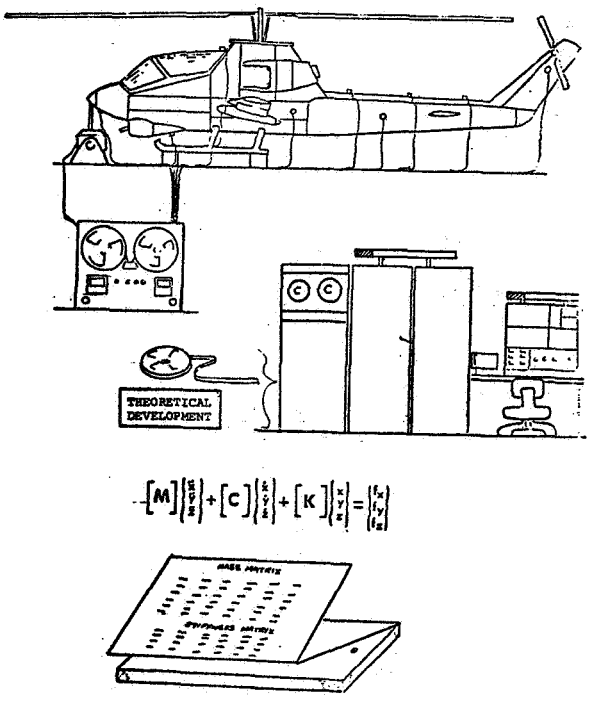

Figure 1. System Identification Process

The usefulness and numerical soundness of the theoretical development was demonstrated through a computer simulation of an experimental program, including a typical and reasonable degree of measurement error. To test the sensitivity of the method to measurement error, a series of computer experiments were conducted incorporating typical and reasonable degree of measurement error. The results indicate that accurate identification of structural parameters from dynamic test data can be achieved with presently available measurement techniques and equipment.

Description of the Theory

Derivation of the Single Point Iteration Process

As presented in References 1 and 2, the mobility of a structure at forcing frequency, ω, is given by

$$[Y] = [\Phi]\left[Y^*_{i_\omega}\right][\Phi]^T \qquad (1)$$

With excitation at station k, the responses at station j, including k, are obtained. These provide the k-th column of the mobility at a particular forcing frequency ω_1:

$$\{Y_{j(k)\omega_1}\} = \begin{matrix}\partial y_1/\partial f_1 \\ \{\partial y_2/\partial f_1\} \\ \vdots \\ \partial y_J/\partial f_1\end{matrix}_{\omega_1}$$

$$= \sum_{i=1}^{N} Y^*_{i\omega_1}\phi_{ki}\{\phi\}_i = [\Phi]\{Y^*_{i\omega_1}\phi_{ki}\} \qquad (2)$$

where $1 \le j \le J$ and $1 \le i \le N$.

This represents a column of mobility response each element of which is the response at a generalized coordinate on the structure with excitation at station k and at forcing frequency ω_1. Similarly, with the exciter remaining at station k, the k-th column of the mobility at another frequency, ω_2, can be obtained.

$$\{Y_{j(k)\omega_2}\} = \begin{matrix}\partial y_1/\partial f_2 \\ \{\partial y_2/\partial f_2\} \\ \vdots \\ \partial y_J/\partial f_2\end{matrix}_{\omega_2}$$

$$= \sum_{i=1}^{N} Y^*_{i\omega_2}\phi_{ki}\{\phi\}_i = [\Phi]\{Y^*_{i\omega_2}\phi_{ki}\} \qquad (3)$$

The columns of mobility response represented by (2) and (3) may be combined into one matrix

$$[\{Y_{j(k)\omega_1}\}\{Y_{j(k)\omega_2}\}]$$

$$= [\Phi][\{Y^*_{i\omega_1}\phi_{ki}\}\{Y^*_{i\omega_2}\phi_{ki}\}]$$

$$= \underset{JxN}{[\Phi]}\underset{NxN}{[\phi_{ki}]}\underset{Nx2}{[\{Y^*_{i\omega_1}\}\{Y^*_{i\omega_2}\}]} \qquad (4)$$

Generally, for p forcing frequencies where $1 \le p \le P$,

$$\underset{JxP}{[Y_{j(k)p}]} = \underset{JxN}{[\Phi]}\underset{NxN}{[\phi_{ki}]}\underset{NxP}{[Y^*_{ip}]} \qquad (5)$$

If J > P, Equation (5) is set of more equations than unknowns for which there is no solution. In this situation, Equation (5) can then be written as

$$[Y_{j(k)p}] = [\Phi][\phi_{ki}][Y^*_{ip}] + [R_{jp}] \qquad (6)$$

where R_{jp} is the residual associated with the j-th station and the p-th forcing frequency.

As described in References 1 and 2, the imaginary displacement mobility is usually significantly affected by modes associated with natural frequencies in proximity to the forcing frequency. Reference 3 indicates that accurate estimates of the modal vectors may be obtained by considering only the effects of modes proximate to the forcing frequency. Therefore, the analysis will employ only Q modes, where Q is less than N. The imaginary displacement mobility may be expressed as:

$$[Y^I_{j(k)p}] = [\Phi][\phi_{ki}][Y^{*I}_{ip}] + [R_{jp}] \qquad (7)$$

Since each column of $[Y^{*I}_{ip}]$ is associated with a particular frequency, the dominant element of each row of the matrix will be the modal mobility measured at the forcing frequency in proximity to a particular natural frequency. Normalizing the rows of the aforementioned matrix on the largest element yields

$$[S_{ip}] = [1/Y^{*I}_{in}][Y^{*I}_{ip}] \qquad (8)$$

where Y^{*I}_{in} is the maximum value of the i-th row. Equation (7) may be rewritten, incorporating Equation (8)

$$[Y^{I}_{j(k)p}] = [\phi][\phi_{ki}Y^{*I}_{in}][S_{ip}] + [R_{jp}] \quad (9)$$

The matrix Equation (9) has no solution, however, an approximation to a solution may be defined as that which makes the Euclidian norm of the matrix of residuals a minimum. The modal vector matrix with respect to which the Euclidian norm of the residuals is a minimum is obtained through use of the pseudoinverse, and is given by

$$[\phi] = [Y^{I}_{j(k)p}][S_{ip}]^{+}\left[\frac{1}{\phi_{ki}Y^{*I}_{in}}\right] \quad (10)$$

where $[S_{ip}]^{+}$ is defined as the generalized inverse or pseudoinverse of $[S_{ip}]$ and is defined by

$$[S_{ip}]^{+} = [S_{ip}]^{T}([S_{ip}][S_{ip}]^{T})^{-1} \quad (11)$$

In Equation (10) each diagonal element of $\left[\frac{1}{\phi_{ki}Y^{*I}_{in}}\right]$ simply multiplies the corresponding column of the modal matrix. Since each modal vector is normalized on the largest element in the vector, the effect of the aforementioned multiplication is negated and Equation (10) can be reduced to

$$[\phi] = [Y^{I}_{j(k)p}][S_{ip}]^{+} \quad (12)$$

The [S] matrix can be accurately estimated from knowledge of only the forcing frequencies and the natural frequencies. Equation (12) will be solved utilizing matrix iteration techniques. At each successive iteration a solution is found that minimizes the Euclidian norm of the residual matrix with respect to the newly found matrix of either [S] or [ϕ]. The basic algorithm used in the matrix iteration procedure for the q-th iteration becomes

$$[\phi^{(q)}] = [Y^{I}][S^{(q-1)}]^{+}$$

and

$$[S^{(q)}] = [\phi^{(q)}]^{+}[Y^{I}] \quad (13)$$

Determining the Modal Parameters

The real modal impedance at forcing frequency ω_p can be written as

$$Z^{*R}_{i\omega_p} = \frac{Y^{*R}_{i\omega_p}}{(Y^{*R}_{i\omega_p})^2 + (Y^{*I}_{i\omega_p})^2} \quad (14)$$

Substituting the real and imaginary displacement mobility as given in Reference 1 yields

$$Z^{*R}_{i\omega_p} = K^{*}_{i}(1 - \omega_p{}^2/\Omega_i{}^2) \quad (15)$$

From Equation (15) it is observed that the modal impedance is a linear function of the square of the forcing frequency. The forcing frequency at which the modal impedance becomes zero is, therefore, the natural frequency. From a least squares analysis of modal impedance as a function of forcing frequency squared, proximate to the natural frequency, the generalized stiffness of the i-th mode and the natural frequency of the i-th mode can be calculated.

The generalized mass associated with the i-th mode is given by

$$m^{*}_{i} = K^{*}_{i}/\Omega_i{}^2 \quad (16)$$

The structural damping coefficient may be determined from

$$g_i = \left(\frac{\omega_p{}^2}{\Omega_i{}^2} - 1\right)\frac{Y^{*I}_{i\omega_p}}{Y^{*R}_{i\omega_p}} \quad (17)$$

Models

There are two basic types of dynamic mathematical models describing structures. The first type described as "Complete Models" considers as many modes as degrees of freedom. The second type labelled "Truncated Models" considers fewer modes than points of interest on the structure. Using the methods described herein, it is possible to identify either a complete model or a truncated model.

For the completed model the modal matrix [ϕ] is square. However, in the case of the truncated model the modal matrix [ϕ] is rectangular having J rows corresponding to the points of interest and Q columns associated with the mode shapes, where J > Q.

Truncated Models

Consider a rectangular identified modal matrix which has J rows indicating the points of interest on the structure and Q columns representing the modes being considered where J > Q. The influence coefficient matrix for the truncated model is given by

$$[C_{TR}] = [\phi]\left[\frac{1}{K_i^*}\right][\phi]^T \qquad (18)$$

The above matrix is singular being of rank Q and order J. The mass, stiffness and damping matrices for the truncated model are

$$[m_{TR}] = [\phi]^{+T}[m_i^*][\phi]^+$$

$$[K_{TR}] = [\phi]^{+T}[K_i^*][\phi]^+$$

$$[d_{TR}] = [\phi]^{+T}[g_i K_i^*][\phi]^+ \qquad (19)$$

The classical modal eigenvalue equation has the analogous truncated form

$$[C_{TR}][m_{TR}]\{\phi_i\} = \frac{1}{\Omega_i^2}\{\phi_i\} \qquad (20)$$

Complete Models

For the complete model the identified modal vector matrix is square, having the same number of degrees of freedom as mode shapes, thus J = Q. The influence matrix is given by

$$[C] = [\phi][1/K_i^*][\phi]^T = \sum_{i=1}^{N} 1/K_i^*\{\phi_i\}\{\phi_i\}^T \qquad (21)$$

The mass, stiffness and damping matrices for the complete model are similar to those of Equation (19), except that the matrices are square.

$$[m] = [\phi]^{-T}[m_i^*][\phi]^{-1}$$

$$[K] = [\phi]^{-T}[1/K_i^*][\phi]^{-1}$$

$$[d] = [\phi]^{-T}[g_i K_i^*][\phi]^{-1} \qquad (22)$$

Full Mobility Matrix

The full mobility matrix of either complete or truncated models is given by

$$[Y] = [\phi][Y_i^*][\phi]^T \qquad (23)$$

Computer Test Simulation

The usefulness and numerical soundness of the theoretical development was demonstrated through a computer simulation of an experimental program. Approximately 400 computer experiments were performed in the study. A twenty-degree-of-freedom lumped mass beam type representation of a helicopter supported on its main landing gear and tail gear was used to generate simulated mobility test data. Each of the coordinates was allowed a transverse degree of freedom. The concentrated mass and stiffness parameters of the beam are shown in Table I, with EI varying linearly between stations and with 5 percent structural damping.

Simulated Errors

System Identification theories of any practical engineering significance must be functional with a reasonable degree of experimental error. Therefore, a typical and reasonable degree of measurement error ranging to ±15% random error uniformly distributed and 15% bias error, was incorporated in the simulated test data. Both random and bias error were applied to the real and imaginary components of the displacement mobility data. The levels of error applied are consistent with those inherent in the present state-of-the-measurement art.

Models

The number of degrees of freedom of a physical structure is infinite. Therefore, the usefulness of model identification, necessarily with a finite number of degrees of freedom, using impedance testing techniques, depends on the ability to simulate the real structure with a small mathematical model.

Several size models, containing from 5 to 15 degrees of freedom, were synthesized from the simulated test data incorporating the specified experimental error. Table II describes the various models used in the analysis. The model stations used in the models refer to the corresponding stations in the twenty point specimen.

Identified Models

Typical generalized mass identifications are shown in Tables III, IV and V. Table III presents results for several different five point models. The model designations refer to the descriptions presented in Table II. Data are also

presented for the twenty point specimen with zero experimental error. Thus, a basis of comparison is established with the theoretically exact control model of the beam representation of the helicopter. It is apparent that no outstanding differences exist among the identified generalized masses for the models considered for comparison. Table IV presents similar data for the nine-point models studied. The generalized mass distribution associated with each of the models is in excellent agreement with the twenty point model results.

Table V describes the results of the computer experiments conducted employing the twelve point models. The results are satisfactory except for the identification of the generalized masses of the tenth and eleventh modes. However, the generalized masses associated with these modes are extremely small in comparison with the remaining modal generalized masses. An examination of the tenth mode shape revealed a lack of response at all points of interest on the structure other than the first station. Therefore, the effect of the tenth mode is difficult to evaluate in the calculation of the generalized parameters. Computer experiment 309 yielded a negative generalized mass for the tenth mode. All computer experiments that failed in this respect gave drastically unrealistic values of generalized mass. Ordinarily, in a situation where the generalized mass was unrealistic, use of different stations for the model improved the identification.

TABLE I. 20-POINT SPECIMEN DESCRIPTION

Sta No.	1	2	3	4	5	6	7	8	9	10	11	12	13	14	15	16	17	18	19	20
Sta (In.)	0		60		120		160		200		240		280		320		370		430	
		30		100		140		180		220		260		300		340		400		460
Mass ($Lb\text{-}Sec^2/In.$)	.029		3.67		2.18		2.385		2.08		.910		.170			.070		.095	.210	
		1.05		3.71		2.18		2.59		1.56		.260		.085		.060		.120		.150
EI ($Lb\text{-}In.^2 \times 10^{10}$)	.35		.35		1.95		4.37		5.80		4.425		3.07		2.05		.975		.55	
		.35		1.20		3.00		5.70		5.60		3.6		2.60		1.60		.65		.50
Springs to Ground (Lb/In.)						10000												10000		

TABLE II. MODEL DESCRIPTION

	Stations Used																			
Model	1	2	3	4	5	6	7	8	9	10	11	12	13	14	15	16	17	18	19	20
5A	x					x				x					x					x
5B	x					x					x					x				x
5C	x					x				x					x				x	
5D		x				x						x			x				x	
9A	x	x				x	x			x			x			x		x		x
9B	x		x			x		x			x			x			x		x	x
9C		x	x			x	x			x			x			x		x		x
12A		x	x	x	x	x		x		x		x		x		x		x		x
12B	x	x	x		x	x		x		x		x		x		x		x		x
12F	x	x	x		x	x		x			x		x		x		x		x	

TABLE III. IDENTIFICATION OF GENERALIZED MASSES, 5 X 5 MODEL OF 20 X 20 SPECIMEN

Model	5A	5B	5C	5D	1**
Computer Experiment Number	296	297	292	295	-
Random Disp. Error	±5%	±5%	±5%	±5%	0
Bias Disp. Error	+5%	+5%	+5%	+5%	0
Random Error Seed	13	13	13	13	-
Mode	Generalized Masses (Lb-Sec^2/In.)				
1	8.544	8.538	8.543	8.568	8.534
2	4.506	4.506	4.619	4.610	4.449
3	.494	.494	.494	.493	.495
4	1.048	1.047	1.050	.994	1.087
5	.653	.653	.651	.629	.630

** From 20 x 20 Specimen

TABLE IV. IDENTIFICATION OF GENERALIZED MASSES, 9 X 9 MODEL OF 20 X 20 SPECIMEN

Model	9A	9B	9C	20 Pt
Computer Experiment Number	300	303	304	1**
Random Disp. Error	±5%	±5%	±5%	0
Bias Disp. Error	+5%	+5%	+5%	0
Random Error Seed	13	13	13	-
Mode	Generalized Masses (Lb-Sec^2/In.)			
1	9.000	9.015	9.043	8.534
2	4.350	4.335	4.513	4.449
3	.472	.472	.472	.495
4	1.042	1.042	1.138	1.087
5	.551	.549	.584	.630
6	.786	.783	.723	.743
7	1.154	1.243	1.120	1.177
8	1.401	1.411	1.396	1.412
9	.787	.708	.791	.786

** From 20 x 20 Specimen

TABLE V. IDENTIFICATION OF GENERALIZED MASSES, 12 X 12 MODEL OF 20 X 20 SPECIMEN

Model	12B	12F	12A	20 Pt
Computer Experiment Number	312	311	309	1**
Random Disp. Error	±5%	±5%	±5%	0
Bias Disp. Error	+5%	+5%	+5%	0
Random Error Seed	13	13	13	-
Mode	Generalized Masses ($Lb/Sec^2/In.$)			
1	8.474	8.464	8.518	8.534
2	4.556	4.510	4.492	4.449
3	.488	.487	.487	.495
4	1.150	1.151	1.103	1.087
5	.596	.597	.595	.630
6	.722	.724	.777	.744
7	1.182	1.113	1.159	1.177
8	1.232	1.242	1.215	1.412
9	.797	.743	.789	.786
10	1.203	1.043	-.564	.043
11	.093	.104	.0103	.172
12	1.177	1.119	1.147	1.050

** From 20 x 20 Specimen

Response From Identified Model

One of the most essential requisites of relating a discrete parameter system to a continuous system is model response fidelity over a given frequency range of interest. The finite degree of freedom model must accurately reproduce the dynamic response of the infinite degree of freedom structure over a specific number of modes. Figures 2a and 2b show typical real and imaginary driving point acceleration response respectively for the five point model. The "exact" curve represents the simulated experimental data for the twenty point structure, obtained with zero error. The frequency range encompasses the first five elastic natural frequencies. Figures 3 and 4 present similar results for typical nine and twelve point models, respectively. The computer experiments for which results are presented incorporated a ±5 percent random and a +5 percent bias on the real and imaginary displacement mobility data. As evidenced by the figures, the various models yielded satisfactory reidentification of the twenty point specimen simulated dynamic response data.

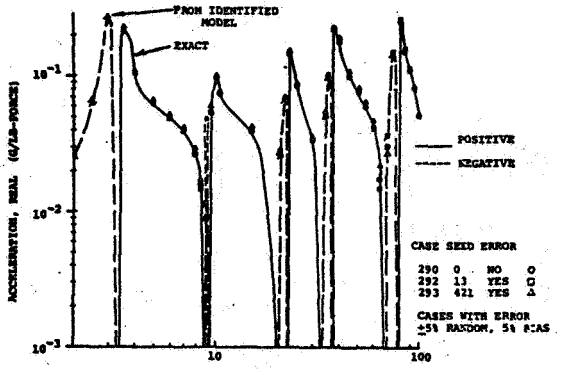

Figure 2a. Effect of Error on Five-Point Model Identification of Real Acceleration Response; Driving Point at Hub

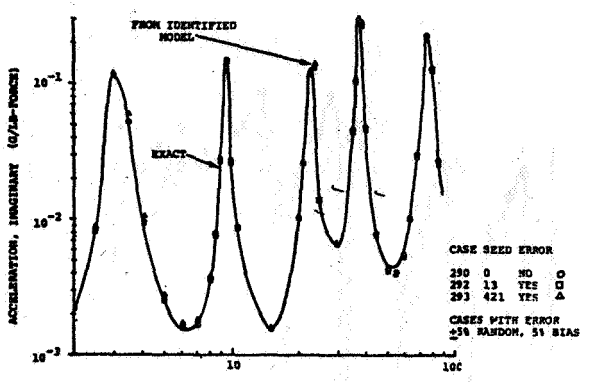

Figure 2b. Effect of Error on Five-Point Model Identification of Imaginary Acceleration Response; Driving Point at Hub

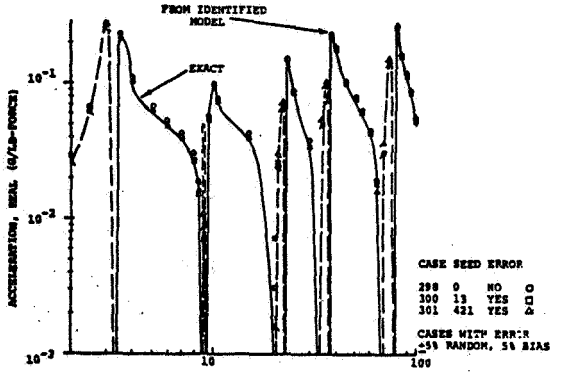

Figure 3a. Effect of Error on Nine-Point Model Identification of Real Acceleration Response; Driving Point at Hub

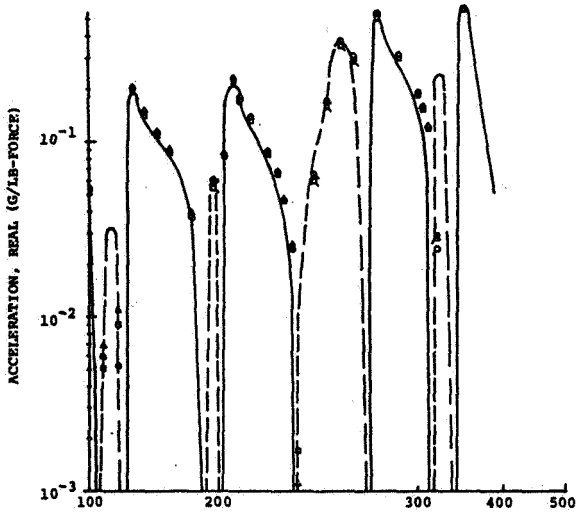

Figure 3a - Continued

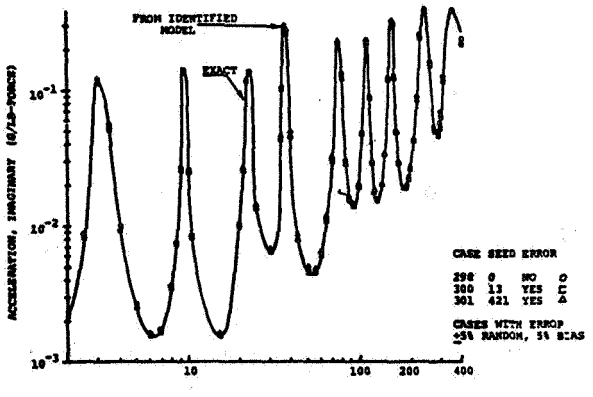

Figure 3b. Effect of Error on Nine-Point Model Identification of Imaginary Acceleration Response; Driving Point at Hub

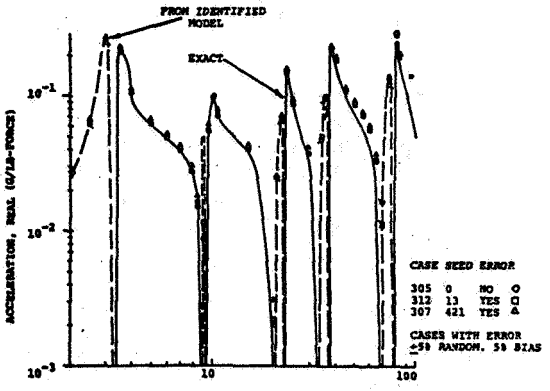

Figure 4a. Effect of Error on Twelve-Point Model Identification of Real Acceleration Response; Driving Point at Hub

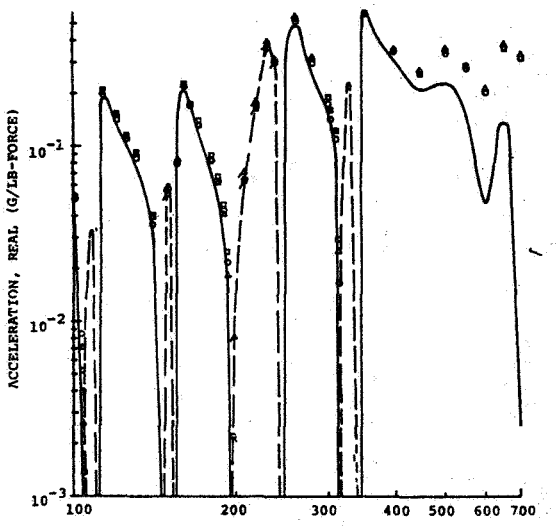

Figure 4a - Continued

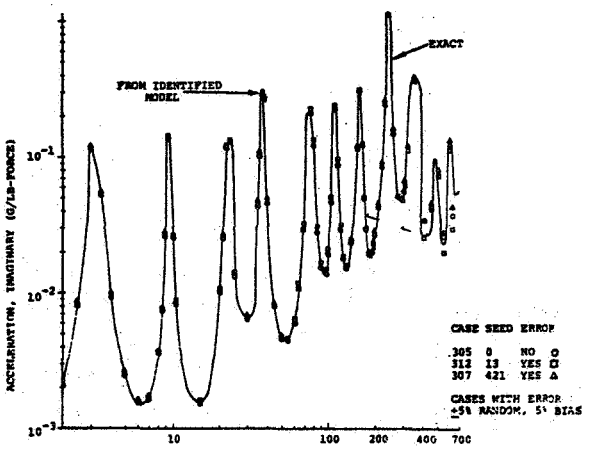

Figure 4b. Effect of Error on Twelve-Point Model Identification of Imaginary Acceleration Response; Driving Point at Hub

Conclusions

1. Single point excitation of a structure yields the necessary mobility data to satisfactorily determine the mass, stiffness and damping characteristics for a mathematical model having less degrees of freedom than the linear elastic structure it represents.

2. The method does not require an intuitive mathematical model and uses only a minimum amount of impedance type test data.

3. The eigenvector or mode shape associated with each natural frequency is also determined.

4. Computer experiments using simulated test data indicate the method is insensitive to the level of measurement error inherent in the state-of-the-measurement art.

References

1. USAAMRDL Technical Report 70-6A, THEORY OF STRUCTURAL DYNAMIC TESTING USING IMPEDANCE TECHNIQUES, Flannelly, W.G., Berman, A. and Barnsby, R. M., U. S. Army Air Mobility Research and Development Laboratory, Fort Eustis, Virginia, June 1970.

2. USAAMRDL Technical Report 72-63A, RESEARCH ON STRUCTURAL DYNAMIC TESTING BY IMPEDANCE METHODS - PHASE I REPORT, Flannelly, W.G., Berman, A. and Giansante, N., U. S. Army Air Mobility Research and Development Laboratory, Fort Eustis, Virginia, November 1972.

3. Stahle, C.V., Jr., PHASE SEPARATION TECHNIQUE FOR GROUND VIBRATION TESTING, Aerospace Engineering, July 1962.

ENGINE/AIRFRAME INTERFACE DYNAMICS EXPERIENCE

C. Fredrickson
Senior Engineer

Boeing Vertol Company
Philadelphia, Pa.

Abstract

Recent experience has highlighted the necessity for improved understanding of potential engine/airframe interface dynamics problems to avoid costly and time-consuming development programs. This paper gives some examples of such problems, and the manner in which they have been resolved. It also discusses a recent program in which contractual engine/airframe interface agreements have already proven helpful in the timely prediction and resolution of potential problems.

In particular, problems of engine/drive system torsional stability, engine and output shaft critical speeds, and engine vibration at helicopter rotor order frequencies are discussed, and test data and analyses presented. Also presented is a rotor/drive system dynamics problem not directly related to the engine.

General

This paper is an attempt to highlight some recently encountered problems in the area of helicopter engine and drive system dynamics. In comparison to the number of technical papers published in the area of rotor and blade aeroelasticity and stability, and fuselage vibration reduction schemes, there are relatively few indeed dealing with engine/airframe dynamics.

The paper does not present highly sophisticated methods of solution for these problems. It instead shows that solutions were attained by the application of basic engineering principles to state-of-the-art analytical and test techniques. Also, having encountered these problems, we are more cognizant of these potential "show-stoppers," the manner in which they manifest themselves, and the available courses of corrective action. It is essential that the knowledge gained through these programs be judiciously applied to new helicopters, and growth versions of existing models.

Engine/Drive System Torsional Stability

The usual stability requirements that dictate fuel control gain limits are complicated by the flexibility of the helicopter drive system and by the dynamics of a gas turbine engine. The interaction of the helicopter rotor and drive system, engine, and fuel control requires careful attention if a good or even workable fuel control is to be achieved. In the case of the T55-L-11 engine and the CH-47C aircraft, these items were growth versions of existing components. There was no requirement for new control concepts since operation had been successful on previous models. However, the fuel control gains had to be carefully re-evaluated for the new power levels.

Computer simulation of the CH-47C rotor system with the T55-L-11 turbine engine was accomplished before initial flight tests began. The simulation indicated favorable engine/control stability. However, as pointed out in Reference (1), unacceptable oscillations in engine shaft torque and rotor RPM were observed during initial flight tests (Figure (1)). These torque oscillations were audible, disconcerting to the flight crew, and were observed only in hover and on the ground (not in forward flight). The frequency of the oscillation was also higher than the predicted drive system torsional natural frequency.

Since the torsional instability was not predicted by the computer simulation, a study of pertinent system parameters was undertaken. It was discovered that the only parametric change having a significant effect on torsional stability was the slope of the blade lag damper force-velocity curve below the preload force level. When this curve was artificially "stiffened" beyond its actual limits, as shown in Figure (2), the oscillation was reproduced. This fact suggested that by "softening" the actual damper preload slope, the oscillation might be suppressed. Once analytically reproduced, the oscillation could be eliminated by simulating a fuel control with a reduced steady state gain and a slowed time constant. The computer analysis, therefore, revealed two potential solutions to the torsional oscillation problem: a lag damper modification and a fuel control modification.

Flight tests with a set of lag dampers with significantly reduced preload slope, together with the original fuel controls, were conducted. These tests revealed that the torque oscillation was

apparently suppressed. However, since the lag dampers were on the aircraft for ground resonance reasons, this significant load change reduced damping capacity and produced some degradation in the ground resonance characteristics of the helicopter. Therefore, damper modification to remedy torque oscillation was rejected.

Fuel controls with a 30% reduction in steady-state gain were flight tested, and yielded acceptable torsional stability. However, this degraded to marginal instability in colder ambient temperatures. Controls incorporating a gain reduction plus an increase in time constant provided acceptable engine torque stability in the cold and over the entire engine operating envelope. Fuel control frequency response curves are shown in Figure (3). Pilots also noted that engine response to input power demands was not perceptibly degraded with these slowed-down controls. Therefore, this fuel control modification was considered an acceptable production fix.

Representation of the lag damper with just the force-velocity curve in the engine/drive system/fuel control simulation had been shown to be insufficient to accurately reproduce the torque oscillation phenomenon. Therefore, a more accurate math model of the damper was deemed necessary for further analysis, and for a more complete understanding of the problem. The derivation of the upgraded lag damper math model is shown in Reference (1). Inclusion of this lag damper math model into the torsional stability computer simulation accurately reproduced the torque oscillation with the original fuel controls. Frequency of oscillation, phasing and magnitude of damper force, shaft torque oscillation, and fuel flow fluctuation were now simulated accurately. Final simulation may be seen in Figure (4). The primary difference between this damper simulation and the earlier version is that the new model included the hydraulic spring effect of the damper.

The reduced gain-increased time constant fuel control fix has provided satisfactory torsional stability for the CH-47C production fleet. However, several early production aircraft reported instances of a "pseudo-torque oscillation". This phenomenon is a torque split, followed by a low amplitude torque oscillation of the high torque engine. The problem was traced to high levels of vibration affecting the internal workings of the fuel control. Vibration at cross shaft frequency caused an instantaneous increase in the effective gain of the control, increasing its torque output with respect to the other engine, and making it susceptible to torsional instability. The problem was resolved by closely monitoring cross shaft vibration, and with minor fuel control component modifications.

During the latter part of the torque oscillation program, it became apparent that the engine and airframe manufacturers can easily coordinate their efforts to prevent this type of incompatibility. Lycoming has now provided Vertol with a mathematical model of the engine and fuel control system, so that rotor/drive system design changes may be evaluated for their effect on torsional stability. It is equally important that as accurate a representation as possible of the rotor and drive system be given to the engine manufacturer.

There has been some mention in recent years about the possibility of using a zero torsional stiffness coupling (Reference (2)) to effectively isolate the engine from the rotor drive system, thereby precluding torque oscillation. At this time, potentially high developmental costs, uncertainty of transient behavior, and added weight to the drive system seem to rule out the z.t.s. coupling. However, continued research may yield an acceptable concept that may be the design solution for torsional instability for the next generation of increasingly larger, faster and more complex VTOL rotorcraft.

Engine Vibration at Helicopter Rotor Frequencies

The CH-47/T55 engine installation is "hard-mounted", as shown in Figure (5). It employs two front mounts on a yoke at the engine inlet housing, and an aft vertical support link at the engine diffuser flange. The outboard yoke airframe point is connected to take out high fore-aft maneuver loads. Engine vibration had rarely been a problem on the CH-47A and B models with this type installation.

However, field service reports indicated an increase in engine, engine component and engine mount vibration-related problems with the installation of the T55-L-11 and -11A engines in the CH-47C helicopter. These problems led to a full scale engine and strain survey, the purpose of which was to determine the dynamic characteristics of the engine installation, especially the vibration/strain relationships. The engine survey (Reference (3)) provided a wealth of information concerning the CH-47C engine/airframe interface dynamic characteristics. In particular, the survey identified rotor 3/rev as the predominant excitation frequency in the engine mounting system.

Also, inlet housing stresses and drag strut load increased significantly with frequency (rotor speed), as if approaching a resonance, as shown in Figure (6). As a result of this discovery, a ground shake test was recommended to define the characteristics of the apparent engine/airframe mode being excited by rotor 3/rev. The shake test setup is shown in Figure (7).

The CH-47C/T55-L-11 engine shake test revealed a 14.2 H_z rigid body yaw mode. Installation of -11A engines (an additional 40 lbs.) caused a .4 H_z downward shift in modal frequency, and a twofold increase in 3/rev inlet housing strains. Additional testing showed that reducing drag strut bolt torque could lower the engine yaw mode frequency into the CH-47 operating range (11.5 to 12.5 H_z). Complete elimination of the drag strut lowered the mode to 7.5 H_z, well below the CH-47C operating range. Shake test frequency sweeps are shown in Figure (8). Removal of the drag strut, however, is not a practical solution. It is needed to assure acceptable cross shaft alignment under high maneuver G and jet thrust loads. The solution, therefore, was to retain the drag strut, but slot one end to eliminate dynamic stiffness for small amplitude motions, resulting in a structurally detuned installation.

Flight evaluation of the slotted drag strut was desired, and the Model 347 research helicopter was available as a testbed. The 14 H_z yaw mode fell within the operating n/rev frequency range (14-16 H_z) of the four-bladed Model 347 and, therefore, it would be possible to verify the inflight placement of the mode. However, rotor speed sweeps of from 210 to 240 RPM with the standard strut failed to show a peak inlet housing stress response in the expected frequency range. Reducing rotor RPM still further finally located the engine yaw mode at 13.2 H_z.

Installing the slotted drag strut on one engine completely eliminated the 13 H_z peaks, and resulting 4/rev inlet housing stresses were reduced by as much as 75%. Lateral 4/rev vibration at the engine diffuser showed as much as an 85% reduction. These load and vibration reductions are illustrated in Figure (9).

It is noteworthy that analytical efforts to predict the installation dynamic characteristics met with limited success. This analysis first made use of assumed values of fuselage backup structure stiffness, and later used values calculated from a finite element structural model of the entire fuselage. However, the accuracy of these stiffness values is a function of idealization accuracy and validity, and end condition assumptions. The analytical predictions began to resemble the actual test results only when static load-deflection test data at the engine support points was used in the analysis. It is important here to point out two other factors that contributed to the CH-47C engine vibration stress problem; the increase in normal rotor RPM from the A to C model to improve the flight envelope resulted in a higher forcing frequency, and the increasing engine weight and inertia of the more powerful engine moved the resonant frequency downward.

Engine bending was not a contributing factor in this installation. In engine installations where it is a factor, the analysis becomes much more complex. Close coordination between engine and airframe manufacturers, through engine/airframe interface agreements, will be necessary to accurately describe the installed engine dynamics in this case.

In the overall design of an engine installation, it is imperative to choose the engine dynamic characteristics (isolated, detuned or hard mounted) such that output shaft alignment is not jeopardized. Or, conversely, output shaft couplings must be tailored to the vibratory environment of the engine. In an isolated engine installation (where most engine modes are placed well below predominant forcing frequency), output shaft couplings with high misalignment capability must be employed. In a hard-mounted or detuned installation, low misalignment couplings, such as the Thomas coupling, may be utilized.

Rotor/Drive System B/Rev Torsional Resonance

The Boeing Vertol Model 347 research helicopter is a derivative of the CH-47C Chinook helicopter, the primary differences being a 30 inch higher aft pylon, a 100 inch longer fuselage, and an increase in rotor blades from 3 to 4 per rotor (Reference (4)). A Holzer torsional analysis of the CH-47C revealed natural modes at roughly .3/rev, .9/rev, 4.1 and 4.2/rev; therefore, the Chinook was considered to be free from b/rev torsional resonance (3/rev in this case). A similar analysis on the Model 347 revealed almost identical non-dimensional torsional frequencies, despite a lengthened aft rotor shaft and forward synchronizing shaft, and a reduction in rotor RPM. There was some concern about the proximity of the third and fourth torsional modes to b/rev (4/rev in this case). However, it was believed that forcing levels and

phasing would not be sufficient to excite these modes. The Model 347 drive system torsional modes are shown in Figure (10).

The Model 347 program was flown successfully, until the aircraft was flown at high gross weights. Here, high 4/rev blade chordwise bending moments in transition and high speed forward flight became a structurally limiting factor. Examination of flight test data revealed that the chordwise bending moments of all four blades on each hub were exactly in phase. Data also revealed substantial rotor shaft 4/rev torque fluctuations, with the forward and aft rotor systems opposing each other as shown in Figure (11), and 4/rev chordwise bending moments increasing sharply with RPM, as if approaching a resonance (Figure 12).

Analytical parametric studies were conducted to evaluate the effect of various system modifications on the apparent 4/rev resonance. Modifications such as forward and aft rotor shaft stiffness changes, synchronizing shaft stiffness changes and effective lag spring stiffening were all found to be effective to some extent. However, these changes were rejected due to the magnitude of change required to move the resonance and sensitivity to RPM changes. A much more acceptable modification was found to be raising the blade uncoupled chordwise bending natural frequency. On the CH-47C, this blade frequency was just above 5/rev; consequently, the largest blade bending loads are at 5/rev. However, with these same blades on the Model 347, the largest blade bending loads were at 4/rev, indicating the blade/drive system coupling effect.

Both blade softening and stiffening were investigated. It was found that decreasing the blade chordwise bending frequency was more effective in moving the drive system resonance than the same percentage increase, as shown by the Figure (13) analysis. But it was felt that this blade softening would present too great a structural degradation problem in the blade. Hence, raising the blade chordwise frequency, and with it the coupled blade/drive system torsional resonance, was the design goal. Analysis revealed that a 4 H_z increase in blade natural frequency would result in satisfactory detuning of the blade/drive system resonance.

The most effective location to attempt a chordwise frequency increase is at the trailing edge. It was necessary in this case to add on a material of high stiffness and minimum weight, such that chordwise balance and CF loads are not grossly affected. The design selected consisted of top and bottom boron fiber doublers bonded to the stainless steel trailing edge from 30% to 70% span, and boron skins applied to several blade boxes. The benefit of the boron stiffening is twofold, for in addition to increasing the chordwise frequency to avoid resonance, strength is increased.

The addition of boron stiffening moved the blade uncoupled flexible chordwise frequency from 5.26/rev to over 6/rev. This resulted in a shift in the blade/drive system natural frequency to over 4.2/rev (at 235 RPM) or to 4.3/rev (at 220 RPM). This was sufficient to preclude high 4/rev amplification, since blade chordwise trailing edge loads are now highest at 6/rev (the uncoupled blade frequency).

This problem does not fall strictly into the category of engine/airframe interface dynamics. However, the influence of the engine in the drive system dynamics, and the potential impact of such a problem on the engine cannot be ignored. For example, to accurately predict drive system modes, the power turbine inertia must be accurately known.

Engine Output Shaft Critical Speed Analysis

The Boeing Vertol Heavy Lift Helicopter prototype will incorporate three Detroit Diesel Allison XT701-AD-700 turboshaft engines. These engines have been developed from the Allison 501-M62B as part of a program to procure representative engines for the HLH Advanced Technology Component (ATC) dynamic systems test rig. Many helicopters built in the past were designed around existing engines. However, in the case of the HLH, initial development of the engine is to be fully coordinated by the prime contractor; hence, development of both engine and airframe will be in parallel. The HLH engine program is discussed in Reference (5).

A development problem was encountered during the program which involved the engine/airframe output drive shaft interface. The original design of the engine output shaft was a short splined shaft with the torquesensor mounted within the main frame of the engine. Based on more detailed engine nacelle design, it was requested that the splined shaft interface be moved forward to reduce inlet blockage and to facilitate inspection of the shaft coupling. This change was agreed upon, and the drive shaft connection was moved to a point 17 inches forward of the front face of the engine. The torquesensor was also housed in the resulting engine "nose". A cutaway view of the torquesensor and housing is shown in Figure (14).

The original shafting concept on the HLH was to drive into the main transmission directly, without right angle gearboxes, resulting in a substantial weight savings. A layout of the original HLH engine/mixbox shaft configuration is shown in Figure (15). The original engine-to-mixbox shafting consisted of two 7.25 inch diameter sections of equal length with a single bearing support point. However, in an attempt to further reduce inlet blockage and reduce weight, the shaft diameter was reduced to 6 inches. This decision was based on preliminary analytical trade studies which used an initial estimate of engine flexibility. Critical speed placement was analyzed to be more than 25% above normal operating speed (11,500 RPM).

As the detailed design of the engine progressed and was included in the critical speed analysis, it became apparent that the anticipated critical speed margin would not be realized. The analysis was expanded to include the torquesensor, its housing, bearings, and effective engine radial and moment flexibility. This more detailed analysis, performed at Detroit Diesel Allison and confirmed by Boeing Vertol, revealed the shaft/torquesensor whirl mode in the area of 12,500 - 13,000 RPM, or only about 10% above normal operating speed. The analytical mode shapes and frequencies are shown in Figure (16).

Working together, both companies conducted parametric analyses to evaluate various potential fixes. Prime candidates were inlet housing and torquesensor housing stiffness increases, a shorter engine nose, auxiliary support struts, stiffened torquesensors, plus combinations; however, when they were analyzed in combination with a complete engine dynamic model, none proved satisfactory. In fact, with the complete engine model, the critical speed of the original configuration was around 10,200 RPM, below normal operating speed. The mode involved substantial whirl of the torquemeter housing, some shaft bending and some case bending, and was very sensitive to output shaft coupling weight and unbalance.

This analysis revealed that the only practical solution was a drastic shortening of the torquesensor and housing, such that the shaft adapter is an integral part of the engine output shaft, and the flexible coupling is now only 5.3 inches from the front face of the engine. Due to the increased distance between the engine and combining transmission, the output shaft was changed to a 3-section configuration. This also reduced the amount of weight hung off the engine. Analysis of this configuration placed the natural mode at about 14,200 RPM, which was basically power turbine conical whirl interacting to some extent with the torquesensor shafting. Another mode at about 17,200 RPM showed compressor conical whirl with rotor, power turbine and case participation. Forced response analysis showed both these modes were only mildly responsive to mass unbalance at the output shaft coupling, as shown in Figure (17). This indicates that the desired shaft/engine dynamic decoupling has been accomplished.

It is interesting to note how design decisions not directly related to engine shaft dynamics provided constraints to the solution of the interface problem. For example, the decision to move the shaft interface well forward of the engine front face led to the long torquesensor housing design, which brought about the shaft/torquesensor whirl problem in the first place. Also, the engine/shaft interface could not be moved very much closer to the engine front face without shortening the torquesensor. Since torquesensor accuracy is a function of length, the decision to drastically shorten the torquesensor and housing was made with reluctance, since torquesensor accuracy had to be compromised to some extent.

Another interesting aspect of this problem is the fact that the critical speed of the engine-to-mixbox shafting could not be accurately analyzed until the complete engine dynamics were included. This is where the engine/airframe interface agreement in effect between Boeing Vertol and Detroit Diesel Allison has been instrumental. It has led to excellent working agreements between the companies that have helped to reveal, analyze and solve this potential problem before it reached the hardware stage. Preliminary shaft critical speed work was done at Boeing Vertol. However, when it became apparent that engine dynamics must be included to accurately predict the critical speeds, all work was done jointly with Allison.

Conclusions

(1) Helicopter engine/drive system torsional instability may be prevented if care is taken to accurately represent both engine and rotor systems in the analysis, including such effects as hydraulic compressibility of the blade lag damper.

(2) Accurate analysis and/or shake testing of all engine installations, whether hard mounted, detuned, or isolated, is required to determine potential engine vibration and stress problem areas.

(3) Helicopter rotor blades and drive systems must be designed such that blade lag flexibility does not couple

with drive system torsional flexibility to produce a resonance at the number of rotor blade's frequency (b/rev).

(4) Formal engine/airframe interface agreements have already proven beneficial in the timely resolution of potential interface dynamics problems.

References

1. Fredrickson, C., Rumford, K. and Stephenson, C., FACTORS AFFECTING FUEL CONTROL STABILITY OF A TURBINE ENGINE/ HELICOPTER ROTOR DRIVE SYSTEM, 27th National American Helicopter Society Forum, Washington, D.C., May 1971.

2. Vance, J. M. and Gomez, J., VIBRATORY COMPATIBILITY OF ROTARY-WING AIRCRAFT PROPULSION COMPONENTS, 29th National American Helicopter Society Forum, Washington, D.C., May 1973.

3. Boeing Vertol Company, D210-10348-1, CH-47C/T55-L-11 ENGINE VIBRATION AND STRAIN SURVEY, Kumpel, M., October 1971.

4. Hooper, W. E. and Duke, E., THE MODEL 347 ADVANCED TECHNOLOGY HELICOPTER, 27th National American Helicopter Society Forum, Washington, D.C., May 1971.

5. Woodley, D. and Castle, W., HEAVY LIFT HELICOPTER MAIN ENGINES, SAE Technical Paper 730920, October 1973.

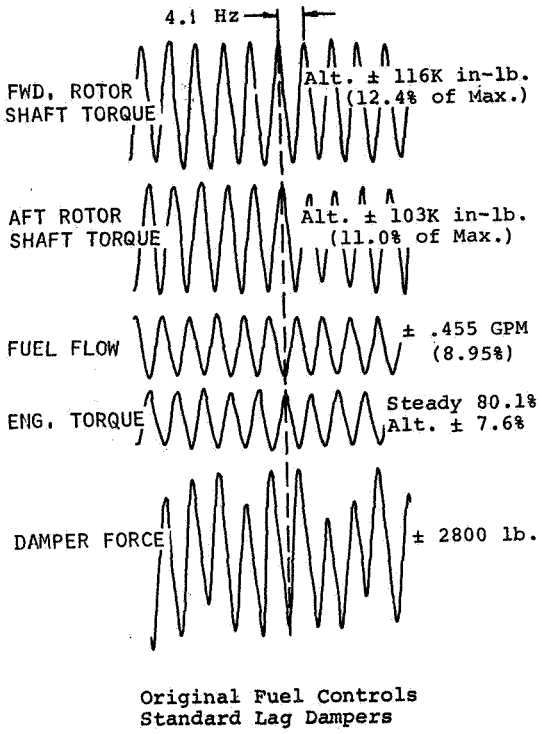

Figure 1. Torque Oscillation Flight Test Data

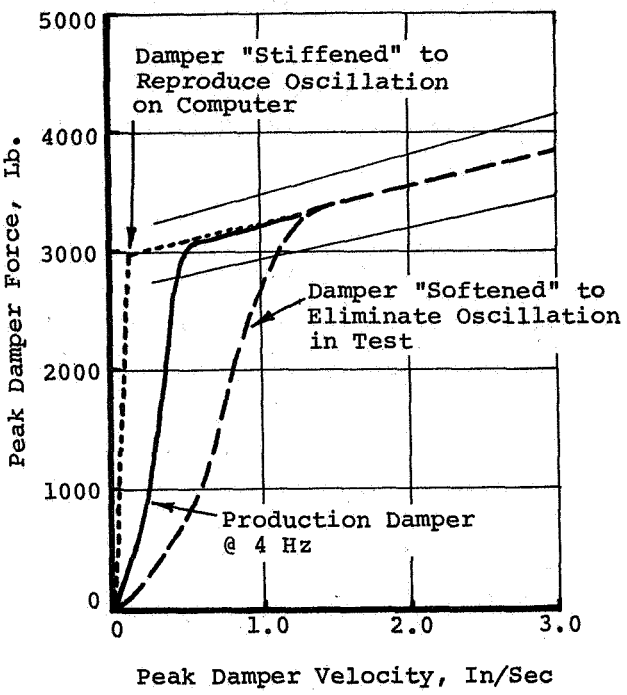

Figure 2. Lag Damper Force-Velocity Curves

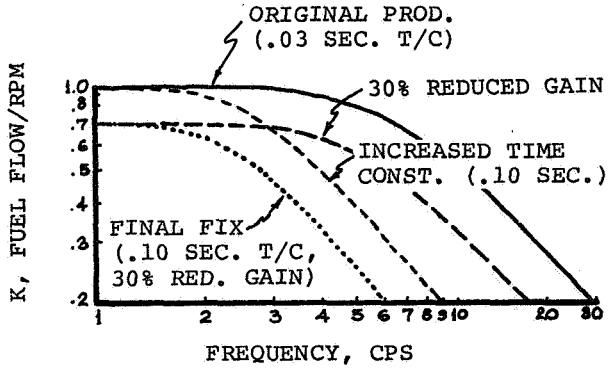

Figure 3. Fuel Control Frequency Response

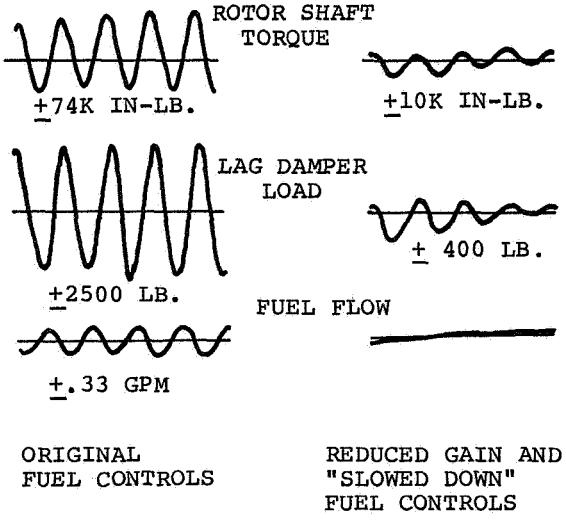

Figure 4. Final Torque Oscillation Simulation

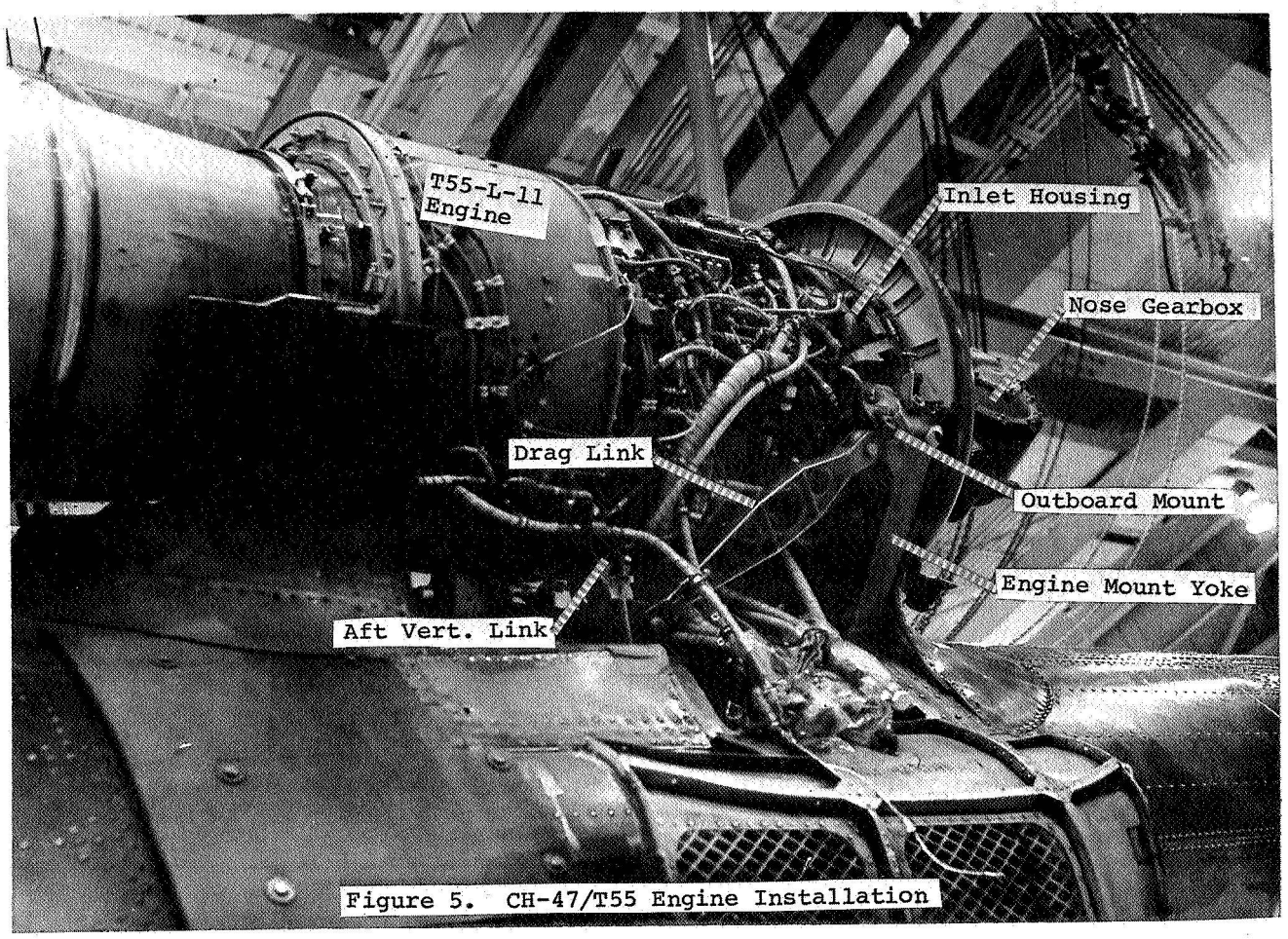

Figure 5. CH-47/T55 Engine Installation

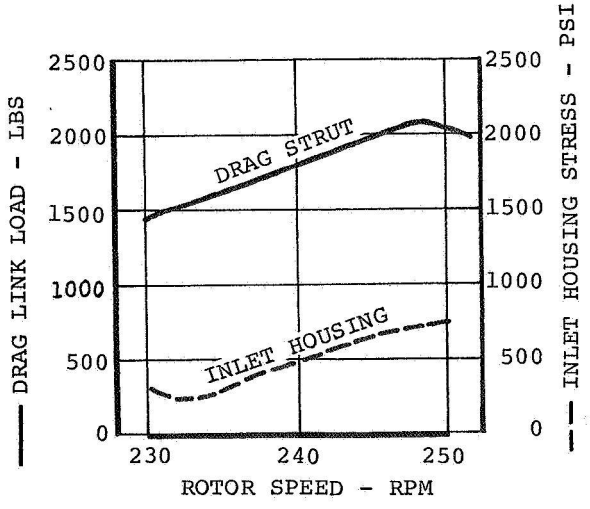

Figure 6. Inlet Housing Stress &
Drag Link Load vs. RPM

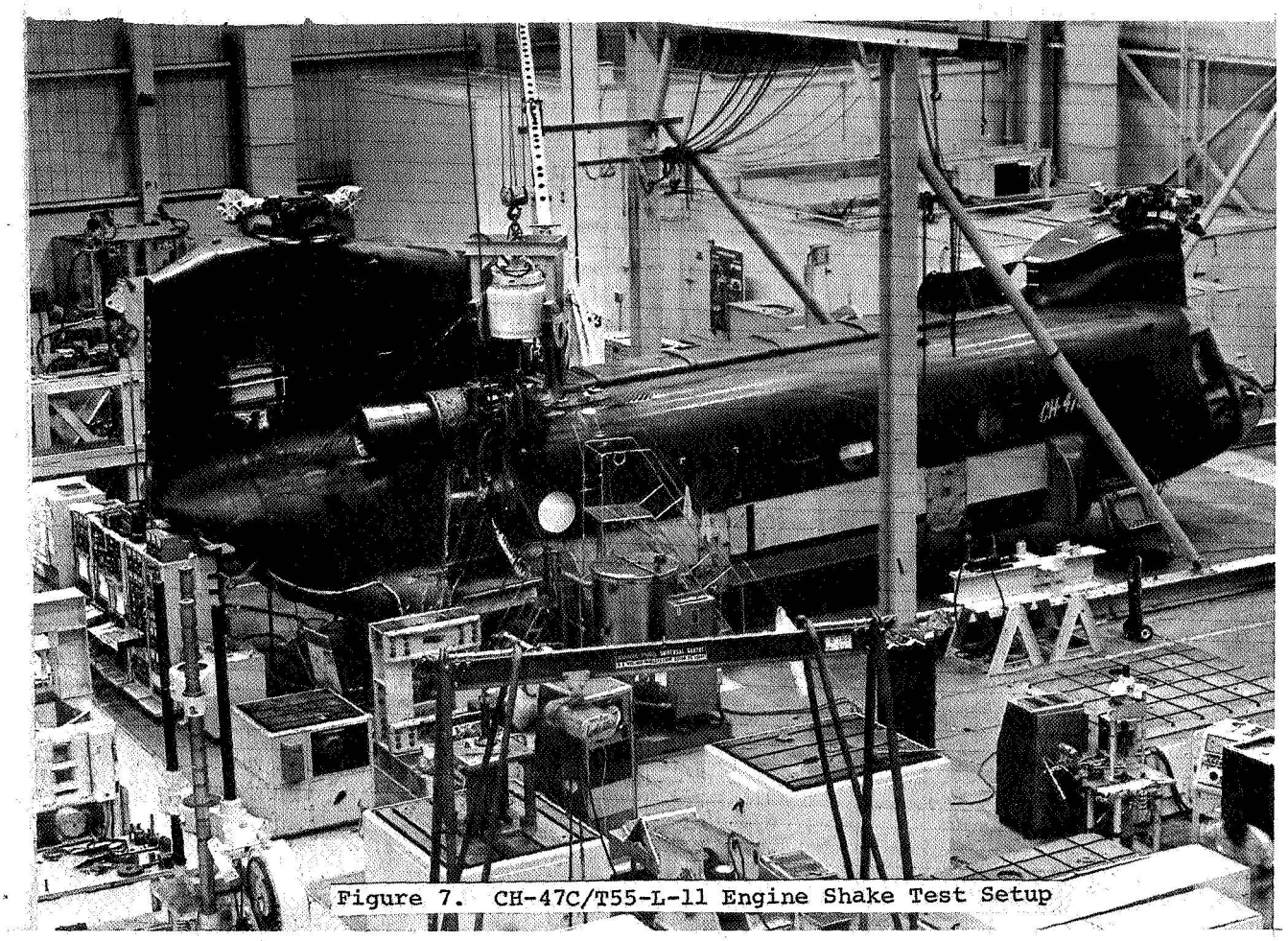

Figure 7. CH-47C/T55-L-11 Engine Shake Test Setup

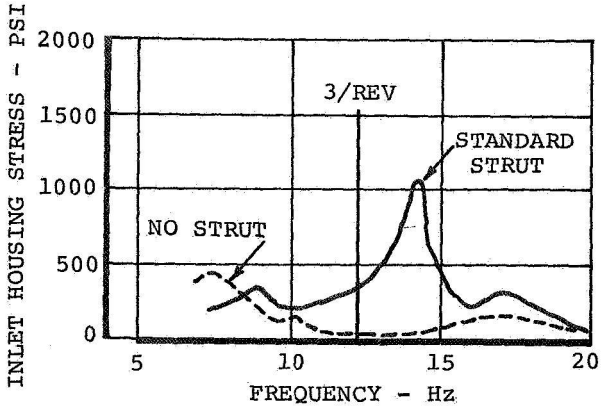

Figure 8. CH-47C/T55-L-11 Engine Shake Test Results

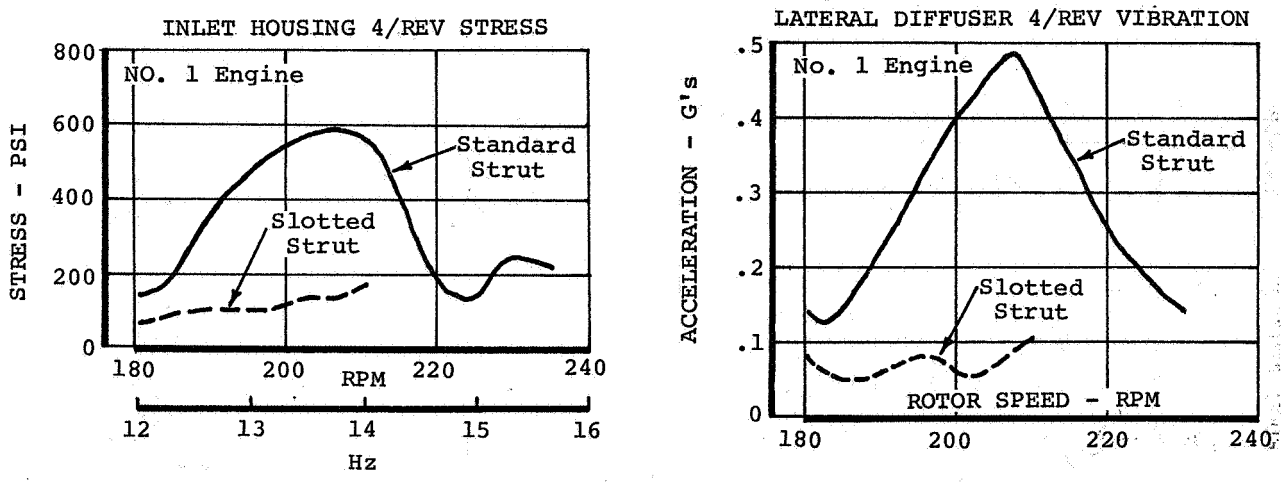

Figure 9. Vibration and Stress Reductions with Slotted Drag Strut

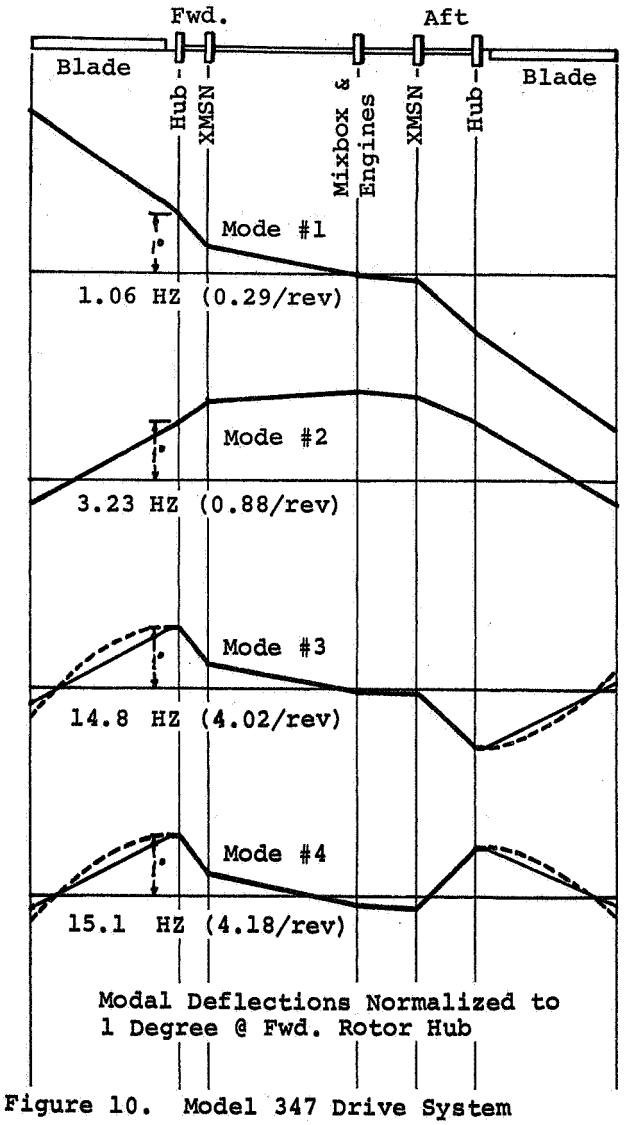

Figure 10. Model 347 Drive System Torsional Modes

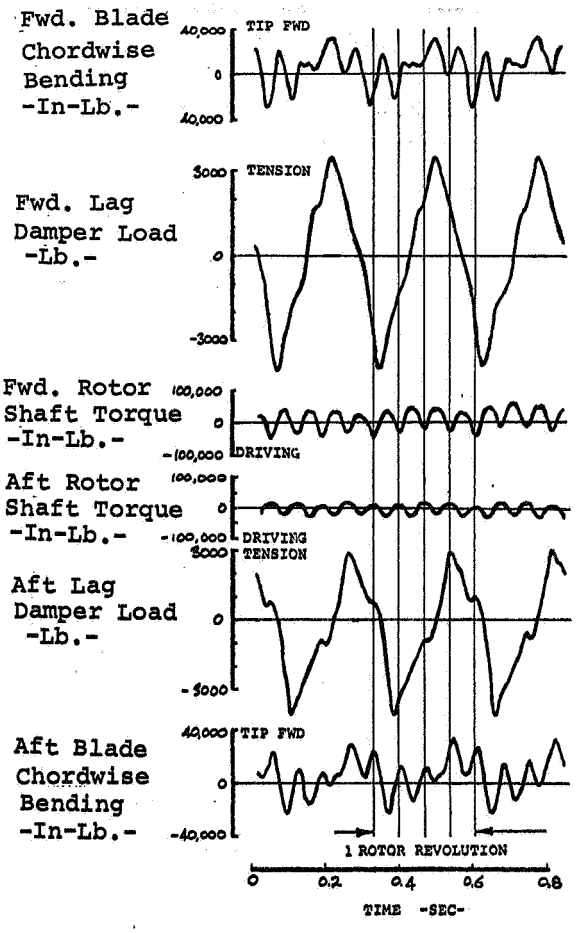

Figure 11. Model 347 Rotor/Drive System Flight Test Data

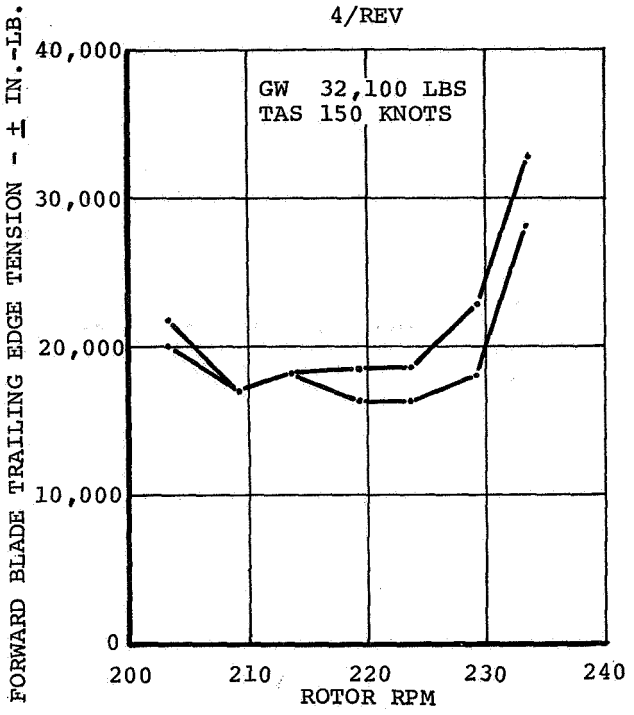

Figure 12. Model 347 Blade Chordwise Bending Moment vs. RPM

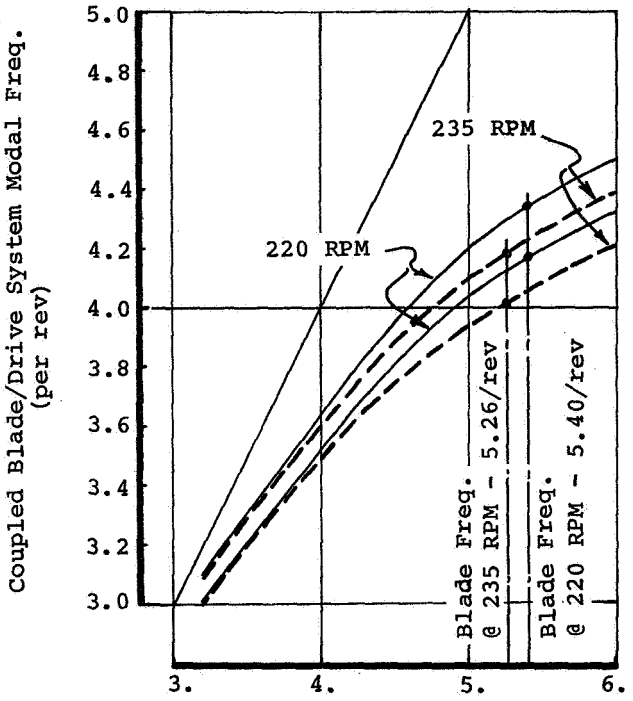

Figure 13. Effect of Chordwise Blade Bending Frequency on Model 347 Drive System Modes

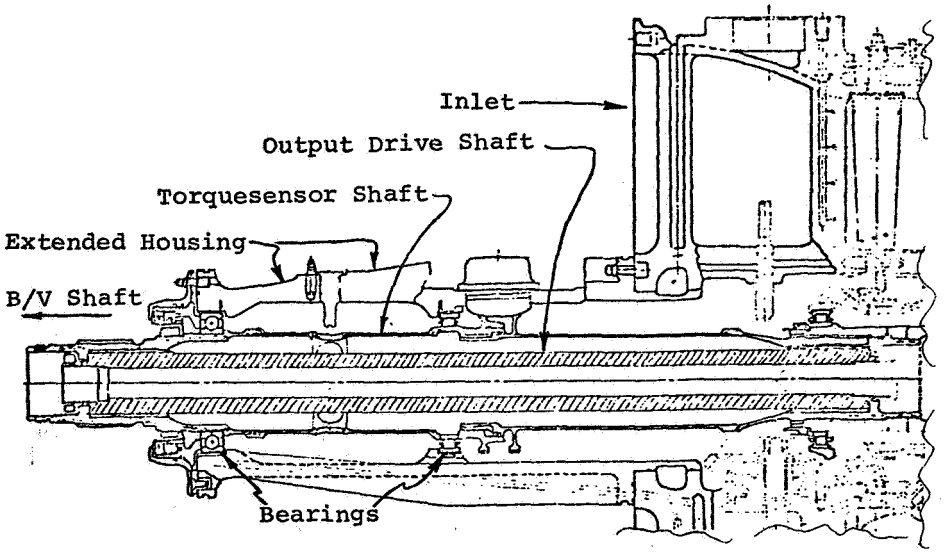

Figure 14. Original 501-M62B Torquesensor Configuration

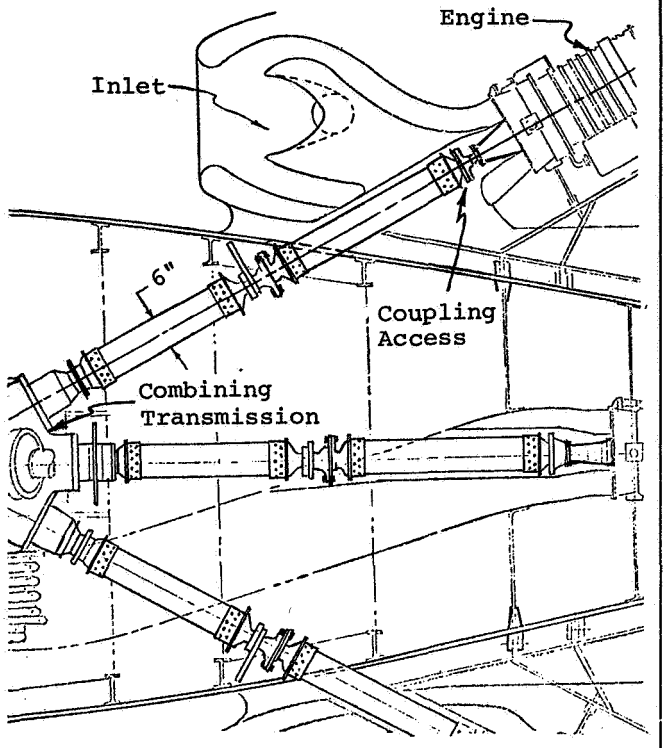

Figure 15. Original HLH Engine to Combiner Box Shafting

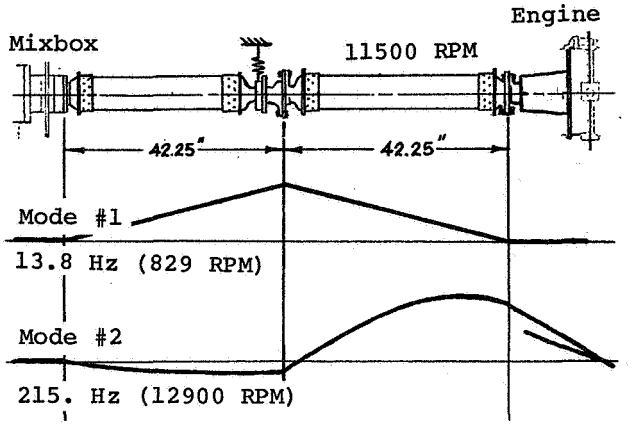

Figure 16. Preliminary Engine/Shaft Dynamic Analysis showing Torquesensor/Shaf Conical Whirl Mode

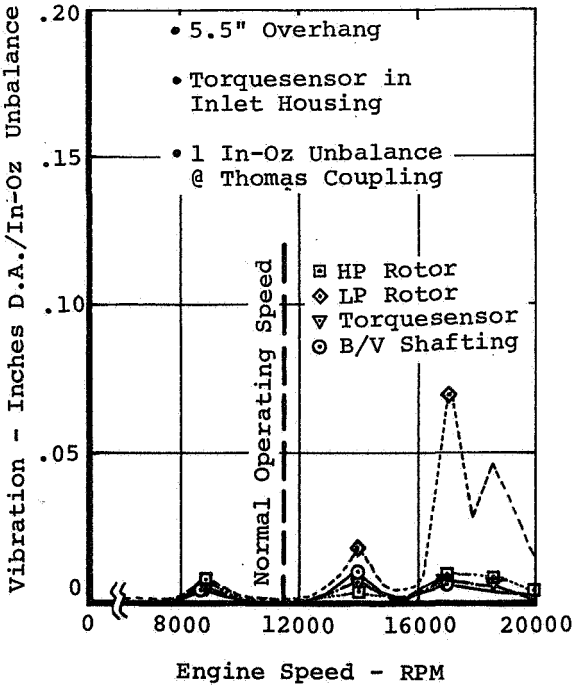

Figure 17. Final HLH Engine/Shaft Analysis - Response to Unbalance

HINGELESS ROTOR THEORY AND EXPERIMENT ON VIBRATION REDUCTION BY PERIODIC VARIATION OF CONVENTIONAL CONTROLS

G. J. Sissingh and R. E. Donham
Lockheed-California Company
Burbank, California

Abstract

The reduction of the n per rev. pitch-, roll- and vertical vibrations of an n-bladed rotor by n per rev. sinusoidal variations of the collective and cyclic controls is investigated. The numerical results presented refer to a four-bladed, 7.5-foot model and are based on frequency response tests conducted under an Army-sponsored research program. The following subjects are treated:

- Extraction of the rotor transfer functions (.073R hub flapping and model thrust versus servo valve command, amplitude and phase)
- Calculation of servo commands (volts) required to compensate .073R hub flapping (3P and 5P) and model thrust (4P)
- Evaluation of the effect of the vibratory control inputs on blade loads
- Theoretical prediction of the root flapbending moments generated by o to 5P perturbations of the feathering angle and rotor angle of attack.

Five operating conditions are investigated covering advance ratios from approximately 0.2 to 0.85. The feasibility of vibration reduction by periodic variation on conventional controls is evaluated.

Summary

For several operating conditions covering advance ratios from approximately 0.2 to 0.85, the control inputs required to counteract the existing 4P pitch, roll and vertical vibrations are calculated. The investigations are based on experimental vibration and response data. As the tests were part of and added on to a larger hingeless rotor research program, only a few operating conditions with essentially zero tip path plane tilt were investigated because of limited tunnel time. At the test rotor speed (500 rpm) the rotor blade mode frequencies were 1.34P, first flapping, 6.3P, second flapping, and 3.6P, first inplane.

This work was conducted under the sponsorship of the Ames Directorate of the U. S. Army Air Mobility R&D Laboratory under Contract NAS2-7245. The authors gratefully acknowledge the assistance of Mr. David Sharpe, the AMRDL Project Engineer, and Messrs. R. London and G. Watts of Lockheed in conducting the experimental portion of this work.

Presented at the AHS/NASA-Ames Specialists' Meeting on Rotorcraft Dynamics, February 13-15, 1974.

It should be noted that there was no instrumentation to measure the vibratory pitching and rolling moments. These moments were obtained by properly adding up the flap-bending moments of the four blades at 3.3 in. (0.073R) which were measured separately. This means, the effects of the inplane forces, vertical shear forces and blade torsion have been ignored. These are important influences in current hingeless rotor designs. The inplane 3P and 5P shear forces are of particular interest. However, the experimental data obtained for a model hingeless rotor system provides the beginning of at least a partial data base for the investigation of vibration attenuation of such systems through periodic variation of conventional controls.

Generally speaking, the control inputs required for flapping (hub moment) sourced vibration elimination are smaller or about of the same magnitude as those used for the frequency response tests. Their amplitudes lie, depending on flight condition and advance ratio, between 0.2 and 3 degrees. With the exception of the $\mu = 0.851$ case, for which the results are somewhat in doubt (the response tests to lateral cyclic pitch and the corresponding baseline data were inadvertently run with 0.3-degree collective pitch differential), the control inputs required for vibration reduction drastically reduce the 3 and 5P, and have only a minor effect on the 2P flexure flap-bending moments. Chord-bending moments and blade torsion generally increase.

The theoretical predictions mentioned refer to forced-response influence coefficients. They are based on the first two flapping modes. The blade root flap-bending moments (0P through 5P) which result from unit perturbations of blade feathering angle and rotor angle of attack have been calculated. The solution provides for intermode coupling through the 17th harmonic by analytic solution of the two-degree-of-freedom system, utilizing constant coefficient and loading descriptions over ten-degree azimuth sectors. In each solution case, the rotor reached steady-state motion in eight revolutions. In that time the least converging second mode flapping motion converged to a minimum of four significant figures.

Evaluation of the test data reveals two types of shortcomings, which should be avoided in future tests. First, the data given are based on a single test and have not been verified. Second, in some cases, the baseline and frequency response tests were not run successively.

From the data available, the approach is promising, especially for the low and medium advance ratio range. At higher advance ratios ($\mu \sim 0.8$), the control inputs required for vibration reduction may become prohibitive.

Notation

A, B	quantities describing cos 4ψ and sin 4ψ components of actuator input for frequency response tests, volt, see Table II and Equation (1)

C, D — quantities describing responses to A and B, in.-lb and lb, respectively, see Equation (1)

E, F, G, H — blade loads due to unit actuator input, in.-lb/ volt, see Equation (13)

$K_1 \ldots K_{18}$ — gains of rotor response, see Table I

m — calculated flapbending moment at 3.3 in., in.-lb,

$$m = m_o + \Sigma m_{ns} \sin n\psi + \Sigma m_{nc} \cos n\psi$$

M, L, T — 4P vibratory pitching moments, rolling moments and thrust variations, in.-lb and lb, respectively; subscript e denotes existing vibrations to be compensated, subscript control describes effects of oscillatory control inputs.

$$M_e = M_s \sin 4\psi + M_c \cos 4\psi$$

$$L_e = L_s \sin 4\psi + L_c \cos 4\psi$$

$$T_e = T_s \sin 4\psi + T_c \cos 4\psi$$

$\theta_{nominal}$ — nominal collective pitch, degrees

θ_o, θ_s, θ_c — oscillator inputs for collective, longitudinal and lateral cyclic pitch, volt

$$\theta_o = \theta_{os} \sin 4\psi + \theta_{oc} \cos 4\psi$$

$$\theta_s = \theta_{ss} \sin 4\psi + \theta_{sc} \cos 4\psi$$

$$\theta_c = \theta_{cs} \sin 4\psi + \theta_{cc} \cos 4\psi$$

$\tau_1 \ldots \tau_{18}$ — lag angles of response, degrees, see Table I

Ω — rotor angular velocity, sec^{-1}

ψ — azimuth position of master blade, rad

$$\frac{C_{RM}}{a\sigma} = \frac{\text{Blade Root Moment, STA (o)}}{\pi R^3 \rho(\Omega R)^2 a\sigma}$$

where

$a = 5.73$

$\rho = 0.002378$ slugs/ft^3

$\sigma = 0.127$

"Compensating Control Inputs" define those which reduce the existing 4P pitching moments, rolling moments and vertical forces of a given flight condition to zero.

The analysis deals with the concept of vibration reduction by oscillatory collective and cyclic control applications. Several related aspects of this problem are treated. The foremost are the determination of the proper control inputs and their effect on the vibratory blade loads. These studies are based on frequency response tests conducted on a 7.5 foot-diameter, four-bladed, hingeless rotor model, the results of which are published in Appendixes C and D of Reference 1. The subject matter covered, apart from the items listed below, is an abridged version of these appendixes.

Other subjects treated are (a) the calculation of blade loads, based on test data, due to vibratory control command applications; (b) the theoretically determined eigenvalues, at 10-degree azimuth intervals, of the first and second flapping modes, at $\mu = 0.191$, 0.45 and 0.851; (c) the computed single-blade root flap-bending moment, Sta 0, harmonic influence coefficients at $\mu = 0.191$, 0.45 and 0.851; and (d) a limited comparison of the theoretical loads with experiments.

The general case of vibration control will include the effects of lateral and fore-and-aft shear forces at blade passage frequency. These forces can be as influential as the pitch and roll moment and thrust oscillations in causing fuselage vibrations. Thus, in general, five rotor vibratory inputs are to be controlled by manipulation of three controls. Although the five vibratory inputs cannot be nulled individually with three controls, their combined contribution to the fuselage vibration can be controlled. Thus, the general application will involve control of fuselage vibration at three points; say two vertical vibrations and one roll angular vibration. This general application implies the use of adaptive feedback controls. Although the present paper is limited to the more simple case outlined herein, the general application to the control of any three suitable quantities will be apparent.

Although prior investigations of the use of higher harmonic pitch control on teetering and offset hinge rotors have been conducted to investigate improved system performance and also for vibration attentuation (References 2, 3 and 4), this is believed to be the first experimental and theoretical hingeless rotor study of the use of periodic variation of conventional controls for vibration attentuation. The use of 2P feathering to improve rotor performance is not included as part of this work.

Transfer Functions Involved

As a distinction must be made between control applications in phase with sin 4ψ and cos 4ψ, there are six control quantities available, i.e., θ_{os}, θ_{oc}, θ_{ss}, θ_{sc}, θ_{cs} and θ_{cc}, to monitor the pitching moments, rolling moments and vertical forces. This means the dynamic system investigated, which consists of rotor, control mechanism and oscillators used, is characterized by 18 gains K_p and lag angles τ_p. The subscripts p (p = 1 through 18) are defined by Table I.

TABLE I
GAINS AND LAG ANGLES OF RESPONSE
TO OSCILLATORY CONTROL APPLICATIONS

	θ_{os}	θ_{oc}	θ_{ss}	θ_{sc}	θ_{cs}	θ_{cc}
M	$K_1\tau_1$	$K_2\tau_2$	$K_3\tau_3$	$K_4\tau_4$	$K_5\tau_5$	$K_6\tau_6$
L	$K_7\tau_7$	$K_8\tau_8$	$K_9\tau_9$	$K_{10}\tau_{10}$	$K_{11}\tau_{11}$	$K_{12}\tau_{12}$
T	$K_{13}\tau_{13}$	$K_{14}\tau_{14}$	$K_{15}\tau_{15}$	$K_{16}\tau_{16}$	$K_{17}\tau_{17}$	$K_{18}\tau_{18}$

As indicated, K_3 is defined as the amplitude ratio M/θ_{ss} and τ_3 is the lag angle of M with respect to θ_{ss}. For convenience, the dimensions used are identical with those of the computer output, i.e., oscillator voltage for input, in.-lb for M and L, lb for the thrust variation T. This means the dimensions of K_p are

K_1 through K_{12}	in.-lb/volt
K_{13} through K_{18}	lb/volt

The phase angles τ_p are given in degrees, τ_p is positive if the response lags.

Although the investigations deal exclusively with 4P control variations, some general remarks may be in order. The general case involves sinusoidal collective and cyclic control variations with the frequency $n\Omega$ where n can be any positive number.

If n is an integer, the rotor excitations repeat themselves after each rotor revolution which means that the responses of each revolution are identical. This is true for any number of rotor blades but does not necessarily mean that all blades execute identical flapping motions. The latter is true only if n equals the number of rotor blades or is a multiple of the blade number. Only for these cases does a truly time independent response with invariable amplitude ratios K and lag angles τ exist.

Extraction of Gains and Lag Angles from Experiments

As for all response tests conducted, the oscillator input contained both sin 4ψ and cos 4ψ-components; always two amplitude ratios K and two lag angles τ are involved. Therefore, each time a set of two tests must be evaluated. According to Table II, the input is characterized by the quantities $A_1\ B_1\ A_2\ B_2$ and the response by $C_1\ D_1\ C_2\ D_2$.

If the rotor responds to cos 4ψ excitations with the gain K_j and the lag angle τ_j (j = even number) and to sin 4ψ excitations with K_i and τ_i (i = odd number), input and output are related by the equations

$$\left.\begin{aligned} A_1 K_j \cos(4\psi - \tau_j) + B_1 K_i \sin(4\psi - \tau_i) &= C_1 \cos 4\psi + D_1 \sin 4\psi \\ A_2 K_j \cos(4\psi - \tau_j) + B_2 K_i \sin(4\psi - \tau_i) &= C_2 \cos 4\psi + D_2 \sin 4\psi \end{aligned}\right\} \quad (1)$$

TABLE II
INPUT AND OUTPUT NOTATIONS

Test	Input	Response
#1	$A_1 \cos 4\psi + B_1 \sin 4\psi$	$C_1 \cos 4\psi + D_1 \sin 4\psi$
#2	$A_2 \cos 4\psi + B_2 \sin 4\psi$	$C_2 \cos 4\psi + D_2 \sin 4\psi$

To calculate the unknowns $K_i\ K_j\ \tau_i$ and τ_j, a component analysis is used. The gains $K_i\ K_j$ are expressed as

$$\left.\begin{aligned} K_i &= (R_i^2 + I_i^2)^{1/2} \\ K_j &= (R_j^2 + I_j^2)^{1/2} \end{aligned}\right\} \quad (2)$$

See also Figure 1 which shows the oscillatory pitching moments due to combined θ_{ss} and θ_{sc} control applications. The moments generated are presented by rotating vectors where cos 4ψ is positive to the right and sin 4ψ positive down. This means, the vector positions shown refer to $\psi = 0$. By definition, the quantities $R_{i,j}$ characterize the responses in phase with the excitation and $I_{i,j}$ those out of phase. The latter are positive if the response leads. As indicated, there are altogether four responses involved which are combined to the resultant M.

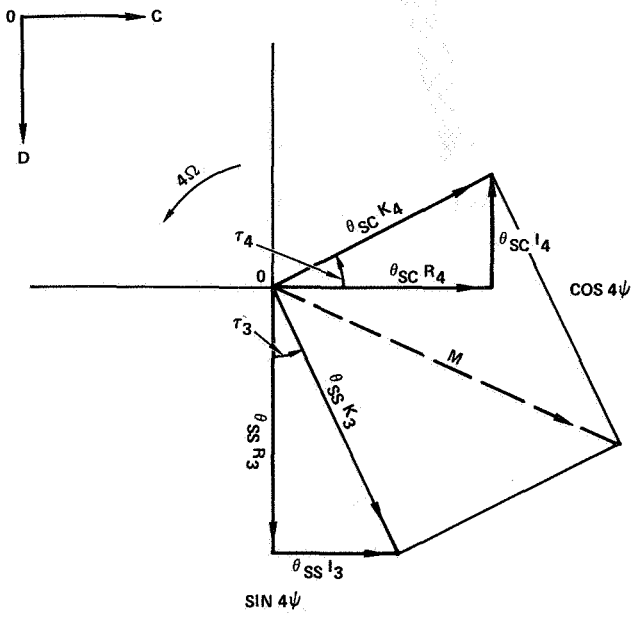

Figure 1. Vector Diagram Showing Pitching Moment Due to θ_{ss} and θ_{sc} Control Applications

Inserting Equation (2) into Equation (1) leads to

$$\left.\begin{aligned} R_i &= \frac{A_1D_2 - A_2D_1}{A_1B_2 - A_2B_1} \\ I_i &= \frac{A_1C_2 - A_2C_1}{A_1B_2 - A_2B_1} \\ \tan\bar{\tau}_i &= |I_i/R_i| \quad 0 < \bar{\tau}_i < \pi/2 \end{aligned}\right\} \quad (3)$$

and

$$\left.\begin{aligned} R_j &= \frac{C_1B_2 - B_1C_2}{A_1B_2 - A_2B_1} \\ I_j &= \frac{B_1D_2 - B_2D_1}{A_1B_2 - A_2B_1} \\ \tan\bar{\tau}_j &= |I_j/R_j| \quad 0 < \bar{\tau}_j < \pi/2 \end{aligned}\right\} \quad (4)$$

In both cases

$$\begin{array}{lll} \tau = +\bar{\tau} \text{ for } & R>0 & I<0 \\ = -\bar{\tau} & R>0 & I>0 \\ = \pi + \bar{\tau} & R<0 & I>0 \\ = \pi - \bar{\tau} & R<0 & I<0 \end{array}$$

Check of Calculated K_i K_j τ_i and τ_j Values

If so desired, Equation (1) can be used to check the calculated values of K_i K_j τ_i and τ_j. Splitting up these equations into sin 4ψ and cos 4ψ components leads to the following four expressions which must be satisfied

$$\left.\begin{aligned} A_1 K_j \cos\tau_j - B_1 K_i \sin\tau_i &= C_1 \\ A_1 K_j \sin\tau_j + B_1 K_i \cos\tau_i &= D_1 \\ A_2 K_j \cos\tau_j - B_2 K_i \sin\tau_i &= C_2 \\ A_2 K_j \sin\tau_j + B_2 K_i \cos\tau_i &= D_2 \end{aligned}\right\} \quad (5)$$

Oscillatory Control Inputs Required

The six oscillator inputs available have to be selected so that their responses satisfy the requirements, whatever they may be. By definition, the vibratory control inputs result in the following pitching moments, rolling moments and vertical forces (n = 4):

$$\begin{aligned} M_{control} = &+\theta_{os} K_1 \sin(n\psi - \tau_1) \\ &+\theta_{oc} K_2 \cos(n\psi - \tau_2) \\ &+\theta_{ss} K_3 \sin(n\psi - \tau_3) \\ &+\theta_{sc} K_4 \cos(n\psi - \tau_4) \\ &+\theta_{cs} K_5 \sin(n\psi - \tau_5) \\ &+\theta_{cc} K_6 \cos(n\psi - \tau_6) \end{aligned} \quad (6)$$

$$\begin{aligned} L_{control} = &+\theta_{os} K_7 \sin(n\psi - \tau_7) \\ &+\theta_{oc} K_8 \cos(n\psi - \tau_8) \\ &+\theta_{ss} K_9 \sin(n\psi - \tau_9) \\ &+\theta_{sc} K_{10} \cos(n\psi - \tau_{10}) \\ &+\theta_{cs} K_{11} \sin(n\psi - \tau_{11}) \\ &+\theta_{cc} K_{12} \cos(n\psi - \tau_{12}) \end{aligned} \quad (7)$$

$$\begin{aligned} T_{control} = &+\theta_{os} K_{13} \sin(n\psi - \tau_{13}) \\ &+\theta_{oc} K_{14} \cos(n\psi - \tau_{14}) \\ &+\theta_{ss} K_{15} \sin(n\psi - \tau_{15}) \\ &+\theta_{sc} K_{16} \cos(n\psi - \tau_{16}) \\ &+\theta_{cs} K_{17} \sin(n\psi - \tau_{17}) \\ &+\theta_{cc} K_{18} \cos(n\psi - \tau_{18}) \end{aligned} \quad (8)$$

$$\left.\begin{aligned} M_{control} &= -M_s \sin 4\psi - M_c \cos 4\psi \\ L_{control} &= -L_s \sin 4\psi - L_c \cos 4\psi \\ T_{control} &= -T_s \sin 4\psi - T_c \cos 4\psi \end{aligned}\right\} \quad (9)$$

To reduce the existing vibrations, the moments and forces generated must counteract M_e, L_e and T_e, i.e.,

Equations 6 through 9 lead to six linear equations, (10), for the unknowns θ_{os}, θ_{oc}, θ_{ss}, θ_{sc}, θ_{cs} and θ_{cc}.

Effect on Blade Loads

An objective of the investigations is to determine the effect of the compensating control input on the blade loads, i.e., on the following measured quantities:

- flapbending at 3.3 in.
- flapbending at 13.15 in.
- chordbending at 2.4 in.
- torsion at 9.28 in.

In all cases the 2 to 5P content of the loads is of interest. The first task is to determine from the response tests the contribution of each of the six possible 4P control inputs to these loads. Again, two sets of data are required. The vibratory control applications used and the resulting n^{th} harmonic of the load considered are written as follows:

Test	Input	Resulting Load (in.-lb)
#1	$A_1 \cos 4\psi + B_1 \sin 4\psi$	$C_{n1} \cos n\psi + D_{n1} \sin n\psi$
#2	$A_2 \cos 4\psi + B_2 \sin 4\psi$	$C_{n2} \cos n\psi + D_{n2} \sin n\psi$

(11)

$$\begin{bmatrix} +K_1\cos\tau_1 & +K_2\sin\tau_2 & +K_3\cos\tau_3 & +K_4\sin\tau_4 & +K_5\cos\tau_5 & +K_6\sin\tau_6 \\ -K_1\sin\tau_1 & +K_2\cos\tau_2 & -K_3\sin\tau_3 & +K_4\cos\tau_4 & -K_5\sin\tau_5 & +K_6\cos\tau_6 \\ +K_7\cos\tau_7 & +K_8\sin\tau_8 & +K_9\cos\tau_9 & +K_{10}\sin\tau_{10} & +K_{11}\cos\tau_{11} & +K_{12}\sin\tau_{12} \\ -K_7\sin\tau_7 & +K_8\cos\tau_8 & -K_9\sin\tau_9 & +K_{10}\cos\tau_{10} & -K_{11}\sin\tau_{11} & +K_{12}\cos\tau_{12} \\ +K_{13}\cos\tau_{13} & +K_{14}\sin\tau_{14} & +K_{15}\cos\tau_{15} & +K_{16}\sin\tau_{16} & +K_{17}\cos\tau_{17} & +K_{18}\sin\tau_{18} \\ -K_{13}\sin\tau_{13} & +K_{14}\cos\tau_{14} & -K_{15}\sin\tau_{15} & +K_{16}\cos\tau_{16} & -K_{17}\sin\tau_{17} & +K_{18}\cos\tau_{18} \end{bmatrix} \begin{bmatrix} \theta_{os} \\ \theta_{oc} \\ \theta_{ss} \\ \theta_{sc} \\ \theta_{cs} \\ \theta_{cc} \end{bmatrix} = \begin{bmatrix} -M_s \\ -M_c \\ -L_s \\ -L_c \\ -T_s \\ -T_c \end{bmatrix} \quad (10)$$

If nonlinear effects are excluded, the n per rev load variation due to unit control application in phase with

$$\left.\begin{array}{ll} \text{(a)} & \cos 4\psi \text{ amounts to } (E_n \cos n\psi + F_n \sin n\psi) \\ \text{(b)} & \sin 4\psi \qquad\qquad (G_n \cos n\psi + H_n \sin n\psi) \end{array}\right\} \quad (12)$$

In these expressions

$$\left.\begin{aligned} E_n &= \frac{B_2C_{n1} - B_1C_{n2}}{A_1B_2 - A_2B_1} \\ F_n &= \frac{B_2D_{n1} - B_1D_{n2}}{A_1B_2 - A_2B_1} \\ G_n &= \frac{A_1C_{n2} - A_2C_{n1}}{A_1B_2 - A_2B_1} \\ H_n &= \frac{A_1D_{n2} - A_2D_{n1}}{A_1B_2 - A_2B_1} \end{aligned}\right\} \quad (13)$$

If $\theta_{\xi s}$, $\theta_{\xi c}$ (ξ = o, s, c) denote the vibratory control inputs used, the increments of the n^{th} harmonic of the load considered are

$$(\Delta\text{load})_n = (\theta_{\xi c} E_n + \theta_{\xi s} G_n) \cos n\psi + (\theta_{\xi c} F_n + \theta_{\xi s} H_n) \sin n\psi \quad (14)$$

Evaluation of Experiments

Flight Conditions Investigated

The methods outlined in the previous sections are applied to the following five operating conditions for which test data are available:

TABLE III
OPERATING CONDITIONS INVESTIGATED

μ	$\theta_{nominal}$	α	C_T/σ
0.191	12°	-5°	0.102
0.239	4	-5	0.028
0.443	4	-5	0.011
0.849	10	-5	-0.005
0.851	4	-5	-0.013

In all cases the shaft angle of attack is $\alpha = -5^o$ and the rotor is trimmed so that essentially $a_1 = b_1 = 0$. As can be seen, the tests cover the advance ratio range from approximately $\mu = 0.2$ to $\mu = 0.85$. The case $\mu = 0.191$ is characterized by $\theta_{nominal} = 12^o$ and $C_T/\sigma = 0.102$, the latter figure indicates a relatively high specific loading. In contrast, at the advance ratios $\mu = 0.849$ and 0.851 the rotor is practically unloaded, i.e., no steady lifting force is generated. The 4P vibrations associated with the various test conditions are listed in Table IV. The moments are given in inch-pounds and the vibratory forces in pounds.

These moments were obtained by properly adding up the flap-bending moments of the four blades at 3.3 in. which were measured separately. This means, the effects of the in-plane forces, vertical shear forces and blade torsion have been ignored.

TABLE IV
VIBRATORY MOMENTS AND FORCES
TO BE COMPENSATED

μ	0.191	0.239	0.443	0.849	0.851
M_s	0.3805	- 1.7207	2.6149	20.0483	3.5349
M_c	- 0.5301	- 0.4113	- 0.5208	- 4.5724	- 8.4341
L_s	12.2080	1.3725	- 6.7626	9.4647	-10.5154
L_c	2.2180	- 1.9145	- 3.7399	- 31.1214	-17.2626
T_s	0.1979	- 0.1089	0.0304	1.9247	0.8838
T_c	- 0.2013	- 0.0865	0.0556	- 0.0048	- 0.8626

Gains and Lag Angles

The rotor response characteristics are calculated by applying equations (2, 3, 4) to the test data available. The results available are listed in Table V. As pointed out previously, the values given include the effect of the actuator used. Some general statements can be made. It is obvious that for $\mu = 0$. the gain and lag angle of the responses to sin 4ψ- and cos 4ψ-type control applications must be the same. For $\mu \neq 0$ this is no longer true, and one would expect that the spread between K_iK_j and $\tau_i\tau_j$ (see equations (3), (4)) widens with increasing advance ratio. Further, according to classical rotor theory which neglects blade stall, the nominal collective pitch setting has no effect on the frequency response characteristics.

Generally speaking, the K_iK_j and $\tau_i\tau_j$ values given in Table V differ very little. It appears however, that at higher advance ratios (compare columns for $\mu = 0.849$ and 0.851) the collective pitch has a larger effect than anticipated. It is also possible that the error of the baseline data described in the summary may play a role.

Oscillator Inputs Required

Equation (10) is used to calculate the inputs required to

(a) generate unit amplitudes of pure pitching moments, rolling moments and vertical forces and

(b) compensate the existing vibrations

The results are given in Tables VI and VII. They show that, as to be expected, the oscillatory inputs required for vibration reductions generally increase with increasing advance ratio. Surprisingly, the rotor collective pitch setting seems to play a larger role than the steady lift generated. See also Table VIII which summarizes the results obtained and lists the operating conditions investigated in the order of decreasing vibrations. The first column shows the relative magnitude of the vibratory moments generated and the last column the approximate amplitude of the blade pitch variation required to compensate the vibrations. The amplitude of the pitch variation produced per volt oscillator input changes with the control loads and

TABLE V
GAINS AND LAG ANGLES DERIVED FROM EXPERIMENTS
(K_p - in.-lb/volt, τ_p - degrees)

	$\mu = 0.191$		$\mu = 0.239$		$\mu = 0.443$		$\mu = 0.849$		$\mu = 0.851$	
p	K_p	τ_p	K_p	τ_p	K_p	τ_p	K_p	τ_p	K_p	τ_p
1	5.617	42.3	1.099	125.6	2.236	120.5	4.798	72.0	4.094	116.5
2	6.126	44.0	1.141	149.1	2.791	129.3	4.787	72.6	3.487	135.6
3	17.571	- 9.6	52.416	- 30.1	42.237	- 28.7	18.537	- 19.8	43.319	- 5.1
4	26.019	- 45.4	47.991	- 37.3	40.073	- 30.1	20.329	- 41.5	37.081	12.7
5	30.696	155.7	59.416	182.9	45.186	188.4	33.002	183.4	26.170	214.2
6	32.505	181.7	77.408	193.2	61.144	180.8	21.085	180.0	38.661	184.5
7	2.856	136.0	4.246	81.9	8.166	86.5	2.472	102.1	10.097	93.1
8	1.507	98.4	5.083	67.1	8.077	66.9	3.412	144.7	7.979	62.9
9	35.384	213.4	59.420	198.8	43.846	181.4	44.506	200.5	48.081	176.2
10	41.674	185.8	51.280	198.6	39.383	195.7	48.473	201.0	40.850	187.7
11	45.953	116.6	76.875	108.3	78.512	101.8	67.268	134.4	88.540	94.7
12	61.589	131.5	86.361	99.3	80.995	95.7	61.288	141.5	90.934	95.3
13	6.879	45.6	5.420	51.4	8.928	39.2	8.188	35.8	9.340	38.5
14	7.211	43.7	6.195	46.4	8.999	35.9	8.906	36.1	9.651	35.6
15	6.635	245.2	4.275	205.9	2.571	195.2	5.976	215.0	3.623	184.0
16	6.033	218.3	3.962	208.1	3.123	188.7	4.775	229.5	1.977	185.4
17	13.000	127.3	7.596	94.3	7.632	76.7	13.261	133.1	11.188	86.9
18	10.057	128.6	8.176	97.4	8.381	92.2	7.953	126.3	11.101	90.7

the type of control ($\theta_0, \theta_s, \theta_c$) used. Therefore, the conversion factor varies and the last column of Table VIII is given only to indicate the approximate amplitudes involved.

With one exception, the vibratory control applications required were smaller than those used for the frequency response tests. The exception is the case with the highest vibration level encountered for which the compensating controls required were approximately 15 to 20% higher than the inputs used for the 4P frequency response tests.

Blade Loads

The calculation of the effect of the compensating control inputs on the blade loads is based on Equations (13) and (14). The first step is to calculate, for each specific case, the quantities E_n through H_n (n = 2, 3, 4, 5). See Table IX which refers to $\mu = 0.849$ and lists the sin $n\psi$ and cos $n\psi$ components of the various loads due to unit control (volt) application. The table shows, for instance, that at the advance ratio $\mu = 0.849$, a ±1 volt variation of θ_{ss} produces 3P chordwise bending moments of the magnitude

$$(-91.77 \sin 3\psi + 7.15 \cos 3\psi) \text{ in.-lb}$$

As the control inputs required for vibration reduction have been previously calculated, their effects on the blade loads can be determined by adding up the various contributions. The reader is referred to Table X which applies to the flapbending moment at 3.3 in. for the case $\mu = 0.849$. Given are the original loads without vibratory control application, the individual contributions and the sum. The last column shows the amplitudes without and with compensating control input. A summary of the loads is represented in Table XI. Generally speaking, chordbending, blade torsion and the 4P flap-bending moments of the root flexure increase with increasing advance ratio. The 3 and 5P flap-bending moments of the flexure are, by nature, reduced and the 2P flap-bending moments are least affected. From the limited data available, it appears that the 4P chordwise- and 5P torsion moments may be the critical load for this configuration, inasmuch as the natural frequencies are close to these values.

As mentioned previously, it is assumed here that the pitching and rolling moments are solely caused by the flapbending moments of the root flexure which were individually measured and properly combined by a sin-cos potentiometer. This means, the only source for the troublesome 4P moments in the nonrotating system are the 3 and 5P flap-bending moments at 3.3 in. For four identical blades, it follows that elimination of the 4P pitching and rolling moments requires that the sin 3ψ, cos 3ψ, sin 5ψ and cos 5ψ components of the flap-bending moments at 3.3 in. are reduced to zero. As the four blades behave differently, this ideal condition will practically never be fulfilled.

In the preceding paragraphs the flapbending moment of a specific blade, with consideration of the compensating control input, was calculated. To a certain extent, these predicted loads can be used as an independent check. As an example, the case $\mu = 0.849$ is treated. According to Table IV the amplitudes of the 4P pitching and rolling moments to be compensated are

$$M = 20.56 \text{ in.-lb}$$
$$L = 32.52 \text{ in.-lb} \qquad (15)$$

The calculated 3 and 5P flap-bending moments with consideration of the compensating control input amount to (see Table VII),

$$m_{3s} = 0.6233 \text{ in.-lb}$$
$$m_{3c} = -1.1833$$
$$m_{5s} = -1.9266 \qquad (16)$$
$$m_{5c} = 0.3099$$

The amplitudes of the resulting 4P pitching and rolling moments are

$$M = 3.14 \text{ in.-lb}$$
$$L = 5.91 \text{ in.-lb} \qquad (17)$$

TABLE VI
OSCILLATOR INPUTS REQUIRED (VOLT) TO GENERATE PURE sin 4ψ- AND cos 4ψ- COMPONENTS OF PITCHING MOMENTS, ROLLING MOMENTS AND VERTICAL FORCES

μ	$M_{control}$ *	θ_{os}	θ_{oc}	θ_{ss}	θ_{sc}	θ_{cs}	θ_{cc}
0.191	$M_{s,\ control} = 1$	+0.0143	- 0.0485	+0.0508	+0.0290	- 0.0296	+0.0241
	$M_{c,\ control} = 1$	+0.0117	- 0.0123	- 0.0055	+0.0283	- 0.0219	- 0.0098
	$L_{s,\ control} = 1$	- 0.0177	- 0.0236	- 0.0113	+0.0052	- 0.0169	+0.0073
	$L_{c,\ control} = 1$	+0.0042	- 0.0071	- 0.0209	- 0.0200	+0.0003	- 0.0147
	$T_{s,\ control} = 1$	+0.0922	+0.1380	- 0.0490	- 0.0302	+0.0252	- 0.0232
	$T_{c,\ control} = 1$	- 0.1044	+0.1164	+0.0123	- 0.0210	+0.0235	+0.0081
0.239	$M_{s,\ control} = 1$	+0.0028	- 0.0069	+0.0299	+0.0219	- 0.0111	+0.0211
	$M_{c,\ control} = 1$	+0.0109	+0.0028	- 0.0096	+0.0206	- 0.0154	- 0.0070
	$L_{s,\ control} = 1$	- 0.0023	- 0.0108	- 0.0056	+0.0203	- 0.0167	+0.0078
	$L_{c,\ control} = 1$	+0.0128	- 0.0029	- 0.0245	- 0.0243	- 0.0008	- 0.0210
	$T_{s,\ control} = 1$	+0.1356	+0.1337	- 0.0053	- 0.0155	+0.0072	- 0.0128
	$T_{c,\ control} = 1$	- 0.1436	+0.1085	+0.0168	+0.0070	+0.0091	+0.0100
0.443	$M_{s,\ control} = 1$	- 0.0019	- 0.0053	+0.0255	+0.0116	- 0.0069	+0.0145
	$M_{c,\ control} = 1$	+0.0053	+0.0011	- 0.0023	+0.0331	- 0.0168	- 0.0004
	$L_{s,\ control} = 1$	- 0.0057	- 0.0067	- 0.0021	+0.0253	- 0.0135	+0.0126
	$L_{c,\ control} = 1$	+0.0120	- 0.0028	- 0.0155	- 0.0084	- 0.0093	- 0.0112
	$T_{s,\ control} = 1$	+0.1020	+0.0732	- 0.0088	- 0.0094	- 0.0018	- 0.0138
	$T_{c,\ control} = 1$	- 0.0714	+0.0941	+0.0071	- 0.0108	+0.0171	- 0.0024
0.849	$M_{s,\ control} = 1$	+0.0049	- 0.0240	+0.0338	+0.0179	- 0.0229	+0.0182
	$M_{c,\ control} = 1$	+0.0149	- 0.0149	- 0.0109	+0.0487	- 0.0271	- 0.0222
	$L_{s,\ control} = 1$	- 0.0124	- 0.0137	- 0.0120	+0.0074	- 0.0118	+0.0024
	$L_{c,\ control} = 1$	+0.0052	- 0.0056	- 0.0072	- 0.0121	+0.0006	- 0.0123
	$T_{s,\ control} = 1$	+0.1050	+0.0698	- 0.0211	+0.0037	+0.0017	- 0.0214
	$T_{c,\ control} = 1$	- 0.0772	+0.1079	- 0.0034	- 0.0305	+0.0221	+0.0031
0.851	$M_{s,\ control} = 1$	+0.0001	- 0.0081	+0.0191	+0.0122	- 0.0077	+0.0109
	$M_{c,\ control} = 1$	+0.0082	- 0.0055	- 0.0126	+0.0290	- 0.0135	- 0.0055
	$L_{s,\ control} = 1$	- 0.0080	- 0.0107	- 0.0043	+0.0117	- 0.0057	+0.0098
	$L_{c,\ control} = 1$	+0.0113	- 0.0102	- 0.0069	+0.0028	- 0.0137	- 0.0037
	$T_{s,\ control} = 1$	+0.1016	+0.0599	- 0.0087	+0.0109	- 0.0130	- 0.0091
	$T_{c,\ control} = 1$	- 0.0682	+0.0998	+0.0034	- 0.0143	+0.0189	- 0.0058

* in.-lb

TABLE VII
OSCILLATOR INPUTS REQUIRED (VOLT)
TO COMPENSATE EXISTING 4P- VIBRATIONS

μ	0.191	0.239	0.443	0.849	0.851
θ_{os}	0.1683	0.0394	0.0146	0.0457	0.0300
θ_{oc}	0.3121	0.0224	-0.0490	0.2354	-0.2726
θ_{ss}	0.1746	0.0090	-0.1400	-0.7980	-0.3275
θ_{sc}	-0.0133	-0.0293	0.1273	-0.5881	0.3498
θ_{cs}	0.2052	-0.0026	-0.1176	0.4610	-0.3549
θ_{cc}	-0.0651	-0.0180	0.0056	-0.8308	-0.0428

TABLE VIII
VIBRATION SUMMARY

Rel. Vibration Level	μ	θnominal	C_T/σ	Ampl. of Pitch Variation
1	0.849	10^o	-0.005	$\sim 3.0^o$
0.58	0.851	4	-0.013	2.0
0.32	0.191	12	0.102	0.8
0.21	0.443	4	0.011	0.5
0.08	0.239	4	0.028	0.2

Decreasing Vibration Level

TABLE IX
EFFECTS OF UNIT 4P OSCILLATOR INPUT ON BLADE BENDING
AND TORSION MOMENTS (in-lb). $\mu = 0.849$

$\mu = 0.849$	Input	sin 2ψ	cos 2ψ	sin 3ψ	cos 3ψ	sin 4ψ	cos 4ψ	sin 5ψ	cos 5ψ
Flapbending 3.3 in.	θ_{os}	0.3815	- 2.6028	- 1.1212	+ 1.9467	+ 0.0022	1.6252	- 0.4640	+ 0.2286
	θ_{oc}	- 0.7265	- 0.7428	- 2.1170	- 0.9082	- 1.7646	0.1744	+ 0.4336	- 0.2014
	θ_{ss}	- 20.1796	- 7.1252	0.4843	10.9746	9.2290	- 1.4705	- 12.1221	- 16.4408
	θ_{sc}	1.4455	- 18.6069	- 11.8793	0.8771	1.9670	9.2946	+18.4710	- 13.1116
	θ_{cs}	- 15.0717	19.2091	- 1.7568	+ 13.3006	4.4390	13.0827	24.2022	- 18.4700
	θ_{cc}	- 11.0041	- 12.5052	- 12.2451	- 3.9250	- 11.5818	6.8481	17.1269	+18.2863
Flapbending 13.15 in.	θ_{os}	- 3.1446	0.01156	+ 0.0644	- 6.4289	0.5673	- 5.5966	- 2.6912	- 5.2806
	θ_{oc}	0.4488	- 3.3139	+ 5.7587	- 0.6033	7.2213	1.7289	4.4109	- 1.9638
	θ_{ss}	- 13.1131	- 1.6401	- 9.4439	11.4718	2.7493	1.6368	20.3552	30.4485
	θ_{sc}	- 3.1093	- 10.4663	- 13.7168	- 7.3647	- 0.7250	4.6008	- 31.6355	23.4534
	θ_{cs}	- 15.3541	3.9011	- 20.8842	- 14.1583	- 4.0272	- 4.6816	- 53.1766	36.9531
	θ_{cc}	- 3.7738	- 10.2279	7.2742	- 11.8491	2.4534	1.0036	- 30.9619	- 33.3918
Chordbending 2.4 in.	θ_{os}	- 5.2318	5.1653	18.4997	- 66.4765	8.5046	- 2.0555	6.0027	8.6689
	θ_{oc}	- 0.3311	2.6008	55.9170	15.3823	8.5503	12.5308	- 10.1401	4.6381
	θ_{ss}	- 23.2604	3.6649	- 91.7693	7.1537	- 12.9172	- 5.1116	- 13.8450	7.4174
	θ_{sc}	4.7043	- 8.0015	- 37.9514	- 71.7419	6.5301	- 16.8130	- 4.2184	- 12.8505
	θ_{cs}	- 25.0714	15.3009	- 59.7492	- 177.5673	41.5059	- 80.7110	- 5.8153	- 27.4052
	θ_{cc}	- 2.0059	- 7.7253	77.1483	- 7.0902	68.5358	26.5134	7.7451	- 28.5566
Torsion 9.28 in.	θ_{os}	0.1891	0.0544	- 0.2460	0.5652	- 1.0733	0.2665	0.1925	0.0465
	θ_{oc}	0.0788	- 0.1531	- 0.1960	- 0.2328	- 0.6076	- 1.0110	0.0102	0.01822
	θ_{ss}	0.4975	0.2685	- 0.9271	- 1.5838	- 0.0498	1.4606	15.6374	13.1496
	θ_{sc}	- 0.6976	- 0.7498	3.0700	- 1.4345	- 1.0039	0.9952	- 11.8807	15.1709
	θ_{cs}	0.8756	- 0.0250	- 1.5421	- 0.9968	- 1.9762	1.0423	- 14.6088	21.3914
	θ_{cc}	- 0.8745	- 0.9375	2.1226	- 2.5792	- 1.3255	- 1.2713	- 17.9657	- 13.8937

Comparison of Equations (15) and (17) shows that the vibratory pitching moment is reduced to approximately 15 percent and the rolling moment to approximately 18 percent of its original value. This indicates that the various blades behave differently and that the goal of zero 4P pitch-roll and vertical vibrations is achieved by cancellation of the effects of the four blades.

Analytical Formulation and Calculated Results

The aeromechanical characteristics of the High Advance Ratio Model (HARM) has been analytically described in 2 degrees of freedom. These are based on the first and second flapping modes which have been approximated by polynomial fits of finite element determined mode shapes. The first and second mode shape approximations used are given by

$$\phi_1 = 2.292x^2 - 1.292x^3$$

and

$$\phi_2 = -10.21x^2 + 20.78x^3 - 9.57x^4$$

where

$x = \frac{r}{R}$; the non-dimensional radial station.

The aerodynamics are based on classical quasi-steady incompressible strip theory. The reverse flow region is fully accounted for, but stall effects have been neglected, as described in Reference 5.

TABLE X
EFFECT OF VIBRATION COMPENSATION ON FLAPBENDING MOMENT (in-lb) AT 3.3 in. $\mu = 0.849$

n		cos n	sin n	Amplitude
2	W/O Vibration Control	-92.7652	17.2338	94.35
	Contribution of θ_o	- 0.0559	- 0.1536	
	θ_s	16.6165	15.2507	
	θ_c	19.2393	2.2002	
	TOTAL	-56.9653	34.5311	66.61
3	W/O Vibration Control	- 1.1732	-14.7883	14.83
	Contribution of θ_o	- 0.1248	- 0.5496	
	θ_s	- 9.2715	6.5928	
	θ_c	9.3862	9.3684	
	TOTAL	- 1.1833	0.6233	1.34
4	W/O Vibration Control	- 0.1403	- 3.5448	3.55
	Contribution of θ_o	0.1153	- 0.4152	
	θ_s	- 4.2868	- 8.5191	
	θ_c	0.3317	11.6713	
	TOTAL	- 3.9801	- 0.8078	4.06
5	W/O Vibration Control	3.2312	2.2658	3.95
	Contribution of θ_s	- 0.0370	0.0809	
	θ_s	20.8199	- 1.1807	
	θ_c	-23.7042	- 3.0926	
	TOTAL	0.3099	- 1.9266	1.95

TABLE XI
SUMMARY OF OSCILLATORY BLADE LOADS (IN.-LB)
WITHOUT AND WITH VIBRATION COMPENSATION

Operating Condition	μ	Flapbending at 3.3 in.				Flapbending at 13.15 in.				Chordbending at 2.4 in.				Torsion at 9.28 in.			
		n = 2	n = 3	n = 4	n = 5	n = 2	n = 3	n = 4	n = 5	n = 2	n = 3	n = 4	n = 5	n = 2	n = 3	n = 4	n = 5
Without Oscillatory Control Input	0.191	30.1	4.4	1.6	3.5	16.0	1.9	3.0	4.3	21.0	2.2	8.3	19.4	1.2	0.7	0.4	0.6
	0.239	10.5	0.6	0.2	0.9	5.3	1.7	0.9	1.2	4.6	2.0	11.0	2.6	0.5	0.2	0.3	0.2
	0.443	16.4	2.7	0.1	1.6	9.2	3.2	0.4	3.5	9.4	1.7	10.5	7.7	0.9	0.6	0.3	0.2
	0.849	94.4	14.8	3.6	4.0	55.9	3.6	9.5	5.9	31.5	31.4	13.1	14.6	6.8	4.1	0.9	0.3
	0.851	18.9	8.6	1.5	3.1	17.7	4.6	3.4	5.8	17.4	10.9	18.9	10.7	3.3	2.4	0.7	0.4
With Oscillatory Control Input	0.191	29.6	1.1	2.9	0.4	16.1	4.4	5.0	3.0	19.2	22.7	10.9	3.9	1.0	1.2	0.4	4.5
	0.239	10.3	0.4	0.3	0.7	5.3	1.9	0.8	1.5	4.7	3.0	11.5	2.1	0.5	0.3	0.3	1.2
	0.443	12.3	1.3	1.3	1.1	7.5	2.7	0.5	1.3	7.7	3.5	13.6	8.7	0.8	1.4	1.4	1.7
	0.849	66.6	1.3	4.1	2.0	41.7	1.3	2.4	2.1	15.7	68.8	38.9	22.3	6.5	4.4	0.8	3.1
	0.851	20.2	2.4	6.5	4.1	16.5	3.8	7.0	2.5	17.5	13.6	75.6	7.0	2.3	4.0	0.7	3.5

The method of solution provides for intermode harmonic coupling through the 17th harmonic. This is accomplished by obtaining transient solutions of the 2-degree-of-freedom description of the rotor system described as constant coefficient linear differential equations over 10-degree sectors of the rotor azimuth.

The values of the coefficients for the system of differential equations evaluated in this work have been determined at the center of the sectors i. e., at 5^{o}, 15^{o}, 25^{o}, etc.

The basis for the analytical formulation is founded on Shannon's sampling theorem which says that the discrete signal is equivalent to the continuous signal, provided that all frequency components of the latter are less than 1/2T cycles per second, T being the time between instants at which the signal is defined, (References 6 and 7). Since the solution also provides for a completely general transient solution, it can be used to calculate a Floquet solution by specializing the initial conditions. This has been done for the square spring oscillator case studied by M. A. Gockel and reported in the AHS Journal in January 1972. The problem statement which is exactly describable by this theoretical method was shown to yield the identical Floquet solutions as those reported. It is important to note that should the system be unstable, the harmonic balance method of solution would not directly reveal this instability.

Briefly, the initial conditions at the beginning of a sector are determined by calculating the terminal conditions for the previous sector which are then used to initialize the new sector. It has been found that essentially arbitrary conditions can be used to start the solution and that excellent steady-state conditions have been obtained for the conditions examined in six rotor revolutions. For each solution case presented, the rotor has been solved for eight revolutions to ensure that the second flapping mode contribution to the response has converged to a steady-state value accurate to at least four significant figures. The program is used to calculate closed-form analytic solutions over each 10-degree sector and therefore is not dependent on a particular method of numerical integration. (See Appendix A.) The method, however, when applied to the analysis of steady-state conditions, does require that sufficient solution time be calculated so that initial transients are dissippated to ensure that steady-state equilibrium is achieved (Reference 8).

The test configuration experimentally examined with respect to 1P flapbending distributions at $\mu = 0$, including centerline measurements, has been compared with this analysis procedure on Figure 2, utilizing the two-mode description. This is a limited use of the analysis technique to establish test/analysis correlation. It is believed that the absence of time-dependent aerodynamics quasi-steady, largely accounts for the phase error in response. The centerline shaft moment measured was 0.75 of the calculated (a = 5.73). This may be due to the relatively low inflow of the test condition.

In general this correlation, including the spanwise distribution, appears reasonable.

The eigenvalues of each 10-degree sector are evaluated as part of the method. These are summarized in Tables XII, XIII, and XIV versus azimuth the $\mu = 0.191$, 0.45, and 0.85 where the real and imaginary parts of the eigenvalues have been normalized by the noted natural-mode frequencies. The negative aerodynamic spring effects over azimuth $90 < \Psi < 270$ as well as the positive stiffening from $270 < \Psi < 90$ are as expected more pronounced on the first mode frequency. The effects of reduced aerodynamic spring and damping are also seen on the retreating side. These results show that both damping as well as frequency variations occur around the azimuth which influence the rotor response with harmonic excitations.

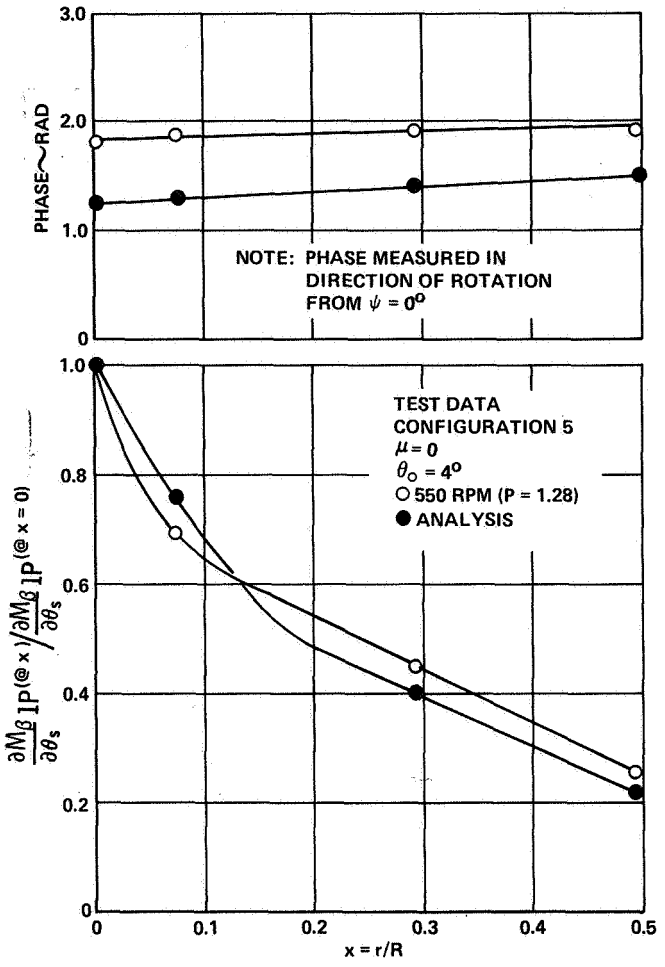

Figure 2. One-Per-Rev Blade Radial Flap-Bending Moment Distribution at $\mu = 0$.

The rotating frequencies and properties of the flapping modes noted in Tables XII, XIII, and XIV analytically describe the 7.5-ft-diameter rotor, configuration (5), 500-rotor-rpm condition for which all harmonic feathering tests were conducted. In an effort to further improve analytic correspondence with test data the slight change of the second flapping mode frequency resulted from matching collective blade angle selection at the test conditions. Details of the test model are given in References 9, 10 and 11.

The harmonic components of the blade root flap-bending moment (0P through 5P) were calculated for these advance ratios for unit perturbation of blade feathering angle at θ_{1c}, θ_{1s}, θ_{2c}, θ_{2s}, θ_{3c}, θ_{3s}, θ_{4c}, θ_{4s}, θ_{5c}, θ_{5s}, as well as for unit change in θ_o and α

The single non-dimensional blade root, centerline flap-bending moment harmonic influence coefficients resulting from harmonic feathering are summarized in matrix form in Tables XV, XVI, and XVII for $\mu = 0.191$, 0.45, and 0.85. These are based on harmonic analysis of the moment at each condition for 36 equally spaced (10-degrees apart) azimuth intervals. Single-blade

TABLE XII
NORMALIZED EIGENVALUES* AT EACH 10-DEGREE AZIMUTHAL SECTOR FOR $\mu = 0.191$

		P = 1.34		P = 6.38	
SECTOR	Ψ^o	R_1	I_1	R_2	I_2
1	5	-.204	1.024	-.155	1.002
2	15	-.212	1.022	-.163	1.002
3	25	-.220	1.019	-.170	1.002
4	35	-.227	1.014	-.177	1.002
5	45	-.233	1.007	-.183	1.001
6	55	-.238	.999	-.187	1.001
7	65	-.242	.990	-.190	1.000
8	75	-.244	.980	-.192	1.000
9	85	-.245	.970	-.193	.999
10	95	-.244	.960	-.192	.998
11	105	-.242	.951	-.190	.998
12	115	-.239	.943	-.186	.997
13	125	-.234	.937	-.182	.997
14	135	-.228	.933	-.176	.997
15	145	-.221	.930	-.169	.996
16	155	-.213	.930	-.162	.996
17	165	-.205	.932	-.154	.996
18	175	-.197	.935	-.146	.997
19	185	-.188	.940	-.138	.997
20	195	-.180	.945	-.130	.997
21	205	-.172	.952	-.123	.997
22	215	-.165	.958	-.116	.998
23	225	-.159	.965	-.111	.998
24	235	-.154	.971	-.106	.998
25	245	-.150	.978	-.103	.999
26	255	-.148	.984	-.101	.999
27	265	-.147	.989	-.100	1.000
28	275	-.148	.995	-.101	1.000
29	285	-.150	.999	-.103	1.000
30	295	-.154	1.005	-.107	1.001
31	305	-.158	1.010	-.111	1.001
32	315	-.164	1.014	-.117	1.001
33	325	-.171	1.018	-.124	1.002
34	335	-.179	1.021	-.131	1.002
35	345	-.187	1.023	-.139	1.002
36	355	-.195	1.025	-.147	1.002

*SECTOR EIGENVALUES ARE GIVEN BY:

$$(R_1 + I_1\, i)\ (1.34\Omega)$$

AND $(R_2 + I_2\, i)\ (6.38\Omega)$

computed root flap-bending moment influence coefficients at $\mu = 0.45$ are compared with experimental 0.073R single-blade data, in parentheses, from Reference 1 and 12 in Table XVIII.

These appear reasonable when shear effects are considered.

It is important that the general character of these influence coefficients be established in future tests. These tests should be structured to permit measurement to confirm these distributions.

TABLE XIII
NORMALIZED EIGENVALUES* AT EACH 10-DEGREE AZIMUTHAL SECTOR FOR $\mu = .45$

		P = 1.34		P = 6.2	
SECTOR	Ψ^o	R_1	I_1	R_2	I_2
1	5	-.215	1.087	-.167	1.007
2	15	-.234	1.088	-.186	1.007
3	25	-.252	1.084	-.203	1.007
4	35	-.269	1.075	-.218	1.006
5	45	-.283	1.059	-.232	1.005
6	55	-.295	1.037	-.242	1.004
7	65	-.303	1.011	-.250	1.002
8	75	-.309	.982	-.255	1.000
9	85	-.311	.951	-.256	.998
10	95	-.310	.920	-.254	.996
11	105	-.305	.891	-.249	.995
12	115	-.297	.867	-.240	.993
13	125	-.285	.850	-.229	.992
14	135	-.271	.839	-.215	.991
15	145	-.255	.837	-.200	.991
16	155	-.237	.842	-.182	.991
17	165	-.218	.854	-.164	.992
18	175	-.197	.870	-.145	.992
19	185	-.177	.889	-.126	.993
20	195	-.158	.909	-.108	.994
21	205	-.139	.928	-.092	.995
22	215	-.123	.945	-.078	.996
23	225	-.109	.960	-.068	.997
24	235	-.098	.972	-.061	.998
25	245	-.089	.982	-.057	.998
26	255	-.085	.990	-.056	.999
27	265	-.083	.997	-.055	1.000
28	275	-.084	1.003	-.056	1.001
29	285	-.089	1.011	-.058	1.001
30	295	-.078	1.018	-.062	1.002
31	305	-.108	1.027	-.069	1.003
32	315	-.122	1.038	-.079	1.003
33	325	-.138	1.049	-.093	1.004
34	335	-.156	1.061	-.110	1.005
35	345	-.175	1.072	-.129	1.006
36	355	-.195	1.081	-.148	1.006

*SECTOR EIGENVALUES ARE GIVEN BY:

$(R_1 + I_1\, i)$ (1.34Ω)

AND $(R_2 + I_2\, i)$ (6.20Ω)

TABLE XIV
NORMALIZED EIGENVALUES* AT EACH 10-DEGREE AZIMUTHAL SECTOR FOR $\mu = .85$

		P_1 = 1.34		P_2 = 6.20	
SECTOR	Ψ^o	R_1	I_1	R_2	I_2
1	5	-.231	1.192	-.040	1.014
2	15	-.267	1.209	-.048	1.015
3	25	-.301	1.212	-.055	1.016
4	35	-.332	1.200	-.061	1.015
5	45	-.360	1.171	-.067	1.013
6	55	-.382	1.126	-.071	1.010
7	65	-.399	1.065	-.074	1.006
8	75	-.409	.992	-.076	1.002
9	85	-.413	.911	-.076	.997
10	95	-.411	.826	-.076	.992
11	105	-.402	.745	-.073	.988
12	115	-.387	.675	-.070	.984
13	125	-.366	.625	-.065	.982
14	135	-.339	.603	-.060	.980
15	145	-.308	.611	-.053	.980
16	155	-.274	.645	-.040	.981
17	165	-.237	.698	-.039	.983
18	175	-.199	.759	-.031	.986
19	185	-.160	.822	-.023	.989
20	195	-.123	.879	-.016	.992
21	205	-.090	.925	-.012	.993
22	215	-.062	.954	-.011	.994
23	225	-.043	.970	-.012	.996
24	235	-.034	.977	-.014	.997
25	245	-.032	.983	-.015	.998
26	255	-.032	.990	-.015	.999
27	265	-.033	1.000	-.016	1.000
28	275	-.032	1.009	-.015	1.000
29	285	-.032	1.016	-.015	1.001
30	295	-.034	1.021	-.014	1.002
31	305	-.043	1.028	-.012	1.004
32	315	-.061	1.040	-.011	1.006
33	325	-.088	1.063	-.013	1.007
34	335	-.120	1.094	-.017	1.008
35	345	-.156	1.130	-.024	1.010
36	355	-.193	1.165	-.032	1.012

*SECTOR EIGENVALUES ARE GIVEN BY:

$(R_1 \pm I_1\, i)$ (1.34Ω)

AND $(R_2 \pm I_2\Omega)$ (6.20Ω)

TABLE XV

$\frac{C_{RM}}{a\sigma}$ – BLADE ROOT (STA 0) BENDING MOMENT INFLUENCE COEFFICIENT MATRIX FOR μ = 0.191 (P_1 = 1.34, P_2 = 6.38)

	$C\beta_0$	$C\beta_{1C}$	$C\beta_{1S}$	$C\beta_{2C}$	$C\beta_{2S}$	$C\beta_{3C}$	$C\beta_{3S}$	$C\beta_{4C}$	$C\beta_{4S}$	$C\beta_{5C}$	$C\beta_{5S}$
$\Delta\alpha$	.0034	.0009	-.0016	-.0001	-.0001	0	0	0	0	0	0
$\Delta\theta$	.0132	.0049	-.0111	-.0007	-.0005	-.0001	0	0	0	0	0
$\Delta\theta_{1S}$	.0036	.0057	-.0225	-.0018	-.0003	0	.0002	0	0	0	0
$\Delta\theta_{1C}$	-.0005	-.0213	-.0045	-.0001	.0018	.0002	0	0	0	0	0
$\Delta\theta_{2S}$	0	-.0056	-.0004	.0018	.0031	.0014	-.0009	.0002	.0003	0	0
$\Delta\theta_{2C}$	-.0003	-.0005	.0057	.0031	-.0018	-.0009	-.0014	.0003	-.0002	0	0
$\Delta\theta_{3S}$	0	-.0001	.0004	.0001	.0002	-.0046	-.0012	.0015	-.0014	.0001	.0003
$\Delta\theta_{3C}$	0	.0004	0	.0002	-.0001	-.0012	.0046	-.0014	-.0015	.0003	-.0001
$\Delta\theta_{4S}$	0	0	0	0	.0001	-.0010	.0017	-.0076	-.0026	.0017	-.0020
$\Delta\theta_{4C}$	0	0	0	.0001	-.0001	.0017	.0009	-.0026	.0076	-.0020	-.0017
$\Delta\theta_{5S}$	.0119	0	0	0	0	.0002	.0002	-.0015	.0024	-.0101	-.0033
$\Delta\theta_{5C}$	0	0	0	0	0	.0002	-.0002	.0024	.0015	-.0033	.0101

TABLE XVI

$\frac{C_{RM}}{a\sigma}$ – BLADE ROOT (STA 0) BENDING MOMENT INFLUENCE COEFFICIENT MATRIX FOR μ =.45 (P_1 = 1.34, P_2 = 6.20)

	$C\beta_0$	$C\beta_{1C}$	$C\beta_{1S}$	$C\beta_{2C}$	$C\beta_{2S}$	$C\beta_{3C}$	$C\beta_{3S}$	$C\beta_{4C}$	$C\beta_{4S}$	$C\beta_{5C}$	$C\beta_{5S}$
$\Delta\alpha$	.0085	.0053	-.0089	-.0010	-.0012	-.0004	-.0004	-.0001	-.0001	0	0
$\Delta\theta$	.0160	.0135	-.0276	-.0038	-.0029	-.0009	-.0004	-.0001	-.0002	0	0
$\Delta\theta_{1S}$	.0087	.0102	-.0292	-.0048	-.0016	-.0004	.0007	-.0006	0	0	0
$\Delta\theta_{1C}$	-.0011	-.0226	-.0034	-.0004	.0046	.0011	.0002	.0001	.0003	0	0
$\Delta\theta_{2S}$	0	-.0130	-.0006	.0006	.0046	.0036	-.0020	.0009	.0015	-.0002	.0002
$\Delta\theta_{2C}$	-.0015	-.0024	.0142	.0043	.0001	-.0020	-.0035	.0015	-.0009	.0001	.0002
$\Delta\theta_{3S}$	0	0	.0023	.0004	.0010	-.0057	-.0032	.0038	-.0036	.0008	.0016
$\Delta\theta_{3C}$	-.0002	.0022	-.0002	.0007	-.0001	-.0033	.0057	-.0036	-.0038	.0016	-.0008
$\Delta\theta_{4S}$	0	-.0001	0	.0003	.0007	-.0026	.0042	-.0090	-.0046	.0043	-.0048
$\Delta\theta_{4C}$	0	0	0	.0004	0	.0042	.0026	-.0046	.0090	-.0048	-.0043
$\Delta\theta_{5S}$	0	0	0	0	.0003	.0008	.0008	-.0038	.0058	-.0118	-.0055
$\Delta\theta_{5C}$	0	0	0	0	.0003	.0008	-.0009	.0058	.0038	-.0054	.0118

TABLE XVII

$\frac{C_{RM}}{a\sigma}$ – BLADE ROOT (STA 0) BENDING MOMENT INFLUENCE COEFFICIENT MATRIX FOR μ = .85 (P_1 = 1.34, P_2 = 6.20)

	$C\beta_0$	$C\beta_{1C}$	$C\beta_{1S}$	$C\beta_{2C}$	$C\beta_{2S}$	$C\beta_{3C}$	$C\beta_{3S}$	$C\beta_{4C}$	$C\beta_{4S}$	$C\beta_{5C}$	$C\beta_{5S}$
$\Delta\alpha$	.0201	.0227	-.0296	-.0056	-.0102	-.0037	-.0039	0	-.0021	0	-.0015
$\Delta\theta$	.0253	.0378	-.0598	-.0141	-.0155	-.0061	-.0039	0	-.0032	-.0003	-.0018
$\Delta\theta_{1S}$	.0192	.0278	-.0490	-.0117	-.0114	-.0036	-.0004	-.0019	-.0014	-.0005	-.0001
$\Delta\theta_{1C}$	-.0024	-.0258	-.0015	-.0012	.0085	.0035	.0008	.0003	.0022	0	.0009
$\Delta\theta_{2S}$	-.0006	-.0229	-.0007	-.0026	.0079	.0081	-.0034	.0024	.0054	-.0019	.0016
$\Delta\theta_{2C}$	-.0056	-.0110	.0308	.0084	.0067	-.0026	-.0064	.0052	-.0019	.0013	.0023
$\Delta\theta_{3S}$	-.0003	-.0014	.0076	.0010	.0035	-.0088	-.0082	.0100	-.0084	.0033	.0049
$\Delta\theta_{3C}$	-.0009	.0060	0	.0029	-.0009	-.0084	.0089	-.0084	-.0100	.0048	-.0033
$\Delta\theta_{4S}$	-.0005	-.0004	.0003	.0013	.0008	-.0067	.0087	-.0135	-.0100	.0112	-.0100
$\Delta\theta_{4C}$	-.0004	.0002	-.0002	.0007	-.0014	.0087	.0067	-.0100	.0134	-.0101	-.0112
$\Delta\theta_{5S}$	0	.0001	.0006	.0002	-.0003	.0029	.0023	-.0088	.0124	-.0167	-.0115
$\Delta\theta_{5C}$	0	.0006	-.0002	-.0003	-.0002	.0023	-.0029	.0124	.0088	-.0116	.0167

TABLE XVIII
BLADE ROOT (STA 0) BENDING MOMENT (IN-LB)/DEG INFLUENCE MATRIX FOR $\mu = .45$
($\Omega = 52.36$, $P_1 = 1.34$, $P_2 = 6.20$)

	β_0	β_{1C}	β_{1S}	β_{2C}	β_{2S}	β_{3C}	β_{3S}	β_{4C}	β_{4S}	β_{5C}	β_{5S}	LIFT
$\Delta\alpha$	19	12	-20	-2	-3	-1 (1)	-1 (-2)	0	0	0 (1)	0 (-1)	6
$\Delta\theta$	36	31	-62	-9	-7	-2 (1)	-1 (1)	0	0	0 (1)	0 (0)	10
$\Delta\theta 1S$	20	23	-66	-11	-4	-1 (1)	2 (-2)	-1	0	0 (1)	0 (0)	6
$\Delta\theta 1C$	-2	-51	-8	-1	10	3 (0)	0 (1)	0	1	0 (0)	0 (0)	0
$\Delta\theta 2S$	0	-29	-1	1	10	8	-5	2	3	-1	0	0
$\Delta\theta 2C$	-3	-5	32	10	0	-5	-8	3	-2	0	0	-1
$\Delta\theta 3S$	0	0	5	1	2	-13	-7	9	-8	2	4	0
$\Delta\theta 3C$	0	5	-1	2	0	-7	13	-8	-9	4	-2	0
$\Delta\theta 4S$	0	0	0	1	2	-6 (0)	9 (6)	-20 (-8)	-10 (-5)	10 (-5)	-11 (-1)	0
$\Delta\theta 4C$	0	0	0	1	0	9 (6)	6 (-2)	10 (-4)	20 (7)	-11 (-6)	-10 (3)	0
$\Delta\theta 5S$	0	0	0	0	1	2	2	-9	13	-27	-12	0
$\Delta\theta 5C$	0	0	0	0	1	2	-2	13	9	-12	27	0

Full-Scale Control Loads

The feasibility of active vibration attenuation depends on the capability of the rotor to generate cancelling shaft moments and shears while control forces and displacements remain within acceptable limits.

Since full-scale data are the most relevant from the standpoint of hardware test background, the CL 840/AMCS (Advanced Mechanical Control System) Cheyenne rotor configuration, at a gross weight of 20,000 and with a rotor shaft moment of 100,000 in.-lb, was analyzed for hovering flight to gain a numerical measure of how loads compare with limits. In this analysis three higher harmonic blade-feathering excitations, 3P, 4P and 5P, were examined to determine the relationships among control loads, shaft moments and shear forces. The Lockheed Rotor Blade Loads Prediction Model was used for this analysis; 68 finite elements were used to describe the system. The calculated results, based on 1-degree excitation levels, are summarized in Table XIX.

TABLE XIX
CL 840 ANALYSIS -
SHAFT AND BLADE LOADS DUE TO ONE-DEGREE
OF HIGHER HARMONIC BLADE-FEATHERING MOTIONS

	FEATHERING FREQUENCY						
	3φ		4φ		5φ		Endurance
	Amplitude	Phase	Amplitude	Phase	Amplitude	Phase	Limit, in.-lb
Shaft Forces							
4P H-force	380 lb	61°	40 lb	59°	310 lb	34°	
4P Y-force	380 lb	84°	40 lb	83°	310 lb	12°	
4P Pitching Moment	22,000 in.-lb	83°	0		108,000 in.-lb	8°	325,000
4P Rolling Moment	22,000 in.-lb	16°	0		108,000 in.-lb	76°	
4P Thrust	0		3000 lb	40°	0		
Blade Root Torsion * Harmonic							
Steady	-3800 in.-lb		-4000 in.-lb		-3900 in.-lb		
1P	210 in.-lb	11°	210 in.-lb	11°	220 in.-lb	11°	15,500
2P	80 in.-lb	49°	50 in.-lb	42°	50 in.-lb	39°	
3P	1500 in.-lb	15°	70 in.-lb	82°	40 in.-lb	84°	
4P	130 in.-lb	47°	13,300 in.-lb	88°	400 in.-lb	57°	
5P	20 in.-lb	27°	80 in.-lb	35°	7800 in.-lb	10°	

* Pitch link forces are internal loads between the blade and swashplate and therefore self-cancelling.

The calculated root torsion moments shown in the table reflect both the feathering moments at the primary exciting frequency and the interharmonic coupling terms; as expected, the latter are considerably less. Pitch link loads can be determined by multiplying the root torsion moment by 0.1 (to account for all applicable geometry); endurance limit of the pitch link load is 1550 pounds.

The 7.5-foot hingeless rotor model data showed that 0.2 to 0.6-degree cyclic angle excitation levels were required. Study of CL 840 test data indicates that similar blade excitation would be expected with a full-scale, four-bladed rotor. The CL 840 data are not yet published in documents that can be referenced, however, this material is expected to be published during 1974.

In summary, full-scale data founded on endurance limit considerations indicate that internal blade loads and control loads will not limit the trim flight use of periodic variation of conventional controls for vibration attenuation.

Conclusions

The present report is a preliminary evaluation of the concept of vibration reduction by properly selected oscillatory collective and cyclic control applications. The investigations are based on experimental frequency response data covering advance ratios from approximately 0.2 to 0.85.

Because there was no instrumentation for the measurement of the pitch and roll vibrations, these values were obtained by properly adding up the flap-bending moments at 3.3 inches. Any other quantity representing pitch/roll vibrations can be compensated for in the same fashion.

The calculated control inputs required for vibration reduction stay within acceptable limits. For four of the five conditions tested they are smaller than the values used for the frequency response tests. The blade pitch variations required for vibration alleviation vary, depending on the advance ratio, less than 1° for $.2 \leqslant \mu \leqslant .45$ and $\sim 3^{\circ}$ for $\mu = .85$.

As to be expected, the compensating controls greatly affect the blade loads, i.e., torsion, flap- and chordwise bending. With regard to flap-bending at 3.3 inches (root flexure), the following statements can be made:

- 3 and 5P flap moments were, by command, drastically reduced
- 2P flap moments were least affected. These were the largest oscillatory loads.
- 4P flap moment increments generally increased with increasing advance ratio, but were small relative to the 2P flap moments.

As a general rule, chordwise bending and blade torsion increments also increase with the advance ratio. At lower μ values the loads are not critical. It is concluded that the concept investigated is primarily suited for low and medium advance ratios, i.e., for the speed-range of present day rotary wing aircraft. The latter application appears promising and further studies and tests are suggested. Instrumentation to determine rotor vertical and inplane shear forces should be incorporated in such future tests. Also a system with a first inplane frequency in the vicinity of 1.5P in combination with a flapping frequency of 1.1P should be tested at conventional advance ratios to provide experimental data representative of current designs.

References

1. London, R. J., Watts, G. A., and Sissingh, G. J., EXPERIMENTAL HINGELESS ROTOR CHARACTERISTICS AT LOW ADVANCE RATIO, NASA CR-1148A, December 1973.
2. USAAVLABS Technical Report 69-39, SUPPRESSION OF TRANSMITTED HARMONIC VERTICAL AND INPLANE ROTOR LOADS BY BLADE PITCH CONTROL, Balcerak, J. C., and Erickson, J. C., Jr., Ft Eustis, Virginia, July 1969.
3. ASRL - Technical Reference 150-1, HIGHER HARMONIC BLADE PITCH CONTROL FOR HELICOPTER, Shaw, John Jr., Massachusetts, December 1968.
4. USAAVLABS Technical Reference 70-58, WIND TUNNEL INVESTIGATION OF A QUARTER-SCALE TWO-BLADED HIGH-PERFORMANCE ROTOR IN A FREON ATMOSPHERE, Lee, Charles; Charles, Bruce, and Kidd, David, Ft Eustis, Virginia, February 1971.
5. Sissingh, G. J., DYNAMICS OF ROTORS OPERATING AT HIGH ADVANCE RATIOS J. American Helicopter Society, 13(3) July 1968.
6. C. E. Shannon, COMMUNICATION IN THE PRESENCE OF NOISE, Proc. IRE, Vol. 37, January 1949, p.11.
7. DeRusso, P. M., Roy, R. J., and Close, C. M., STATE VARIABLES FOR ENGINEERS, New York, John Wiley and Sons, Inc. 1967, p. 6-9.
8. Donham, R. E., Subsection titled "RESPONSE OF HELICOPTER ROTOR BLADES TO GUST ENVIRONMENTS" in NUCLEAR HARDENING SURVIVABILITY DESIGN GUIDE FOR ARMY AIRCRAFT. This report is being prepared by the B-1 Division of Rockwell International under Army Contract DAAJ02-73-C-0032.
9. Kuczynski, W. A., Sissingh, G. J., RESEARCH PROGRAM TO DETERMINE ROTOR RESPONSE CHARACTERISTICS AT HIGH ADVANCE RATIOS, LR 24122, February 1971, prepared under Contract NAS 2-5419 for U. S. Army Air Mobility Research and Development Laboratory,Ames Directorate, Moffet Field, California.
10. Kuczynski, W. A., Sissingh, G. J., CHARACTERISTICS OF HINGELESS ROTORS WITH HUB MOMENT FEEDBACK CONTROLS INCLUDING EXPERIMENTAL ROTOR FREQUENCY RESPONSE, LR 25048, January 1972, prepared under Contract NAS 2-5419 for U. S. Army Air Mobility Research and Development Laboratory,Ames Directorate, Moffet Field, California. (Volumes I and II).

11. Kuczynski, W. A., EXPERIMENTAL HINGELESS ROTOR CHARACTERISTICS AT FULL SCALE FIRST FLAP MODE FREQUENCIES LR 25491, October 1972, prepared under Contract NAS 2-5419 for U. S. Army Air Mobility Research and Development Laboratory, Ames Directorate, Moffet Field, California.

12. Watts, G. A. and London, R. J., VIBRATION AND LOADS IN HINGELESS ROTORS, Vol. I and II, NASA CR-114562, September 1972.

Appendix A

The transient response solution of a system described by constant coefficient linear differential equations is developed in this appendix. The single-degree-of-freedom case with arbitrary initial conditions and solution of the general case for an nth order system with both zero and nonzero initial conditions is reported.

Given the single degree of freedom:

$$A\frac{d^2\beta}{dt^2} + B\frac{d\beta}{dt} + C\beta = F(t) \tag{1}$$

where A, B, and C are constants, then

$$A\mathcal{L}\left(\frac{d^2\beta}{dt^2}\right) + B\mathcal{L}\left(\frac{d\beta}{dt}\right) + C\mathcal{L}(\beta) = \mathcal{L}(F(t))$$

where $\mathcal{L}$ is the Laplace transform operator. This yields

$$(As^2 + Bs + C)\,\beta(s) = F(s) + \beta(0)(As + B) + \dot{\beta}(0)A \tag{2}$$

or

$$\beta(s) = \frac{F(s) + \beta(0)(As + B) + \dot{\beta}(0)A}{As^2 + Bs + C}$$

If a positive constant step load of magnitude + L is the form of F(t), then

$$\mathcal{L}(F(t)) = F(s) = \frac{+L}{s}$$

and

$$\beta(s) = \frac{L}{A(s)(s-\alpha)(s-\gamma)} + \frac{\beta(0)As}{A(s-\alpha)(s-\gamma)} + \frac{\beta(0)B + \dot{\beta}(0)A}{A(s-\alpha)(s-\gamma)} \tag{3}$$

Where $\beta(0)$ and $\dot{\beta}(0)$ are the values of the variable β at time $t = 0$ and α, γ are the roots of $s^2 + Bs/A + C/A$, $\beta(s)$ transformed back into the time plane is accomplished through use of the inverse Laplace transform of the form $\frac{P(s)}{Q(s)}$

where

P(s) = polynomial of degree less than n

and

$$Q(s) = (s-\alpha_1)(s-\alpha_2)\ldots(s-\alpha_n)$$

where $\alpha_1, \alpha_2, \ldots \alpha_n$ are all distinct, this yields

$$\beta(t) = \sum_{k=1}^{n} \frac{P(\alpha_k)}{Q'(\alpha_k)} e^{\alpha_k t} \tag{4}$$

In the case cited

$$Q(s) = A(s)(s-\alpha)(s-\gamma)$$

where

$$\alpha_1 = 0$$

$$\alpha_2 = \alpha$$

$$\alpha_3 = \gamma$$

and

$$P(s) = L + \left[\beta(0)A\right]s^2 + \left[\beta(0)B + \dot{\beta}(0)A\right]s$$

Therefore

$$\beta(t) = \sum_{k=1}^{n} \frac{P(\alpha_k)}{Q'(\alpha_k)} e^{\alpha_k t}$$

$$\beta(t) = \frac{L}{A(-\alpha)(-\gamma)} + \left[\frac{L + \left[\beta(0)A\right]\alpha^2 + \left[\beta(0)B + \beta(0)A\right]\alpha}{A(+\alpha)(+\alpha-\gamma)}\right]e^{\alpha t} + \left[\frac{L + \left[\beta(0)A\right]\gamma^2 + \left[\beta(0)B + \beta(0)A\right]\gamma}{(A)(+\gamma)(\gamma-\alpha)}\right]e^{\gamma t} \tag{5}$$

Extension to the general case is accomplished as follows. Given the general determinantal equation:

$$\left\{s^2[A] + s[B] + [C]\right\}\left\{\beta(s)\right\} = \left\{F(s)\right\} \tag{6}$$

Where the elements of matrix A, B, and C are constants, using Cramer's Rule:

$$\beta_i(s) = \frac{\left|\begin{array}{l}\text{Denominator with}\\ \text{Column i replaced by } F(s)\end{array}\right|}{\left|s^2[A] + s[B] + [C]\right|} \tag{7}$$

Expanding

$$\left|s^2[A] + s[B] + [C]\right|$$

yields

$$A_o(s-\alpha_1)(s-\alpha_2)\ldots(s-\alpha_n) \tag{8}$$

where

A_o = Coefficient of highest power term

α_i (i = 1 . . . n) are the eigen values (roots) of the determinantal equation

Case 1 - Zero Initial Conditions

Assume $\beta_i(0)$ and $\dot{\beta}_i(0)$ for all i are both zero and that a positive unit load acts on β_e and that the response of β_f is to be determined. Then

$$\left\{F(s)\right\} = \left\{\begin{array}{l}+\ 1/s \text{ in row e with all other} \\ \text{rows equal } \underline{0}\end{array}\right\}$$

Defining

$$\left| s^2[A] + s[B] + [C] \right|_{(e,f)} \tag{9}$$

as the original determinantal equation with Row e and Column f removed and all the remaining rows and columns moved up and to the left, respectively, this forms a determinantal equation of one less order.

Based on the earlier development in the s-plane

$$\mathcal{L}\left(\beta_f(t)\right) = \frac{a_o}{s} + \frac{a_1}{s-\alpha_1} + \frac{a_2}{s-\alpha_2} + \ldots + \frac{a_n}{s-\alpha_n}$$

and in the time plane

$$\beta_f(t) = a_o + a_1 e^{\alpha_1 t} + a_2 e^{\alpha_2 t} + \ldots + a_n e^{\alpha_n t} \tag{10}$$

where

$$a_o = \frac{(-1)^{(e+f)}\, D(o)_{e,f}}{A_o \prod_{i=1}^{n} \alpha_i}$$

and

$$a_j = \frac{(-1)^{(e+f)}\, D(\alpha_j)_{e,f}}{\alpha_j A_o \prod_{i=1}^{n} (\alpha_j - \alpha_i)} \qquad i \neq j$$

A_o is determined by the relationship

$$D(o) = A_o \prod_{i=1}^{n} \alpha_i$$

$D(o)_{e,f}$ and $D(\alpha_j)_{e,f}$ are formed from the original determinantal equation with Row e and Column f removed and all the remaining rows and columns moved up and to the left, respectively, evaluated at o and α_j. The α_j are the roots of the original determinantal equation before Row e and Column f were removed. These roots are assumed distinct, an unimportant limitation for most physical systems. Note that this solution does not preclude instability either aperiodic or oscillatory.

In practice the eigenvalues are obtained prior to the formation of the coefficients and are examined to verify the distinct character of the eigenvalues.

Scalar multiplication of this solution provides the result for the nonunit loading case. Summation of solutions obtained for loadings at each coordinate can be used to provide the general solution for this case where $\beta_i(0)$ and $\dot{\beta}_i(0)$ for all i are both zero, i.e., that the initial conditions at time zero are all zero.

In most applications the restriction that the initial conditions are zero is an unacceptable constraint and this condition has been relaxed; the solution follows.

Case 2 - Nonzero Initial Conditions

The general form of F(s) now becomes:

$$\left\{F(s)\right\} = \left\{\frac{L_i}{s}\right\} + \left\{ s[A] + [B] \right\}\left\{\beta_i(0)\right\} + \left\{[A]\left\{\dot{\beta}_i(0)\right\}\right\} \tag{11}$$

where L_i are the forces applied at each coordinate β_i and $\beta_i(0)$ and $\dot{\beta}_i(0)$ are the positions and rates of the coordinates at time zero (initiations of the solution). In this case place the column $s\{F(s)\}$ into the column location of the coordinate for which the response is desired without reduction of the order. Then

$$P(s) = \left| \begin{array}{c} \text{Column i} \\ \downarrow \\ s\left\{F(s)\right\} \end{array} \right| \tag{12}$$

where all other terms are

$$\left| s^2 [A] + s[B] + [C] \right|$$

and

$$Q(S) = A_0(s-\alpha_0)(s-\alpha_1)\ldots(s-\alpha_n) \tag{13}$$

where the α's are the eigenvalues of the determinantal equation

$$\left\{ s \left| s^2[A] + s[B] + [C] \right| \right\} = 0$$

Then

$$\beta_i(t) = \sum_{k=0}^{n} \frac{P(\alpha_k)}{Q'(\alpha_k)} e^{\alpha_k t} \tag{14}$$

where s = 0 and the remaining eigenvalues of the general determinantal equation form the set of α_k's, and A_0 is determined by the relationship

$$D(0) = A_0 \prod_{i=1}^{n} \alpha_i \tag{15}$$

as given in Case 1.

FOREWORD TO THE SUPPLEMENT

This supplement includes questions and answers following the papers of Sessions I through IV and all of the material of Session V. Questions and answers, as well as panel members' prepared comments were transcribed from tape recordings. This material has been carefully checked and minor changes have been made for clarification. Where the meaning may have been ambiguous, editorial comments are bracketed. Panel members have checked their comments for accuracy and made minor corrections in the transcript where required.

R. A. Ormiston
Technical Chairman

WELCOME

Clarence A. Syvertson
Deputy Director
Ames Research Center, NASA

Dr. Mark is out of town, so I have been asked to substitute. I guess most of you have been here at Ames before but in spite of that I would like to welcome you to the Ames Research Center. I'm very pleased, the whole center is very pleased, that the specialists in this field of rotor dynamics picked Ames for the site of this meeting. I'm certainly not an expert in your field but from all I can see the field of rotor dynamics represents one of the most technically difficult and most challenging fields in modern aeronautics. I looked over the papers that will be presented and it seems, in spite of all the difficulties, that some real progress is being made in the field. I think that is very encouraging. I also noticed that you have papers by representatives of virtually every major rotorcraft manufacturer in the country, by representatives from the Ames and Langley Research Center, and by representatives from the Ames, Langley, and Eustis Directorates of the U. S. Army Air Mobility R&D Laboratory. I think that it's this broad representation from all the organizations throughout the country concerned with these problems that really makes meetings like this especially fruitful. I hope you find the papers interesting and the meeting productive. And again, in spite of the fact that you've probably been here before, I'd like to welcome you to Ames Research Center. Thank you.

OPENING REMARKS

E. S. Carter, Meeting General Chairman
Chief of Aeromechanics
Sikorsky Aircraft

First, I would like to acknowledge the indispensable contributions from NASA that have made this meeting possible. The AHS is not an affluent organization and NASA has provided not only the facilities, but the printed brochure, the manpower to staff the registration tables, the bus service for the tours, and our hardworking administrative chairman, Jim Biggers. When the meeting was first conceived by Bob Wood's AHS Dynamics Committee, it was hoped that the Army could also co-sponsor this meeting. A significant factor in selecting Ames as a location was the presence here of the rotary wing dynamics research team in the Army Ames Directorate which has probably the most sharply focused rotorcraft dynamics program to be found anywhere within the government research agencies. It developed that the Army cannot officially co-sponsor a meeting such as this, but they have provided the technical chairman, Dr. Bob Ormiston. To Bob must go the credit, not only for having a good bit to do with initiating the meeting in the first place, but for following through with the excellent technical program which you are about to hear.

The rotorcraft dynamics problem, which this meeting addresses, is perhaps the most challenging, most complex and technically sophisticated challenge that can be found short of the biological sciences. The problem is well illustrated by Slide 1 which I have borrowed from a paper by Bob Tapscott at the Civil Transport meeting at the Langley Center in November 1971. It also illustrates all of the ingredients of the problem that we will be addressing in the next two days: the air mass dynamics problem, which because of its four dimensional (time variant) characteristics, virtually defies visualization; the lifting surface problem with its skewed flow, unsteady effects, and centrifugally pumped boundary layer which can't possibly be reproduced in two dimensional wind tunnel tests; the blade dynamics, complicated not only by the centrifugal field, but by the difficult coupling effects introduced by built-in or elastic twist; the fixed to rotating coordinate transformation problem that immensely complicates the airframe and rotor interactions; and finally, the aeroelastic characteristics of the body itself with its large concentrated masses, unsymmetrical offsets and very large cutouts.

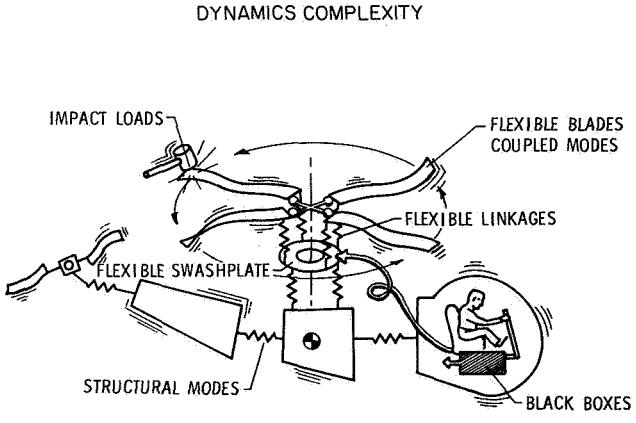

Slide 1.

For the next two days we'll be assessing the state of the art and our ability to handle each of these problems and on Friday we will have a chance to back off and overview the whole situation. Bob Ormiston's paper in this final session is, as far as I know, unique in the comparison it makes between all of our competitive methods addressed to a single problem. Finally, in the panel sessions, our ultimates customers, the designers and the service users, will be given an opportunity to tell us what we're doing wrong.

DINNER ADDRESS

WHAT CAN THE DYNAMICIST DO FOR FUTURE ARMY AIRCRAFT?

Paul F. Yaggy
Director, U. S. Army Air Mobility R&D Laboratory
Moffett Field, California

The terms "rotary wing aircraft" and "dynamics" are synonomous. All dynamics are not rotary wing, but all rotary wings are dynamic. Every consideration of the rotorcraft structure includes dynamic phenomena in some form. One cannot talk of the utility and economy of rotorcraft without considering the impact of dynamics on structural vibrations, passenger comfort and ride quality, pilot handling qualities, safety, and wearout and life cycle of critical components. Some have been so derisive in their comments as to say that the rotorcraft in many respects is an effective inherent fatigue testing machine.

Now you may object to an analogy as harsh as that, but you would be hard pressed not to admit that there is much semblance in fact to support it. For this beautifully sophisticated and integrated machine with its vertical flight capability has a nasty attribute of creating its own hostile environment as it attempts translation flight. We speak of the rotor operating through the vortices shed from its rotating blades, producing large amplitude nonsteady loads; not unlike a wheeled vehicle bouncing over a corduroy road. This would be problem enough, but these first order loads produce highly interactive, coupled phenomena throughout the structure from the rotor through the shaft to the drive system, the fuselage, the control system, the instruments, and even the pilot's posterior resting on his seat. All of these motions are important, but their relative importance is not easily determined. Ability to adequately account for dynamic phenomena has had a pronounced influence on the development of rotorcraft, particularly on its most prevalent derivative, the helicopter.

It is both interesting and revealing to consider the role of dynamics in the history and development of rotary wing aircraft. For convenience, let us consider them in five decades from that before 1940 to the current decade of the '70's.

Prior to 1940, development efforts were more of a novelty than an orderly plan. The Berliner, Focke, Flettner, Sikorsky, and others made brilliant achievements in vertical flight, while Cierva identified some of the basic problems and restrictions of rotary wings with his autogyro. The immediate goal of this period was simply the demonstration of some type of successful, controlled flight, an elusive goal which many failed to attain. It is interesting that many of the dynamic problems we wrestle with today were readily identified in that period. Rotor vibration, high blade vibratory stresses, "ground resonance," air resonance, blade flutter, stick vibration, and short life of critical components were all readily apparent. Lacking sophisticated analytical tools and methods, the stalwart pioneers of the day turned to empirical approaches which further proved their genius as they incorporated dampers, blade balancing techniques, and other modifications to improve system dynamics of their marvelous machines.

Based on these early efforts, the decade from 1940 to 1950 witnessed a great acceleration of more orderly development for the helicopter. So many advances were made in this period that it is almost startling to consider them in retrospect. The full range of rotor configurations was investigated; single, coaxial, tandem, and jet driven rotors were experimented with by industrial groups such as Bendix, Platt-Lepage, McDonnell, Aeronautical Products, Piasecki, Hiller, Kaman, Bristol, Cierva, and others. Some that reached production included Flettner, Focke, Sikorsky, and Bell.

Novelty gave way to utility in this decade, even though much was exploratory in nature. Included were wire laying, shipboard operations, courier duty, observation and air ambulance operations. Utility was limited by the reciprocating engine with its awkward volume envelope and high specific weight. This was but one of the limitations with which the designer had to cope and which restricted operational vehicles to maximum capabilities of 80 knots, 6 passengers and significantly reduced altitude and hot day performance. This decade, too, was plagued by the now all too familiar dynamic problems of high vibration levels, rotor instabilities, blade weaving, blade flutter, and a very limited life of dynamic components. Typical lifetimes ran about 75 hours before removal for discard or overhaul; a high price to pay for the unique vertical flight capability.

Significant research and development efforts were undertaken in this decade to cope with blade structural and dynamic analyses and rotor airflow and wakeflow analyses. However, the complexity of the mathematical models overtaxed the computational capabilities of the day and necessary linearization of the problem masked many of the important characteristics.

In the decade from 1950 to 1960, the number of variants in helicopter design began to diminish as the most optimal designs began to be apparent. Utility was increased by applying new found technology and methodology for design. A new source of power, the turbine engine was appearing which would give a more optimum volume envelope and eliminate the vibration input of the reciprocating engine. This transition to turbine power, with its improved specific weight and fuel consumption, was destined to revolutionize helicopter utility and capability.

The helicopters of the '50's were produced in large quantities under the impetus of the Korean War and their new found military utility. Payload capability increased to 20 passengers. Performance reached the ability to hover at 6000 feet and 75-degrees F. Allowable vibration criteria were quantified and defined by military specification. Bold new life goals for dynamic components were

set at 1000 hours before removal. Although some reached these levels, many still barely attained 250 hours. Utility of the vehicle was the primary gain of this period, but the plaguing restrictions resulting from dynamic phenomena still produced high costs and restricted performance.

In the decade just past, 1960-1970, the gas turbine completely supplanted the reciprocating engine in helicopters with a resulting increase in payload and range. Payload exceeded 5000 pounds, carried at speeds in excess of 200 miles per hour in test flights. Hover was attained at 6000 feet and 95-degrees F. Life of dynamic components was somewhat improved, even to on-condition removal for some parts, but the spread of lifetimes for dynamic components still ranged from 250 to 1000 hours. Although the established vibration criteria was met in part by some helicopters, vibration problems still plagued the designer. Unpredicted rotor instabilities and coupled phenomena still occurred with surprising regularity, quite often with disastrous impact to vehicle and development program. Flight speeds were increased by improved power ratios. However, this only served to further increase the dynamics problem, since at these higher speeds stall induced loads, stresses and vibrations became the key limiting factors in determining critical speeds and maneuvers. Use of the helicopter for combat, with requirements for greater agility, further sharpened the awareness of these limitations and focused greater attention on the dynamic constraints.

Now what of this decade in which we reside. Our research and development efforts, based on our newly acquired computational capability and advanced technology, have given us promise that we can achieve greatly increased performance, utility, and agility from our new helicopter system developments. Driven by military requirements, we have accepted the challenge to also survive in the hostile environment of the battlefield. To do this, reliability, maintainability, availability, and detectability all must reach new levels. Among these criteria, nonsteady phenomena become most critical factors. Improvements in capability and cost now become the challenge primarily of the dynamicist and he will determine success or failure.

Then where are we now in making these advances? Early helicopters had accepted low component life, high vibration, and marginal performance. Predictive techniques at that time were based on relatively simple analytical and experimental models. Technological advance was slow, based on the empiricism of rudimentary experiment. We have exploited to the maximum that past technology with its simple representations of rotor dynamics and flow fields. The old barrel of empiricism is bare. The greater demands for agility, longer life, and lower vibration demand new advances in dynamics from basic and applied research and development. A rededication to innovative methodology for aerodynamics, rotor flows, dynamics, and their coupling in interdisciplinary systems is necessary to meet the demands of the forthcoming generations of helicopters. Only significant advances in the comprehension of dynamic phenomena will meet the need for a technological base for desired future growth of capability.

Three specific areas of emphasis suggest themselves in considering the scope and direction for future technological development.

First, intensive effort is required in both the evolution of global analytical models which describe the dynamics of the helicopter and in the more specific interpretive models which describe the physics of the phenomena in more detail. Results of both of these modelling efforts must be verified continually by experiments with both model and full-scale tests. The improved comprehension of physical phenomena from interpretive models must be integrated into the global models in a timely manner as they are verified.

Second, the adequacy of the forcing functions, which are the inputs for the foregoing models, must be improved. These forces result from aerodynamic loads generated on the rotor blades, which are often highly nonlinear in nature. Unlike fixed wing aircraft, in helicopter flight these regions of nonlinear loading are penetrated deeply and periodically by the rotor blade. The generation of these loads results from the complex flow field in which the rotor operates. Here again, adequate mathematical models must be generated to predict these dynamic loadings and the models must be verified by experiment. When correlation is attained, we must assure timely efforts to include these descriptions into the inputs of the global and interpretive dynamic analyses.

Last, but by no means least, we must demonstrate true professional acumen to sensitize our efforts to the gain to be expected. Expressed in other terms, we must assess the gain to be made by more accurate models against the cost to obtain that gain. The last few percent of accuracy may well not be worth the cost. Our goal should be to produce predictive techniques for the designer to assure sufficient accomplishment of performance goals without the surprises of instabilities and shortened component life which have plagued us for now five decades, but without the cost of even one degree of sophistication more than required for that goal.

The discipline of dynamics shares the preeminence with that of structures as offering the greatest potential for advanced helicopter capability in this decade and the next. The assemblage at this symposium is the hope of that achievement. May you rise to the challenge and show its worth!

SESSION V

APPLICATION OF DYNAMICS TECHNOLOGY TO HELICOPTER DESIGN

Panel 1: Prediction of Rotor and Control System Loads

Panel Members

Peter J. Arcidiacono, Moderator	Head of Rotor Systems Design and Development, Sikorsky Aircraft
William D. Anderson	Research and Development Engineer, Lockheed California Company
Richard L. Bennett	Assistant Group Engineer, Aeromechanics, Bell Helicopter Company
Wayne Johnson	Research Scientist, USAAMRDL, Ames Directorate
Andrew Z. Lemnios	Chief Research Engineer, Kaman Aerospace Corporation
Richard H. MacNeal	President, The MacNeal-Schwendler Corporation
Robert A. Ormiston	Research Scientist, USAAMRDL, Ames Directorate
Frank J. Tarzanin, Jr.	Chief, Rotor Loads Unit, Boeing Vertol Company
Richard P. White, Jr.	Executive Vice President and Director of Engineering, Rochester Applied Science Associates, Inc.

COMPARISON OF SEVERAL METHODS FOR PREDICTING LOADS ON A HYPOTHETICAL HELICOPTER ROTOR

Robert A. Ormiston
Research Scientist

Ames Directorate
U. S. Army Air Mobility R&D Laboratory
Moffett Field, California 94035

ABSTRACT

Several state-of-the-art methods for predicting helicopter rotor loads were used to calculate rotor blade loads including airloads, bending moments, vibratory hub shears, and other parameters for a hypothetical helicopter rotor. Three different advance ratios were treated: $\mu = 0.1, 0.2$, and 0.33. Comparisons of results from the various methods indicate significant differences for certain parameters and flight conditions. Trim parameters and flapwise bending moments show the smallest variations, while chordwise bending moments, torsional moments, and vibratory shears show moderate to large differences. Torsional moment variations were most sensitive to advance ratio. Analysis of the results indicates that the differences can be attributed to all three fundamental parts of the problem: numerical solution methods, structural dynamics, and aerodynamics.

INTRODUCTION

The prediction of rotor loads is one of the most difficult analytical problems in rotary wing technology since it involves a highly nonlinear aeroelastic response problem. Rotor loads, however, are basic to helicopter design because vibratory forces and moments from the rotor largely determine fatigue life, reliability, flight envelope limits, and ride comfort. Ultimately, rotor loads have a large impact on the cost of the vehicle. Much effort has been devoted to the development of sophisticated methods for calculating rotor loads, but these methods necessarily depend on empiricisms and approximations because the aerodynamic and structural phenomena involved are not completely understood.

Needed progress in the development and refinement of these methods is often hindered for several reasons – the inherent difficulties of the problem, the specialization of different methods to treat different rotor types, the scarcity of reliable experimental data, and the difficulty in transferring experience gained by different investigators using different methods. As a result, it is difficult to accurately assess the state-of-the-art or to reach a consensus on the areas that require special attention. One proposal to partly overcome these difficulties is to specify a standard problem for calculating and comparing results of several loads prediction methods. This approach would focus attention on common, as well as individual, problem areas, permit sensitizing or "calibrating" different methods with respect to one another, and provide a new and broader basis for transferring experience.

Several rotor loads specialists jointly agreed to undertake a project of this type for presentation at the AHS/NASA-Ames Specialist's Meeting on Rotorcraft Dynamics. This paper summarizes the main results. The project was made possible only by the enthusiastic cooperation of these specialists and the support of helicopter manufacturers and other organizations. The principal individual contributors were Wayne Johnson, USAAMRDL, Ames Directorate; Richard L. Bennett, Bell Helicopter Co.; Frank J. Tarzanin, Jr., Boeing Vertol Co.; James R. Neff, Hughes Helicopters; A. Z. Lemnios, Kaman Aerospace Corp.; John Gaidelis, Lockheed California Co.; Michael P. Scully, M.I.T.; J. J. Costes, O.N.E.R.A.; Peter J. Arcidiacono, Sikorsky Aircraft; and A. J. Landgrebe, United Aircraft Research Laboratories.

Experimental data are not available for establishing the accuracy of any one loads prediction method; therefore, all interpretations and conclusions are based solely on relative comparisons of the results.

STANDARD PROBLEM SPECIFICATION

The standard problem was defined on the basis of inputs from all contributors. The basic philosophy was to emphasize aerodynamic phenomena by choosing a simple structural configuration. Most of the analytical difficulties are associated with aerodynamics, and interpretations of the results can be made simpler by removing unnecessary structural details.

Presented at the AHS/NASA-Ames Specialist's Meeting on Rotorcraft Dynamics, Moffett Field, California, February 13-15, 1974.

A conventional articulated rotor was chosen, with three rectangular blades having 10° twist, an NACA 0012 airfoil section, and coincident flapping and lead-lag hinges with 4% offset. The blade is uniform in stiffness with coincident mass center, aerodynamic center, shear center, and feathering axis to minimize aeroelastic coupling effects. Complete details are given in the Appendix. A tip speed of 750 ft/sec ($M = 0.672$) and rotor lift coefficient $C_L/\sigma = 0.0897$ were chosen for three basic flight speeds: Case A at 250 ft/sec ($\mu = 0.333$) to emphasize retreating blade stall flutter, Case B at 150 ft/sec ($\mu = 0.20$) for a typical unstalled flight condition, and Case C at 75 ft/sec ($\mu = 0.10$) in the transition flight regime to emphasize vortex wake-induced blade loads.

In addition to the three basic cases, several additional specialized cases were defined. These include selective combinations of rigid blade motion, linear aerodynamics, and uniform downwash in contrast to the most general case that includes elastic blade response, nonlinear aerodynamics, and nonuniform downwash. The particular combinations treated are listed in Table 1. Nonlinear aerodynamics is defined here to include the effects of unsteady stall, compressibility, and spanwise flow on the airfoil lift, drag, and moment coefficients. Linear aerodynamics is defined somewhat arbitrarily as inviscid, incompressible, steady-state, two-dimensional airfoil theory with a skin friction drag contribution ($c_l = 2\pi\alpha$, $c_d = c_{d_o}$, $c_m = 0$). Nonuniform downwash is based on either a linear rigid wake geometry or a nonlinear distorted wake geometry determined by self induction.

CONTRIBUTORS

Results were contributed by the organizations listed in Table 2. A code is assigned to each one to identify results in the figures that follow. Where applicable, the name of the computer program is also included. These programs encompass a rather wide variation of sophistication and capability. Several are multi-use "global" programs that include rotor loads prediction as one of several capabilities. Others were developed primarily for predicting rotor loads. Three methods (noted by asterisks) are specialized programs, not intended for routine rotor loads predictions, but are included here to broaden the comparisons.

Only the main results from the large body of contributed data are presented. The complete results include azimuthal variations, at several radial locations, of flapwise and chordwise bending moment, lift, drag, and pitching moment airloads, angle of attack, downwash, root torsional moments, and blade tip elastic torsion deflection; radial distributions of oscillatory bending moments and harmonics of the lift airloading; root vibratory shears; and trimmed rotor forces, power, flapping angles, control angles, and distorted wake geometry. The complete results are compiled in Ref. 1.

MATHEMATICAL MODELS

Pertinent features of the numerical solution methods, structural dynamics, airfoil aerodynamics, and downwash modeling of the various rotor loads prediction methods are summarized in Tables 3 and 4. This information does not necessarily describe the complete capabilities of each program; it refers only to program features applied to the present calculations. A more detailed discussion of various methods may be found in Refs. 2 to 6. Each method falls into one of four basic categories, depending on the form of the equations of motion (modal or finite element) and the method of solution (harmonic or numerical integration).

Numerical Solution Methods

The numerical integration solution method integrates the equations of motion in time from an arbitrary, assumed initial condition until a suitably converged solution is achieved. A variety of initial conditions, convergence criteria, convergence rates, integration methods, step sizes, etc., is used. The harmonic response solution methods generally calculate structural response using airload harmonics based on previously assumed blade motion and structural response. Iterations between the response and airloads continue until a converged solution is achieved.

Structural Dynamics

Modal equations are obtained from the partial differential equations of a rotating beam, and the generalized coordinates of the normal modes are the system degrees of freedom. Finite element equations are based on the force and moment equilibrium of a lumped mass or elemental segment of the blade and each element requires several degrees of freedom. In either the modal or the finite element representation, the coupling between degrees of freedom is important. This is difficult to summarize and the information in Table 3 is far from definitive. Substantial differences do exist, mainly in regard to coupling of the chordwise or torsional motion. Different methods are also used to calculate blade bending moments, although complete information is not included in Table 3.

Aerodynamics

Airfoil aerodynamics and induced downwash are determined by a variety of methods. Static airfoil properties are usually based on experimental data, using a table look-up procedure, with unsteady wake effects approximated by Theodorsen theory below stall. Unsteady aerodynamics in the stall regime, i.e., dynamic stall, is treated by several semiempirical methods (Refs. 7-11) in Table 4. The

effects of yawed flow on lift and drag are included for some methods. The rotor loads programs used for Cases A1, C1, and C2 include a variety of methods for calculating nonuniform induced downwash (Refs. 12-15) (Table 4). Most are based on a lifting line theory with a finite element (potential vortex filaments) representation of the trailed and shed vorticity. Induced velocities are calculated from the Biot-Savart law.

The unsteady potential flow of a finite-bladed rotor in forward flight actually encompasses both unsteady airfoil aerodynamics and wake-induced downwash. However, the near and far shed wake contributions are often treated separately. The near shed wake can be approximated either by using Theodorsen theory for the airfoil aerodynamic coefficients or by considering an approximate near shed wake sheet segment as part of the wake system. The ONERA method uses a doublet acceleration potential theory that implies a continuous vorticity sheet, with both shed and trailed vorticity emanating from each blade. Other refinements of several of the methods include viscous tip vortex core representations, lifting surface theory for close blade/vortex passage, and wake distortion effects due to mutual self-induction of the vortex filaments.

THE QUESTION OF VALIDITY

An important question must be addressed when one attempts to compare numerous results from sophisticated computer programs that require many input parameters. To what extent are the results affected by errors in programming input data, errors in selecting program options, differences in calculating intermediate steps (such as natural modes and frequencies), or approximations (possibly unspecified) in the program that do not meet the standard problem specification? Of course, it is impossible to verify completely that all calculations have met the specified conditions. And this must always be kept in mind as a possible explanation for differences in the results. However, it is useful to examine the static airfoil data and the blade natural frequencies to check the consistency of certain basic ingredients in the calculations.

Static Airfoil Data

The static, two-dimensional, NACA 0012 lift, drag, and pitching moment coefficients used for the different methods are compared in Fig. 1 for a Mach number of 0.5. The differences, especially at high angles of attack, indicate that there is not a universal consensus on static data of the NACA 0012 airfoil. Data for $M = 0.2$ and 0.9 (not shown) exhibit smaller and greater differences, respectively, than the $M = 0.5$ data. For Cases A1-A6 at $\mu = 0.33$, the maximum retreating blade angle of attack is about 13° to 14° at $M \cong 0.23$; therefore, the differences in static airfoil data are not considered to substantially affect the comparison of the results.

Blade Natural Frequencies

The blade mass and stiffness properties were chosen to provide blade frequencies typical of existing helicopter rotors. Predictions by the different methods are compared in Fig. 2 for the lower frequencies of the blade rotating in vacuo. For this condition, the pitch angle at 0.75R is zero, the blade static deflections are virtually zero, and coupling terms are very small. Furthermore, in many cases, coupled frequencies* were not calculated. Fully coupled (flapwise, chordwise, torsion) results are denoted by a single asterisk, partly coupled results (flapwise, chordwise) are denoted by double asterisks, and uncoupled results by triple asterisks. The results are fairly close for the fundamental elastic bending frequencies, but a more significant variation, about 10%, exists for the first elastic torsion frequency. The frequency differences for bending should not appreciably affect the comparisons of the results, but the torsion differences are more troublesome since stall flutter is sensitive to torsion frequency.

COMPARISON OF RESULTS

Only a small sample of the results is presented, but this is sufficient to illustrate and support the main conclusions of this study. Results are included for trim conditions, oscillatory bending moments, vibratory shears, and azimuthal variations of selected parameters. Trim conditions were specified in terms of the rotor lift, propulsive, and side forces. The required control angles and resulting blade flapping response and shaft power are also included. In several instances, a complete series of results is not available for comparison. This indicates that a calculation was not applicable or that specific output parameters were not available from a particular loads program. In certain instances, when results for a specific case were not available, another case was substituted to broaden the basis for comparisons. This was done only when departures from the specified case are presumed to have only a minor effect on the comparisons.

Case A3

The advance ratio of 0.333 and elastic blade motion, dynamic stall, and uniform downwash are included. Considering the extreme operating condition, the trim conditions (Fig. 3) are in reasonable agreement, although the specified zero side force was not

*The coupling included for the natural frequencies is not necessarily the same as the coupling included for calculating forced response (see Table 3).

accurately achieved by all the programs. The radial distribution of oscillatory flapwise and chordwise bending moments is presented in Fig. 4. The flapwise moments compare reasonably well, considering the flight condition.

Chordwise moments show larger differences. First, there is a substantial variation in magnitude along the blade and, second, there is a qualitative difference in behavior at the blade root where the moments either increase to a large finite value or vanish. In the first case, differences can result from at least three factors: (1) dynamic stall aerodynamics, (2) structural/inertial coupling effects (primarily flapwise/chordwise structural coupling), and (3) the method of calculating bending moments (in the case of modal equations). The effects of dynamic stall are considered to be less important for chordwise moments than for flapwise moments (see Cases A5 and B1 below); however, significant differences in structural coupling are present. For modal methods, bending moments can be calculated from internal structural moments of the blade deflection equation (by summing the modal moment distributions for each generalized coordinate) or from a spanwise integration of the applied inertial and aerodynamic loads acting on the blade. With a limited number of modes, the latter method is more accurate.

The second difference in the chordwise bending moments is associated with the lead-lag damper. The LCC calculations using finite element equations, with and without the lead-lag damper, show that the damper increases the chordwise moments at the root compared with the zero moment boundary condition for a pin-end beam without damping. The BHC and SA methods use modal equations and exhibit zero bending moment at the blade root (lead-lag damper was not omitted). This could be a result of the way the bending moments are calculated. Integrated blade loadings, including the damper moment, would give a root moment, whereas a summation of modal moment distributions would not. This is because normal modes determined in vacuo cannot satisfy the pin-end boundary condition with a viscous damper (unless complex modes are used) and the moment must be zero at the hinge for each mode.

Azimuthal variations in bending moments at $r = 0.5$ (Figs. 5 and 6) show general agreement of the basic waveforms with some variations, particularly chordwise. The 1/rev flapwise moment is mainly due to blade twist. The azimuthal variation of the lift airloading at $r = 0.8$ (Fig. 7) begins to show the influence of dynamic stall flutter for the retreating blade and therefore some significant differences are evident.

The clearest evidence of dynamic stall occurs in the elastic tip torsion deflection (Fig. 8). Each method, with the possible exceptions of ARC and HH, clearly predicts stall flutter behavior, but the character and amplitude of the motion shows substantial differences, probably due largely to differences in the semiempirical unsteady aerodynamic stall modeling. The HH result could be interpreted as stall flutter and the low amplitude may be due to the relatively small static pitching moment coefficient at stall. The sensitivity of stall flutter behavior to details of the solution method is shown by the two BHC calculations for tip torsion deflection. Results for two different azimuthal integration step sizes are shown, $\Delta\psi = 4°$ and $10°$. The $10°$ azimuth increment reduces the peak torsion response by $5.5°$, or about half. An increment of $6°$ (not shown) reduced the torsion response by about $2°$. Chordwise bending moments were only moderately influenced by integration step size, and flapwise bending moments only very slightly.

The first five sine and cosine harmonics of the vertical and horizontal shears acting on the hub in the rotating coordinate system are shown in Fig. 9. The first harmonic components are nearly proportional to the rotor tip path plane tilt and reflect the trim propulsive and lateral forces, respectively. Since lateral trim variations are present (Fig. 3), the large variation in the first cosine harmonic of vertical shear is not surprising. Generally, the vibratory shears show relatively large variations between the different methods, but again this represents the most extreme flight condition.

Case A5

This case is identical to Case A3, except that the airfoil coefficients are based on linear theory, excluding stall, unsteady aerodynamics, and compressibility as defined above. These results help explain the results of Case A3 by removing the contributions of stall. Spanwise distributions of the oscillatory bending moments are shown in Fig. 10. The flapwise moments and their variations are both reduced compared to Case A3. The average of the chordwise moments was not substantially changed, but chordwise moment variations actually increased. Note that the nonstandard shaft angle for KAC could contribute to reduced chordwise Coriolis excitation. The lack of airfoil stall strongly suggests that the large differences in chordwise bending moments may be caused by differences in the structural/inertial coupling terms in the equations of motion and the lead-lag damper noted above for Case A3. The azimuthal variations of lift and drag airloading at $r = 0.8$ (Fig. 11) show only minor variations. The effects of dynamic stall on the lift observed in Case A3 are not present and the minor variations in the drag airload are not sufficient to account for the differences in the chordwise bending moment.

The blade elastic tip torsion deflection (Fig. 12) is substantially reduced without dynamic stall. Not all the results, however, met the Case A5 specification of zero pitching moment coefficient ($c_m = 0$). Results for SA and HH retained the linear quasisteady contribution of pitch rate damping; BV retained the apparent inertia aerodynamic term. BHC, KAC, and LCC used zero pitching moment coefficient. Notwithstanding these inconsistencies, the results illustrate possible evidence of anomalous behavior arising from the numerical solution method. BHC and KAC appear to have undamped torsion oscillations while HH shows a numerically unconverged solution; the specified value of zero pitch damping may be a contributing factor. Differences in the steady and 1/rev torsion imply again that differences exist in structural inertial/coupling terms in the equations of motion.

The above conclusions are also supported by the vibratory shears shown in Fig. 13. These shears are not greatly reduced from Case A3, indicating that stall is not the only contributor to vibratory shears at high advance ratio. A clear explanation for the

remaining differences is not available. Possibilities include the structural/inertial coupling, differences in the numerical solution method, or differences in the lateral trim condition. Particularly disturbing are the substantial differences even for lower harmonics of the vibratory shears.

Case B1

This case is identical to Case A3 except that the advance ratio is reduced to 0.2 where retreating blade stall becomes much less significant. Nonlinear aerodynamics, elastic blade motion, and uniform downwash are included. Only the results for trim and the oscillatory blade bending moments are shown (Figs. 14 and 15), and these results substantiate the findings from Cases A3 and A5. For example, the chordwise moments show substantial differences that cannot be attributed to stall aerodynamics because the angle of attack of the retreating blade is generally well below stall.

Cases C1 and C2

For these cases, the advance ratio is reduced to 0.1 and rotor loads are dominated by interactions between the blades and trailing tip vortices in the wake. The few results included emphasize the wake-induced velocities and blade lift airload. Cases C1 and C2 both include nonlinear aerodynamics, elastic blade motion, and nonuniform downwash. Case C2 includes a rigid wake geometry for determining downwash velocities and Case C1 includes a more general distorted wake. At the low advance ratio, blade stall is virtually nonexistent and elastic blade motion is not large; hence the main effects can be attributed to the wake. Several of the methods used for Cases C1 and C2 did not include the specified airfoil aerodynamics and elastic blade modeling as noted in Tables 3 and 4, but these exceptions are not considered to be significant.

The induced downwash for Case C2, with the rigid wake, is given in Fig. 16. Three methods (BV, MIT, UARL) use a finite element potential vortex system and direct application of the Biot-Savart law. The BHC method uses a semiempirically modified momentum theory and the OR method uses the doublet acceleration potential theory that implies a continuous sheet of vorticity behind each blade. Results from the four potential theory methods are similar, except the BV result is approximately 1/5 the magnitude of the others. This is due to an arbitrary reduction in the strength of the wake vorticity, which was found to give better correlation with blade loads measurements. All the results show the typical increase in downwash at the rear of the rotor and decrease at the front. The blade lift airload (Fig. 17) also shows reasonable agreement, especially with respect to lift impulses caused by close blade/vortex interactions. Particularly interesting is the qualitative agreement of the finite vortex method (UARL), the mixed finite vortex/sheet vorticity method (MIT), and the sheet vorticity method (OR). The BV result reflects the reduced wake circulation strength, but the same blade/vortex interactions are discernable.

Results for Case C1 with the distorted wake are given in Figs. 18 and 19. The distorted wake is induced into a position close to the rotor disc plane and the results become more sensitive to the details of the prediction method. For example, the downwash variations for UARL are increased due to the closer proximity of the wake vortices, but high frequency variations were also introduced in part by the numerical solution method. The MIT lift airload impulses from the blade/vortex interactions would be considerably larger without the use of a lifting surface method that scales down the airloads.

Summary Results

A useful summary can be obtained by plotting results for Cases C2, B1, and A3 as a function of advance ratio. Figure 20 shows oscillatory flapwise and chordwise bending moments ($r = 0.5$) and blade root torsion moments. The results for Case A5 are also included to emphasize the effect of stall in comparison with Case A3 results. The differences in flapwise moment are not large and they increase only moderately with speed as retreating blade stall begins. The increased BHC moments at $\mu = 0.1$ are attributed to the semiempirical correction of downwash for the effect of blade tip vortices. The chordwise moments show large differences for all three speeds and also for linear aerodynamics, implying that stall is not the cause of the differences. Root torsion moments (equivalent to elastic tip torsion deflection and pitch link loads) are very sensitive to retreating blade stall and hence advance ratio. These results are not surprising in view of the number of different semiempirical dynamic stall models currently in use. Since torsion moments typically grow rapidly after a certain threshold speed is reached, small differences in this threshold speed could contribute to the large variations at $\mu = 0.33$. The straight lines joining the data points are not intended to suggest the actual functional variation, but only to indicate continuity between the data points of different methods.

INTERPRETATIONS AND ASSESSMENTS

It is not uncommon for rotary wing analysts and researchers to assume that rotor blade structural dynamics is well understood and that the main obstacle to accurate prediction of rotor loads is an incomplete understanding of rotor aerodynamics, particularly dynamic stall. This is certainly true to an extent, but it nevertheless reflects a tendency to focus on one aspect of the problem and overlook other areas in need of attention as well. The above results and comparisons show that limitations for rotor loads prediction exist in all three main areas: (1) numerical solution methods, (2) structural dynamics, and (3) aerodynamics. A more detailed interpretation and assessment of the above results in terms of these three main subjects is given below.

Numerical Solution Methods

The results illustrate several examples where accuracy was compromised by numerical techniques and procedures used to solve the equations of motion. Considering the complexity of a large number of highly coupled, nonlinear equations, difficulties of this type are not surprising. Additional examples of numerical problems were found in subjective reactions expressed by contributors in the preliminary stages of calculating their solutions. In several cases, unexpected difficulties were encountered in achieving converged solutions, in reaching the desired rotor lift levels or in avoiding apparent blade motion instabilities. In several cases, these difficulties were resolved by adjustments to numerical details in the solution method or arbitrary deviations from the standard problem specifications. In most instances, problems of this type occurred for the high-speed flight condition. Little discussion of these problems appears in the literature, but they appear to be significant.

Structural Dynamics

One of the main results of the comparisons was the large differences in chordwise bending moments and vibratory shears even when nonlinear aerodynamic phenomena were absent or negligible. This clearly indicates that important differences exist in the structural dynamic modeling, probably due, in part, to different assumptions and approximations for structural/inertial coupling and, in part, to an inadequate fundamental knowledge of the mechanics of a flexible rotating beam. In the first place, there is insufficient information about the approximations used and this contributes to difficulties in drawing meaningful conclusions. It is evident that for conditions of minimum coupling, i.e., a beam rotating in vacuo at zero pitch angle, the lower natural bending frequencies show relatively good agreement. It also appears that chordwise bending moments are highly sensitive to flapwise/chordwise coupling. For example, the methods that calculated uncoupled chordwise moments, BV and KAC, generally showed the lowest results. It is difficult, however, to draw more substantive conclusions about other important structural/inertial coupling terms, such as bending/torsion coupling. Nevertheless, the results indicate that structural coupling effects are significant, that different approximations and assumptions are in common use, and that the validity of these approximations needs to be examined more closely.

Also, fundamental questions can be raised concerning blade structural dynamics. Certainly, this subject is much better understood than nonlinear aerodynamic phenomena. However, the development of nonlinear structural equations for bending and torsion of slender beams is still in progress. The widely accepted work of Houbolt and Brooks (Ref. 16) provides only linear equations of motion. A recent derivation of nonlinear equations of motion by Dowell and Hodges (Ref. 17) points out some of the difficulties involved in more complete treatments. These involve assumptions in neglecting higher order terms, nonlinear strain displacement relations, warping of beam cross sections, etc.

Different methods used to calculate blade bending moments also contributed to differences in the results. These moments must be carefully evaluated, particularly when using the modal equations of motion. Results of the modal methods did not show the expected increase in chordwise bending moments near the blade root because of the lead-lag damper.

Aerodynamics

Although probably not a substantial source of inaccuracy, the degree of variation in the NACA 0012 airfoil coefficients was unexpected, and certainly should be remedied. The differences in the stall flutter torsion response of the rotor blade were not unexpected because the present semiempirical methods for calculating dynamic stall aerodynamics are quite different.** Improvements will depend on future research into very basic aerodynamic phenomena. Although it is impossible to interpret the present rotor loads predictions in terms of detail aerodynamic phenomena, it is well understood that three-dimensional aerodynamics, yawed flow or sweep effects on drag and stall, and blade vortex interactions need much more attention. The rotor wake significantly influences rotor loads at low to moderate speeds. Several different methods are currently in use and again many of the assumptions and approximations need to be examined more closely.

CONCLUSIONS AND RECOMMENDATIONS

The present results have shown that there is certainly much to be gained from direct comparisons of helicopter rotor loads prediction methods. A clearer perspective of the state-of-the-art is now available and this alone should promote further improvements and advances in the state-of-the-art. The results also show that, for extreme operating conditions; the different rotor loads methods predict results with significant differences for some parameters. The following general conclusions summarize the results with respect to the relative quantitative accuracy of these methods:

(1) Rotor forces, power, control positions, and blade flapping generally showed small to moderate differences.

**W. Johnson (Ref. 18) presents comparisons of rotor loads predictions where only the dynamic stall methods are varied. The calculations are for the high-speed flight condition (Case A) of the rotor configuration developed here. The results obtained complement the present comparisons.

(2) Flapwise bending moments showed small to moderate differences that increase with advance ratio.

(3) Chordwise bending moments showed moderate to large differences for all advance ratios. This is attributed to structural dynamics.

(4) Torsional response showed moderate to large differences, especially at high advance ratio. This is attributed to dynamic stall aerodynamics.

(5) Blade root vibratory shears showed large to very large differences. Significant differences occurred even with linear aerodynamics and a satisfactory explanation is not available.

(6) At $\mu = 0.1$, the blade lift and downwash calculated by different methods show qualitatively similar results, including blade/vortex interactions. Differences were largest for the distorted wake calculations.

(7) It is concluded that differences in the results arise from all three basic areas: numerical solution methods, structural dynamics, and aerodynamics.

Based on the discussions and conclusions above, the following recommendations are made for possible ways to improve rotor loads prediction methods:

(1) Standard comparisons should be continued. Sensitivity to additional configuration parameters should be determined and comparisons for trend behavior should be made.

(2) Additional investigation should be undertaken in greater detail to resolve questions raised by the present results. At the present time, it is not possible to sort out and assess all the assumptions and semiempirical factors in the problem by examining the resultant rotor loads. This applies to comparisons between different methods and to correlations with experimental data as well. Computer experiments should be used to study specific isolated aspects of the solution methods and structural dynamics. The accuracy of approximations and validity of specific assumptions should be determined.

(3) Fundamental experimental research should be continued to investigate dynamic stall, blade/vortex interactions, and three-dimensional flow effects. Special experiments should be designed to isolate and simulate specific aspects of the total rotor aerodynamic problem. This will eventually aid in the development and validation of analytical modeling for individual aspects of the total aerodynamic problem.

(4) Ultimately [after some progress is made with items (2) and (3) above], it will be useful to check rotor loads prediction methods with experimental data from wind-tunnel tests of a large-scale rotor. For maximum benefit, these tests should be performed on a rotor specially designed and fabricated to eliminate all nonessential complexities, and thus enhance the chances for meaningful correlations. Also, a new design could avoid some of the operating stress limitations of existing flightworthy rotor systems and permit testing at more extreme operating conditions. Sufficient instrumentation would be essential to measure all important parameters including steady and vibratory hub forces, blade airloads and stresses, and wake-induced velocities.

REFERENCES

1. Ormiston, R. A., "Compilation of Results of Several Loads Prediction Methods for a Hypothetical Helicopter Rotor," NASA report to be published.

2. Anon., Specialists Meeting on Helicopter Rotor Loads Prediction Methods, Milan, Italy, March 1973, AGARD Conference Proceedings No. 122.

3. Johnson, W., "The Effect of Dynamic Stall on the Response and Airloading of Helicopter Rotor Blades," Journal of the American Helicopter Society, Vol. 14, No. 2, April 1969.

4. SADSAM User's Manual, MSR 10, The MacNeal-Schwendler Corp., Los Angeles, Calif., Dec. 1970.

5. Costes, J. J., "Calcul des Forces Aérodynamiques Instationnaires sur les Pales d'un Rotor d'Hélicoptère," La Recherche Aérospatiale, No. 1972-2 (March-April). (See also AGARD Report No. 595, April 1972.)

6. Scully, M. D., "Computation of Helicopter Rotor Wake Geometry and Its Influence on Rotor Harmonic Airloads," M.I.T. Aeroelastic and Structures Research Laboratory Report (to be published).

7. Ham, N. D. and Garelick, M. S., "Dynamic Stall Considerations in Helicopter Rotors," Journal of the American Helicopter Society, Vol. 13, No. 2, April 1968.

8. Carta, F. O., Casellini, L. M., Arcidiacono, P. J., and Elman, H. L., "Analytical Study of Helicopter Rotor Stall Flutter," Paper presented at the 26th Annual National Forum of the American Helicopter Society, Washington, D. C., 1970.

9. Tarzanin, F. J., Jr., "Prediction of Control Loads Due to Blade Stall," Journal of the American Helicopter Society, Vol. 17, No. 2, April 1972.

10. Harris, F. D., Tarzanin, F. J., Jr., and Fisher, R. K., Jr., "Rotor High Speed Performance, Theory vs. Test," Journal of the American Helicopter Society, Vol. 15, No. 3, July 1970.

11. Ericsson, L. E. and Reding, J. P., "Dynamic Stall of Helicopter Blades," Journal of the American Helicopter Society, Vol. 17, No. 1, Jan. 1972.

12. Miller, R. H., "Rotor Blade Harmonic Airloadings," AIAA Journal, Vol. 2, No. 7, July 1964.

13. Johnson, W., "A Lifting Surface Solution for Vortex Induced Airloads," AIAA Journal, Vol. 9, No. 4, April 1971.

14. Landgrebe, A. J., "An Analytical Method for Predicting Rotor Wake Geometry," Journal of the American Helicopter Society, Vol. 14, No. 4, Oct. 1969.

15. Davenport, F. J., "A Method for Computation of the Induced Velocity Field of a Rotor in Forward Flight, Suitable for Application to Tandem Rotor Configurations," Journal of the American Helicopter Society, Vol. 9, No. 3, July 1964.

16. Houbolt, J. C. and Brooks, G. W., "Differential Equations of Motion for Combined Flapwise Bending, Chordwise Bending, and Torsion of Twisted Nonuniform Rotor Blades," NACA Rept. 1346, Oct. 1958.

17. Dowell, E. H. and Hodges, D. H., "Nonlinear Equations of Motion for the Elastic Bending and Torsion of Twisted Nonuniform Rotor Blades," NASA Technical Note to be published.

18. Johnson, W., "Comparison of Three Methods for Calculation of Helicopter Rotor Blade Loading and Stresses Due to Stall," NASA report to be published.

APPENDIX

Rotor Configuration

Radius	25.0 ft	Blade mass/unit length	0.25 slugs/ft
Chord	1.83 ft	Polar mass moment of inertia/unit length	0.03 slug-ft^2/ft
Number of Blades	3	Flapwise mass moment of inertia/unit length	0.001 slug-ft^2/ft
Solidity	0.070	Chordwise mass moment of inertial/unit length	0.029 slug-ft^2/ft
Twist, Linear	-10° (from r = 0 to 1.0)	Polar area moment of inertia	0.003 ft^4
Lock number (a = 5.73 rad)	7.49	Flapwise bending stiffness	30×10^6 lb-in.^{2}
Airfoil	NACA 0012	Chordwise bending stiffness	400×10^6 lb-in.^{2}
Blade root cutout	3.75 ft (r = 0.15)	Torsional rigidity	30×10^6 lb-in.^{2}
Flap hinge offset	1.0 ft (r = 0.04)	Feathering axis location	0.25c
Lead-lag hinge offset	1.0 ft (r = 0.04)	Elastic axis (shear center)	0.25c
Control system kinematic pitch-flap and pitch-lag coupling	0.0	Center of mass	0.25c
Lead-lag damper (ideal viscous damping about the lead-lag hinge)	3.0×10^3 ft-lb-sec	Tension axis	0.25c

Operating Conditions

Tip Speed	750 ft/sec	Drag (parasite area)		25 ft²	
Speed of sound	1117 ft/sec	Side force		0.0	
Density	2.378×10^{-3} slug/ft³		Case A	Case B	Case C
Shaft angle of attack	0.0°	Forward velocity, ft/sec	250	150	75
Rotor lift coefficient, C_L/σ	0.0897	Advance ratio	0.333	0.20	0.10
Lift	16,500 lb	Advancing tip Mach number	0.895	0.806	0.739

Nomenclature

c	blade chord
c_d	airfoil section drag coefficient
c_l	airfoil section lift coefficient
C(k)	Theodorsen unsteady aerodynamic function
C_L	rotor lift coefficient
c_m	airfoil section moment coefficient
C_P	rotor power coefficient
M	Mach number
r	dimensionless blade radius, 0 at center of rotor, 1.0 at tip
α	airfoil section angle of attack
λ_i	dimensionless induced downwash velocity, positive down
μ	advance ratio
σ	rotor solidity
ψ	blade azimuth (when lead-lag angle equals zero)
α_s	shaft angle of attack, pitch-up positive
$\beta = a_0 - a_{1s} \cos \psi - b_{1s} \sin \psi$	blade flapping angle with respect to shaft axis system, positive up
$\theta_{0.75} = \theta_0 - A_{1s} \cos \psi - B_{1s} \sin \psi$	blade pitch angle, shaft axis system, positive leading edge up

Coordinate Systems and Sign Conventions

Blade torsion deflection	positive leading edge up
Rotor forces	shaft axis system, positive thrust force up, propulsion force forward, side force toward right
Lift and drag airload	shaft axis coordinates, positive up and toward blade trailing edge
Flapwise/chordwise bending moment	airfoil principal axis coordinate system, positive for tension in blade lower surface and leading-edge, respectively
Vibratory hub shear	forces acting on hub in rotating shaft axis coordinate system; vertical force positive up, horizontal force positive toward blade trailing edge; harmonics of positive Fourier series

Table 1.– Special Cases

Case	μ	Structure	Aerodynamics	Downwash
A1	0.33	Elastic	Dynamic stall	Rigid wake
A3		Elastic	Dynamic stall	Uniform
A5		Elastic	Linear aerodynamics	Uniform
A6		Rigid	Linear aerodynamics	Uniform
B1	0.2	Elastic	Dynamic stall	Uniform
C1	0.1	Elastic	Dynamic stall	Distorted wake
C2		Elastic	Dynamic stall	Rigid wake

Table 2.– Contributors

Contributor	Code	Program Name
Ames Research Center*	ARC	– – –
Bell Helicopter Company	BHC	C81
Boeing Vertol Company	BV	C60
Hughes Helicopters	HH	SADSAM
Kaman Aerospace Corporation	KAC	6F
Lockheed California Company	LCC	3110
Massachusetts Institute of Technology*†	MIT	– – –
Office National d'Études et de Recherches Aérospatiales*	OR	– – –
Sikorsky Aircraft	SA	Normal Modes
United Aircraft Research Laboratories	UARL	Normal Modes

*Specialized program.

†Calculations performed under NASC Airframe Division Contract N00019-73-C-0378.

TABLE 3.

NUMERICS AND SOLUTION PROCEDURE										STRUCTURAL DYNAMICS			
Code	Method for Solving Equations of Motion	Convergence Criteria for Blade Motion or Rotor Forces	Initial Conditions for Blade Motion or Rotor Controls	Computer and Approximate CPU Run Time	Radial Points for Aerodynamic Forces	Integration Step Size $\Delta\psi$ or No. of Forcing Function Harmonics	Integration Method or Azimuth Points to Define Airload Harmonics	Revolutions or Aero/Structural Iterations for Convergence	Remarks	Equations of Motion	Modes Included or Finite Elements	Total Degrees of Freedom	Structural and Inertial coupling of Modes or Finite Elements
ARC	Harmonic Response	None	Rigid flapping from Gessow and Myers	IBM 360/67 170 sec	9	10	24	6	Thrust assumed perpendicular to tip path plane to obtain propulsive and side forces to trim	Modal	*Rigid Flapping* 1 Flapwise 1 Torsion	3	*Uncoupled. Nonrotating* torsion mode.
BHC	Numerical Integration	None	Initial trim obtained from elastic blade response to 1/rev aero forces	IBM 360/65 2-7 min	20	15° (A3, 4°)	4 cycle Runge-Kutta	5		Modal	Rigid Flapping Rigid Lead-Lag 2 Flapwise 1 Chordwise 1 Torsion	6	Fully coupled normal modes. Bending moments determined from modal moment distributions.
BV	Harmonic Response	None	Rigid blade motion from simple trim program	IBM 360/65 6 min	15	10	24	10	Interharmonic coupling of aerodynamic forcing function neglected	Finite Element	20	Coupled flap/pitch 60, Chordwise 40	Coupled flap/pitch. Uncoupled chordwise. Approximate torsion moment due to chordwise bending. Structural effects of twist and pitch of principal axes neglected.
HH	Numerical Integration	Generally when subharmonic response $\leq$ 1% of largest harmonic response	$\chi,\dot{\chi},\ddot{\chi}=0$	CDC 6600 77 sec	11	3.6°	Newmark β	~18	Thrust assumed perpendicular to tip path plane for trim	Finite Element	11	37	Fully coupled.
KAC	Integrating Matrix Operator	Thrust ± 50 lb Prop. Force ± 20 lb Side Force ± 10 lb	Estimated from linearized equations	IBM 360/40 1 hour	16		24	5-10		Modal	Rigid Flapping Rigid Lead-Lag 1 Flapwise 1 Torsion	4	Fully coupled. Bending moments determined from uncoupled equations at zero pitch.
LCC	Harmonic Response	No angle changes more than .00001 rad per revolution	Estimate based on interpolation of several trial runs	IBM 360/91 4.2 min	18	10	36	~3		Finite Element	32	Coupled flap/chord 64	Flapwise and chordwise bending fully coupled. Torsion structural response from flap and chord bending. Torsion dynamics neglected.
MIT	Numerical Integration	$\Delta\beta,\Delta\dot{\beta} < .00001$ rad, rad/sec	Rigid flapping from Gessow and Myers	IBM 370/165 Rigid wake 40-70 sec Free wake 5.5-6.5 min	6	15°	Houbolt Finite Difference	5	Thrust assumed perpendicular to tip path plane to obtain propulsive and side forces to trim	Modal	Rigid Flapping 1 Flapwise	2	Uncoupled. Approximate polynomial bending mode shape.
O.N.E.R.A.	Harmonic Response	None	Linear flapping solution	IBM 360/67 200 sec (Downwash Matrix 1.5 hr)	5	6	13	5	Iteration required only to obtain lead-lag response	Rigid body dynamics	Rigid Flapping Rigid Lead-Lag	2	Uncoupled structurally and inertially.
SA, UARL	*Numerical Integration*	$\Delta\chi \leq .001$ *rad* $\Delta\dot{\chi} \leq .001$ rad/sec ΔLift $\leq$ 200 lb ΔProp. Force $\leq$ 50 lb $\Delta\theta_0, \Delta A_{1s} \Delta B_{1s} \leq 3°$ for var. inflow	*Rigid flapping and* controls from NASA CR-114	*UNIVAC 1108* ~9 min (Distorted wake 16 min)	15	5°	*Modified* Euler	5-10		Modal	Rigid Flapping Rigid Lead-Lag 3 Flapwise 2 Chordwise 1 Torsion	8	Uncoupled normal modes obtained for zero pitch and twist. Structural coupling terms included as forcing functions in modal equations.

TABLE 4.

AIRFOIL AERODYNAMICS						DOWNWASH								
Code	Unsteady Aerodynamics Below Stall	Dynamic Stall: Lift	Dynamic Stall: Moment	Dynamic Stall: Drag	Yawed Flow Effect	General Method	Number of Trailing Vortex Elements	Azimuth Interval for Trailing Wake Elements	Number of Trailing Vortex Spirals	Near Shed Wake (See "Unsteady Aerodynamics Below Stall" column of Airfoil Aerodynamics)	Number of Far Shed Wake Vortex Elements	Core Size	Vortex Dissipation	Distorted Vortex Elements
ARC	Theodorsen, modified for unsteady velocity.	Ham and Garelick, Ref. (7) No compressibility correction.			No yawed flow effect	Lifting line vortex theory, rigid wake.	6	30°	2	Sheet vorticity	12 per revolution	Tip vortex 0.025R. All elements 0.1R.	None	
BHC	Lift: Theodorsen, C(k) = 1. Moment: Carta *et al.*, Ref. (8).	Tarzanin, Ref. (9)	Carta *et al.* Ref. (8)	Harris *et al.*, Ref. (10)	Drag and $C_{\ell_{max}}$, Ref. (10)	Modified momentum theory.	Downwash proportional to radius with a cosine ψ azimuthwise variation. Tip vortex represented by increased downwash for $r \geq 0.8$, and $45° \leq \psi \leq 165°$ or $255° \leq \psi \leq 315°$. *Magnitude of mean, cosine component, and tip vortex effect are semiempirical functions of advance ratio.*							
BV	Theodorsen	Tarzanin, Ref. (9)	Tarzanin, Ref. (9)	Harris *et al.*, Ref. (10)	Drag and $C_{\ell_{max}}$, Ref. (10)	Lifting line vortex theory, rigid wake.	Two vortices at tip and root.	15°	2	None	None	None	None	
HH	First order time lag approximation to Theodorsen.	Ericsson and Reding, Ref. (11)	Ericsson and Reding, Ref. (11)	Steady-state drag only	$C_{\ell_{max}}$, Ref. (10)	Uniform downwash for present calculations.								
KAC	Theodorsen, C(k) = 1.	Steady-state only			No yawed flow effect	Uniform downwash for present calculations.								
LCC	Theodorsen	Tarzanin, Ref. (9)	Tarzanin, Ref. (9)	Harris *et al.*, Ref. (10)	Drag and $C_{\ell_{max}}$, Ref. (10)	Uniform downwash for present calculations.								
MIT	Approximation to Theodorsen, Ref. (12).	Harris *et al.*, Ref. (10)			$C_{\ell_{max}}$, Ref. (10)	Lifting line vortex theory, free wake. Lifting surface theory for close blade/vortex interaction.	Two vortices at r = 0.4 and 1.0 *plus tip trailing* sheet vorticity for 0.6 to 0.9 < r < 1.0 *and about one* spiral in length	15°	4	Sheet vorticity 15° in azimuth behind blade midchord, Ref. (12)	12 per revolution	Tip vortex 0.0075 c Root vortex 0.2 c Far shed wake 0.105 c	*Tip vortex* bursts to 0.3 c core size after *close* blade/vortex interaction	*Tip vortex*
O.N.E.R.A.	*Linear unsteady* potential theory for lift. Constant friction drag coefficient.	No stall			No yawed flow effect	Linearized doublet acceleration potential theory	Implicit in theory is continuous spiral sheet of wake vorticity emanating from a single bound vortex of each blade and convected downstream by resultant of *freestream velocity and mean* induced velocity vectors. Both shed and trailing vorticity components are implied.							
SA, UARL	Carta *et al.*, Ref. (8).	Carta *et al.*, Ref. (8), M = 0.2. Scaled up to M = 0.5 for compressibility. For $\alpha > 27°$, quasi-steady for all M.		Steady-state drag only	No yawed flow effect	Lifting line vortex theory, free wake.	10	15°	5–8	None	None	1/3 c	None	*Tip vortex*

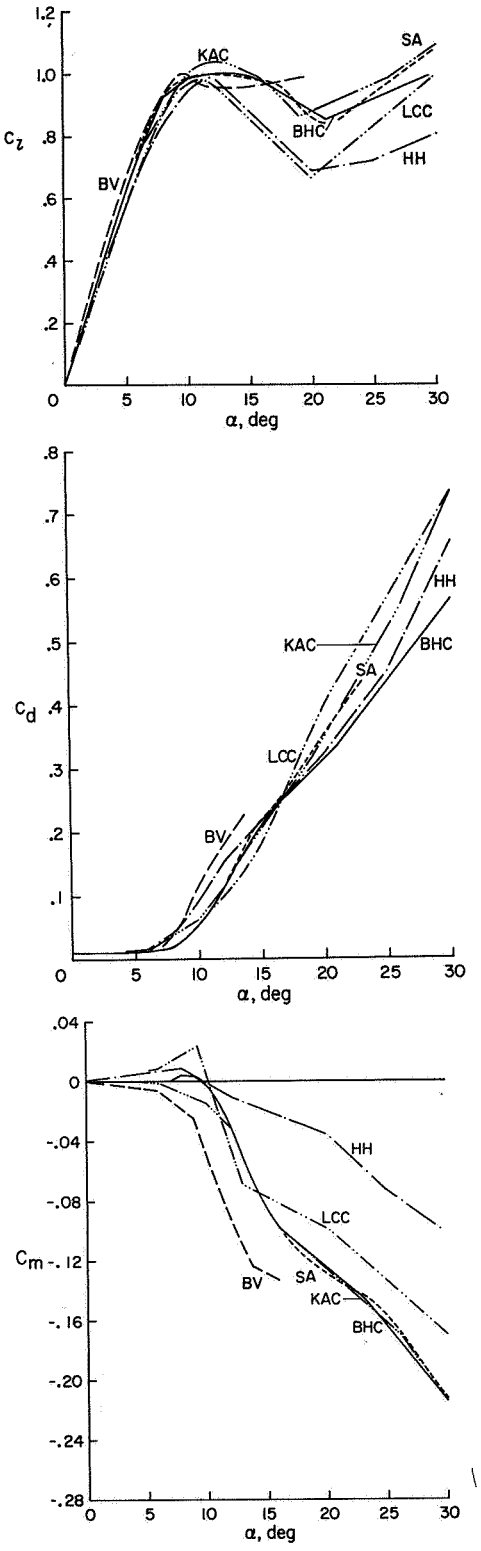

Fig. 1.– NACA 0012 airfoil section lift, drag, and pitching moment coefficients at M = 0.5 used for different methods.

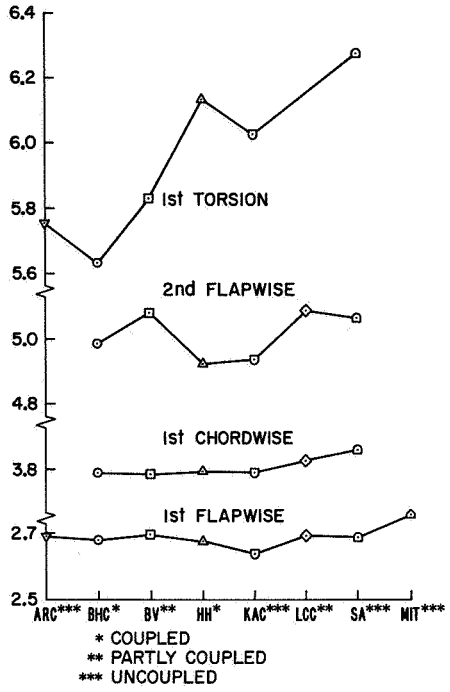

Fig. 2.– Rotor blade rotating natural frequencies in vacuo, $\theta_{0.75} = 0°$.

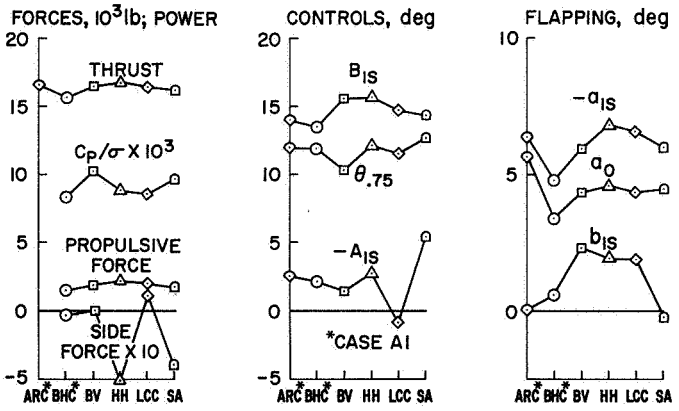

Fig. 3.– Trim parameters, Case A3.

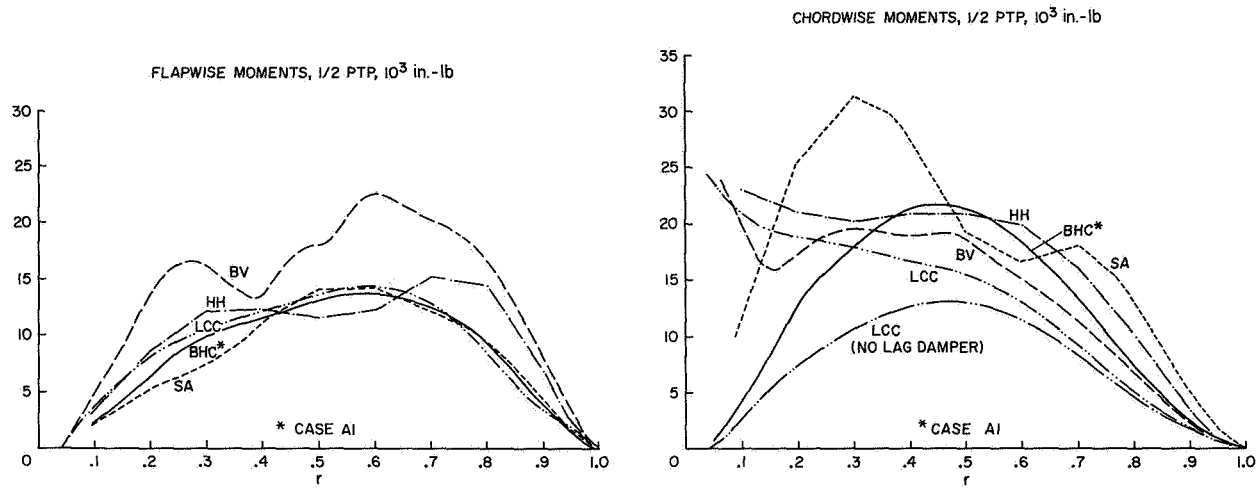

Fig. 4.– Oscillatory blade bending moments, Case A3.

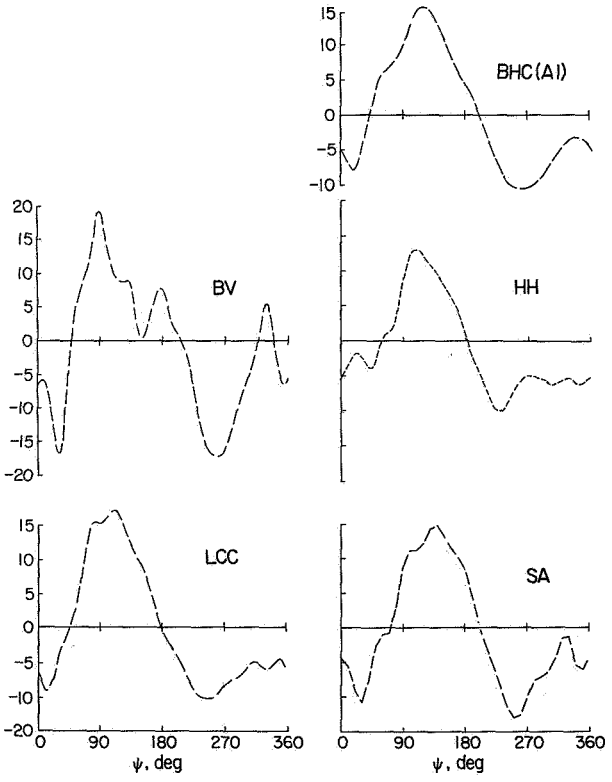

Fig. 5.– Flapwise bending moment (in.-lb) vs. azimuth; r = 0.5, Case A3.

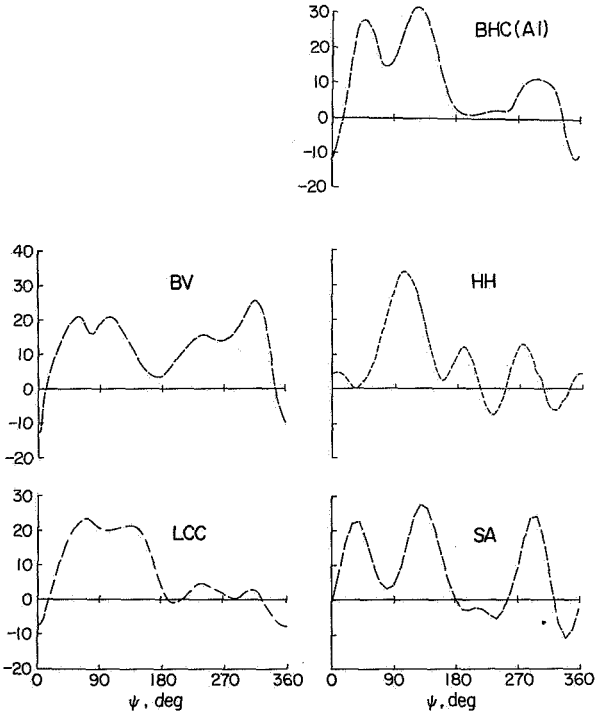

Fig. 6.– Chordwise bending moment (in.-lb) vs. azimuth; r = 0.5, Case A3.

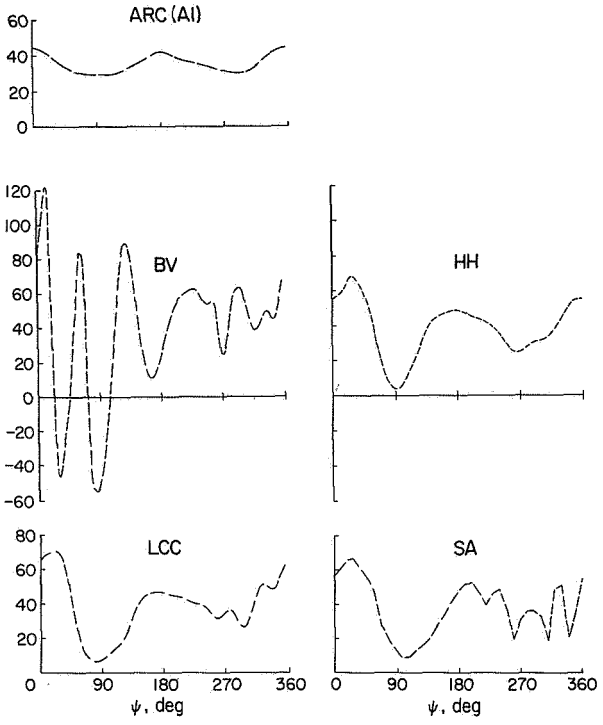

Fig. 7.– Lift airload (lb/in.) vs. azimuth; r = 0.8, Case A3.

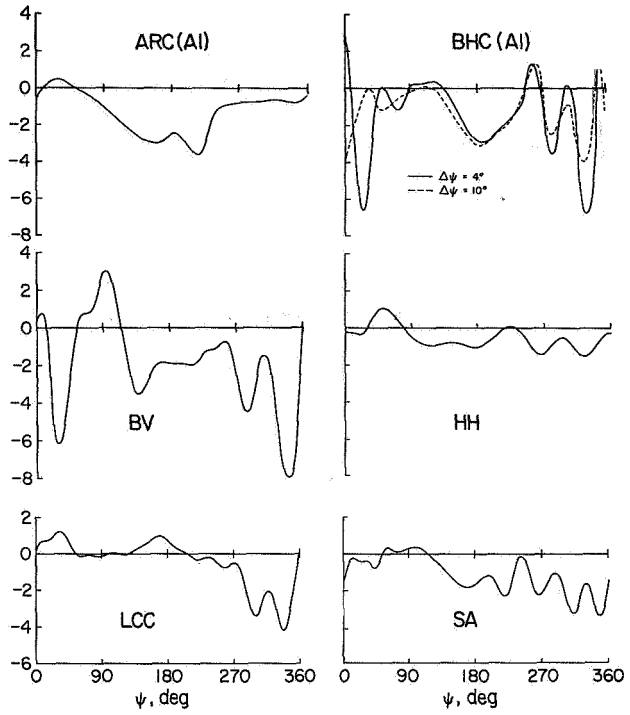

Fig. 8.– Blade tip elastic torsion (deg) vs. azimuth, Case A3.

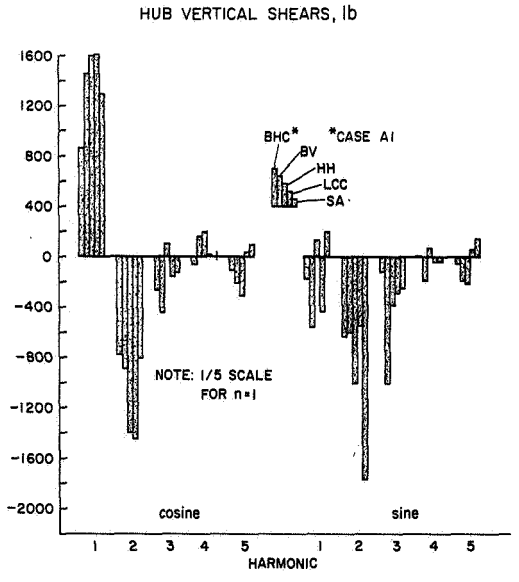

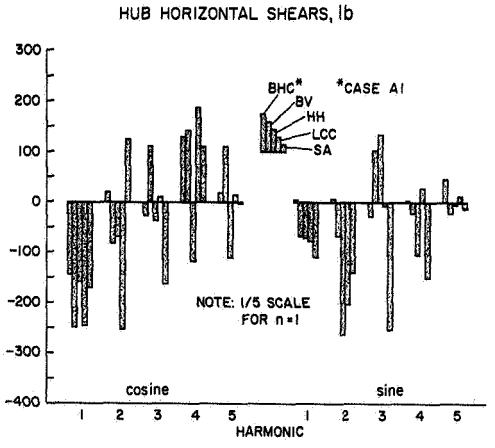

Fig. 9.– Harmonics of hub vibratory shears, Case A3.

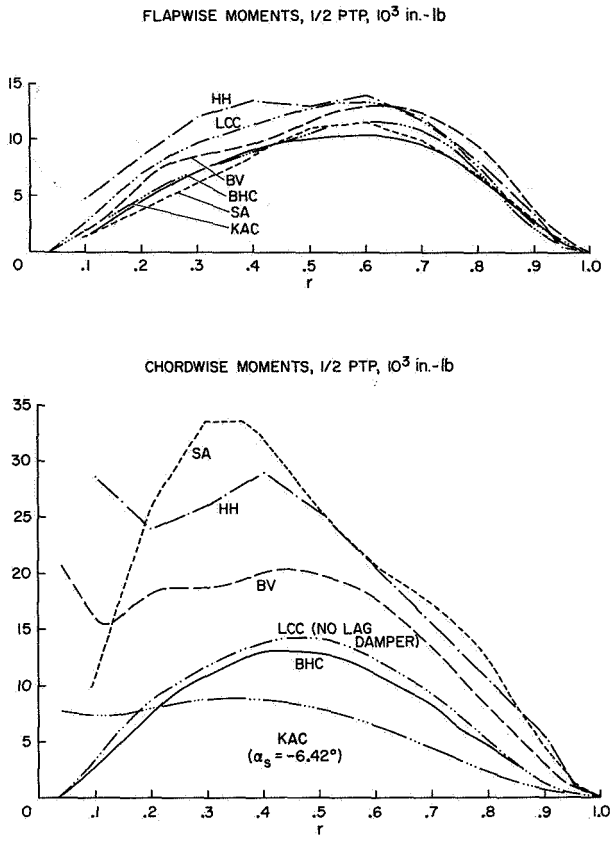

Fig. 10.– Oscillatory blade bending moments, Case A5.

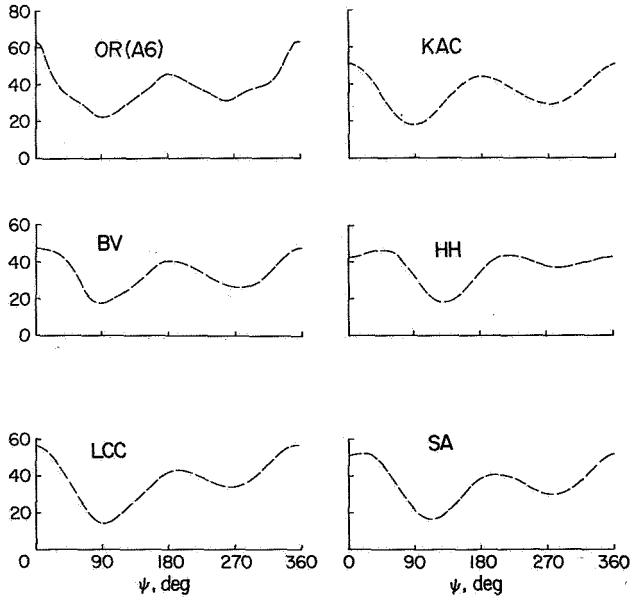

Fig. 11(a).– Lift airload (lb/in.) vs. azimuth; r = 0.8, Case A5.

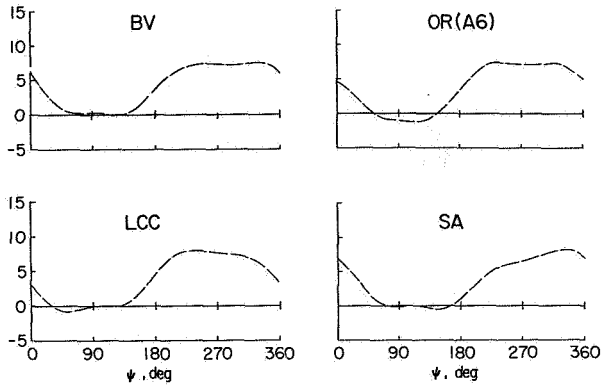

Fig. 11(b).– Drag airload (lb/in.) vs. azimuth; r = 0.8, Case A5.

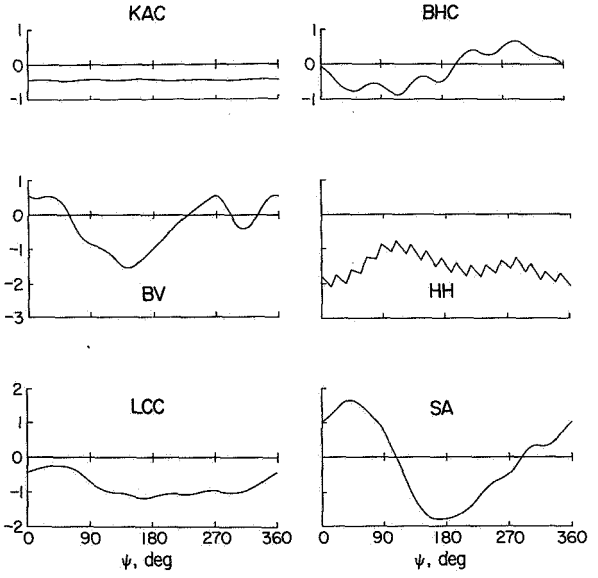

Fig. 12.– Blade tip elastic torsion (deg) vs. azimuth, Case A5.

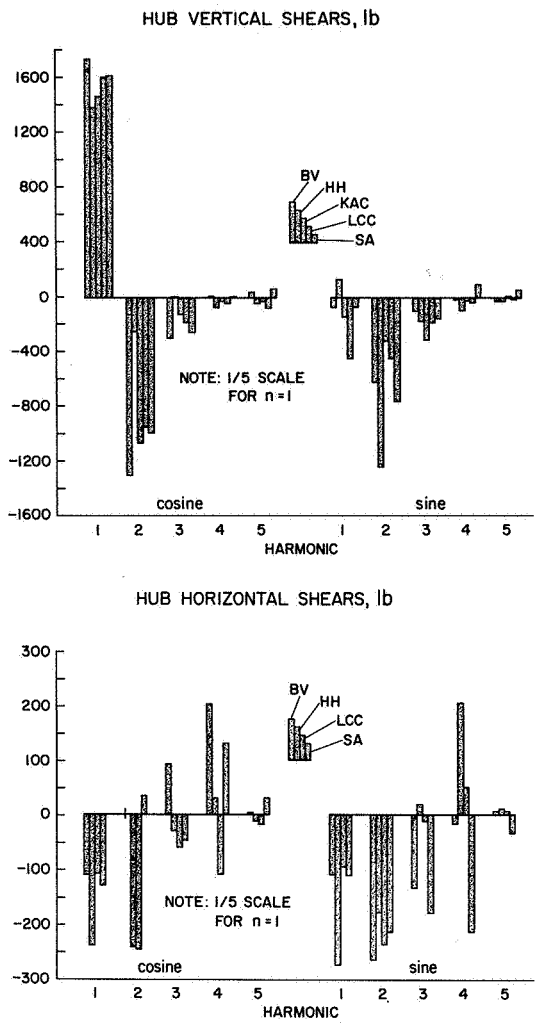

Fig. 13.– Harmonics of hub vibratory shears, Case A5.

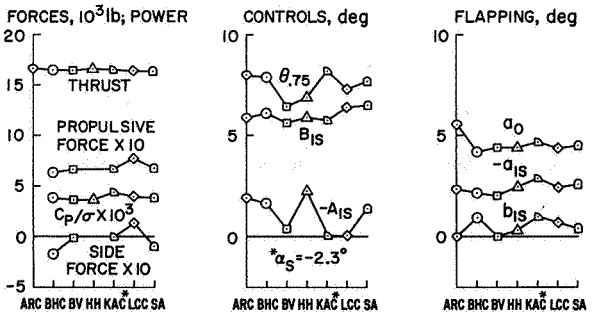

Fig. 14.– Trim parameters, Case B1.

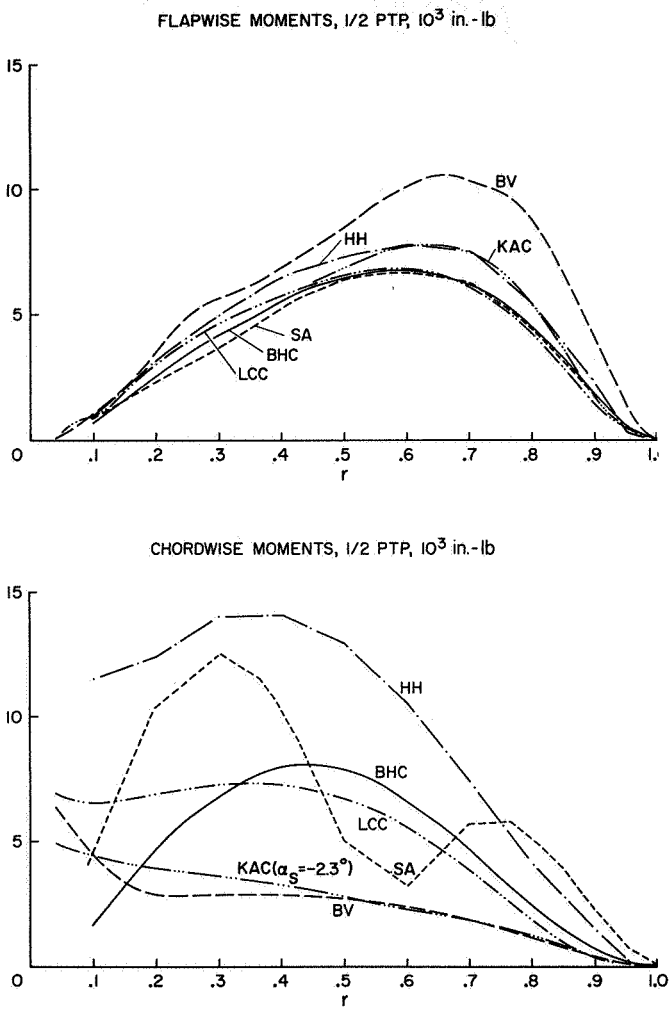

Fig. 15.– Oscillatory blade bending moments, Case B1.

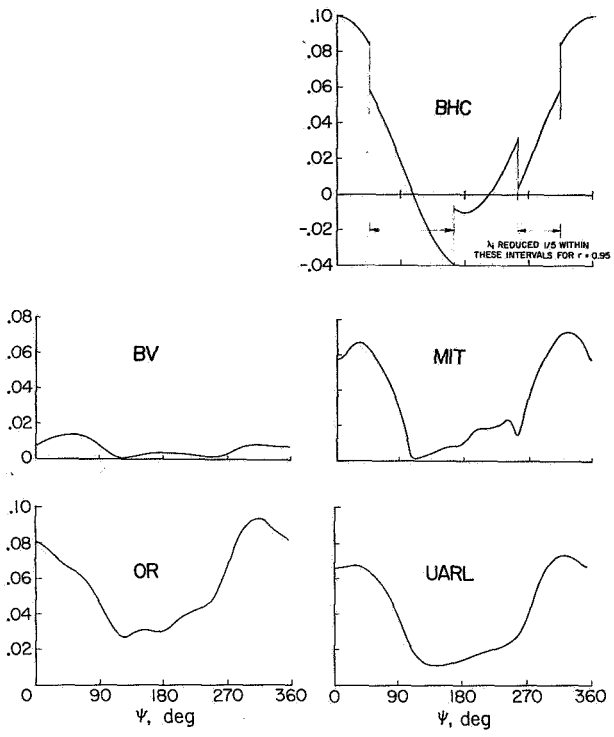

Fig. 16.– Induced downwash, λ_i, vs. azimuth; r = 0.95, Case C2, rigid wake.

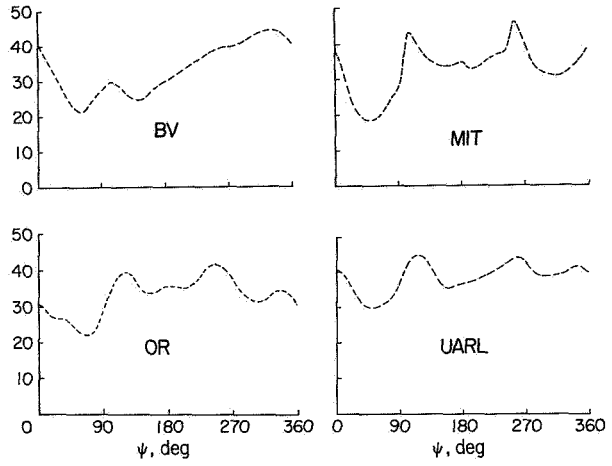

Fig. 17.– Lift airload (lb/in.) vs. azimuth; r = 0.95, Case C2, rigid wake.

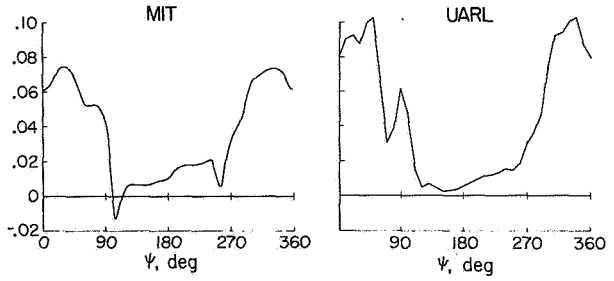

Fig. 18.– Induced downwash, λ_i, vs. azimuth; r = 0.95, Case C1, distorted wake.

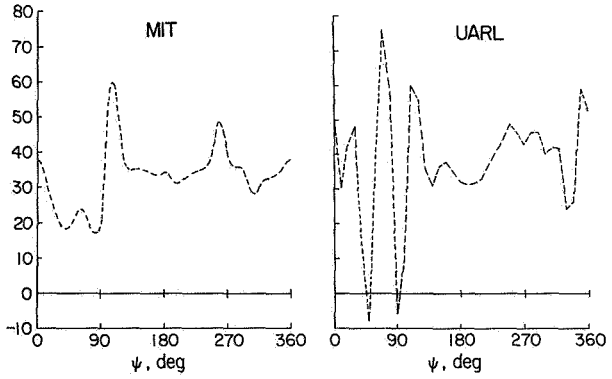

Fig. 19.– Lift airload (lb/in.) vs. azimuth; r = 0.95, Case C1, distorted wake.

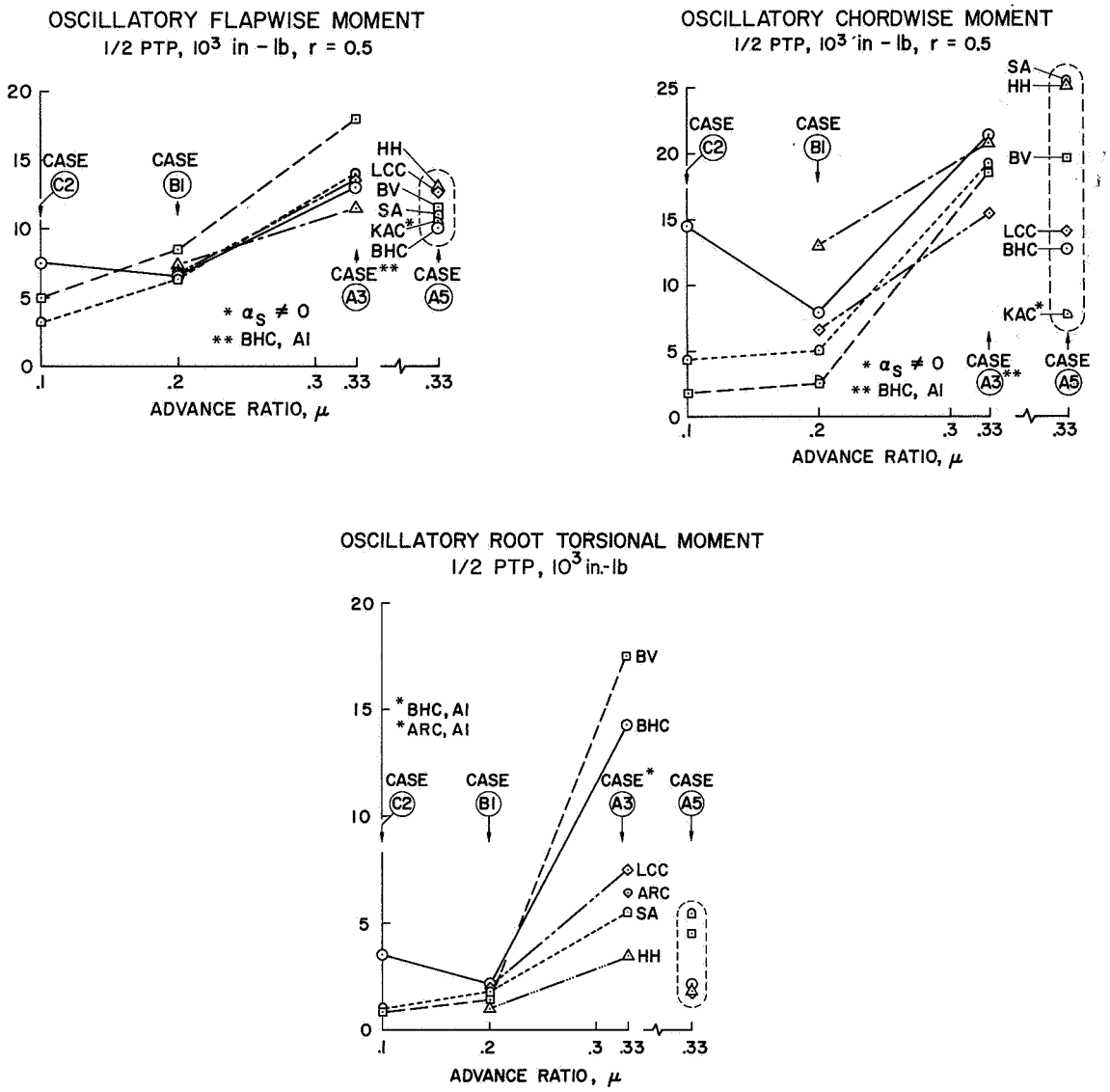

Fig. 20.– Summary of blade oscillatory moments vs. advance ratio.

DISCUSSION

Panel 1: Prediction of Rotor and Control System Loads

Moderator Arcidiacono: First of all, I would like to extend my personal congratulations to Bob Ormiston for the very fine job that he did in coordinating the efforts that went into this paper. To my knowledge, this is the first serious attempt at a comparative study of the various rotor aeroelastic and loads analyses available to the industry. We all know that any analysis at any point in time is the product of a set of assumptions, and I am sure that most of us involved in developing these analyses have wondered at one time or another just how we were doing relative to the other fellow, or whether his analysis would correlate better with our particular test experience. I'm equally sure that in trying to establish our relative positions, we have been frustrated – I know I have been at times – in trying to assess the available literature with its inevitable limited description of assumptions forming the basis for any particular analysis. Or, perhaps – I have been frustrated by the fact that, and I have been guilty of this myself – that the list of assumptions referred to in describing an analysis just refers the reader to a list of references that have to be tracked down. I'm also sure that you have probably heard the phrases that the analysis was fully coupled and that variable inflow is included, and that unsteady aerodynamics were included, without really being sure of or having the time to dig into the details that were necessary to understand the procedures being employed. I think that the mere existence of these frustrations means that technology transfer has, to a certain degree, been inhibited and this in itself, to my mind, is a perfectly adequate justification for Bob Ormiston's paper, because now without any words or *fol de rol*, these are the results, and one can certainly at least calibrate his own analysis relative to other analyses. We have seen the results of the paper now and comments are certainly in order. We have on our panel people who, at least recently, have been responsible for translating $F = ma$ into a useful rotor analysis. These have been introduced by Troy, and I have asked that each panel member speak for 5 minutes, and if time permits, address generally the following subjects: Correlation of their analysis with tests, identification of any clearly unusual trends noted in their own particular results, and perhaps make suggestions for how further checking of analyses of these types could be done. After the prepared comments, we will turn the floor open for discussion and I'm sure there will be a lot of discussion. Now, we are going to take the panel members in alphabetical order, and Bill Anderson will talk first.

Prepared Comments

William D. Anderson
Research-Development Engineer
Lockheed California Co.

First of all, I'd like to again extend appreciation to Bob for the fine job he did here. I'd also like to extend recognition to John Gaidelis back home for his work as a key person in developing the Lockheed rotor loads program, and also really in performing the analyses that were reported here. The Lockheed rotor loads program used in this particular study is a finite element analysis which is capable of up to about 75 spanwise stations. We generally use on the order of 40 or 50. In this particular analysis, as was indicated, we used 23 stations due to the uniformity of the blade characteristics. The analysis is fundamentally a steady maneuver and steady level flight type of analysis and it is incapable of doing a transient maneuver, but we feel that transient maneuvers are equally critical in the design of rotary wing vehicles. We do have another program which most of you are familiar with in name anyway, and that is Rexor, which is much more expensive to run and was not applied because this study was primarily associated with steady flight conditions. The Rexor program is a modal analysis; it does represent the total coupled rotor and airframe. I would also like to say there is one thing that it does include which was brought up earlier in one of the discussions. It does include the reorientation of the structural principal axes which means that it is fully capable of including all the periodic (structural) effects as well. Both programs include stall aerodynamics basically as Tarzanin and Harris have developed. The Rexor program is solved by a numerical integration method and the program that was used here is basically a harmonic response type of analysis which converges in 3 to 4 rotor revolutions. At this time I would like to show some correlation that we have had on some AH-56 data using the program that was actually used in this study. Could I have Slide 2, please.

Slide 2 shows chordwise bending and flap bending at approximately 60% rotor span, and chord bending and flap bending at approximately 6% of rotor span versus equivalent air speed with test data out to 210 knots, which is a little over 220 knots true air speed. The dots and the solid lines represent the cyclic loads. The dots are test data; the solid lines are analysis. The open circles and dashed lines represent steady loads, again test and analysis. You can see fairly good comparison in both the cyclic and the steady loads as a function of forward speed. There is some conservatism in the predicted cyclic loads as we go out in speed for the flapping moments at the 6% span.

Slide 3 shows blade torsion moments at approximately 45% span, as a function of speed, again the cyclic and steady moments are shown with fairly good correlation. Shown also are the steady and cyclic pitch link loads as a function of speed, and the steady collective servo force which is a control load measured in a stationary coordinate system. This of course is sensitive to c_{m_o} of the blade, blade tabbing, etc. Slide 3 shows finally the cyclic collective control loads versus speed. I think that these results show fairly good correlation of the program with Lockheed experience.

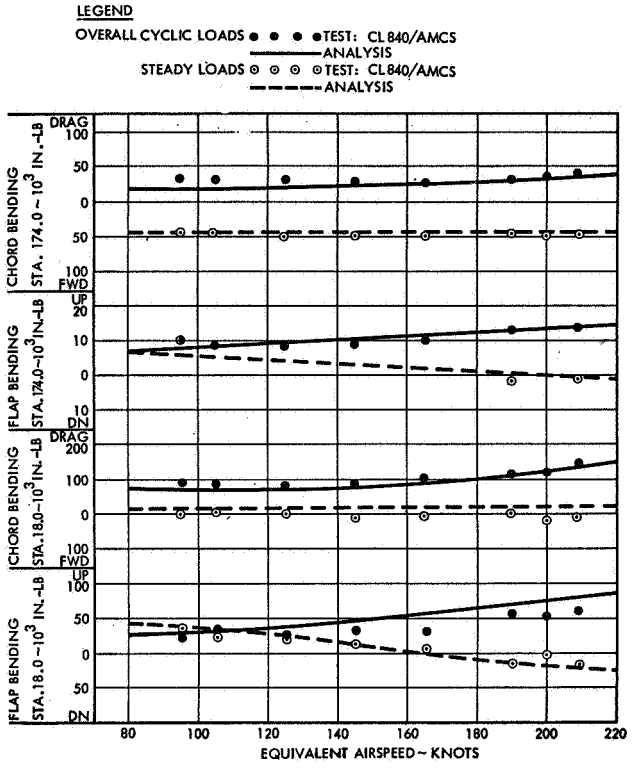

Slide 2.

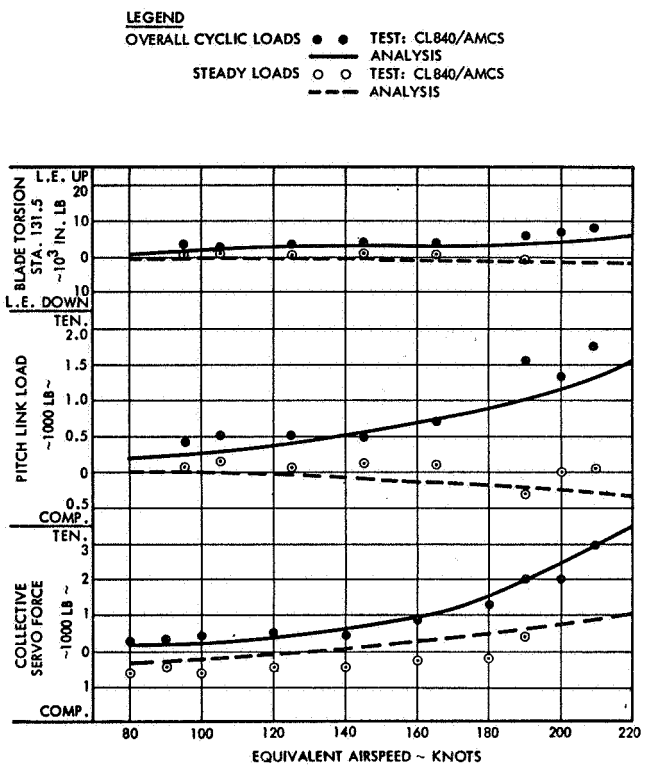

Slide 3.

I would like to say that, relative to the results of the prepared paper, one question that comes to mind is how can we have so many different definitions of the basic NACA 0012 airfoil that has been around for several years? I would also say that the treatment of the lag damper seems to require a little more scrutiny as evidenced by the root bending moments for chordwise bending. I'm not too familiar with how some of the other programs are solved, particularly the modal ones, and I would like to point out that in a modal solution you have to be extremely careful in how the loads are integrated. If one uses the second derivative of the deflection to get internal loads it leads to fairly large discrepancies. And in a modal solution it does take a spanwise integration of each load element times a moment arm to come up with fairly realistic flapwise and chordwise moment distributions.

I would also like to add that with regard to a fallout of rotor loads, vibration that is, it would seem that until a more consistent type of rotor loads prediction method is developed that the prediction of vibration will leave a little bit to be desired, I believe. And finally, I feel that this effort supports the need for the development of a considerably more comprehensive and universal rotorcraft simulation model which is capable of predicting rotor loads and I think it should even be comprehensive enough to be used in the prediction of airframe vibration.

Peter J. Arcidiacono
Head of Rotor Systems Design and Development
Sikorsky Aircraft

I would like to show you some of our correlation, but before getting into that, Slide 4 just shows the relative position of the Sikorsky results, compared to the other analyses on the flapwise, chordwise, and the torsional responses. The Sikorsky results are the solid symbols and the bars indicate the range of the maximum flapwise moment predicted for the B and A cases. The Sikorsky flapwise results tend to be in the mid to low range on flapwise, in the high range on chordwise, and in the mid to low range on the torsion.

In looking at those results I don't think I was surprised by them, generally speaking, except for the result on chordwise, and the reason for that was that we were on the high end and our experience has been that we have tended to underestimate chordwise

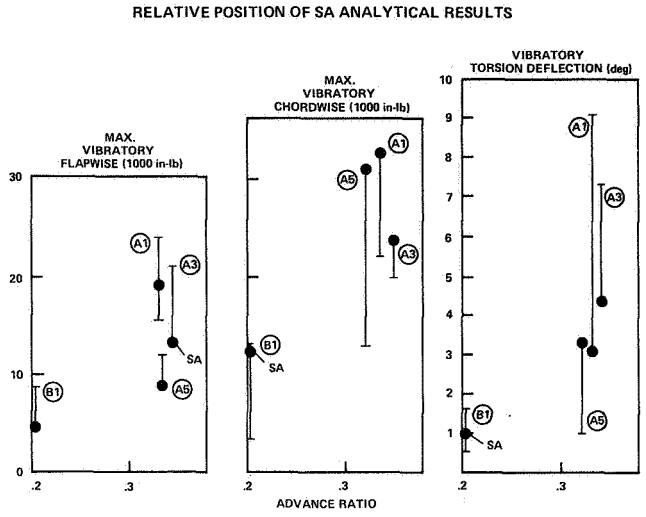

Slide 4.

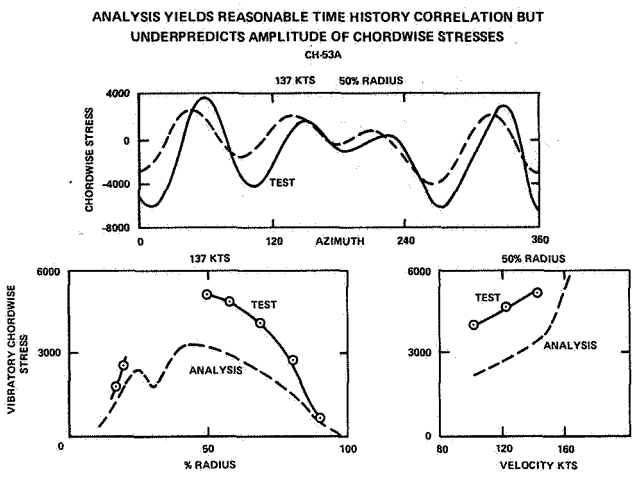

Slide 5.

stresses. I have illustrated that point here on Slide 5 where, for the CH-53A helicopter, we have the time history of chordwise stress at 50% radius. Down here we have the peak vibratory stress as a function of radius, test and analysis, and finally over here we have the vibratory stress as a function of velocity, test and analysis. As you can see, we have been under-predicting chordwise stresses.

Slide 6 is flapwise stresses, and these have been pretty good as far as our experience is concerned, particularly when variable inflow and unsteady aerodynamics have been included, and this shows the peak-to-peak response versus radius and versus velocity. The time history correlations – you saw some of them presented by Ray Carlson the other day – are equally good.

In Slide 4 we were on the low end as far as torsion response was concerned and that tends to be consistent with our experience in correlating with our test information. Slide 7 shows the vibratory control load as a function of speed, in this case for the CH-53A, for two different C_T/σ's, test and analysis. The slide also shows the correlation for two different aircraft, differing primarily in the amount of blade twist. I think this illustrates the point that most of the comparisons that you have seen in Bob's paper are comparisons on an absolute basis, and as we all know, an analysis can still be extremely useful if it can predict qualitative trends, and this we feel is the case here.

Slide 8 summarizes my observations and recommendations. I think the exercise was useful and interesting. I was surprised at

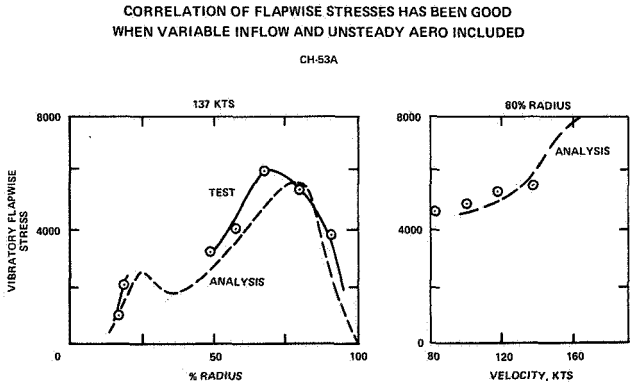

Slide 6.

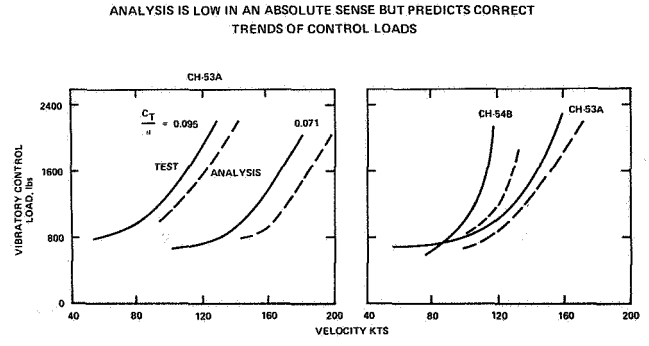

Slide 7.

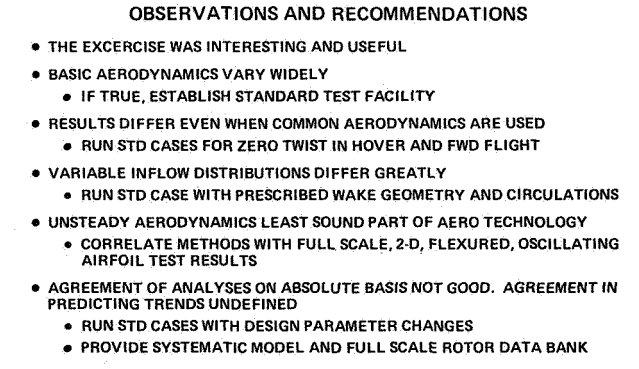

Slide 8.

the 0012 airfoil steady-state data variations, and if that's really true, even after the passage of 10 or 15 years, I think it is ample justification to establish some sort of a standard test facility. However, even when the aerodynamics were pretty much the same, the results differed and I think this seems to suggest the need for running cases with zero twist in hover and in forward flight. I was also somewhat surprised about the variable inflow part of the problem. I had thought there was more agreement on basic technology for variable inflow than perhaps there is. Certainly Cornell Aero Labs showed over 10 years ago that the general trends of inflow could be predicted, and yet even at this late date people either aren't availing themselves of that technology or they don't believe it. Assuming that technology is in hand, I would think some sort of standard case using prescribed wake geometry and prescribed circulations would help isolate questions in that area. I think unsteady aerodynamics is the least sound part of the aerodynamic technology and I agree with Bob Ormiston on doing such tests as full-scale oscillating flexured airfoils, the airfoils being well instrumented. And finally the point I made a moment ago: on an absolute basis the agreement of the analyses in certain areas is not terrific. I think we ought to define how well these analyses predict qualitative trends and I would suggest several standard cases in which systematic parameter variations are made.

Richard L. Bennett
Assistant Group Engineer, Aeromechanics
Bell Helicopter Company

C-81 is a global program that we use at Bell Helicopter that was conceived and brought about to be a useful design tool. I would like to point out that this study that we have just gone through only exercised about 20% of the total program. This study didn't say anything about the maneuvering flight capabilities, the stability routines, or the second rotor analysis. The use of C-81 is widespread, and inhouse it is run on a completely open shop basis, so anyone who wants to can run the program. Consequently, I don't know all of the uses. I do know the uses when they have some difficulty, so one week I made a list of the cases that were brought in for diagnosis. There was the Cobra at 1.9 g's; the Model 301 stability study, there were some questions on the fifth scale articulated rotor in a wind tunnel, another question concerning a C-81 run on an elevator sizing study on the Huey, and finally there were some cases being run for the "Drees Special." At Bell Helicopter the "Drees Special" is the windmill.

I think in this area there is a real need for meaningful correlation studies, and I think that there are four necessary requirements to accomplish this task. The first is that we must have an accurate mathematical model, sound in theory and well programmed. Second, there must be an accurate source of input data that is readily available. Many of these programs, C-81 included, sometimes call for input data that are just a wee bit fuzzy. Third, there has to be a source of test data that can be certified. And fourth, there has to be compatibility of the above three items.

One of the questions that comes up is, why the proliferation of so many different rotor analyses? I think part of it has come about because someone writes $I\ddot{\beta}$. They go out to the flight test, they get their results, and they try to compare the measured and the calculated, and naturally they don't compare. So what is the obvious conclusion? Let's start over again and write $I\ddot{\beta}$ in a different coordinate system. Maybe that will help.

Right now at Bell Helicopter we are in the middle of a correlation study using the results obtained from a 1/5 scale 4-bladed articulated rotor that was tested by Sikorsky Aircraft. We set out with very noble intentions on this contract. Sikorsky did a tremendous job in gathering the data, the physical properties of the blade – mass, stiffness – and they conducted a two-dimensional wind tunnel test to get the airfoil properties, and then they went into the tunnel. In our correlation effort it suddenly became very apparent that there are aerodynamic considerations for the model rotor that are not included in C-81, because we could get nowhere near the C_T/σ measured, using the 2-D airfoil data.

Also, we are in the process of trying to come up with a definition of: What is correlation? By definition, all correlation is good, it's fair, or it's excellent. At Bell, when someone asks me about correlation, I usually tell them that correlation, like beauty, is in the eye of the beholder. So we must come up with a good definition, a workable definition of correlation. I would propose as a continuation of this study started by Bob Ormiston to continue in the same general approach that we started on the Sikorsky correlation program, and I would propose the fabrication and test of a full-scale 0012 rotor system with known physical properties. Quite often the question comes up – what is the torsional rigidity of a UH-1D main rotor blade? This is a very complicated question. I can assure that the results calculated by C-81 will be no better than those input data. So let's go through the process on a 0012 blade. I would next think that we should take that rotor system into a vacuum chamber test similar to what NASA Langley is doing. We should then take that airfoil into a two-dimensional tunnel for tests, because in regard to what Pete said, there's a wide variety of c_ℓ and c_d. The last point I want to make is I feel that in the helicopter business – in the loads prediction – there is a field that hasn't been brought to bear, and that is statistics. The statistical design of wind tunnel tests, and the statistical treatment of the measured data. I feel that if we can continue our correlation efforts, meaningful correlations, we can establish the integrity of these global type programs, and in the final result we will come up with a better and a cheaper helicopter.

Wayne Johnson
Research Scientist
USAAMRDL, Ames Directorate

The results Dr. Ormiston has shown us have included many different assumptions and it's my own conclusion that the multitude of different results from current programs may be traced to the fact that we are dealing with phenomena that in many cases are on the edge of the current state-of-the-art, in structures and dynamics, and particularly in aerodynamics, and I'd like to concentrate my comments on a couple of the aerodynamic elements. Even a calculation with everything fixed but the representation of airfoil lift, drag, and moment coefficients at stall levels – even that comparison shows significant differences using the various dynamic stall models available. You find that the prediction of the overall performance parameters at high thrust is about the same, but there are still differences, from 30-50% in the peak-to-peak torsion and bending moments. And when you get down to the detailed characteristics of the aerodynamic lift and moment variation, you find that those differ very greatly, so it is quite evident that considerable fundamental research remains to be done in this area, and I think the state-of-the-art is in a similar position with vortex induced loads. It is interesting that both of these problems involve viscous three-dimensional aerodynamics which I think is probably the basic reason that they are so complicated and difficult to solve.

I believe that some additional calculations of the type shown by Dr. Ormiston might be useful to isolate the specific differences as much as possible. In other words, concentrating on just the differences in the structural or the aerodynamic models. It has to be recognized, however, as I am sure all the members on this panel do now, that these calculations involve a considerable amount of work. It would also be very helpful to have some more detailed descriptions of the capabilities and limitations and assumptions of the existing methods. That alone would go a long way toward improving the assessment of the existing programs.

One thing that is required in the area of experimental rotor airloads work, I think, is a greater attempt to measure more elements in this complicated interactive system. For example, besides just the blade airloads and blade motion, a simultaneous measurement also of the wake tip vortex geometry and induced velocity and the blade stresses is needed as well. With more information about the intermediate steps, it would allow a more direct assessment of the existing methods and also facilitate the development of better methods. It is clear, of course, that conducting such a test would be quite a job.

Andrew Z. Lemnios
Chief Research Engineer
Kaman Aerospace Corporation

In light of Bob Ormiston's comparison of all the analyses to date, I would suggest that perhaps we should modify Newton's second law to $F = Kma$ where K is a function of the individual investigator. Along those lines, incidentally, I would like to apologize to Bob for not getting our results to him in time to be included in his presentation but they will be included in the written version of his paper. I would just very briefly like to explain the aeroelastic loads program that we use at Kaman, and how we couple that into our blade bending moments program. It is primarily a harmonic analysis program.

Slide 9 shows primarily what we call our rotor blade design loop, and as you can see, we get our inputs from our various departments, our weights group and our stress group to give us our weight and stiffness distributions. From our weights department we get a breakdown of the blade weight as a function of many rotor stations and, obviously, our computer program can't handle that so we have to re-configure the whole blade and that takes a few days or even a few weeks perhaps, especially for the nonlinear type of mass distributions we are talking about. I'd like to get into a little bit more of that later on. Also, the same thing from our stress group and then finally after we have all of our physical characteristics we go through and get our blade statics and dynamics and go into our aeroelasticity and trim program which is what we call our 6F program, six modes of freedom. This is then used to evaluate blade stability from a linear standpoint and then we go into a nonlinear iteration procedure which is basically a harmonic analysis to calculate the airloads over a trimmed condition, and we force rotor trim to user specified hub forces and we just allow the control inputs to vary until we do get those forces at the hub. We then output all of the rotor performance characteristics. The airloads are then harmonically analyzed from the aeroelasticity program and are input into what we call our blade bending program, which is again basically a harmonic analysis, and these are used as forcing functions to generate the flapwise responses and edgewise

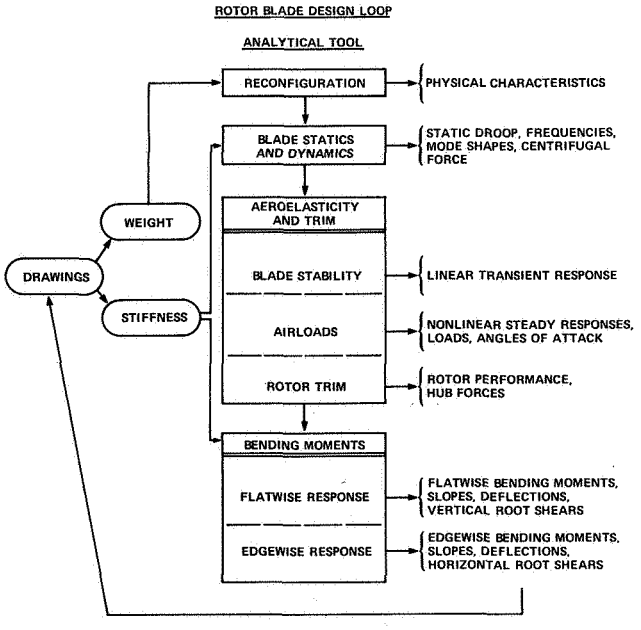

Slide 9.

responses of the entire rotor system. Slide 10 shows basically what is involved in the aeroelasticity program. We have the six modes – four rigid body modes – used for the stability analysis. Also, when we get into the nonlinear equations we incorporate all of the higher order nonlinear terms. For airfoil data we have tables of c_ℓ, c_d, and c_m as a function of angle of attack and Mach number. We do not have the unsteady airfoil data that were generated either by Sikorsky or Vertol, we just have an approximation using Theodorsen derivatives which are truly applicable only in linear incompressible flow.

COUPLED BLADE MOTIONS

- *FLAPPING
- *FEATHERING
- *LAGGING
- *SERVO FLAP
- *FLAPWISE BENDING
- *TORSION

COUPLED INERTIA TERMS

- *CORIOLIS ACCELERATIONS
- *HIGHER ORDER NONLINEAR TERMS

REAL AIRFOIL DATA

- *ANGLE OF ATTACK
- *FLAP ANGLE
- *MACH NUMBER

Slide 10.

I would like to echo Bill Anderson's comments regarding the lag damper. We have found that the lag damper characteristics are some of the least known characteristics that not only we but other manufacturers have, or don't have. For example, it has been assumed in most instances that when you talk about a damping rate for a lag damper you have a constant damping rate, and this is applicable over the entire range of frequencies. Well, this is quite valid and it's very good when you are talking about the rigid body lag mode. However, if you are going to apply a lag damper to a system, unfortunately it also works in the first edgewise mode and the second edgewise mode, and your lag damper has a very nasty dropoff characteristic in damping rate as you go up in frequency, and a very equally nasty buildup in liquid spring rate as you go up in frequency. So your higher frequency edgewise modes could be seeing effectively a cantilever root condition rather than a pin-ended damped root condition. This is something I think that needs to be further investigated and also something that needs further definition as far as the lag dampers themselves are concerned. Pop off valves and nonlinear characteristics of the lag damper are things that we all recognize physically, but yet we don't model very accurately in a mathematical sense.

I would like to ditto again Bill and Pete's comments regarding steady and unsteady airfoil data. I highly recommend that we get some government agency back in the business again of generating some very reliable and useful airfoil data, both steady and unsteady.

Richard H. MacNeal
President
The MacNeal-Schwendler Corporation

I'm basically a stand-in for Jim Neff who did the actual work, so it perhaps is a little less self-serving if I add my congratulations to Bob Ormiston for what I consider to be a landmark achievement.

Pete Arcidiacono sent around a letter to all of us prospective panelists in which he solicited some written comments and I didn't get around to sending mine in, but I think the questions he asked are very good, so I will repeat the questions, and I will give my particular answers.

First question: What general type of correlation have you experienced in the prediction of flatwise, chordwise, and torsional moments at conditions near maximum steady flight speed? I'm a little hesitant to answer that one in view of the lack of correlation we have seen. Until I came here today I used to think that we got around 25% agreement between the peak values as measured in flight test and as calculated by SADSAM. In some cases I'm sure it's true, perhaps in others it is not.

Second question: What do you feel are the most important potentially critical assumptions (if any) of your program in each of the following areas? Aerodynamics: It obviously has to be in connection with the static airfoil characteristics, I believe the moment coefficient is probably the most important one and the one that is least well known. Also, in connection with the method of dynamic stall which is used, which quite apparently, if you look at the results in detail, show that quite a lot of differences must exist in this area. Dynamics: In our program SADSAM – it is a fully coupled method – the most important assumption that we make is that the mechanical coupling effects are linearized about an average, deformed blade position, with one exception, which is that the Coriolis effects are treated in a nonlinear fashion. Method of solution: We use the SADSAM program which I might say is available at public data centers in case anyone wishes to use it. It is the only method of the group that was shown that at the same time uses a transient method of analysis in the time domain coupled with a non-modal solution. There are certain advantages to this I believe. In the first case, the transient method will show any potential instabilities whereas the harmonic method will not necessarily do that, and the direct method as opposed to modal avoids the problem of the lag hinge damper – not showing sufficiently high stresses.

Third question: Which of the following would you recommend for evaluation of the various programs? (a) Further analytic computations using standard cases: Yes, I believe we should as a first instance try to resolve the discrepancies between the various

calculations. This maybe means peeking at the answers, which would be fundamentally experimental. (b) Experiments: I believe we ought to have wind tunnel tests on a simplified rotor where we know the facts about it very well. In the area of fundamental technology, we should do a great deal more to try to get common aerodynamic data.

Question 4: What do you think has led to the current situation which is characterized by a multitude of programs yielding quite different results? Answer in 25 words or less. I can answer it in six words. First three words: Immaturity of the technology. Second three words: Lack of communication.

Five: Do you feel that we or the government should be working toward a single rotor loads analysis following the general precedents set by NASTRAN? Now, I have a privileged position in answering this question because I worked on NASTRAN. I have a one-word answer to this question: No.

Six: Is there any other major point that you would wish to make? The major point I'd like to make: Please carry on.

Frank J. Tarzanin, Jr.
Chief, Rotor Loads Unit
Boeing Vertol Company

Due to time limitations, I would like to discuss the program correlation for most of the time, and then just quickly go through the other issues. First, I would like to address the flap bending moment problem. Here we have, Slide 11, alternating flap bending moment data versus radial position for the H-34 helicopter. This data was obtained in the Ames full-scale tunnel and the reason we used the wind tunnel data was that we had a wide range of airspeeds from 100 knots to 175 knots, and hopefully we elminate some of the turbulence effects that are experienced in flight tests. The solid line represents the predicted flap bending moment envelope, and the four dots represent the test results. As you can see, the theory generally overpredicts in every case and the highest over-prediction occurs at the high airspeed, generally in the middle of the blade. This over-prediction is not a major concern, since the results are conservative when compared with wind tunnel data, and generally fall well within the bounds of the flight data scatter. In other words, were you to actually get a flight data envelope there would be quite a bit of scatter in it and the analysis would fall within that scatter.

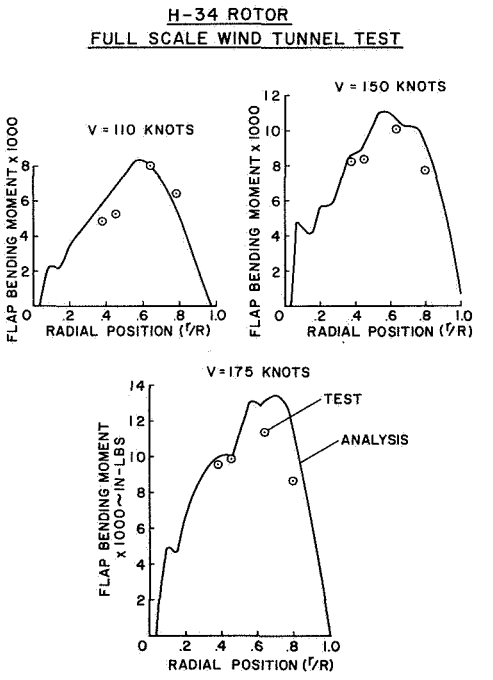

Slide 11.

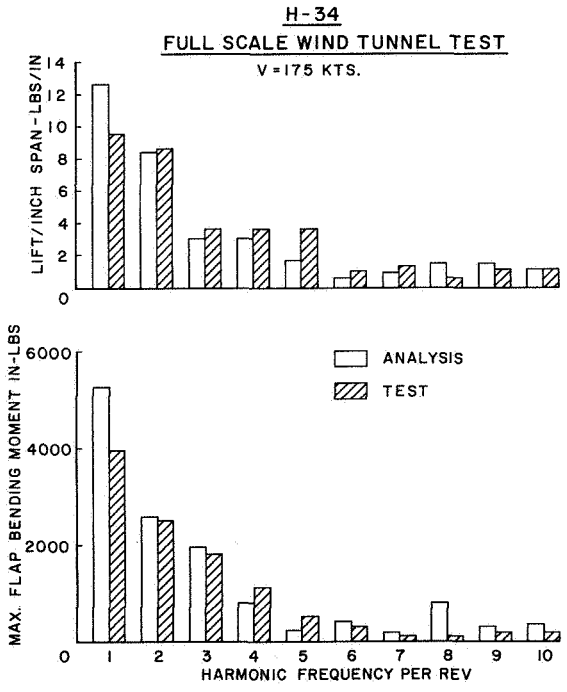

Slide 12.

Slide 12 compares the lift and the flap bending moment harmonic components for the H-34 rotor. This is at the airspeed condition of 175 knots and the radial position is at 65% span, which is where we had the large over-prediction at the 175 knot condition. The analysis is represented by the open bars and the test results by the hash bars. As you can see, the analysis overpredicts the 1 per rev and this explains that the flap bending moment envelope over-prediction is primarily due to the 1 per rev. Now, the 1 per rev is over-predicted in the middle of the blade and not at the root and the tip. I don't know why. If you look at the second, third, and

fourth harmonic components, there is really very good correlation. You can tell that the correlation tends to go downhill quite a bit as you get out to the higher harmonics, and it becomes clear from looking at this that you could expect to predict vibration for rotors with a small number of blades, but as you get out to a higher number of rotor blades the expected correlation I think would go down.

Slide 13 shows the 3 per rev vertical hub loads versus airspeed and the phasing of these hub loads versus airspeed for the CH-46 helicopter. Now, this data was obtained by directly measuring the loads in the hub drive system, the main shaft. The main shaft was instrumented with gauges and then cross-calibrated to get out all the coupling effects, so this is directly measured data. The analysis is the dashed line and the test, the solid line. As you can see, there is really very good correlation, both in the magnitude and the phase, and this is expected if you look at the H-34 results and notice that there was really good correlation – when you look at the 3 per rev airloads and the 3 per rev flap bending moments. And you would expect if you went to a five or seven blade rotor the correlation wouldn't be as good.

Next I would like to discuss the pitch link load correlation. Now, all the previous pitch link load theory/test comparisons that we have shown, were compared with either model wind tunnel data or what we called smooth flight data. Now that was when we carefully went through the flight data and checked the flight cards and found flights where the data was very repeatable and the air was smooth, very little turbulence. In these conditions we found that we either predicted the loads or we were a little high, so this time we tried to just take scatter bands, just a number of flights at a given condition and compare the loads with the scatter of the flight test data.

In Slide 14, we have the CH-47C helicopter at 46,000 lbs. gross weight, 4 in. aft cg, and the C_T/σ of the aft rotor is 0.102. The solid lines represent the range of the measured pitch link loads for five flights. These are supposedly all the same conditions. As you

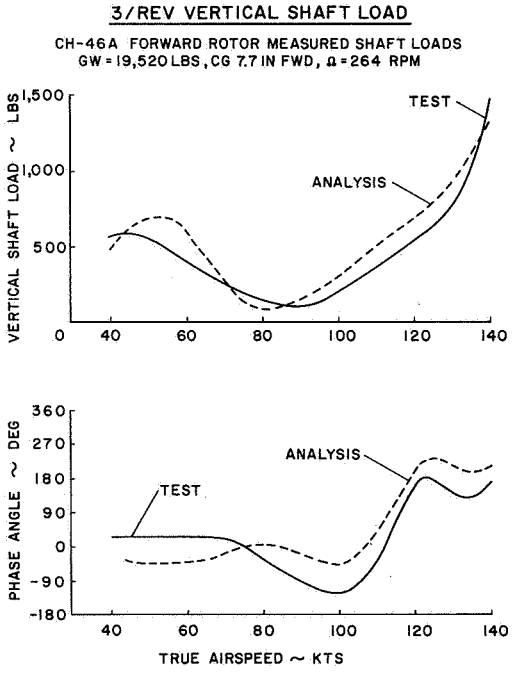

Slide 13.

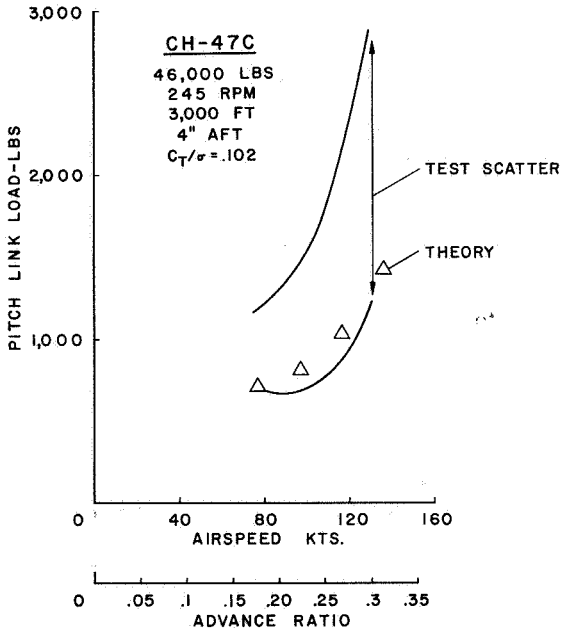

Slide 14.

can see, the theory now predicts just the bottom of the scatter band, so clearly there are turbulence effects and so on that are just raising the loads. In Slide 15, we have the same thing for 50,000 lbs. gross weight, again this is for three flights. Again, a very large scatter band and the analysis is just predicting the lower end of this band.

Last, and you can see why it's last, is the chord bending moment in Slide 16. Typically, we have not been able to predict the chord bending moment. Here we have chord bending moment versus airspeed. This is the maximum bending moment, and the analysis is predicting only about 40% to 60% of that load. Now, we have done a number of investigations and discovered that the equivalent viscous damping at the root end plays a very important role in determining what the maximum loads are. As you can see in the lower figure, we have been able to bring this predicted chord bending moment up to the test data by raising the equivalent viscous damping from 23,000 to 60,000. Now, really this is not an appropriate way to represent the damping. It is a much more complicated phenomena. There is a pre-load, there is a frequency effect, and an equivalent viscous damping doesn't seem to be adequate. Other things that may affect it are the actual chordwise stiffness. If you try to calculate chordwise stiffness, you have to consider if the

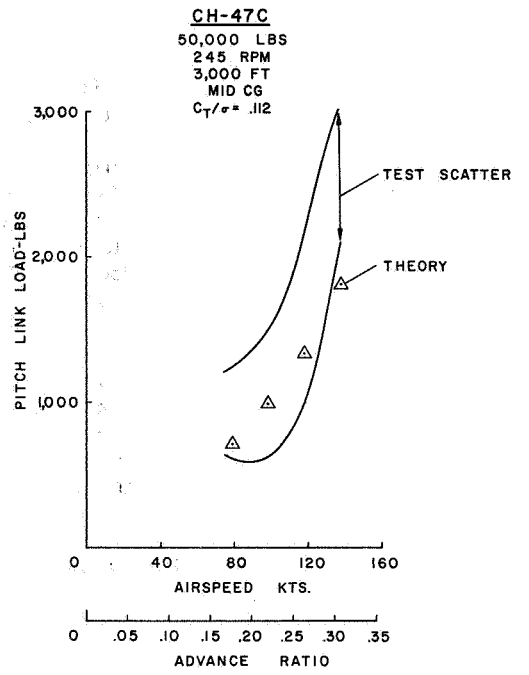

Slide 15.

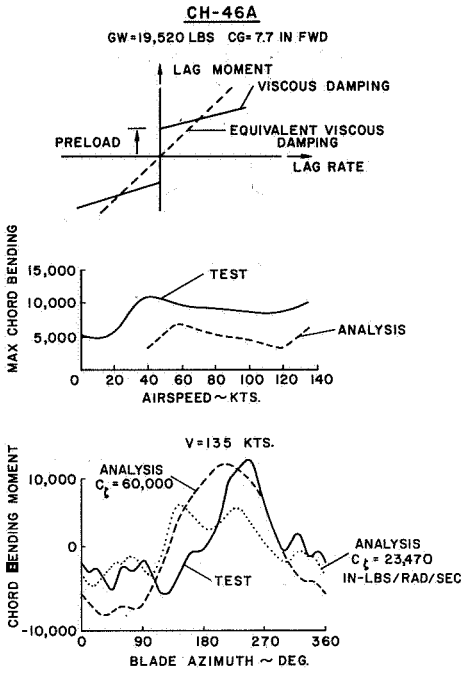

Slide 16.

trailing edge is buckling, or how effective are the skins, and so on. Another thing is the coupling. The C-60 program does not couple chord bending. It is coupled in flap/pitch, and chord bending is done at the end, uncoupled, and this may play a role, and finally the drive system. Charlie Fredrickson has shown that the drive system could play a very important role in determining the coupled modes of the chord bending. So this summarizes the correlation.

I'd like to make one little comment on the downwash. On the downwash plots it was shown that the Boeing Vertol analysis was predicting about 1/10 of the induced velocity at the 80% radial station. We use an analysis very similar to Sikorsky's and what happened was that when we originally did the calculations, we had the same order of magnitude results for downwash that they had. But we had some flight data where we flew the CH-47C, which is a tandem, and varied the pitch attitude until we got the downwash from the forward rotor to run right into the aft rotor. When we tried to correlate with these loads we found that the theory was greatly over-predicting the flap bending moment. We went back, scratched our heads, and tried to figure out why. Well, we started iterating the downwash on itself. In other words, we let the downwash prediction affect the lift distribution and that would then give a new downwash distribution, which we fed back again on the lift, and we continued doing this iteration and we discovered that the tip vortex strength went down to somewhere between 1/6 and 1/10 of its original value, depending on the flight condition. So when we put that back into the analysis – at that worst condition – we found out that the load was now correlated. We then ran the normal separated conditions where the vortex was not running right back into the next blade and we found the correlation was still O.K., so we continued using this method of iterating the downwash on itself.

One final thing – I think we should continue with this work.

Richard P. White, Jr.
Executive Vice President and Director of Engineering
Rochester Applied Science Associates, Inc.

As you probably noticed, I don't have any results up there. We at RASA have been working for about 6 years in developing various computer programs for rotor loads prediction, and free wakes, for NASA. I just couldn't find a way to finance this study, but I thought it would be very interesting if we could have because I'm not as discouraged as some of the other panelists. In the work that we have been doing we haven't really had the opportunity to have our own type of hardware to try to correlate data with. In the correlation we have obtained in the development and checkout of these programs, we have had to use what is published, i.e., what is available without all the background behind it. In doing that we have found that you have to look in very great detail at certain things you might not expect. I think that many times in the industry, probably when they are working with their own rotor system they can find a way that they can turn a knob to obtain very good correlation with their rotor system. I think this is why I am not so discouraged. You might have gotten the feeling that from the results that you saw, that rotor loads prediction analysis ain't worth a "Billy-be-damned." I don't think that's true. I think within each company, the way they have developed their programs for their rotor

systems, and the knowledge they have of their rotor systems, I think, and some of them have shown this, that the use of their program for their rotor systems does a far better job than it would do, necessarily, for somebody else's rotor system. In some respects that's not too surprising, because a lot of the input is a function of art and not science.

A couple of comments that I do want to make. What did surprise me in the results was that since (how much it might be laid to the difference in airfoil characteristics I don't know) the first three harmonics of loading are generated just by the trim control settings and q, I was surprised to see the large variation in the predicted results of the various theories and I can't lay it to the analysis being developed for one theory or another. It's too fundamental and too basic. A number of years ago, using published loads data taken for the H-34, UH-1A, and the XH-51, I worked out a non-dimensionalizing parameter that had advance ratio and loads and the loading functions of the load that the total rotor system was carrying, and I found a very interesting thing. Here we had three different types of rotor systems, three different types of characteristics that were rather dramatically different. The first three harmonics of the sine and cosine functions laid right on top of each other. So there is not a big difference in these lower harmonics of the rotor and I'm a little surprised that we can't do a better job of prediction. A lot of the work and association that I have had with rotor loads has been the inclusion of wake analyses, free wake effects, and I think from what you saw today, the wake effect is an important effect. The free wake as compared to the prescribed wake is an important effect, and it's kind of surprising to me as well that on the two prescribed wake calculations that were done, the induced velocity distributions were so different. Maybe we're having trouble computing what the strength of the tip vortex is. I think that the reason for the work that has been done by a number of investigators starting way back with Ray Piziali and Frank DuWaldt, was based on the premise that you ought to be able to predict the lower harmonics of rotor loading very well, and I think maybe 10 years ago we were doing a better job maybe than we are indicating now. So what did we do? We said, "Gee, what you need is the wake effects in there to get the higher harmonic loading functions," and Frank and Ray showed that this could be done and then the industry picked it up and they worked it in their own way, which they should have done, and maybe because we have complicated the program so damn much to get the higher harmonics in, we have screwed up all the lower harmonics. I don't believe it. If the majority of the industry is computing the loads for their own rotor system, I expect almost excellent agreement and I'd believe the agreement in the lower harmonics. I do think there is more work that needs to be done, and I think Bob ought to take the responsibility for it and I think he ought to get himself a fairly refined rotor system, build the blades, incorporate the structural features and things that are needed in it, put instrumentation all over the place, and run some very controlled experiments to investigate the various areas that were proposed in the calculations that were conducted, and then he should spend the rest of his life analyzing that data so we would have some good consistent data. He opened up the Pandora's box, now he's got to get all the pieces in it [so] that we all have something to work with. He needs the induced velocity distribution, the loads, the responses, etc. I think it would be very bad if we did what we did in the past with the H-34, the UH-1A, the XH-51, all the data was collected, it was all tabulated and put in thick reports and everybody got a copy and it went up on the shelf and that's the last time anybody really looked at it, except if they are looking for one particular point. I think in many respects that was a waste of money. All that data was there but never really analyzed. I would hate to see it repeated again.

SURVEY OF PANELISTS

Panel 1: Prediction of Rotor and Control System Loads

Moderator P. J. Arcidiacono posed five questions to the members of Panel 1 before the meeting. A summary of the responses was to be presented at the conclusion of the panel discussion, however time was not available for this. The responses are pertinent to the attendee's questions and the panelists' discussion and warrant inclusion in these Proceedings. Responses to the questions were optional and not all members responded. The following summary of their responses was prepared by the moderator.

1. What general type of correlation have you experienced in the prediction of flatwise, chordwise and torsional moments at conditions near maximum steady flight speed?

   - Flatwise moments (3 replies: Boeing, Kaman, Sikorsky): Predictions quoted to be within ±10%.
   - Edgewise moments (2 replies: Boeing, Sikorsky): Predictions low by 20 to 40%.
   - Torsion moment (4 replies: Boeing, Sikorsky, Kaman, RASA): Results inconsistent, indicating this is the most difficult to predict.

2. What do you feel are the most important potentially critical assumptions (if any) of your program in each of the following areas?

   - Aerodynamics (5 replies): Unsteady aerodynamics were *unanimously* chosen as being of concern.
   - Dynamics (5 replies): Most answers indicated a concern as to whether all of the dynamic coupling terms had been included.
   - Method of solution (This refers to the techniques used to solve whatever dynamic and aerodynamic equations have been deemed worthy of solution): Not much concern expressed here but two replies indicated that the harmonic method may result in some limitations.

3. Which of the following would you recommend for further evaluation of the various programs?

   a) Further analytical computations using standard cases: Five of seven responding endorsed further work here. (This time a funded effort, however.)

   b) Experiments

      1) Rotor: General agreement on need for systematic detailed data on large scale rotors tested in the 40 X 80 wind tunnel. Only one response also recommended smaller scale model tests as well.

      2) Fundamental technology: Steady and unsteady airfoil tests by NASA were the only specific tests recommended. In general, industry members appeared to favor rotor tests at this time rather than fundamental technology work.

4. What do you think has led to the current situation which is characterized by a multitude of programs yielding (in some areas) quite different results? (25 words or less)

   This has resulted from the basic evolutionary nature of the scientific method which calls for hypothesis, correlation with test, revised hypothesis, test, etc. The process has tended to go on relatively independently in each company. The resulting analyses are molded by the data available to each group. To the extent that the data correspond to different configurations which may emphasize different aspects of the same overall problem, different groups will inevitably evolve somewhat different methods. This situation has been aggravated by the lack of systematic test data (and funds in some cases) against which to thoroughly correlate the analysis. Perhaps when all things are considered, the comparisons are really fairly close.

5. Do you feel that we or the Government should be working toward a single rotor loads analysis following the general precedents set by NASTRAN?

   Seven replies received: Three no, two yes and two possibly. In general, there seemed to be some desire for such a program but a great deal of skeptism as to whether it was practical or even possible. There was concern as to whether any program could be general enough to anticipate all future configurations. For example, if such a program had been developed 10 years ago, would it have included all the hingeless rotor design variables since found to be important? One of the no responses stated that the money would be better spent supporting systematic rotor parametric tests. Also, of particular interest was the response of Dick MacNeal, who, of course, has been directly involved with NASTRAN. He was definitely opposed.

QUESTIONS AND ANSWERS

Panel 1: Prediction of Rotor and Control System Loads

Bob Wood, Lockheed California Co.: I would like to again congratulate Bob for the study and also make several comments. In particular, I would like to just raise the question that has frequently been brought up, if we had a standardized method. I think if we had a standardized method, I think we would still face this F = Kma point that was brought up by the panel to some extent. There are, within each rotor system, variables that would have to be introduced by the manufacturers that would not be included in the model. Let me give several examples: Leading edge balance bars. Some of the manufacturers, for example, integrate these intergrally into the spar, which means that the CF load is picked up integrally along the blade. Others let all of that CF load be transferred right to the tip, which means then that you have a moment. That probably would not be incorporated in a universal model. Secondly, the lag damper, of course, also varies from manufacturer to manufacturer, and generally may have a relief valve and is highly nonlinear. Another aspect that we at Lockheed got involved in was in implementing the Bell C-81 global program. We found that in using it, of course it was developed for a hard swashplate control system, so we had to take one whole section of that program and remove it to put in the gyro control and the flapping feedback which are characteristic of the Lockheed rotor system. So I think even if we had a standardized method it would be tailored as it was picked up by the manufacturers. But I am curious with respect to Dick MacNeal's comment, having been one of the primary participants in the NASTRAN thing, as to what his reason is for saying no to having a standardized method since we are actually saying here that we would like to have standardized input but non-standardized methods. I'd like to hear your comment, Dick, if I could.

MacNeal: I see I didn't get away with my one-word answer. I think that there is great virtue in diversity, particularly when there is a great deal of doubt as to the physics of the problem, the methods of analysis, etc. If we settle on one particular approach, we will all use it and we will all go over the cliff together like lemmings going into the sea.

Frank Harris, Boeing Vertol: Well, I have been over to the wind tunnel for the last 4 years and now I'm here and I think this problem sort of looks like a charcoal broiled steak, it's very well done on the outside and pretty damn bloody in the inside. I can't help but tell you that as the proceeding went on here I got madder and madder and madder, and I'll tell you why. I'm here at a dynamics meeting and yet at the conclusion I hear that everything is going to work fine if we get the dynamic stall. There's Ericsson to blame, Reding to blame, Tarzanin, Carta, "None," and Harris, and I refuse to sit here and accept the blame for what is obviously a problem. Then you complained that the wake isn't correct, so you are going to work on Piziali and DuWaldt and Scully at your next meeting probably. I think this is an excellent table that you have summarized here, but I don't think there is a guy in the room here, or two guys in the room that could write the equations from Lagrange, or work a list of equations of ma, and I personally wouldn't go one step further until I could see somebody write down ma. You've got a good chance to do it, you don't have any air particles to contend with, it's all structure. So maybe there ought to be 5 guys that sit down and if those 5 guys could write and then program successfully and numerically evaluate just ma, I would be willing to consider the problem further.

Frank DuWaldt, Calspan Corp.: I have to observe that when industry does its internal comparisons it seems to do much better, and I would like to suggest that this is because they are tuned to their configurations by economics. Therefore my comment is that what we have seen today is the range of disposable ignorance and this is the part that you use to make your configuration look good to everybody else inside.

Bob Wagner, Hughes Helicopters: I think I must take some exception to Frank Harris' comments. But the thing that I saw and felt this morning was a kind of structural connection between what the analysts are getting and what happens in the real world. Maybe the connection is only metaphysical and I think it must be, but those of us who at times have had the problem of taking helicopters off the production line and getting them to a proper degree of smoothness to be delivered, these machines are built presumably to the same specifications, the same drawings, and everything else. Yet, there is as much difference in the behavior of those machines in the real world as is indicated by the differences in the predictions of supposed identical components here. That would result then, in a proposal to perform an analysis, not on identical components, but on components which differ within manufacturing tolerances, and I would not care which analysis is used there. But some of the vibration characteristics that we experience I am sure are related to the differences in the components themselves and not to the differences of the methods of analysis.

Ray Piziali, Vizex, Inc.: Some of the comments have been made by the panel members on how we should make our correlations. I think if you look at what has been done over the years, rather gross comparisons are made. If we all compare the lift values that were predicted up here, they compare very well; if you look at the time history of the lift at one radial station, they don't look quite as good, and if you look at the radial distribution of a given harmonic of the lift, the comparisons become worse and worse. Now for the application for which you are going to use your program, your predictive technique, some things are more important than others so we have no need to look at some of the detail. However, if you are trying to improve your analysis so that you can use it in many different applications, I think we must look at these details, look at the radial distribution of the harmonics of the load, the differences in the generalized force in each degree of freedom, etc.

Ken Amer, Hughes Helicopters: I would like to follow up on Dick MacNeal's comment in answering the question of why he thought that there was such a wide disparity among the various programs, and three of his words were "lack of communication." Right now, as a result of lack of communication, in essence we are each the judge of the accuracy of our own program, and human beings being that way we generally convince ourselves that our programs are pretty good. I would like to suggest that under government sponsorship a critical cross-evaluation of programs. In other words, pick pairs of companies and pay each of the two companies to evaluate the other company's program. Personally, I would rather be criticized and embarrassed by someone else finding an error in my program rather than, on the day my helicopter flies, being embarrassed by finding out I failed to predict the blade loads correctly.

SESSION V

APPLICATION OF DYNAMICS TECHNOLOGY TO HELICOPTER DESIGN

Panel 2: Control of 1/Rev Vibration

Panel Members

William F. Wilson, Moderator	Senior Dynamics Engineer, Bell Helicopter Company
Dale F. Benton	Superintendent of Helicopter Maintenance, Tenneco, Inc.
Raymond G. Carlson	Supervisor, Rotor Dynamics Section, Sikorsky Aircraft
R. J. van der Harten	Deputy Managing Director, KLM Noordzee Helikopters B. V.
Robert Jones	Principal Research Engineer, Kaman Aerospace Corporation
James J. O'Leary	Chief of Dynamics, Boeing Vertol Company

THE USER'S PROBLEM

Operational Viewpoint on Control of One-Per-Rev-Vibrations

R. J. van der Harten
Deputy Managing Director
KLM Noordzee Helikopters B. V.

Our company operates 3 Sikorsky S-61N helicopters on a 24 hr, fully IFR certified, service to oilrigs, and for harbor pilots, to ships on the North Sea. This virtually unrestricted day and night service requires the highest technical reliability of the airframe, its components, instruments and electronics, which can only be achieved by maintaining constant low vibration levels. Also it became clear, when IFR operations became more extensive, in particular for the harbor pilot service, that the tolerance of the crew for vibrations decreased with the increase in workload.

Together with the National Laboratory (NLR) we measured the vibration levels, which we had been able to achieve in two of our aircraft on the basis of pilots acceptance, one being acceptable in one-per-rev (3.4 Hz), but barely acceptable in 5 per-rev (17 Hz) levels, and the other being acceptable in 5-per-rev, but barely acceptable in one-per-rev levels. It was found that:

- pilots accepted only 3.4 Hz acceleration levels at or below 0.005 g laterally and vertically, and 17 Hz acceleration levels at or below 0.07 g laterally and 0.02 g vertically. Higher 17 Hz levels are mainly objectionable, because they cause blurring of instruments and are very fatiguing.

- an increase in 3.4 Hz acceleration levels will increase 17 Hz levels.

With the present S-61N rotor technology, the desired one-per-rev vibration levels could be maintained with a tracking flag method, which I developed as an analysis aid for rotor problems, when in 1955 I had the honor to be Jan Drees experimental test pilot and "ad hoc" vibration engineer for the development of the "Kolibri" ramjet helicopter. Basically this method consists of:

1. Tracking the rotorblades at low and high *rotor rpm* at low pitch, to obtain a reading of changes in track of the blades in relation to each other with rpm changes, thus with airspeed. Trailing edge adjustments were then made to obtain constant track between low and high rpm, being careful to obtain the minimum stick shake (for reversible controls), caused by unequal aerodynamic moment coefficients of the blades.

2. Tracking at low and high *collective pitch* at high rotor rpm, to obtain a reading of a change in track indicating a chordwise balance problem, requiring a change in blade inplane position, relative to each other for two bladed rotors, or indicating an out of phase condition for articulated rotors, which can only be corrected with blade track changes. This is called the phase (or lag) tracking method, indicating that tracking is carried out for best phase instead of track. This is a major point. This discovery became the basis for attaining as low as practical vibration levels possible with the present state-of-the-art.

The method requires very skilled pilots and engineers, and vibrographs if the pilot cannot feel and analyze vibration changes correctly, and can be rather time consuming.

When I was responsible as chief test pilot for a U. S. Army overhaul program of their helicopters, the method was also used successfully on Sikorsky helicopters. As Sikorsky balances their blades dynamically to close tolerances on the rotor tower for equal mass and aerodynamic moments, vertical one-per-rev vibrations were only a problem if blades had been repaired badly, or damaged in handling at the trailing edge. Preventing this last problem with good workshop procedures, only lateral one-per-rev's had to be tackled. A lateral one-per-rev occurs mainly when unequal lift/drag properties of the blades, or damper characteristics, are involved, causing out of phase conditions. If the differences are not too extreme, changes in track of the blades, corresponding to the indications at low and high pitch, and carefully observing the change in vibration level at each adjustment will bring the blades in phase. The correct position in phase will be indicated when vibration levels are below perceptible and/or the blade will maintain correct track, relative to the other blades at low and high collective pitch (e.g., on the S-61N, a 1/4 in. down adjustment in track will decrease blade lag 1/4 in. at the tip). Of course, when using the flag method, it is necessary to make certain that dampers and rotorhead are in good condition, and blades are matched with less than 1000 flight hours difference. When correctly tracked for best phase in this manner, low and high blades may be up to 1 inch apart in track. The aircraft will then be smooth throughout its flight envelope and only needs a retrack if a blade is changed. If you have more than 1 inch out of track you may have trouble with vortices striking the other blades, giving a 5-per-rev vibration.

When the aircraft and it's components became older, however, it was more and more difficult to obtain the best results, because the reason for the "out of phase" condition could not be made visible. Thus it became too much of a trial and error method. Also when using the flag method on the S-61N, it was only possible to obtain a reasonable high collective pitch reading when the wind was calm, due to the turbulent and heavy downwash, which at the length of the tracking flagpole to be used, could lead to blade-tip damage.

Thus we started an investigation of tracking equipment, which would allow the average pilot and mechanic to analyze and solve out of phase problems, which meant that the blade position in phase and track should be made visible even at the highest possible collective pitch position. The best solution seemed to be a stroboscopic system. Tests were carried out with the assistance of the NLR which proved that with this system, out of phase conditions could be made visible even at high collective pitch and wind conditions up to 20 knots. It was however very difficult to analyze the phase pattern, due to the large distance of the blade tips to the cockpit and, even with a concentrated light beam, it was only usable at night. Also the 5 strikers, required for the magnetic pickup to trigger the stroboscope, caused false and erratic phase readings.

Around that time the Naval Air Service, which also became interested in our trials, was approached by the German firm Drello, that, under contract with the German Army, was developing a TV monitored stroboscopic tracking system. This system seemed to present the solutions for most problems because:

- it could be used in daylight.
- it used electronic phase control to keep the reflectors on the monitor, when changing rpm, thus blade phase position.
- it could present selected blade pairs for comparison.
- it presented the pattern of the blades on a monitor, which could be placed in the cockpit, thus enabling the pilot and mechanic to observe the changes of blade pattern with different rpm and pitch conditions.
- it used a photocell to trigger the stroboscope, and thus prevented the inaccuracy found with strikers. This also saves the time for installing the strikers and magnetic pickup.

Last but not least the system was offered at half the price of the Chicago Aerial Industries tracker as used by Sikorsky, which is more accurate. Thus we developed the system with Drello to its present stage, and acquired the first production type tracker in the beginning of last year.

The first actual analysis and track adjustment with the prototype equipment was carried out in 1972 under supervision of Mr. Andy Lapaty, Supervisor of the aerodynamic test section of Sikorsky Aircraft. I must mention that at that time Sikorsky did not believe that track changes that small could cause proportional phase changes. The aircraft concerned was measured for one-per-rev acceleration levels before and after phase tracking. At 100 knots and 120 knots the former lateral acceleration levels of respectively 0.008 g and 0.012 g were found to have decreased to 0.004 g or less. Measurements of the second aircraft which had been phase tracked before revealed even lower figures, namely 0.000 g at 100 knots and 0.0025 g at 120 knots. This last aircraft had already flown 300 hours after the last tracking. In fact, one aircraft flew 600 flight hours without changing its one-per-rev levels, and could have carried on without retrack, except for the fact that a blade had to be changed. Sikorsky has checked the phase tracking method on the rotor tower and on production aircraft confirming these very satisfactory results.

As adjustments for best phase are made for the low to high pitch pattern indications, sometimes a slight increase in lateral one-per-rev levels, when on the ground has to be accepted. In the case of the first aircraft this increased from 0.011 to 0.012 g. It may be noted that vibration levels at low pitch on the ground are not an indication of the actual vibration level in flight. After a phase track therefore a hover is always carried out to ascertain that the one-per-rev is within limits. In-flight trackings have never been found to be necessary when using the phase tracking method, nor accelerometer checks, as best phase always corresponds with best *lateral* vibration levels. The Drello blade tracker is only used, after the blades are tracked first in the normal way with the flag, when the one-per-rev levels are found to be unacceptable by the maintenance pilot or by other pilots on normal flights. Installation, analysis of a problem and readjustment takes from 1 to 2 hours presently, depending on the type of trouble.

Since the introduction in May 1972, the equipment has been used 12 times. Practically all major one-per-rev troubles with our aircraft have been found to be caused by damper discrepancies. It should be mentioned that these discrepancies also can cause an increase in one-per-rev levels with increased coning and flapping (high altitude, gross weight and turbulence), which are particularly disturbing to pilots when flying in IMC.

In one case one damper, giving an erratic pattern in phase was found to be scored, one damper to be leaking badly internally and two leaking to a lesser degree, all on one aircraft. This aircraft even developed a vertical one-per-rev, probably due to the badly leaking damper which, without the Drello tracker could not easily have been located, even if it was noticed that this one-per-rev only appeared at high pitch at airspeeds over 100 knots, thus had to be caused by a damper. The equipment also makes it possible to predict incipient damper troubles indicated by lagging, leading or erratic behavior within still acceptable limits which are approximately a 1/4 inch out of phase condition to both sides of normal phase. This has been proven on one aircraft, where approximately 200 flight hours after this condition was noticed, we had to change the damper in question because of vibration complaints, which solved the problem. It also recently solved a vertical 5-per-rev problem in 2 aircraft, when scored dampers were located and changed. It is therefore a first rate accident prevention tool and has saved us quite a lot of time in analyzing a problem, assessing its danger to flight safety immediately, and correcting the problem at a suitable time or directly in between operational flights.

We still have a lot to learn, and this will take time as we have to wait for a problem to occur and then, by analyzing and correcting it, step by step, develop methods in such a way that reproducible results can be obtained to solve specific problems, so that instructions can be made for the mechanics and maintenance pilots to recognize and solve the different problems as presented on the monitor, even without the use of accelerometer indications.

General Equipment Specification

The Drello Blade tracker, model SKB 483, is designed to track helicopter blades. It consists essentially of a flashlight-stroboscope of high intensity, and a television unit. It permits accurate observation of the individual rotor blade tips for high/low and leading/lagging errors. Observation of up to 6 rotor blades is possible, and satisfactory results can be obtained with tracking in bright daylight.

Scotchlite foil targets are attached to the blade tips, Slide 17. These targets will reflect incident light in the direction of the light source. This means that when the stroboscope flashes are directed on the blade tips from a distance of 10 to 20 m, Slide 18, they will be reflected in the direction of the lamp. Owing to the high light intensity of the flashes, the targets will reflect sufficient light even under bright sky conditions to have the built-in television camera in the reflector produce contrasted pictures on the monitor for easy evaluation.

Slide 17.

The televised observations of the targets has certain advantages over the direct observation method, such as:

- Accurate evaluation of the full scale images of the targets by applying a graticule to the monitor screen, Slide 19.
- Observation of the target images from any desirable position, as for instance from the helicopter cockpit, Slide 20.
- The tracking operation can be observed by several persons at the same time.

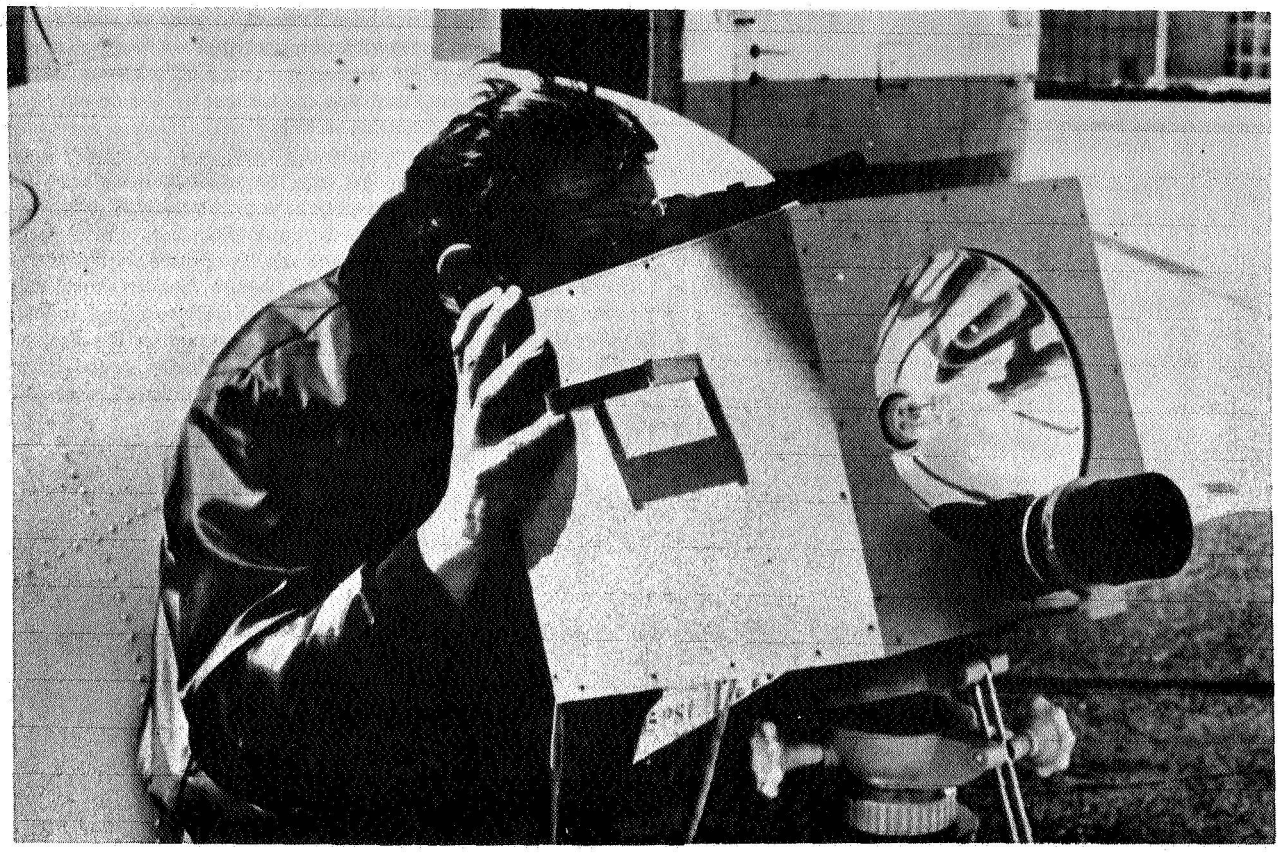

Slide 18.

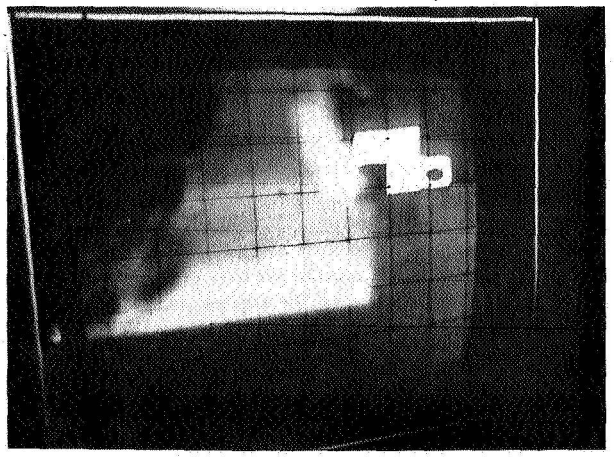

Slide 19.

The flashes are triggered by a pulse light-barrier placed on the ground underneath the rotor and directed vertically against the sky. The light-barrier having a small aperture angle, the flashes are triggered with great accuracy as soon as the leading edge of the blade passes over the light-barrier. The actual triggering pulse to the stroboscope can be delayed electronically with a potential meter thus correcting horizontal movements of the blades with changes of rotor rpm and pitch enabling the pilot to keep the blade reflectors on the monitor, while vertical movements of the blade reflectors are corrected by cyclic pitch.

To determine lead/lag errors of the blade tips, the pulse light-barrier has to be offset by one blade section.

When operating the equipment with switch "TRIGGERING" in position 3, no reference pulse transmitter is needed. Selector switch "BLADE NO." is set to the number of blades on the rotor for cyclic counting of the blades. With this method it is not possible to choose the blade which is to start the cycle. It is, therefore, necessary to use differently shaped targets for identification of the blades. By means of switches "BLADES–PRESELECTION" any desirable pairing of the blades is possible.

Button "BLADE–SKIPPING" permits to offset the pairing by one section, e.g., if blades 1-2 had been preselected, the pairing will then apply to blades 2-3, 3-4, etc.

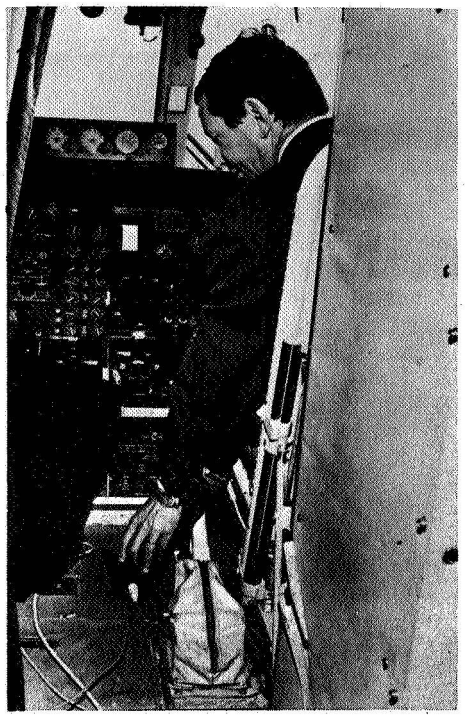

Slide 20.

Concluding Remarks

For 2 days, I have been listening to your excellent lectures on research to improve vibration control. I am happy that at last the manufacturers are becoming concerned with vibrations. I hope that from my story, you can see that we also do our best to improve on your somewhat wobbly product. Give us a chance by listening to and acting upon our complaints and don't be too skeptical about them. We have to make a living with your product, which may ultimately be your living also. I strongly feel that the present state-of-the-art could provide us with blades and dampers which remain accurate and troublefree until they reach a reasonable T.B.O., which would prevent unnecessary one-per-rev problems – keeping our aircraft on the ground when they should fly. I know the industry recognizes the problems, but to my mind are weary to perfect existing systems which we have to work with and in which we have invested hundreds of thousands or even millions of dollars.

THE USER'S PROBLEM

Dale F. Benton
Superintendent of Helicopter Maintenance
Tenneco, Inc.

After listening to all these fine presentations I would like to make a few statements which concern the people who put the work you gentlemen are doing into practical use. I have heard a lot of statements about the term assumption. Well, in our field it has to be a fact, we can't assume something is going to work. We have to make it work because the people we carry do not like it if it does not ride like a 707. And we are faced with a lot of problems. We are able to correct many of them, for others, there is nothing we can do. We just have to live with them.

One of our most common problems is the 1/rev vibration which is usually left to the operator to take care of, to keep his ship free of this vibration. This can be done in several ways, but we have to rely upon a refined method to assure the lowest level of vibration. I have called upon the Chadwick-Helmuth Company, Inc. for support with their electronic tracking and balancing devices, that are working very well for us at this time. I would say it is giving us improvements of up to three times the life of some parts. A very important part of the increased life is the tail rotor and drive shaft bearings. By using this machine we have up to three times less parts usage as well as manhours to keep the systems functioning. This is true for all rotating systems, the engines, and other parts, just due to 1/rev vibration getting out of hand. We have had to go to the manufacturers with these problems because we are very limited in the field. We needed a backup and Chadwick-Helmuth supports us in this area.

I feel that there are any numer of people here who are doing fine work but have probably never ridden in a helicopter out in the field when it's in service. I think this might be helpful, I feel that there is a gray area between your work and the area that is connected with the operation of the aircraft. I talk to some people and they say, "Yes this is my area, but that's not my problem." You talk to the other people and they say, "This is not my area, it's their problem." So when it comes into service we are left holding the bag. I think this panel is a good idea, but I think you should do a little more of what we operators do in the field. We have a real close relationship, even with our competitors, and we listen to each other's problems and try to work them out, because after all we are all in the same business and we have to make it go. I feel that you are doing a great job but possibly we are trying to advance too far without continuing to work out our past problems. We say, "This is good enough, this is all we can do." Well, I don't really believe this. I think there is enough knowledge and technical equipment available for us to go ahead and develop a much smoother system. Thank you.

TECHNICAL ASPECTS OF 1/REV VIBRATION

William F. Wilson
Senior Dynamics Engineer
Bell Helicopter Company

There are five topics that I want to talk about. Before I get into these topics, I have four slides of a test that we ran at the Army Aeronautical Depot Maintenance Center where we actually ran through a series of four rotors and made some step-by-step adjustments to see the sensitivities of various parameter adjustments that can be made on a rotor: sweeping, balancing, tabbing and rolling the blades.

Slides 21 and 22 show the effect of blade balance on a UH-1D helicopter at 80 knots. Slide 21 for the spanwise balance shows how much 2 ounces of blade weight will produce in terms of pylon motion. Now this is vertical motion measured at the pylon at 1 per rev. Similarly, Slide 22 shows the chordwise sweep adjustment and the effect of adjusting the drag brace. An interesting thing that we observed in that test concerns the correspondence between tab and pitch link adjustments. Slides 23 and 24 show the vibration level measured at the pilot's seat at 80 knots airspeed on both aircraft. Each step in Slide 23 represents 1/2° tab angle change. You will notice that 1/2° for a little tab out on the tip of the rotor causing a change of .04 g's. Keep that in mind when we talk about levels in a minute. Slide 24 shows that for 4 minutes of blade pitch change the vectors are in virtually the same direction. This indicated to me that the difference between tab and roll changes in a blade were pretty small. I mean they virtually give the same effect. I don't have the plot at 120 knots, but there is a slight air speed effect difference with the tab. It does increase with air speed slightly, but it's not a significant change.

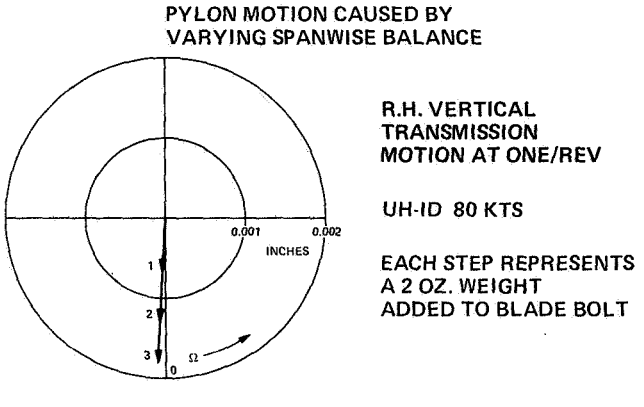

Slide 21.

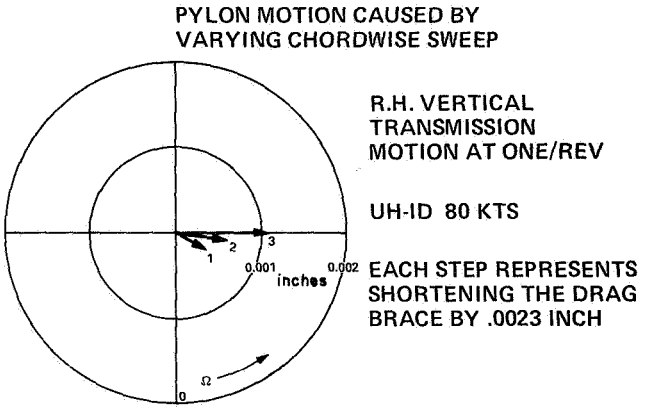

Slide 22.

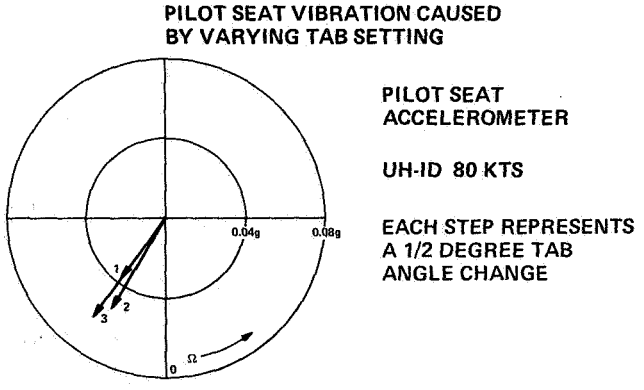

Slide 23.

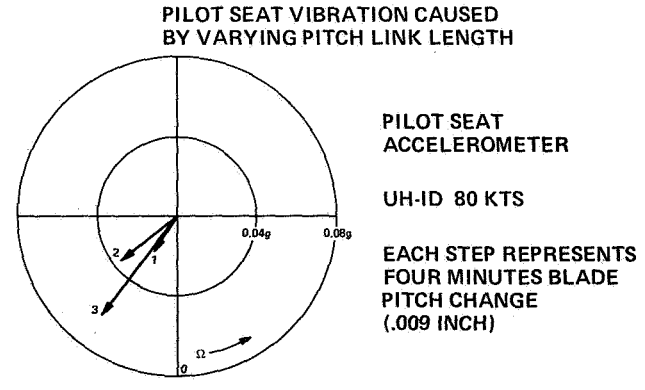

Slide 24.

DISCUSSION

Panel 2: Control of 1/Rev Vibration

Moderator Wilson: The first topic is what levels should we be shooting for? I have a couple of slides, Slide 25 is from a 1964 NASA report* on bioastronautics and it shows perception levels in the 3-5 Hz range of about .0025 to .0030 g's. Now this is the kind of number that Mr. van der Harten has been talking about. What can you feel? It doesn't check with what my experience in helicopters has been. It's surprising that you can feel down that low, but it's possible that for IFR we may have to go there. You can see that unpleasantness starts around .03 g's but the perception level is an order of magnitiude lower than where it becomes unpleasant. So the question becomes: What is the goal?

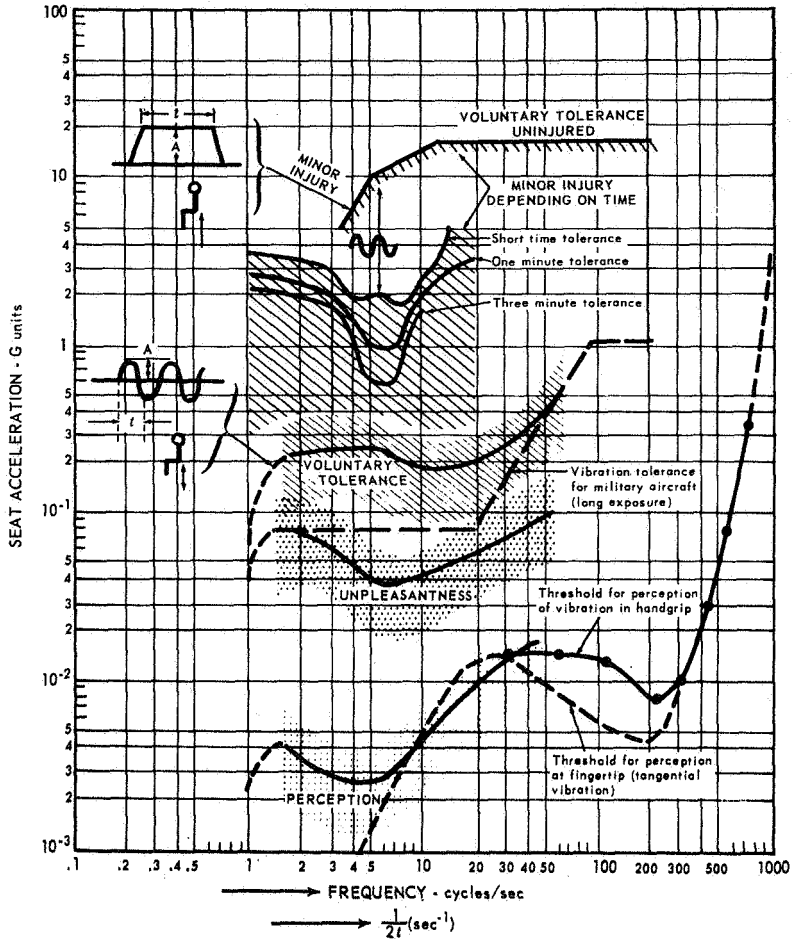

Slide 25.

Consider just the 3-1/2 to 6 Hz range and what various people have said over the years about what the level should be. Slide 26 is self-explanatory. Our experience is that people won't start adjusting rotors until vibration gets above .03 g, that's about where they will begin to think, "Well, we've got to do a rotor adjustment" and they can generally reduce it to that range. But, I have not really seen the case where they can really feel down below .01 g, because the other frequencies bothered them to the point that they don't do that. I would like to ask the panel members for their reaction. What should the desired goal be for a vibration level at main rotor 1 per rev and should the levels vary with rpm?

Carlson: Mr. van der Harten has done an excellent job of either describing us or exposing us, depending upon your overall attitude, I guess. We are able to achieve and ought to aim at levels on the order of .005 g and that experience shows that levels on the order of .01 g are felt by the individual in the aircraft. These are levels that are achievable as Mr. van der Harten has indicated and I would

*Bioastronautics Data Book, Edited by Paul Webb, NASA SP 3006, 1964.

imagine then that this is our aim. In order to reach them, it is a complicated process and all of us have to work hard at it. Now, I'm only able to speak of the levels of our aircraft which have 1 per rev that is rather low. They are under the levels of normal body resonance and I am unable to answer with regard how this enters into the other aircraft which have higher rotor speeds. I'll pass it on to others at this stage.

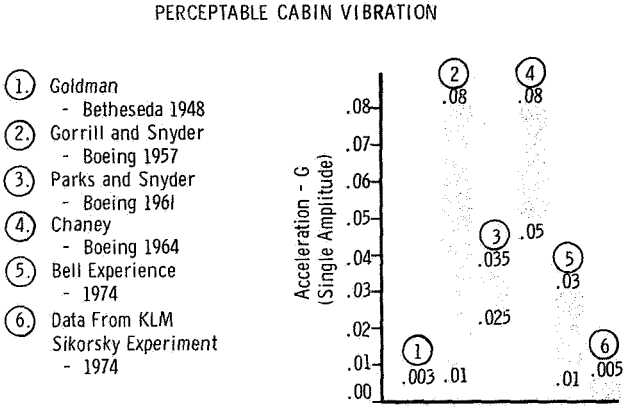

Slide 26.

Jones: The UH-2 has automatic tracking which we will be getting into later. From an actuation standpoint the automatic tracker actuates at .014 g's so therefore in theory we are keeping our helicopter within .014 g's of 1 per rev. It has hysteresis in the system so that when it gets down to about .007 g the actuator cuts off and then does not start again until the level reaches .014 g's. Now as far as frequency goes, I think Bell and Kaman are approximately in the same area. Bell runs at about 5.4 Hz, at least in their UH-1, which again is the human factors problem. Our UH-2 is approaching that. I think we are about 4.3 or 4.4 Hz from a 1 per rev standpoint, so we are at least approaching this. So I assume there would have to be some form of rpm variation on acceptable levels. And to really illustrate this, again in our development of our UH-2 helicopter, we had a vertical bounce on the ground, which we worked very hard to get rid of, but I couldn't even tell you how we did, it just seemed to disappear, but we did get rid of it. That vertical bounce was very near the human factors problem area, the test pilots could hardly write on their knee pads, so levels can be quite important.

O'Leary: I would just like to make a few comments in a couple of areas. One is that the newer specs – as we relate what's happened to the vibration spec requirements at 1 per rev – have obviously driven us all down towards attaining better levels, as we come from the .15 g's down to the .05 g's of the AR-56 and the later generation aircraft specs. We have done pilot seat shake testing under controlled conditions and reported this at various symposiums. This has shown that levels like .02 g and .03 g are acceptable for what our experienced pilots consider long term operation – for an excellent or outstanding qualitative assessment of the aircraft. It is assumed that it would not affect them operationally or fatigue them. I think the important thing that we found from our own flight experience on some of our later helicopters is that as the n per rev levels are being driven down to meet .05 g's at b per rev or n per rev, the awareness of the 1 per rev is greater than it was before. They are complaining more about other frequencies now that we are getting rid of the ones that used to be up in the .3-.4 g range. In fact our testing showed that when we did the testing by individual frequencies and attained levels that would receive an outstanding rating for long period operation and then took the same attained g levels at each frequency – taking the same g level that gave an individual rating of outstanding and adding just 1 per rev, 4 per rev, and 8 per rev together, the rating became completely unacceptable. So in the presence of other frequencies, the requirements for 1 per rev are even lower than perhaps we thought in the past. Our current goal was around the .03 g range and it has been demonstrated I think on one of our tandems and on the BO-105 that those kind of levels are attainable.

Wilson: You can see that we have some disagreement among ourselves as the load calculators do, as to what the flight levels are. Now experience has shown to me in the flight tests that we have done that the .01 to .03 range is attainable on most rotors and we are somewhat in agreement with Vertol on that line.

Our next topic for discussion, I want to keep very brief. The question is: What is being done by industry to insure that these goals are being met? We are doing two things at Bell. We are looking into the possibility of automatic devices. We have had a couple of programs in the last two years. We are also doing work on the blades themselves and trying to make better blades using what we call closed cavity bonding tools that will give better control of contour and twist in our rotors. Recent tests have shown that at least on a first-try basis for the first 10 or 15 blades we have made, we haven't needed a tab. We've just been rolling them into track and going, and it has been very successful and satisfying to date. Would you all care to make any comments on this?

O'Leary: I would just amplify the point about the closed mold process for controlling the airfoil contour. We really feel that that has been demonstrated on aircraft like the BO-105 and our tilt rotor Model 222. There is another area that we also are concentrating on and that is the control of the fuselage frequencies around 1 per rev. On our large tandems, generally from an air resonance standpoint, we have lower limits on where these frequencies can be placed and that generally assures that you are not going to have a frequency for the lowest mode, especially for very large helicopters like the heavy lift, that will be coincident with 1 per rev at some operating condition. So there are structural changes that Dick Gabel will talk about later actually being installed on this aircraft to keep the modes closest to 1 per rev above 1.6 to 1.7 per rev. On our other helicopters we are consciously aware of keeping the amplification of these modes whether they be above 1 per rev or below 1 per rev to some nominal value like 2 and we are so conscious of it that, for our current aircraft, we plan to shake test the aircraft to assure in fact that the fuselage modes are far from 1 per rev so that any residual loading won't be amplified by the structure itself.

Jones: The only comment that I really have is that, although right at the moment I don't get in with our service group or our manufacturing groups, we do keep our blades in very close tolerance, and as far as the stated question: "Are we doing something about

it?" Well, I sure feel that Kaman has at least done something about it in the fact that we do have automatic tracking in flight on all of our UH-2 helicopters, so that track is maintained in flight.

Carlson: I'm only able to add here, I guess, that at Sikorsky we work hard at the initial balance and tracking of the blades in that each blade is balanced with weights at the tip and chordwise we have tabs on our blades which are used. We have a master set of blades to track each of them against and then ultimately each blade is tracked. These all give us what are in general reasonably smooth levels. I would add a small item, I suppose it ought to be brought out that it isn't only the blades that enter into this, it's the hub as well in that we have to have our hubs lined up and well made also.

Jones: May I just interject something here, I just want to beat Sikorsky out on one point here. We don't have a master blade, we have a master master blade.

Carlson: We also have that.

Jones: Oh, do you! I got a big kick out of it. I didn't realize we had a master, master blade, and that is the blade that we whirl to get a master blade which we then use to whirl blades to meet tolerances. I assume then when the master blade wears out, we whirl another one to get another master blade, to the master master blade.

Wilson: Concerning that subject, we will talk a little more about whirl testing in just a minute. I would like to go to the next slide and if we can I would like to keep the comments very brief on this subject. Really I would like to find out whether we are in favor of or not in favor of electronic tracking and balancing devices for correcting main rotor and tail rotor balance. The question is: What about electronic tracking and balancing devices? Can we save dollars for the operator?

Benton: We are definitely sure that electronic devices are good. Some of these are really expensive but they are valuable to the operators in dollars saved. We used to take a 1 per rev out of the ship until we would get into 2 per rev that we were unable to do anything about and then they failed. So many of us thought we were inducing the 2 per rev so we would leave the 1 per rev to cover up something that you folks had stopped short of and left in. So with this electronic machine we found out that we were actually hurting ourselves by covering up the 2 per rev.

van der Harten: Well, our good friends at Sikorsky build a wonderful aircraft. Their S-61 is considered as a kind of DC-3. We'll let that alone, I think, but we don't have that problem which you have, Mr. Benton, not as much I should say, but we save a lot of money by controlling vibration. The only thing you need is time to do it, so you need a quick analyzing method and that's what we have been trying with the Drello method. Also, you run into problems if you are not able to observe carefully what the phase is doing and what the track is doing. And I always hear track, track, track – I don't care about track. As long as my blades run the same paths through angles of attack and through changes of airspeed, I couldn't care less. The only thing I worry about: If I go too far out of track – let's say 2 inches, that's about the ultimate limit, the maximum limit we have flown – you will get into the same trouble as Mr. Benton is talking about, you will get into trouble with the n per rev. Apparently you get vortices hitting the other blades. That is a theory, my good friend Andy Lapaty would say, "You are theorizing again, prove it to me." Well, that's our problem, to prove these things, but we find out things and I think it's up to the industry to prove what is really happening and we hope that you will do it and give us the equipment to quickly get through it. But in talking about dollar savings, 1 per rev causing 5 per rev, or 5 per rev being caused by taking out a 1 per rev, in our case – when we were able to prevent that, after a lot of experimenting – we found a big saving, in the other expensive indicators and VGI's, unscheduled removals. You are talking about $1,000 repair every time. If you save that for five years, and it was more than that I can tell you, you have saved $5,000. If the equipment cost $10,000, it takes you two years to get out of it, and the main thing is that you don't have your aircraft on the ground all the time because the pilots come back and complain about them.

Benton: If I may I would just like to add one thing. Talking about dollars saved, with the electronic devices we can usually do a ship in four hours say, but before we had them, sometimes it would take 3 or maybe even 4 days to work out a problem, so that's a big savings in time, and the machine off of the job, and that is many dollars.

Wilson: To go on to the next topic: What about whirl testing blades against a master? Does it pay off since airspeed cannot be simulated? Here is something that the operators don't get into, some manufacturers do. We haven't whirled a blade at Bell I guess in 10 years on anything but a helicopter. The other manufacturers here all whirl every blade that they build. They talk about whirling against the master and bending their tabs and getting them set. I would like to see if they really think it's justifiable since airspeed is not present on the whirl stand. Maybe we don't understand what you are doing.

O'Leary: We do whirl our blades and we do adjust the tip weight to take care of chordwise moment, and we also adjust tabs to take care of rpm variations, and also track the blades within pretty close tolerances. I think the general philosophy and the general occurrence has been less time is spent on inflight tracking if we do that. That doesn't mean that we never do inflight tracking, but less time is spent on that and less flights are required for that. We really think we are reducing the number of variables for the inflight tracking problem when we take into account these things such as balance, chordwise, spanwise, and the effect of rpm, and therefore we will reduce the number of inflight tracks that we have to make.

Jones: Again, I'm just going to have to say that I agree with Jim O'Leary. I just want to point out, I think Kaman possibly has more of a tracking problem than other conventionally controlled rotors. We use a servo-flap; this means a very soft torsional system for our control. It means I think that our tolerances have to be much better; therefore, we do rely upon whirling and really matching blades. We also have one other item we have to match and that is not just the blade but we have to match our servo-flaps and so therefore we really feel we have to do this. From the standpoint of costing I have no answer for that aspect except I think that if we did not do that we'd really have tracking problems. And again, we really do rely upon the automatic tracker with the inflight system.

Carlson: Well, I would only want to point out one item here. I suppose it holds that the more blades that there are on a rotor the harder it is to track it wholly on the aircraft. It's almost impractical if there are a large number of blades as we have, and our answer is that all of our blades are tracked against the master.

Wilson: I think it would be to their interest to run some programs to see – we have run programs – to see where various factors have entered into the cost of helicopters and I'm certain that whirl testing does enter into the cost of blades. Just like balancing or anything else enters into it, and with the electronic tracking that we are doing now maybe that's a possibility that they might be thinking about.

O'Leary: I think a comment that I would like to add to that is that – with the new generation of blades where we really feel that the airfoil contour control can be much better maintained with better production processes such as closed molds – in fact this change with airspeed will be less of an effect and has been less of an effect on aircraft that do this. And therefore by tower tracking and getting all the variables out, the one remaining variable which is this characteristic of the airfoil, differences will be minimized.

Wilson: We have one more topic. The question came up with Kaman's rotor and with ours also, we've been experimenting with automatic trim devices. We've looked at electric pitch links. We made one system that would automatically bring the rotor in track in flight. You could bend the tab up or down by 4 degrees and still track the rotor by adjusting the pitch length. We had both manual and automatic control so that we could feed back an accelerometer signal into it. We decided after we got to that point that the question was really: Does the operator really want automatic trim devices? Does he need them?

van der Harten: Well, flying Sikorsky helicopters, I would say we wouldn't need that because if you set your blade on the ship and if the blades stay like they are – I mean do not crack up somewhere and have to be taken off, or if the dampers do not go out of whack which is the most important problem, internal leakage, valves and things like that – then you don't have to change track, the aircraft will remain smooth. If the blades would hold out without having to change them for 2000 hours I'm pretty sure I wouldn't track the aircraft for 2000 hours. If the dampers wouldn't give any trouble. Actually it is different on Bell helicopters and aircraft that do not have pre-tracked rotor blades. I think that what we have found that the pre-tracked rotor blade will not change its characteristics for quite a number of hours and will remain interchangeable. The main problem is that the dampers go out of whack.

Benton: I really don't see the need for automatic pitch change links, etc. It's an added expense, and to the people in the field and for many one-aircraft-operators, it's just an added complication and expense to them. I will go back to one thing and agree with Bill Wilson, if they could do away with the tabs and hold the blades to a little closer tolerance. The tabs are continually getting bent, a man throws a tie-down strap on, he bends the blade, they run it into the wall, or they will bend it during installation. So we have built-in trouble to start with, but as far as the automatic tabs are concerned – no I don't think we need them.

Jones: I sort of agree with the operators, an automatic system could be expensive from the standpoint of maintenance and so forth, but how about some form of indicator so you would maybe know at least which blade is a problem, which one is high and which one is low, not necessarily an automatic tracker but at least this would tell you where the blade is in flight and when you came down you could possibly do something about it.

Benton: The pilot usually tells you that when they get out a little bit.

Jones: Well, do they know which one it is really?

Benton: No, but that's where the electronic device comes in. We can throw it on in about 30 minutes and we can tell immediately what has happened. Then for a one man-hour job, we could maybe replace this automatic device we would put on for many dollars.

van der Harten: Well, I disagree a little bit, but that's mainly because of flying larger helicopters and thinking about airline use of helicopters. There it would be nice from the flight safety standpoint to have an indication that something has gone wrong in the rotor head. The articulated rotor is the smoothest rotor system you can fly, especially if your blades are pre-tracked as well as they are at Sikorsky. Your problem is when something goes wrong in the rotor head itself, dampers again. I am fed up with dampers after I have found so many with our Drello tracking system. If you have a system in your aircraft that we will show you that the blades are going wrong in phase rather than in track which could be shown by photocells or something like that in the fuselage, and the aircraft was big enough to take the expense, I would say do it, but that's for bigger aircraft mind you.

Wilson: Well, of course the size of the device may be pretty small. Even on a 206 which is a 3,000 lb machine, we might be able to afford a pound or two for keeping the rotor in track if we can afford so many other pounds for so many other things as we have often done in the past.

QUESTIONS AND ANSWERS

Panel 2: Control of 1/Rev Vibration

Bill Paul, Sikorsky Aircraft: I have a comment on Mr. Wilson's comments. First of all, I think when your vibration level gets as low as it is getting to on the Noda-Magic system, I think you will find that you might require more careful control of your track, particularly in the commercial environment. That's my observation, but it may not be correct. I think that 1 per rev is a very subjective thing, it depends on what you are used to. If you are used to – as Mr. van der Harten is, as well as he knows – a very low vibration level, then .005 g is not acceptable. If you are at .01 g to begin with, you might have thought .005 g was fantastic. The second point is, Mr. O'Leary's comment, I don't think we are going to improve 1 per rev. I may be wrong, but my observation is that with cambered airfoils, where we are now talking about 9,000 in-lb versus 900 in-lb for symmetric airfoils, that even though you are exercising better control, the control almost has to be precise and I don't mean just precise coming out of the barn, but precise after a few thousand hours of flying, maybe a few hundred hours anyway. So one of the things that I would suspect is going to happen with cambered airfoils is that – and we are all using them, by the way – is that you are going to see more out of track in forward flight, and the problems may not occur on the ground or on a whirl stand. The same thing holds true with higher twist blades and I think that will show up so I think that we are coming into an era where we might find more of the out of track taking place – I mean out of track in this sense, high speed, and not so much the 1 per rev concern. Finally when you talk about composites, and we are all using those as well, you damn well know that control of the weight is very difficult even with molding techniques that we have, so I think the problem is just beginning in a different era.

O'Leary: I think from the weight standpoint the tolerances on the balancing chordwise and spanwise that we will use with these blades is even more stringent than we had in the past which recognizes that fact.

Dick MacNeal, MacNeal-Schwendler Corp.: I believe Mr. O'Leary that you were the only one who mentioned the problem of 1 per rev structural resonance. I would like to ask whether you would care to comment on the problems posed by extremely heavy wing stores such as long range fuel tanks.

O'Leary: I guess my only comment is that if they can change the characteristics of a structure to move modes closer to 1 per rev, then obviously you would have to consider means to avoid that.

Dick Gabel, Boeing Vertol: Speaking about the tracking again versus the vibration level, we have also had a lot of experience where in special programs to improve track on test vehicles, we have taken great pains to match pitching moments and pitch link loads and tabs and a whole raft of things. We've gotten the vibration level down at the expense of getting blades out of track, which is often possible, because if there are discrepancies from blade to blade you can do better by putting them out of track than in track to get the g's down, but when we do so the pilots turn out to be more concerned about that disturbing shadow out there than they are about the 1 per rev, so its really a balance between the aesthetics of it and the g's of it.

Jones: May I just make a point about that. Again, when I talk about our automatic tracking, admittedly we are tracking to g level and not track. However, I've never heard that comment from our pilots. I just sort of want to make the statement that we haven't run into that one specifically.

van der Harten: Well I don't think the pilots are bothered about blades out of track. We are talking about flying real IFR, I mean going up with no visibility, letting down with no visibility, and at the last moment seeing where you are going to land, take off, vice-versa again, turbulence, everything. They don't care about blades off track, we have flown with blades out of track, no problem there. They do care about vibration, because vibration disturbs the high work that they have when flying under those conditions. So if you can do it by bringing your blades out of track, and maybe for the bigger ones by getting automatic control in there, to reach the higher speeds without 1 per rev vibration, then do it. I'm getting scared a little bit that in the future technology you are calculating a higher 1 per rev load, which I heard from the first question. I think this should be prevented at all cost if you want helicopters to be acceptable to passengers, since they are used to vibration levels of 707's and 747's. The second thing is the pilots will be bothered very much by it and we still don't know the effects if you are on longer flights and you have to cope with vibration levels that are shaking you up. It is all at the wrong frequency, 1 per rev, 5 per rev, it is all between 2 and 20 Hz and, as is proven in many reports that does something to your body system, and how much we don't know.

SESSION V

APPLICATION OF DYNAMICS TECHNOLOGY TO HELICOPTER DESIGN

Panel 3: Integrating Dynamic Analysis and Helicopter Design

Panel Members

William F. Paul, Moderator	Chief Engineer, Sikorsky Aircraft
Rodney W. Balke	Assistant Group Engineer, Dynamics, Bell Helicopter Company
Richard Gabel	Manager, Rotor Technology Staff, Boeing Vertol Company
J. Ford Johnston	Senior R&D Engineer, Lockheed California Company
James R. Neff	Chief of Dynamic Analysis, Hughes Helicopters

DISCUSSION

Panel 3: Integrating Dynamic Analysis and Helicopter Design

Moderator Paul: We are not going to spend too much time on formal discussions this morning because I think this has to be an interactive panel in discussion with you. Therefore, what we are going to do is to spend 5 minutes, each of us, summarizing our position as to where we stand with integrating dynamic analysis into the design and where we think we should be going, and then open the discussion to the floor because I think that's where the most fruitful discussion should take place. So, I would like to proceed immediately with Mr. Rod Balke and have him present his position.

Prepared Comments

Rodney W. Balke
Assistant Group Engineer, Dynamics
Bell Helicopter Company

The design process that we are all immersed in can be broken down into three basic phases: the concept formulation, the iterative design loop, and the final design and documentation (Slide 27). I have chosen, as a format, to take you through a three-month response to a military RFP. The concept formulation may already be complete at the receipt of the RFP. The final design and documentation we know from experience will take 1 to 1-1/2 months. This leaves approximately 1-1/2 months for the iterative design loop. For the dynamicist, as you know, that's where it's at. Now we are going to talk a little bit about – what it's like, where it's at – to make a few points, and hope to stimulate some discussion.

To set the stage, Slide 28, we have requirements for rotor frequency placement, loads, stability, and requirements for vibration control, which for Bell is generally a rotor isolation system. For the fuselage we have frequency placement and vibration levels, for the drive system we have frequency placement and stability. We have major programs in each of these areas. As you have heard, we use C-81 for rotor work. We have NASTRAN available, although detail modeling must be done. We do start in many cases, particularly in the vibration control area, with simple 1 or 2 degree-of-freedom systems to keep that gut feel.

DESIGN PROCESS
(3 MO. RFP RESPONSE)

CONCEPT FORMULATION
(USUALLY COMPLETE AT RECEIPT OF RFP)

ITERATIVE DESIGN LOOP
(APPROX. 1-1/2 MO.)

FINAL DESIGN/DOCUMENTATION
(APPROX. 1-1/2 MO.)

Slide 27.

TO SET THE STAGE

ROTOR	
– FREQUENCY PLACEMENT	MYKLESTAD
– LOADS	C81
STABILITY	DYN5
VIBRATION CONTROL	
– ROTOR ISOLATION SYSTEM	NASTRAN
FUSELAGE	
– FREQUENCY PLACEMENT	NASTRAN
VIBRATION LEVELS	
DRIVE SYSTEM	
FREQUENCY PLACEMENT	NASTRAN
STABILITY	HYBRID

Slide 28.

The first pass, Slide 29, the rotor frequencies, begins with extrapolated parameters and assumed hub impedance. The loads begin with level flight and maneuvers using the existing program version. The vibration control begins with the development of a NASTRAN model of the isolation system on a rigid fuselage, the point being to keep it simple. The fuselage vibration, again a simple NASTRAN stick model. We start program modifications at this point or new programs as required. Slide 30, the tempo picks up a bit; the rotor frequencies, the first real parameters become available, but we are still using assumed hub impedance. We find that maneuvers are taking too much time, we go to a fallback position and switch to a hybrid version of C-81. For vibration control we obtain hub impedances from the NASTRAN model. This goes back to what Jim Staley was pointing out, the need for integrating the hub impedance from the fuselage analysis into the rotor system, combining the rotor analysis with a program such as NASTRAN. For fuselage vibration, we develop a 2-D model of the fuselage and start a 3-D model. The tempo continues and we've got to hurry to meet the schedule here, Slide 31. We get a parameter update, we now have some hub impendances, we complete the loads and forward them to rotor stress. We obtain rotor excitation forces to apply to the fuselage. We combine the vibration control and the fuselage vibration into one 3-D model; we must now freeze program modifications. We then come up to the 4th pass, Slide 32. The fatigue group finds some minor stress problems, the rotor is beefed up in this area. For vibration control we apply the rotor forces and get the first look at the vibration picture, and suddenly we are struck with the design freeze and no further changes are made. Now the points being made are that we should keep the model simple consistent with the design status, which provides fallback positions. We should support the

analysis with model tests and correlation, particularly for checking out new analyses. We should not support that desire to make another pass, because it has to be documented; and we do need an integrated rotor/fuselage analysis.

FIRST PASS

ROTOR
- FREQ – EXTRAPOLATED PARAMS. AND ASSUMED HUB IMPEDANCE
- LOADS – LVL FLT AND MANEUVER/EXISTING PROGRAM

VIBRATION CONTROL
- DEVELOP NASTRAN MODEL ON RIGID FUSELAGE

FUSELAGE VIBRATION
- DEVELOP SIMPLE NASTRAN STICK MODEL

PROGRAMS
- START MODIFICATIONS

Slide 29.

SECOND PASS

ROTOR
- FREQ – FIRST PARAMS AVAILABLE/ASSUMED HUB IMPEDANCE
- LOADS – MANEUVERS TAKING TOO MUCH TIME, SWITCH TO HYBRID VERSION OF C81

VIBRATION CONTROL
- OBTAIN HUB IMPEDANCES FROM NASTRAN MODEL

FUSELAGE VIBRATION
- DEVELOP 2-D MODEL OF FUSELAGE
- START 3-D MODEL

Slide 30.

THIRD PASS

ROTOR
- FREQS – PARAM. UPDATE + HUB IMPEDANCE
- LOADS – COMPLETED LOADS FORWARDED TO ROTOR STRESS
- OBTAIN ROTOR EXCITATION FORCES

VIBRATION CONTROL AND FUSELAGE VIBRATION
- COMBINE ISOLATION SYSTEM AND FUSELAGE INTO 3-D MODEL

PROGRAMS
- FREEZE MODIFICATIONS

Slide 31.

FOURTH PASS

ROTOR
- FATIGUE GROUP FINDS SOME STRESS PROBLEMS
- ROTOR IS BEEFED UP IN THIS AREA.
- NO FURTHER CHANGES MADE.

VIBRATION CONTROL AND FUSELAGE VIBRATION
- APPLY ROTOR FORCES AND OBTAIN FIRST LOOK AT VIBRATION PICTURE.

DESIGN FREEZE

Slide 32.

Richard Gabel
Manager, Rotor Technology Staff
Boeing Vertol Company

I'll limit my remarks to one portion of the design integration process, Slide 33, the rotor loads to airframe analysis, and it parallels certainly what Rod Balke has just shown. The upper part of Slide 34 is a flow diagram. You apply criteria on frequencies and stresses and compute frequencies and go around that loop until you modify the blade for those requirements. Then, concentrating on the vibratory loads going into the fuselage, the lower set of plots show some vibratory hub loads. We try to have as a backup to all those computer programs – which as you saw this morning are "very unreliable," other methods to make sure that we are conservative in the prediction of the vibratory loads. And one that we have been finding quite useful is models where we scale the hub loads from dynamic models. As a backup to even that we have also used the supply of information from previous aircraft and scaled that to the new aircraft, where that's possible. We look at all those and take the highest and work from there.

On Slide 35, looking at the airframe, in the work on the HLH we first established the maneuver loads and vibratory loads for the airframe. We do a preliminary shear moment diagram in the old fashioned way, work with design in sizing the original stringers and frame and then as that begins to solidify we get more detailed in the model that's used and start to use NASTRAN as shown on the next slides. There's a whole series of them, it's so complicated now that we break up the fuselage into pieces even in this preliminary design stage. There's the forward pylon, Slide 36, and the forward cabin, Slide 37, and the next one, Slide 38, is the aft cabin and finally, Slide 39, the rear pylon on the HLH. Of course that's because it's such a huge aircraft. The way this impacts design is that nowadays we size stringers and frames to the NASTRAN prediction and get that solid line of EI, Slide 35 – grouping it on the EI as a simplification. We specify the strength and dynamics requirements, and then we judge the results with the very same model. The use of one model has been a very big improvement. We used to have multi-programs and have legislated those out of existence pretty much and stuck with NASTRAN for one basic model for both stress and dynamics use. Now it is established that the vibration requirement

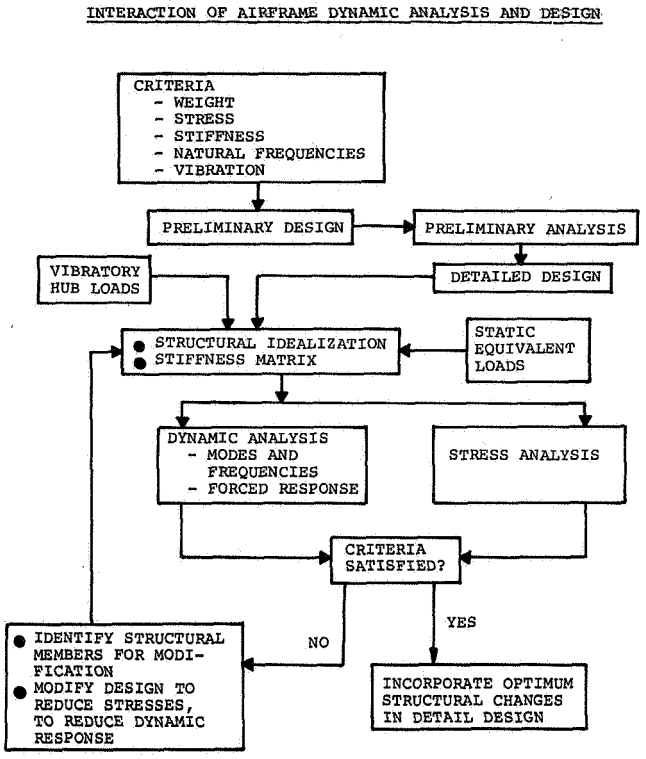

Slide 33.

is different and we are faced with working out the differences between the two of them. And here we have been able to stiffen the fuselage in the area at mid station around 600 so as to beef up the stringers to satisfy the vibration requirement where it's obviously greater than the strength requirement, and then at the frame 200 to 400 region where the vibration says it should be softer than the strength, we compromise by considering cutouts in the airframe to accomplish the softness without compromising the strength. Another advantage of these NASTRAN type programs is that you get very detailed stress information on each member, and hopefully the airframe will be lighter by virtue of the analysis having gotten so involved.

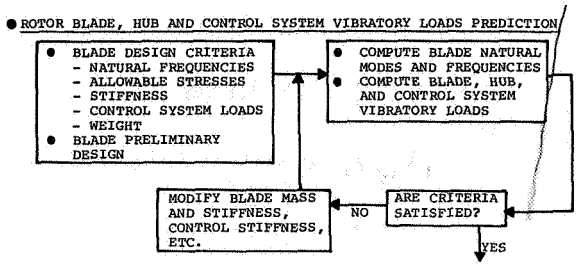

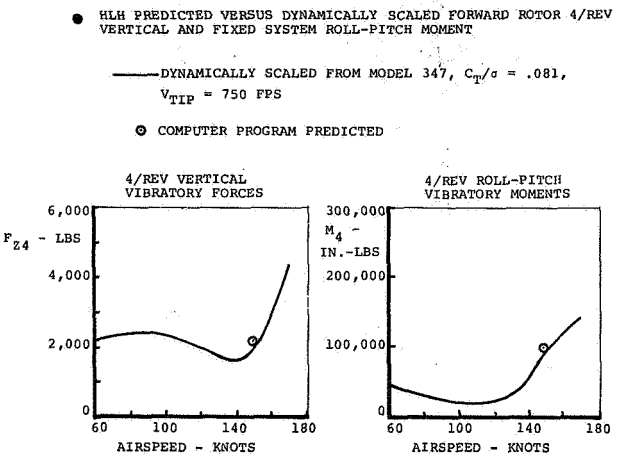

Slide 34.

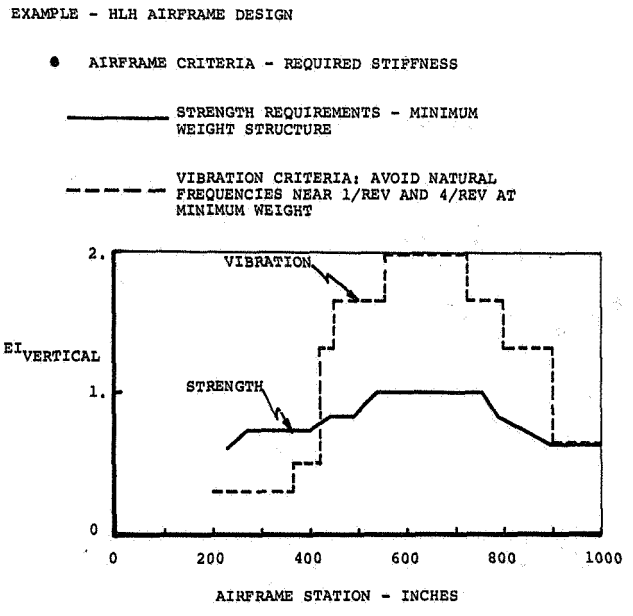

Slide 35.

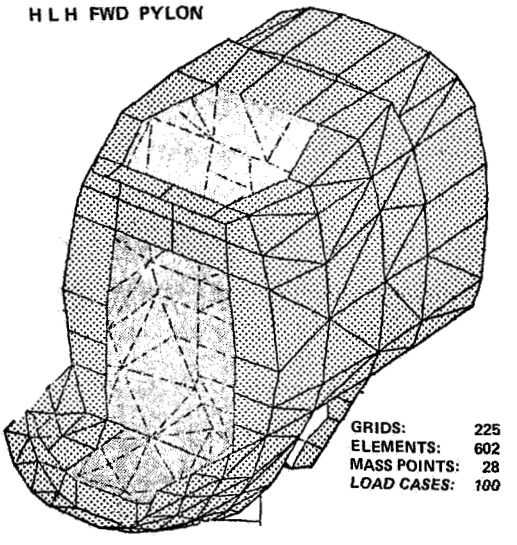

Slide 36.

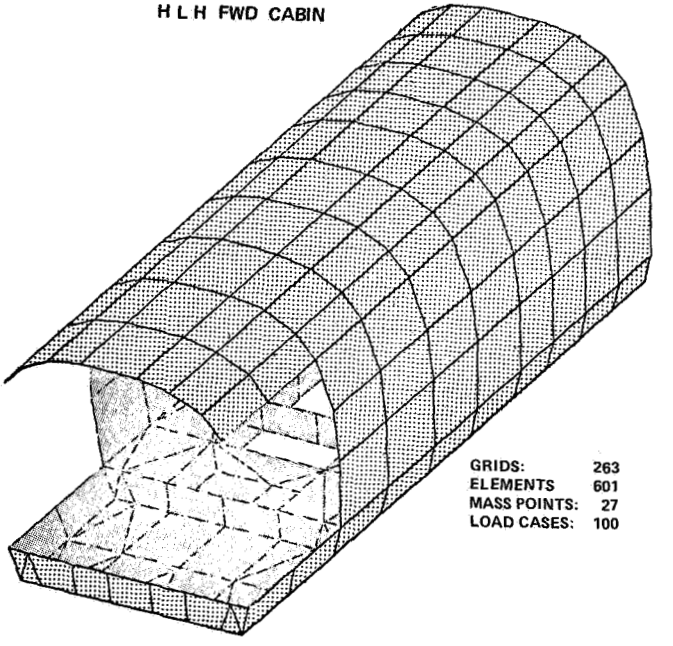

Slide 37.

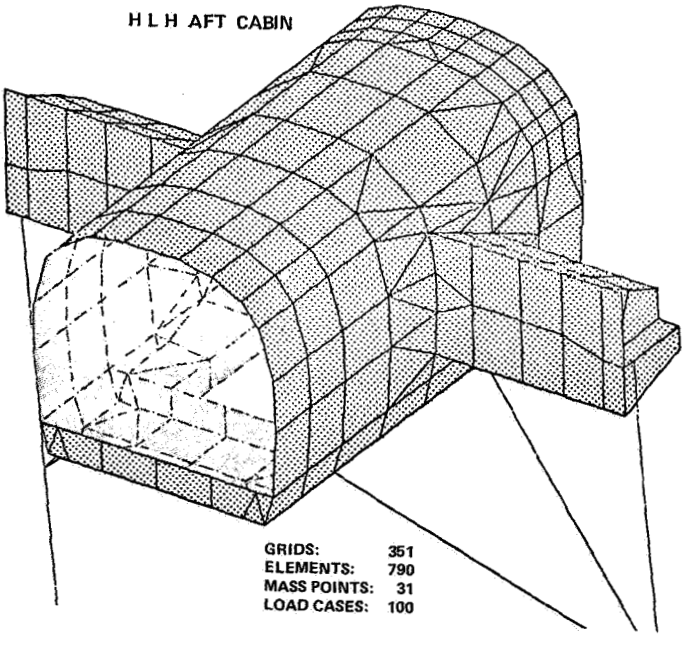

Slide 38.

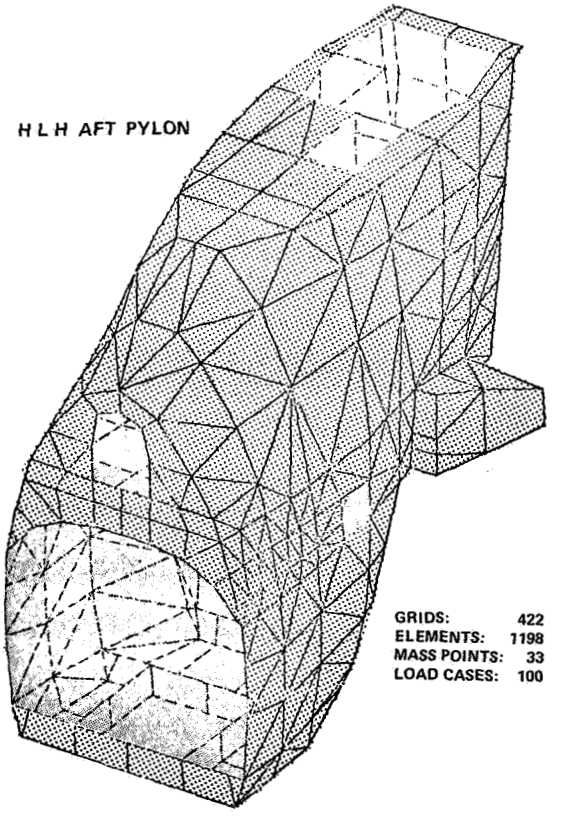

Slide 39.

J. Ford Johnston
Senior R&D Engineer
Lockheed California Company

A year or so ago I was able to participate in a very successful program, the AH-56 AMCS, and what I observed there led me to some thoughts on the management and the attitudes of the dynamicist in such a program. I found this program was one in which the dynamicist was very closely in the loop and participated in the preliminary design, and carried on through. And rather than go into the details of how this is done, I thought I would like to talk about some of the principles that were evident to me in this process.

CLOSING THE LOOP AT LOCKHEED

WE HAVE TO:

BE AN ACTIVE ELEMENT IN THE LOOP

HELP ESTABLISH THE DESIGN CRITERIA

BE RIGHT, NOT CONSERVATIVE

DEVELOP A TRACK RECORD FOR "RIGHTNESS"

BE MEANINGFUL – COMMUNICATE

WE USED AN OMBUDSMAN

Slide 40.

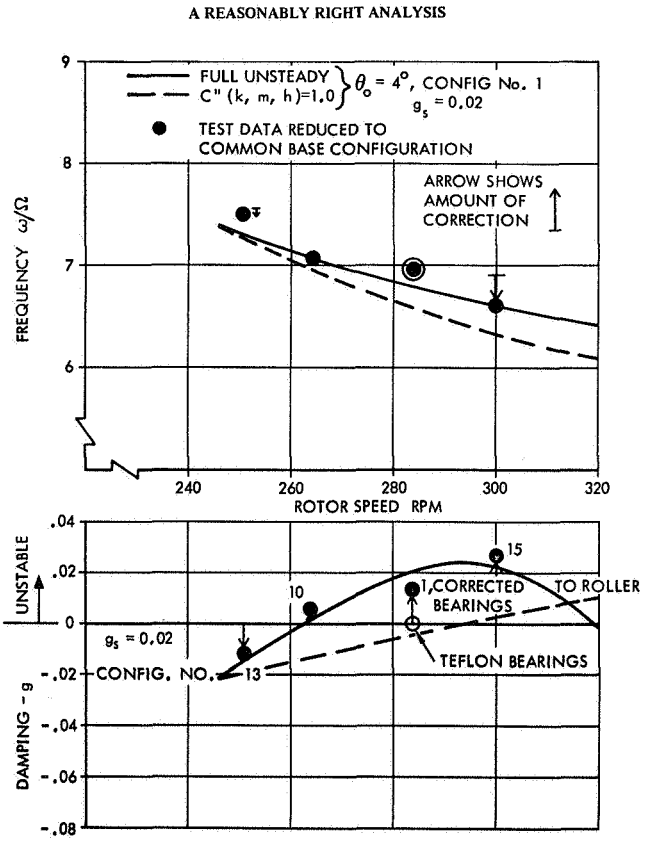

Slide 41.

Slide 40. I found that the dynamicist has to be a very active element in the loop, to help establish the design criteria, and in order to be this and to do this, he has to be right; he has to be as nearly right as he can and not give himself margins of conservatism. And he has to have developed a track record for being right so that management can pretty well depend on his inputs, and then of course he has to change from the nomenclature that he uses with his fellows and be able to communicate to the design people, the aerodynamicists, etc. Having been in that position I put in this last part that we call the ombudsman. It's a term to indicate a man who can help you at City Hall if your case is right, and since I was in that position as staff to the director of engineering, I was able to say, "Yes, that makes sense," or, "Let's have another go at that." And I think that it's very useful for the dynamics group to be able to work against a chief engineer who has a background and experience in dynamics. Now, just to illustrate a couple of points, if I could have the next slide, please.

This one I call a reasonably right analysis, Slide 41. It came early in the development of the AH-56 and it pointed to the fact that we had a potential 7P flutter problem. What we had in the beginning was the dashed line to illustrate linear analysis, and just recent we completed – as reported in one of our contractor reports* – a full wake analysis, and that was pretty good, it showed good correlation. Actually the first analysis alerted us to the problem, and showed us the ways in which we could fix it, so I considered that pretty good.

Slide 42. That was unfortunately conservative, it is a re-do. Put yourself in the position that you are looking at the analytical curve in the absence of the test data because the rotor hasn't been whirled yet. You look at that analysis and you say, "With a little bit of spread that could be unstable within the expected overload gross weight range of the vehicle," and so it affects your

---

*"Rotor Blade Wake Flutter" by W. D. Anderson and G. A.Watts, Lockheed Report LR 26213, Lockheed California Co., Prepared for U. S. Army Aviation Systems Command and USAAMRDL, Ames Directorate, Contract No. DAAJ01-73-C-0286 Mod. P00005, Dec. 1973.

Companion Reports:

"The Reactionless Inplane Mode of Stiff-Inplane Hingeless Rotors" by J. F. Johnston and F. Conner, LR 26214, Dec. 1973.

"Flight Test and Analytical Data for Dynamics and Loads in a Hingeless Rotor" by R. E. Donham and S. V. Cardinale, LR 26215, Dec. 1973.

"Flying Qualities of a Gyro-Controlled Hingeless-Rotor Compound Helicopter" by A. J. Potthast and A. W. Kerr, LR 26216, Dec. 1973.

risk analysis of this system, and this is a second go around in which a more conservative look was taken at the couplings involved. The first analysis goes down closer to the 0.02 range prediction-wise and when the test results came out we breathed a sigh of relief, but nonetheless it cost us quite a bit.

Slide 43 is one that Bill Anderson showed you yesterday and it was an excellent example to me of the communication of taking the results not of a root locus plot but of turning that into terms that other people can see, roll rate per inch of stick and inplane loads per inch of stick. You can see that too small a blade droop angle would get you into a loads problem and into multiple problems of roll response, and too large a droop angle would get you into a possible excessive response, a too lightly damped roll mode. The actual design value of 2° droop was taken.

THIS ANALYSIS WAS UNFORTUNATELY CONSERVATIVE

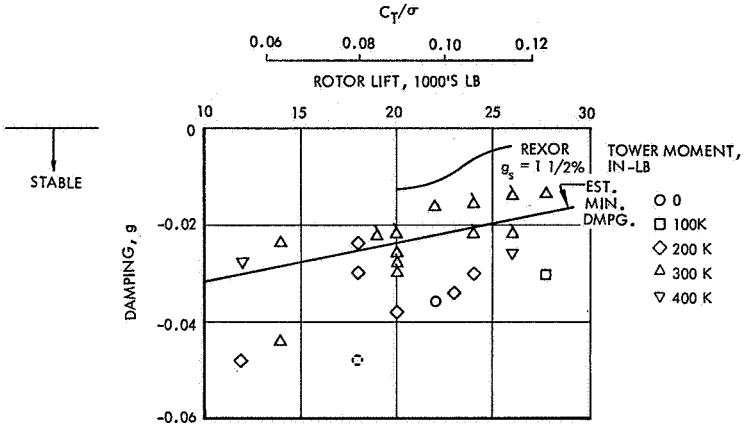

Slide 42.

THIS PRESENTATION GOT THE POINT ACROSS

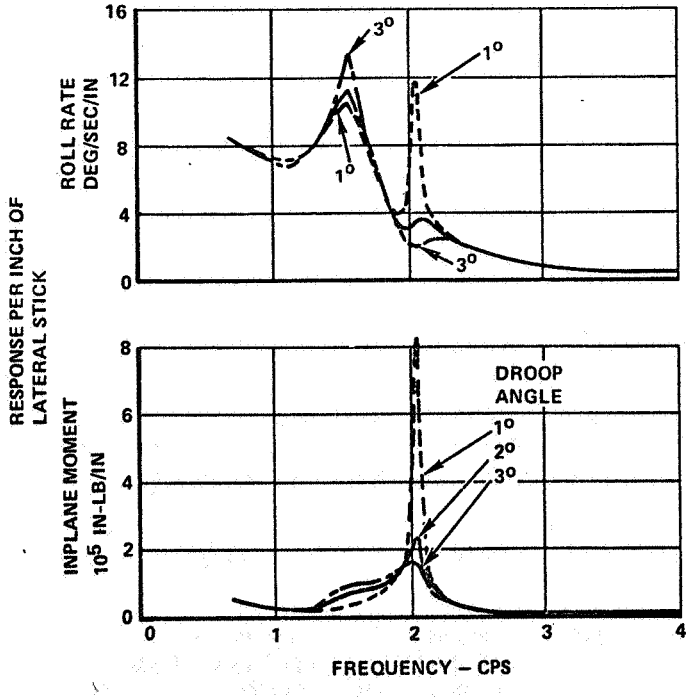

Slide 43.

James R. Neff
Chief of Dynamic Analysis
Hughes Helicopter

I think the basic problem is a matter of getting inputs from a dynamic analysis into the initial stages of the design at the earliest possible time, and this is a very serious problem and one where we need to have programs that may not be quite as rigorous as NASTRAN or the global programs, and that we can get some information put together and get some data together in order to affect the initial stage of the design. Providing these inputs usually requires extensive variations of parameters to be made on structures whose characteristics are loosely defined and in a state of flux. The airframe at that point is not well defined, stores configurations are usually not defined, they certainly are being changed. So we need analysis methods that are inexpensive and require a minimum amount of input data preparation in order to meet design schedule deadlines. Sufficient rigor of the analysis must be retained to assure accuracy of results, at least consistent with the level of definition of structure existing in the initial design stages. You have to have enough accuracy in your analysis to be able to depend on it to some extent. As the design proceeds and becomes solidified, more detailed and rigorous methods are justified. The programs we are using at Hughes to do this are SADSAM and NASTRAN. Another thing that we use in the early stages is, as Dick Gabel mentioned, quite a bit of scaling from existing test data and from models. May I have the first slide, please.

Slide 44 is supposed to be faintly humorous, I know my boss laughed the first time he saw it, but maybe it's more a crying matter than a laughing matter. Anyway that's about the kind of problem that we face in trying to meet the requirements of the design people.

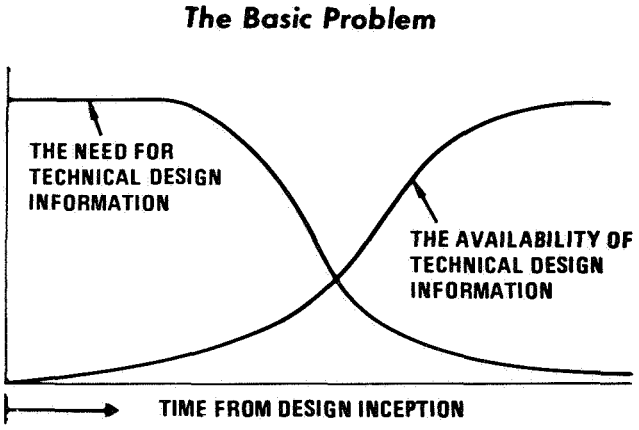

Slide 44.

FINITE ELEMENT PROGRAMS

	SADSAM	NASTRAN
PROBLEM SIZE LIMIT	80 D.O.F.	PRACTICALLY UNLIMITED
TYPE OF MODEL USED	LINEAR BEAM AND TORSION ELEMENTS ("STICK MODEL")	THREE DIMENSIONAL; FRAMES, PLATES, SHELLS
INFORMATION REQUIRED	GROSS SECTION PROPERTIES, GEOMETRICAL LAYOUT, MASS DISTRIBUTION	DETAIL ELEMENT PROPERTIES, GEOMETRY, AND MASS DISTRIBUTION
TIME TO OBTAIN AND ASSEMBLE INFORMATION	DAYS TO WEEKS	WEEKS TO MONTHS
COSTS TO RUN TYPICAL PROBLEMS		
• NORMAL MODES	$10 to $80	$50 – $400
• DAMPED MODES	$15 to $40	—
• FREQUENCY RESPONSE	$6 PLUS $1.00 PER FREQUENCY	$50 – $500
• TRANSIENT RESPONSE	$20 to $50	—
SPECIAL CAPABILITIES	TRANSIENT RESPONSE OF NONLINEAR SYSTEMS, ROTATING COORDINATE TRANSFORMATION (GROUND RESONANCE, ETC.), COMPLEX CONSTRAINTS	

Slide 45.

Slide 45 is a little example here of the two types of analysis that we are using and a comparison to give an indication of what they are being used for and why. The SADSAM program is limited in size of course and NASTRAN is practically unlimited. In the case of SADSAM, linear beam and torsion elements or stick models are used. This is a simplified analysis and it's more adaptable to getting some early answers out. With NASTRAN we set up three-dimensional problems with frames, plates and shells, and of course it is rigorous and by the end of the design we need this type of analysis. The information required: Cross-section properties, geometrical layout and mass distribution – those are gross section properties – for SADSAM. This is information that you can get together fairly rapidly. In NASTRAN, detailed element properties, geometry and mass distribution; it takes quite a bit of time to get this ready and it's been my experience at least that we don't have that type of information ready in time to apply it early in the design when it's really needed. The cost to run these programs is a significant factor in that you need to make variations of parameters and you need to run a lot of cases. If you have a program that costs you a stack of money to run one case and you want to run 20 cases, you pretty soon run out of budget, and of course we have stringent budgets to meet, I think that's true of everybody. We have some special capabilities with SADSAM of course which are not available in NASTRAN. We can do transient response of nonlinear systems, we do rotating coordinate transformations for ground resonance, and conceivably we could match fuselage impedance to the rotor. We have not actually used it in that sense so far, but we could. We can put in complex constraints which also would help solve the rotor fuselage interaction problem.

Slide 46. These are the problems that we apply the programs to. For main and tail rotors, we get natural frequencies, response to flight loads, steady stability, and mechanical stability, using SADSAM both for preliminary design, and final design and substantiation. There is quite a difference I think between the type of program you need early in the design and later on for final substantiation. For the fuselage and fixed aerodynamic surfaces we use SADSAM to solve for natural frequencies, response to flight loads, unsteady

TYPES OF PROBLEMS

PROBLEMS	SADSAM	NASTRAN
MAIN AND TAIL ROTORS		
• NATURAL FREQUENCIES	A,B	
• RESPONSE TO FLIGHT LOADS	A,B	
• STABILITY (FLUTTER AND DIVERGENCE)	A,B	
• MECHANICAL STABILITY (GROUND AND AIR RESONANCE)	A,B	
FUSELAGE AND FIXED AERODYNAMIC SURFACES		
• NATURAL FREQUENCIES	A	B
• RESPONSE TO FLIGHT LOADS	A	B
• STABILITY (FLUTTER AND DIVERGENCE)	A,B	

A = PRELIMINARY DESIGN

B = FINAL DESIGN AND SUBSTANTIATION

Slide 46.

stability – flutter and divergence, in the preliminary design stages. Then we use NASTRAN for the final design and substantiation of fuselage natural frequencies and responses to flight loads and to determine vibration levels.

William F. Paul
Chief Engineer
Sikorsky Aircraft

As moderator, I'm going to wind up the session with a few minutes of discussion and observations. I'm going to address myself solely to the rotor designer's challenge and problems because I think he is in a unique position. He has a product which is very difficult to change and which is very vital to the helicopter, and yet he is very reliant on everyone else's input to it. I think that's very much different from the problems that you have in the airframe or even in the transmission area where you tend to control your own destiny. In this area, and having been there, I'm faced with the first problem which is kind of a dichotomy. On the one hand, you can't afford to make a mistake, even with respect to picking something as small as the trailing edge strip, whether it be graphite or fiberglass to control edgewise frequency, because if you do make that mistake, you probably won't discover it until the aircraft is flying, but you've already qualified the rotor blades and you have spent a great deal of money in that qualification program. So even a small a problem like that begins to trouble you. On one hand then you need to have the best tools you can get. On the other hand – the dichotomy part – the requirement for innovation in rotor design won't wait for documentation and correlated analysis.You've got to proceed, even though you don't have that analysis, so that's what the designer is faced with. In my case, and our case at Sikorsky, I guess we handle this problem by wanting to get as many methods as possible to exercise in order to examine the decisions that we make. Anywhere from the most simplistic to the most sophisticated, and what we are really looking for is the red flag. We make the decisions on the basis of the fundamentals, but try to find out where the red flags are, where the problems are and then trace those down and make sure they are believable. Now, I would like to show you one example of how in the past we might have made a wrong decision but using advanced technology – and I really mean that, advanced technology, particularly with respect to unsteady aerodynamics – we were able to make a design decision that we wouldn't have made in the past.

Slide 47. This is a composite blade which we are developing now, and we had to make a decision on the airfoil, whether it would be cambered or symmetrical – that's really a cambered airfoil with a reflex trailing edge to reduce the control moment. The elastic tip deflection in degrees is plotted versus blade azimuth angle, and this is an indication of what the blade tip is doing and what the control loads are doing. Now, the attractiveness of a symmetrical airfoil is the lower load, and when you look at the performance from an L/D point of view, particularly on the advancing side, it didn't look like the symmetrical or cambered airfoil had much difference, so when we used the steady aerodynamics and the constant inflow the result would indicate that the decision should be made for the symmetric airfoil because of the same performance and the lower control loads.

Slide 48 is the same case but run with unsteady aerodynamics and variable inflow. It took a week to get this plot but we were willing to wait that week. Running time to us is not that important when we are running the first or second cases. Two things happened. First of all, we saw a general increase in the steady moment, but more importantly, the symmetrical airfoil exhibited a high frequency oscillation; you can call it stall flutter if you want. Now, the question is whether to believe this information, that's what the designer faces, and that's where we spent the month to try to understand this result. Was it the input data, was it the information that we had, or was it in fact true. We did find out, as a matter of fact, that the symmetrical airfoil in Slide 47 did in fact have stall except that torsional tip deflection and the control load didn't show it.

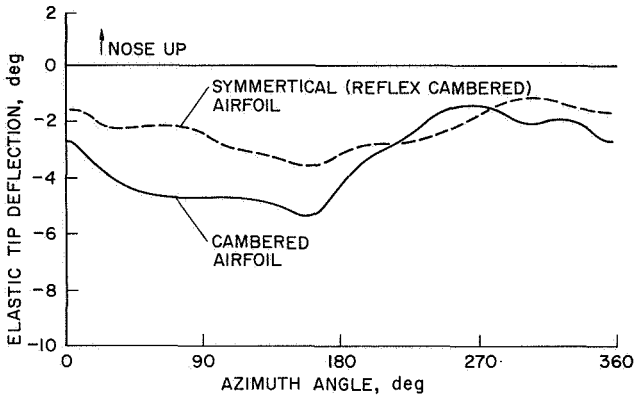

Slide 47.

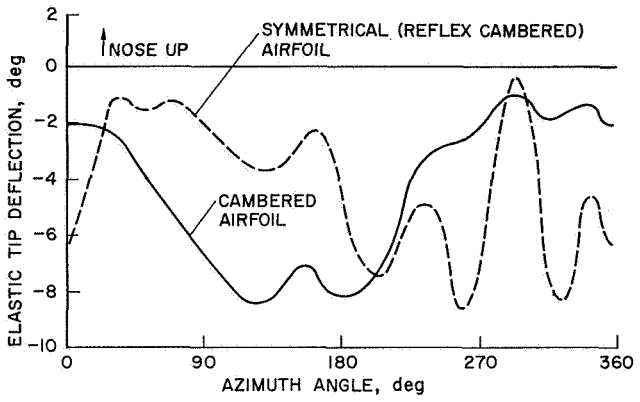

Slide 48.

But in Slide 48, what happened was that the stall showed up in the stall flutter because we used unsteady aerodynamics and variable inflow. So having looked at this thing and dissected the problem – we spent a month doing it – we finally made the decision to go to the cambered airfoil, and accept the larger steady moment but the vibratories would be considerably lower. Now, two messages come up here. First of all, we are using advanced technology in design. We've got to use it. If it's available, we will use it, and we are. Secondly, I think you have made fantastic strides, regardless of the inaccuracies, the qualitative trends are there, and that's what we are looking for. You have made fantastic strides in getting unsteady aerodynamics and variable inflow into our programs. And I think that this is a very profound thing because in the past I remember that looking at the difference between steady and variable inflow there were very small effects, but it seems like the incorporation of unsteady aerodynamics and its impact on stall has had a very profound effect on our decision making process. But the other item and the thing that I would like to ask you to do please is to be sure that in your programs you have the ability to dissect the problem. We've got to understand the answer that you get. There's no question about it. We will not make a decision based solely on computer output, so if it takes us a month to get that answer, we might have to make an arbitrary decision before then. That is a problem and an area where you must concentrate your efforts.

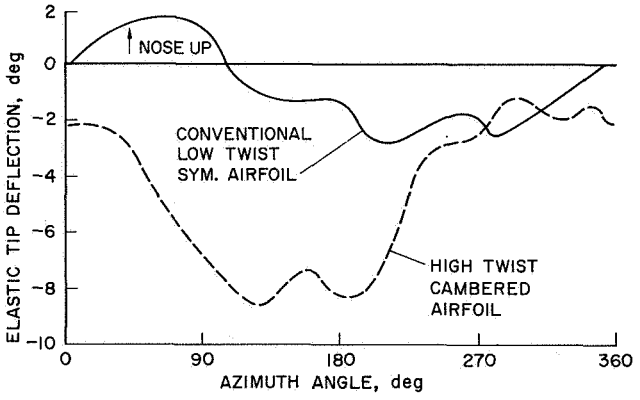

Slide 49.

Now, Slide 49 shows the same thing, the elastic windup versus azimuth, but what we are looking at here is a conventional low twist blade with a symmetrical airfoil, no camber whatsoever, and the same airfoil that we showed before, the high twist cambered airfoil. Now, the main point I want to get at here is that on the advancing side we are running angles of about 6°-8°, now maybe this is not right, maybe it's 4°-6° or 6°-8° or 8°-10°, I don't know, but the key thing is that we are showing that with the high twist blade and the cambered airfoil and the kind of aspect ratio blades that we make, you are going to get a significant elastic windup of the blade, particularly at high speed. Now, in doing so we've got to incorporate this sort of information into our performance decks, because when you go to ask the performance engineer for the computation of performance he gives you the information where the line is right across here, the rigid blade analysis. Generally speaking, that's true since he has his own computer decks. So the point I would like to emphasize here is that I think the aeroelastics must get into performance and performance engineers must begin to quote performance information based on the dynamic information.

Slide 50 is a typical plot of the frequency versus rotor speed, 4 per rev, 5 per rev, 6 per rev, the various lines, and the two modes, these are coupled modes as it turns out, flapwise and edgewise. Now, why do I show this simple plot? Because I don't think we really know how to measure the edgewise natural frequency of a rotor blade. And I'm still concerned that we don't know how to do that in spite of the advances we have made in other areas. And a typical example we had here, there's a dot right here and that dot is the rap test or shake test that we had statically. We expected the information flow along this line and what these dots show are the actual test data that we had on the whirl stand. It's actually worse than this. I should have redrawn the plot, because the departure from that line, it's very significant, the slope differences. The key point is that if you operate at this rpm, what do you believe? Do you believe the analysis, or do you believe the test data, or do you extrapolate this information on up? Now what happened was that we were not able to determine the edgewise frequency because I think we were exciting the control system to try to find the

frequency, or we were putting sheets below the rotor to try to provide some sort of excitation, and the problem is you don't know what the edgewise force is, so you can't normalize the edgewise displacement to the edgewise force to determine what the edgewise frequency really is, and you get a great deal of coupling from the flapwise mode, particularly with a high degree of twist. So if there is any deficiency in the fundamentals, I would say that we should concentrate on defining better methods of determining the rotating edgewise natural frequency.

Now, going to the simpler analysis, Slide 51. We have developed a computer aided design program for rotor blades. It has the ability to select any different airfoil, all the airfoils are in the data bank, and it also allows you to vary the cg-ac offset, compute values of inertia, stiffness, etc., and it saves a great deal of time, particularly on the computation of statics.

We have also incorporated in this, Slide 52, a menu to allow you to select the forward flight condition and actually perform a forward flight analysis of loads and dynamics based on a simplified Normal Modes program, a couple of flapwise modes, one edgewise mode, one torsion mode, constant inflow, but it's a great tool for the designer. Now what he selects here is the velocity and the air density and all the parameters that one needs and on the output side, is the trim condition and it shows that you do in fact need trim.

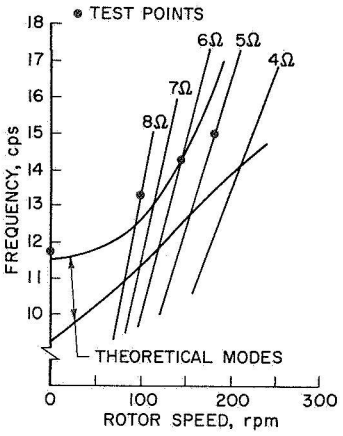

Slide 50.

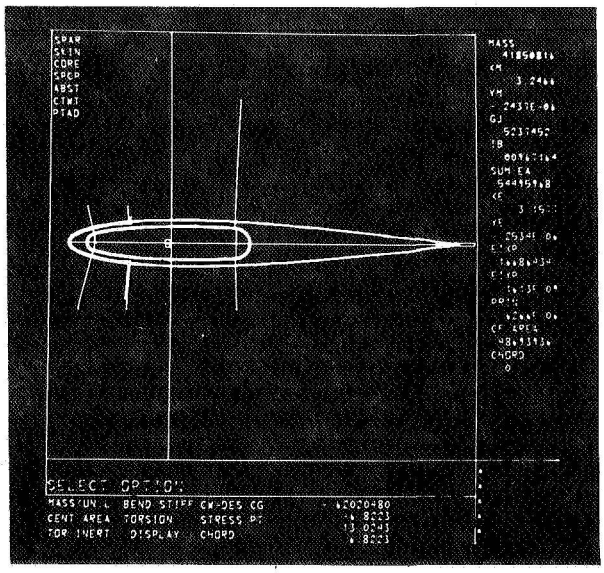

Slide 51.

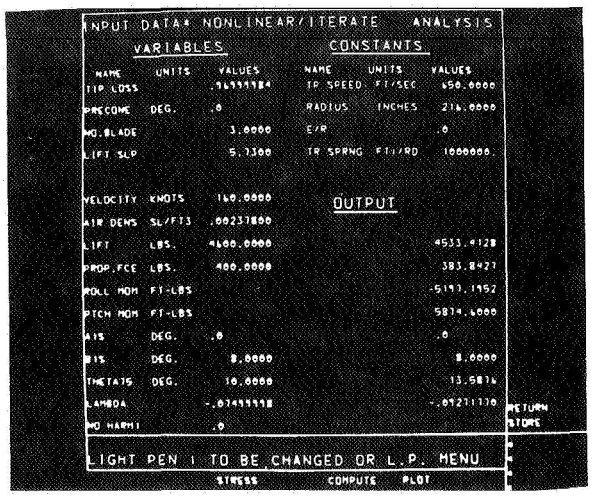

Slide 52.

Then, of course, Slide 53, he is able to predict and see the stresses versus span, the blade motions versus azimuth, or any element that is available in the batch computer process. The advantage here is that the designer is allowed a degree of freedom he never had before and that is – at least using simplified methods – to iterate the design around to something that is optimum for him, but having in there the constraints the dynamicist has to place on him. I remember when we first got this program running, we had one of our most senior designers, and honestly he was really more of a most senior draftsman – because the designer of a rotor blade often is the guy sitting back in Aeromechanics – but in this particular case, we got this 10 year designer in front of the tube, he got out the edgewise natural frequency, it turned out to be 3.9 per rev and he knew that wasn't acceptable. I asked him, "What do you do about it," and he didn't know, but we worked with him and we got the

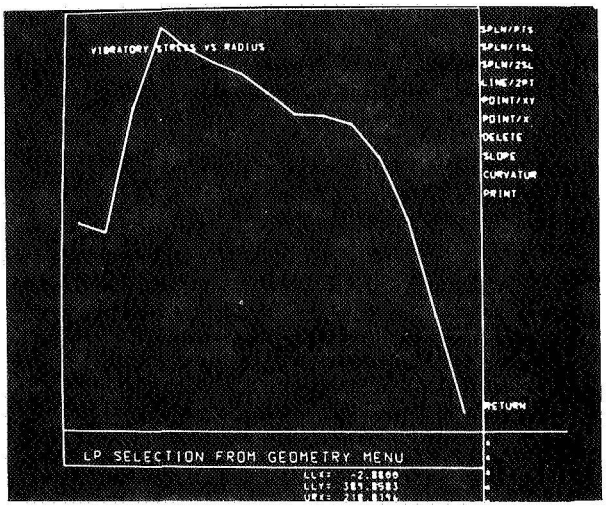

Slide 53.

mode shape plotted out on the tube, he was able to apply some masses and stiffness distributions and optimize the frequency, optimize the stress, and the cost, and the weight, and the reliability, and the rest of it. And this is what we are going to try to do more and more of, encourage our young engineers, and some of the older ones, to becomes designers and not draftsmen, by giving them some of these fundamental tools in the CRT.

I'd like to make one final point on one subject we haven't covered at all, and that's vibration, n per rev vibration. I think the biggest challenge we face is the new challenge the government has given us which is ±.05 g's with n per rev and although I know this is maybe not the area we should be discussing – or maybe we should be discussing it – this is the area we are going to have to concentrate on, I feel. When I looked at the correlation of the various different methods I saw on the first panel this morning, I wasn't startled at the differences between the stresses and motions, but I was very much startled by the very significant differences in the rotor loads, particularly at frequencies of 4, 5, and 6 per rev. Jan Drees if you are out there you know there has been a lot of criticism about two-bladed rotors but the one advantage is that certainly you could predict the loads and you look at the 4, 5, and 6 per rev that we have here and you look at what our dynamicists are doing in terms of looking at the proper phasing and the modes and the contributions and it looks like a waste of time when you look at the variations that we have here. I think it is a very, very serious problem and not one that is going to be completely solved by vibration control devices and I look forward to maybe having some sort of a session some day on just that subject.

Finally, in concluding my remarks, I would say that from a rotor designer's point of view, or any designer's point of view, he needs all the analysis he can get. He needs the sophisticated and the simple, and at face value you might say that that's very expensive, but when you consider the impact of that decision and the investment that you are making in a helicopter, it's a very, very small investment and one that's worthwhile, I think. That concludes our formal discussion, and we are looking forward to some stimulating questions and comments from the audience.

QUESTIONS AND ANSWERS

Panel 3: Integrating Dynamic Analysis and Helicopter Design

Bob Wagner, Hughes Helicopters: I would like to make a comment that I think arises mostly from Rod Balke's presentation relative to the lack of time, lack of information, and the ulcers that arise during the proposal. And I would propose that there not be any dynamics analysis present in a proposal. Since the information on which to base a firm analytical solution is agreed is not available at that time, it would appear then that we are producing a whole bunch of fiction to be read by other people who attempt meaningfully to assess the same. Rather, I believe, that if we were told in a proposal, "Tell me how you are going to analyze these structures, first give me a delineation and an expression how you are going to do it, what methodology, and second, how are you going to handle the problems when they arise in flight tests?" Those two questions, I think, if we were to spend 100 pages each in describing those to the government or to the customer, rather than the 100 pages of analytical printouts, etc. that we now supply, I think that we would be better off.

Balke: I'd like to comment on that just briefly. Of course, as you know, the requirement comes from the military for analysis in the proposal, however, my experience has been that you do need some lead time even with crude parameters to begin to get a feel for what ballpark you are in, particularly when you are working with designs that deviate from previous designs. And secondly, I agree with you, I think maybe a lot of effort should be diverted into a better follow-through in correlating shake tests with the analysis, updating the analysis, to give you a good handle on any future work that needs to be done.

Glid Doman, Boeing Vertol: My question ties right in with Bob's. I wonder if the panel or the room feels that the customer should allow more time during design competitions, or perhaps that we need to induce him to encourage a different philosophy. Would we really do better with more time?

Gabel: I'd like to comment on both of them. I think a lot depends on the energy and perhaps the defensiveness of the contractor on certain points during a proposal. In our UTTAS preparation, the big issue of course was the stability of the hingeless rotor, and we put out a massive effort during that proposal in which we did a huge analytical job, plus a huge model job which went into the proposal, and hopefully we convinced the government evaluators that we had done a good job and the aircraft would be stable. Now, there is an example where probably we could almost stop at that point. We had done such a vast job of preparation and modeling on that issue in the proposal, that what has developed since then, in the actual design of the aircraft has really been sort of minor parameter variations beyond that. So, I don't believe that it's true that proposals have to be goodness and mercy, but rather they can be much more factual with our advanced technology of today.

Doman: That was done despite a large lack of time.

QUESTIONS AND ANSWERS

Session I – Rotor System Dynamics

Chairman: Kurt H. Hohenemser, Washington University
Co-chairman: James R. Neff, Hughes Helicopters

Paper No. 1

HINGELESS ROTOR FREQUENCY RESPONSE WITH UNSTEADY INFLOW

D. A. Peters
USAAMRDL, Ames Directorate

Kurt Hohenemser, Session Chairman: First of all, for a hingeless rotor, say, with one of the usual flapping frequencies of 1.05 or 1.1 or something like that, you have three modes really to consider: You have the advancing mode, which is somewhere on the order of magnitude of frequency of 2.0 and you have the coning mode which is around 1.0 or 1.05 and then you have the regressing mode, which is on the order of 0.2 or something like that. Now, would it be correct to say that for the advancing mode, and for the coning mode, you should really forget about the inflow? While for the regressing mode, you can use, without too much error, the quasi-steady approximation? This is my first question.

Peters: In general, you are correct about the advancing and regressing modes. From [Fig. 6] one can see that induced flow is not important for the advancing mode, while quasi-steady induced flow is adequate for the regressive mode (.2/rev) except at very low C_T/σ in hover. The coning mode, however, which is near 1 per rev, is in the region where unsteady induced flow could be a significant factor in rotor response.

Hohenemser: Well, my next question is the following: In these programs like Rexor and the C-81, by Lockheed and Bell, actually time delays were used for the inflow. Now, did you compare the time delays that were used in the industry with the time delays that come out of the potential theory that you used?

Peters: As far as the Lockheed program, we did not check the time delay they used. However these potential flow time delays, the one for thrust was used in an early report [Ref. 8] where they did transient response – put in a step in collective pitch and watched how the thrust came up – and that correlated well with that data. The time constant for roll and pitch, the K_I, correlated well with the data that Professor Hohenemser had gotten at Washington University, but the potential flow theory is just for zero lift and I'm sure that once lift is on the rotor these values may change considerably.

Hohenemser: So, in other words, you are saying for the higher advance ratio, you have not made a comparison, or rather the lags that have been put in into Rexor or C-81, really have nothing to do at all with your potential lag, is that what you are saying?

Peters: That's right.

Hohenemser: Maybe we could take the opportunity here by somebody who is familiar with Rexor or C-81 to say something about the lag times that were actually put in there. Maybe somebody else made a comparison with what Mr. Peters had.

Jan Drees, Bell Helicopter Co.: I can speak only for a development we had in C-81 which was in connection with a study on gust response and we felt we had to put in a model to represent the induced flow change due to thrust change when you fly into a gust. We took into account two effects, one was kind of looking at the large scale induced flow field assuming a sudden change in lift which was done progressively [and would be] felt in the wake and we made calculations for how the induced velocity would change with time, at various advance ratios. There you find that if you change the collective pitch or you have a sudden change in thrust, that of course the wake will initially not know all this so you work with the induced flow that pertains to the previous lift value. And then gradually it will change to the new value and if you think in terms of a collective pitch change, initially you would develop a lot more lift but that would die out after a little while. Now, that would lead to very large lift overshoots, which you actually can measure in say a hovering rotor. And I think NASA has done some work in this respect. But you have to take into account also the near wake effects if you have a sudden change in lift on the blade. You have a starting wake behind the blade which tries to reduce the lift, momentarily, so that for very high and sudden inputs, and high frequencies also, you're more into the non-steady blade aerodynamics and that will mitigate the lift overshoot. But we found more or less the same conclusion that the effects are most pronounced at the low advance ratios.

Bob Ormiston, AMRDL, Ames Directorate: I just have one question, Dave: The method that you discussed is based on a fairly simple wake model, and there is a lot of work being done on unsteady aerodynamics and downwash theory in other areas of the industry, and I wonder if you could contrast these methods with the method you are using in respect to the differences in applications with these methods.

Peters: Yes, most of the prescribed wake and free wake programs for the induced flow, as was mentioned before, have to do with high frequency response, and with the shed wake of the blade and the fine details of the induced flow [for] rotor airloads, where this

model is just concerned with the low frequency response and just the gross effects. But these programs could be used to develop the L matrix. Remember the L matrix relates induced flow to the thrust and roll moment. These programs could conceivably be used to determine the nine elements in that matrix, to determine a better induced flow model as a function of thrust and advance ratio.

Dick Bennett, Bell Helicopter Co.: Would the techniques that you have used also be applicable to an articulated rotor or is there something special that makes it only relevant to a hingeless rotor?

Peters: Of course the methods would be applicable to an articulated rotor, but of course it's not as important a problem because the articulated rotor does not develop as large a moment so therefore the effect of induced flow would in general be smaller. But if you have a sizeable offset and do develop moments, then it could be used, it is not restricted to hingeless rotors.

Paper No. 2

DYNAMIC STALL MODELING AND CORRELATION WITH EXPERIMENTAL DATA ON AIRFOILS AND ROTORS

R. G. Carlson and R. H. Blackwell
Sikorsky Aircraft

G. L. Commerford
United Aircraft Research Laboratories

P. H. Mirick
USAAMRDL, Eustis Directorate

Ray Piziali, Vizex, Inc.: Could you comment on the apparent, at least it appeared to be an apparent contradiction between your two dimensional comparisons and those you obtained on the rotor. If I interpret it right, your comparisons with the two dimensional tests indicated less aerodynamic damping from your predicted technique. The amplitude of the response appeared to be larger than the test data, whereas it appeared to be just the opposite in the full-scale rotor correlations.

Carlson: Are you speaking of our tests of the oscillating model?

Piziali: Yes, the airfoil.

Carlson: I wish I was able to answer that, to be perfectly honest. I don't really have the answer. It could have to do with the property of the airfoil model and of the fact that it isn't actually a two-dimensional model but you know has end effects.

Piziali: It could be in the three-dimensional effect?

Carlson: Yes. Possibly that's it.

Kurt Hohenemser, Session Chairman: May I ask you a question. I didn't quite understand, could you explain once more what is the basis of the time unit in your time delay method? I have the impression that you really should use a different unit if you go along the blade span. Is it based on the rotational time or on what is it based, that unit of 6? [τ^*, Fig. 1]

Carlson: It is based on the local inflow over each rotor element, each element of the blade along the radius. In other words, it's the Ωr – where r is the radius to the element – plus the local airspeed over the blade element.

Hohenemser: I see. So actually in real time, the delays are different along the blade?

Carlson: They are. Well this is probably a problem that it has, actually there isn't enough interaction between the elements on the blade. And each one is stalling on its own at a different instant.

Hohenemser: Also I noticed you had one graph without any scales on it for damping. Was that left out purposely?

Carlson: No, it's in the paper, I think. Actually our visual aids were rushed at the end here and it was left out.

Hohenemser: It might be interesting to show this once more and explain to us what the scales actually are.

Carlson: O.K., that's [Fig. 3] – The bottom of the trough here curves at a mean incidence angle of approximately 20°. The damping begins at drop off in the area of 12°. [Below that] I basically have potential flow, and the damping that's associated with it, and at higher angles it drops off. The magnitude of the damping – it's a non-dimensional term and I would have to refer to one of the earlier references for description of it.

John Ward, NASA Langley: Ray, how did you handle unsteady drag in these calculations?

Carlson: Well, this isn't handled at all, actually. In all of this, all we have is the drag that you pick up from two-dimensional steady tests, that's all. Now, this is an area that ought to have more work and it's an area that I suspect will help us out in giving more accurate edgewise response that we have had. However, it is an area that isn't handled in here.

Tarzanin, Boeing Vertol: In your time delay theory, you have a separated flow c_ℓ vs. α. You didn't talk about it here, but you do in the paper. How is that determined?

Carlson: It's based in part on looking at the hysteresis loops of blades and in looking at a blade in terms of the lift that it would have if the flow was purposely fully separated and the magnitude we had here was on the order of sin 4 α.

Tarzanin: So you didn't simply put a line through the bottom of the loops.

Carlson: No.

Tarzanin: Second question: Has the α, A, B method changed significantly from the previous reported results?

Carlson: No, we have altered the means of scaling it and I left this out. We are using it on other airfoils, basically scaling the hysteresis loops around the two-dimensional characteristics of other airfoils. If there is any improvement in the method, it is in this area.

Tarzanin: Has it been a Mach number correction?

Carlson: It is in there, in a way, but –

Tarzanin: The same method essentially as before, right, you just did a $1/\sqrt{1-M^2}$ correction?

Carlson: Yes, that's all it has in there, right.

Tarzanin: So in the theory, improvement is due to the downwash, essentially.

Carlson: It is actually, yes, we have worked harder at modeling it and using as accurate a model of it as we are able to.

Glid Doman, Boeing Vertol: I'm wondering if in the analysis of the flight test data – [the] interpretation of the flight test data push rod loads – you've looked into the possible interrelationship of the loads in the stalling blade to those in the adjacent pushrod, in terms of swashplate motion. The hypothesis being that the rotor might not have flutter at all, but you might be seeing the stall load in the stalling blade appearing in the adjacent push rod.

Carlson: We have looked at it and all of our blades are acting comparably at equal azimuth angles.

Doman: The swashplate is moving?

Carlson: It is. Really, I haven't any indication that this is the cause of it. I suspect we could look into it more but – well there isn't any indication of it that I am aware of.

Jan Drees, Bell Helicopter Co.: We are always struggling with the question: Do you have to include yawed flow effects, like Frank Harris showed that you should many years ago? In your correlation studies, are you using this?

Carlson: No. It isn't in here.

Drees: And why not?

Carlson: Well, that's even harder to answer but we haven't put it in and it is interesting and I don't know how major an item it actually is. It's on our list of items to look at as a possible improvement area.

Drees: Usually the effect is that it reduces the stall effects. It would make the correlation worse.

Carlson: Well, that's possible.

Marcel Kretz, Giravions Dorand: I would like to know to what extent the similarity conditions were respected during your tests? As far as the Reynolds number is concerned, for instance, and the reduced frequency.

Carlson: Well, in the tests the Reynolds number isn't accurate, it isn't representative of the actual aircraft. However, the reduced frequencies – in the model that is torsionally sprung, the mass and inertia of the airfoil are all accurately scaled. However, it is a small

model and it is off in the Reynolds number that we had. Our scaling of the unsteady aerodynamics in each instance, is about the two-dimensional steady data of the actual model that I was using, and this is also accurate.

Kretz: Second question, did you run into flutter during your tests?

Carlson: Yes – well it depends on your meaning of the word. Is a high torsional oscillation at the natural frequency flutter? If it is, yes. There is a question here, is it stall flutter or is it a high amplitude response of the blade due to an impressed moment at an instant. I have a little of each acting, I think. I have a change of exitation as I enter stall and I also have a negative aerodynamic damping entering in to build up this oscillation afterwards. From that angle, I have a little of each and it's a little hard to split off which is which here.

Kretz: Are those oscillations explained by your theory?

Carlson: Yes, I am able to pick up the amplitude and the overall physical characteristics of this oscillation. From this angle it is explained, yes.

Bill Wilson, Bell Helicopter Co.: In one of your earlier slides, probably the third or fourth slide, you showed in the time delay, that you had three different scales going from low frequency to high frequency, would you care to put some numbers on those frequencies, please?

Carlson: Well those are actually made up in my head from looking at typical hysteresis loops. I'm actually hard pressed to put a number on any of them.

Piziali: With regard to the apparent discrepancy between the two-dimensional and three-dimensional comparisons, you mentioned in your full-scale comparisons that the computations included the induced velocity variation. Was this induced velocity variation compatible with the solution at each instant of time or was it like a fixed inflow distribution, non-uniform, but fixed in time? The reason for the question is that it's possible, maybe, that since the blade does not stall over its entire span, you may be getting damping from the wake over the unstalled portions of the span in your analysis.

Carlson: Well, it is handled in iteration, actually, and there really isn't the total instantaneous interaction there. I run the blade response program for the blade loadings and motion, then I use it to describe a model of the wake. This, in turn, describes the inflow over the rotor and then I run the blade response history over again, and if it isn't altered appreciably, then I hold that I have a reasonably accurate modeling of the inflow. If it is altered, then I iterate again on the modeling of wake and the inflow. And I have.

Paper No. 3

COMPUTER EXPERIMENTS ON PERIODIC SYSTEMS IDENTIFICATION USING ROTOR BLADE TRANSIENT FLAPPING–TORSION RESPONSES AT HIGH ADVANCE RATIO

K. H. Hohenemser and D. A. Prelewicz
Washington University

Earl Hall, Systems Control, Inc.: Did you have any convergence problems using the extended Kalman filter? This is one of the major criticisms of this approach when it is applied to realistic data.

Hohenemser: Well, I can tell you something else that is in the paper and that I didn't mention here. We first used a very simple equation, namely Mathieu's equation, of a periodic system which had much less periodicity than the system that we used later, and we tried to apply a nonlinear estimation where the parameters and the state variables were estimated at the same time, and that converged only if you really knew pretty well the values of the parameters. So if we really put relatively large errors in there, and if we were not very careful to match the initial covariances with the initial values of the estimates, that actually did diverge. But with this linear estimator, we didn't have any problems with divergence at all. Only after smoothing the data with a digital filter. Well the convergence, I guess, is always there because as soon as the covariance matrix components go to zero, you just don't get any change of data any more. So it converges, obviously, as soon as the P components are all zero. But, of course, it converges to a wrong number.

Hall: Did you do any investigation on the confidence bounds of the parameter estimates you were getting? In particular, did you investigate what the effect of the pre-processing filters was on the confidence bounds of the parameter estimates?

Hohenemser: No, we didn't do that at all. Of course, in order to do that, we really would have to have gone through a lot of analysis, I mean either do it theoretically, we didn't do that, or we could have done it experimentally by just running these things a number of times but we didn't do that. Well, we ran it maybe two or three times and they all looked about alike, like the one that we showed you, but that of course doesn't mean that we actually got confidence bounds.

Hall: In the paper you mentioned selecting elements of the information matrix or the interpretation of the information matrix here P, and looking at elements of that and possibly figuring out problems related to identifiability. Have you considered alternately using the elements of the sensitivity function themselves, $\partial H/\partial a$, in order to give an indication of those modes which are and are not excited?

Hohenemser: No, we didn't do that here. Since the system is relatively simple, we have only these two modes and so you have to be sure that both of these modes are well excited, obviously, and that was the reason why we had these two gusts, first the gust up and then the gust down, in order to make sure that they are both well excited. We first tried it with only one gust and that didn't always give us good results, so you have to be sure that you have sufficient excitation in the system, in order to get a good result. That is quite clear.

Professor Bryson, Stanford University: I think it is a very commendable beginning in using this type of technique for a complicated problem. I think that Earl Hall has indicated that the real problem is a lot harder and I think you are aware of that, too, that the modeling errors creep in and you have to make some estimates, using this type of theory, of some white noise or some colored noise that enters into the process equations themselves. And if you then use accelerations as your measurements there's a further complication, namely that your measurement noise is correlated with the process noise because the accelerations contain them. This has been handled too but it's still a long way, it seems to me, from these beginnings to a system that will work on measured real data.

Hohenemser: Well, we'll see. We are presently running wind tunnel tests and want to try it out in the real world. But, of course, we tremendously exaggerated the measurement noise here. Actually our wind tunnel measurements are much more accurate than what we assumed here, so I would hope that the modeling errors that we will obviously have in the wind tunnel tests, will compensate, somehow, the tremendously exaggerated measuring errors that we have assumed in our computer studies.

Paper No. 4

DYNAMIC ANALYSIS OF MULTI–DEGREE–OF–FREEDOM SYSTEMS USING PHASING MATRICES

R. L. Bielawa
United Aircraft Research Laboratories

A. Z. Lemnios, Kaman: In the model that you investigated with the aft chordwise cg position, did you assume coincidence between the aerodynamic center, the elastic axis, and the quarter chord?

Bielawa: I assumed that the aerodynamic center was at the quarter chord.

Lemnios: Therefore, you had a detrimental cg-ac offset effectively?

Bielawa: Yes, I was introducing it purposely because I knew *a priori* that this would demonstrate the instability very well. I might add that the equations that I used are intended only to demonstrate the mechanisms of the matrices and are not intended to break new ground in that area.

Lemnios: Following this, one more question. You therefore had an aerodynamic spring effect basically from the torsion mode being fed into your bending or flapping modes. Did you have a corresponding – I don't see how you could have – but did you have a corresponding term of an aerodynamic stiffness due to moment in the torsion mode as well?

Bielawa: No. You do get a centrifugal moment, of course.

Dick Bennett, Bell Helicopter Co.: I was wondering about the applicability of the method to forward flight and second, have you done any work in adapting this method to understanding what you get out from a Floquet type of analysis?

Bielawa: Well the answer to the second one is simpler, no, I haven't. I would answer the first question by saying the method is not geared to any kind of a rotor eigensolution problem. It's geared to a more general class. If you can describe the equations of motion as a series of constant coefficient matrices, that is all you really need.

Hohenemser, Session Chairman: Well I think Dr. Bielawa really deserves congratulations for a very simple and very effective means of making the complicated relations between the various dynamic variables visible and I have the feeling that this method will really lead to very large progress in really understanding these complex connections that we have in instability problems. Thank you, Dr. Bielawa.

Paper No. 5

SOME APPROXIMATIONS TO THE FLAPPING STABILITY OF HELICOPTER ROTORS

J. C. Biggers
NASA/Ames Research Center

Peretz Friedmann, UCLA: I have one comment which I would like to make. I don't really see in what way your conclusions differ from the work which is given in the various papers by Professor Hohenemser because if I can recall your conclusions correctly, conclusion number one said that fixed coordinates give more insight and all I can say about this conclusion is that insight is something which varies from person to person and some people can get insight also using Floquet theory. That's not really that important. And the second conclusion is that for low advance ratios you can consider the equations to be constant coefficient equations which is essentially mentioned a few times in Professor Hohenemser's papers, and the third conclusion is that at high advance ratios you have to go to more complicated methods which is again a comment made in Professor Hohenemser's papers. So what really is different from what you show?

Biggers: O.K. Professor Hohenemser's work mentioned the constant coefficient, kind of as an aside – incidentally: Here it is. But I wanted to take a little harder look at it. I found it a little bit surprising that it would work on the articulated type of rotor which Professor Hohenemser had not mentioned in his work. I was not terribly surprised that it worked well on the hingeless [rotor] but you notice that with the articulated rotor, there is a very large frequency and damping change. Whereas, with the hingeless rotor, I had to greatly expand the scales on these plots to show the effects clearly – so the changes in frequency and damping on the hingeless machine are not very high. But with the articulated rotor, you get some very significant changes and the constant coefficient approximation for the low frequency modes, does a surprisingly good job.

David Peters, AMRDL, Ames Directorate: I think it's not correct to say the hingeless rotor doesn't show the effects and the articulated does. It depends on the Lock number and P. And for any P value you can find a Lock number where these effects are big and other Lock numbers where the effect is small.

Biggers: That's true.

Peters: The same with the articulated rotor as you found, at a Lock number of 6 no periodic effects, hardly at all, at the low advance ratios. But [if] you get exactly the right Lock number then you can get the effects.

Biggers: Right. This is more clear from some of the other figures that are in the paper. The γ-μ plane, I think, shows it pretty clearly.

Earl Hall, Systems Control, Inc.: As you know, I've been associated with Floquet analysis for some time. I guess I've had a question thrown at me many times. There's been a lot of mathematical work done on the only method available for solving linear differential equations with periodically varying coefficients. But I think particularly with respect to the frequency entrainment which is associated with half of the basic cyclic variation, there is still in my mind and I think perhaps for many of the people in this room [a question]: What experimental verification do we have that such a frequency entrainment exists and how does it manifest itself in an actual helicopter? Is there anybody who has some information along those lines? I mean, the thing is there, whatever it is, it's there, but what does it look like?

Maurice Young, University of Delaware: I would simply like to suggest that since the constant coefficient method works so well at the very low advance ratios, why not use it once again with a simple perturbation in advance ratio? In effect, you have the low, or zero μ solution, you perturb it once in the first power of advance ratio, and I would think you would have an excellent approximation without the complications of the periodic coefficient differential equations.

Biggers: O.K. that has been done by Wayne Johnson in one of the references in my paper, and that work is very useful. So that technique is also available. The other thing about the equations that I discussed, is whether you use it in the constant coefficient or with the periodic coefficient, the non-rotating degrees of freedom do include all blades.

Young: What benefit, if any, in this type of approximation, could be gained by reducing the differential equations to a standard form, eliminating the middle term, or the damping term, by a proper transformation?

Biggers: You mean, a state variable form? Oh, O.K. The Hill's equation form. I don't know, I didn't look at that. One thing is that – one point I want to make on this thing is that there are undoubtedly cases where the approximation will not work. There are other cases where it is a very good approximation. And the point is there are still going to be a lot of cases where all the standard techniques that have been developed through the years can be used. But you need to check them using Floquet theory or some similar device.

Hall: If I might express a theoretical point of view, this question of transforming a periodic system to a constant system is treated extensively under the theory of Liapunov transformations. This says, that if you have a periodic system, there does exist a constant coefficient system which will represent the response of that. This Liapunov transformation by the way has the rather nice theoretical

property that it is almost impossible to find. However, it might be interesting to see whether or not approximations such as this can be interpreted in terms of Liapunov transformations and if that is the case, perhaps the degree of applicability of such transformations could be extended such that they would have more application to the interpretation of flight test results. Just a comment. Thank you.

Hohenemser, Session Chairman: I might mention something with respect to Dr. Hall's question. If you go back to the Lockheed history, they very definitely had that one and a half per rev that comes in from the Floquet theory so it has been observed in hardware, it's not that it's just theoretical.

Pete Arcidiacono, Sikorsky Aircraft: A more practical question: Have you exercised your analysis and made these comparisons for four, five, and six bladed rotors and come up with an estimate of what advanced ratio you feel the constant coefficient method would work? In a three-bladed rotor you show it's only like 2/10ths, 3/10ths advance ratio.

Biggers: No, except for the coupling that might come in due to slightly different flow fields due to different numbers of blades, I think you can look at the γ-μ planes that are in the written version of the paper and get a fair idea of the places where you can expect trouble from periodicity.

Arcidiacono: Did you look at the higher number of blade problem?

Biggers: No, I looked at the 4-bladed and that is in the written version of the paper and as far as the constant coefficient approximation is concerned, it looks just like this one [the 3-blade case] except you have another degree of freedom which is blades one and three up and two and four down. You know, differential coning kind of thing, and for that one, when you do the approximation all the periodicity goes away, it decouples from all the others and it looks just like the hover rotors so that was not much use.

Arcidiacono: Thank you, I would like to compliment you on your paper. I think you've made a very real attempt to communicate the results of your work to the audience.

Hohenemser: I agree with this. Let me say one more word on this. Maybe this should be in the form of a question: Isn't it correct that below the branch point in the complex plane, not when its on the real axis, but if you have a branch point in the complex plane, and you are, with your parameter, below that branch point, then the constant coefficient approximation seems to be quite good. But once you are beyond that branch point where you had actually a single complex root of the Floquet transition matrix, then you have to be careful. Sometimes the constant coefficient approximation might be useful but it may also not. Would you agree with this?

Biggers: That's correct. If it turns out to be a case where it does turn the corner you have to be careful and examine it.

Frank DuWaldt, Calspan Corp.: Kurt, I'd like to first of all congratulate Jim again on the paper. There was a study in which the expansion was made in advance ratio, and in which we tried to interpret some old flutter results that we had which appeared to us to support the belief that the integer and half integers are in fact experimentally identifiable in forward flight flutter cases. The work was reported at the Air Force Flight Dynamics Laboratory V/STOL Conference in Las Vegas in September of 1969.

Biggers: Thank you.

Hall: That was the work of Daughaday and DuWaldt at Cornell [Aeronautical Laboratory]. That was what he [DuWaldt] was referring to which was done on a model.

Paper No. 6

FLAP–LAG DYNAMICS OF HINGELESS HELICOPTER BLADES AT MODERATE AND HIGH ADVANCE RATIOS

P. Friedmann and L. J. Silverthorn
University of California, Los Angeles

David Peters, AMRDL, Ames Directorate: I have one comment and one question. The comment is on the radial flow term. I don't know if radial flow is the best term to call it. In every paper I have seen on flap-lag in forward flight, except I think an earlier one of your's and Pin Tong's, it's in there and it's not called radial flow. It has to do [with the fact] that the blade is not at ψ but it's at $\psi + \zeta$ because of the inplane motion, you must take that into account. The question is that there are two assumptions you made in the beginning in order to get what you call the gut feel and the one assumption was that you use the hover value of trim of β_0, and no cyclic pitch or no β_s or β_c trim. And also the assumption that you used the hover induced flow rather than the forward flight induced flow. And from the work we've done, those kind of assumptions will actually give qualititatively inaccurate results, and I was wondering how limited you think your conclusions are, based on those two assumptions?

Friedmann: As you realize, I am very honest in presenting my results, and that is why I showed you how important collective pitch is. And as you well know, if you are aware of my report which was funded by AMRDL-Ames when I was at MIT, I started out by putting in trim and then after that experience with the trim procedure, I came up with the conclusions that using trim gives you a kind of effect which has a tendency to mask the effects associated with: a) periodic coefficients, and b) what is the effect of including the lag

degree of freedom. In order to be even more honest, I have now a program which does it with the trim procedure and its quite significant and its very case dependent. It's difficult to generalize.

Earl Hall, Systems Control, Inc.: With all due respect Professor Friedmann, many of the results that you presented were also in Reference 10, of your document. I would like to ask one question. I have also been working recently in a problem similar to what you have described here. It is for others to go into the details of that. But one recurring problem that we have faced, and I would like to know if you found a solution to it, is how to determine what frequency you actually have. In other words, Floquet theory has an ambiguity to it in frequency. Now there are analytical and experimental techniques for determining these. I'm just curious if you have attempted to address this problem in your work, or have done what we've done which is rely on some of the more expensive computational procedures to determine the frequency.

Friedmann: O.k. I'll answer your questions starting with the first part. I am very well aware of your report and I have been aware of it for a long time. And, I should also be honest in saying that from your report, I did not get a satisfactory gut feeling and that's why I decided to look at this thing, too. And I think you would agree with me that when you worked on this problem, you were more control systems oriented than helicopter blade dynamics oriented, and that's why maybe some of the gut feeling was missing. And regarding your second question, my recipe which I don't consider to be a good one, or the best one, but it's the one which for me works, is that I start my computations at μ equal to zero and I usually know what's going on at hover and that's how I physically identify the various modes and I simply trace them. And when they split, I still easily can keep track of them. That's the only method which as far as I know works.

Hall: That appears right now to be the only method. You can do it by other methods but they can assume all the storage of a 360 computer.

Hohenemser, Session Chairman: Maybe I should mention in this respect, I believe that what he really did has not very much to do with periodic coefficients at all because that has been done before using these multi-blade coordinates that Mr. Biggers told us about, and when you use constant coefficients, you also find that instability. There's a lot of literature available from Lockheed and from the people at Boelkow and from Westland and so on where they determined the lag instability and now it is also known from the literature that the inflow has a tremendously large effect. Now, you used a very, very simple inflow model that has no non-uniformity in the longitudinal direction. Now it has been established in literature that the non-uniformity of the inflow has a large effect on the stability of the inplane motion. And also it has been established in the literature, that the elastic lag-flap-torsion coupling is one of the main parameters that enters into the stability problem and you have also neglected that so I think, really, you are still quite a bit away from really getting close to the actual blade stability, but nevertheless, the thing that you are doing is very valuable because it is certainly including more than many other people have done.

Jan Drees, Bell Helicopter Co.: Since this radial flow is such an important parameter – I still don't understand what it is and I don't have a gut feeling for what you mean there – could you explain what it is?

Friedmann: Let me tell you what the term is. If you want to think in terms of an articulated blade, it's simply a beta times zeta term times $\mu^2 \cos^2 \psi$ term which arises in the aerodynamic term associated with a lag degree of freedom.

Hohenemser: I think it's a term that most people have included. It's just a new name for it.

Maurice Young, University of Delaware: Just one last point. I think in some of these individual blade dynamic studies, there's always a temptation to say that the blade is a cantilever, as you have done and many of us have done before. I'd like to suggest the concept of reduced mass, that is, not assuming that the fuselage is of infinite mass. In other words, a moderate refinement will produce the same sorts of changes that some of these other parameter variations produce. So, I'd suggest that when you have these infinite hub mass calculations, with a little bit more work you can re-interpret them in terms of a real hub mass.

Bob Ormiston, AMRDL, Ames Directorate: I think we are really a very long way from understanding the true nature of the problem and qualitatively whether stability or instability exists in forward flight even for the flap-lag system without the torsion. I think in that sense that we have to look at these results and say we really don't know what's going on yet. I'd like to amplify a little bit what Dave Peters was remarking about. He was talking about some of his work. Using somewhat different assumptions on trim and some of the same basic assumptions, some grossly different stability behavior was observed. So I think there is some question about the interpretation of these results and there's going to be a considerable amount of effort that has to be done to really resolve some of these. One more point is that in the paper it's mentioned that droop has a large effect on stability in hover and I don't understand the reason for this, it's quite contrary to some of our results. We've used several approximations for flap-lag stability in hover, and we definitely do not see a strong sensitivity to droop or, as we define it, preconing.

Friedmann: The Lockheed people claim that droop has a very large effect. That's all I can tell you.

Ormiston: I'd like to say that the Lockheed work, as far as I understand it, does include the torsion degree of freedom and that is probably the most important factor here because of the way it couples with the flap bending and lag bending and directly influences stability. So droop and precone are very important factors if you're considering the full flap-lag-torsion problem. But for flap-lag – I can't say anything about forward flight – but in hover, our results show it doesn't have an effect that's appreciable.

QUESTIONS AND ANSWERS

Session II – Helicopter Vibration and Loads – Theory

Chairman: E. Roberts Wood, Lockheed-California Company
Co-chairman: G. Alvin Pierce, Georgia Institute of Technology

Paper No. 7

CORRELATION OF FINITE–ELEMENT STRUCTURAL DYNAMIC ANALYSIS WITH MEASURED FREE VIBRATION CHARACTERISTICS FOR A FULL–SCALE HELICOPTER FUSELAGE

I. J. Kenigsberg and M. W. Dean
Sikorsky Aircraft

R. Malatino
Naval Air Systems Command

David Peters, AMRDL, Ames Directorate: You mention in the beginning, you used the philosophy of building up the fuselage from components. I take it you reduce out degrees of freedom and then add them together. Had you thought of calculating the mode shapes of the smaller components, and then using modal composition to get the overall mode shapes of the structure?

Kenigsberg: Well, that's the method of substructuring. What I was referring to is the structural modeling techniques and the allocation (and the location) of dynamic degrees of freedom to each component, under the assumption that you had correlation. Then you added something like a sponson. Model that, represent your mass distribution, add that to your structure either as a complete addition or by substructural analysis, and compare the correlation. If now there's a degradation in correlation it has to be an error in the modeling technique for the last element added, because everything else is correct. But this can be applied whether you use substructuring or not. This was a test and correlation approach.

Marcel Kretz, Giravions Dorand: The first question, did you make any attempt to evaluate the damping of your structure?

Kenigsberg: No, we did not during the course of this shake test, but during other tests that we have run on other vehicles, we have found the percent critical damping on fuselage modes varies from about 3% to about 6%.

Kretz: It's purely experimental?

Kenigsberg: Based on experiment, that's correct.

Kretz: The second question, what is the accuracy of your theoretical evaluation, in general?

Kenigsberg: On the fuselage first vertical bending mode, first lateral bending mode, and transmission modes, we had an average error between predicted frequency and measured frequency of 3% to 4%.

Bill Nettles, AMRDL, Eustis Directorate: Irwin, I don't know exactly how to paraphrase this but in looking at the calculation accuracy you've got with the system without the appendages [stripped vehicle], you had a relatively complex system where the individual elements were of significance to the problem. Now did you in fact, when you added these other lump masses in given areas, actually diminish the significance of the smaller components, and in essence, create a simpler problem, thereby allowing a more accurate solution, if you will. Did you actually go from a very complex problem of small elements to a new superimposed problem which included the small elements but which became predominated by the large masses?

Kenigsberg: Well the answer to your question is yes, we did by adding the ballast, attack a simpler problem. We did not change the structural representation, we added the ballast. What we were trying to analyze in the stripped configuration, was a shell structure with a limited number of dynamic degrees of freedom. We only applied 200 dynamic degrees of freedom and we were getting modes well over 2,000 cpm. We were trying to develop modeling techniques which could be applied to the helicopter. The helicopter has a large transmission, a concentrated mass. It has a large concentrated mass at the tail rotor, so we can safely say that the modeling techniques we've evolved as a result of this will apply when analyzing the helicopter, but if you went out and tried to analyze the shell of a space vehicle, they would not apply.

Nettles: My question is, I guess, do the two different configurations actually represent two different problems. One in which the ability to predict accurately is a good deal more difficult than the other case?

Kenigsberg: Yes, in the stripped vehicle we would have to go to a much higher number of dynamic degrees of freedom in order to get the level of correlation that we achieved. They are two different problems.

Bob Donham, Lockheed California Co.: In your model analysis, you mention the essentially plate restraint that you placed on the forebody which you think affected the behavior of the pitch degree of freedom of the transmission. I think you might have said something about the mass effect, and I was thinking more of the elastic properties of the root restraint of the transmission. You might comment on that.

Kenigsberg: The point I was trying to make is that from our experience, the transmission pitch mode is to a great extent controlled by the frames immediately below the transmission and the mass and inertia of the transmission. And if you completely strip a vehicle and go to a shell representation, and try to predict the mode shapes and the frequencies there, then the point I'm trying to make is that it's not fair to take a shell structure and make a beam out of it and try and get an accurate prediction of that mode. However, as we kept that same modeling assumption in the analysis, representing the full fuselage as a beam; when we added the fully assembled transmission, or the equivalent of a fully assembled transmission, in that case we got excellent correlation.

Donham: Yes, I think that clarifies the question. I guess really the point that I understand you to make is that you have to get a sufficient distance from the transmission base to be able to get the elastic properties of that support.

Kenigsberg: Maybe I should reemphasize that if you were analyzing a vehicle without a rear cargo ramp, then all you need consider is a detailed finite element model, for example, spanning about 8 bays about the transmission region. That would give you an accurate prediction of the fuselage mode and the transmission mode.

Donham: You mention that you had considered the panels to be non-buckled. I noticed in some of the maneuvers that you've made with the aircraft, that the panels are heavily buckled. What's the relevance here to your prediction, or have you made some calculations to assess that effect?

Kenigsberg: Well, vibration levels always change in maneuvers, but when we design the vehicle from a vibration standpoint, we're designing for the 1 g level flight condition which is basically an unbuckled state.

Bob Wagner, Hughes Helicopters: Presumably, you had a tremendous amount of detailed information relative to section properties.

Kenigsberg: That is correct.

Wagner: Now, would you care to comment on the accuracy, that you might have in the course of preparing a proposal where you haven't got so much detail information.

Kenigsberg: All right, I should have emphasized then and I didn't, and I'll do it right now, that I believe that in order to get this level of correlation you have to have accurate structural data. And in developing the input for these analyses we actually went through the drawings one by one and generated the frame properties, the stringer areas, the skin thicknesses, the moment of inertia of the frames, and input it to the analysis. I believe that during a proposal effort, you would not have that type of accuracy, and I think therefore, from a time standpoint, we all have to give consideration to integrating our structural design analyses, and our dynamic analyses, so that as rapidly as possible, the structural data base required for the dynamic analysis, could be updated. This is why we're going away from the FRAN analysis and beginning to use the NASTRAN analysis for dynamics because we're using that for stress as well, and if we can combine the two we can get an accurate structural data base in the most rapid fashion. But it does require an accurate representation of the structure.

Paper No. 8

COUPLED ROTOR/AIRFRAME PREDICTION METHODS

J. A. Staley and J. J. Sciarra
Boeing Vertol Company

Dick Bennett, Bell Helicopter Co.: Are your externally applied air loads treated only in terms of harmonics of 1 per rev and 2 per rev?

Staley: Yes, this analysis as indicated here would be performed one harmonic at a time, in other words we would only feed back one harmonic of hub motion into this analysis, and ideally we should consider effects of other harmonics, their effects on the vibratory hub loads.

Vincent Piarulli, Pi-Rad, Inc.: In your optimization techniques, if you start looking at more than just getting the response to 4 per rev, what is your criteria going to be for optimizing?

Staley: Well, the more things you try to satisfy at one time, the more difficult the problem becomes. The approach that was basically mentioned here was an attempt to identify structural members which could be changed to move particular resonances either above or below a particular exciting frequency. Conceivably, modes that would be excited at say, 4 per rev on a 4-bladed helicopter would not necessarily be involved in response at 1 per rev so that if we could identify members which could be changed to modify the frequency of one mode without affecting the frequency of another mode then that would be the optimum condition. That's not always possible, but usually there are some members which affect a particular mode without having a great affect on another mode. At this point, I don't think the solution to this problem has been completely put into closed form, and people are using a more or less trial and error approach to this problem.

Bill Nettles, AMRDL, Eustis Directorate: You said that there were something like 1849, I think, structural mass degrees of freedom. My question [is], since numbers like this stick in people's minds long after the subtleties of your program: Do you in fact have a dependency in your so-called structural degrees of freedom, that you can somehow reduce down such that you are using the term degrees of freedom loosely, are they truly degrees of freedom? Do you really have 50 degrees of freedom to begin with?

Staley: Well, I'm not certain I completely understand your problem. As pointed out in the earlier paper, in the 3-dimensional model there are certain constraints that you have to try to work against and these are usually defining the shape of frames in the model and things of this nature which require the large number of degrees of freedom in the original structural model, merely to get the stiffness representation due to effects of shape of the model. Once those are obtained, then reduction of many degrees of freedom can be accomplished without too much effect on the lower modes of the final system. Am I answering your question? I believe your question is do we need all these structural degrees of freedom if we are only going to use 200 of them in the final analysis? Is that what you are asking?

Nettles: My question was, since you go through this reduction, do you in fact use 1849 degrees of freedom?

Staley: Oh, yes, if we break down the matrix equations into a set which has – if we look at the modal representation with no forces on the right hand side, and we partition these equations into a set with no masses on the left hand side and a set corresponding to the masses, you can see that the only things that couple the equations are terms in the stiffness matrix, so that we can more or less express a final reduced set of equations in terms – in other words there is a relationship between the reduced degrees of freedom and the final retained degrees of freedom in the final set of equations and that allows us to eliminate some of these degrees of freedom from the matrix to bring it down to a size which we can handle in the eigenvalue solution. So all of them are actually used, nothing is lost in the structural representation, assuming that the mathematics can be performed accurately.

Piarulli: There was one more question I had that I also had wanted to ask the previous speaker. In your simulation of the fuselage, or body of the aircraft, do you take advantage of any symmetries of the structure?

Staley: Well, NASTRAN can take advantage of symmetry. I'm not certain exactly how far we have gone with this, but there are features within NASTRAN which can analyze a structure which is symmetrical. In other words, you would only have to provide structural mass input data for half of the structure say, if it were symmetrical, and the program would then fill in the remaining portion of the final stiffness matrix based on the assumption of symmetry. So those features are in NASTRAN I understand. I'm not certain that we've taken advantage of them or whether we have complete symmetry in our structures so that we can.

Paper No. 9

HELICOPTER GUST RESPONSE INCLUDING UNSTEADY AERODYNAMIC STALL EFFECTS

P. J. Arcidiacono and R. R. Bergquist
Sikorsky Aircraft

W. T. Alexander, Jr.
USAAMRDL, Eustis Directorate

A. Z. Lemnios, Kaman Aerospace Corp.: Peter, let me congratulate you on a very well presented paper, I think it was a very interesting piece of work. I did have a question on your gust penetration work. Did you look at the combination of advance ratio and rotor rpm whereby you could actually get a blade going into and out of the gust or did you treat the gust penetration as a solid actuator disc which then penetrates the gust?

Arcidiacono: Well, we looked at several advance ratios, the gust profiles were as you saw them. Most of the results were for the sine squared gusts, and there was a fixed wavelength on that gust. We looked at advance ratios up to .5, so we in effect varied the rate of penetration. It was a four bladed rotor and those parameters define when a particular blade will penetrate what part of the gust. And [if] each blade was considered separately, the results showed that the blade would actually travel downstream faster than the gust front was proceeding across the disk, the blade would move out of the gust front.

Lemnios: In other words, the gust alleviation factor that you quoted, for 50% did include the effect of perhaps a blade moving in and out of the gust in any one revolution.

Arcidiacono: Yes, it did.

Jan Drees, Bell Helicopter Co.: In reading over your paper, the effect of dynamic stall was mentioned as one of the important factors. In our study that parallels pretty much your study, we came up with similar conclusions. We were using the Wagner and Kussner functions on each blade in order to simulate the dynamic effects of sudden encounters of each blade. And of course this alleviated the load from the blades and on the helicopters. I wonder if you've looked at that to see if that compares with the dynamic effects that you incorporated in your model?

Arcidiacono: As I understand the work that was done at Bell, the effects that you just described were included, but those are primarily potential flow effects and they tend to alleviate the buildup of loads in potential flow. It was my understanding that the dynamic stall effects, the non-potential flow effects, were not included in the Bell work.

Drees: That is correct.

Arcidiacono: And that works against you, it allows the rotor to build up a larger load factor and we had, in effect I think, both effects included in our analysis through the use of the α, A, B method. Your second question?

Drees: This is not so much a question as a comment. You've just looked at single-rotor helicopters and came to the conclusion that the airframe motions were not all that important. In our study, we also included the effect of a tandem rotor and I think there we found a much bigger effect since during the penetration of the gust the front rotor will first experience the gust and the aircraft will have time to pitch up a little bit and we found an increase in load level because of that. Maybe somebody from Vertol could comment on this. And then we looked at alleviation factors and we found that δ_3 and a bobweight in the collective system could substantially reduce the effects of gust.

Arcidiacono: I think those are two good points. We didn't consider the tandem at all and obviously it will take more time for the gust to encompass the entire aircraft. As far as the bobweight part of the problem is concerned, we did the entire thing controls fixed because we felt that was a more general, and perhaps easier problem.

Hohenemser, Washington University: My question really has been answered already, by what Jan Drees said but I wanted to ask you what really is the difference between your analysis and the analysis that they did there. I thought they were doing that with the first versions of C-81 and I wasn't aware that stall wasn't involved in it. I thought they had also stall in it.

Arcidiacono: I pointed out, that as far as I understand, we have included unsteady stall aerodynamics in the problem.

Hohenemser: That's the main difference?

Arcidiacono: Yes, as far as I can see. Of course, as you see on Friday, there may be other differences that aren't so apparent.

Dave Brandt, Boeing Vertol: Pete, to the best of your knowledge, has this analysis or any analysis that's similar to this, ever designed so much as one rivet on any piece of flightworthy hardware in the helicopter industry?

Arcidiacono: To the best of my knowledge, I think the answer is no. And that's why I pointed out that, however, for commercial applications the ride comfort part of the problem still is of interest.

Brandt: Then you need a control system in the SAS. Well, may I just make the comment that before we fall into the trap that our fixed-wing brothers have, let us dispense with this topic before somebody drives that idiotic power spectral density jazz down our throats, there are better ways to waste a lot of money than this topic.

Peretz Friedmann, UCLA: I have a question of curiosity. You use a longitudinal gust, and for case for rotor blade which has rotational symmetry, it always bothered me – why not consider simultaneously a lateral gust and a longitudinal gust? Maybe that is a worse case than the one we have been looking at. What is your feeling about this?

Arcidiacono: Perhaps you are right. Looking at those effects was beyond the scope of our study and concerning Dave Brandt's comment, I'm not sure that they should be looked at.

Paper No. 10

APPLICATION OF ANTIRESONANCE THEORY TO HELICOPTERS

F. D. Bartlett, Jr. and W. G. Flannelly
Kaman Aerospace Corporation

Irwin Kenigsberg, Sikorsky Aircraft: Is it absolutely necessary for the anti-resonant isolator to have both an inertial and elastic element or can you just have an elastic element?

Bartlett: You will have to have both inertial and elastic elements because it is from the stiffness type element and the mass type element that the frequency is defined.

Kenigsberg: Could the inertial element be the transmission itself? If the elastic element were mounted under the transmission?

Bartlett: Well, the anti-resonant isolator is designed such that it is independent of the, say, the non-isolated body. So that it would have its own internal degrees of freedom.

Leo Kingston, Bell Helicopter Co.: I wonder, is there a significant mathematical difference between your description of the anti-resonant system and a shaker system which has a closed loop feedback? Or several shakers, of course, which may be placed in several places on the fuselage with a closed loop.

Bartlett: I don't have an answer to that question at this time.

Bob Wagner, Hughes Helicopters: I don't want to appear stupid certainly, but maybe I'm speaking for more of the members than for fewer of the members if I would ask if there is a simpler way of explaining the principles of the anti-resonance devices that we have just heard?

Bartlett: Admittedly, the subject of anti-resonance theory is complicated. Since joining Kaman and studying anti-resonance theory, I have found that no matter how many times I read the subject, I learn something new. Now, as to whether or not we can simplify this theory, I see no reason to simplify it. We do not simplify conventional matrix iteration techniques when we solve for resonances and normal modes and this technique is simply an extension of that by which we solve for those points in the structure that have zero motion for forces along generalized coordinates which we are interested in. So, if you look at the DAVI system itself as an independent and decoupled dynamic system, the resulting equations are not as difficult to understand. However, the overall picture looking at the isolated structure and the non-isolated structure and taking all degrees of freedom into account, is more complicated, yes.

Leonard Foster, Lord Kinematics: By way of further explanation, are you not talking similar to earlier papers on structural analysis using NASTRAN to tune the structure, in that you are placing critical stations at nodal points?

Bartlett: We're not placing nodal points, we are forcing nodal points.

Foster: Well, that's what I'm referring to. I'm trying to get at an explanation of actually – You have an association between what you're talking about and doing a structural analysis or a finite element analysis, in reducing the response at different stations. Am I off base there or is there a correlation between tuning the structure, and what you are talking about with anti-resonances?

Bartlett: Well, we do tune the structure to have an anti-resonance using the vibration isolator.

Foster: O.K. Well, that's the point I wanted to make.

Bob Jones, Kaman Aerospace Corp.: I think to maybe clarify the issues a little bit – and I'm not really up on the theory even though I work with Bart – I sort of agree with the gentleman who just spoke before. It really is a structural dynamics problem. Bart was only using say, anti-resonance isolators or dynamic absorbers to illustrate the problem. But it is a structural dynamics problem from the aspects that eigenvalues for antiresonances can be obtained and by structural dynamics you could force a nodal point at a given point of the structure, such as Bart was saying, at the pilot seat. Therefore, in design, this capability of calculating anti-resonances and putting anti-resonance at a specific point, could be of major value. So it is a structural dynamics problem, and not really an anti-resonant vibration isolator or vibration absorber problem, per se.

Al Pierce, Session Co-Chairman: If there are no other questions, I would like to comment, myself. And that is in the light of simplified explanations. Simplified explanation is only arrived at through understanding. And I think this paper deserves some congratulations as much as it has clarified many techniques of resonance and anti-resonance approaches in one organized piece of work. Thank you, Bart.

Paper No. 11

THE EFFECT OF CYCLIC FEATHERING MOTIONS ON DYNAMIC ROTOR LOADS

K. W. Harvey
Bell Helicopter Company

Dick Gabel, Boeing Vertol: Can you comment on what portion of the load increase is due to the aerodynamics? I gather that there are two effects here, the aerodynamics and the dynamic effect of this adverse tuning at 3 per rev. Well, I presume then that you did not have flapping aerodynamics from cycling, resulting from cycling, prior to this. Can you comment on what portion of that load increase is aerodynamic?

Harvey: Yes. There was a single set of aerodynamic forces that were taken from C81 and of course the aerodynamic cyclic effect is treated in there. But our representation in that program, consists of an airfoil shell that oscillates around a non-feathering elastic blade structure. The collective pitch is represented and a built-in twist is represented for the elastic blade structure, but the cycling motion of the elastic structure is not. The airfoil shell does oscillate which is required to balance the air load moments to maintain steady-state flight or precess the rotor to some other position. But just a single set of air loads were used for both cases, with and without cyclic.

Peretz Friedman, UCLA: I'm wondering why in the plots which you have of the natural frequency versus rpm, you have no numbers on the vertical coordinates, both in your slides and in the paper?

Harvey: You can obtain those directly. The scale is labeled from zero to 300 rpm and then the 1, 2, 3, and 4 per rev lines are shown so that you can construct the values very readily. I didn't feel that lends anything to the significance of the placement. But the magnitudes can be obtained directly.

Gene Hammond, AMRDL, Langley Directorate: In the data that you present, you present out-of-plane degrees of freedom and in-plane degrees of freedom, but nothing on the torsional degree of freedom. Is there a reason first of all for leaving out the torsion, and secondly, do you expect to see any effect on the torsional response from your cyclic feathering?

Harvey: Are you talking about blade torsion degree of freedom?

Hammond: Yes.

Harvey: Well, I included strictly the rigid body degree of freedom in blade torsion mode. The reason that it's not in there is just because of the development cycle of the program. I intended that that would be one of the next items included. And yes, I do expect some effect when that is included, particularly if that elastic motion derives from say, a control deflection as opposed to a blade twist, because it does seem to be that the most important consideration is the geometric angle of the blade structure that's closest to the feathering bearing. That's the principal item affecting this effect.

Marcel Kretz, Giravions Dorand: You showed on one of the slides that the feathering modified the bending moment in the blade. Can you give the configuration of the rotor and especially the advance ratio of the rotor for this case?

Harvey: I'm not sure I got the question. The flight condition for this set of air loads was a King Cobra which is our upgraded Huey Cobra flying at 150 knots, and the rotor rpm was 300, so I think that's about .2 or .25 advance ratio, somewhere in there.

Kretz: Can you give an idea of the influence of the advance ratio on the bending moment in the blade?

Harvey: No, I cannot, I've just run that one case. Most of the study to date has been to try to gain some sort of decision as to whether or not this effect was significant and we have not run very many cases. We're not automated to the point that we can very easily, at this point.

Dave Brandt, Boeing Vertol: I don't understand why the aerodynamic damping doesn't show up in your analysis so that you would predict your damped resonance at something like 3.1 per rev. What's missing in the analysis that doesn't permit that?

Harvey: We have that represented in the analysis, but it's a question of the trade-off between computer time and so forth. We have certainly aeroelastic effects and aerodynamic damping in the present C81 family of programs. In this particular study, I excluded it so that it would not mask the structural damping effects, the apparent damping effects due to structural feathering.

Paper No. 12

CONTROL LOAD ENVELOPE SHAPING BY LIVE TWIST

F. J. Tarzanin, Jr.
Boeing Vertol Company

P. H. Mirick
USAAMRDL, Eustis Directorate

Kip Cheney, UARL: Paul [Mirick], that was a good paper, I really enjoyed it. One question that I had that you didn't address was the frequency of response. I was busy counting bumps on your curve there. I know on some of the 5 and 7 per revs, it looked like it was responding at 5 and 7 per rev, but the 3 and 4 per rev blades weren't responding at 3 or 4 per rev.

Tarzanin: If you look at all the wave forms, you can see for the lower C_T/σ's evidence of the lower frequency spiking. But as you get deep into stall you tend to see a higher frequency appearing which is traceable to the second torsional mode. So you have participation of both the first torsional and second torsional mode in the very high C_T/σ conditions.

Peter Arcidiacono, Sikorsky Aircraft: Frank [Tarzanin], and Paul, you've varied the torsional stiffness and torsional inertia independently – it looked like – on one of your figures. It looked as though the reduction in the torsional inertia led to higher control loads, did I interpret that figure correctly?

Tarzanin: Earlier we did some work where we varied pitch inertia, control system stiffness, and blade torsional stiffness, and combinations thereof, and we got a very gross trend which showed that the lower frequency blades reduced the loads and the high frequency blades had higher loads. But there was a great deal of scatter, especially down at the low frequency end. You're right here in that when we went to the low frequency end and looked at changing pitch inertia there were actually increases.

Arcidiacono: I raise that point because we had a companion study to this and we found that – our analysis at least – predicted that reducing the torsional inertia reduced the torsional loads, and was a more dramatic effect than the torsional frequency.

Mirick: On your analysis you also – when you looked at torsional frequency – you coupled it with control system stiffness, didn't you, Pete?

Arcidiacono: We made independent changes and combined changes as well. We're going to get into it on Friday, the comparison of various analyses, and this is one opportunity to at least examine the effect, the qualitative effect, or prediction of the two analyses with regard to a particular design parameter change and I was interested in that one point.

Tarzanin: We may not disagree. It depends I think on where you started from. Because if you start at the higher end, if you go to around 7 per rev and then reduce the inertia, I think you can reduce the load.

Arcidiacono: I think we differ in some areas.

Leo Kingston, Bell Helicopter Co.: I'd first like to congratulate you on an excellent paper. At least I enjoyed it very thoroughly. I wonder whether you can help me a little bit. In the beginning of the paper you differentiated between the effects that you could achieve by changing control stiffness or by changing torsional stiffness of the blade. You showed that you apparently got the best results by varying the blade stiffness. I wonder whether you could elaborate a little bit to give me the rationale for why this was the best trend.

Tarzanin: I wish I knew. I'm looking into it now and I just fall back to some of the work we did earlier where, when we changed everything we were able to get loads to go up and down using all methods. However, why torsional stiffness reduces loads the most, I don't know.

Ray Piziali, Vizex Inc.: I may have missed a point. For each of the different torsional stiffness blades that you examined – and made comparisons – were the rotor trim conditions of forces and rolling and pitching moments maintained?

Tarzanin: As the study was first done, the cyclic pitch boundary was matched and thrust was matched. In other words, side force and propulsive force could vary. We went back at the extreme conditions, and retrimmed the rotors, and found that the trends didn't change but it significantly affected the power. Originally, when we left the cyclics the same, it started showing that the softer blades had a great advantage in power. But when we went back and retrimmed them, they all appeared to have the same power boundaries.

Maurice Young, University of Delaware: I'm puzzled and a little concerned at the presentation of the results in absolute terms, rather than using reduced frequency. I have a concern that what looks good on this particular rotor with its particular load distribution and chord and so forth, might be ruinous on another rotor system. In effect, have you tried to sift these factors out in terms of that standard parameter?

Tarzanin: No, I haven't.

Jim McCroskey, AMRDL Ames Directorate: I presume some of that problem of the rise in pitch link loads at the low natural frequency is due to compressibility phenomena, and hence would tend to go away if you reduced the rpm. But of course, that would make stall flutter worse on the retreating blade. And I wonder if you have looked any at the trade-off in that direction?

Tarzanin: No, again I haven't looked at that.

McCroskey: Do you have any feel for how that would go?

Tarzanin: It seems reasonable, it's clearly the advancing blade problem which is associated with speed. You can see that it is very, very speed sensitive, so yes, it makes sense.

McCroskey: Well, I think it has to be that, because I don't believe the pitching moment characteristics of a cambered airfoil flying upside down are that much different from one flying right side up, in low speed flow. So it must be the fact that when the cambered airfoil is flying at negative angle of attack, it has pretty bad shock wave characteristics on the lower surface.

Tarzanin: Oh, you are saying it's just due to drag.

McCroskey: No, it's not drag. It changes the center of pressure.

Tarzanin: No, it's not the pitching moment. The pitching moment, per se, is restoring, it's goodness.

McCroskey: But Paul said it was a nose down pitching moment, and I presume he means [that] nose down for the negative angle of attack is like a divergent moment.

Tarzanin: The load results from the fact that on the advancing blade, the tip is lifting down. And you have a shape like this [blade tip deflected down]. Then you take your drag [moment], and you bring that thing nose down again, well that nose down twist makes the lift more down again. Which again gives you more moment, so if your torsional stiffness is too low you just wind this thing right up. It's very similar to divergence, yes.

Bill Nettles, AMRDL, Eustis Directorate: I think with regard to Jim's question, even if what he's saying is true, I don't think your analysis accounts for it in the aerodynamic data at the tip. So I don't think – well I may be wrong, but I don't believe it accounts – you remember all the bit about the aspect ratio effect and all that – so there's no major change in center of pressure as your data is now put together.

Tarzanin: We've looked into aspect ratio effects at the tip and we do have tables that account for it and that doesn't seem to be a significant factor here. I think if we got to very high Mach numbers that would be true.

Nettles: O.K. There's another question that I want to ask you. Your conclusion, and I'm not sure I necessarily agree, is that you can – using this rather complex mathematical model as a design tool, a useful design tool at this point – qualitatively predict something with regard to the stall flutter boundaries and the torsional characteristics. Do you think, that now in retrospect perhaps understanding the problem a little better, that you could prepare a simplified model which would accomplish the same particular objective?

Tarzanin: Do you mean a non-computer model like some kind of parameter?

Nettles: Something along the lines of the simplified models that we've discussed, that perhaps could be done by hand or maybe would only require minimal usage of the computer.

Tarzanin: It certainly sounds feasible. I guess it is a matter of work and time to work something like that out.

QUESTIONS AND ANSWERS

Session III – Rotor/Vehicle Dynamics

Chairman: Peter J. Arcidiacono, Sikorsky Aircraft
Co-Chairman: William E. Nettles, USAAMRDL, Eustis Directorate

Paper No. 14

ROTOR AEROELASTICITY COUPLED WITH HELICOPTER BODY MOTION

Wen-Liu Miao
Boeing Vertol Company

H. B. Huber
Messerschmitt-Bölkow-Blohm Gmbh

Kurt Hohenemser, Washington University: I have two questions. First, what is really different in your present conclusions, from the ones you had in your various previous works? I have the superficial impression that everything is really more or less the same, you just have more data and have correlation with your new tests, but it seems that there are no surprises in it. But maybe I didn't quite catch it. And the second question is this was all based on the rotating system, you have very low damping ratios of 1% or so, I assume this is all based on the rotating reference system. Now those are the damping values without any structural damping, is that right, you have eliminated structural damping in your presentation?

Miao: O.K. The second question first. The model blade has 1/2% inplane structural damping and all the data presented here have 1/2% inplane structural damping. And because of the construction of the model, we know the blade has less damping than the full-scale blade. We have tested the BO-105 full-scale blade, it has more damping, at least 1%. It has data scatter but can go as high 3%, so the data shown here is, in a way, not representative of a full-scale blade. Now, to answer your first question, as far as I remember, there are two papers [that were] presented on this. One is for very small scale model, of 28 inch diameter. Another is the BO-105 full-scale data and on the BO-105 the parameter variation is impossible. This one is 5-1/2 ft in diameter and I believe the data is more reliable. Something that is always of concern, say what is the cyclic [pitch] influence on the stability, do you really have to include cyclic pitch in the analysis of air resonance? But this test data seems to indicate that the air resonance mode is not really influenced by that. And we also varied the control system stiffness. We showed that we will have a favorable trend versus collective pitch, when the collective pitch increased to a certain amount, because there is blade elastic pitch-flap-lag coupling. Then at high collective, because of the induced drag, the trend turns again. Now the control system stiffness will minimize that, for the high control system stiffness. This has never been shown before.

Hohenemser: But this is all based on the same analysis. You could have gotten all this data with what you did a year and two years ago, is that right?

Miao: No, the analysis I am showing here, is mostly the Blama analytical model [Messerschmitt-Bolkow-Blohm] which Huber used to correlate with the BO-105 data.

Hohenemser: Yes, but he used that in the presentation of the last program, too.

Miao: Yes.

Bob Wagner, Hughes Helicopters: Would you conclude that the modal damping ratios that you show are proportional to the 0.5% damping that you showed about the virtual lead lag hinge, is that a fair statement? In other words, does the modal damping ratio appear as a product of some other dampings of which the lead-lag damping would be a component?

Miao: If you refer to the old Coleman's criteria –

Wagner: That's right.

Miao: – the product of damping from the oleo and from the blade lag damping – we really didn't look at it that way. But I believe that because the blade has a very powerful flap damping, in a way you can think of it as oleo damping, and the lag damping in here is more or less very minimized. I don't know what would happen if I had zero blade lag damping in there. But we did do the analysis theoretically by varying the blade inplane damping, I can go down to zero damping and the mode is still stable.

Wagner: That would indicate then that the modal damping is not only a product of components, but a sum of say the flapwise damping perhaps.

Miao: Well, I think the way that Coleman reached the conclusion on the product of damping, he ignored all the aerodynamic effect in there.

Wagner: That's right, he did.

Miao: Right. But I think the air is important in there. You can never get zero damping.

Bob Ormiston, AMRDL, Ames Directorate: I have two questions, Jerry. First, the trim condition in forward flight. Was the model in trim and propulsive force, or what were the conditions during those tests?

Miao: Let's see, trim and propulsive force.

Ormiston: In other words, it was matched at some drag coefficient for the air frame.

Miao: Right.

Ormiston: I have another general question about some of the past work of both yourself and Mr. Huber. If I'm correct in remembering, I think some of the past work for stability in hover, showed that in your results there is an instability in the lead-lag mode at high collective pitch. And in some of the work that Mr. Huber has done, this instability does not appear unless the effects of stall are included. I wonder if you can comment on this, and if I have stated it correctly, maybe resolve the point for me.

Huber: This was a question already at Washington [AHS Forum] last year, and up to now we have no exact [explanation] of these differences. In our theory, which brings only the stall instability in the very high thrust region, this new instability reached at moderate g levels without stall, does not come out. We are looking for this effect – I cannot give you a clear answer to that. But it seems that this curve [versus] g, which Jerry [Miao] showed, compares better to test results.

Ormiston: In other words there still is a question that could be resolved?

Huber: Yes.

Miao: But, I think in a way, actually, the data we show there versus very high collective pitch, very high, I mean, and it shows a downward trend. We have eliminated the stall effect in there – you still will have it and it is caused by induced drag. But I think maybe if you included stall this thing would happen earlier. Could be.

Paper No. 15

AN APPLICATION OF FLOQUET THEORY TO PREDICTION OF MECHANICAL INSTABILITY

C. E. Hammond
USAAMRDL, Langley Directorate

Dick Bielawa, UARL: From your results, it sort of looks to me like what you have with one blade damper inoperative, that you have a one-bladed rotor and the rest of the blades comprising part of the pylon mass. Do you think it might work to apply the Coleman analysis to an equivalent system, where you now have a one-bladed rotor without a damper and the rest of the blades not responding and comprising part of the pylon mass?

Hammond: Let me give you an answer to it and see if I can give you a satisfactory answer. The answer is – directly to your question, I'm not sure, but one thing that comes to mind is the fact that one of the criteria that Coleman gives for completely doing away with the mechanical instability is to have the lag frequency of the blade greater than 1 per rev. That criteria is applied to a blade which has no damper on it. If you put damping on it, that's a very conservative requirement. All right, so to treat the situation that you ask about, it would say that if I had my blade with no damping, if I can somehow get its frequency above 1 per rev, maybe I can eliminate the problem. I have some results that show that you can eliminate the problem before you get that high, so I'm not really sure how to answer your question other than to tell you that I have some results where I've changed the lag spring on the blade to try to get the frequency up above 1 per rev to see what effect it has. And the instability actually goes away before you get as high as a 1 per rev lag frequency.

Bielawa: I don't think you understand my question. I don't expect an answer. I'm just sort of asking you to consider it, that you might get an approximation to the problem very simply by treating the whole system as one wherein you have a reduced mass rotor, where you only have a one bladed rotor mass. It does not have any damping so your mass ratio will be reduced from what it would be if you considered all of the rotor mass.

Hammond: You want me to run a one bladed rotor now?

Bielawa: Well, it sort of looks like you might be able to get an approximation to the solution using the Coleman results for an equivalent system. I don't know whether it will work or not, but it is an idea that was suggested to me by the responses that you showed.

Maurice Young, University of Delaware: As a follow-up on the previous question, it seems to me that the system in either case is a linear one and that the loss of one damper is, in effect, a perturbation in one of the system coefficients. So that the solution should form a continuum and if you use the perturbation technique alluded to during one of yesterday's sessions – if you have a stable system to begin with, the first perturbation should give you a direct estimate of the loss in damping for the system, due to the failure of one damper.

Hammond: I think that that's possibly true. The thing with that approach is that you have to go through and set up the perturbation equations and do the perturbation analysis, whereas if you use the Floquet results everything comes out from the basic equations.

Young: Well, perturbation analysis doesn't really require any additional analysis because the characteristic part of the equation is identical from perturbation to perturbation. In effect, the perturbation produces a forcing function for the correction term. So it's a relatively straightforward calculation.

Hammond: Right.

Vince Piarulli, Pi-Rad, Inc.: Gene, to go back to the question before this one, maybe you could look at that by taking a good look at the modal response that you are getting on the other blades. If they are all moving in phase then he's probably right that you could simulate it by one blade and lump the other blades in with the hub. But if not, if you are seeing that they are acting differently, then that won't be true.

Hammond: Right. One of the things that I have not done, is to look at detail at what each blade is doing. Even though the time history doesn't really indicate instability, I think that it would show the phasing between the blades.

Bart Kelley, Bell Helicopter Co.: Maybe I didn't get it through my thick skull as you were explaining, but the collective drag mode with all the motion in the blades – this was the symmetrical hub – would be torsional then on the mast, or on the shaft, right? And a torsional stiffness should be included in the analysis there. That's one part of the question, and the other part is, this might also modify the anisotropic hub case. I just wondered whether that consideration is included or whether you were assuming a "cast iron" rpm that absolutely cannot vary – an infinitely stiff shaft driving this thing.

Hammond: It's a "cast iron" rpm. It's exactly the same as the Coleman and Feingold analysis, except that now I take one of the dampers off, and look at a non-isotropic rotor. I think the rpm will change and certainly the effect of a torsionally soft mast will have some effect on the problem.

Paper No. 16

THEORY AND COMPARISON WITH TESTS OF TWO FULL–SCALE PROPROTORS

W. Johnson
USAAMRDL, Ames Directorate

A. Lemnios, Kaman Aerospace Corp.: I may have missed the point, Wayne, but did you mention what the wing incidence was during these tests?

Johnson: The wing incidence for the theoretical and most of the experimental results presented, was zero. In the tests and in the theory we have varied wing incidence up to about 20 degrees. It has relatively little effect on high inflow proprotor dynamics. The main influence of the wing aerodynamics is on the damping due to angle of attack change when you have vertical bending motion.

Lemnios: I was just wondering if perhaps it did have a significant effect on the stabilizing characteristics at the resonant frequencies that you pointed out in there, in other words, at the low speeds zero incidence condition, you indicated that you had an instability occurring at the 50 kt condition on the Boeing rotor, I believe it was.

Johnson: O.K. Well, that is simply a resonance with the vertical bending frequency and the only effect that it might have is as you change the orientation of the inplane motion with respect to the wing vertical bending and chordwise bending direction. You might change that a little bit. I don't believe that we investigated that experimentally as I recall. I would not expect it to have a significant effect over the range of angle of attacks involved.

Bob Donham, Lockheed California Co.: I think the paper is really a very fine piece of work and I think it's very interesting. I do have a question relative to the effect you observed in the powered flight versus the autorotation flight case. The question is, do you believe there is an effect of whether or not the thrust vector on the rotor is positive or negative, so that if we had used power and put a large negative thrust vector in the sense of a braking action, would that have produced stability?

Johnson: The influence of the lift and drag on the blade in high inflow aerodynamics is relatively small compared to the lift changes due to angle of attack perturbations. In fact, that's one of the things I meant by the "rotor" aerodynamic model that I referred to. The comparison of the autorotation and powered cases that were shown in the curves you saw today in fact, neglected the thrust terms on the blade. In general, the conclusion is that the effect you mentioned is small for high inflow aerodynamics. On the other hand of course, for hover aerodynamics, that may be another matter, certainly.

John McCloud, NASA Ames: Wayne, could you comment on the experimental accuracy of determining damping? Your last slide showed some pretty horrible scatter for a condition where we were trying to find out if we were stable at 192 knots in our wind tunnel. Is this related to the difficulty referred to earlier of getting information on stability from time histories?

Johnson: It's not the same thing that was referred to in the last paper, because the distinction that was made in the last paper was in the behavior of constant coefficient and periodic coefficient systems. In the matter of interpreting the periodic coefficients. In this case, it is involved in the question of interpreting experimental transient traces for the wing motion. That is what is involved. The way these damping levels were measured in this case, was to excite the wing motion with an aerodynamic vane; we'd oscillate the vane on the wing tip until we got a sizeable wing motion then we would stop the vane and then watch the decay of the strain gauge [output] measuring the wing motion. Now at high speeds you have enough turbulence in the tunnel to excite these big proprotors quite a bit, and that together with the rather low damping level indicated for the air resonance behavior, made the interpretation of the decay rate of these transient curves rather difficult. Now there are techniques available to get better experimentally determined damping ratios out of either the transient motion or out of transfer functions. This simply indicates that it would be a good idea to look seriously at these.

John Bloomer, Bloomer Flying Saucer Co.: I wanted to ask you about the possible application of your theory to a jet flap proprotor. Would it be, do you think, applicable to a jet flap proprotor of about the same dimensions?

Johnson: The only thing that comes to mind is the important factor, the change in the lift on the blade section with angle of attack. That's the dominant factor in the rotor aerodynamics and I'm not really that familiar with jet flaps to know whether you could just get by with using a higher effective lift curve slope or maybe you have to do a little bit more detail there. Basically, I think the dynamics involved would probably remain the same.

Paper No. 17

EXPERIMENTAL AND ANALYTICAL STUDIES IN TILT–ROTOR AEROELASTICITY

R. G. Kvaternik
NASA/Langley Research Center

Bob Thresher, Oregon State University: We have a particular interest at Oregon State in wind machines and both you and the last speaker operated your rotors as essentially windmills. I wondered if you would have any comments on potential problems, particularly at low inflow ratios which might be the regime of operation for a wind machine?

Kvaternik: Very low inflow ratios? We, experimentally of course, have not done anything there and although I've done a lot of analytical studies, even in the windmilling case they've all been essentially restricted to the fairly large inflow ratios typical of airplane operation of the tilt rotor.

Thresher: You don't have any intuitive feel then for potential problems in that area?

Kvaternik: No, I wouldn't want to venture a guess.

Jeff MacDonald, AMRDL, Eustis Directorate: I was wondering if you had an opportunity to make lateral control inputs on the model to determine if the rotor inplane motion coupled with the wing motion and provided any high frequency tendency for the pylon to couple in the model?

Kvaternik: I haven't put any oscillatory inputs into the equations, at this point.

MacDonald: Or to the model?

Kvaternik: No, we didn't have that particular capability in the model at that time.

Paper No. 18

COMPARISON OF FLIGHT DATA AND ANALYSIS FOR HINGELESS ROTOR REGRESSIVE INPLANE MODE STABILITY

W. D. Anderson and J. F. Johnston
Lockheed California Company

Jerry Miao, Boeing Vertol: I find your paper very interesting because it is a stiff inplane rotor and is different from a soft inplane rotor. Now I have two questions. The first one is a definition of your regressive inplane mode. Is that a mode which is the rotor speed subtracted by the lag frequency? And the second question is, on the last slide you showed test data of the regressive mode damping and also of roll mode damping. How do you obtain those test data? Do you measure it from the roll trace and one from the lag trace?

Anderson: Well the first question. The inplane frequency in the rotating coordinate system on a stiff inplane system is, of course, above rotational speed so if you looked at a regressive mode in the rotating system, you would subtract rotational speed from it and you'd still end up with a regressive mode in the stationary system and the frequency of that mode would be the inplane frequency less rotational speed. So if you have a 1.5 P inplane frequency, the frequency would be 0.5 P. The advancing mode would come out at 2.5 P or the inplane frequency plus rotational speed. Does that answer the first question?

Miao: Yes, it does. But the result we provide is also the regressive inplane mode.

Anderson: O.K., right, on the soft inplane system, the frequency is below rotational speed of course, and in the rotating system it's a regressive inplane mode, whereas, when you go through the transformation of that mode into the stationary system, you'll find that it turns out to be advancing in stationary coordinates. I mean I hope you find that out.

Miao: The second question is where do you get the damping from? From the last slide. [Fig. 25]

Anderson: The experimental technique there is done by the pilot instituting usually a control reversal of the lateral stick. We call it a stick doublet and this may be an inch, inch and a half or two inches of lateral stick, at different frequencies. Usually we have him do it at one-half cps, one cps, and one and one half cps, and the pilot we've had flying, for that particular test anyway, seems to hit these things right on. From that we take the data and first do a hand analysis but then we use a process that we call a moving block analysis which tries to isolate the single frequency. I reported a little bit on that at the AHS Forum last year. Using Fourier transform techniques we try to isolate the specific frequencies and also the amplitude of those frequencies with time in order to determine the log decrement or damping of each mode.

Miao: Well, my question is here, when you analyzed the damping from the roll mode, does it have a frequency in the fixed system? And when you analyze the regressive lag mode, the frequency is in a rotating system – from a different trace?

Anderson: O.K., I understand what you mean. No, the damping in each case indicated has been resolved to the fixed coordinate system. For the roll damping, basically we look at roll rate to just get that; for the inplane however, we take the blade measurements in the rotating coordinate system and resolve or sum them together in such a way that we end up with a cyclic inplane bending moment by appropriate summation of the blades in the rotating coordinate system. If you sum blades 1 and 3, you will end up with – I'm sorry – if you difference blades 1 and 3 you will end up with a cyclic mode and likewise on blades 2 and 4. So using that data we have a cyclic which does include 1 per rev and 3 per rev and 5 per rev and so on but we do a Fourier analysis on that at different intervals of time and plot the amplitude of that versus time.

Kurt Hohenemser, Washington University: This is just a comment I want to make, with respect to the definition of droop and sweep. These are not dimensionless quantities and I think it is really basically wrong to use them. There is a big pitfall in it. It should be really expressed as a percentage of the chord shift, say the cg shift, in percentage of chord. Isn't it true that in the XH-51, you had no problems at all with this system and I think you had 2-1/2° sweep or something, and in the AH-56 you did get into problems because the percentage chord shift was not the same, but rather the sweep was the same? I think one should try to really use non-dimensional quantities in the description of the systems. That is really my comment.

Anderson: I think you have a very good point, Dr. Hohenemser.

Paper No. 19

HUB MOMENT SPRINGS ON TWO–BLADED TEETERING ROTORS

W. G. O. Sonneborn and J. G. Yen
Bell Helicopter Company

Jim Hayden, U.S. Army Aviation Systems Test Activity: Thanks for an excellent paper. It was my understanding that the original underslung feathering axis was put in to reduce Coriolis loads. Will not the additional underslinging bring back that problem?

Sonneborn: The question of Coriolis loads in a two-bladed rotor is at least a difficult one. In our analysis, we did include the computation of Coriolis loads in using the assumption that the vector of rotation is lined up with the rotor mast; you will find one gentleman in the audience, Mr. Harvey, who gave a paper yesterday, who would violently disagree with this assumption, and assume because of the relative inertias between engine and the rotor and the relative softness of the mast, that 1 per rev Coriolis motions arising out of coning and flapping, do not apply to a two-bladed teetering rotor. I have in the paper an additional figure that shows how the chord loads are influenced by additional underslinging and hub restraint. The change in chord loads appear to be very small compared to what we see being induced by airloads. I would think that the small amounts of additional underslinging that are required to balance the moments about a point below the hub, are insignificant in changing the chord loads.

Ken Amer, Hughes Helicopters: This is probably a related question. You said that when you flew the OH-58, although you did not change the underslinging, you did not get a significant increase in vibration because the blades were acting like a dynamic absorber by inplane bending. Was there a significant effect on blade chordwise stress in your flight test of the OH-58?

Sonneborn: Well, the inplane bending was changed. If you look in the paper you can see some results that show that the inplane bending was changed. However, once airloads and the inplane bending due to the dynamic absorber response are considered together, there is a phase difference, and for small amounts of hub restraint the chord loads actually go down because they are out of phase with those induced by airloads. And again, if we compare the chordwise loads that are introduced by airloads at V_H level flight conditions, they are significantly higher than those required for the dynamic absorber action to balance this 23% additional control power. Again, the chord loads are changed, yes, but the change is insignificant, it does not produce a structural problem.

Kip Cheney, United Aircraft Research Laboratories: Two questions. What effect did spring have on the fundamental flapping frequency and also did you measure root stresses, flatwise stresses, what were they?

Sonneborn: In answer to the first question, I do not know exactly. However, the amount of restraint that we provided I would guess would be in the order of 1.01 or maybe 1.02 per rev, very small. And the flatwise stresses are increased, correct.

Cheney: To what level?

Sonneborn: I am not able to answer that right now, but if you go to a 50% increase in additional control power, they have to be considered in the design, definitely.

Marcel Kretz, Giravions Dorand: I would like to ask a question concerning the possibility to build a rigid two-bladed rotor. Once you introduce a spring constraint, it's a question of degree, to what extent the two-bladed rotor becomes a rigid rotor. In your opinion, is it feasible to have a rigid rotor, in this case?

Sonneborn: A completely rigid two-bladed rotor?

Kretz: That's right.

Sonneborn: That would be unstable on a soft pylon. That is a matter of degree. I gave a reference in my paper that might help you in that respect. In our hybrid computer studies we could go to very high spring stiffnesses and even in the model we could lock out the teetering hinge completely, the flexibility provided by the coning flexures was sufficient to prevent instability. So you can go rather far. It doesn't appear to be a practical consideration.

QUESTIONS AND ANSWERS

Session IV – Helicopter Vibration and Loads – Applications

Chairman: James J. O'Leary, Boeing Vertol Company
Co-Chairman: William G. Flannelly, Kaman Aerospace Corporation

Paper No. 21

VERTICAL–PLANE PENDULUM ABSORBERS FOR MINIMIZING HELICOPTER VIBRATORY LOADS

K. B. Amer and J. R. Neff
Hughes Helicopters

Irwin Kenigsberg, Sikorsky Aircraft: In general, when applying a dynamic absorber to a system, the absorber will drive the attachment point to zero with the tuned frequency. Since the attachment point is outboard on the blade, it's not immediately evident that the root shear must go to zero. Could you explain further why the root shear goes to zero, and why you believe a more outboard station would be more effective? Question number two is, in your paper you discuss effective mass. Could you define that more completely?

Amer: I don't believe I said that the root shear was literally driven to zero. I said it was reduced significantly. You're right that because the pendulum is not literally at the flapping hinge, it couldn't literally drive it to zero, I don't believe. So it does not drive it to zero, but it does reduce it theoretically by roughly two thirds – practically, by roughly a half. Your question about mass ratio, Jim, why don't you take it.

Neff: Your question was about the effective mass?

Kenigsberg: The mass ratios that are in the paper are not clearly defined.

Neff: The mass ratio shown there is the relative proportion of the modal mass, just looking at it from a modal standpoint.

Kenigsberg: Is that the ratio of the mass of the absorber to the generalized mass of the mode? There are two mass ratios given. One is a mass ratio and one is a modal mass ratio.

Neff: The modal mass ratio is the portion of the modal mass contributed by the absorber. The other one is just the actual mass of the absorber and the actual mass of the blade.

Kenigsberg: I see. Two other questions. The modes that you had were quite close to 3 and 5 per rev. In a hypothetical case if it were a three-bladed rotor system and you put the absorbers on at 2 per rev and at 4 per rev with your modes at 2.7 and 4.8, would the absorber have been as effective, or do you believe it would have been more sensitive to tuning, or off tuning, from the principal harmonic?

Amer: I would say the effect of the absorber would be less significant because you're not near a resonant frequency. I could also say that from practical experience, we also build a three-bladed rotor system on our 269 helicopter, and it is much less of a vibration problem. In other words, we did not have to go to pendulum absorbers in there to achieve a smooth helicopter. So it takes a combination of both proximity to blade resonance as well as a specific number of blades to result in the vibration problem.

Kenigsberg: One other question, if I may. What was the effect on your 3 per rev and 5 per rev flatwise stresses following the addition of the absorber?

Neff: There was very little effect. There could have been a slight increase, it was negligible overall.

Jim Staley, Boeing Vertol: I also have two questions. You mention the problem in the approach to hover. What was the experience with the pendulums in vibration in that condition, and also, what direct measurements do you have of the effectiveness in reducing the 3 and 5 per rev components of the rotor blade root shears?

Amer: You mean during the approach to hover?

Staley: No, in all conditions. But you didn't cover the approach to hover condition. What was that experience, and then in general, what was your experience in the 3 and 5 per rev components of blade root shear reduction as far as measurements indicated?

Amer: Well, answering the second question first, we never did measure root shears specifically. The only measurements that were made were blade stresses and cockpit responses. As far as the first question, during the approach to land condition, to my knowledge, we only had qualitative pilot opinion.

Staley: Did you have any measurement of pendulum amplitude during steady state and transient conditions? Pendulum flap amplitude?

Amer: To this extent, as originally installed, we would occasionally – you notice the pendulums are below the blades – as originally installed, we would occasionally see evidence of contact between the pendulum and the underside of the blade. We then had to put some stops. So I would say 95+% of the time it's less than about 20° amplitude. Occasionally, during a severe maneuver, the pendulums will try to exceed 20° and will hit their stops.

Glid Doman, Boeing Vertol: This is perhaps in the line of an historical note and on your comment Ken about the use of these pendulums being a first. It ties back to the question about effective pendulum driving its attach point to zero. In 1944, we flew these things on the R6, on the swashplate. A pendulum at the base of each pushrod. They were tuned to enforce a zero for 2 per rev and 4 per rev. We elected to use two and they enforced absolute zero conditions at the base of the pitch link until we switched blades and put some of our worst blades upon the machine and the pendulum was overpowered and put out of tune. We added another half pound and we were back to utter enforcement of no motion. This was, of course, on a machine with no servos, no irreversibles, and it was a wonderful thing for the pilot. The advent of servos had made us forget this.

Amer: Well, it sounds like an interesting way to get your control force vibration down to zero. What I was talking about was getting the overall helicopter vibration reduced.

Paper No. 22

THE EVALUATION OF A STALL–FLUTTER SPRING–DAMPER PUSHROD IN THE ROTATING CONTROL SYSTEM OF A CH–54B HELICOPTER

W. E. Nettles
USAAMRDL, Eustis Directorate

W. F. Paul and D. O. Adams
Sikorsky Aircraft

A. Z. Lemnios, Kaman Aerospace Corp.: Bill [Nettles], and also Bill Paul, and Dave Adams from Sikorsky, I think you have done very fine work on this damping in pitch, I find it quite interesting. I do have a three-part question, however. I was wondering, had you considered in your analysis what the sensitivity would be to mismatched pitch dampers, what would happen if one of the pitch dampers did fail, and in fact, did you measure the pitch damping rates of the dampers to see how well they were matched?

Nettles: I'll answer your last question, first. We built something like nine dampers. We took the dampers which were best matched. Frankly, I don't recall the numbers, but they were relatively close. In the whirl test and in the flight test of the vehicle, we were able to get a rotor system which tracked reasonably well. We had a little trouble in the whirl test, because we didn't know at first how you track such a rotor, but we learned how to do it, and in flight test the rotor system was well tracked. With regard to a mismatch occurring in flight, we talked about it, but I'm not sure how you would analyze it. Certainly it would cause a problem But we don't believe it would cause a catastrophic loss of the aircraft. As far as the total loss of one, that's a good question. Now I will say this, in order to check out what would happen if we lost damping, in the whirl test we bled the dampers. We were flying on nothing but the spring. Never noticed a thing.

Session Chairman O'Leary: Any other questions? Frank Harris.

Nettles: Frank, you told me you wouldn't do it.

Frank Harris, Boeing Vertol: I guess I should just say Hi, Bill – is that what you are saying? I think it's an excellent example of exploratory testing and I'm pleased to hear that you are going to gather more points with which to look at this problem because acquiring stall data in straight and level flight is fairly non-repetitive kind of situation, and then to also be tackling the problem in a banked maneuver makes it even more of a chance for data scatter, but I'm very encouraged by your results. There was one area that I thought was interesting. I have sort of calibrated eyeballs on the torsion waveform, and I noticed that in the advancing quadrant of the disc, the pitch link is shown to be in tension. Maybe my eyeballs are uncalibrated, is there a sign problem there or is the tension load on the advancing side of the disc consistent with that kind of a rotor system?

Nettles: Let me ask Pete Arcidiacono what he thinks about that. The reason that I ask for Pete is that this becomes a critical point with regard to the accuracy of the analysis, more so than the significance of the effect on the damper itself.

Pete Arcidiacono, Sikorsky Aircraft: I think it's reasonably consistent. It's an uncambered blade and usually we have found with our waveforms that there is a nose-down pitching moment that occurs as you go into stall on the retreating side, and as the average moment due to stall relieves itself, the blade tends to spring back and overshoot on the advancing side and then comes back and finally enters into stall again. It would be different with a cambered blade.

Nettles: I wouldn't hang my hat on the quantitative accuracy of this analytical data. I wouldn't hang my hat on the quantitative accuracy of any of the analytical data from this type of program. But we went through a great deal of soul searching, and it is at this point when you do the proper amount of soul searching and use the proper ingenuity – whether you're talking Normal Modes or for that matter, C-60 – that you can use it as a design tool. In this particular case I think it was quite adequate for accomplishing the purpose intended.

Paper No. 23

MULTICYCLIC JET–FLAP CONTROL FOR ALLEVIATION OF HELICOPTER BLADE STRESSES AND FUSELAGE VIBRATION

J. L. McCloud, III
NASA/Ames Research Center

Marcel Kretz
Giravions Dorand

Bob Wagner, Hughes Helicopters: On one of the last slides, the second from the end, I believe, where you showed the comparison between the blade stresses and the vibrations. Do you feel a little uneasiness when you see the blade stresses going down but the vertical vibration going up? Is there not some kind of implied contradiction there, John?

McCloud: No, I don't think there's a contradiction there – it isn't the greatest, this isn't what I would like – I'd like them both to go down together. But in my experience with other systems, and I was going to ask this question of Bill Paul and Bill Nettles, when I've added dampers in the system, it has chased the loads someplace else, into the blades for example. That's all I can say – I don't find it contradictory.

A. Z. Lemnios, Kaman Aerospace Corp.: In order to perhaps amplify somewhat on John [McCloud's] statement, we're in the process of completing a study of putting in some multi-cyclic flap control on our controllable twist rotor. And with the dual control system such as that, we do have an optimization problem whereby we can maintain trim with many, many combinations of collective and cyclic on both the inboard and onboard end. We have been putting in 2, 3, and 4 per rev on the servo flap and the blade and we can get reductions of the shears transmitted to the hub. We do get some slight increases in bending moments, perhaps a little bit of increase in horsepower, 1 or 2 percent increase in horsepower, and peak angles of attack stay relatively about the same. What we are talking about here in trying to maintain optimum contours of many parameters at the same time. Now, you are going to benefit some of these parameters, but you will also get some detriments in the other parameters.

McCloud: I think the real reason, Mr. Wagner, is, that we really haven't made the load uniform all over the disc. To do this, we would need a system which would give us radial control that is, variation in a radial sense as well as azimuthally. And I think until we do that, we will not be able to get rid of all the vibration at one time, all of the bad things.

Paper No. 24

IDENTIFICATION OF STRUCTURAL PARAMETERS FROM HELICOPTER DYNAMIC TEST DATA

N. Giansante and W. G. Flannelly
Kaman Aerospace Corporation

Gene Hammond, AMRDL, Langley Directorate: First of all, is the method you describe applicable to rotating structures. Secondly, have you ever tried it on such a structure?

Giansante: No, I'm sure it's applicable to rotating structures but I think this is one of the main points of interest for most helicopters right now, is getting impedance data for the rotor, or mobility data for the rotor.

Hammond: When you say you are checking the structure sinusoidally, is there any particular frequency you are using or are you sweeping the frequency?

Giansante: We are sweeping.

Irwin Kenigsburg, Sikorsky Aircraft: Having defined the mass matrix and the stiffness matrix from the test data, do you have any plans for determining the modifications required for the stiffness matrix to reflect changes in the structure during the vibration reduction program?

Giansante: Well, I think perhaps this might be accomplished from substructure analysis.

Kenigsberg: You mean integrating analytical methods into the system identification technique?

Giansante: I think the two would complement one another, yes.

David Peters, AMRDL, Ames Directorate: I have two questions. First, what would you consider to be the difference in using white noise input rather than sweeping in sinusoidal excitations, using this method? Would it be feasible?

Giansante: Well, we would have to define frequencies, we would have to define the natural frequencies of the system, first of all – at least approximate natural frequencies. This method can be implemented only using data proximate to the natural frequencies. So you have to force at a particular frequency of excitation which is very close to each of the natural frequencies.

Peters: Of course, white noise contains all frequencies.

Giansante: Well, we would be exciting all the modes one time then.

Peters: Right, and then by frequency analyzing the output, you can find what the output is at that frequency.

Giansante: I suppose that might be an application.

Peters: The second question is, in one of the earlier slides, you mention an iteration technique of matrices in connection with the pseudo inverse, do you mean you're iterating on the pseudo inverse?

Giansante: No. We're using the pseudo inverse as a vehicle for the iteration.

Peretz Friedmann, UCLA: You mentioned when Gene Hammond asked you a question that you are sweeping and when Peters asked you a question you told him that you are exciting at the natural frequency. So, either/or, you can't have both.

Giansante: We are sweeping from the point of view that we are sweeping to discrete frequencies and taking data at these discrete frequencies, which are in proximity to the natural frequencies. That's true, we are not sweeping over the complete frequencies.

Friedmann: O.K., because I saw that on the first slide, you had S equal to the natural frequency and the exciting frequency, both statements.

Giansante: The S matrix, as I defined it there, was only a function of the natural frequencies and forcing frequencies.

Friedmann: So, do I understand correctly that if you want to find the natural frequencies of a structure, where you don't have the slightest idea where they are, you can't use this method.

Giansante: That's right.

Bill Wilson, Bell Helicopter Co.: We ran a correlation study about a year or so ago, on an AH-1J, using NASTRAN and modeling NASTRAN with the shake test of the AH-1J. We were able to do pretty well out to about 22, 23 Hz. The modes in between there and 100 Hz as you have there on the model, are considerably more complex than we have yet defined, I mean we're still modeling to try to get higher in frequency. Do you feel that damping in these higher frequency modes, and you showed in your beam – a very undamped beam by the way and I don't think any fuselage structure is going to be that way – but do you foresee that this method will handle the complex damping terms that are going to arise, in the higher frequencies?

Giansante: Yes, that should present no problem at all. As a matter of fact, the beam representation we used had approximately 5% structural damping. At each of the modes, we inserted that much, 5% structural damping.

Paper No. 25

ENGINE/AIRFRAME INTERFACE DYNAMICS EXPERIENCE

C. A. Fredrickson
Boeing Vertol Company

John Bloomer, Bloomer Flying Saucer Company: How did you match the torque in the three engines?

Fredrickson: We are working the problem in the fuel control unit and we feel we have a satisfactory solution.

Bob Donham, Lockheed California Company: I think the paper and the presentation were excellent. I have a question about how you balance the engine-to-combiner gearbox shafting in view of the fact that it is 6 in. in diameter and operating at 11,500 rpm.

Fredrickson: We are having some problems with vibration but not necessarily in balancing the shafts. End fixity at the combining transmission contributed to the shaft vibration problem but balancing is not as great a problem. The shafts are now roughly only 25 in. to 30 in. long and therefore are operating further from the bending critical speed.

Donham: I asked the question because we experienced a problem with a similar shaft on a test stand that was not successful. This shaft was about 6 in. in diameter, 40 in. long, and operated at 13,500 rpm. The problem was in balancing the thin walled tube. It was balanced by adjusting weight on the end fittings but this did not prevent vibrations due to dynamic unbalance caused by imperfection in the tube wall and transient torque loads. We eventually went back to a small diameter precision ground shaft. This is feasible because it doesn't really have to be any larger than the torque meter shaft.

Fredrickson: We are having some problems right now with an installation on one of the transmission test stands. It's a problem of end fixity. I was just wondering how many bending critical speeds did you go through with this new shaft installation?

Donham: Our shaft, the new installation, you mean on the stand?

Fredrickson: Yes.

Donham: The final one was operating above the bending critical speed. And the problem we ran into originally was that we ended up with a first torsion mode between these two opposite ends, which had been shaved off to balance them, and the shaft, when it got to twisting, started oscillating and it just shook the devil out of everything.

Fredrickson: Very interesting.

Bob Wagner, Hughes Helicopters: Are the HLH engines soft mounted or not?

Fredrickson: The plans for the prototype right now are for a hard mount installation. But we have been doing work to find out what type of mounts we should put in there, in case of any problems. In other words, we do have a back-up design including a de-tuned and isolated engine installation. But the plans right now are for a hard mounted installation.

Paper No. 26

HINGELESS ROTOR THEORY AND EXPERIMENT ON VIBRATION REDUCTION BY PERIODIC VARIATION OF CONVENTIONAL CONTROLS

G. J. Sissingh and R. E. Donham
Lockheed-California Company

John Bloomer, Bloomer Flying Saucer Co.: Yes, I was wondering, I understand there were several Lockheed rigid rotor helicopters that did come apart in the wind tunnel or experimentally. Is this theory going to help alleviate the problem?

Donham: No, I think the areas of activity you are talking about are not at all related to this information. As a matter of fact, in a somewhat different vein however, I would like to point out that the magnitudes of these angles we are talking about, relative to the control harmonics, appear to be small. In an autopilot functional mode you are not committing very much authority to such systems, and I think in that sense, they look like they could be very, very attractive with minimum risk to the aircraft.

Bloomer: You mean to say that this system that you are describing could potentially improve the stability of the rigid rotor that was used in that particular helicopter?

Donham: No, our subject is not related to stability. We are really related to forced response here, for a system that is already a stable operating system.

Sissingh: I would like to make some general comments about this subject and about the idea. We have in principle, our rotor, which gives us our vibration – put this rotor in a box. Out comes vibrations of all types, all the frequencies and so on. And we have six control inputs available, the sine 4ψ and cosine 4ψ variations of collective and two cyclics. And we have the choice to reduce six quantities to zero. So you can select what you want. In our cases, we selected the vertical forces and the pitching and rolling moment as we describe them. It is not necessary that these vertical forces and pitching and rolling moments be made to go to zero at the same point of the helicopter, in principle. In general, you would do that. But in principle, you could reduce the vertical forces at point A to zero, the rolling moments at B, and for pitching moments at C. We did not calculate response data and all our investigations are based on experimental data. We use our frequency response data to calculate the input to obtain the required output. In this case, we try to reduce, or to counteract the existing vertical vibration, pitching moment, and rolling moment.

Rod Balke, Bell Helicopter Co.: I may have missed it, but what was the consideration of torsional stiffness of the model blades? And is this a factor?

Donham: This particular model is extremely stiff in torsion. I can't give you a figure but I suggest that it's over 8 per rev. It's quite high. My comment was – well, it's a good comment – that the model behavior, I think, was not at all influenced by the torsional rigidity of the blades, so we were giving this blade angle to the full span of the rotor blade.

Dick MacNeal, MacNeal Schwendler Corp.: I'd be interested in a comment regarding your opinion of the feasibility of an adaptive control system to perform these functions.

Donham: Well, I'll be honest in telling you that I haven't made such a study. I think, to be quite frank, Dick, the sense of our work to date has been to establish this: if I knew how to steer it, would I be able to make it? I think John McCloud is shedding some light on it and I think he believes he could make it, and I think the majority of the people here believe that you can do it. I think though the basic issue is, can you do it and handle the varied conditions you encounter? I'm kind of optimistic that you could actually make an adaptive control system that would automatically relieve this moment, and to be honest again, the reason I believe that, Dick, is that the authority levels you have to have, I think, are sufficiently low that you can actually, I guess the word is, play with it. I think it can be done.

Ray Rose, Honeywell Inc.: I understand from what Dr. Sissingh stated, that you can concentrate on a particular load at a frequency that you would like to reduce. I was wondering if you do concentrate on one particular load, is there some limit of control that you have to exercise to be sure that you don't cause another load to diverge at another frequency?

Sissingh: Theoretically, you can do anything. What is practical, of course, I don't know. If the theoretical problem can be solved, you can concentrate on six quantities which reduce to zero, in theory.

Donham: I guess I would add one remark to that. I can't imagine from a gut feeling – that's been used a lot but I think it is a good expression – how could it be the case that we could experience loads? I think most of us know full well, that if the rotor system is actually exceeding its endurance limits in trimmed flight it is in a great deal of difficulty. So it seems rather surprising to me to imagine – unless we had a very unusual event here – that we could get into serious difficulty in that area.

LIST OF ATTENDEES

David O. Adams
Sikorsky Aircraft

H. R. Alexander
Boeing Vertol Company

Kenneth B. Amer
Hughes Helicopters

William D. Anderson
Lockheed California Company

Peter J. Arcidiacono
Sikorsky Aircraft

Rodney W. Balke
Bell Helicopter Company

Jewel B. Barlow
University of Maryland

Lawrence D. Barrett
Boeing Vertol Company

Felton D. Bartlett, Jr.
Kaman Aerospace Corp.

William G. Basham
U. S. Army

Paolo Bellavita
Costruzioni Aeronautiche Giovanni Agusta

Richard L. Bennett
Bell Helicopter Company

Dale F. Benton
Tenneco, Inc.

Marvin S. Berger
U. S. Army Aeronautical Depot Maintenance Center

Richard L. Bielawa
United Aircraft Research Laboratories

James C. Biggers
NASA–Ames Research Center

B. J. Bird
Bell Helicopter Company

John H. Bloomer
Bloomer Flying Saucer Co.

H. Peter Borie
Sikorsky Aircraft

William G. Bousman
Ames Directorate, USAAMRDL

David E. Brandt
Boeing Vertol Company

Herbert H. Brimmer
Lockheed Missiles and Space Company, Inc.

James H. Brown, Jr.
U. S. Army

William R. Bryant
U. S. Army Foreign Science and Technology Center

Arthur E. Bryson
Stanford University

James A. Burke
HQ, USAAMRDL

Marvin W. Buss
U. S. Army Aviation Systems Command

Raymond G. Carlson
Sikorsky Aircraft

E. S. Carter
Sikorsky Aircraft

James R. Chadwick
Chadwick-Helmuth Company, Inc.

David P. Chappell
U. S. Army Aviation Systems Command

M. C. Cheney
United Aircraft Research Laboratories

Sing Chu
NASA–Ames Research Center

J. J. Costes
Office National d'Études et de Recherches Aérospatiales

Samuel J. Craig
Systems Technology Inc.

W. L. Cresap
Bell Helicopter Company

John P. Cress

H. C. Curtiss
Princeton University

Roland Dat
Office National d'Études et de Recherches Aérospatiales

Gary L. Davis
U. S. Army

John M. Davis
Bell Helicopter Company

Robert C. Ditrich
Lord Kinematics

Glidden S. Doman
Boeing Vertol Company

Robert E. Donham
Lockheed California Company

Jan M. Drees
Bell Helicopter Company

Frank DuWaldt
Calspan Corporation

David Victor Ellis
Westland Helicopters Limited

Robert F. Forsyth
U. S. Army Aviation Systems Command

Leonard W. Foster
Lord Kinematics

David J. Fowler
U. S. Army

Charles A. Fredrickson
Boeing Vertol Company

Juanita Frick
Ames Directorate, USAAMRDL

Peretz Friedmann
University of California, Los Angeles

Richard Gabel
Boeing Vertol Company

Troy M. Gaffey
Bell Helicopter Company

G. H. Gaonkar
Southern Illinois University

Nicholas Giansante
Kaman Aerospace Corporation

Donald P. Gleiter
U. S. Naval Air Development Center

Mike Gockel
The MacNeal-Schwendler Corporation

Jerry H. Grantham
Lord Kinematics

W. Earl Hall, Jr.
Systems Control, Inc.

C. E. Hammond
Langley Directorate, USAAMRDL

Franklin D. Harris
Boeing Vertol Company

Gary Hartwick
Pi-Rad Inc.

Keith W. Harvey
Bell Helicopter Company

James Hayden
U. S. Army Aviation Systems Test Activity

Robert E. Head

David H. Hickey
NASA–Ames Research Center

Dewey H. Hodges
Ames Directorate, USAAMRDL

Kurt H. Hohenemser
Washington University

Helmut Huber
Messerschmitt-Bolkow-Blohm GmbH

Shukry K. Ibrahim
Honeywell, Inc.

F. H. Immen
HQ USAAMRDL

Nelson K. Itterly
U. S. Army Aviation Systems Command

David S. Jenney
Sikorsky Aircraft

Wayne Johnson
Ames Directorate, USAAMRDL

J. F. Johnston
Lockheed California Company

Robert Jones
Kaman Aerospace Corporation

Clarence T. Jones
U. S. Army

Daniel D. Kana
Southwest Research Institute

Gerd Kanning
NASA–Ames Research Center

David H. Kaplan
Bell Helicopter Company

Neville F. K. Kefford
Sikorsky Aircraft

Bartram Kelley
Bell Helicopter Company

Mark W. Kelly
NASA–Ames Research Center

Irwin J. Kenigsberg
Sikorsky Aircraft

Paul Kesling
Lockheed California Company

David Key
HQ, USAARMDL

Edward J. King
GTE Sylvania, Inc.

Leo Kingston
Bell Helicopter Company

Douglas G. Kirkpatrick
U. S. Naval Ship Research and Development Center

Marcel Kretz
Giravions Dorand

Raymond Kvaternik
NASA–Langley Research Center

Anton J. Landgrebe
United Aircraft Research Laboratories

A. Z. Lemnios
Kaman Aerospace Corp.

Richard B. Lewis
U. S. Army Aviation Systems Test Activity

Karl Luken
U. S. Army

H. I. (Jeff) MacDonald
Eustis Directorate, USAAMRDL

Richard H. MacNeal
The MacNeal-Schwendler Corporation

George Maggos
Naval Air Systems Command

Martin D. Maisel
Ames Directorate, USAAMRDL

Ray Malatino
Naval Air Systems Command

John L. McCloud III
NASA–Ames Research Center

Barnes W. McCormick
Pennsylvania State University

W. J. McCroskey
Ames Directorate, USAAMRDL

Joseph H. McGarvey
Eustis Directorate, USAAMRDL

Dennis P. McGuire
Lord Kinematics

Ronald B. McIntosh
U. S. Army

Walt McIntyre

Wen-Liu Miao
Boeing Vertol Company

Paul Mirick
Eustis Directorate, USAAMRDL

Richard L. Mohr
Systems Control, Inc.

Gilbert G. Morehouse
Ames Directorate, USAAMRDL

H. Andrew Morse
Ames Directorate, USAAMRDL

David E. Mowbray
British Embassy

Mike Munguia
U. S. Army Aeronautical Depot Maintenance Center

A. W. Myers
Bell Helicopter Company

James R. Neff
Hughes Helicopters

William E. Nettles
Eustis Directorate, USAAMRDL

James J. O'Leary
Boeing Vertol Company

Robert A. Ormiston
Ames Directorate, USAAMRDL

William F. Paul
Sikorsky Aircraft

Robert E. Peskar

David A. Peters
Ames Directorate, USAAMRDL

Wayne Petrie
U. S. Army

J. J. Philippe
Office National d'Études et de Recherches Aérospatiales

Vincent J. Piarulli
Pi-Rad Inc.

G. Alvin Pierce
Georgia Institute of Technology

Raymond Piziali
Vizex, Inc.

M. F. Platzer
U. S. Naval Postgraduate School

Richard K. Pollock
U. S. Army

James A. Poore
U. S. Army Hughes Plant Activity

Curtis J. Poree Jr.
U. S. Army

Robert D. Powell, Jr.
Eustis Directorate, USAAMRDL

A. LeRoy Pucker
Lord Kinematics

John P. Rabbott, Jr.
Ames Directorate, USAAMRDL

B. M. Rao
Texas A&M University

Kenneth R. Reader
U. S. Naval Ship Research and Development Center

Gunther Reichert
Messerschmitt-Bolkow-Blohm GmbH

Barclay T. Resler

Stephen A. Rinehart
Pi-Rad, Inc.

Raymond E. Rose
Honeywell, Inc.

Samuel W. Russell

Warren E. Schmidt
Lord Kinematics

Fredric H. Schmitz
Ames Directorate, USAAMRDL

Daniel P. Schrage
U. S. Army

Robert G. Schwendler
The MacNeal-Schwendler Corporation

Michael P. Scully
Massachusetts Institute of Technology

David L. Sharpe
Ames Directorate, USAAMRDL

John L. Shipley
Langley Directorate, USAAMRDL

G. J. Sissingh

Charles E. Smith
Oregon State University

Walter G. O. Sonneborn
Bell Helicopter Company

M. E. Southgate
British Embassy

Richard Spivey
Bell Helicopter Company

Francis E. Spring, Jr.
U. S. Army Aviation Systems Command

James A. Staley
Boeing Vertol Company

Irving C. Statler
Ames Directorate, USAAMRDL

Robert E. Steinwedel
Lord Kinematics

W. Z. Stepniewski
Boeing Vertol Company

K. G. Sunding
Lord Kinematics

Brian E. Swan
NASA–Ames Research Center

Peter Talbot
Ames Directorate, USAAMRDL

Frank J. Tarzanin
Boeing Vertol Company

Robert W. Thresher
Oregon State University

Andrew T. Trenka
Vizex, Inc.

William J. Twomey
Office National d'Études et de Recherches Aérospatiales

George F. Unger III
Naval Air Systems Command

V. V. Utgoff
U. S. Naval Academy

R. J. van der Harten
KLM Nordzee Helikopters B.V.

Henry R. Velkoff
HQ USAAMRDL

Robert A. Wagner
Hughes Helicopters

John F. Ward
NASA–Langley Research Center

George A. Watts
Lockheed California Company

Lawrence E. Wessman
U. S. Army

Richard P. White, Jr.
Rochester Applied Science Associates, Inc.

Bradford H. Wick
NASA–Ames Research Center

Joseph B. Wilkerson
U. S. Naval Ship Research and Development Center

Robert M. Williams
U. S. Naval Ship Research and Development Center

Robert Elliot Wilson
Oregon State University

William F. W on
Bell Helicopter Company

Robert A. Wolfe
U. S. Army Aviation Systems Command

Edward R. Wood
Lockheed California Company

Clifton Wrestler, Jr.
U. S. Army Materiel Command

Jing G. Yen
Bell Helicopter Company

Maurice I. Young
University of Delaware

Steven E. Zalesch
Naval Air Systems Command

☆ U.S. GOVERNMENT PRINTING OFFICE: 1974—635-043/25

NATIONAL AERONAUTICS AND SPACE ADMINISTRATION
WASHINGTON, D.C. 20546

OFFICIAL BUSINESS
PENALTY FOR PRIVATE USE $300

SPECIAL FOURTH-CLASS RATE BOOK

POSTAGE AND FEES PAID
NATIONAL AERONAUTICS AND SPACE ADMINISTRATION
451

U.S.MAIL

POSTMASTER: If Undeliverable (Section 158 Postal Manual) Do Not Return

"The aeronautical and space activities of the United States shall be conducted so as to contribute . . . to the expansion of human knowledge of phenomena in the atmosphere and space. The Administration shall provide for the widest practicable and appropriate dissemination of information concerning its activities and the results thereof."

—NATIONAL AERONAUTICS AND SPACE ACT OF 1958

NASA SCIENTIFIC AND TECHNICAL PUBLICATIONS

TECHNICAL REPORTS: Scientific and technical information considered important, complete, and a lasting contribution to existing knowledge.

TECHNICAL NOTES: Information less broad in scope but nevertheless of importance as a contribution to existing knowledge.

TECHNICAL MEMORANDUMS: Information receiving limited distribution because of preliminary data, security classification, or other reasons. Also includes conference proceedings with either limited or unlimited distribution.

CONTRACTOR REPORTS: Scientific and technical information generated under a NASA contract or grant and considered an important contribution to existing knowledge.

TECHNICAL TRANSLATIONS: Information published in a foreign language considered to merit NASA distribution in English.

SPECIAL PUBLICATIONS: Information derived from or of value to NASA activities. Publications include final reports of major projects, monographs, data compilations, handbooks, sourcebooks, and special bibliographies.

TECHNOLOGY UTILIZATION PUBLICATIONS: Information on technology used by NASA that may be of particular interest in commercial and other non-aerospace applications. Publications include Tech Briefs, Technology Utilization Reports and Technology Surveys.

Details on the availability of these publications may be obtained from:

SCIENTIFIC AND TECHNICAL INFORMATION OFFICE

NATIONAL AERONAUTICS AND SPACE ADMINISTRATION

Washington, D.C. 20546